

THE JOURNAL OF PHYSICAL CHEMISTRY

Volume 74, Number 23 November 12, 1970

Linear Regression Models in the Study of Charge-Transfer Complexation	Robert A. LaBudde and Milton Tamres	4009
The Aggregation of Arylazonaphthols. I. Dimerization of Bonadur Red in Aqueous and Methanolic Systems	Alan R. Monahan and Daniel F. Blossey	4014
Electron Spin Resonance Studies of Free Radicals Formed from Orotic Acid	Jürgen Hüttermann, John F. Ward, and L. S. Myers, Jr.	4022
Electron Paramagnetic Resonance Study of 4-Alkyl- <i>o</i> -benzosemiquinones	J. Pilarř	4029
An Exact Solution to the Rate Equation for Reversible Photoisomerization	Joseph Blanc	4037
The Photochemistry of Peroxodiphosphates. The Oxidation of Water and Two Alcohols	Roger J. Lussier, William M. Risen, Jr., and John O. Edwards	4039
The Photochemistry of Pentafluorobenzene in the Vapor Phase	Kh. Al-Ani and David Phillips	4046
Infrared Studies of the Matrix Isolated Photolysis Products of PF ₃ H and P ₂ F ₄ and the Thermal Decomposition Products of P ₂ F ₄	Jeremy K. Burdett, Leslie Hodges, Virginia Dunning, and Jerry H. Current	4053
Effect of Various "Dry Electron" Scavengers on the Radioluminescence of Indole in Polar Solution	H. B. Steen	4059
Effect of the Solvent on the Kinetics of Diazotization	Z. A. Schelly	4062
The Reduction of Ruthenium(III) Hexaammine by Hydrogen Atoms and Monovalent Zinc, Cadmium, and Nickel Ions in Aqueous Solutions	G. Navon and D. Meyerstein	4067
The Reactions of Methyl Benzoate and Methyl Formate with Hydrogen Bromide and Hydrogen Iodide	Richard K. Solly and Sidney W. Benson	4071
Kinetics of the Shock-Initiated Decomposition of 1,1-Difluoroethylene	J. M. Simmie and E. Tschuikow-Roux	4075
Recoil Tritium Reactions with Methyl Isocyanide and Methyl Cyanide. Estimates of Energy Deposition for the T-for-H Reaction	C. T. Ting and F. S. Rowland	4080
Energy Transfer in Alkali Halide Matrices	Mohan Khare and Everett R. Johnson	4085
Thermal Decomposition of the Perchlorate Ion in a Potassium Chloride Matrix	I. C. Hisatsune and D. G. Linnehan	4091
Ultrasonic Absorption in Aqueous Solutions of Polyethylene Glycol	L. W. Kessler, W. D. O'Brien, Jr., and F. Dunn	4096
Electron Spin Resonance Spectra and Catalytic Activity of Molybdenum Oxide on Various Supports	K. S. Seshadri and L. Petrakis	4102
Molecular Structure of Dilute Vitreous Selenium-Sulfur and Selenium-Tellurium Alloys	A. T. Ward	4110
Solute and Solvent Structure Effects in Volumes and Compressibilities of Organic Ions in Solution	L. H. Laliberté and B. E. Conway	4116
Diffusion of Several Transition Metal Ions in the Adsorbed Layer of Sodium Polyacrylate As Studied by Polarography	Hiroyuki Kojima and Shizuo Fujiwara	4126
Electronic Spectra of the Oxyanions of Selenium in Solution	A. Treinin and J. Wilf	4131
Formation of Ions and Excited States in the Laser Photolysis of Solutions of Pyrene	J. T. Richards, G. West, and J. K. Thomas	4137

Reduction of Cobalt(III) in Cobaltamines Induced by the Decomposition of Persulfate Ion James Dee White and H. Taube	4142
Chemisorption of Hydrogen and Ethylene and Hydrogenation of Ethylene on Zinc Oxide D. Narayana, Jagdish Lal, and V. Kesavulu	4150

NOTES

A Kinetic Study of the Reactions of Water with Sodium and Cesium in Methylamine R. R. Dewald and O. H. Bezirjian	4155
Vapor Phase Association of Methanol. Vapor Density Evidence for Trimer Formation Venghuot Cheam, Sutton B. Farnham, and Sherril D. Christian	4157
A Proton Nuclear Magnetic Resonance Technique for Determining the Surface Hydroxyl Content of Hydrated Silica Gel Victor M. Bermudez	4160
A Formulation of the Reaction Coordinate Kenichi Fukui	4161
Intramolecular Hydrogen Bond Formation in <i>o</i> -Trifluoromethylphenol Frank C. Marler, III, and Harry P. Hopkins, Jr.	4164
Diaphragm Cell Diffusion Studies with Short Prediffusion Times Michael J. Pikal	4165

COMMUNICATIONS TO THE EDITOR

Photodissociation of an e_{aq}^- Complex in Hydrogen-Saturated Alkaline Solutions C. Gopinathan, E. J. Hart and K. H. Schmidt	4169
Isentropic Compressibility of Ideal Solutions Gary L. Bertrand and Larry E. Smith	4171
Electronic Excitation Energy Transfer in Dye-Polyanion Complexes R. B. Cundall, C. Lewis, P. J. Llewellyn, and G. O. Phillips	4172
Chemical Equilibrium and the Anti-Helmholtz Function. A Statistical Interpretation D. K. Hoffman	4174
Intramolecular Energy Relaxation. A Novel and Direct Test of the RRR-RRKM Postulate J. D. Rynbrandt and B. S. Rabinovitch	4175

AUTHOR INDEX

Al-Ani, K., 4046	Edwards, J. O., 4039	Kessler, L. W., 4096	O'Brien, W. D., Jr., 4096	Seshadri, K. S., 4102
Benson, S. W., 4071	Farnham, S. B., 4157	Khare, M., 4085		Simmie, J. M., 4075
Bermudez, V. M., 4160	Fujiwara, S., 4126	Kojima, H., 4126	Petrakis, L., 4102	Smith, L. E., 4171
Bertrand, G. L., 4171	Fukui, K., 4161	LaBudde, R. A., 4009	Phillips, D., 4046	Solly, R. K., 4071
Bezirjian, O. H., 4155	Gopinathan, C., 4169	Lal, J., 4150	Phillips, G. O., 4172	Steen, H. B., 4059
Blanc, J., 4037	Hart, E. J., 4169	Laliberté, L. H., 4116	Pikal, M. J., 4165	Tamres, M., 4009
Blossey, D. F., 4014	Hisatsune, I. C., 4091	Lewis, C., 4172	Pilař, J., 4029	Taube, H., 4142
Burdett, J. K., 4053	Hodges, L., 4053	Linnehan, D. G., 4091	Rabinovitch, B. S., 4175	Thomas, J. K., 4137
Cheam, V., 4157	Hoffman, D. K., 4174	Llewellyn, P. J., 4172	Richards, J. T., 4137	Ting, C. T., 4080
Christian, S. D., 4157	Hopkins, H. P., Jr., 4164	Lussier, R. J., 4039	Risen, W. M., Jr., 4039	Treinin, A., 4131
Conway, B. E., 4116	Hüttermann, J., 4022	Marler, F. C., III, 4164	Rowland, F. S., 4080	Tschuikow-Roux, E., 4075
Cundall, R. B., 4172	Johnson, E. R., 4085	Meyerstein, D., 4067	Rynbrandt, J. D., 4175	Ward, A. T., 4110
Current, J. H., 4053	Kesavulu, V., 4150	Monahan, A. R., 4014	Schelly, Z. A., 4062	Ward, J. F., 4022
Dewald, R. R., 4155		Myers, L. S., Jr., 4022	Schmidt, K. H., 4169	West, G., 4137
Dunn, F., 4096		Narayana, D., 4150		White, J. D., 4142
Dunning, V., 4053		Navon, G., 4067		Wilf, J., 4131

ANNOUNCEMENT

On the last two pages of this issue you will find reproduced the table of contents of the October 1970 issue of the *Journal of Chemical and Engineering Data*.

Martin Karplus AND Richard N. Porter

Join Our P-Chem Paperback Picture

ATOMS AND MOLECULES

An Introduction for Students of Physical Chemistry

MARTIN KARPLUS, *Harvard University*

RICHARD N. PORTER, *University of Arkansas*

640 Pages. Illustrated. \$17.50 Cloth, \$7.95 Paper

This textbook, based on lectures given originally by Martin Karplus at Columbia University, is intended for the part of a beginning undergraduate sequence in physical chemistry concerned with basic principles of quantum theory and their application to atoms and molecules. It has been supplemented with material developed and taught by the authors over a period of years.

The writing style often forgoes the succinctness of purely mathematical exposition to explain *in words* the meaning and utility of a principle before it is formulated mathematically. Many examples of applications are from the recent literature of physical chemistry and chemical physics. Problems reinforce and extend the textual material and are of sufficient number and variety to allow the individual instructor flexibility in his emphasis.

The discussion of atomic and molecular structure goes beyond that of any available physical chemistry text, but these topics are treated in a style that places them within the context of the elementary course rather than in a more advanced course in quantum theory. In addition, the systematic and integrated treatment of van der Waals interactions, ionic bonds, transition metal complexes, and covalent bonds is unique in its organization with respect to open and closed shell interactions of atoms and ions.

The book should prove to be an effective bridge between the bonding principles taught in general chemistry and beginning organic chemistry and the subject matter of a first-year graduate course in quantum chemistry. Sufficient examples and applications of the principles make the book useful also to students for whom the elementary physical chemistry course is the terminal course in the subject.

Round Out Your Physical Chemistry Class Picture from this Gallery . . .

UNDERSTANDING PHYSICAL CHEMISTRY

Second Edition

ARTHUR W. ADAMSON, *University of Southern California*
528 Pages. \$12.50 Cloth, \$4.95 Paper

THE CALCULUS OF CHEMISTRY

With an Introduction to Computer Programming

JAMES NEWTON BUTLER, *Formerly University of British Columbia*

DANIEL GUREASKO BOBROW, *Massachusetts Institute of Technology*

160 Pages. Color Illus. \$12.50 Cloth, \$3.95 Paper

MOLECULAR THERMODYNAMICS

RICHARD E. DICKERSON, *California Institute of Technology*

450 Pages. \$15.00 Cloth, \$4.95 Paper

RATES AND MECHANISMS OF CHEMICAL REACTIONS

W. C. GARDINER, JR., *University of Texas*

350 Pages. \$15.00 Cloth, \$4.95 Paper

QUANTUM MECHANICS IN CHEMISTRY

Second Edition

MELVIN W. HANNA, *University of Colorado*

250 Pages. \$15.00 Cloth, \$4.95 Paper

THERMAL PROPERTIES OF MATTER

WALTER KAUZMANN, *Princeton University*

Volume I: Kinetic Theory of Gases

262 Pages. Illus.

Volume II: Thermodynamics and Statistics, With Applications to Gases

284 Pages. Color Illus. \$12.50 Cloth Each, \$4.95 Paper Each

INTRODUCTION TO CHEMICAL THERMODYNAMICS

IRVING M. KLOTZ, *Northwestern University*

262 Pages. Illus. \$4.95 Paper

SEVEN SOLID STATES

An Introduction to the Chemistry and Physics of Solids

WALTER J. MOORE, *Indiana University*

224 Pages. Illus. \$12.50 Cloth, \$4.95 Paper

INTRODUCTION TO CRYSTALLOGRAPHY

DONALD E. SANDS, *University of Kentucky*

165 Pages. \$15.00 Cloth, \$4.95 Paper

Just Published . . .

NUMERICAL TABLES OF TWO-CENTER OVERLAP INTEGRALS

EDWARD A. BOUDREAUX and LIONEL D. DUREAU, *Louisiana State University* L. CHOPIN CUSACHS, *Tulane University*

432 Pages. \$25.00 Cloth

This complete set of numerical values of overlap integrals required in molecular orbital calculations makes it possible for researchers to carry out any study where overlap integrals are required. The tables preclude the need for a com-

puter, and remove the traditional restriction of the types of atoms involved. Included are all possible combinations of orbital parameters encountered in any practical type of overlap computation.

Individual orders must be prepaid and total a minimum of \$10.00. Deduct 20%; we pay postage.



W. A. BENJAMIN, INC.

TWO PARK AVENUE • NEW YORK, N.Y. 10018

PROJECT SEED DEMONSTRATES ACS CONCERN

The Knoxville News-Sentinel-May 1970

b. About Dioxolenium Ions

Austin-East Senior Helps Write Scientific Paper

An Austin-East High School senior is the co-author, along with a UT assistant chemistry professor and a UT student, of a scientific paper with a tongue-titling title, "Relative Stabilities of Mono- and Dioxolenium Ions."

Arkansas Gazette-June 1970



She's Part of Project Catalyst

Kathleen Watts, who will be a senior this fall at Fayetteville, is one of several high school students in the nation participating in Project Catalyst, a program of the American Chemical Society that is designed to motivate disadvantaged students and encourage them to continue their education. Miss Watts, daughter of Mr. and Mrs. W. H. Watts of Fayetteville (her father is pastor of the Old Wire Road Church of Christ), is spending the summer doing chemical research at the University of Arkansas under a \$500 American Chemical Society grant. Her project concerns identification of compounds formed when electrons strike a liquid surface.

Laramie Daily Boomerang-July 1970



a Laramie student, 401 South 10th, associated with the University of Wyoming, chemistry of

natural plant poisons or toxins. The student's summer job has been made possible through the national office of the American Chemical Society, committee on chemistry and public affairs. (UW photo)

The Christian Science Monitor-June 1970

Helping high schoolers

Efforts of the business community to help disadvantaged kids often go unheralded. Consider the project of the American Chemical Society to move 100 high school students from poor neighborhoods to college campuses this summer.

Under "Project Catalyst" each boy or girl will receive a grant of \$500 and work directly with professors of chemistry and their research teams in serious scientific research. Launched as a pilot project in 1968 with 10 students, it is entirely supported by voluntary contributions from individual members of the American Chemical Society.

The students, going to 64 universities in 44 states, find they can overcome severe educational handicaps. They learn to mas-

ter slide rules, elements of computer programming, and the use of laboratory equipment. And a lot of them go back to their senior year in high school with a new determination to go on to college. The professors involved find they have a better understanding of how disadvantaged youths are motivated and think.

American Chemical Society members also support, by voluntary contributions, such programs as the finding of summer jobs in the chemical industry for disadvantaged college freshmen and sophomores. The blanket title for nine such summer projects is "Project Seed" (Subcommittee on the Education and Employment of the Disadvantaged). Rightly named!

Project SEED is a unique ACS activity that helps the local community and provides an opportunity for direct financial support by ACS members. To succeed it must have your interest and your continuing support through a positive commitment of your time and your funds. Please fill out the coupon and send it with your contribution to:

**American Chemical Society
1155 16th Street, N.W.
Washington, D.C. 20036**

PROJECT SEED:

Enclosed please find my contribution in the amount of \$ _____ to support the continuation of ACS Project SEED programs.

NAME _____

STREET _____

CITY & STATE _____

ACS Local Section _____

Please enclose with your donation made payable to ACS PROJECT SEED.

THE JOURNAL OF PHYSICAL CHEMISTRY

Registered in U. S. Patent Office © Copyright, 1970, by the American Chemical Society

VOLUME 74, NUMBER 23 NOVEMBER 12, 1970

Linear Regression Models in the Study of Charge-Transfer Complexation

by Robert A. LaBudde and Milton Tamres

Department of Chemistry, University of Michigan, Ann Arbor, Michigan 48104 (Received November 4, 1969)

Linear regression models are analyzed in the determination of equilibrium constants, K , and extinction coefficients, ϵ , of charge-transfer complexes. Criteria for separating K and ϵ from the $K\epsilon$ product in weak complexes are refined. For strong complexes where linear approximations lead to large error, equations are developed which permit reasonable corrections to be made from a knowledge of the experimental conditions.

Introduction

In recent years there has been a growing number of spectrophotometric studies of charge-transfer (CT) complexes in the vapor phase.¹⁻⁶ The experimental techniques generally are more involved than are those in solution and, consequently, the determination of the thermodynamic and spectral characteristics of the CT complexes are subject to greater uncertainty. First, concentrations may not be as precise because very small amounts of reagents are involved in many cases, and they may have to be determined by means other than weighing. Second, because of the interest in learning about solvent effects,⁷ many of the vapor studies to date have focused on the relatively nonvolatile acceptor molecules such as iodine^{1,3,4b,6} and tetracyanoethylene⁴ because of the many solution data already available for these acceptors. This has necessitated the vapor studies to be made at higher temperatures, a condition less favorable for complexation. Third, while pressure cells have been used for some contact CT observations in the vapor phase,^{8,9} they have not yet been employed to study more stable CT complexes. Until they are, the maximum concentration of the system in vapor studies will remain less than $10^{-1} M$, and more often closer to $10^{-2} M$.

Since vapor phase results are more directly related to theory,¹⁰ they are more likely to be quoted, which is all the more reason for keeping the above limitations in mind. Person¹¹ has focused on the difficulty in obtaining a meaningful separation of the equilibrium con-

stant, K , and the extinction coefficient, ϵ , when the extent of complexation is low. More recently, Deranleau¹² has stated that a reasonably low per cent error in K is possible only if the component of smaller concentration is between ~ 20 and 80% complexed, a situation which surely is not met in many of the vapor as well as some solution studies. In this paper we reexamine these concepts and, assuming the favorable situation of only 1:1 complexation, a criterion is de-

(1) (a) F. T. Lang and R. L. Strong, *J. Amer. Chem. Soc.*, **87**, 2345 (1965); (b) E. I. Ginns and R. L. Strong, *J. Phys. Chem.*, **71**, 3059 (1967).

(2) (a) J. Prochorow and A. Tramer, *J. Chem. Phys.*, **44**, 4545 (1966); (b) J. Prochorow, *ibid.*, **43**, 3394 (1965).

(3) (a) J. M. Goodenow and M. Tamres, *ibid.*, **43**, 3393 (1965); (b) M. Tamres and J. M. Goodenow, *J. Phys. Chem.*, **71**, 1982 (1967); (c) M. Tamres, W. K. Duerksen, and J. M. Goodenow, *ibid.*, **72**, 966 (1968); (d) W. K. Duerksen and M. Tamres, *J. Amer. Chem. Soc.*, **90**, 1379 (1968).

(4) (a) M. Kroll and M. L. Ginter, *J. Phys. Chem.*, **69**, 3671 (1965); (b) M. Kroll, *J. Amer. Chem. Soc.*, **90**, 1097 (1968).

(5) (a) S. D. Christian and J. Grundnes, *Nature*, **214**, 1111 (1967); (b) J. Grundnes and S. D. Christian, *J. Amer. Chem. Soc.*, **90**, 2239 (1968); *Acta Chem. Scand.*, **22**, 1702 (1968).

(6) A. A. Passchier and N. W. Gregory, *J. Phys. Chem.*, **72**, 2697 (1968).

(7) R. S. Mulliken, Proceedings of the Robert A. Welch Foundation Conferences on Chemical Research XI, Radiation and the Structure of Matter, Dec 4-6, 1967.

(8) D. F. Evans, *J. Chem. Soc.*, 1735 (1960).

(9) E. C. Lim and V. L. Kowalski, *J. Chem. Phys.*, **36**, 1729 (1962).

(10) R. S. Mulliken, *J. Amer. Chem. Soc.*, **74**, 811 (1952).

(11) W. B. Person, *ibid.*, **87**, 167 (1965).

(12) D. A. Deranleau, *ibid.*, **91**, 4044 (1969).

veloped separating K and ϵ from the $K\epsilon$ product which is an extension of Person's.

For stronger complexes, the concentrations in the vapor phase and solution are comparable, and more such studies are to be anticipated. In comparing the results in the two phases, it should be recalled that analysis of most of the earlier solution work was based on a linear regression model for a 1:1 complex. It is now known that this model leads to error.^{13,14} In the second part of the paper, equations are given which permit the effects of a linear approximation to be estimated from the experimental conditions, and these are analyzed using known, synthetically generated data.

1:1 Complexes. The vast majority of CT complexes studied have been considered to be of 1:1 composition. Recently, the question has been raised whether only 1:1 complex formation can be assumed from studies involving a limited concentration.^{12,15} Evidence has been given that even hexamethylbenzene-tetracyanoethylene forms both 1:1 and 2:1 complexes,¹⁶ with the former being dominant at the lower concentrations. For weak complexes or a low extent of complexation, the 1:1 species is favored and, for the purposes of this paper, it is assumed to be the only significant interaction. Then

$$K = \frac{C}{(D_0 - C)(A_0 - C)} \quad (1)$$

where D_0 and A_0 are the initial concentrations of donor and acceptor, respectively, and C is the equilibrium concentration of the complex. If it is further assumed that the only absorbing species are A, D, and C in the region studied spectrophotometrically, with molar extinction coefficients ϵ_A , ϵ_D , and ϵ_C , respectively, the Beer-Lambert relation for the complexation is

$$OD = \epsilon_A[A_0 - C] + \epsilon_D[D_0 - C] + \epsilon_C C \quad (2)$$

Let

$$OD' = OD - \epsilon_A A_0 - \epsilon_D D_0$$

$$\epsilon' = \epsilon_C - \epsilon_A - \epsilon_D$$

Then (2) becomes

$$OD' = \epsilon' C \quad (3)$$

Combining (3) with expression 1 gives the well-known relation

$$\frac{A_0 D_0}{OD'} = \frac{1}{K\epsilon'} + \frac{1}{\epsilon'} [A_0 + D_0] - \frac{OD'}{\epsilon'^2} \quad (4)$$

Since this relation is symmetric in A_0 and D_0 , it is expedient analytically to make the following transformations¹⁷

$$\alpha = (A_0 + D_0)/2$$

$$\beta = \frac{D_0}{A_0} \left(\text{or } \frac{A_0}{D_0} \right)$$

where β is chosen to be greater than one. Substitution in (1) and (4) gives, respectively

$$C^2 - (2\alpha + 1/K)C + \frac{4\alpha^2\beta}{(1 + \beta)^2} = 0 \quad (5)$$

and

$$\frac{4\alpha^2\beta}{(1 + \beta)^2 OD'} = \frac{1}{K\epsilon'} + \frac{2\alpha}{\epsilon'} - \frac{OD'}{\epsilon'^2} \quad (6)$$

The assignment

$$Y = \frac{A_0 D_0}{OD'} = \frac{4\alpha^2\beta}{(1 + \beta)^2 OD'} \quad (7)$$

sometimes will be referred to for convenience.

Weak Complexes. A linear approximation of relation (4) [or (6)] is commonly used in the statistical estimation of stability constants from spectrophotometric data, *i.e.*

$$Y \simeq \frac{1}{K\epsilon'} + \frac{2\alpha}{\epsilon'} \quad (8)$$

which is of the form

$$Y = a + b2\alpha \quad (9)$$

from whence

$$a = \frac{1}{K\epsilon'}; \quad b = \frac{1}{\epsilon'} \quad (10)$$

and

$$K = \frac{b}{a}; \quad \epsilon' = \frac{1}{b} \quad (11)$$

For very weak complexes, $1/K$ is large; the linear term in (8) vanishes in relation to the constant term. Since K and ϵ' can be determined separately only to the significance of the linearity of (9), some criterion governing the reliability of (11) is important. Person¹¹ suggested a criterion of

$$D_0 \simeq 2\alpha \geq 0.1/K \quad (\text{or } 2\alpha K \geq 0.1) \quad (12)$$

This is based on a standard deviation (σ) of 1% and a confidence level of 99% (or 3σ). Person extended this to 10σ by considering that very few data points are available.

Since the confidence level varies with the number of data points, one refinement would be to take this into account.¹⁸ Also, the error limits in a linear regression depend on the range covered in the x -coordinate. Thus

(13) N. J. Rose and R. S. Drago, *J. Am. Chem. Soc.*, **81**, 6138 (1959).

(14) M. Tamres, *J. Phys. Chem.*, **65**, 654 (1961).

(15) D. A. Deranleau, *J. Amer. Chem. Soc.*, **91**, 4050 (1969).

(16) P. J. Trotter and D. A. Yphantis, *J. Phys. Chem.*, **74**, 1399 (1970).

(17) For the case when $D_0 \gg A_0$, *i.e.*, the treatment of Benesi-Hildebrand, *J. Amer. Chem. Soc.*, **71**, 2703 (1949), then $\alpha \simeq D_0/2$.

(18) E. L. Heric, *ibid.*, **73**, 3496 (1969).

the range of the variable 2α should be considered and not just its magnitude.

Several statistical estimators can be used to test if the data are linearly dependent on α as given by (9). One choice might be the correlation coefficient r ; an equivalent choice might be the student- t value for the slope b . The evaluation of K and ϵ' is not considered acceptable if the statistic r is not significantly greater than zero at the $100(1 - \gamma)\%$ level, where γ is the maximum acceptable probability that the observed dependence of Y on 2α is spurious. In this paper γ will be taken as 0.05 (*i.e.*, the 95% confidence level).

The test can be applied in reverse fashion by asking, "For which minimum value of K is significance still possible at the 95% level?" Suppose the variable Y has 95% confidence intervals $Y \pm \Delta Y$. Then let

$$\eta = \frac{\Delta Y}{Y}$$

which is the convenient measure of the precision of the data.

If, as often is the case in spectrophotometric studies the errors in A_0 , D_0 , and cell length can be neglected,¹⁹ then $\eta = \Delta OD'/OD'$, which is the same as Deranleau's¹² $\eta = \Delta \text{Abs}/\text{Abs}$. This is equated in his treatment with $\Delta s/s$, where s is the fraction complexed of the component present in smaller concentration. For a fixed Δs , η varies over the entire range of complexation. It is this variation which leads to the conclusion that for $\Delta s = 0.01$ the error in ϵ rises rapidly when complexation is less than 20%. Similarly, errors in K rise rapidly outside the range 20–80% complexation, as is evidenced from eq 1 when $D_0 \gg A_0$; *i.e.*, large errors in K occur when C is very small or very large, and the smallest error occurs when $C = A_0/2$.

However, this applies only to the situation where the same experimental procedure is used over the entire range of complexation. It should be possible to have a small η for a very low extent of complexation by using a more sensitive method to detect differences. Spectrophotometrically, this is achieved by varying the cell length, so that η remains essentially constant over the entire range of measurements.

If $\pm 1\%$ error limits on Y are taken over the full range of 2α and these limits correspond to a 95% confidence level, then $\eta = 0.01$.²⁰ It follows from the definition of the correlation coefficient, if L is the range of the variable 2α , only those values of K which satisfy

$$KL \geq \frac{\eta r_\gamma}{(1 - r_\gamma^2)^{1/2}} = \frac{\eta t_\gamma}{(N - 2)^{1/2}} \quad (13)$$

can have regressions significant at the $100(1 - \gamma)\%$ level, where r_γ is the appropriate critical value of the correlation constant for N data points and t_γ is the appropriate value of the (one-sided) student- t statistic. Equality in (13) occurs when half of the data

points are at each end point of the range L and corresponds to the minimum value of KL for which $100(1 - \gamma)\%$ significance may still be attained.

Similarly, the inequality

$$KL \leq \frac{1/2\sqrt{2Nr_\gamma\eta}}{(1 - r_\gamma^2)^{1/2}} = 1/2t_\gamma\eta \left(\frac{2N}{N - 2} \right)^{1/2} \quad (14)$$

governs those KL which do not have $100(1 - \gamma)\%$ significance. Equality in (14) occurs when the least favorable selection of N data points in the range L is made and corresponds to the maximum value of KL for which a significance of $100(1 - \gamma)\%$ may still not be obtained in the regression. Since the Person criterion (12) governs these experiments which must satisfy the conditions for acceptance; the refinement of his criterion is therefore (14).

Values of $(KL)_{\min}$ and $(KL)_{\max}$ from (13) and (14), respectively, for different sample sizes for $\gamma = 0.05$ and $\eta = 0.01$ are given in Table I. For $N = 4$, the

Table I: Minimum and Maximum Critical Values of $[KL]$ at the 95% Significance Level^a

N	$[KL]_{\min}$ $\times 10^2$	$[KL]_{\max}$ $\times 10^2$
4	2.06	2.92
5	1.36	2.15
6	1.07	1.85
7	0.901	1.69
8	0.793	1.59
9	0.716	1.52
10	0.658	1.47
11	0.611	1.43
12	0.573	1.40
13	0.541	1.38
14	0.514	1.36
15	0.491	1.35
20	0.410	1.29
100	0.167	1.18
∞	0.000	1.16

^a For $\eta = 0.01$; this corresponds to approximately $\pm 1\%$ error in Y . For an error of $\pm p\%$ in Y , the entries in this table should be multiplied by p .

value would be close to that of 0.1 given by Person if a 99% confidence level had been used. For illustration, suppose a ten-point sample is taken with an experimental range $L = 0.01$, as may be the case in many vapor phase studies, and separation at the 95% significance level is desired. If $K < 0.658$, even the most optimal design of the experiment will not achieve separation

(19) For inclusion of the various sources of error see W. Wentworth, W. Hirsch, and E. Chen, *J. Phys. Chem.*, **71**, 218 (1967); also P. E. Hammond, *J. Chem. Soc.*, 479 (1964).

(20) If the error limits correspond to a different confidence level, this value should be multiplied by the ratio of the length of a 95% confidence interval to that of the given confidence in terms of standard deviations, *e.g.*, if $\pm 1\%$ error limits are for the 99% confidence level, $\eta = 2\sigma/3\sigma \times 0.01 = 0.067$.

with the desired level of significance. If $K \geq 1.47$, 95% significance will be obtained no matter how the points are chosen within the range. Conversely, if it is known after the fact that significance at the 95% level is not obtained, then it can be stated with regard to the true value of K that it must be less than 1.47.

A point which should be kept in mind is that the use of the values in Table I implies the choice of $\eta = 0.01$. In agreement with Deranleau,¹² a larger η makes it more difficult to determine small K . For some of the vapor phase studies, η may be appreciably larger.

Similar inequalities hold for the error in the slope b .

$$\sigma \frac{\sqrt{2}}{L} \leq \sigma_b \leq \sigma \frac{2}{LN^{1/2}}$$

Therefore, the greater the range L of the points, the smaller the error in the slope. Also, if additional points are chosen near the extremes, the error in the slope will decrease as $N^{-1/2}$; if near the center, more points may not affect the error in the slope.

Strong Complexes. The linear approximation (8) to determine K and ϵ is known to produce error for strong complexes.^{13,14} It is possible, however, to estimate the effect of the approximation. Equation 6 may be rewritten

$$Y = \frac{1}{K\epsilon'} + \frac{2\alpha}{\epsilon'} - \frac{C}{\epsilon'} \quad (15)$$

Assuming for the moment that there is no error in the observations, a linear regression of (15) will then correspond to a linear regression of

$$C = d + 2e\alpha \quad (16)$$

over the point set, and

$$Y = \frac{1}{\epsilon'} \left(\frac{1}{K} - d \right) + \frac{2\alpha}{\epsilon'} (1 - e) \quad (17)$$

If K^* and ϵ^* are the apparent values obtained from relations in (11), then

$$\frac{1}{K^*\epsilon^*} = \frac{1}{\epsilon'} \left(\frac{1}{K} - d \right); \quad \frac{1}{\epsilon^*} = \frac{1}{\epsilon'} (1 - e) \quad (18)$$

or

$$K^* = \frac{K(1 - e)}{1 - Kd}; \quad \epsilon^* = \frac{\epsilon'}{1 - e} \quad (19)$$

If β is a monotonically increasing function of α , then d and e are both positive, although generally quite small. Therefore ϵ^* will be larger than ϵ' by the small factor $1/(1 - e)$. Also, K^* will be larger than the true constant by the factor $(1 - e)/(1 - Kd)$, and for large K it is possible for K^* to be negative.

For small e , C does not vary much, and

$$C \simeq \frac{\overline{OD'}}{\epsilon^*}; \quad \epsilon^* \simeq \epsilon' \quad (20)$$

where $\overline{OD'}$ is the average optical density. Then

$$\frac{1}{K^*} \simeq \frac{1}{K} - \frac{\overline{OD'}}{\epsilon^*} \quad (21)$$

i.e., the last term is an "average" correction for the term omitted from the full eq 4. Rearranging

$$\frac{K^*}{K} \simeq \frac{\epsilon^* + \overline{OD'}K^*}{\epsilon^*}$$

Therefore, the fractional error in K can be approximated quite simply from usually readily available data by using the relation

$$\text{fractional error in } K = \frac{K^* - K}{K} \simeq \frac{\overline{OD'}}{\epsilon^*} K^* \quad (22)$$

This expression is in a more convenient form for spectrophotometric studies than a similar one given by Deranleau.^{12,21} It differs from Deranleau's with regard to sign; his fractional error is negative whereas that in (22) is positive since all terms on the right-hand side are positive. The difference is due to retaining $2\alpha = D_0 + A_0$ in this paper, whereas Deranleau used $2\alpha \simeq D_0$.^{12,17} If, as is common, C increases with α (*i.e.*, $e > 0$), then (22) will overestimate the fractional error in K .

Improved estimates of K and ϵ' can be obtained by estimating d and e directly from the experimental data. This can be done by approximating C from the linear terms of its Taylor series expansion (after solving for C in eq 5). Letting α_m and β_m be the mean values of α and β , respectively, it can be shown that the following expressions for d and e are obtained for the two cases.

Case 1. The species of lower concentration is held constant (a common procedure for CT studies in solution).

$$d = \frac{2\alpha_m^2\beta_m}{S_m(1 + \beta_m)^2} \left[\frac{\alpha_m}{\alpha_m + \frac{1}{2K^*}} \times \left\{ 1 - \frac{2\alpha_m\beta_m}{(1 + \beta_m)^2 \left(\alpha_m + \frac{1}{2K^*} \right)} \right\} - \frac{1}{\beta_m} \right] \quad (23)$$

$$e = \frac{\alpha_m\beta_m}{S_m(1 + \beta_m)^2} \left[\frac{\beta_m + 1}{\beta_m} - \frac{\alpha_m}{\alpha_m + \frac{1}{2K^*}} \right] \quad (24)$$

Case 2. β varies independently of α (*i.e.*, A_0 and D_0 vary independently).

$$d = \frac{2\alpha_m^2\beta_m}{S_m(1 + \beta_m)^2} \left[\frac{\alpha_m}{\alpha_m + \frac{1}{2K^*}} \times \left\{ 1 - \frac{2\alpha_m\beta_m}{(1 + \beta_m)^2 \left(\alpha_m + \frac{1}{2K^*} \right)} \right\} - 1 \right] \quad (25)$$

(21) Deranleau's expression can be rewritten as

$$\frac{K' - K}{K} \simeq - \frac{\overline{OD'}}{\epsilon^* D_0}$$

$$e = \frac{\alpha_m \beta_m}{S_m(1 + \beta_m)^2} \left[2 - \frac{\alpha_m}{\alpha_m + \frac{1}{2K^*}} \right] \quad (26)$$

where, in both cases

$$S_m = \left(\alpha_m + \frac{1}{2K^*} \right) \times \left[1 - \frac{2\alpha_m^2 \beta_m}{(1 + \beta_m)^2 \left(\alpha_m + \frac{1}{2K^*} \right)^2} \right] \quad (27)$$

Some general points can be made for cases 1 and 2. Clearly $e > 0$ for both cases. When case 2 holds, $d < 0$ and e is maximized. When case 1 holds, e is minimized; and for β_m moderately large and $\alpha_m > 1/2K^*$, $d > 0$ and e vanishes.

It should be noted that only estimates α_m and β_m are needed to calculate d and e , and hence to calculate corrected values of K and ϵ' .

$$K = \frac{K^*}{1 - e + K^*d}; \quad \epsilon' = \epsilon^*(1 - e) \quad (28)$$

If desired, an iterative procedure can be used for further refinement.

These relations were examined using synthetic data. Seventeen representative samples were chosen for varying magnitudes K and ϵ' . The value of K , ϵ' , $\alpha_m \beta_m$, and \overline{OD}' for each sample is listed in Table II. Effort was made to keep the optical densities of the samples within typical experimental range. All samples correspond to sets of eight concentrations, except for number 2 which consists of only six concentrations. In order to isolate the systematic trend with the value of K , samples number 1-16 were chosen to obey case 1; sample number 17 was included as an example of case 2. Values of K^* and ϵ^* were calculated from eq 8, and d and e were calculated from a regression of eq 16. These may be compared with d and e (called d^* and e^* in Table II) calculated from (23) and (24) for numbers 1-16, and from (25) and (26) for number 17. The values of d^* and e^* listed are the final values of four successive iterations of the equations, and the final corrected values of K^* from (28) are given for comparison. The error in K^* was usually of the order of that predicted by (22).

As can be seen from samples 1-14, the systematic error in K^* increases rapidly as K increases, the error being less than 1% for $K < 100$. The error in ϵ^* is small when case 1 holds. The calculated values of d^* and e^* from case 1 give good estimates of d and e . In samples 5 and 15 and in 8 and 16, the only difference within the pairs is in the magnitude of α_m and β_m . A smaller error for ϵ^* in samples 15 and 16 is obtained, in accordance with eq 24. In samples 13 and 14, for very large K , d becomes greater than $1/K$

Table II: Comparison of True and Calculated Values of Parameters

Sample ^a	K	ϵ	$\alpha_m \times 10^3$	$\beta_m \times 10^{-2}$	\overline{OD}'	K^* ^b	ϵ^* ^b	$d^* \times 10^4$	$e^* \times 10^3$	$d^{*d} \times 10^4$	$e^{*e} \times 10^3$	K_{cor}^f
1	1.0	15000	325	13.0	2.86	0.9999	15003	6.972	0.190	7.730	0.1836	1.0000
2	20.0	15000	1.01	1.00	0.0115	19.99	15006	0.082	0.370	0.0022	0.3697	19.997
3	100	15000	10.5	2.10	0.871	100.2	15017	3.410	1.138	4.500	1.051	99.855
4	500	15000	2.30	0.450	0.958	506	15094	3.529	6.218	4.537	4.932	497.0
5	1000	20000	0.890	0.213	0.978	1016	20240	2.779	11.86	2.827	11.59	998.9
6	5000	20000	0.680	0.217	1.015	6259	20139	4.134	6.903	4.067	6.825	5016.4
7	10000	20000	0.350	0.130	0.841	14879	20244	3.360	12.07	3.167	12.94	10204
8	15000	30000	0.235	0.225	0.493	18264	30261	1.239	8.625	1.368	6.488	14690
9	20000	30000	0.235	0.225	0.514	27332	30222	1.368	7.353	1.464	5.604	19600
10	30000	30000	0.233	0.300	0.404	45734	30124	1.156	4.127	1.211	3.113	29492
11	40000	30000	0.233	0.300	0.414	78186	30101	1.225	3.344	1.256	2.663	39493
12	50000	30000	0.233	0.300	0.421	136830	30085	1.271	2.811	1.284	2.373	49677
13	75000	30000	0.233	0.300	0.430	-1.929 × 10 ⁷	30060	1.339	2.011	0	0	0
14	100000	30000	0.233	0.300	0.434	-266000	30047	1.375	1.565	0	0	0
15	1000	20000	1.11	0.435	0.606	1014	20102	1.901	5.065	2.220	5.161	996.7
16	15000	30000	1.10	1.09	0.571	20664	30010	1.829	0.339	1.848	0.3439	14958.
17	1000	20000	0.941	0.089	4.92	705.7	25029	-13.23	200.9	-5.107 ^h	81.70 ⁱ	799.9

^a Sample consists of eight data points, except number 2 which has only six. ^b Calculated from (11). ^c Calculated from (16). ^d Calculated from (23). ^e Calculated from (24). ^f Corrected K , calculated from (28). ^g Could not be calculated because K is negative. ^h Calculated from (25). ⁱ Calculated from (26).

and K^* becomes negative. The corrected values of K^* for samples 1-16 are quite good. The much poorer result for sample 17 using eq 25 and 26 is due to the large variations in α and β which makes the Taylor series approximation more in error.

Acknowledgment. This work was supported in part by a grant from the National Science Foundation, NSF GP-6429. One of the authors (R. A. L.) expresses his appreciation for two NSF Undergraduate Research Participation Awards.

The Aggregation of Arylazonaphthols. I. Dimerization of Bonadur

Red in Aqueous and Methanolic Systems

by Alan R. Monahan* and Daniel F. Blosssey

Research Laboratories, Xerox Corporation, Xerox Square, Rochester, New York 14608 (Received April 17, 1970)

The absorption spectra of the sodium salt of Bonadur Red in aqueous and methanolic solutions were analyzed in terms of monomer-dimer equilibria in the concentration range 10^{-6} to 10^{-4} mol l.⁻¹. The dimerization constants, $K_{eq} = c_d/c_m^2$, are $(8.00 \pm 2.73) \times 10^3$ and $(1.25 \pm 0.01) \times 10^4$ l. mol⁻¹ for the methanol and water systems, respectively. The absorption spectra of the pure monomer and pure dimer in the two solvents were calculated. The splitting and relative strengths of the dimer bands were used along with the strength of the monomer band to calculate the relative orientations of the two dye molecules in the dimer. Assuming a parallel plane dimer configuration, the twist angle between the dye molecules was calculated to be $43 \pm 10^\circ$ for the dye-methanol system and $63 \pm 1^\circ$ for the dye-water system. The spacing between the molecules was calculated to be 4.6 ± 0.2 Å in methanol and 4.3 ± 0.0 Å in water. In addition, for the dye-methanol solution, the dimer splitting was 2700 ± 200 cm⁻¹ with the midpoint between the H- and J-dimer bands red-shifted by 200 ± 100 cm⁻¹ from the monomer peak. For the dye-water solution, the splitting was 2200 ± 100 cm⁻¹ with the midpoint red-shifted by 800 ± 100 cm⁻¹ from the monomer peak. These findings are consistent with a greater degree of overlap of the electron wave functions between the molecules in the dimer in water than in methanol. The general similarities between the dimerization in aqueous and methanolic systems led to the suggestion that hydrogen bonding may be responsible for aggregation. This was partially supported by the exothermic heats of dimerization of 5.7 ± 1.0 kcal (mol dimer)⁻¹ for both solutions.

Introduction

It is well documented in the chemical literature that the dimerization of dyes and formation of higher order aggregates in solution and the solid state is responsible for dramatic color changes,¹ enhanced photosensitizing properties,² etc. Azo compounds were chosen for this investigation because they form the largest class of organic pigments, and their detailed spectroscopy has not been studied in solvents capable of promoting aggregation.

Non-Beer's law behavior for the solution spectra of organic dyes is generally attributed to aggregation of the dye molecules. Aggregation of dye molecules, as measured by deviations from ideality, has been found in limited classes of solvents for concentration ranges typically of the order of 10^{-6} to 10^{-4} M. To form the simplest aggregate, the dimer, the dye-dye interaction must be strong enough to overcome any other forces which would favor solvation of the monomer. Thus nonpolar solvents are presumably to be preferred over

polar solvents because, the lower the dielectric constant of the solvent, the less the screening of the dye-dye interaction by the solvent.^{3,4} In actuality, water forms the system from which the largest body of information has been accumulated concerning dye aggregation processes. Because water does not have as low a dielectric constant as nonpolar solvents but still is a host for dye aggregations, it has been said to be anomalous.⁵ Aggregation has been observed in alcoholic systems,⁶

* To whom correspondence should be addressed.

(1) (a) E. S. Emerson, M. A. Conlin, A. E. Rosenoff, K. S. Norland, H. Rodriguez, D. Chin, and G. R. Bird, *J. Phys. Chem.*, **71**, 2396 (1967); (b) W. West and S. Pearce, *ibid.*, **69**, 1894 (1965).

(2) G. R. Bird, B. Zuckerman, and A. E. Ames, *Photochem. Photobiol.*, **8**, 393 (1968).

(3) K. Sauer, J. R. Lindsay Smith, and A. J. Schultz, *J. Amer. Chem. Soc.*, **88**, 2681 (1966).

(4) R. B. McKay and P. J. Hilson, *Trans. Faraday Soc.*, **63**, 777 (1967).

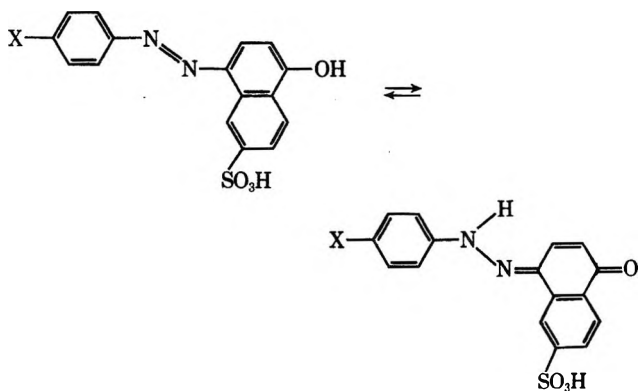
(5) M. J. Blandamer, M. C. R. Symons, and M. J. Wooten, *ibid.*, **63**, 2337 (1967).

particularly at low temperatures, but to a lesser degree than in water. Some authors feel that the solvent can participate in the dimer bonding (e.g., hydrogen bonding *via* hydroxyl groups), although solvation generally interferes with dimerization.⁷ In the case of water, the dye-dye interaction is probably not the major force driving the molecules toward aggregation; instead the strong solvent-solvent interaction, no doubt, tends to exclude the dye molecules from solution and causes them to aggregate.

Spectrophotometric techniques are most often used for studying these phenomena although conductometric techniques,⁸ as well as vapor pressure lowering,⁹ have been found to be useful probes into the nature of these phenomena. Nmr spectroscopy has been used as a particularly powerful technique for studying the specific types of interactions mentioned above.¹⁰ Very briefly, spectrophotometric observations are generally associated with the appearance of new bands as the dye concentration in solution is increased.^{1,7} The new bands are formed at the expense of the high intensity band seen at dilute concentrations. This absorption band is generally the same one observed in solvents displaying Beer's law behavior over extended concentration ranges ($>10^{-5}$).

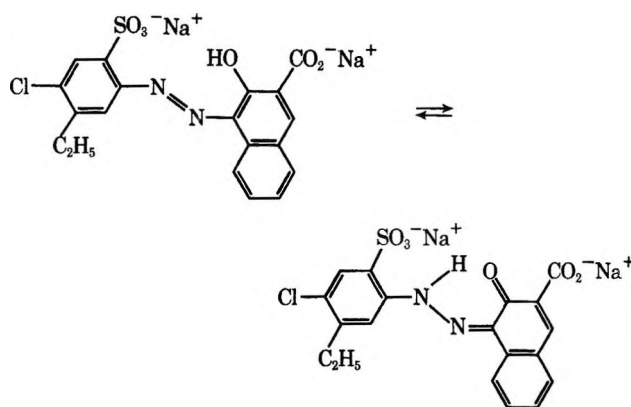
The formation of dimers and higher aggregates of azo dyes (benzoporpurines) was first observed in a qualitative manner by Robinson and Molliet¹¹ in H₂O using conductometric techniques and was later confirmed by Sheppard and Geddes¹² using spectrophotometric methods. Their spectra, as the concentration was increased, showed a slight broadening and loss in intensity; however, no new bands appeared. This behavior was in marked contrast to classes of dyes such as cyanines, fluoresceins, Rhodamine-B, Eosin, porphyrines, and phthalocyanines which were either mentioned or reported in the same paper. In all these systems, distinct new transitions occurred at the expense of the highest intensity, dilute solution bands. In addition to the sparse spectroscopic evidence reported by Sheppard, azo dye aggregation has been observed in mixed molecular systems by Lemin and Vickerstaff.¹³

Zollinger¹⁴ has qualitatively observed dimer formation in H₂O in molecules of the type



This molecule is an arylazonaphthol and is similar to the one reported on in this study, e.g., both dyes exist in solution and the solid state as mixtures of an azo tautomer and a hydrazone tautomer. In the concentration range, 10^{-6} – 10^{-4} M, increasing proportions of the above dye, at any concentration, were in the associated form as the electron-withdrawing nature of group X was increased, i.e., as the fraction of the hydrazone tautomer increases.¹⁵ When X was $-\text{NO}_2$, the hydrazone absorption at $479 \text{ m}\mu$ was superseded by another band at $451 \text{ m}\mu$ as the concentration was increased from 5.0×10^{-6} to 4.0×10^{-4} M. Finally, Fischer and coworkers¹⁶ have qualitative evidence for the possibility of formation of hydrogen-bonded aggregates in cyclohexane for *m*- and *p*-hydroxyazobenzenes. Similar to the dyes in Zollinger's study, these molecules contain OH groups which are labile and capable of intermolecular hydrogen bonding.

In this paper, we report studies on the monomer-dimer equilibrium of the sodium azo dye salt derived from 2-amino-4-ethyl-5-chlorobenzenesulfonic acid and 2-hydroxy-3-naphthoic acid.



The calcium salt of this compound is a common magenta pigment called Bonadur Red. The spectrophotometric techniques used in the past by West and Pearce^{1b} and other workers³ were used as guides in this investigation.

(6) E. Rabinowitch and L. F. Epstein, *J. Amer. Chem. Soc.*, **63**, 69 (1941).

(7) Kh. L. Arvan and N. E. Zaitseva, *Opt. Spectrosk.*, **10**, 137 (1961).

(8) F. H. Holmes and H. A. Standing, *Trans. Faraday Soc.*, **41**, 568 (1945).

(9) S. Arnoff, *Arch. Biochem. Biophys.*, **98**, 344 (1962).

(10) D. J. Blears and S. S. Danyluk, *J. Amer. Chem. Soc.*, **89**, 21 (1967).

(11) C. Robinson and J. L. Molliet, *Proc. Roy. Soc., Ser. A*, **143**, 630 (1934).

(12) S. E. Sheppard and A. L. Geddes, *J. Amer. Chem. Soc.*, **66**, 1995 (1944).

(13) D. R. Lemin and T. Vickerstaff, *Trans. Faraday Soc.*, **43**, 491 (1947).

(14) H. Zollinger, "Azo and Diazo Chemistry," Interscience, New York, N. Y., 1961, pp 311–360.

(15) I. Saito, Y. Bansho, and A. Kakuta, *Tokyo Kogyo Shikensho Hokoku*, **63**, 105 (1968).

(16) (a) G. Gabor, Y. F. Frei, and E. Fischer, *J. Phys. Chem.*, **72**, 3266 (1968); (b) G. Gabor, Y. F. Frei, D. Gegiou, M. Kagonowitch, and E. Fischer, *Israel J. Chem.*, **5**, 193 (1967).

A computer program was developed in this study which effectively separates out monomer and dimer contributions at each concentration without making assumptions pertaining to the nature of the "pure" monomer or dimer absorption spectrum.

Experimental Section

The dye, Na₂ Bonadur, was prepared by standard preparative procedures¹⁴ from 2-amino-4-ethyl-5-chlorobenzenesulfonic acid (American Cyanamid) and 2-hydroxy-3-naphthoic acid (Pfister). The former was recrystallized twice from a sodium acetate-deionized water solution and the latter compound twice from isopropyl alcohol.

The synthesized dye was recrystallized from distilled water after several distilled water washings and dried under vacuum at 60° for 12 hr. (Anal. Calcd for Na₂ Bonadur: C, 47.65; H, 2.75; N, 5.86. Found: C, 48.00; H, 2.71; N, 5.89.)

Spectra were run immediately after solution preparation on a Cary Model 14R automatic spectrophotometer using 0.1-, 1-, 5-, and 10-cm matched quartz cells. Low temperature and temperature-dependent spectra were taken in a 5-cm all-quartz absorption cell. The cell was fitted with an outer Dewar jacket and an inner cell for liquid nitrogen or thermostated water. For equilibrium measurements the cell was controlled ($\pm 0.2^\circ$) by circulation of water from an external thermostat. Water used for the solution spectroscopy was distilled from an all-glass system. The methanol was spectroquality solvent obtained from Matheson Coleman and Bell and was used without further purification.

The freshly distilled water used in the experiments initially had a pH of 6.95 ± 0.05 but, due to CO₂ absorption, the water stabilized at a pH of 6.00 ± 0.05 after a period of 20 min. All spectroscopic results quoted for water were at solution temperatures of $22 \pm 1^\circ$ and a pH of 6.00 ± 0.05 . To observe if there was any mild pH effect on the spectra, the pH was varied between 6 and 8 by adding NaOH with no noticeable changes in the spectra. Effects of large pH changes (pH 3 to 11) along with substituent effects on the monomer-dimer equilibrium and dimer structure will be the subject of a future publication.¹⁷ In reference to the dye structure, it is most likely that the molecules exist as contact ion pairs. This can be inferred from the work of Zaugg and Schaeffer¹⁸ in which they observed solvent-induced electronic spectral shifts of the solution spectra of a series of alkali salts of phenols and enols. They found that a wide variety of organometallic salts having a pK_a range of 2 to 11 exist as contact (intimate) ion pairs in water and ethanol whereas stronger solvating agents such as DMF, DME, THF, etc., are required to produce solvent separated ion pairs.

Results and Discussion

Concentration Dependence. The concentration dependences of the absorption spectra of the sodium salt

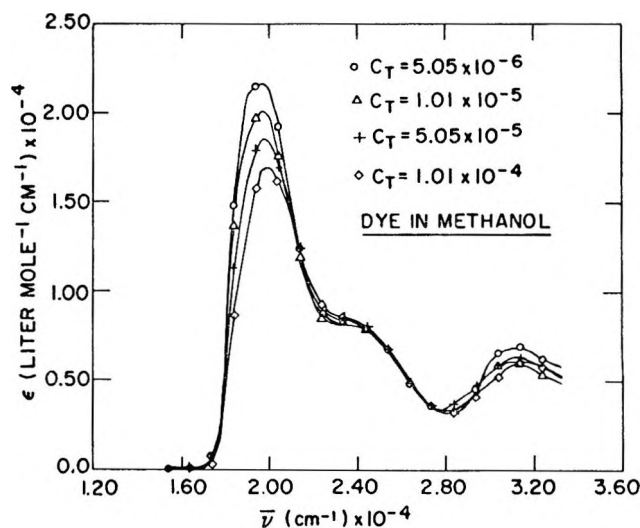
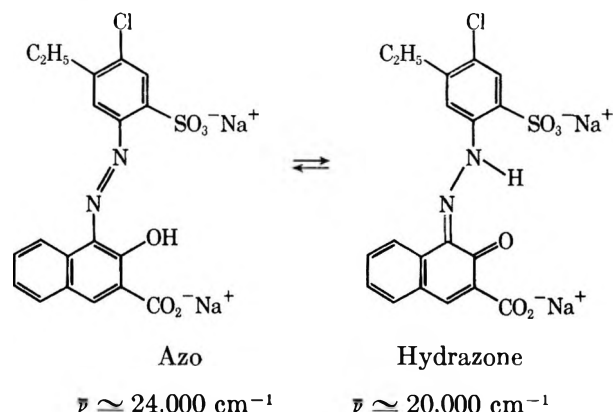


Figure 1. Concentration dependence of Na₂ Bonadur in methanol. All spectra obtained at 22°. The symbols on curves in this figure and following figures for notation purposes only.

of Bonadur Red (hereafter called Na₂ Bonadur) in methanol and water are shown in Figure 1 and 2, respectively. Spectra in both solvents were characterized by an intense monomer peak at 20,000 cm⁻¹ with a shoulder at 24,000 cm⁻¹. The major peak is assigned to the quinone-hydrazone tautomer of the dye and the shoulder to a vibrational satellite of the hydrazone^{16b} and partly to contributions from the corresponding azo tautomer, *viz.*



In this type of molecule, the hydrazone tautomer always absorbs at lower energy than that of the azo tautomer.¹⁴ In addition, *o*-hydroxyaryazonaphthols, independent of substituent and solvent, nearly always contain a majority concentration of the quinoid tautomer.^{16b} It is not the purpose of this paper to discuss the ramifications of the tautomerization of azo dyes and general spectroscopy since this has been the subject of voluminous reports.^{14, 16b} However, it is stressed that the assignment

(17) A. R. Monahan, N. J. Germano, and D. F. Blossey, unpublished work.

(18) H. E. Zaugg and A. D. Schaeffer, *J. Amer. Chem. Soc.*, **87**, 1857 (1965).

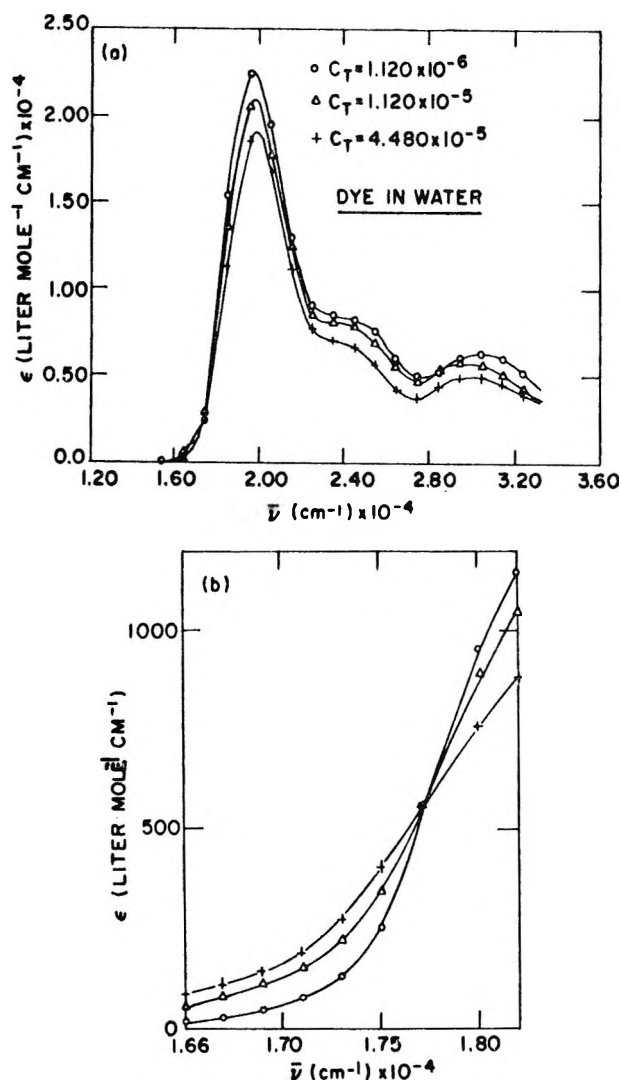


Figure 2. (a) Concentration dependence of Na_2 Bonadur in water. (b) Expanded scale showing isosbestic point.

of the high intensity band to that of the hydrazone was made with a high degree of confidence. This is based largely on past work and the strong carbonyl absorption of this compound in the infrared at 1620 cm^{-1} .¹⁴

The concentration dependence of the dye-methanol system was characterized by a slight blue shift of the absorption peak with increasing concentration. Also, a uniform loss in intensity was observed with the exception of a crossover at $22,000\text{ cm}^{-1}$. The maximum concentration of $1.01 \times 10^{-4}\text{ M}$ is roughly the limit of solubility of the molecule in methanol. The spectral concentration dependence in water was somewhat similar with the exception of a slight gain in intensity on the red tail of the hydrazone absorption with increasing concentration. Although the Bonadur compound is soluble in water in excess of 10^{-3} M , solutions in excess of 10^{-4} yielded nonuniform spectral changes with further increases in concentration. Therefore, it was not unreasonable to assume that above 10^{-4} , aggregates other than dimers were being formed (*i.e.*, trimers,

tetramers, etc.).^{1b} Additional evidence supporting this assumption will be presented during the data analysis.

Monomer-Dimer Equilibrium. It has been demonstrated in the past^{1b,3} that monomer-dimer equilibria follow the law of mass action

$$c_d/c_m^2 = K_{eq} \quad (1)$$

where K_{eq} is the equilibrium constant, c_d is the dimer concentration, and c_m is the monomer concentration. This equation has been found to be valid for several dye systems in both aqueous and nonpolar solvents. Since it takes two monomer units to make up one dimer unit, the dimer concentration is given by

$$c_d = (c_t - c_m)/2 \quad (2)$$

where c_t is the total dye concentration. This equation restricts the application of mass law to only a monomer-dimer equilibrium. By combining eq 1 and 2, both c_d and c_m may be determined as functions of the total concentration c_t and the monomer-dimer equilibrium constant K_{eq} . The molar extinction coefficient ϵ_t in $\text{l. mol}^{-1}\text{ cm}^{-1}$ is a function of the total concentration c_t and dependent on the relative concentrations of the monomer and dimer species. If the concentration range can be controlled so that only the monomer and dimer species are present, then ϵ_t may be expressed as the sum of a term due to absorption by the monomer species and a term due to the absorption of the dimer species. If ϵ_m is the monomer molar extinction coefficient and ϵ_d is the dimer molar extinction coefficient *per monomer unit* then the molar extinction coefficient ϵ_t may be related to ϵ_m and ϵ_d as

$$c_t \epsilon_t = c_m \epsilon_m + 2c_d \epsilon_d \quad (3)$$

The factor of two in front of the dimer contribution in eq 3 is needed because c_d is the concentration of dimer units and ϵ_d is the dimer molar extinction coefficient per monomer unit. ϵ_d was expressed this way so that direct comparison of the molecular oscillator strengths in the monomer and the dimer species could be made. Combining eq 1, 2, and 3 gave ϵ_t as a function of the total concentration c_t , the equilibrium constant K_{eq} , and the monomer and dimer extinction coefficients ϵ_m and ϵ_d

$$\epsilon_t = \left[\frac{\sqrt{1+2x}-1}{x} \right] \epsilon_m + \left[\frac{1+x-\sqrt{1+2x}}{x} \right] \epsilon_d \quad (4)$$

where $x = 4K_{eq}c_t$. For $x \ll 1$, ϵ_t is approximately equal to ϵ_m ; thus, in principle, it should be possible to achieve a solution at low concentrations in which only the monomer species exist. In reality, there is a lower concentration limit below which the optical density of the solution is too small a quantity to measure accurately. The dimer spectrum and equilibrium constant could be

calculated quite simply if the pure monomer spectrum were known,^{1b,3} but for our concentration range of dye solutions, it was not possible to attain a dilute enough solution to have the pure monomer species. For other dyes,^{1b} the pure monomer species can be attained in methanol, but for sodium Bonadur solutions the dye-methanol and dye-water solutions behave very much the same. Negligible solubility in other solvents made it necessary to develop an alternative approach.

The analysis of monomer-dimer equilibria *via* spectroscopy is especially adaptable to computer methods. It could even be said that analysis by hand is not only too tedious but that it also may give erroneous results. In this calculation, the best-fit monomer spectrum ϵ_m , the dimer spectrum ϵ_d , and equilibrium constant K_{eq} were calculated simultaneously by using eq 4 to fit the spectrum at several concentrations c_t . The standard deviation in K_{eq} was then found using the best-fit ϵ_d and ϵ_m to find K_{eq} at each concentration. If the standard deviation in K_{eq} was within reasonable limits, then the validity of the mass law of eq 1 was confirmed, and the calculation was internally consistent. For any equilibrium constant K_{eq} , a best-fit monomer and dimer spectrum could be calculated; the problem was in finding the best one. The best-fit monomer and dimer spectra for a given K_{eq} were used in eq 4 to calculate an average standard deviation between the data at all concentrations c_t and the best-fit result. To find the best K_{eq} , this standard deviation was minimized. It has been our experience that the calculated monomer and dimer spectra were strongly dependent on the choice of equilibrium constant K_{eq} . Conversely, the resulting standard deviation which was minimized was only weakly dependent on the equilibrium constant K_{eq} . Thus, *if the pure monomer spectrum is not attainable*, many calculations are necessary to find the best K_{eq} which, without using a computer, is not feasible. To reiterate, the computational method used was as follows. (1) Vary K_{eq} in a systematic manner. (2) For each K_{eq} , calculate the best-fit ϵ_m and ϵ_d at each wavelength using eq 4. (3) Using the best-fit monomer and dimer spectra for the given K_{eq} , calculate the average standard deviation between the experimental ϵ_t and the best-fit ϵ_t for the data at all concentrations. (4) Compare the standard deviations for various choices of K_{eq} and choose the K_{eq} that gives the minimum standard deviation. (5) Use the monomer and dimer spectra calculated at the best K_{eq} to calculate a best K_{eq} for each concentration c_t . (6) Calculate the standard deviation in K_{eq} . If the standard deviation in K_{eq} was within reasonable limits, then the calculation was considered to be internally consistent.

To be certain that a true monomer-dimer equilibrium was taking place (*i.e.*, no higher aggregates are present), care was taken in choosing the allowable concentration range for the dye in solution. For a dye concentration of less than 5×10^{-5} mol l.⁻¹ in water, the resulting

equilibrium constants were within 1% of each other. Increasing the range to 2×10^{-4} mol l.⁻¹ caused the resulting equilibrium constants to deviate by more than 100% from one another. Thus, for dye concentrations greater than 5×10^{-5} mol l.⁻¹ in water, there are, no doubt, higher order aggregates (trimers, tetramers, etc.) being formed which are altering the spectra. Usually, it was quite easy to see the concentration at which larger aggregates are being formed because the spectra changed systematically up to that point. Beyond that, new changes in the spectra were observed. This concentration provides an upper bound on the dye concentration above which the data were unacceptable for studying monomer-dimer equilibria.

The best-fit monomer and dimer spectra are shown in Figures 3 and 4 for the dye-methanol and dye-water

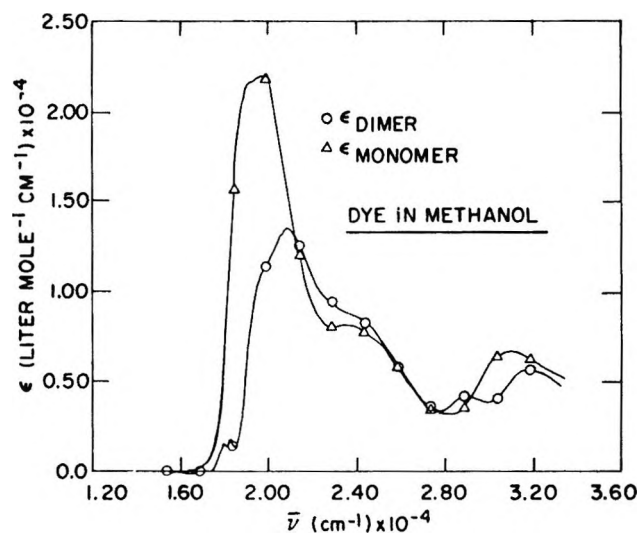


Figure 3. Calculated absorption spectra of pure monomer and dimer in methanol. Dimer spectrum plotted per monomer unit.

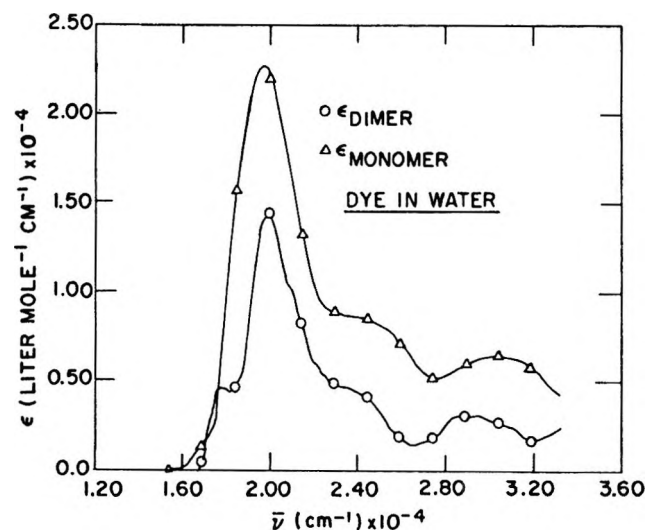


Figure 4. Calculated absorption spectra of pure monomer and dimer in water. Dimer spectrum plotted per monomer unit.

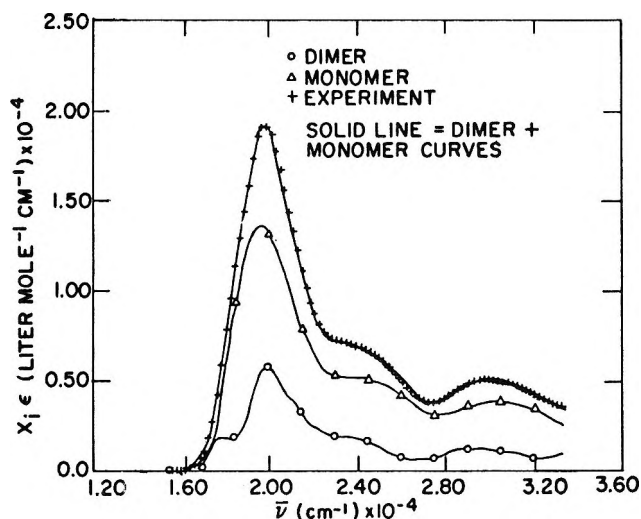


Figure 5. Sample best-fit spectrum showing resolved monomer and dimer contributions to the total spectrum; x_i mole fraction of individual species. Figure shown is for dye in water at a concentration of $4.48 \times 10^{-6} \text{ mol l.}^{-1}$.

solutions, respectively. The best fit was obtained at equilibrium constants of $K_{\text{eq}} = 8.00 \times 10^3 \text{ l. mol}^{-1}$ for the dye-methanol solution and $K_{\text{eq}} = 1.25 \times 10^4 \text{ l. mol}^{-1}$ for the dye-water solution. Figure 5 shows, for a given dye concentration in water, a sample best fit of monomer and dimer contributions compared with the experimental spectrum at that particular concentration.

To show that the calculation is internally consistent, the monomer and dimer spectra shown in Figures 3 and 4 were used to calculate equilibrium constants for each concentration. The results of this calculation are given in Table I. Figure 6 shows the agreement with a simple monomer-dimer equilibria by graphical display of eq 1 in logarithmic form.

Dimer Structure. When two dye molecules come together to form a dimer unit, the monomer absorption peak is split into two peaks: the H band (higher en-

Table I: Precision of Equilibrium Constants As Check on Validity of Calculation

Dye concentration	Std dev in $\epsilon_t \times 10^{-4}$	$K_{\text{eq}} \times 10^{-4}$
Dye in Methanol at 22°		
$K_{\text{eq}} = (8.00 \pm 2.73) \times 10^3 \text{ l. mol}^{-1}$		
5.05×10^{-6}	0.021	0.450
1.01×10^{-5}	0.023	1.191
5.05×10^{-6}	0.013	0.670
1.01×10^{-4}	0.010	0.874
Dye in Water at 22°		
$K_{\text{eq}} = (1.25 \pm 0.01) \times 10^4 \text{ l. mol}^{-1}$		
1.12×10^{-6}	0.011	1.259
1.12×10^{-5}	0.018	1.247
4.48×10^{-6}	0.008	1.251

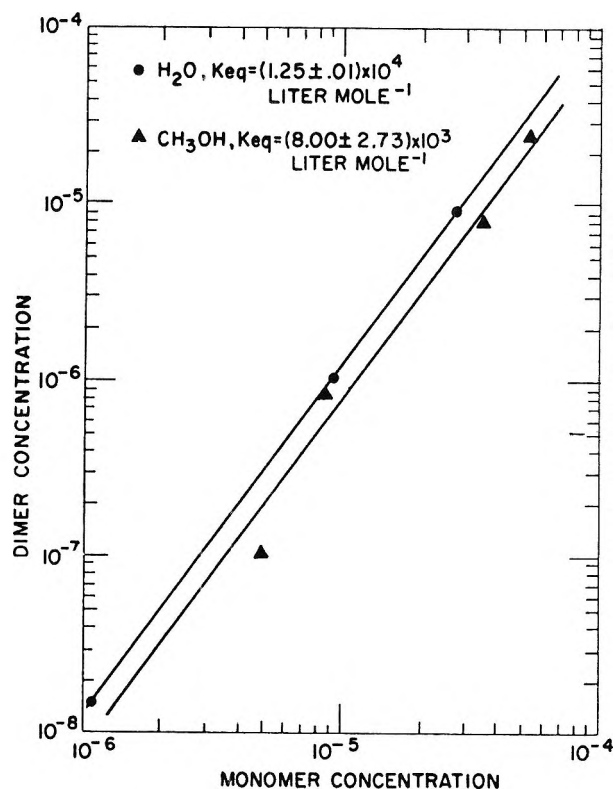


Figure 6. Plot of $\log c_d$ vs. $\log c_m$ for aqueous and methanolic solutions of Na_2 Bonadur. Solid lines drawn with theoretical slopes of 2.

ergy) and the J band (lower energy).^{19a} Even though the J band is small, we have definite evidence for its existence in the dye-water system. (1) There is a reproducible isosbestic point at $17,700 \text{ cm}^{-1}$. This is shown in Figure 2b. (2) At higher dye concentrations a small resolved peak (band) appears near $18,000 \text{ cm}^{-1}$. This is shown in Figure 7. The existence of the J band in the dye-methanol system could be questionable since it occurs on the steep edge of another band which could cause computational errors and no isosbestic point is observable on the longer wavelength side of the monomer peak (see Figure 3). However, at 77°K , a resolved band appears which is also presented in Figure 7. Therefore, independent spectral measurements qualitatively support the dimer spectra computed from the concentration dependences. The peak positions for the monomer and dimer spectra and the splittings are given in Table II. For the dye-methanol solution, the splitting $\Delta\bar{\nu}$ was $2700 \pm 200 \text{ cm}^{-1}$ with the midpoint between the H and J bands being red-shifted by $200 \pm 100 \text{ cm}^{-1}$ from the monomer peak. For the dye-water solution, the splitting $\Delta\bar{\nu}$ is $2200 \pm 100 \text{ cm}^{-1}$ with the midpoint between the H and J bands red-shifted by $800 \pm 100 \text{ cm}^{-1}$ from the monomer peak. The splitting $\Delta\bar{\nu}$ is caused by a dipole-dipole interaction between the adja-

(19) (a) M. Kasha, H. F. Rawls, and M. Ashraf El-Bayoumi, *Pure Appl. Chem.*, **11**, 371 (1965); (b) K. K. Rohatgi, *J. Mol. Spectrosc.*, **27**, 545 (1968).

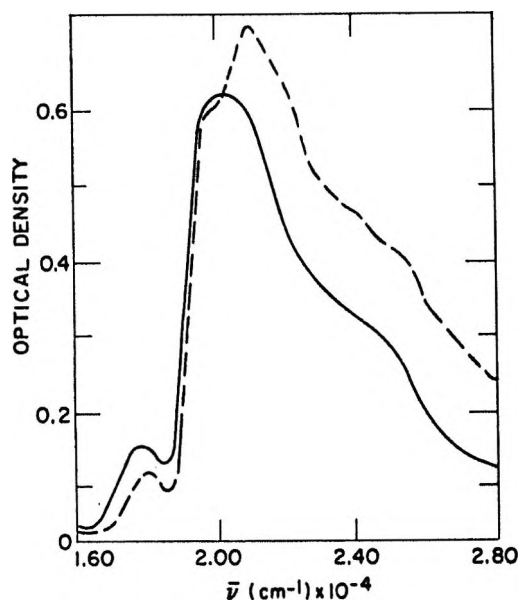


Figure 7. Absorption spectra of Na_2 Bonadur: —, ca. 4×10^{-4} M in water at 22° , 1-cm path; ---, ca. 8×10^{-5} M in methanol at 77°K , 5-cm path.

Table II: Spectral Peak Positions and Splitting for Monomer and Dimer Species

	Dye in methanol	Dye in water
Monomer peak, cm^{-1}	$19,700 \pm 50$	$19,600 \pm 50$
Dimer H-band peak, cm^{-1}	$20,900 \pm 100$	$19,900 \pm 50$
Dimer J-band peak, cm^{-1}	$18,200 \pm 100$	$17,700 \pm 50$
Splitting $\Delta\bar{\nu}$, cm^{-1}	$2,700 \pm 200$	$2,200 \pm 100$

cent molecules in the dimer. The resulting splitting is related to the spacing and directional orientation of the adjacent molecules. The relative orientation of the two molecules also determines the relative strengths of the H band and the J band. The splitting $\Delta\bar{\nu}$ and the relative strengths of the two dimer bands were used to calculate the dimer structure, *i.e.*, the relative orientations and the spacings of the molecules. The shift of the midpoint between the H and J bands relative to the monomer peak position is undoubtedly related to the degree of overlap of the electron wave functions between the two molecules. Unfortunately, there is no simple theory with which this can be correlated. The fact that the midpoint of the split bands shifts more in water than in methanol indicated that the water forces the molecules closer together and, indeed, this fact was borne out by the calculated spacing using the splitting $\Delta\bar{\nu}$ and the relative strengths of the split bands.

A schematic drawing of the parallel plane dimer and the energy levels of the monomer and dimer are shown in Figure 8. The parallel plane dimer configuration was chosen for two reasons. (1) The planar character of

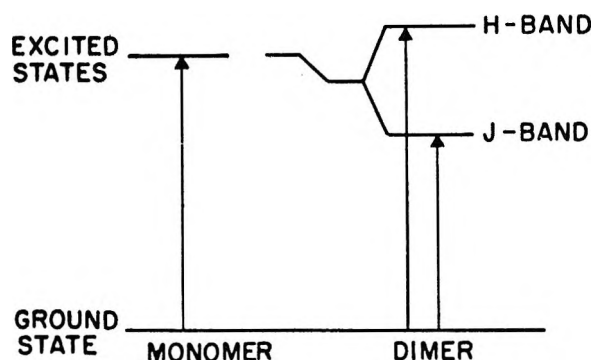
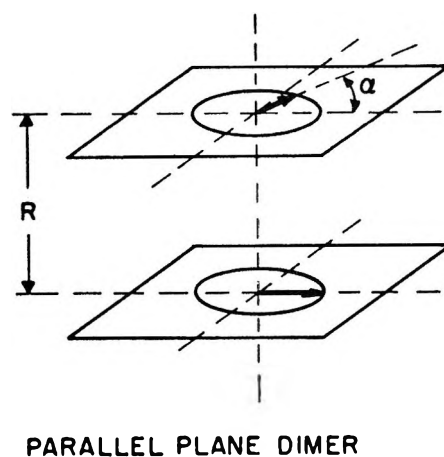


Figure 8. Schematic of parallel plane dimer showing twist angle α and separation R with corresponding energy diagram for monomer and dimer electronic energy levels and optical transitions.

the dye molecules suggests a stacking character as the most stable configuration. (2) This configuration is a simple configuration¹⁹ that allows both H-band and J-band absorption with a larger H band than J band. This model is undoubtedly oversimplified, but it is instructive to evaluate the dimer structural parameters which can be calculated by using this model. Because of the asymmetry of the charge groups on the single molecule, it is unlikely that the molecules in the dimer are exactly coplanar, but the molecules are assumed to be coplanar in the following calculation so that the other structural features of the dimer can be calculated. The arrows represent the transition dipole moments in the individual molecules with the moments being at an angle α to one another. The molecules are separated by a distance R . The energy level diagram shows the first excited state and the ground state of the monomer. When two molecules aggregate to form a dimer, the ground state is assumed to be unaffected but the excited state is split by a dipole-dipole interaction between the molecules.^{19b} The splitting $\Delta\bar{\nu}$ from molecular exciton theory^{19b} is given by

$$\Delta\bar{\nu} = \frac{2D \cos \alpha}{hcR^3} \text{ (in cm}^{-1}\text{)} \quad (5)$$

where D is the monomer dipole strength, h is Planck's constant, and c is the speed of light. The monomer dipole strength is related to the oscillator strength by

$$D = \frac{3hce^2}{8\pi^2mc^2} \cdot \frac{f}{\bar{\nu}} = 1.07 \times 10^{-14} \frac{hcf}{\bar{\nu}} \text{ (in erg cm}^3\text{)} \quad (6)$$

where $\bar{\nu}$ is energy in cm^{-1} , m is the electron mass, and f is the oscillator strength. Solving for the intermolecular distance R in terms of the oscillator strength f , the splitting $\Delta\bar{\nu}$, and the monomer peak energy $\bar{\nu}$ in cm^{-1} gives

$$R = \left[\frac{2.14 \times 10^{10} (\cos \alpha) f^{-1}}{\bar{\nu} \Delta\bar{\nu}} \right]^{1/2} \text{ (in } \text{\AA}\text{)} \quad (7)$$

The oscillator strength f was determined by integrating the molar extinction coefficient ϵ over the monomer band

$$f = 4.32 \times 10^{-9} \int_{\text{band}} \epsilon(\bar{\nu}) d\bar{\nu} \quad (8)$$

where the energy $\bar{\nu}$ is given in cm^{-1} . The dipole strength for the H band of the dimer is given by $D(1 + \cos \alpha)$ and the dipole strength for the J band of the dimer is given by $D(1 - \cos \alpha)$; thus the angle α may be determined from the relative oscillator strengths of the split bands

$$\alpha = 2 \tan^{-1} (\bar{\nu}_H f_J / \bar{\nu}_J f_H)^{1/2}$$

where $\bar{\nu}_H$, $\bar{\nu}_J$, f_H , and f_J are the peak positions and oscillator strengths for H band and J band in the dimer spectrum. The oscillator strengths and dimer structure are given in Table III. The dipole strength D

Table III: Oscillator Strengths and Dimer Structure

	Dye in methanol	Dye in water
Monomer f	0.323 ± 0.003	0.347 ± 0.000
H band of dimer f	0.198 ± 0.003	0.219 ± 0.000
J band of dimer f	0.027 ± 0.015	0.072 ± 0.002
R , \AA	4.6 ± 0.2	4.3 ± 0.0
α , deg	43 ± 10	63 ± 1

for each solution was $D = (3.49 \pm 0.03) \times 10^{-35}$ erg cm^3 for the dye-methanol solution and $D = (3.77 \pm 0.00) \times 10^{-35}$ erg cm^3 for the dye-water solution.

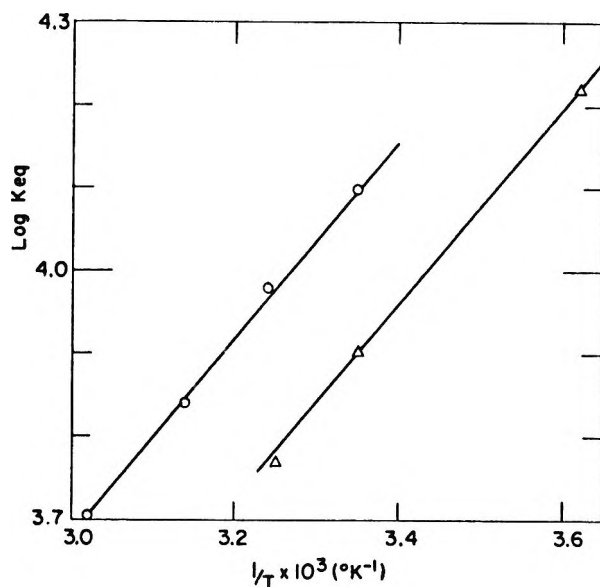


Figure 9. van't Hoff isochores for Na_2 Bonadur: O, water; Δ , methanol.

Although the theoretical basis of the point dipole model represents a great oversimplification of the intermolecular interaction for these complex molecules, it was interesting to compare the dimer parameters of the dye in the two solvent systems. The larger shift in midpoint (relative to the monomer peak) between the split transitions in water compared to the methanol system was most likely a result of the greater degree of orbital overlap.^{19a} This was also supported by a smaller spacing between molecular planes in water as calculated from the dimer split bands relative to the monomer band. Since the molecules are closer, the larger twist angle in water as compared with methanol probably balances the repulsive forces between like charges on the two monomer species.

Authors in the past have suggested the importance of hydrogen bonding in dye aggregation processes.²⁰ It seems probable that forces of this magnitude were operative because the temperature dependences of the systems reported here yielded exothermic heats of dimerization of 5.7 ± 1.0 kcal (mol dimer)⁻¹. The van't Hoff isochores showing the temperature dependences of K_{eq} in the two solvent systems are shown in Figure 9.

(20) (a) S. E. Sheppard and A. L. Geddes, *J. Amer. Chem. Soc.*, **66**, 2003 (1944); (b) K. K. Rohatgi and G. S. Singhal, *J. Phys. Chem.*, **70**, 1695 (1966); (c) L. V. Levshin, Yu. A. Mittsel, and T. D. Slavnova, *Bull. Acad. Sci. USSR*, **32**, 1336 (1968).

Electron Spin Resonance Studies of Free Radicals Formed from Orotic Acid¹

by Jürgen Hüttermann,^{2a,b} John F. Ward, and L. S. Myers, Jr.

Laboratory of Nuclear Medicine and Radiation Biology, and the Department of Radiology, University of California, Los Angeles, California 90024 (Received May 27, 1970)

The paramagnetic species produced in orotic acid (uracil-6-carboxylic acid) by irradiation of single crystals and polycrystalline material as well as by reaction with hydroxyl free radicals in an aqueous system have been studied by electron spin resonance (esr) spectroscopy. Three species were observed in the spectra of the crystals, two of them free radicals associated with the orotic acid molecule and the third, cupric ions resulting from radiation effects on crystal impurities. The spectra of the latter were not investigated in full detail. One of the free radicals is formed by hydrogen addition in the 5 position of the pyrimidine ring, leaving an unpaired electron in a $2p_z$ orbital of carbon atom $C_{(6)}$. The couplings of the two β -hydrogen atoms at the 5 position are 22.8 and 34.2 G, respectively. The principal values of the g tensor are 2.0023, 2.0066, and 2.0031. The second radical results from a hydrogen added to an oxygen of the carboxyl group, giving rise to interaction of the radical electron on carbon $C_{(7)}$ with two hydroxyl protons. The hyperfine couplings of the latter are almost axially symmetrical with one $A_{||} \simeq 12$, $A_{\perp} \simeq 0$ G, and the other $A_{||} \simeq 6$, $A_{\perp} \simeq 0$ G. The g tensor of this radical has principal values of 2.0022, 2.0090, and 2.0047. The spectra obtained from irradiated polycrystalline orotic acid can be explained on the basis of the same two radicals. Hydroxyl free radicals produced by the $Ti^{III}-H_2O_2$ reaction add to the 5 position of orotic acid in acidic aqueous solution. The unpaired electron on carbon $C_{(6)}$ interacts with the β proton on $C_{(5)}$ to produce a doublet of 11.8-G spacing. Each doublet line is further split into three main lines with component spacing of 2.3 G by interaction with the ^{14}N nucleus in 1 position.

Introduction

When nucleic acid constituents in the solid state are exposed to ionizing radiation at room temperature, a major pathway of radiation damage has been shown by electron spin resonance (esr) spectroscopy to be the addition of a hydrogen atom to the unsaturated bonds of the ring of the base molecule.³⁻⁹ Formation of this kind of radical is the predominant type of base damage in purines. However, other radicals are found in significant amounts in pyrimidines. Recent single crystal studies have revealed that in a number of pyrimidine derivatives a radical is formed which involves hydrogen atom addition to one of the keto oxygens.^{5,7,10} Production of such radicals has interesting radiobiological implications since it would cause destruction of the hydrogen-bonding scheme in double-stranded DNA. A third type of pyrimidine radical is generated by reactions involving substituents at the 5,6-double bond. Thus, in thymine a hydrogen atom is removed from the 5-methyl group.⁶

To obtain more information about the various mechanisms of radiation damage in pyrimidine derivatives we extended our investigations to orotic acid, a compound which is derived from uracil by replacement of the 6 hydrogen by a carboxyl group. ESR spectra of irradiated single crystals were used to identify the radicals formed in the solid state. The studies were complemented by investigation of irradiated polycrystalline material and of the radicals formed by reaction of hydroxyl free radicals with the compound in an aqueous system.

droxyl free radicals with the compound in an aqueous system.

Experimental Section

Single crystals of orotic acid monohydrate (Calbiochem A grade) were grown from aqueous solutions as plates, weighing about 10 mg, by repeatedly seeding small crystals in fresh mother liquor. The average crystal dimensions obtained were about $5 \times 2 \times 1$ mm. To our knowledge no data have appeared on the crystal structure and molecular parameters of this compound. Preliminary Weissenberg diagrams reveal that the crystals are triclinic with space group $P\bar{1}$ and two molecules per unit cell assuming a density of 1.5. The two molecules are related by a center of symmetry. In analogy

(1) This work was supported by Contract AT(04-1) GEN-12 between the Atomic Energy Commission and the University of California.

(2) (a) On leave from Lehrstuhl für Physik, Fachbereich Biologie, Universität Regensburg, Germany. (b) To whom correspondence should be addressed at Laboratory of Nuclear Medicine and Radiation Biology, 900 Veteran Avenue, Los Angeles, Calif. 90024.

(3) C. Alexander, Jr., and W. Gordy, *Proc. Nat. Acad. Sci., U. S.*, **58**, 1279 (1967).

(4) B. Pruden, W. Snipes, and W. Gordy, *ibid.*, **53**, 917 (1965).

(5) H. Dertinger, *Z. Naturforsch. B*, **22**, 1266 (1967).

(6) J. Hüttermann, *Int. J. Radiat. Biol.*, **17**, 249 (1970).

(7) J. Hüttermann and A. Müller, *ibid.*, **15**, 297 (1969).

(8) J. Hüttermann, *Z. Naturforsch. B*, **24**, 1648 (1969).

(9) J. Cook, J. Elliott, and S. Wyard, *Mol. Phys.*, **13**, 49 (1967).

(10) W. Snipes and B. Benson, *J. Chem. Phys.*, **48**, 4666 (1968).

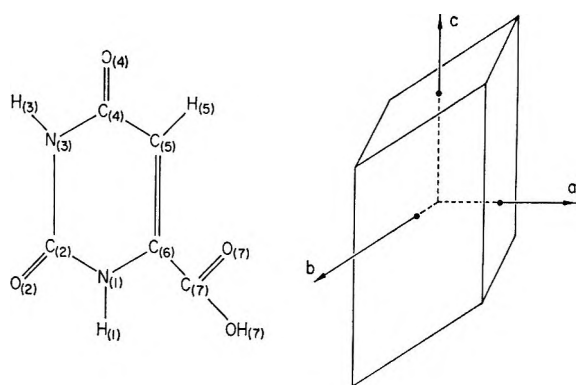


Figure 1. Representation of orotic acid molecule and orotic acid monohydrate single crystal showing numbering system and orthogonal esr reference axes a , b , and c , respectively.

to uracil and thymine it can be assumed that the molecule is in the diketo form. Figure 1 shows the orotic acid molecule and the numbering system used in this paper, as well as the external form of the crystals and the orthogonal abc axis system used for esr measurements.

It should be noted that the relatively large crystals used in this investigation exhibited a slightly yellow color although the small seeding crystals appeared colorless.

The crystals were exposed to radiation from a ^{60}Co γ source at doses between 10 and 60 Mrads. ESR spectra were recorded as first derivatives of the absorption using a Varian 4502 spectrometer operating at about 9-GHz (X-band) microwave frequency. The three lines of Fremy's salt ($g = 2.0055$, $\Delta H = 13$ G) were employed as a standard for calibrating g factors and hyperfine splittings. The spectral data were evaluated by the procedure of Schonland¹¹ and Lund and Vänngräd.¹² Calculations were made on an IBM 360 computer.

Hydroxyl free radicals were generated in aqueous solution with the $\text{Ti}^{\text{III}}-\text{H}_2\text{O}_2$ system following mainly the standard procedure given by Dixon and Norman.¹³ The solutions were 0.004 M with respect to orotic acid. To avoid competition of H_2O_2 for OH radicals, concentrations of 0.015 M H_2O_2 and 0.005 M Ti^{III} were used. OH radicals react with chloride ions in acid solution to give Cl_2^- ion radicals^{14,15} which have an intense esr signal interfering with the lines from solute radicals. Thus we used $\text{Ti}_2(\text{SO}_4)_3$ (LaMotte Chemical Products Co.) as Ti^{III} source instead of TiCl_3 which is usually employed. All solutions were thoroughly bubbled with nitrogen gas. The pH was adjusted with concentrated H_2SO_4 and was measured with a Beckman pH meter before and after mixing of the two reactants.

Results and Discussion

Three different paramagnetic species, labeled A, B, and C are observed in the irradiated orotic acid single crystals as is shown in the esr spectrum of Figure 2.

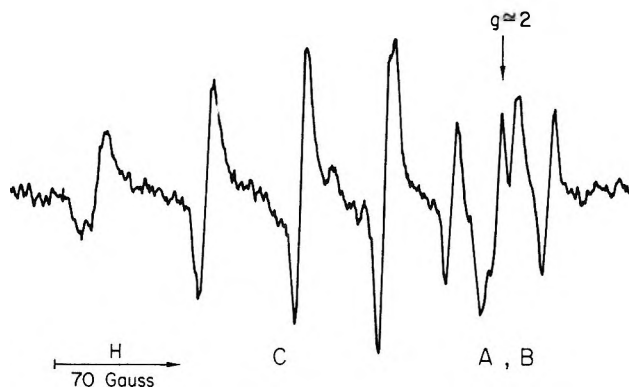


Figure 2. First derivative esr spectrum of orotic acid crystal exposed to about 40 Mrads at ambient temperature showing three distinct line groups A, B, and C. Spectra are taken at X-band frequency at 300°K. Magnetic field H is in ab plane.

Two of the species (A and B) are stable for at least several months and display a superimposed hyperfine spectrum near $g = 2$ which is typical for organic free radicals. The spectrum of the third, C, which is represented by the first four lines at low field in this orientation, decays slowly at room temperature and appears at much higher g factors.

Radical Species A. The $g = 2$ section of room temperature spectra of orotic acid crystals irradiated with about 40 Mrads is shown for two orientations of the crystal in Figure 3. The magnetic field is in the ab plane of the crystal, the angle between the two orientations being 120°. In the upper spectrum, a group of four lines, labeled B, is seen to be superimposed on a spectrum with broader lines, the outer components of which are marked by arrows. The number of lines of the latter group, which is referred to as A in the following cannot be inferred from the upper spectrum of Figure 3. In the lower spectrum, the four lines of B have collapsed to a singlet and a third line of A is seen to appear, marked by a double arrow. Since this line is not placed in the center of the two outer lines of A, symmetry suggests that the number of lines in group A is four. This is indicated by the bars given under the lower spectrum in Figure 3. The fourth line appears as a shoulder on the singlet.

Variation of the incident microwave power or the temperature of esr measurements of crystals irradiated at room temperature does not separate the lines of A and B. Likewise, heat-annealing at 510°K for several minutes (which did not visibly damage the crystals) and storage of the annealed crystals for a week decreased both line groups equally. However, irradiation of the crystals at 77°K and measurements at 170 or 300°K

(11) D. Schonland, *Proc. Phys. Soc.*, **73**, 788 (1959).

(12) A. Lund and T. Vänngräd, *J. Chem. Phys.*, **42**, 2979 (1965).

(13) W. T. Dixon and R. O. C. Norman, *J. Chem. Soc.*, 3119 (1963).

(14) M. Anbar and J. K. Thomas, *J. Phys. Chem.*, **68**, 3829 (1964).

(15) J. F. Ward and L. S. Myers, Jr., *Radiat. Res.*, **26**, 483 (1964).

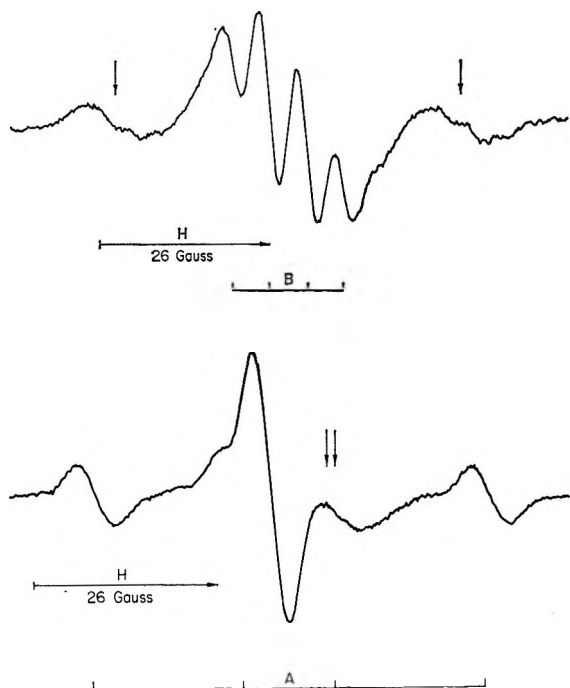


Figure 3. Free-radical section of esr spectra of orotic acid crystals for two different orientations showing species B and A as indicated by the bars beneath the spectra. Experimental conditions otherwise as in Figure 2.

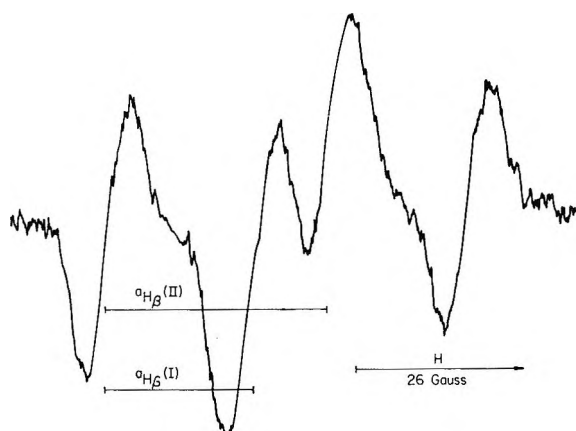


Figure 4. First derivative esr spectrum of orotic acid crystal exposed to 15 Mrads at 77°K, stored at 300°K for several days, and reirradiated at 77°K with 20 Mrads. Temperature of measurement is 300°K. Magnitudes of coupling $a_{H\beta}(I)$ and $a_{H\beta}(III)$ refer to radical structure II for species A.

results in spectra in which the $g = 2$ section consists dominantly of the lines of species A, as is shown in the spectrum of Figure 4 (cf. the legend for details of experimental conditions). Indeed, four lines of about equal intensity are seen to represent group A. On rotation of the crystal in the ab plane the splitting of these lines is nearly isotropic. This is in accord with the isotropic total spacing of the lines of group A as measured by the distance of its outermost lines (cf. arrowed lines in spectrum of Figure 3) in the spectra of the crystals which were irradiated at room temperature. These findings

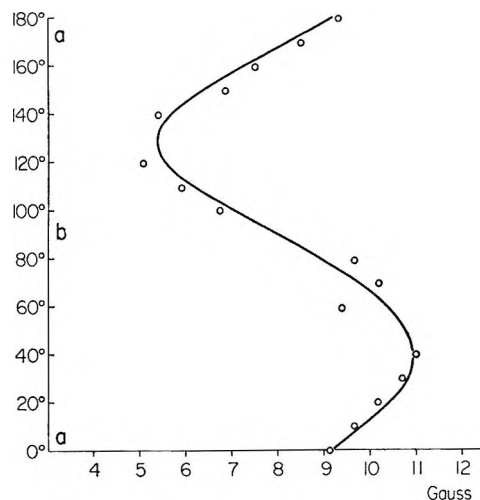


Figure 5. Variation of width of outer lines of group A with magnetic field H in ab plane of orotic acid crystals.

indicate that the unpaired electron of the radical giving rise to group A interacts with two protons in β position with couplings of $a_{H\beta}(I) = 22.8$ G and $a_{H\beta}(II) = 34.2$ G.

The width of the lines of group A is subject to marked changes with crystal orientation. Figure 5 shows this variation for the two outer lines of A on rotation of the crystal in the ab plane. Because of the angular π symmetry of the line-width variation in this plane, unresolved site splitting of magnetically nonequivalent molecular sites in the crystal cannot account for this feature. Instead, poorly resolved anisotropic hyperfine splitting resulting from interaction of the unpaired electron with other nuclei is assumed to be present.

Figure 6 shows the variations of the g factors for group A in the three crystal planes, measured from the position of the center of the two outer lines of this group. The g tensor is characteristic of a radical with its unpaired electron localized mainly in a carbon $2p_z$ orbital.

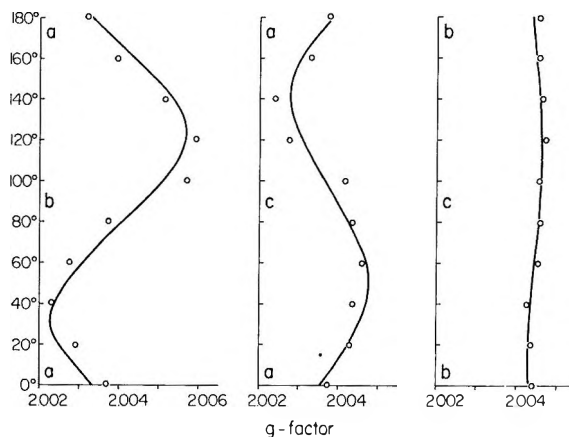


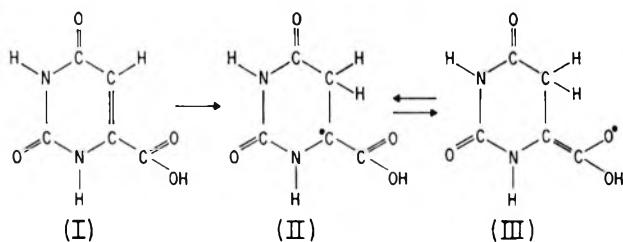
Figure 6. Variation of g factors of group A in three planes of orotic acid single crystals. The open circles are the experimental points, the solid lines the theoretical curves based on the data given in Table I.

Table I: Characteristics of ESR Spectra of Radical II in Orotic Acid under the Various Experimental Conditions

	Principal values	Direction cosines		
		a	b	c
A. Single Crystals				
<i>g</i>	2.0023	0.85	0.51	-0.10
	2.0066	-0.47	0.69	-0.59
	2.0031	-0.20	0.51	0.84
$a_{H\beta}$ (I)	22.8 G	Isotropic		
$a_{H\beta}$ (II)	34.5 G	Isotropic		
B. OH· + Orotic Acid in Aqueous Solution (pH 1.6-2.5)				
<i>g</i>	2.0035			
$a_{H\beta}$	11.8 G			
$a_{N\beta}$	2.3 G			

All features of group A can be accounted for by assuming that the corresponding radical is formed by addition of a hydrogen to the 5 position of the 5,6-double bond of the orotic acid molecule, leaving an unpaired electron in the $2p_z$ orbital of ring carbon $C_{(5)}$ (radical II).

The hyperfine spectrum arises from the interaction of the electron with the two methylene protons attached to carbon $C_{(5)}$. The additional unresolved splitting may in part result from the interaction with the ^{14}N nucleus in the 1 position



The two β protons on $C_{(5)}$ do not couple equally. Assuming sp_2 bonding to $C_{(5)}$ the dihedral angle θ of the $C_{(5)}\text{-H}$ direction with respect to the plane perpendicular to the π orbital of the unpaired electron must be different for each of the two protons. The angles are related by

$$\theta_2 = 60^\circ - \theta_1$$

The couplings of the β hydrogens are related to the spin density $\zeta_{C\alpha}$ on the α carbon and the dihedral angles θ by the semiempirical equation of Heller and McConnell¹⁶

$$a_{H\beta} = \zeta_{C\alpha} \cdot A_0 \cdot \cos^2 \theta$$

Inserting the numerical values of the two couplings and using 58.5 G for the constant A_0 ¹⁷ yields

$$\theta_1 = 41^\circ \quad \theta_2 = 19^\circ \quad \zeta_{C\alpha} = 0.67$$

for the dihedral angles and the spin density. The comparatively small value of the latter can be explained by resonance structure III of radical II in which some unpaired spin density is localized on the carboxyl oxygen.

Since the hyperfine couplings of radical II have proved isotropic in the single crystal, irradiated polycrystalline material of orotic acid should yield roughly the same spectrum for this group as the crystal spectra. Figure 7 shows the spectrum obtained from polycrystalline orotic acid exposed to 6 Mrads at room temperature. It consists of four lines with spacings approximately equal to those of group A lines in the crystal (cf. Figure 4). Two major differences are apparent. The center lines are unequal in intensity and are themselves larger than the two outermost lines. The latter effect is explained by *g*-factor averaging resulting from random orientations of the radicals in the polycrystalline material while the former is due to the presence of radical species B as will be discussed in the next section. Therefore, both the spectra of the single crystals and of the polycrystalline material are compatible with the proposed structure II for the lines of group A.

A spectrum of four hyperfine lines with about the same component splittings as in Figure 7 (18 and 34 G) has been reported for orotic acid exposed to thermal hydrogen atoms¹⁸ and attributed to a radical resulting from hydrogen addition to the 6 position of the pyrimidine ring. The similarity of the hyperfine couplings to those reported here suggests that the hydrogen atoms were at the 5 position in that case also.

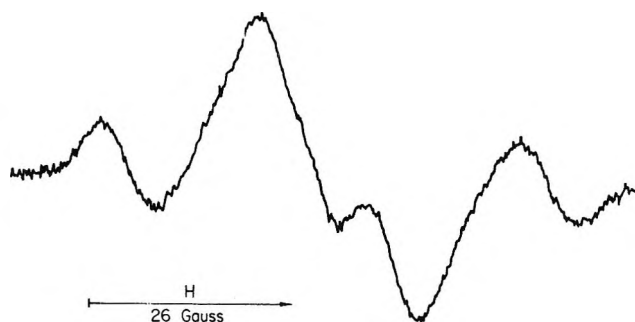


Figure 7. First derivative esr spectrum of polycrystalline orotic acid exposed to 6 Mrads at 300°K. Spectrum taken at X-band frequency at room temperature.

The esr spectrum obtained from the reaction of hydroxyl free radicals with orotic acid in acid aqueous solution is shown in Figure 8a. Variation of the pH from 1.6 to 2.5 produced little spectral change. Since these values are close to the *pK* value of the carboxyl group of orotic acid (2.4), either (1) the ionization of the carboxyl group does not affect the distribution of the unpaired electron, or (2) the *pK* value of the radical resulting from OH attack differs greatly from that of the parent compound. The spectrum consists of two

(16) C. Heller and H. McConnell, *J. Chem. Phys.*, **32**, 1535 (1960).

(17) R. W. Fessenden and R. H. Schuler, *ibid.*, **39**, 2147 (1963).

(18) D. E. Holmes, R. B. Ingalls, and L. S. Myers, Jr., *Int. J. Radiat. Biol.*, **13**, 225 (1967).

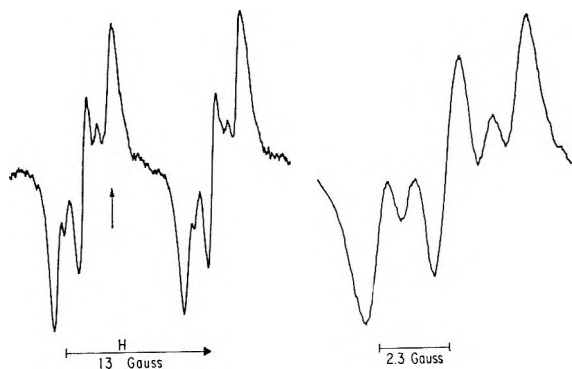


Figure 8. (a) First derivative esr spectrum produced by reaction of OH· free radicals with orotic acid in aqueous solution at pH 2.4. Arrow indicates position of center line of Fremy's salt ($g = 2.0055$). (b) Trace of high-field line of main doublet of spectrum in (a) at slower scan rate and with optimized resolution.

main hyperfine lines with a spacing of 11.8 G centered at a g factor of 2.0035. Figure 8b gives the trace of one of the doublet lines recorded at a slower scan speed under conditions of maximum resolution and using a computer of average transients. Three lines of about equal intensity with component spacing of 2.3 G are seen to constitute each of the doublet lines. The spectrum is therefore assigned to the same type of radical as structure II with the difference that one of the hydrogen atoms at the 5 position is, of course, replaced by a hydroxyl group. The triplet splitting then stems from interaction of the unpaired electron on carbon atom $C_{(6)}$ with the nuclear spin of the nitrogen in the 1 position, whereas the main doublet hyperfine spectrum is due to coupling of the β proton attached to carbon atom $C_{(6)}$. The rather small value of this coupling (11.8 G) may be accounted for by assuming that the planar ring structure of the orotic acid molecule is distorted upon attachment of the hydroxyl group. The direction of this distortion is such, that the dihedral angle of the $C_{(5)}-H$ bond with the π -orbital axis on $C_{(6)}$ is closer to 90° than it is after addition of a hydrogen atom. The latter effect has also been observed for reactions of hydroxyl free radicals with other pyrimidine bases in aqueous solution.¹⁹ A low spin density on $C_{(6)}$ may also feasibly contribute to the small doublet splitting. Neither of these two factors can be defined in a more quantitative way from the experimental data obtained.

The two satellite lines of minor intensity which appear to the left and right of the center line of the triplet (Figure 8b) do not fit into the radical scheme outlined above. They cannot be due to addition of hydroxyl free radicals to another ionic form of orotic acid since their intensity does not vary over the pH range investigated. These lines may result from an additional radical which, however, must have the same main doublet splitting and g factor as that described

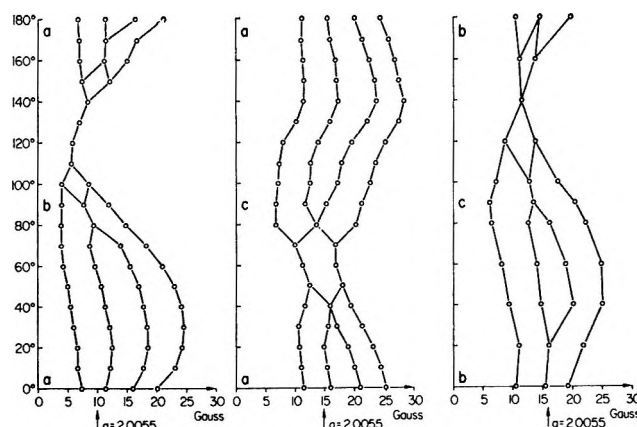


Figure 9. Variation of all hyperfine lines of group B in three planes of orotic acid single crystals. Open circles represent the positions of the lines with regard to the magnetic field given as the abscissa of the curves.

above. A radical of a different chemical structure meeting these requirements is most unlikely. Therefore, we propose that a geometrical isomer of the same OH adduct radical of type II is present. The source of this isomerism may be the nonplanarity of the radical.

Radical Species B. In contrast to the isotropic behavior of the lines of radical II the hyperfine spectrum of species B in the single crystals varies markedly with orientation (Figure 3). The number of lines belonging to this group was found to be one, two, three, or four. The lines of the doublet and the quartet patterns have about equal intensities; those of the triplet have an intensity ratio 1:2:1.

Figure 9 shows the variations of the lines with orientation. When they approach, their position becomes uncertain because of the line widths. This uncertainty is minimized by a numerical least-squares fit of the experimental values in deriving the hyperfine splittings from these data. The lines are symmetric around one center of gravity for all orientations in the three planes. Thus, one radical accounts for all lines. This is in agreement with the results of varying the microwave power and the temperature of measurement, as well as with heat-annealing experiments. Furthermore, the variations of all lines in each plane exhibit angular π symmetry. Therefore, the radical must occupy only one site in the crystal. Examination of the lines in all crystal planes reveals that they are due to the interaction of the unpaired electron with two protons. Figure 10 gives the variations of the splittings of these protons H_1 and H_2 (cf. radical IV) in the three crystal planes. The couplings are approximately axially symmetric with values between about 0 and 6, and 0 and 13 G, respectively. These values are characteristic for protons adjacent to an oxygen atom in a $>\dot{C}-OH$ radical fragment. The only position in the orotic acid

(19) C. Nicolau, M. McMillan, and R. O. C. Norman, *Biochim. Biophys. Acta*, **174**, 413 (1969).

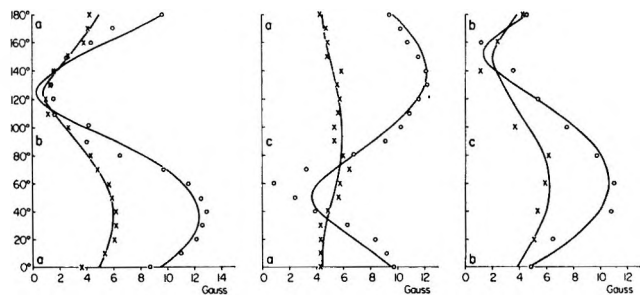
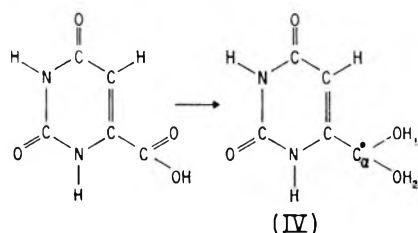


Figure 10. Variation of hydroxyl proton splittings of proposed radical structure IV (of group B) in three planes of orotic acid single crystals. The open circles and the crosses are the experimental values of proton couplings H_1 and H_2 , respectively; the solid lines represent the calculated curves.

molecule which can account for these features is the carboxyl group. Therefore, the radical under consideration is proposed to be of the form IV



The variations of the g factors of radical IV in the three crystal planes are shown in Figure 11. Comparison with the data of Figure 6 show that the g factors of radical IV are slightly higher than those of the hydrogen addition radical. This effect is expected for $>\dot{C}-OH$ vs. $>\dot{C}-C<H_p$ radical fragments.²⁰

For axial symmetry of both hydroxyl proton couplings in radical IV the isotropic components $a(I)$ and $a(II)$ and the anisotropic components $b(I)$ and $b(II)$ of the couplings can be obtained from the equation

$$A_{||} = a + 2b$$

$$A_{\perp} = a - b$$

with $A_{||}(I) = 12.1$ G, $A_{\perp}(I) \cong 0$ G, $A_{||}(II) = 5.96$ G, and $A_{\perp}(II) \cong 0$ G. (Both A_{\perp} values of 0 G are esti-

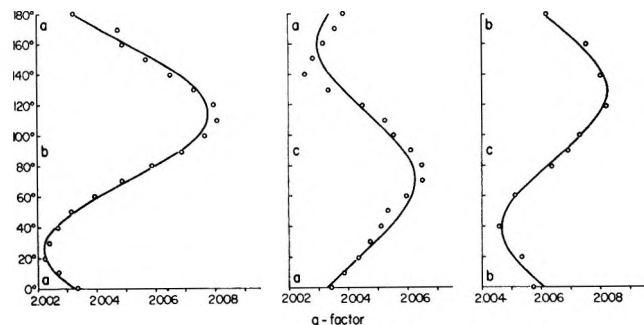


Figure 11. Variation of g factor of radical structure IV (of group B) in three crystal planes of orotic acid single crystals.

mates since they cannot be inferred positively from the spectra because of the width of the lines.) The components obtained by the above equation are $a(I) = b(I) = 4.03$ G and $a(II) = b(II) = 1.98$ G.

The anisotropic component $b(I)$ can be used for an estimate of the spin density, $\zeta_{C\alpha}$, assuming that this dipole coupling arises only from unpaired electron density on carbon $C_{(7)}$. Using the approximate relationship²¹

$$b(I) = 28.2 \cdot \zeta_{C\alpha} / r^3$$

and taking r as 1.74 \AA , $\zeta_{C(7)}$ is found to be 0.74. The dihedral angles θ_I and θ_{II} for the two OH bonds with respect to the π -electron orbital can be found by inserting the isotropic hydroxyl proton couplings $a(I)$ and $a(II)$ into the relation²⁰

$$a = (B_0 + B_1 \cos^2 \theta) \cdot \zeta_C$$

With the constants $B_0 = -2.5$ G and $B_1 = 40$ G as proposed by Henn and Whiffen we obtain

$$\theta_I \cong 63^\circ \text{ and } \theta_{II} \cong 70^\circ$$

Table II gives the data for the g tensor and the hyperfine couplings of radical IV together with the direction cosines.

Table II: Principal Values of g Tensor and Hyperfine Splittings (in Gauss) of Radical IV in Single Crystals of Orotic Acid

	Principal values	Isotropic component	Direction cosines		
			a	b	c
g	2.0022		0.92	0.38	-0.01
	2.0090		-0.36	0.76	-0.54
	2.0047		-0.15	0.53	0.84
$A_{OH}(II)$	$A_{ } = 5.96$	1.98	0.14	0.53	0.84
	$A_{\perp} \cong 0$		-0.49	0.78	-0.40
$A_{OH}(I)$	$A_{ } = 12.1$	4.03	0.81	0.43	-0.41
	$A_{\perp} \cong 0$		-0.59	0.66	-0.46

It remains to discuss the difference in the proton couplings of the two hydroxyl groups adjacent to carbon $C_{(7)}$ in radical IV. The differences in the isotropic components of the couplings must result from differing dihedral angles which the OH bonds make with the π orbital on C_{α} . The anisotropic components of the hydroxyl proton coupling is proportional to the inverse cube of the distance r between the proton and the radical electron on C_{α} . In the undamaged orotic acid molecule, both oxygens of the carboxyl group take part in hydrogen bonding to neighbor molecules. It can be assumed that, in the corresponding radical IV, one

(20) D. Henn and D. Whiffen, *Mol. Phys.*, **8**, 407 (1964).

(21) H. Zeldes, G. Tammell, R. Livingston, and R. Holmber, *J. Chem. Phys.*, **32**, 618 (1960).

hydrogen bond is still intact, whereas the other has been broken upon radical formation. Thus, the distances r_1 and r_2 would be different for the two hydroxyl protons with r being longer for the proton which takes part in hydrogen bonding.

It is not clear whether the mechanism of formation of this radical is associated with addition of atomic hydrogen to the oxygen. Possibly, it is due to a protonation of a negatively charged radical. The proton may well stem from the hydrogen bond by which the oxygen is bound to a neighboring molecule. This assumption draws support from the fact that exposure of orotic acid in the polycrystalline state to thermal hydrogen atoms does not result in the formation of radical IV. Instead, only the addition reaction to the 5,6-double bond takes place.¹⁸

No quantitative investigations of the concentrations of the different species in the spectra have been carried out, but the yield of radical IV appears to be much higher than that of II when the crystals are irradiated at room temperature. Low temperature irradiation, however, reduces its contribution strongly.

In the spectrum of the irradiated polycrystalline sample of orotic acid (Figure 7), radical IV is present, too. The hydroxyl proton hyperfine splittings collapse to a singlet under these conditions, which, because of the higher g factor overlaps mainly with the second left line of radical II causing the intensity unsymmetry of the spectrum which was mentioned in the previous section.

Species C. A group of four hyperfine lines, labeled C, is present in the spectra of irradiated orotic acid single crystals at both 77°K and room temperature (*cf.* Figure 2 for one 300°K spectrum). This group appears at much higher g factors than the lines of groups A and B, reflecting a strong spin-orbit interaction which leads to the assumption that the spectrum must be due to a paramagnetic ion with nuclear spin 3/2. Since neither the unirradiated crystals, nor the unirradiated or irradiated polycrystalline orotic acid display this hyperfine spectrum, it must result from an impurity in the single crystals whose paramagnetism becomes apparent as a result of the irradiation. Emission spectra of the single crystals revealed the presence of about 70 ppm copper as the largest impurities.

Our investigation of the lines of group C in the ab plane of the single crystals were sufficient to make certain that the four-line spectrum arises from single Cu^{2+} ions. The g factor varies between 2.065 and 2.166 and the hyperfine spacing of the quartet components between 44 and 108 G in this plane. Figure 12 shows the four lines in an orientation with maximum hyperfine splitting. The outer quartet lines are seen to be split into doublets due to the difference of the magnetic moments of the isotopes ^{63}Cu and ^{65}Cu . No further analysis of the Cu^{2+} spectrum is attempted here since the $S = 1/2$, $I = 3/2$ system of cupric ions has

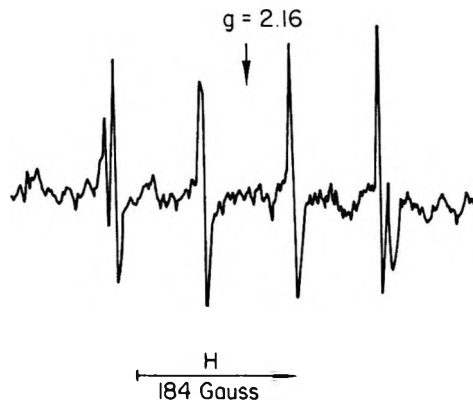


Figure 12. First derivative esr spectrum of group C in single crystals of orotic acid showing Cu^{2+} hyperfine lines and isotopic splittings of ^{63}Cu and ^{65}Cu nuclei.

been investigated recently in an irradiated single crystal of cupric acetate.²²

We assume that the copper is an impurity in the mother liquor. Since at neutral pH orotic acid is ionized, some molecules may crystallize as the nonmagnetic cuprous orotate. Radiation can then convert cuprous into cupric ions, which would give rise to the observed spectra. Possibly, the presence of cuprous ions causes the slight yellow color of the unirradiated orotic acid single crystals which was mentioned in the Experimental Section.

Conclusions

Of the three paramagnetic species observed in irradiated single crystals of orotic acid, two have been shown to be free radicals involving the orotic acid molecule whereas the third is the result of a copper impurity present during crystallization. One radical, structure II, is formed by hydrogen addition to the carbon atom $\text{C}_{(5)}$. In aqueous solution hydroxyl free radicals add to the 5,6-double bond at the 5 position to give the OH analog of structure II. The other radical observed in single crystals of orotic acid involves a hydrogen attached to the oxygen of the carboxyl group, structure IV. The spectra obtained from polycrystalline orotic acid can be explained on the basis of radicals II and IV.

Nearly all unsaturated pyrimidine bases investigated in the solid state form hydrogen addition radicals at the 5,6-double bond after γ irradiation which are equivalent to those produced upon exposure of the compounds to thermal hydrogen atoms.¹⁸ The source of the attacking hydrogen in the case of ionizing radiation is usually not revealed since hydrogen abstraction radicals are not observed. Radical II in single crystals of orotic acid is of this type. However, the radical structure IV which involves the carboxyl group was not detected upon exposure to thermal hydrogen atoms¹⁸ which suggests that there is an alternate mechanism for its formation.

(22) D. Morton-Blake, *J. Phys. Chem.*, **73**, 2964 (1969).

We propose that it is formed by the breakage of a hydrogen bond after addition of an electron to the molecule. $>\dot{C}-OH$ radicals of this kind are produced in the DNA constituent cytosine⁵ and in 5-halouracils.⁷ The hydrogen-bonding scheme of nucleic acids provides a pathway for the production of this type of radicals. Thus, anions could mediate their damage *via* breakage of a hydrogen bond which would lead to a local weakening of the double-stranded structure of DNA.

While this report was being prepared, an esr study of irradiated single crystals of orotic acid was published by Horan and Snipes.²³ On the basis of spectra differing from those reported here, these authors conclude that only one radical is present and that it results from abstraction of a hydrogen atom from the nitrogen in the 1 position. Surprisingly, no hydrogen addition to the 5,6-double bond is reported. We assume, that the differing esr spectra result from differences in the crystals

investigated. Such differences are obvious, since these authors report the occurrence of magnetically inequivalent molecules which are not observed in the triclinic crystals analyzed here. The crystals grown by Horan and Snipes from a mixture of ethanol and 0.8 *M* NH_4OH most probably are the diammonium salt of orotic acid.

Acknowledgments

We wish to thank G. Alexander of this laboratory for carrying out the impurity analysis and E. Maverick and D. Davis (Crystallography Section, Department of Chemistry, University of California, Los Angeles) for taking the Weissenberg patterns. Furthermore, we are indebted to Professor A. Müller (Lehrstuhl für Physik, Universität Regensburg, Germany) for helpful discussions and criticism of the manuscript.

(23) P. Horan and W. Snipes, *Radiat. Res.*, **41**, 24 (1970).

Electron Paramagnetic Resonance Study of 4-Alkyl-*o*-benzosemiquinones

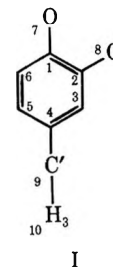
by J. Pilarř

Institute of Macromolecular Chemistry, Czechoslovak Academy of Sciences, Prague, Czechoslovakia
(Received March 30, 1970)

The epr spectra of a member of 4-alkyl-*o*-benzosemiquinones in an aqueous alcoholic and aprotic medium were measured and analyzed. The values of the parameters h_o and k_{CO} were suggested for the calculation of the spin densities of these radicals by the McLachlan method. The comparison of the calculations and experiments shows that the spin densities on the aromatic ring carbon atoms in positions 3 and 6 of *o*-benzosemiquinone are positive. Changes of magnitude of the splitting constants of β protons of various alkyl substituents were interpreted on the basis of the Stone and Maki theory of the hindered internal rotation.

Introduction

The formation of *o*-benzosemiquinone anion radicals in the course of the atmospheric oxidation of pyrocatechols in an alkaline aqueous alcohol was first confirmed by Hoskins¹ and Adams, *et al.*,² using the epr method. Stone and Waters,³ who studied the epr spectra of *o*-benzosemiquinones systematically, obtained in the series of 4-alkyl-*o*-benzosemiquinones a well-resolved spectrum of the 4-methyl derivative, but they failed to analyze the spectra of the 4-isopropyl and 4-*tert*-butyl derivatives. Trapp, *et al.*,⁴ did not succeed in determining exactly the splitting constant of one of the protons of the aromatic ring in a poorly resolved spectrum of 4-*tert*-butyl-*o*-benzosemiquinone. In all the papers referred to in this paper, *o*-benzosemiquinones were prepared by the oxidation of pyrocatechols in an alkaline polar medium.



In the calculations of spin densities in *o*-benzosemiquinone Vincow and Fraenkel^{5,6} found that spin densities calculated by the McLachlan method⁷ were in

- (1) R. Hoskins, *J. Chem. Phys.*, **23**, 1975 (1955).
- (2) M. Adams, M. S. Blois, and R. H. Sands, *ibid.*, **28**, 774 (1958).
- (3) T. J. Stone and W. A. Waters, *J. Chem. Soc.*, 1488 (1965).
- (4) Ch. Trapp, Ch. A. Tyson, and G. Giacometti, *J. Amer. Chem. Soc.*, **90**, 1394 (1968).

considerably better agreement with the experimental data than those calculated by a simple HMO method. Vincow⁶ suggested the most suitable values for the parameters h_o and k_{CO} which determine the magnitude of the Coulomb integral of the oxygen atom and the value of the resonance integral of the C–O bond. Calculations involving these parameters led him to a conclusion that the spin densities on the carbon atoms of the aromatic ring in positions 3 and 6 were negative. Trapp, *et al.*,⁴ attained a comparatively good agreement between the experimental and calculated values of the spin densities in their investigation of *o*-benzosemiquinones substituted with methyl and *tert*-butyl groups, although in the calculations involving the HMO method they did not consider the possible occurrence of negative spin densities in these radicals and although they used the values of the parameters h_o and k_{CO} suggested by Vincow⁶ for calculations made by the McLachlan method. Calculations performed by Pople, *et al.*,⁸ using the INDO approximation of the SCF–MO method, and by Edwards and Grinter⁹ by the unrestricted Hartree–Fock method do not lead to a good agreement between the calculated and experimentally determined splitting constants of the protons of the aromatic ring of *o*-benzosemiquinone.

In this paper results are presented which were obtained in the investigation of oxidation transformations and antioxidative efficiency of pyrocatechols^{10,11} and which concern primary radical intermediates of the air oxidation of 4-alkylpyrocatechols in alkaline aqueous alcohol. We concentrated our attention particularly on the experimental determination of the effect of alkyl substituents and solvent on the distribution of the spin density in the aromatic ring of 4-alkyl-*o*-benzosemiquinones and on the verification of the quantum chemical methods of spin density calculations to give an adequate description of the changes observed.

Experimental Section

Materials Used. All pyrocatechol derivatives were chromatographically pure. Pyrocatechol and 4-*tert*-butylpyrocatechol were commercial products (British Drug Houses); the other derivatives were prepared in the laboratory according to literature.^{12–15} Quinones were obtained by the oxidation of the corresponding derivatives of pyrocatechol with silver oxide in anhydrous ether. The other chemicals were analytical purity grade. Acetonitrile was purified by a method described previously;¹⁶ the other solvents were purified by distillation prior to use.

Production of Radicals. Derivatives of pyrocatechol were oxidized in 75% aqueous methanol by air–oxygen dissolved in the solvent under normal pressure and at room temperature in the flow arrangement. A solution of the pyrocatechol derivative under study (10^{-3} M) and the 20% solution of potassium hydroxide (KOH) in 75% aqueous methanol were mixed in a glass mixing

cell placed in close vicinity to the measuring cavity of an epr spectrometer. The mixture was then passed through the cavity resonator by means of a glass capillary. Each time, the flow rate of the reaction mixture through the cavity (1–5 ml/min) was adjusted so as to achieve the best record of the spectrum of the radical investigated.

o-Benzoquinone and its 4-methyl derivative were electrolytically reduced in acetonitrile with 0.1 M tetrabutylammonium perchlorate. The concentration of quinones in the solution was 10^{-3} to 10^{-4} M. With respect to the low stability of the forming *o*-benzosemiquinones the electrolysis had to be carried out in the resonator cavity directly using the flow arrangement. The quinone solution flowed from a container, in which it was kept under nitrogen atmosphere, through the glass capillary of the electrolyzer, of about 1.5 mm o.d., with fused-in platinum electrodes. The anode was situated immediately before the resonator cavity, and the cathode was placed directly in the cavity of the spectrometer. The epr spectra were measured during the contemporary flow electrolysis. The electrode voltage and the flow rate were adjusted so as to attain the most resolved record of epr spectra (usually 10–15 V at a flow rate lower than 1 ml/min).

Measurements and Analysis of the Epr Spectra. The spectra were measured with the JES-3B epr spectrometer (JEOL Tokyo) operating in the X band at room temperature. An aqueous solution of Fremy's salt ($a^N = 13$ G)¹⁷ and *p*-benzosemiquinone in alkaline aqueous alcohol ($a^H = 2.368 \pm 0.001$ G)¹⁸ were used as calibration standards. The analysis of spectra in which no overlap of the neighboring spectral lines occurred was carried out directly; spectra having an insufficiently resolved hyperfine structure were analyzed by comparison with simulated spectra. Simulated spectra were calculated using computers Ural and Minsk, by the modified Stone and Maki¹⁹ method provided that the shape of the

(5) G. Vincow and G. K. Fraenkel, *J. Chem. Phys.*, **34**, 1333 (1961).

(6) G. Vincow, *ibid.*, **38**, 917 (1963).

(7) A. D. McLachlan, *Mol. Phys.*, **3**, 233 (1960).

(8) J. A. Pople, D. L. Beveridge, and P. A. Dobosh, *J. Amer. Chem. Soc.*, **90**, 4201 (1968).

(9) T. G. Edwards and R. Grinter, *Mol. Phys.*, **15**, 367 (1968).

(10) I. Buben and J. Pospíšil, *Collect. Czech. Chem. Commun.*, **34**, 1991 (1969).

(11) J. Pilař, I. Buben, and J. Pospíšil, *ibid.*, **35**, 489 (1970).

(12) J. Pospíšil and V. Ettl, *ibid.*, **24**, 341, 729 (1959).

(13) A. L. Ramizov, *Zh. Org. Khim.*, **28**, 2530 (1958).

(14) E. Späth and H. Quietensky, *Chem. Ber.*, **60**, 1888 (1927).

(15) I. Buben, Thesis, Institute of Macromolecular Chemistry of Czechoslovak Academy of Sciences, Prague, 1968.

(16) O. Ryba, J. Pilař, and J. Petráněk, *Collect. Czech. Chem. Commun.*, **33**, 26 (1968).

(17) G. E. Pake, J. Townsend, and S. I. Weissman, *Phys. Rev.*, **85**, 682 (1952).

(18) B. Venkataraman, B. G. Segal, and G. K. Fraenkel, *J. Chem. Phys.*, **30**, 1006 (1959).

(19) E. W. Stone and A. H. Maki, *ibid.*, **38**, 1999 (1963).

Table I: Splitting Constants of the Investigated *o*-Benzosemiquinones (in gauss)

Derivative	a_1^H	a_2^H	a_3^H	a_6^H	Reference
Unsubstituted ^a	0.95 ± 0.04	3.65 ± 0.04	3.65 ± 0.04	0.95 ± 0.04	2
4-Methyl ^b	0.7	4.4^g	3.7	1.4	3
4-Methyl ^c	0.25	5.1^g	4.0	1.0	3
4- <i>tert</i> -Butyl ^d	0.3 ± 0.1	0.32 ± 0.03^h	3.80 ± 0.02	1.17 ± 0.02	4
Unsubstituted ^e	0.87 ± 0.02	3.75 ± 0.05	3.75 ± 0.05	0.87 ± 0.02	
4-Methyl ^e	0.25 ± 0.01	4.80 ± 0.05^g	3.85 ± 0.05	1.05 ± 0.02	
4-Ethyl ^e	0.30	3.70^i 0.20^j	3.70	1.00	
4-Propyl ^e	0.32 ± 0.01	3.30 ± 0.04^k	3.80 ± 0.05	1.00 ± 0.02	
4-Isopropyl ^e	0.39 ± 0.01	2.21 ± 0.03^l 0.32 ± 0.01^m	3.90 ± 0.05	0.93 ± 0.02	
4- <i>sec</i> -Butyl ^e	0.42 ± 0.01	1.67 ± 0.03^n 0.32 ± 0.01^o	3.84 ± 0.05	1.00 ± 0.02	
4- <i>tert</i> -Butyl ^e	0.42 ± 0.01	0.32 ± 0.01^h	3.96 ± 0.05	0.83 ± 0.02	11
Unsubstituted ^f	1.50 ± 0.03	3.30 ± 0.04	3.30 ± 0.04	1.50 ± 0.03	
4-Methyl ^f	0.80 ± 0.02	4.10 ± 0.05^g	3.72 ± 0.05	1.54 ± 0.03	
4- <i>tert</i> -Butyl ^f	1.16 ± 0.03	0.30 ± 0.02^h	3.90 ± 0.05	1.40 ± 0.03	16

^a Measured in alkaline aqueous ethanol. ^b Measured in a mixture dimethylformamide-water (9:1). ^c Measured in an aqueous solution of sodium hydroxide. ^d Measured in 50% aqueous methanol. ^e Measured in 75% aqueous methanol. ^f Measured in acetonitrile. ^g Splitting constants of protons of the methyl group. ^h Splitting constants of protons of the *tert*-butyl group. ⁱ Splitting constants of two β protons of the ethyl group. ^j Splitting constants of three γ protons of the ethyl group. ^k Splitting constants of two β protons of the propyl group. ^l Splitting constants of the β proton of the isopropyl group. ^m Splitting constants of six γ protons of the isopropyl group. ⁿ Splitting constants of the β proton of the *sec*-butyl group. ^o Splitting constants of five γ protons of the *sec*-butyl group.

spectral lines was Lorentzian. The spin densities of the radicals were calculated with an Elliott-503 computer.

Results and Discussion

Epr Spectra. Unsubstituted *o*-benzosemiquinone and its 4-methyl, 4-ethyl, 4-propyl, 4-isopropyl, 4-*sec*-butyl, and 4-*tert*-butyl derivatives were investigated in the alkaline aqueous methanol medium. The splitting constants determined from the spectra of the unsubstituted *o*-benzosemiquinone (Figure 1a) and its 4-methyl derivative are in good agreement with the data published in literature.^{2,3} The splitting constants for 4-*tert*-butyl-*o*-benzosemiquinone listed in Table I were determined from a spectrum the analysis of which was described in detail elsewhere.¹¹

Spectra that were comparatively well resolved were obtained in the oxidation of 4-isopropyl and 4-*sec*-butyl derivatives of pyrocatechol. An analysis of the measured spectra of 4-isopropyl and 4-*sec*-butyl-*o*-benzosemiquinone (Figures 2a and 3a) demonstrated that these spectra showed a resolved hyperfine structure, owing to an interaction of the unpaired electron with three nonequivalent protons of the aromatic ring and with one β proton and six or five γ protons of the alkyl substituent. The splitting constants determined by the analysis of these spectra are given in Table I, and the corresponding simulated spectra are represented in Figures 2b and 3b.

A quite different character was found with the spectra which were obtained in the oxidation of the 4-ethyl and

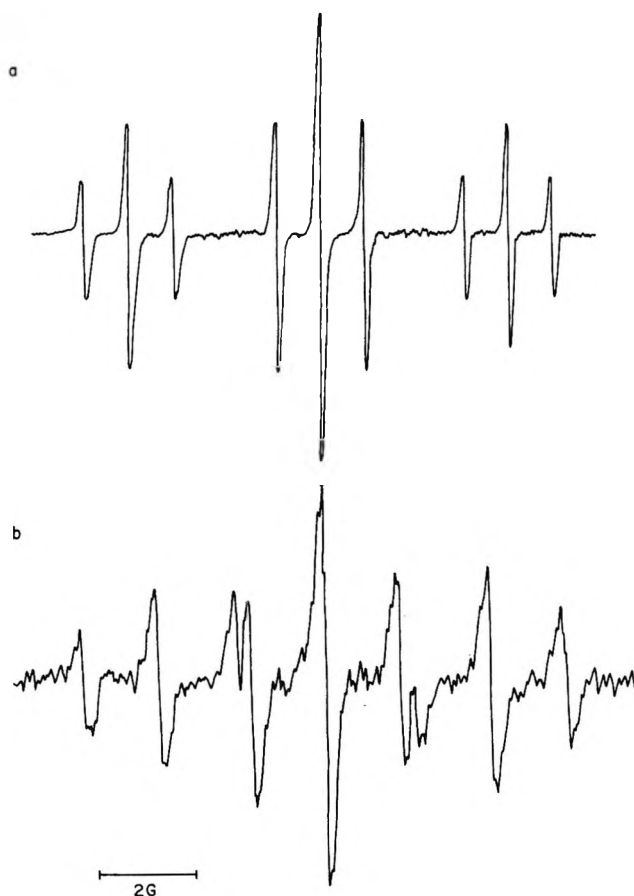


Figure 1. The epr spectrum of unsubstituted *o*-benzosemiquinone: (a) in 75% aqueous methanol; (b) in acetonitrile.

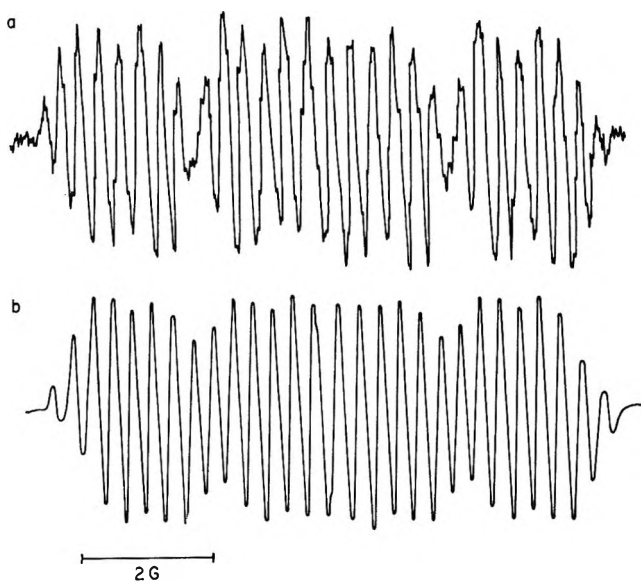


Figure 2. The epr spectrum of 4-isopropyl-*o*-benzosemiquinone in 75% aqueous methanol: (a) experimental spectrum; (b) simulated spectrum ($\Delta H_{1/2} = 160$ mG).

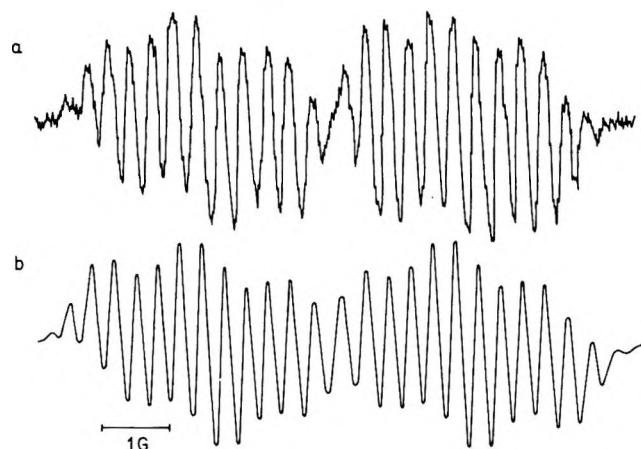


Figure 3. The epr spectrum of 4-*sec*-butyl-*o*-benzosemiquinone in 75% aqueous methanol: (a) experimental spectrum; (b) simulated spectrum ($\Delta H_{1/2} = 280$ mG).

4-propyl derivatives of pyrocatechol. The spectrum of 4-ethyl-*o*-benzosemiquinone consists of eight lines in which further splitting can be seen. Relative intensities of these lines indicate that the spectrum is composed of a quadruplet of doublets. Since we did not succeed in getting a proper resolution of the hyperfine structure, no exact analysis of this spectrum could be made either. The basic quadruplet is probably formed by an interaction of the unpaired electron with one proton of the aromatic ring and with two β protons of the ethyl substituent, which are characterized by splitting constants of approximately the same numerical value. The doublet is probably formed by an interaction of the unpaired electron with another proton of the aromatic ring; the further uncompletely resolved splitting is probably due to the weak interaction of the unpaired electron with the

remaining proton of the aromatic ring and with three γ protons of the ethyl substituent. The splitting constants of this radical listed in Table I are only approximate. The spectrum of 4-propyl-*o*-benzosemiquinone (Figure 4a) has a well-resolved hyperfine structure, which is due to the interaction of the unpaired electron with three nonequivalent protons of the aromatic ring and with two equivalent β protons of the propyl substituent. The lines of the spectrum do not exhibit any indications of a further splitting caused by the interaction of the unpaired electron with the other protons of the propyl substituent. The splitting constants determined by an analysis of this spectrum are also listed in Table I; the corresponding simulated spectrum is represented in Figure 4b.

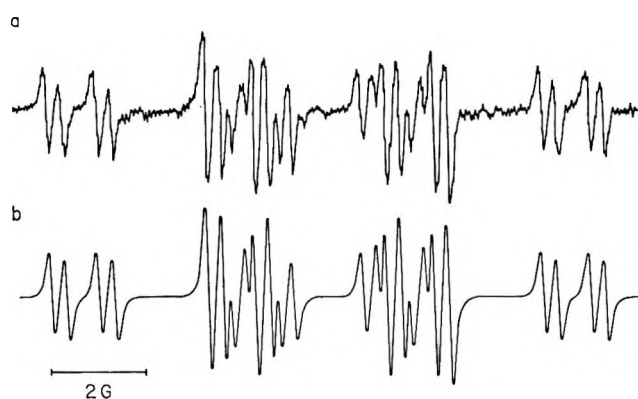


Figure 4. The epr spectrum of 4-propyl-*o*-benzosemiquinone in 75% aqueous methanol: (a) experimental spectrum; (b) simulated spectrum ($\Delta H_{1/2} = 200$ mG).

o-Benzosemiquinone and its 4-methyl and 4-*tert*-butyl derivatives were studied in an aprotic medium. The epr spectrum of the comparatively stable 4-*tert*-butyl-*o*-benzosemiquinone was described in one of our previous papers;¹⁶ in Table I, only splitting constants determined by its analysis are given. The electrolytic reduction of the corresponding *o*-benzoquinones in acetonitrile enabled us to prepare unsubstituted *o*-benzosemiquinone and its 4-methyl derivative as well, which are considerably less stable. The spectra of both radicals are of the same type as their spectra in the aqueous methanol medium, with the exception that the splitting constants differ considerably (Table I), owing to the effect of the solvent. The effect of the solvent on the magnitude of the splitting constants in *o*-benzosemiquinone can be seen in Figure 1. A lower stability of the latter two radicals in acetonitrile under an inert atmosphere is probably due to reactions between radicals, the main role in which can be played by the high spin densities on carbon atoms in positions 4 and 5 of the aromatic ring of *o*-benzosemiquinone, or by a considerable delocalization of the unpaired electron on the protons of the methyl group in its 4-methyl derivative, respectively.

Spin Densities Calculations. From the values given in Table I it is evident that the splitting constants of protons of the aromatic ring determined from spectra of variously substituted derivatives of 4-alkyl-*o*-benzosemiquinone vary with varying substituent in position 4 and with the solvent. If we assume McConnell's relationship²⁰ $a^H = Q_{CH^H} \rho_C^\pi$ to be valid, the changes observed with these splitting constants can only be explained by the fact that the distribution of spin density in the radicals is influenced, on the one hand, by the presence of the individual substituents, and on the other, by various solvents. We tried to verify whether the quantum chemical methods of the spin density calculations could give an adequate description of these changes. Owing to the possible occurrence of negative spin densities in *o*-benzosemiquinones⁶ we chose McLachlan's method⁷ for the calculations, *viz.*, the approximation based on the calculation of two groups of one-electron wave functions. The usual value $\lambda = 1.2$ was used for the parameter λ .

The first preliminary calculations of the spin densities in 4-alkyl-*o*-benzosemiquinones were made using the parameters h_O and k_{CO} suggested by Vincow.⁶ For the description of substituted alkyl groups the induction model of hyperconjugation was used.²¹ The results of these calculations, also with respect to the inadequacy of the chosen method of considering the effect of voluminous alkyl substituents, led us to the conclusion that a better agreement between the splitting constants of the protons of the aromatic ring and the calculated spin densities could be achieved by selecting "better values" for the parameters h_O and k_{CO} . To find these "better values," we calculated the spin densities in the unsubstituted *o*-benzosemiquinone, varying the values of the parameters h_O and k_{CO} in the intervals 1.2–2.6 (by 0.2) and 0.3–2.0, respectively. The ratio of the calculated spin densities on the carbon atoms of the aromatic ring in positions 4 and 3, $A_{43} = \rho_4/\rho_3$, was taken as the first basic criterion to consider the agreement between the splitting constants and calculated spin densities. Its absolute experimental value is given by the ratio of splitting constants of the corresponding protons of the aromatic ring of *o*-benzosemiquinone. In the aqueous methanol medium its value is $|A_{43}^{MeOH}| = a_4^H/a_3^H = 4.3 \pm 0.1$, in acetonitrile it is equal to $|A_{43}^{CH_3CN}| = 2.2 \pm 0.1$. Searching for a further criterion we chose the ratio of the splitting constant of the proton of the aromatic ring in position 4 to the calculated spin density on the carbon atom in this position, *i.e.*, $Q_4 = a_4^H/\rho_4$. We required that the absolute value of Q_4 should lie within the usual limits for the absolute value of the σ - π interaction constant Q_{CH^H} , that is in the interval 24–27 G.

The values of the ratios A_{43} of the calculated spin densities in dependence on the parameter k_{CO} are plotted in Figure 5; the corresponding values of the parameter h_O are given at the individual curves in the figure. For

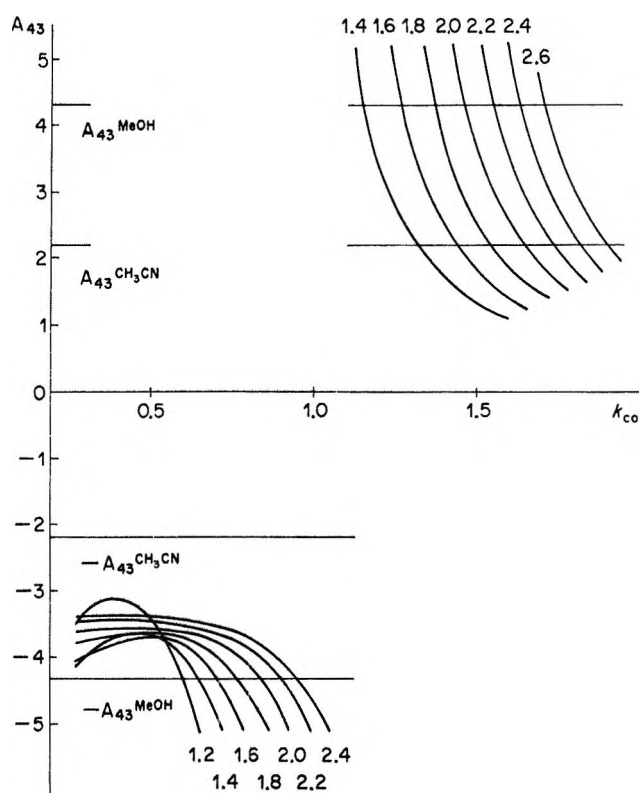


Figure 5. Dependence of the ratio $A_{43} = \rho_4/\rho_3$ of *o*-benzosemiquinone on the value of the k_{CO} parameter of the C-O bond for various values of the h_O parameter of the oxygen atom. (ρ_4 and ρ_3 are spin densities calculated by McLachlan method on the aromatic ring carbon atoms of *o*-benzosemiquinone in positions 4 and 3.)

all the given values of the parameter h_O the calculated spin density on the carbon atom of the aromatic ring of *o*-benzosemiquinone in position 4 is positive and decreases with increasing magnitude of the parameter k_{CO} . The spin density on the carbon atom of the aromatic ring in position 3 is always negative for small values of the parameter k_{CO} and increases up to positive values if k_{CO} increases. It can be seen from Figure 5 that in the region of small values of k_{CO} , where the spin density ρ_3 and the ratio A_{43} are negative, only those pairs of the parameters h_O and k_{CO} can be found for which A_{43} is in agreement with the value $-|A_{43}^{MeOH}|$. In the region of higher values of k_{CO} , where ρ_3 and A_{43} are positive, pairs of the parameters can be found for which the value of the ratio A_{43} agrees with the value $|A_{43}^{MeOH}|$, as well as those for which the value of the ratio A_{43} is identical with the value $|A_{43}^{CH_3CN}|$. It is also evident from this figure that in the latter region the change in the distribution of the spin density in *o*-benzosemiquinone, due to the replacement of an aqueous methanolic medium by an aprotic one (acetonitrile), can be reflected in the calculations by a decrease in the

(20) H. M. McConnell and D. B. Chesnut, *J. Chem. Phys.*, **28**, 107 (1958).

(21) A. Streitwieser, Jr., "Molecular Orbital Theory for Organic Chemists," Wiley, New York, N. Y., 1962.

Table II: Spin Densities in *o*-Benzosemiquinone Calculated by McLachlan Method

Parameters		Position ^a				A_{43}^b	Q_4 , G ^c
h_o	k_{CO}	1,2	3,6	4,5	7,8		
2.00	1.46	0.1992	0.0321	0.1410	0.1276	4.39	26.6
2.20	1.55	0.2058	0.0339	0.1463	0.1140	4.32	25.6
2.40	1.63	0.2116	0.0347	0.1509	0.1028	4.35	24.9
2.60	1.71	0.2158	0.0360	0.1544	0.0938	4.29	24.3
1.64	1.46	0.1581	0.0558	0.1225	0.1636	2.20	26.9
1.80	1.55	0.1650	0.0592	0.1282	0.1476	2.17	25.7
1.96	1.63	0.1712	0.0614	0.1330	0.1343	2.17	24.8
2.14	1.71	0.1777	0.0627	0.1377	0.1219	2.20	24.0
1.30	0.63	0.2087	-0.0307	0.1320	0.1900	-4.30	28.4
1.35	0.64	0.2204	-0.0332	0.1421	0.1707	-4.28	26.4
1.40	0.66	0.2293	-0.0344	0.1495	0.1557	-4.34	25.0

^a Individual positions are designated as shown in structure I. ^b A_{43} is the ratio of the calculated spin densities on the carbon atoms in positions 4 and 3. The values of this ratio determined experimentally from the splitting constants of the corresponding protons of the aromatic ring were 4.31 for *o*-benzosemiquinone in aqueous methanol and 2.20 in acetonitrile. ^c Q_4 is the ratio of the splitting constant of the proton of the aromatic ring in position 4 to the corresponding value of the spin density calculated on the carbon atom of the aromatic ring in the same position.

value of the parameter h_o by roughly 0.4. This finding is in accordance with the conception interpreting the effect of the solvent on the spin density distribution in radicals as a consequence of dipolar interactions between the polar molecules of the solvent and the polar heteroatoms of the radicals. These interactions manifest themselves in a change of electronegativity of the heteroatoms with respect to the rest of the radical.²²

From both regions mentioned above we selected pairs of parameters which allow to calculate the distribution of the spin density on *o*-benzosemiquinone in agreement with the splitting constants according to the other criterion also. The selected pairs of parameters, the spin densities calculated using these pairs and corresponding ratios A_{43} and Q_4 are listed in Table II.

In the calculations of spin densities in 4-alkyl-*o*-benzosemiquinones we used selected pairs of the parameters h_o and k_{CO} , and for the description of alkyl substituents an inductive model of hyperconjugation²¹ (the parameter of the carbon atom of the aromatic ring in position 4 was varied within the limits $h_{C_4} = 0$ to -0.8) was used first. In the calculations involving the parameters h_o and k_{CO} from the region of positive values of the spin density ρ_3 and with h_{C_4} was decreasing, the changes of the calculated spin densities on the carbon atoms of the aromatic ring in positions 3, 5, and 6 were in qualitative agreement with the changes of splitting constants of the corresponding protons of the aromatic ring of a series of 4-alkyl-*o*-benzosemiquinones with increasing volume of the alkyl substituent. We suspected in this case the quantitative disagreement between the changes of these two quantities to be due to the use of a too simplifying model of the voluminous alkyl substituents.

We applied therefore a conjugation model of hyperconjugation for the description of methyl groups in the

calculations of spin densities in 4-methyl-*o*-benzosemiquinone and used the values of parameters suggested by Lazdins and Karplus²³ ($h_{C'} = -0.1$; $h_{H_3} = -0.5$; $k_{CC'} = 0.7$; for the parameter $k_{C'H_3}$, a slightly higher value, *i.e.*, 3.0 was used, and the value of the parameter h_{C_4} was varied in the proximity of -0.1). Table III presents the spin densities calculated with these parameters for the methyl group and with those pairs of parameters h_o and k_{CO} for which the magnitude of the ratio Q_4 (Table II) approaches 27 G. The splitting constants of the aromatic ring protons listed in Table III were determined from the calculated spin densities by means of the McConnell relationship, assuming that $|Q_{CH^H}| = 27$ G. It can be seen from comparison of the splitting constants thus calculated with the splitting constants determined experimentally in both the aqueous methanol and acetonitrile, that a good agreement exists in both media in these cases, where the values of the pairs of parameters h_o and k_{CO} were selected from the region of positive values of ρ_3 (the marginal bi-columns in Table III). A considerably poorer agreement was found between the splitting constants determined from the spin densities which had been calculated with pair of parameters from the region of negative values of ρ_3 (the central bi-column in Table III) and the constants found experimentally in the aqueous methanol. This fact, along with the finding that in the region of negative values of the ratio A_{43} it is not possible to calculate the spin densities of *o*-benzosemiquinone to be in agreement with the experimentally determined splitting constants in acetonitrile, seems to indicate that the spin densities on the carbon atoms of the aromatic ring of *o*-benzo-

(22) J. Gendell, J. H. Freed, and G. K. Fraenkel, *J. Chem. Phys.*, **37**, 2832 (1962).

(23) D. Lazdins and M. Karplus, *J. Amer. Chem. Soc.*, **87**, 920 (1965).

Table III: Calculated Spin Densities^a and Splitting Constants^b of 4-Methyl-*o*-benzosemiquinone

Position ^c	Aqueous methanol				Acetonitrile	
	$h_O = 2.00, k_{CO} = 1.46$		$h_O = 1.35, k_{CO} = 0.64$		$h_O = 1.64, k_{CO} = 1.46$	
	$h_{C_4} = -0.08$	$h_{C_4} = -0.10$	$h_{C_4} = -0.08$	$h_{C_4} = -0.10$	$h_{C_4} = -0.08$	$h_{C_4} = -0.10$
1	0.2064	0.2078	0.2413	0.2552	0.1644	0.1656
2	0.1933	0.1923	0.2052	0.1912	0.1552	0.1547
3	0.0089	0.0053	-0.0529	-0.0579	0.0336	0.0298
4	0.1502	0.1519	0.1700	0.1854	0.1302	0.1317
5	0.1477	0.1490	0.1409	0.1302	0.1295	0.1309
6	0.0387	0.0398	-0.0216	-0.0152	0.0617	0.0627
7	0.1296	0.1300	0.1789	0.1878	0.1665	0.1671
8	0.1192	0.1178	0.1316	0.1153	0.1540	0.1523
9	-0.0016	-0.0016	-0.0020	-0.0018	-0.0015	-0.0015
10	0.0076	0.0077	0.0085	0.0097	0.0065	0.0066
a_{H}	0.24	0.14	1.43	1.56	0.91	0.81
a_{C}	3.99	4.02	3.80	3.52	3.50	3.53
a_{O}	1.05	1.07	0.58	0.41	1.66	1.69
Q_{Me} ^d	32.0	31.6	28.2	25.9	31.5	31.1

^a Calculated using the values $h_{C'} = -0.1$, $h_{\text{H}_1} = -0.5$, $k_{\text{CC}'} = 0.7$, $k_{C'\text{H}_1} = 3.0$ for the parameters describing the methyl group.

^b Splitting constants were calculated from the above spin densities by means of McConnell's relationship, assuming that $|Q_{\text{CH}^{\text{H}}}| = 27$ G. ^c Individual positions are designated as shown in structure I. ^d $Q_{\text{Me}} = a_{\text{Me}}^{\text{H}}/\rho_4$.

semiquinone in positions 3 and 6 are probably positive. So far, however, this conclusion has not been given an experimental evidence.

In the last line of Table III the values are given of the ratio of the splitting constant of the protons of the methyl group to the calculated spin density on the carbon atom of the aromatic ring of 4-methyl-*o*-benzosemiquinone in position 4, $Q_{\text{Me}} = a_{\text{Me}}^{\text{H}}/\rho_4$, the numerical value of which is identical with the absolute value of the hypothetical σ - π interaction constant $Q_{\text{CCH}_3^{\text{H}}}$. In all cases when an agreement between the calculated and experimental values was attained the value Q_{Me} kept in the interval 31.5 ± 0.5 G, and its ratio to the supposed magnitude of the σ - π interaction constant $|Q_{\text{CH}^{\text{H}}}| = 27$ G was 1.17. This result is very close to the value obtained by Claxton, *et al.*,²⁴ in the investigation of *p*-benzosemiquinones substituted with methyl groups.

So far it has not been possible to make similar calculations for 4-alkyl-*o*-benzosemiquinones substituted with higher alkyl groups, since no model has yet been suggested, for voluminous alkyl groups equivalent to the conjugation model for the methyl group. To allow a more accurate selection of the values of parameters h_O and k_{CO} it would be necessary to gather experimental data about the spin densities on the carbon atoms of the aromatic ring in positions 1 and 2 and on the oxygen atoms.

Splitting Constants of the β Protons of Alkyl Substituents. An analysis of the epr spectra of a series of variously substituted 4-alkyl-*o*-benzosemiquinones in the aqueous methanol revealed considerable differences in the magnitudes of the splitting constants of β protons of various alkyl substituents (Table I). The splitting constants of β protons of alkyl groups in the series

methyl, ethyl, propyl, isopropyl, and *sec*-butyl gradually decrease; the magnitude of the splitting constant of the β proton of the *sec*-butyl group being only about 30% of the splitting constant of protons of the methyl group. A modification of the Heller-McConnell relationship $a_{\beta}^{\text{H}} = \langle Q(\vartheta) \rangle \rho_{\text{C}_\alpha}^{\pi}$ suggested by Stone and Maki²⁵ allows to explain the observed changes of the splitting constants of β protons a_{β}^{H} either by a change of the magnitude of the spin density $\rho_{\text{C}_\alpha}^{\pi}$ on the carbon atom of the aromatic ring C_α , to which the alkyl group is attached, or by a change of the time-averaged quantity $\langle Q(\vartheta) \rangle = B_2 \langle \cos^2 \vartheta \rangle$; in the latter expression, B_2 is a constant and ϑ is an angle between the plane containing the axis of the p_z orbital of the C_α carbon atom and the atom C' and the plane containing the atoms C_α , C' , and H_β . Comparatively small changes of the splitting constants of protons of the aromatic ring in position 5 of the series of 4-alkyl-*o*-benzosemiquinones (Table I) seem to indicate that also the changes of the spin density on the carbon atom of the aromatic ring in position 4 (C_α) are by far not large enough to influence the magnitude of the splitting constants of β protons in a decisive manner. According to the Stone and Maki theory of the effect of the hindered internal rotation on the magnitude of the splitting constants of β protons of alkyl substituents,²⁵ the changes of the time-averaged quantity $\langle Q(\vartheta) \rangle$ can be due to the steric interactions between the protons of the π system of the radical, on the one hand, and voluminous alkyl substituents, on the other. Owing to these interactions, all possible mutual orientations of the π system of the radical and alkyl

(24) T. A. Claxton, J. Oakes, and M. C. R. Symons, *Trans. Faraday Soc.*, **63**, 2125 (1967).

(25) E. W. Stone and A. H. Maki, *J. Chem. Phys.*, **37**, 1326 (1962).

Table IV: Splitting Constants of β Protons of Alkyl Substituents in Radicals of Various Types and the Corresponding Values $R/2$

Type of the radical	Alkyl substituent									
	Methyl -CH ₃ a_{Me}^H	Ethyl -CH ₂ CH ₃ a_{β}^H	$R/2^a$	Propyl -CH ₂ CH ₂ CH ₃ a_{β}^H	$R/2^a$	Isopropyl -CH(CH ₃) ₂ a_{β}^H	$R/2^a$	<i>sec</i> -Butyl -CHCH ₂ C ₂ H ₅ a_{β}^H	$R/2^a$	Reference
4-Alkyl- <i>o</i> -benzosemiquinones	4.80	3.70	0.39	3.30	0.34	2.21	0.23	1.8	0.19	
Anion-radicals of nitroalkanes	11.4	9.75	0.43	9.98	0.44	4.60	0.20	3.19	0.14	25
Anion-radicals of 4-alkylnitrobenzenes	3.98	2.96	0.37	1.74	0.22	26
4-Alkylphenoxyis	11.95	10.15	0.42	8.7	0.36	6.0	0.25	4.3	0.18	27

^a The value of $R/2$ is determined by half the ratio of the splitting constant of the β proton of the alkyl group to the splitting constant of the protons of the methyl group attached in the same position to the same system of the π bonds.

substituent are not equally probable; the probability of the occurrence of sterically advantageous (equilibrium) conformations increases, and the magnitude of the time-average value of the quantity $\langle Q(\vartheta) \rangle$ departs from the value $B_2/2$, which it acquires in the case that the alkyl substituent rotates freely. On the assumption that the spin density $\rho_{C_\alpha}^\pi$ remains constant in the series of derivatives substituted with various alkyl groups and that the methyl group attached to the system of the π bonds of the radical rotates freely, it is possible to determine the value $\langle Q(\vartheta) \rangle/B_2$ for each alkyl group as half the magnitude of the ratio of the splitting constant of β proton of the corresponding alkyl group to the splitting constant of protons of the methyl group attached in the same position to the same system of π bonds, $R = a_{\beta}^H/a_{Me}^H$.

Table IV presents a list of splitting constants and corresponding values $R/2$ for β protons of the individual alkyl substituents of a series of 4-alkyl-*o*-benzosemiquinones. For reasons of comparison we also give values determined by the analysis of the epr spectra of the anion-radicals of nitroalkanes²⁵ and 4-alkylnitrobenzenes,²⁶ in the analysis of which the Stone and Maki theory was already used, and values determined from the splitting constants of a series of 4-alkylphenoxyis taken over from a paper by Stone and Waters.²⁷ It is obvious that the values $R/2$ corresponding to a certain alkyl group in each of the four given types of radicals are very close to each other, especially if we realize with certainty that the assumption concerning a constant spin density on the carbon atom C_α is not fulfilled with exactitude. In accordance with the authors of the papers quoted^{25,26} above, the values listed in Table IV can be interpreted in such a way that in all four tabulated series of radicals the equilibrium conformations of alkyl substituents with one β proton are those defined by the angle $\vartheta = 90^\circ$. Within the Stone-Maki model²⁵ from the $R/2$ values given in Table IV it follows that the height of the rotation barrier is near 1 kcal/mol for the isopropyl group and has a slightly higher

value for the *sec*-butyl group. The equilibrium conformations of alkyl substituents containing two β protons are those defined by the angle $\vartheta = 60^\circ$; from the $R/2$ value it follows again that the height of the rotation barrier is near 0.6 kcal/mol for the ethyl group and is again slightly higher for the propyl group.

Conclusion

The epr spectra of a series of 4-alkyl-*o*-benzosemiquinones in aqueous methanol and acetonitrile prepared by air oxidation of pyrocatechols or by electrolytic reduction of *o*-benzoquinones in flow arrangement have been measured and analyzed. It was found that McLachlan's method of calculation of the spin densities could be applied to describe the change in the distribution of the spin density over the aromatic ring of *o*-benzosemiquinones, caused by the effect of alkyl substituents in position 4 and by the solvent, if we pick up for the parameters of the oxygen atom and the C-O bond, *i.e.*, h_O and k_{CO} , the values in the limits ($h_O = 2.0$, $k_{CO} = 1.46 - h_O = 2.6$, $k_{CO} = 1.71$), for the radicals in aqueous methanol. If acetonitrile is used as the medium, then the values are the same for the parameter k_{CO} and lower by 0.4 for the parameter h_O . This calculation shows that the spin densities on carbon atoms of the aromatic ring of an unsubstituted *o*-benzosemiquinone in positions 3 and 6 are positive. A good quantitative agreement with the experimental splitting constants was found for the spin densities calculated in 4-methyl-*o*-benzosemiquinone, using the conjugation model of hyperconjugation and slightly modified parameters of Lazdins and Karplus for the methyl group. It was possible to interpret the observed changes of magnitude of the splitting constants of β protons of alkyl substituents on the basis of the Stone and Maki theory of the hindered internal rotation of alkyl substituents. The interpretation of the

(26) T. M. McKinney and D. H. Geske, *J. Amer. Chem. Soc.*, **89**, 2806 (1967).

(27) T. J. Stone and W. A. Waters, *J. Chem. Soc.*, 213 (1964).

splitting constants of γ protons of alkyl substituents is much more difficult. In the present time, the changes observed can only be considered to be a further proof of an important role played by the hyperconjugation type mechanism in the interaction mechanism of the unpaired electron with the γ protons.

Acknowledgments. I wish to thank Dr. J. Pospíšil for the incentive to complete the present work and also for the derivatives of pyrocatechol which he kindly

supplied. My thanks are also due to Dr. J. Petránek for the preparation of the benzoquinone derivatives and for his valuable comments on the manuscript and discussion, and to Dr. I. Buben, Dr. O. Ryba, and Dr. K. Ulbert for their aid and discussions. The program for the calculation of the spin densities was supplied by courtesy of the coworkers of Dr. R. Zahradník, to whom I am much indebted for his consultation in quantum chemistry. Technical assistance was kindly provided by Mrs. J. Vaňková and Miss V. Hartingerová.

An Exact Solution to the Rate Equation for Reversible Photoisomerization

by Joseph Blanc

RCA Laboratories, Princeton, New Jersey 08540 (Received July 6, 1970)

An exact solution to the differential equation proposed by Zimmerman, *et al.*, for reversible photoisomerization is presented. The kinetic equation is given by a rapidly convergent expansion

$$C_0 \ln |\delta| + \sum_{i=1}^{\infty} C_n \delta^n = -\{(F\Phi_T \epsilon_T t)/y_{\infty}\} + \text{constant}$$

where $\delta = D_{\infty} - D$ and the C_n 's are explicit analytic functions of D_{∞} . A brief discussion of errors is also made.

Research in these laboratories has been reported^{1,2} on reversible photoisomerization of indigoid dyes. Because of our own work and because of relatively large discrepancies in quantum yields which have been reported³ in the central case of stilbene photoisomerization, we have been concerned with obtaining an accurate solution to the kinetic differential equation for reversible photoisomerization which would be amenable to systematic error analysis. It is the principal purpose of this article to exhibit such a solution.

For the photochemical isomerization $T \xrightarrow{h\nu} C$, let D be the optical density at time t , y the fraction of isomer C present at time t , y_{∞} the fraction of C at photostationary state, ϵ_T and ϵ_C molar extinction coefficients of isomers T and C, respectively, at frequency ν , $[A]$ total isomeric concentration (moles/unit volume), F the number of incident einsteins per unit time and unit area, l the optical path length, and Φ_T the quantum yield for the process $T \rightarrow C$. ϵ 's and D 's are to the base e .

In their classic paper, Zimmerman, Chow, and Paik⁴ showed, defining a variable $z \equiv y_{\infty} - y$, that the solution to the photochemical rate equation (in the absence of thermal isomerization) is formally

$$I \equiv \int \frac{D}{1 - \exp(-D)} \frac{dz}{z} = -\left\{ \frac{F\Phi_T \epsilon_T t}{y_{\infty}} \right\} + \text{constant} \quad (1)$$

The slope of I vs. t therefore gives Φ_T multiplied by experimentally determinable parameters. Zimmerman, *et al.*, by an expansion of the integrand in terms of D , obtained an approximation of the form $I = s \ln |z| + rz + uz^2$. They did not give explicit expressions for s , r , or u , which are in fact cumbersome functions of the experimental parameters l , ϵ_T , ϵ_C , y_{∞} , and $[A]$.

A much more transparent approximation can be obtained by rewriting I entirely in terms of D : $D = l[A] \{\epsilon_T + (\epsilon_C - \epsilon_T)y\}$. Defining, in analogy to z , $\delta \equiv D_{\infty} - D$, eq 1 can be rewritten

$$I = \int \frac{D}{1 - \exp(-D)} \frac{dz}{z} = \int \frac{D}{1 - \exp(-D)} \frac{d\delta}{\delta} \quad (2)$$

(1) J. Blanc and D. L. Ross, *J. Phys. Chem.*, **72**, 2817 (1968).

(2) D. L. Ross, J. Blanc, and F. J. Matticoli, *J. Amer. Chem. Soc.*, **92**, 5750 (1970).

(3) For a summary of stilbene quantum yields, see D. L. Ross and J. Blanc in "Photochromism," G. H. Brown, Ed., Wiley-Interscience, New York, N. Y., 1971, Chapter 5, in press.

(4) G. Zimmerman, L-Y. Chow, and U. J. Paik, *J. Amer. Chem. Soc.*, **80**, 3258 (1958).

Using the same expansion as Zimmerman, carried to the same order in D

$$\mathbf{I} \cong \left(1 + \frac{D_\infty}{2} + \frac{D_\infty^2}{12}\right) \ln |\delta| - \left(\frac{1}{2} + \frac{D_\infty}{6}\right) \delta + \frac{\delta^2}{24} \quad (3)$$

The coefficients in this expression appear to be power series in D_∞ , with an uncertain radius of convergence. This approximation suggests, however, that an exact solution of the form

$$\mathbf{I} = C_0 \ln |\delta| + \sum_{n=1}^{\infty} C_n \delta^n$$

where the C_n 's are analytic functions of D_∞ , can be found. If the expansion parameter is taken to be δ , which is the "natural" parameter by analogy with thermally reversible first-order reactions, such an exact expansion can be found with the C_n 's explicit functions of D_∞ .

Before proceeding, define $\gamma \equiv \exp(-D_\infty)$ (therefore $0 \leq \gamma \leq 1$); define $f(0) \equiv (1 - \gamma)^{-1} = 1 + \gamma + \gamma^2 + \dots$ ($\gamma^2 < 1$) and $f(n) \equiv \sum_{m=1}^{\infty} m^n \gamma^m$ and note $f(n+1) = \gamma df(n)/d\gamma$ for $n > 0$. Now rewrite eq 2 entirely in terms of δ , γ , and D_∞

$$\mathbf{I} = \int \frac{-d\delta}{1 - \gamma \exp(\delta)} + \int \frac{D_\infty}{(1 - \gamma \exp(\delta))} \frac{d\delta}{\delta} \equiv \mathbf{I}_1 + \mathbf{I}_2 \quad (4)$$

It is interesting to note that for the limiting case $D_\infty \rightarrow 0$, \mathbf{I} equals \mathbf{I}_1 , exactly, and therefore \mathbf{I}_2 can be viewed physically as a correction for photochemical "back-reaction." \mathbf{I}_1 is a standard integral which equals $\ln(1 - \gamma \exp(\delta)) - \delta$. We are interested, however, in expressing \mathbf{I}_1 as a power series in δ for combination with \mathbf{I}_2 . For $-1 < \gamma \exp(\delta) < 1$, the logarithm can be expanded and $\mathbf{I}_1 = -\delta - \sum_{m=1}^{\infty} (\gamma \exp(\delta))^m / m$; now expand $\exp(m\delta)$ in powers of δ and collect terms in δ^n . The result is, omitting a constant term

$$\mathbf{I}_1 = -\sum_{n=1}^{\infty} f(n-1) \delta^n / n! \quad (5)$$

To obtain \mathbf{I}_2 , expand $(1 - \gamma \exp(\delta))^{-1}$ as $\sum_{k=0}^{\infty} (\gamma \exp(\delta))^k$ (valid for $-1 < \gamma \exp(\delta) < 1$), expand $\exp(k\delta)$ once again, collecting terms in δ^n , then integrate term by term

$$\mathbf{I}_2 = D_\infty f(0) \ln |\delta| + D_\infty \sum_{n=1}^{\infty} f(n) \delta^n / n \cdot n! \quad (6)$$

Thus, as desired

$$\mathbf{I} = \mathbf{I}_1 + \mathbf{I}_2 = C_0 \ln |\delta| + \sum_{n=1}^{\infty} C_n \delta^n \quad (7)$$

with $C_0 = D_\infty f(0)$ and $C_n = (D_\infty f(n) - n f(n-1)) / n! \cdot n$. The first three C_n 's are explicitly $C_0 = D_\infty /$

$(1 - \gamma)$; $C_1 = [\gamma(1 + D_\infty) - 1] / (1 - \gamma)^2$, and $C_2 = \gamma[D_\infty(\gamma + 1) + 2\gamma - 2] / 4(1 - \gamma)^3$. Further coefficients can be obtained recursively if needed: they are not listed here as they are unlikely to be useful in practice since all higher coefficients vanish for large D_∞ and are small for small D_∞ . Equation 7 can be shown to converge for all physically meaningful (non-negative) values of D and D_∞ . I note here only that the proper limits are obtained in the limits $D, D_\infty, \delta \rightarrow 0$ and $D, D_\infty \rightarrow \infty$; $\mathbf{I} = (\ln |\delta|)$ and $(D_\infty \ln |\delta| - \delta)$, respectively. The latter result clearly cannot be obtained from the approximate eq 3.

For $D_\infty = 2$, the approximate (eq 3) vs. the exact (eq 7) coefficients are $C_0 = 2.33$ vs. 2.37 (2% error); $C_1 = -0.833$ vs. -0.796 (5% error) and $C_2 = 0.042$ vs. 0.028 (50% error). The approximation gets rapidly worse as D_∞ exceeds 2 and rapidly better in the opposite direction. Little appears to be gained by using the approximation, although it is quite adequate for many experimental situations.

I now give a brief error analysis, discussing only the logarithmic term which almost always dominates the slope of \mathbf{I} vs. t . For $D_\infty \rightarrow 0$, the fractional error in C_0 , i.e., $\Delta C_0 / C_0$, is $\Delta D_\infty / 2$, where ΔD_∞ is the uncertainty in D_∞ ; this error decreases slowly with increasing D_∞ . If D_∞ is a measured optical density (rather than a calculated one; see below), an upper limit to ΔD_∞ can be taken to be ≈ 0.010 (≈ 0.004 in density to the base 10 units), and uncertainties in quantum yields due to this source should not exceed 0.5%. Previous workers have presumably used the approximation for \mathbf{I} in the form suggested by Zimmerman, *et al.*, i.e., in terms of concentrations and absorption coefficients. Equation 3 or 7 can be recast in terms of these parameters; from the point of view of this paper, this amounts to calculating D_∞ in terms of the other parameters. Error estimates for the C_n 's can be made, but I make no such numerical estimates here as, except for the original work of Zimmerman, *et al.*, insufficient details of experimental methods and data reduction have been given to make such estimates reliably. It should be pointed out, however, that errors of 10% or more could plausibly arise even with standard laboratory practices, unless particular care is taken to eliminate them. For example, inaccuracies in y_∞ and $(\epsilon_T - \epsilon_C)$ of 1% would generate errors of more than 3% each in calculated C_0 with parameters appropriate to stilbene photoisomerization.

Finally, I note that the "method of initial slopes" proposed by Lippert and Lüder⁶ and previously used by us^{1,2} is quite correct in principle, but may be difficult to apply in practice without ambiguity. In short, for conversions small enough that "back reaction" is negligible, and if the photochemical system is initially completely in one isomeric form, the method proposes that the quantum yield be determined from

(5) E. Lippert and W. Lüder, *J. Phys. Chem.*, **66**, 2430 (1962).

$$\Phi = \frac{1}{(\epsilon_C - \epsilon_T)F} \left[\frac{dD/dt}{(1 - \exp(-D))} \right]_{t=0}$$

independent of D_∞ . However, in the face of scatter of experimental data, a criterion is needed for judging over what time interval dD/dt is in fact constant. Such a criterion is clearly available by comparison of

results from eq 7 and from the method of "initial slopes."

Acknowledgments. This work is the result of a collaborative effort on photochromic indigoids with D. L. Ross. I am grateful to J. P. Wittke for a useful critique of the manuscript.

The Photochemistry of Peroxodiphosphates. The Oxidation of Water and Two Alcohols

by Roger J. Lussier, William M. Risen, Jr., and John O. Edwards*

Metcalf Chemical Laboratories, Brown University, Providence, Rhode Island 02912 (Received May 8, 1970)

The photolytic reactions of peroxodiphosphate species in aqueous solution, in aqueous ethanol, and in aqueous 2-propanol produce phosphate plus oxygen, acetaldehyde, and acetone, respectively. Variables, which have been investigated for their influence on stoichiometry and quantum yield, are pH, reactant concentrations, and light intensity. In the water oxidation, the results are comparable to those found in the photolytic oxidation of water by peroxodisulfate; nonchain radical mechanisms apparently are involved in both cases but there are differences in detail. The photolytic oxidations of the alcohols by peroxodiphosphate also proceed by mechanisms involving radical intermediates with chain lengths dependent on alcohol nature and pH. Mechanisms which explain the results are presented.

Introduction

In the course of our studies of inorganic peroxides, important differences between the mechanistic chemistries of peroxodiphosphate¹ and peroxodisulfate² became apparent. One of these differences was the lack of facility of the peroxodiphosphates to undergo homolytic scission.



Thus, peroxodiphosphates do not noticeably oxidize water at 80° or below, although the oxidation of water by peroxodisulfate to form oxygen is a radical process with conveniently measured rates at 60°. Estimates^{1a} indicate that homolytic scission of $\text{S}_2\text{O}_8^{2-}$ is about two powers of ten more rapid than scission of $\text{P}_2\text{O}_8^{4-}$. Furthermore, alcohols are oxidized by peroxodisulfate *via* radical chain mechanisms at 40 to 60°



No comparable oxidation of alcohols by peroxodiphosphate occurs at convenient temperatures.

Battaglia,³ in a survey of ultraviolet spectra of peroxides, has shown that the spectra of peroxodiphosphate ion ($\text{P}_2\text{O}_8^{4-}$) and its protonated forms ($\text{H}_{4-n}\text{P}_2\text{O}_8^{n-}$) are very similar to those of other peroxides.

This similarity of spectra led us to predict that peroxodiphosphates would be activated to radical reactions comparable to those observed with hydrogen peroxide⁴ and peroxodisulfate⁵ at 253.7 nm.

We report here the results of an investigation of the oxidation of water and of aqueous alcohols by photo-

* To whom correspondence should be addressed.

(1) (a) M. M. Crutchfield in "Peroxide Reaction Mechanisms," J. O. Edwards, Ed., Wiley-Interscience, New York, N. Y., 1962, p 46 ff; (b) M. M. Crutchfield and J. O. Edwards, *J. Amer. Chem. Soc.*, **82**, 3533 (1960); (c) Sr. A. A. Green, J. O. Edwards, and P. Jones, *Inorg. Chem.*, **5**, 1858 (1966); (d) M. Andersen, J. O. Edwards, Sr. A. A. Green, and Sr. M. D. Wiswell, *Inorg. Chim. Acta*, **3**, 655 (1969).

(2) For reviews on peroxydisulfate mechanisms, see: (a) A. Haim and W. K. Wilmarth in "Peroxide Reaction Mechanisms," edited by J. O. Edwards, Wiley-Interscience, New York, N. Y., 1962, p 176 ff; (b) D. A. House, *Chem. Rev.*, **62**, 185 (1962); (c) E. J. Behrman and J. E. McIsaac, Jr., in "Mechanisms of Reactions of Sulfur Compounds," Vol. 2, N. Kharasch, Ed., 1968, pp 193-218.

(3) C. J. Battaglia, Ph.D. Thesis at Brown University, 1962.

(4) *Cf.*, M. C. R. Symons in "Peroxide Reaction Mechanisms," J. O. Edwards, Ed., Wiley-Interscience, New York, N. Y., 1962, p 137 ff.

(5) (a) Reference 2a; (b) M. Tsao and W. K. Wilmarth, *J. Phys. Chem.*, **63**, 346 (1959); (c) C. R. Giuliano, N. Schwartz, and W. K. Wilmarth, *ibid.*, **63**, 353 (1959); (d) L. Dogliotti and E. Hayon, *ibid.*, **71**, 2511 (1967); (e) E. Heckel, A. Henglein, and G. Beck, *Ber. Bunsenges. Phys. Chem.*, **70**, 149 (1966); (f) M. H. B. Mariano in "Radiation Chemistry," Vol. I, Advances in Chemistry Series No. 81, American Chemical Society, Washington, D. C., 1968, p 182.

excited peroxodiphosphate which confirm the prediction.

Experimental Section

Chemicals. The $\text{Li}_4\text{P}_2\text{O}_8 \cdot 4\text{H}_2\text{O}$ was prepared by the method of Chulski,⁶ and was 99.5% pure, after recrystallization, as determined by active oxygen analysis. The potassium salt $\text{K}_4\text{P}_2\text{O}_8$ was obtained from FMC Corp. and was 98.5% pure after recrystallization. The water used was distilled, then deionized by passage through a mixed bed resin. Carbonate-free NaOH solutions, used to adjust pH, were prepared according to the method of Kolthoff and Sandell⁷ and stored under nitrogen. The adjustment of solutions to low pH values was achieved by addition of orthophosphoric acid solutions made using Baker and Adamson reagent grade acid and deionized water. No buffer solutions were used. Baker and Adamson reagent grade $\text{K}_2\text{S}_2\text{O}_8$ was used after recrystallization. The alcohols ethanol and 2-propanol were reagent grade and used without further purification, except for deoxygenation. Isotope labeling experiments were performed with ^{18}O -labeled H_2O from Yeda (Israel) and with ^{32}P -labeled PO_4^{3-} from Tracerlab.

Photolysis Experiments. The photolytic reactions were carried out in a 1.0-cm absorption cell, with two fused-quartz windows, which was sealed with a serum cap. The cell was reproducibly positioned exposing both windows in the photolysis chamber with a polyethylene holder, by which the cell was removed after each exposure interval for spectral measurement. The photolytic chamber contained eight low-pressure quartz-enveloped Hg arcs, of 25-W input power, high efficiency, and radiative output comprised 91% of 253.7-nm radiation, arranged cylindrically at a radial distance of 10 cm and enclosed in a 30-cm diameter cylindrical reflector. The cell was positioned axially, and axial air circulation at 70 cubic feet per minute maintained chamber temperature at $25 \pm 2^\circ$. The deaerated reaction solutions of compositions given in the tables were mixed immediately prior to photolysis under an N_2 atmosphere and loaded in the sealed cell via syringe. After each carefully timed exposure to preequilibrated arcs, the reaction cell was placed in a Cary 14 or a Hitachi Perkin-Elmer Model 139 spectrophotometer and the spectrum measured in the 200–300-nm region or at 240.0 nm or 242.5 nm (alcohol reactions) to follow the reaction progress. The pH values of the starting reaction solutions were measured on a Beckman Model G meter. All pH values given in the tables as pH^i are such initial values (before photolysis). The pH was observed to drop in solutions for which $[\text{OH}^-] \ll [\text{P}]_{\tau}^i$, where $[\text{P}]_{\tau}^i$ is the initial peroxodiphosphate total concentration of peroxodiphosphate species regardless of degree of protonation. Photolyses of peroxodisulfate solutions were performed in a similar manner.

Isotope Labeling Experiments. A solution of $\text{Li}_4\text{P}_2\text{O}_8 \cdot 4\text{H}_2\text{O}$ was photolyzed in vacuum-degassed H_2^{18}O -enriched water in a quartz vessel, and the evolved oxygen was collected and analyzed for isotopic distribution with a Hitachi Perkin-Elmer RMU-6D mass spectrometer. A sample of the enriched water was converted to hydrogen peroxide,⁸ decomposed by Ce^{IV} addition,⁹ and the evolved oxygen was similarly isotopically analyzed. Photolysis time for this experiment was 5×10^3 sec. A number of solutions of $\text{P}_2\text{O}_8^{4-}$ and ^{32}P -labeled PO_4^{3-} at pH values from 0.90 to 9.38 were degassed and photolyzed for 300 sec in a quartz tube. Identical samples were kept in the dark. A 10.0-ml aliquot of each solution was treated with 5.0 ml of a mixture 0.15 M in MgCl_2 and 0.15 M in NH_4Cl , then with concentrated aqueous ammonia to the methyl red end point. After standing at 0° for about 1×10^3 sec, each solution was then centrifuged for 30 sec. To scavenge any remaining orthophosphate, 1.0 ml of 0.5 M K_3PO_4 (unlabeled) was added to the 10.00-ml aliquots; precipitation with the excess magnesia mixture occurred. After 30 sec of centrifugation, duplicate 1.0-ml aliquots of supernatant were evaporated on planchets and counted, and a 5.00-ml sample of the supernatant was titrated for peroxodiphosphate. Samples which were assumed infinitely thin were counted using a shielded Geiger tube and Nuclear Instrument and Chemical Corp. Model 161 scaler and corrected for background and sample decay which occurred during the preparation time. The photolyzed and dark solutions were treated identically.

Results

Preliminary experiments in which peroxodiphosphate solutions containing mild reducing agents were photolyzed showed that oxidations are caused by the products of the photoexcitation of $\text{P}_2\text{O}_8^{4-}$; comparable oxidations are not caused by $\text{P}_2\text{O}_8^{4-}$ under dark but otherwise equivalent conditions or under dark but higher temperature (100°) conditions. In order to investigate these reactions in detail, the reaction between photoexcited peroxodiphosphate and water was studied in the pH range 3–14. We consider these results before turning to the reactions involving ethanol and 2-propanol.

Photolysis in Water. The primary oxidized product of the reaction is molecular oxygen, as indicated qualitatively by mass spectrometer and quantitatively by a gas volumetric technique (reproducible to $\pm 5\%$).

(6) T. Chulski, Ph.D. Thesis, Michigan State University, 1953; cf. also C. H. Chong, Ph.D. Thesis, Michigan State University, 1958.

(7) I. M. Kolthoff and E. B. Sandell, "Textbook of Quantitative Inorganic Analysis," Macmillan Co., New York, N. Y., 1943, p 551.

(8) R. E. Ball, J. O. Edwards, and P. Jones, *J. Inorg. Nucl. Chem.*, **28**, 2458 (1966).

(9) (a) C. A. Bunton and D. R. Llewellyn, *Research*, **5**, 142 (1952); (b) M. Anbar, *J. Amer. Chem. Soc.*, **83**, 2031 (1961).

Phosphate was identified by precipitation of $\text{Mg}(\text{NH}_4)\text{PO}_4$. The overall stoichiometry then is



The oxygen evolved from peroxodiphosphate solutions photolyzed in H_2O contained $6.00 \pm 0.11\%$ H_2O^{18} , after correction for the water of hydration of $\text{Li}_4\text{P}_2\text{O}_8 \cdot 4\text{H}_2\text{O}$, whereas the true O^{18} content of the solvent H_2O was found to be $6.14 \pm 0.16\%$. Thus, within the stated error limits, all of the evolved O_2 derives from the solvent water.

The photolysis of peroxodiphosphate in water, carried out as described in the experimental section, was found to be first order in peroxodiphosphate, as shown by the linearity of plots of $\log [P]_T$ vs. irradiation time over two half-lives or more, throughout the pH range 3–11. Representative plots are presented in Figure 1. Here

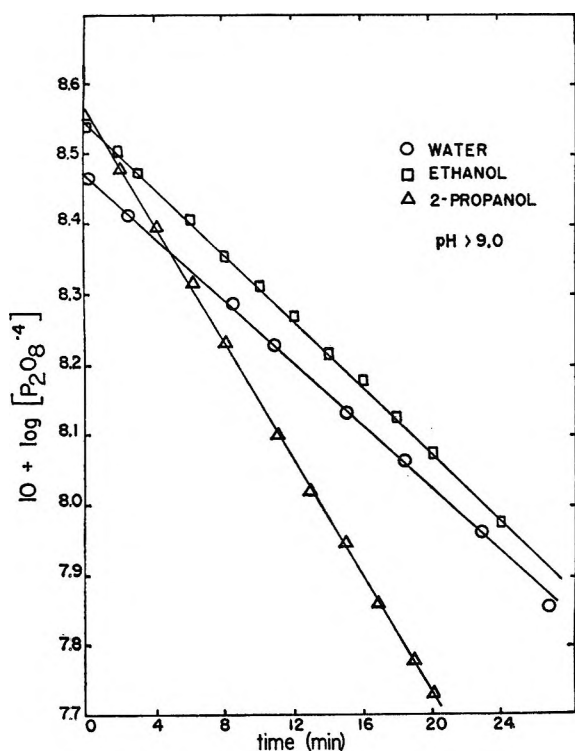


Figure 1. First-order plots for decrease in peroxodiphosphate concentration as a function of time at pH 9.0. The runs are for $\text{P}_2\text{O}_8^{4-}$ in: \circ , pure water; \square , water with ethanol; and Δ , water with 2-propanol.

$[P]_T$ is the total concentration of peroxodiphosphate species, regardless of degree of protonation.

The overall quantum yield ϕ_T was found to be essentially invariant with pH, in the absence of added phosphate or metal ions other than alkali ions, as shown in Table I and Figure 2. The quantum yields were calculated on the basis of $[P]_T$ using the known quantum yield of 0.60 for the photodecomposition of peroxodisulfate⁵ to calibrate the photolysis system. The molar extinction coefficients of $\text{H}_n\text{P}_2\text{O}_8^{8-n}$ ($n = 0, 1, 2, 3$) are

Table I: Dependence of the Overall Quantum Yields (ϕ_T) for Photodecomposition of Peroxodiphosphate upon pH^a

pH ⁱ	$[P]_T^i$, M	ϕ_T
3.12	0.020	0.81
4.96	0.020	0.80
6.42	0.020	0.80
7.84	0.020	0.78
9.10	0.020	0.80
11.40	0.020	0.81
13.35	0.020	0.80
13.74	0.020	0.78

^a $T = 25^\circ$.

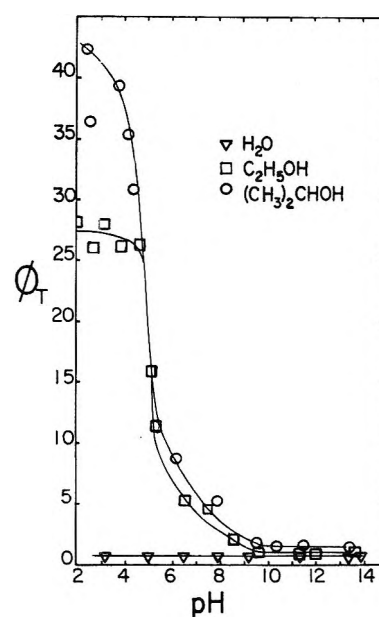


Figure 2. Plots showing the quantum yield as a function of pH. The smoothed curves connect the data for photolysis with: Δ , pure water; \square , water with ethanol; and \circ , water with 2-propanol.

identical to within 2%, an indication that the transition moment for the peroxide absorbance is not greatly affected by the protonation of sites several atoms away. Thus, pH variations of quantum yields which are calculated on the basis (*i.e.*, $[P]_T$) are expected to reflect the dependence of the reaction on hydronium or hydroxyl ion concentration; surprisingly, no such variation was observed.

The data of Table II show that ϕ_T is independent of $[P]_T^i$ in the range $0 < [P]_T \leq 0.050$ M. In addition, ϕ_T does not vary with radiation rates giving rise to light absorptions in the range $3.8\text{--}5.0 \times 10^{16}$ photons sec^{-1} .

Since PO_4^{3-} is a product of the reaction and since Tsao and Wilmarth^{5b} had found that in the photolytic decomposition of peroxodisulfate the addition of moderate amounts of both acid and sulfate decreased the quantum yield, we have investigated the effects of added

Table II: Dependence of the Overall Quantum Yield for Photodecomposition of Peroxidiphosphate on Initial Peroxidiphosphate Concentration $[P]_{T^i}$

$[P]_{T^i}$	pH ⁱ	ϕ_{T^a}
0.020	11.40-13.74	0.80 ^b
0.0403	c	0.77
0.0281	c	0.80
0.0174	c	0.80
0.0120	c	0.79
0.0098	c	0.81

^a $T = 25^\circ$. ^b Average of three values. ^c Enough NaOH added to bring pH to 13.

Table III: Dependence of the Overall Quantum Yield (ϕ_T) for the Photodecomposition of Peroxidiphosphate in Water upon pH in the Presence of Added Phosphate

pH ⁱ	$[P]_{T^i}$, M	$[PO_4^{3-}]_{T^i}$, M	ϕ_{T^a}
2.50	0.020	0.400	0.83
3.31	0.020	0.400	0.79
5.38	0.020	0.400	0.81
6.39	0.020	0.400	0.79
6.60	0.020	0.400	0.81
7.55	0.020	0.400	0.80
8.50	0.020	0.400	0.62
9.59	0.020	0.400	0.57
11.10	0.020	0.400	0.60

^a $T = 25^\circ$.

phosphate and acid in the $P_2O_8^{4-}$ photolysis. The results as shown in Table III indicate that there is no appreciable effect on ϕ_T for acidic or neutral solutions, but ϕ_T is depressed by added PO_4^{3-} in basic solution.

In order to compare more directly the results for the peroxidiphosphate photolyses with those for peroxodisulfate, we have photolyzed peroxodisulfate in the presence of added sulfate and also added phosphate. As shown in Table IV, addition of either SO_4^{2-} or PO_4^{3-}

Table IV: Dependence of the Overall Quantum Yield (ϕ_T) for the Photodecomposition of Peroxodisulfate in Water upon Added Sulfate or Phosphate^{a,b}

pH ⁱ	$[S]_{T^i}$, M	$[SO_4^{2-}]_{T^i}$, M	$[PO_4^{3-}]_{T^i}$, M	ϕ_{T^c}
11.80	0.020	0.400	0.0	0.40
7.00	0.020	0.400	0.0	0.59
2.51	0.020	0.400	0.0	0.17
10.59	0.020	0.0	0.400	0.43
8.31	0.020	0.0	0.400	0.42
5.98	0.020	0.0	0.400	0.52
2.62	0.020	0.0	0.400	0.50

^a $T = 25^\circ$. ^b $[S]_{T^i} = S_2O_8^{2-}$ total concentration, regardless of degree of protonation. ^c Relative quantum yield based on $\phi_T = 0.60$ assumed for photodecomposition of $S_2O_8^{2-}$ in pure water.

resulted in a decrease in the quantum yield in both acidic and basic solutions from the value of ϕ_T in neutral solutions in their absence.

The effect of added PO_4^{3-} on the value of ϕ_T in basic solutions prompted us to compare the extent of exchange between PO_4^{3-} and $P_2O_8^{4-}$ in photolyzed and nonphotolyzed solutions by adding ^{32}P -labeled PO_4^{3-} to $P_2O_8^{4-}$ at various pH values from 0.90 to 9.38. The data of Table V show the results of this experiment.

Table V: Exchange of P^{32} between Phosphate and Peroxidiphosphate under Dark and Photolytic Conditions^{a,b}

pH ⁱ	$[^{32}PO_4^{3-}]_{T^i}$, M	$[P]_{T^i}$, M	A [$P_2O_8^{4-}$] nonphoto- lyzed	A [$P_2O_8^{4-}$] photolyzed
9.38	1.0×10^{-3}	0.020	206	265
6.54	1.0×10^{-3}	0.020	230	206
2.65	1.0×10^{-3}	0.020	255	280
0.90	1.0×10^{-3}	0.020	218	317

^a $T = 25^\circ$. ^b Samples were photolyzed for 5 min before separation. Activity A is in counts $\text{min}^{-1} \text{ml}^{-1}$, and result from triplicate experiments corrected for background of 74 counts min^{-1} .

The average counts ($\text{min}^{-1} \text{ml}^{-1}$) for a photolyzed sample (sum of all pH values) is 267 while it is only 227 for the nonphotolyzed samples. For complete exchange of labeled phosphate the counting rate should be about 1000 counts min^{-1} . The average difference between photolyzed and nonphotolyzed samples was about 40 counts min^{-1} ; thus the apparent exchange under these conditions is about 4%. The exchange percentage is believed to be larger than our experimental error; however, it was not deemed sufficient to warrant further study.

When the photolytic reaction was carried out, the absorbance usually decreased exponentially and plots of $\log [P]_T$ vs. time irradiated were linear for two half-lives or more. With one sample of peroxidiphosphate, however, the absorbance often initially increased, followed by an exponential decrease. Typical absorbance vs. time irradiated curves for the normal case and for the experiments with the one preparation (all in deionized water and carbonate-free base) are shown in Figure 3.

This behavior suggested the presence of an intermediate formed from an impurity in the one batch of peroxidiphosphate. The initial absorbance was more obvious in basic solution than in neutral solution. No distinct maxima or minima in the spectra were observed, but the spectrum appeared to be an enhancement of the peroxide spectrum. The enhancement of absorption was found to be as much as three times that of the peroxide present, and the maximum effect obtained was in time intervals from 30 sec to 180 sec, being sample-dependent. In addition, for those samples in which this phenomenon was observed we noted that O_2 evolu-

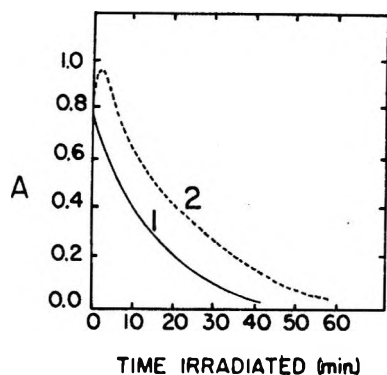


Figure 3. Plots of absorbance at 240 nm as a function of irradiation time for: (—) purified $P_2O_8^{4-}$ in water, and (---) $P_2O_8^{4-}$ containing a small amount of cupric ion in water.

tion continued for periods of an hour or more after termination of photolytic exposure, whereas oxygen evolution normally ceased shortly after cessation of photolysis. After a number of experiments,¹⁰ it was found that the behavior could be matched if a drop of 0.001 *M* copper(II) solution was added to the peroxodiphosphate solution to be photolyzed. It seems likely that the intermediate is a copper(III) and peroxodiphosphate complex. No further study of this complication was carried out.

Photolysis in Presence of Alcohols. The reactions between photoexcited peroxodiphosphate in water and 2-propanol and ethanol separately were studied in the pH range 2–13.5. The primary final products of the oxidations of 2-propanol and ethanol are expected and found to be acetone and acetaldehyde, respectively. They were identified by their characteristic ultraviolet absorptions at 268.0 and 278.0 nm, respectively. In all cases absorbances at long reaction times (t_∞) corresponded to concentrations of acetone or acetaldehyde above 90% of the initial peroxodiphosphate concentration. After each timed exposure to 235.7-nm radiation at 25°, the spectrum of the reaction solution was measured. As shown in Figures 4 and 5, for each reaction, spectra taken after consecutive exposures contained a good isosbestic point for roughly the first two half-lives. This point is 266 nm for ethanol, and for 2-propanol two points, at 257 and 295 nm, are observed. The second (295 nm) isosbestic point for the 2-propanol reaction was not observed unless carbonate was rigorously excluded from the solution. Since the carbonate absorption maximum is in the far-ultraviolet,¹¹ it seemed probable that the difficulty was due to an impurity rather than the carbonate itself.

In the course of the first 1.5 half-lives the formation of acetone (or acetaldehyde) was 98–100% of the loss of peroxodiphosphate, and at long times ($t \rightarrow \infty$) the product concentration corresponded to *ca.* 0.9 $[P]_T^1$. This behavior led us to photolyze the product acetone at 0.3 *M* under analogous pH and temperature conditions. The loss of acetone during 9×10^3 sec of photolysis was

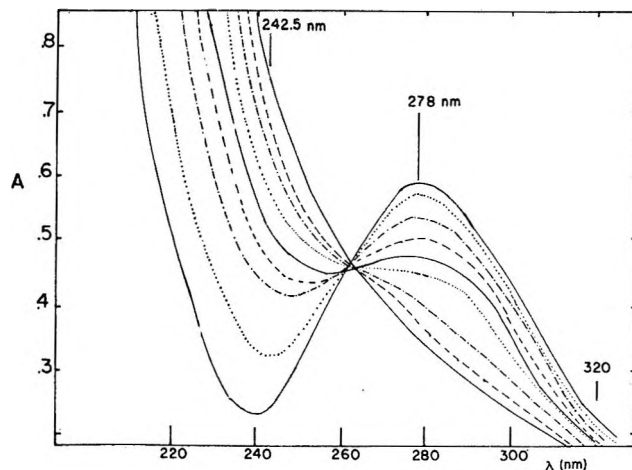


Figure 4. Spectra at various irradiation times for photolysis of $P_2O_8^{4-}$ and aqueous ethanol at pH 10.86.

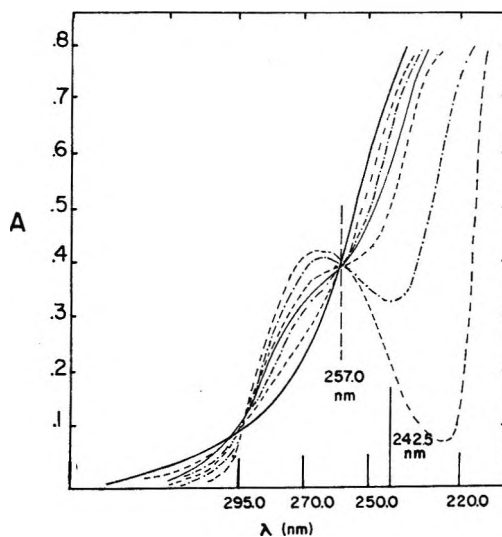


Figure 5. Spectra at various irradiation times for photolysis of $P_2O_8^{4-}$ and 2-propanol at pH 11.76.

15%. The alcohols alone do not appear to undergo any significant photolytic reaction under these experimental conditions.

The decomposition of peroxodiphosphate was first order in $[P]_T$, as observed in the absence of alcohol, with irradiation rates which give absorption rates of 3.8×10^{16} photons sec^{-1} in the reaction cell at the initial peroxodiphosphate concentration used. Plots of $\log [P]_T$ vs. irradiation time were linear, in the presence of either 2-propanol or ethanol, for two half-lives or longer. Dissolved oxygen was found to have an inhibiting effect which is pH dependent, but the nature of this inhibition, whether a chemical or solubility effect was not investigated; and oxygen was rigorously excluded in ex-

(10) Details are presented in R. J. Lussier, Ph.D. Thesis, Brown University, 1969.

(11) E. Hayon and J. J. McGarvey, *J. Phys. Chem.*, **71**, 1472 (1967).

periments leading to the results given in the tables of this paper.

The quantum yields for these reactions were found to be dependent upon both the initial pH and the alcohol concentrations, but in rather different ways. The quantum yield is independent of the alcohol concentration, in the case of each alcohol, if the alcohol concentration is above a limiting value which is different for the two alcohols; some of the data are given in Table VI.

Table VI: Dependence of the Quantum Yield for the Peroxidiphosphate Photolytic Oxidation of 2-Propanol and Ethanol upon Alcohol Concentration

Initial pH	Alcohol concn, M	ϕ_T^a
2-Propanol		
11.40	0.8716	1.7
11.40	0.6550	1.7
11.40	0.3258	1.7
12.10	0.1394	1.7
13.00	0.0697	1.7
11.75	0.0523	1.4
Ethanol		
11.50	0.6870	1.08
11.50	0.3430	1.11
11.50	0.1720	1.09
10.30	0.1374	1.07
10.10	0.0916	1.04
10.10	0.0687	0.86

^a $[P]^i = 0.02 M$; $T = 24^\circ$.

For the reaction with 0.020 M peroxidiphosphate at pH values in the 10–13 range, the limiting concentrations have been estimated to be 0.06 M for 2-propanol and 0.08 M for ethanol.

The pH dependence of the quantum yields, however, is rather striking in view of the results in the absence of alcohols. The quantum yields in the range 9.5–13.0 were found to be constant; under these conditions, ϕ_T is 1.7 ± 0.1 for the 2-propanol photolysis and 1.05 ± 0.08 for that of ethanol. As the pH is lowered below 9.3 the quantum yield increases until about pH 4, where a maximum quantum yield is reached. For 2-propanol the maximum quantum yield is about 43, while for ethanol it is about 27; data are presented in Table VII. Note that the ratio of the quantum yields for the two alcohols in acid (pH 4) is about the same as the ratio of the quantum yields for the two alcohols in basic solution; this ratio is about 1.6. The overall pH dependence of the quantum yield is given in Figure 2 for both alcohols. The curves for the alcohol reactions in Figure 2 have about the same shape, with the increase and leveling off of the quantum yield occurring at about the same pH for both alcohols; thus the principal difference is in the values of the quantum yields.

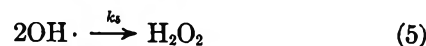
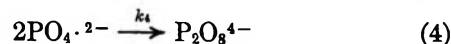
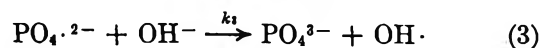
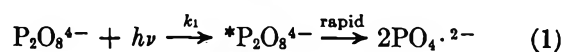
Table VII: pH Dependences of the Quantum Yield for the Peroxidiphosphate Photolytic Oxidations of 2-Propanol and of Ethanol

2-Propanol		Ethanol	
pH ⁱ	ϕ_T^a	pH ⁱ	ϕ_T^b
13.45	1.7	13.60	1.10
13.00	1.7	13.11	1.09
12.75	1.7	12.55	1.09
11.41	1.7	11.89	1.06
10.85	1.7	11.28	1.01
10.41	1.7	10.10	1.04
9.60	1.7	9.49	1.09
9.50	1.7	8.51	2.2
7.85	5.2	7.50	4.7
6.10	8.8	6.45	5.3
4.40	30.8	5.01	15.9
4.11	35.4	5.20	11.1
3.70	39.4	4.52	26.3
2.50	36.4	3.80	26.3
2.41	42.4	3.11	27.9
2.00	32.2	2.71	25.9
		2.00	28.0

^a $[P]_T^i = 0.020 M$; [2-propanol] = 0.0697 M; $T = 25^\circ$.
^b $[P]_T^i = 0.020 M$; [ethanol] = 0.0916 M; $T = 25^\circ$.

Discussion

Mechanism for Photolysis in Water. The experimental results have shown that the reaction is first order in $[P]_T$, with respect to photolytic exposure; that reactions involving H^+ (aqueous) or OH^- (aqueous) do not influence the quantum yield; that a small amount of phosphorus exchange occurs between $P_2O_8^{4-}$ and PO_4^{3-} ; and that essentially all of the oxygen derives from the solvent water. Furthermore, the value of ϕ_T is on the order of one. We propose the following mechanism, consistent with the results, for the aqueous photolysis (with the asterisk denoting a molecule in an excited state).



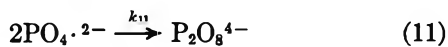
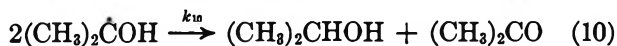
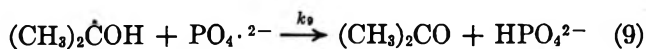
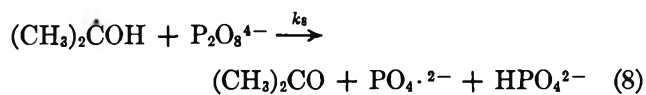
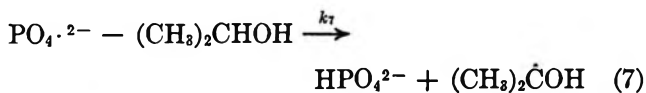
One of the differences between this mechanism and the one proposed for the peroxodisulfate decomposition is the omission of a reaction between H_2O_2 and $P_2O_8^{4-}$. This reaction may occur but our data do not demand it. The present mechanism also differs in the second and third steps. The reaction between phosphate radical and water apparently does not reach equilibrium, since inhibition by phosphate plus acid does not occur.

It is proposed that reactions 2, 3, and 4 account for the loss of PO_4^{2-} . These three steps are competing reactions with step 3 only becoming important in basic solution. The reverse of reaction 3 is postulated as being the reason for the inhibition by phosphate ion in basic solution and the small amount of phosphorus exchange. Apparently, this type of electron exchange becomes less important as the degree of protonation of phosphate increases.

The primary source of the oxygen is postulated to be the decomposition of hydrogen peroxide. Reaction 6 only indicates the overall stoichiometry and does not imply a simple decomposition of hydrogen peroxide. Hydrogen peroxide (and peroxomonophosphate, if formed) must be decomposed rapidly since they could not be detected.

Photolysis in Presence of Alcohols. From the experimental data it appears that there are several mechanistic paths operating, with the acidity of the solution (and therefore the degree of protonation of peroxodiphosphate) influencing the nature of the reaction. From the known photochemical behavior of peroxides,^{4,5} the inhibition by dissolved oxygen,¹² the general reactions of radicals,¹³ and the experimental data, the following mechanisms are proposed.

Basic Solution. In basic solution ($\text{pH} \simeq 9$) the quantum yields in the presence of 2-propanol and ethanol were 1.7 and 1.05, respectively. Since both values are greater than the quantum yield of 0.80 observed for the photolytic decomposition of peroxodiphosphate in aqueous solution, then a multistep process is probably involved and attack of an organic radical intermediate on the peroxodiphosphate must occur. The proposed mechanism is step 1 above plus the following.



The two propagation steps (eq 7 and 8) are reasonable in view of the observations on reactions of several alcohols with peroxides (ref 2, 4, 5d, 12-14). All three termination steps (eq 9 through 11) are consistent with the kinetics and the stoichiometry, but the step



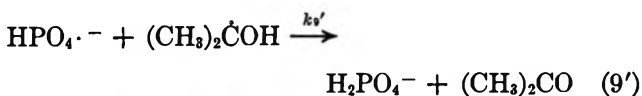
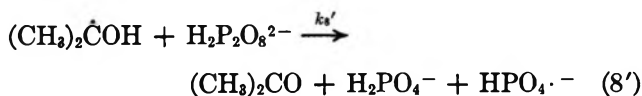
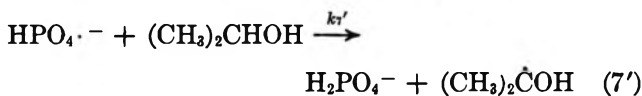
is excluded by the stoichiometry. The same type of mechanism can be invoked for the ethanol oxidation.

The increase of quantum yield in the presence of alcohol is accounted for by the k_8 step wherein the organic

radical attacks peroxodiphosphate ion. Nevertheless the chain length is still short, which is similar to the results obtained for photolysis of hydrogen peroxide in the presence of alcohol.¹⁴ In that study, the data for 2-propanol and ethanol were found to be consistent with a termination step such as eq 10.

An obvious step that might have been included (but was not) in the alcohol oxidations (since it was used in the proposed mechanism for water oxidation) is eq 2. Steps such as eq 7 are known to be very rapid in the reactions of sulfate radical-ion with alcohols.^{5d} Also, the step of eq 2 would be nearly athermal whereas steps such as eq 7 should be exothermic by about 20 kcal mol⁻¹; ¹⁰ therefore, we expect that $k_7 \gg k_2$.

Acid Solution. In acid solution, a longer chain obtains as indicated by the increase in quantum yield for alcohol oxidation; no comparable increase in the water oxidation was observed. The quantum yield in the presence of alcohol began to increase about pH 9, and then kept increasing until about pH 4. The quantum yield appeared to undergo no further increase below pH 4. The first protonation of $\text{P}_2\text{O}_8^{4-}$ begins to occur at about pH 9, and at pH 4 the concentration of $\text{H}_2\text{P}_2\text{O}_8^{2-}$ reaches its maximum.^{1a,b} The proposed mechanism in acid and neutral solution is similar to the mechanism proposed in basic solution, and it is given below.

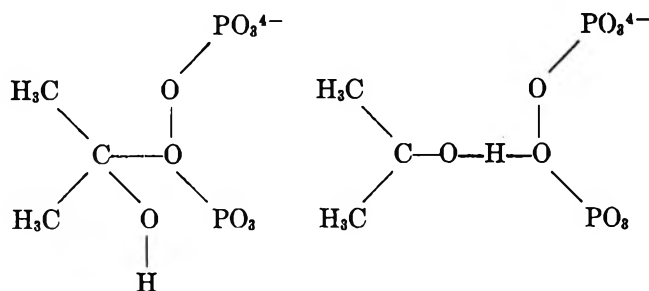


It is to be noted here that the exact nature of the steps is uncertain. A detailed study might, for example, distinguish between the various termination steps. Also, such a study might clarify the reason that pH (or its kinetic equivalent, protonation of peroxodiphosphate) causes a marked change in quantum yield. The attack of the organic radical presents another problem, *i.e.*, the correct choice between the alternative transition states

(12) (a) D. L. Ball, M. M. Crutchfield, and J. O. Edwards, *J. Org. Chem.*, **25**, 1599 (1960); (b) J. O. Edwards, A. R. Gallopo, and J. E. McIsaac, Jr., *J. Amer. Chem. Soc.*, **88**, 3891 (1966); (c) J. E. McIsaac, Jr., and J. O. Edwards, *J. Org. Chem.*, **34**, 2565 (1969); (d) A. R. Gallopo, Ph.D. Thesis at Brown University (1967); (e) L. R. Subbaraman and M. Santappa, *Proc. Indian Acad. Sci.*, **64**, 345 (1966).

(13) (a) E. S. Huyser and D. C. Neckers, *J. Amer. Chem. Soc.*, **85**, 3641 (1963); (b) E. S. Huyser and C. J. Bredeweg, *ibid.*, **86**, 2401 (1964).

(14) J. Barrett, A. L. Mansell, and R. J. M. Ratcliffe, *Chem. Commun.*, 48 (1968).



might be made on the basis of an appropriate study, such as that carried out by Huyser and coworkers¹³ on the induced decomposition of dialkyl peroxides in various media.

We have postulated the existence of the phosphate radical-ions PO_4^{2-} and HPO_4^- on the basis of the chemistry of our reactions and also on the basis of the analogous chemistries of hydrogen peroxide and peroxodisulfate. There is, moreover, independent evidence for the phosphate radical-ions in the peroxodiphosphate oxidation of vanadyl ion,¹⁴ in flash photolysis of phosphates,¹⁵ and in the polymerization of vinyl monomers by peroxodiphosphate alone or in the presence of iron(II) complexes.¹⁶

Other Points. Our data are sufficient to clarify the general behavior of the peroxodiphosphate photolyses.

There are, however, some unresolved points which should be the subjects of further investigation such as (1) the nature of the termination steps, particularly in the acid range for alcohol oxidation, (2) the nature of the copper-containing intermediate, (3) the low quantum yields for alcohol oxidation (compared with the chain length 2000 for 2-propanol oxidation by peroxodisulfate), (4) the specific sites of radical attack in the propagation, and (5) the difference in quantum yield between the alcohol oxidations in basic and acidic solution.

After completion of our manuscript, it came to our attention that Wilmarth and his coworkers also investigated the photochemistry of the peroxodiphosphates. The results of the two investigations, where they overlap, were similar.¹⁷

Acknowledgments. We are grateful to FMC Corp. and AF Office of Scientific Research (Grant No. 1027-66) for financial support, to Charles Morse for technical assistance, and to Professor W. K. Wilmarth for helpful comments. R. J. L. is grateful to the National Science Foundation for a traineeship.

(15) J. R. Huber and E. Hayon, *J. Phys. Chem.*, **72**, 3820 (1968).

(16) E. Chaffee, unpublished results at Brown University.

(17) W. K. Wilmarth, private communication.

The Photochemistry of Pentafluorobenzene in the Vapor Phase

by Kh. Al-Ani and David Phillips*

Department of Chemistry, The University, Southampton, SO9 5NH, England (Received May 21, 1970)

Photophysical processes occurring when pentafluorobenzene vapor is excited at 2700, 2650, 2540, and 2480 Å have been investigated. The quantum yield of fluorescence is very small, being $\Phi_{2700} = 0.04$, $\Phi_{2650} = 0.017$, $\Phi_{2540} = 0.015$, $\Phi_{2480} = 0.016$, and increases at the shortest wavelengths with increase in inert gas pressure. Use of the biacetyl sensitization and *cis*-but-2-ene techniques indicate that a short-lived triplet state of pentafluorobenzene is also formed under these conditions. Some results on pentafluoropyridine are also briefly reported.

Introduction

The photochemistry of several fluorinated aromatic molecules has aroused interest of late. This class of compounds is an interesting series in that all of its members are volatile liquids, enabling a complete study of the effect of substitution upon radiative and nonradiative processes to be carried out in the gas phase. Early work on monofluorobenzene¹ indicated that the fluorescence yield was similar to that of benzene when excited at 2540 Å, and the average yield of sensi-

tized phosphorescence from biacetyl at this wavelength was given as 0.136. This indicated a triplet state yield of 0.88. However, use of spectrofluorometric techniques to repeat this work indicated that the sensitized phosphorescence yield was much smaller, giving an apparent triplet state yield of 0.3.² This latter result

* To whom correspondence should be addressed.

(1) I. Unger, *J. Phys. Chem.*, **69**, 4284 (1965).

(2) M. E. MacBeath, G. P. Semeluk, and I. Unger, *ibid.*, **73**, 995 (1969).

has been verified,³ and the low value has been shown to be caused by singlet quenching of the fluorobenzene by the biacetyl, coupled with difficulties due to the geometry of the optical system in measuring emission yields. These difficulties can be avoided by using the sensitization of the cis-trans isomerization of but-2-ene as a quantitative measure of aromatic triplet state formation, and a value of the triplet state yield at several wavelengths was obtained for fluorobenzene using this compound.⁴ This result has also been checked³ and found to be correct within 10%. Moreover, the apparent singlet self-quenching observed in emission measurements has been shown to be absent by use of the but-2-ene technique.³

Spectrofluorometric techniques have also been used to estimate the fluorescence and triplet state yields of the difluorobenzenes,^{5,6} 1,2,4- and 1,3,5-trifluorobenzenes,⁷ and recently the tetrafluorobenzenes.⁸ Measurements of quantum yields of fluorescence and mean radiative lifetimes were found to be consistent with values expected from a consideration of the symmetry properties of the nominal excited and ground states of the molecules. It was noticed that upon progressive fluorination the fluorescence yields of substituted benzenes gradually reduced in value, that of hexafluorobenzene being very small,⁹ in agreement with values for other perfluoroaromatics.¹⁰ Moreover, as the number of fluorine atoms in the aromatic ring increased, the apparent lifetime of the triplet state was reduced such that difficulty was experienced in obtaining an estimate of the triplet state yield by chemical quenching techniques.

It seemed of interest to study the photochemistry of pentafluorobenzene in order to allow data on the complete series of fluorinated benzenes to be compared. We report here the results of experiments carried out to measure the fluorescence yields and triplet state yields of pentafluorobenzene in the gas phase at 25° at several exciting wavelengths. A preliminary report of this work has been given.¹¹

Experimental Section

The apparatus was similar to that used in the past,^{4,9} and consisted of a conventional high-vacuum system for gas handling, an optical system for selection of exciting wavelengths and detection of absorption and emission of radiation, and a chromatographic setup for analysis of starting materials and products.

The gas handling system was evacuated down to better than 10^{-4} Torr using an Edwards ISC 30A rotary pump with a glass mercury diffusion pump. Springham greaseless stopcocks were used throughout. The reaction vessel was a 60 mm long cylindrical quartz cell of 30-mm diameter, with a centrally placed 20-mm circular side T-window and a cold finger underneath. The vessel was attached to the vacuum system *via* a Pyrex-quartz graded seal and a Springham 4-mm stopcock.

Light from a Hanovia S-100 medium pressure mercury lamp was focused on to the entrance slit of a Hilger and Watts D 330 grating monochromator fitted with a Bausch and Lomb grating blazed at 300 nm and giving a reciprocal dispersion of 25 nm/mm. Light at the selected wavelengths was then focused into a narrow parallel beam which passed through the reaction vessel and was monitored on an RCA 935 phototube. Light emitted at right angles to the exciting beam was sensed by an RCA 1P28 photomultiplier tube. Photocurrents were displayed on a Victoreen 1001 electrometer, and the power supply for the photomultiplier tube was an A.E.I. Type R1184. Corning filters CS 3-71 and CS-54 were interposed between the 1P28 tube and the reaction vessel to isolate the required regions of the spectrum and cut down scattered incident radiation.

Chromatographic analysis was performed on a Pye series 104 chromatograph using flame ionization detection. Separation of the cis and trans isomers of but-2-ene was achieved using a 3.5-m column of 3.5-mm internal diameter packed with saturated silver nitrate in ethylene glycol adsorbed on 60-80 mesh Celite. Analyses of the purity of the starting material were carried out on a 3.5-m Carbowax 20 M column.

Emission quantum yields were measured relative to benzene as a standard. The quantum yield of benzene fluorescence at 2540 Å was taken as 0.18.¹² Triplet state yields for pentafluorobenzene at various wavelengths were also measured relative to that for benzene at 2540 Å of 0.7.¹³

Absorption spectra of pentafluorobenzene were taken on a Unicam SP 800 spectrophotometer, and emission spectra on a Farrand Mk 1 spectrofluorometer.

Materials. Pentafluorobenzene was obtained from Ralph N. Emanuel Ltd. It was shown by vapor phase chromatography to contain 0.4% impurity. Distillation *in vacuo* reduced this, and the material was used without further purification.

Benzene was obtained as chromatography quality from Matheson Coleman and Bell. It contained no impurities detectable by chromatographic techniques.

(3) Kh. Al-Ani and D. Phillips, to be submitted for publication to *J. Phys. Chem.*

(4) D. Phillips, *ibid.*, **71**, 1839 (1967).

(5) F. W. Ayer, F. Greiss, G. P. Semeluk, and I. Unger, *Ber. Bunsenges. Phys. Chem.*, **72**, 282 (1968).

(6) J. L. Durham, G. P. Semeluk, and I. Unger, *Can. J. Chem.*, **46**, 3177 (1968).

(7) G. P. Semeluk, R. D. S. Stevens, and I. Unger, *ibid.*, **47**, 597 (1969).

(8) I. Unger, private communication.

(9) D. Phillips, *J. Chem. Phys.*, **46**, 4679 (1967).

(10) H. M. Rosenberg and S. D. Carson, *J. Phys. Chem.*, **72**, 3531 (1968).

(11) D. Phillips, Kh. Al-Ani, and D. Gray, Proceedings of 5th International Conference on Photochemistry, New York, Sept 1969.

(12) W. A. Noyes, Jr., W. A. Mulac, and D. A. Harter, *J. Chem. Phys.*, **44**, 2100 (1966).

(13) W. A. Noyes, Jr., and D. A. Harter, *ibid.*, **46**, 674 (1967).

cis-But-2-ene was obtained from Cambrian Chemicals Ltd. It contained 0.07% *trans-but-2-ene* as an impurity and was used without attempts at further purification.

Biacetyl was obtained from British Drug Houses Ltd. It was found to be pure and was stored in a blackened bulb at room temperature.

Oxygen was prepared on the vacuum line by heating Analar grade potassium permanganate.

Cyclohexane was spectroquality obtained from British Drug Houses Ltd. It was found to contain 0.2% impurity.

Sulfur Hexafluoride. A cylinder of this gas was obtained from Matheson Ltd. It was shown to be approximately 99% pure and was used without further purification.

Results and Discussion

Fluorescence of Pentafluorobenzene. Figure 1 shows the absorption and fluorescence spectra of pentafluorobenzene compared with those of monofluorobenzene and hexafluorobenzene. It can be seen from Figure 1 that

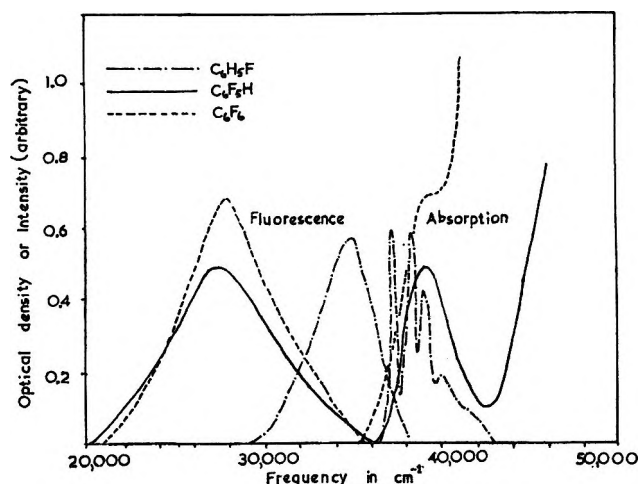


Figure 1. Absorption and fluorescence spectra of some fluorinated benzenes. Path length = 1 cm; C_6H_5F concn = 0.9×10^{-3} mol l.⁻¹; C_6F_5H concn = 3×10^{-3} mol l.⁻¹.

in pentafluorobenzene, as in hexafluorobenzene, there is no evidence of the vibrational structure readily seen in fluorobenzene in absorption. It can also be seen that although the position of the first absorption band in all three compounds is similar, the onset of the second band shifts to longer wavelengths upon progressive fluorination, such that in hexafluorobenzene absorption at wavelengths in the region of 250 nm must produce two excited states, as noted previously.⁹ However, this complication is absent in pentafluorobenzene and integration of the area under the absorption curve for the first band allows an estimate of the mean radiative lifetime of the first excited singlet state of 1.35×10^{-7} sec. Pentafluorobenzene and fluorobenzene both be-

long to the C_{2v} point group for which the radiative transition from the 1B_1 excited state to the 1A_1 ground state is orbitally allowed. The radiative lifetime for pentafluorobenzene obtained above is close to that obtained for fluorobenzene¹ and for other fluorinated benzenes belonging to the same point group.^{5,6,14}

The fluorescence spectrum of pentafluorobenzene excited in the first singlet band is seen to be a broad structureless band extending to much longer wavelengths than that of fluorobenzene. It closely resembles the emission spectrum of hexafluorobenzene in this respect. On a frequency scale, the fluorescence spectrum is a reasonable mirror image of the absorption spectrum and the position of the 0-0 transition can be estimated to be at about 275 nm.

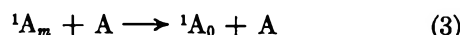
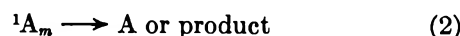
The fluorescence emitted by pentafluorobenzene is very weak compared with that of benzene or fluorobenzene. There can be difficulties in interpretation of results on fluorescence quantum yields in aromatic molecules which have a very structured absorption spectrum, but since pentafluorobenzene shows only a broad structureless absorption band, it is permissible to apply corrections to crude values of apparent quantum yields of fluorescence to account for the geometry of the viewing system. When these are performed, the values for the fluorescence yields of pentafluorobenzene excited at four different wavelengths showed little detectable variation with pressure over the limited pressure range available (1-25 Torr). The mean values of the fluorescence yields are shown in Table I.

Table I: Quantum Yields of Fluorescence of Pentafluorobenzene, Φ_F in the Pressure Range 0-25 Torr, 25°

Wavelength, nm	Φ
272.0 ± 2.5	0.041 ± 0.004
265.0 ± 2.5	0.017 ± 0.002
254.0 ± 2.5	0.015 ± 0.002
248.0 ± 2.5	0.016 ± 0.002

At all wavelengths studied, addition of various inert gases caused the fluorescence quantum yields of pentafluorobenzene to increase slightly. The equations of the best straight lines for the various added gases are shown in Table II. Oxygen differed in that it apparently quenched the fluorescence slightly.

These results may be explained by the following simple reaction mechanism.

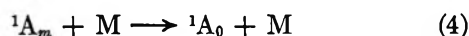


(14) D. Phillips (unpublished results).

Table II: Effect of Added Gases upon Φ_F for Pentafluorobenzene^a

Wave-length, nm	Added gas	Equation of line	Pressure, range, Torr
272 ± 2.5	Cyclohexane	$\Phi_F = 0.041 + 3.49 [M]$	0-50
272 ± 2.5	SF ₆	$\Phi_F = 0.041 + 2.28 [M]$	0-140
262 ± 2.5	Cyclohexane	$\Phi_F = 0.018 + 1.04 [M]$	0-50
265 ± 2.5	SF ₆	$\Phi_F = 0.018 + 0.37 [M]$	0-140
265 ± 2.5	cis-But-2-ene	$\Phi_F = 0.018 + 0.37 [M]$	0-140
265 ± 2.5	O ₂	$\Phi_F = 0.018 + 0.49 [M]$	0-100
254 ± 2.5	Cyclohexane	$\Phi_F = 0.015 + 0.73 [M]$	0-50
254 ± 2.5	SF ₆	$\Phi_F = 0.015 + 0.11 [M]$	0-140
254 ± 2.5	cis-But-2-ene	$\Phi_F = 0.015 + 0.19 [M]$	0-140
254 ± 2.5	O ₂	$\Phi_F = 0.015 - 0.15 [M]$	0-100
248 ± 2.5	Cyclohexane	No discernable trend	0-50
248 ± 2.5	SF ₆	$\Phi_F = 0.019 + 0.08 [M]$	0-140
248 ± 2.5	cis-But-2-ene	$\Phi_F = 0.019 + 0.12 [M]$	0-140
248 ± 2.5	O ₂	$\Phi_F = 0.019 - 0.25 [M]$	0-100

^a Pressure of pentafluorobenzene = 5 Torr throughout. $[M]$ = concentration of added gas in mol/l.⁻¹. It has been assumed that the quantum yield of fluorescence of pentafluorobenzene at a pressure of 5 Torr is the same as the value extrapolated to zero pressure. If any real self-quenching is subsequently shown to occur, the value of Φ_F at zero pressure of inert gas shown in this table must be adjusted accordingly.



where A = aromatic, superscripts refer to multiplicity, subscripts to vibrational energy content, and M = added gas.

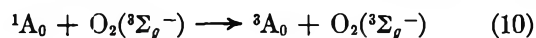
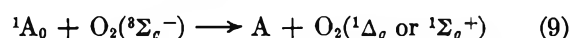
Application of the steady state approximation to this scheme yields the equation for the fluorescence yield at various wavelengths of

$$\Phi_F = \frac{(k_3[A] + k_4[M])}{(k_3[A] + k_4[M] + k_2)} \frac{k_6}{(k_5 + k_6 + k_7)} \quad (8)$$

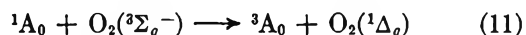
Provided that $k_2 \gg k_3[A] \gg k_4[M]$, this equation can explain the linear dependence of Φ_F upon pressure of inert gas observed at most wavelengths. It should be noted that at the different wavelengths, excited singlet aromatic molecules are prepared with differing amounts of vibrational energy; thus the various values of k_4 will be different at each wavelength, e.g., at 248 nm $k_4[M]$ appears to be vanishingly small. The results imply that the major route for vibrational relaxation is via collision with ground state aromatic molecules; this conclusion has been reached in other studies. It can be noted that as the vibrational energy content of the initially excited state increases, process 4 competes less effectively with process 2. Process 2 has been written as either an internal conversion to the ground state, or as formation of a chemical product, possibly an isomer.

The "Dewar" isomers of pentafluorobenzene have been observed in the photolysis of pentafluorobenzene,¹⁵ although quantum yields have not been determined. In the hexafluorobenzene system, which behaves similarly,^{16,17} the Dewar isomers correlate with the excited triplet state however;¹⁸ thus the "Dewar" isomers observed in the present system may also arise from the triplet state rather than the singlet. This point requires clarification by construction of correlation diagrams for aromatics belonging to the C_{2v} group and will be carried out in a later communication. It suffices to say that isomerizations are likely to arise if the aromatic distorts greatly upon absorption. Inspection of the positions of the absorption and emission maxima in the spectra of both pentafluorobenzene and hexafluorobenzene indicates that there are considerable differences in the geometry of the ground- and excited singlet states of both molecules. It appears not unreasonable therefore to write process 2 as an isomerization and it is hoped to test this hypothesis in subsequent experiments. Reaction 5 has been included because even at wavelengths close to the 0-0 band, fluorescence and triplet state yields are small.

The observed quenching of the fluorescence of pentafluorobenzene by oxygen may be explained by the following two additional steps.



The additional alternative processes



have been ruled out in the benzene system,¹⁹ and may thus also be unimportant here. The quenching effect should lead to an exponential drop in pentafluorobenzene fluorescence with increase in oxygen pressure. However, the effect is small, and the experimental values can be represented by a linear drop.

Triplet State of Pentafluorobenzene. The relative merits of the two techniques available for estimation of triplet state yields of aromatic molecules in the gas phase, those of the sensitized phosphorescence of biacetyl²⁰ and the cis-trans isomerization of but-2-ene,^{21,22}

(15) E. Ratajczak, P. Cadman, and A. F. Trotman-Dickenson, submitted for publication in *J. Chem. Soc. A*; E. Ratajczak, *Rocz. Chem.*, **44**, 447 (1970).

(16) I. Haller, *J. Chem. Phys.*, **47**, 1117 (1967).

(17) A. Bergorni and F. Gozzo, *Chim. Ind.*, **50**, 745 (1968).

(18) D. Bryce-Smith and H. C. Longuet-Higgins, *Chem. Commun.*, 593 (1966).

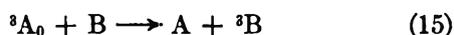
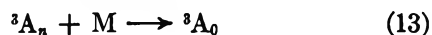
(19) D. R. Snelling, *Chem. Phys. Lett.*, **2**, 346 (1968).

(20) H. Ishikawa and W. A. Noyes, Jr., *J. Chem. Phys.*, **37**, 583 (1962).

(21) R. B. Cundall and T. F. Palmer, *Trans. Faraday Soc.*, **56**, 1211 (1960).

(22) R. B. Cundall and A. S. Davies, *Progr. React. Kinet.*, **4**, 149 (1967).

have been discussed many times. In brief the mechanisms of the methods are shown below.



where B = biacetyl.

In the present system, this leads to an expression for the sensitized phosphorescence yield (Φ_S) of

$$\Phi_S = \frac{(k_3[A] + k_4[M])}{(k_2 + k_3[A] + k_4[M])} \cdot \frac{k_7}{(k_5 + k_6 + k_7)} \cdot \frac{k_{15}[B]}{(k_{14} + k_{15}[B])} \cdot \frac{k_{16}}{(k_{16} + k_{17})} \quad (18)$$

The triplet state yield, Φ_T , is given by

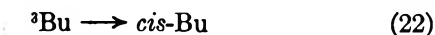
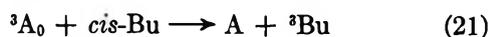
$$\Phi_T = \frac{(k_3[A] + k_4[M])}{(k_2 + k_3[A] + k_4[M])} \cdot \frac{k_7}{(k_5 + k_6 + k_7)} \quad (19)$$

Thus

$$\Phi_S = \Phi_T \cdot \frac{k_{15}[B]}{(k_{14} + k_{15}[B])} \cdot \frac{k_{16}}{(k_{16} + k_{17})} \quad (20)$$

$k_{16}/(k_{16} + k_{17})$ is known, and provided a sufficiently high pressure of biacetyl is used in the system such that $k_{15}[B] \gg k_{14}$, measurement of Φ_S can yield the triplet state yield of the aromatic.

With *cis-but-2-ene*



where Bu = but-2-ene.

The quantum yield of formation of the *trans* isomer $\Phi_{c \rightarrow t}$ is given by

$$\Phi_{c \rightarrow t} = \frac{(k_3[A] + k_4[M])}{(k_2 + k_3[A] + k_4[M])} \cdot \frac{k_7}{(k_5 + k_6 + k_7)} \cdot \frac{k_{21}[\textit{cis-Bu}]}{(k_{14} + k_{21}[\textit{cis-Bu}])} \cdot \frac{k_{23}}{(k_{22} + k_{23})} \quad (24)$$

Thus

$$\Phi_T = \Phi_{c \rightarrow t} \cdot \frac{k_{21}[\textit{cis-Bu}]}{(k_{14} + k_{21}[\textit{cis-Bu}])} \cdot \frac{k_{21}}{(k_{22} + k_{23})} \quad (25)$$

Again, knowing $k_{23}/k_{22} + k_{23}$, and provided $k_{21}[\textit{cis-Bu}] \gg k_{14}$, the triplet state of the aromatic may be measured. For many aromatics it is possible to arrange that a sufficient pressure of the triplet quenching gas is present in the system such that none of the aromatic triplets decay *via* reaction 14. However, for hexafluorobenzene it was found that this process is so rapid

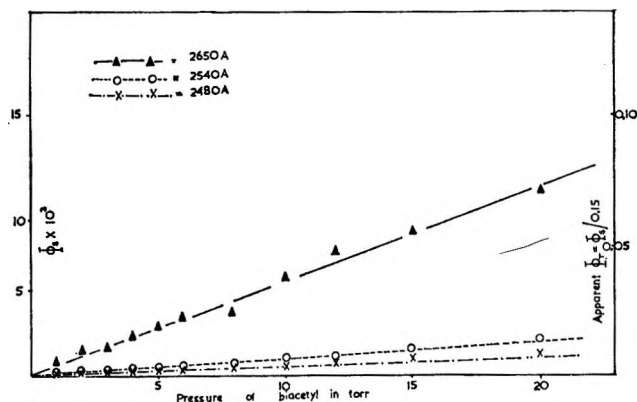


Figure 2. Quantum yield of sensitized phosphorescence from biacetyl (Φ_s) against biacetyl pressure. Pressure of pentafluorobenzene = 5 Torr.

that saturated vapor pressure of biacetyl is unable to compete and totally quench out the triplet state.⁹ Similar results have been obtained with pentafluorobenzene, as shown in Figure 2. Even at high pressures of added biacetyl a radiationless decay process of the pentafluorobenzene triplet dominates, and it is thus impossible to determine the triplet state yield. Similar results have been obtained for 1,3,5-trifluorobenzene.⁷

The use of *cis-but-2-ene* leads to a similar situation, as seen in Figure 3. Addition of even 130 Torr of *cis-but-2-ene* does not produce a leveling off in the sensitized yield of *trans* isomer, indicating that reaction 14 still dominates over reaction 21 at this pressure. Because the experiments do not lead to a value for the triplet state yield of pentafluorobenzene, a value for $k_{23}/k_{22} + k_{23}$, the so-called branching ratio, has not been determined in the present system. Instead the value for benzene of 0.5 has been accepted. Moreover, complications due to the interaction of the quenching gas,

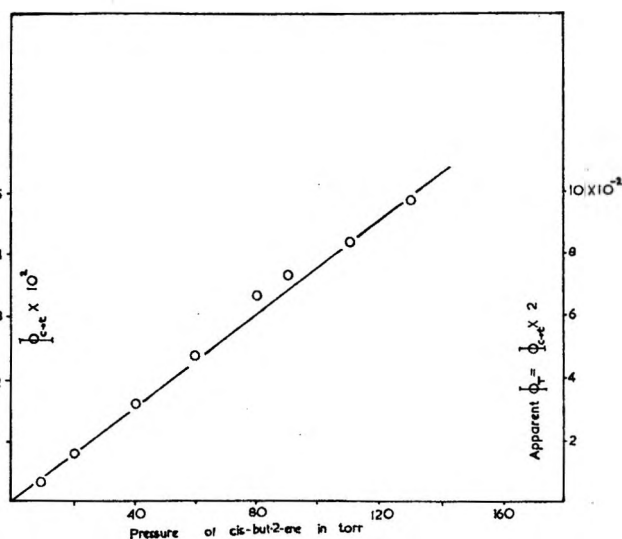
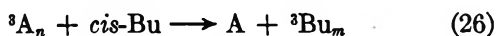


Figure 3. Quantum yield of sensitized *cis-trans* isomerization of but-2-ene ($\Phi_{c \rightarrow t}$) against *cis-but-2-ene* pressure. λ 2650 Å, pentafluorobenzene pressure = 5 Torr.

either biacetyl or *cis*-but-2-ene, with the singlet state of the aromatic have been ignored, since these effects have been shown to be small (cf. Table 2).

The fact that the pentafluorobenzene triplet state appears to sensitize the *cis*-*trans* isomerization of but-2-ene deserves comment, since it implies that the electronic energy level of the aromatic triplet must lie above that of the olefin. However, simple Hückel orbital calculations⁵ show that the triplet level of the fluorine-substituted benzenes should decrease upon progressive fluorination, and competitive quenching experiments show that the triplet energies of 1,2,4-trifluorobenzene⁷ and all of the tetrafluorobenzenes⁸ are lower than that of the butene. Nevertheless, hexafluorobenzene has been shown to sensitize the *cis*-*trans* isomerization of but-2-ene,^{9,16} although this has been attributed to an impurity in the aromatic.²³ Since hexafluorobenzene phosphoresces weakly in EPA glass,⁹ an estimate of the energy level of its lowest triplet, at least under these conditions, is possible. The onset of the phosphorescence is at around 3.50 nm, corresponding to an energy of around 3.5 eV, which is higher than that of the olefin, at 3.12 eV. Unfortunately, in the case of the pentafluorobenzene no phosphorescence was detectable in EPA glass at 77°K, thus no check can be made on the triplet energy level. Localized orbital calculations of the type developed by Murrell²⁴ indicate that the triplet level of pentafluorobenzene should lie lower than those of hexafluorobenzene and 1,2,3,4- and 1,2,3,5-tetrafluorobenzene and the compound may thus have an energy level lower than or at least close to that of the olefin.¹⁴ If this is the case, an alternative explanation for the observed sensitized *cis*-*trans* isomerization of the but-2-ene must be sought. A possible alternative is energy transfer from the triplet state of the aromatic initially formed by intersystem crossing from the singlet state (26). This triplet is vibrationally excited, and could lead to fragmentation of the olefin to form free radicals (27), which will then induce a chain *cis*-*trans* isomerization in the olefin.



Results similar to those have been obtained in other systems such as fluorobenzene³ and trifluoromethyl substituted benzenes,¹⁴ in which it can be shown that the quantum yield of *cis*-*trans* isomerization of the but-2-ene is independent of aromatic over a pressure range from 20 to 2 Torr, but below 2 Torr there is a dramatic increase in the rate of isomerization which can only be due to a chain mechanism. These results

imply that vibrational relaxation of the aromatic triplet is achieved principally by collision with ground-state aromatic molecules. In the present system it is obvious that the lifetime of the pentafluorobenzene triplet is very short; thus a chain mechanism might be expected to persist at higher aromatic pressures than in the fluorobenzene case. It is thus not unreasonable to expect such effects at the pressure of 5 Torr of aromatic used here. However, if a chain mechanism is operative, the rate at which quenching of the aromatic triplets by the olefin is achieved should be less than the observed rate of *cis*-*trans* isomerization of the olefin. This can be tested by competitive quenching experiments in which a mixture of pentafluorobenzene and biacetyl are mixed with an increasing pressure of *cis*-but-2-ene. It has been shown that the olefin does not in any way interact with the triplet biacetyl;¹ therefore any quenching of the sensitized phosphorescence of the biacetyl observed must be due to an interaction of the olefin with the aromatic triplet state. Figure 4 shows the results of such experiments. Slight quenching is observed, but the extent of this quenching is not as large as the corresponding observed rate of *cis*-*trans* isomerization of the olefin. These observations are in accord with the chain mechanism proposed above.

With the long irradiation times used here and the low yields of *trans*-isomer formed, there exists the possibility that the observed *cis*-*trans* isomerization occurs as a dark reaction, as has been noted in some

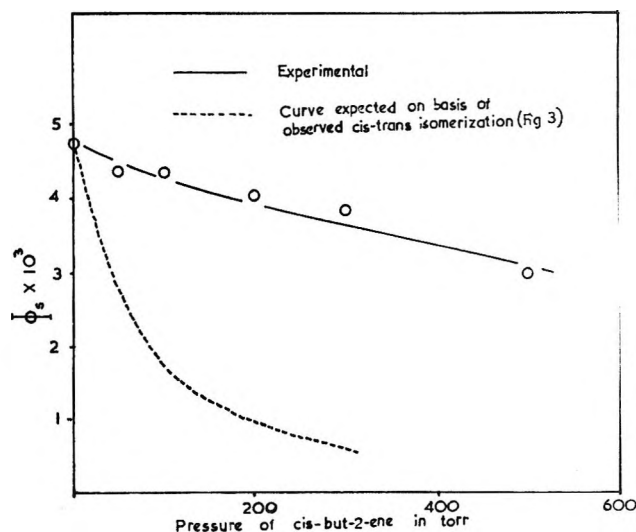


Figure 4. Quenching of sensitized phosphorescence of biacetyl by addition of *cis*-but-2-ene; 2 Torr of pentafluorobenzene, 10 of Torr biacetyl, λ 2650 Å. Dotted curve is result expected if *trans*-but-2-ene arises only *via* energy transfer from aromatic. Experimental curve indicates that chain mechanism must also be important.

(23) R. B. Cundall, private communication.

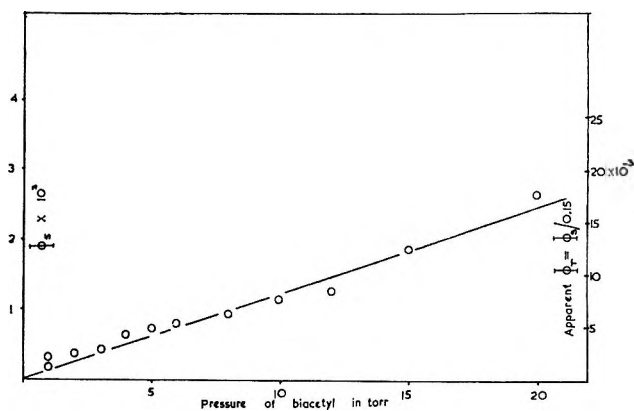
(24) M. Godfrey and J. N. Murrell, *Proc. Roy. Soc. Ser. A*, 278, 57, 64, 71 (1964).

systems.²³ We have attempted to check for this by carrying out blank runs and also by carrying out the experiments with a random selection of pressures of *cis*-but-2-ene, to minimize any effect of cumulative formation of *trans* during storage. The results indicate that the effect is real.

We have also carried out a few experiments on pentafluoropyridine. No fluorescence was detectable with our system, indicating that the compound has a fluorescence yield of much less than 10^{-3} . Clearly, as in the case of pyridine itself, some process occurs which depletes the excited singlet state with a rate constant of $\gg 10^8 \text{ sec}^{-1}$ (if the absorption in pentafluoropyridine is attributed to a π - π^* transition, giving a value for the radiative lifetime of $1 \times 10^{-8} \text{ sec}$).

The possibility that the process which competes with fluorescence is an intersystem crossing to a triplet state must be considered. In the case of pyridine itself²⁵ attempts to measure the quantum yield of triplet state formation using the sensitization of the *cis*-*trans* isomerization of but-2-ene²¹ led to the conclusion that such yields were small in the region of n - π^* absorption and very small in the region of π - π^* absorption. However, it must be noted that the success of this method depends upon the lifetime of the triplet state to be measured. It has been shown that for fluoroaromatics with short-lived triplet states even a very high concentration of olefin does not capture all of the aromatic triplets. It is thus essential in any study to carry out an investigation of the effect of pressure of added olefin in order to obtain meaningful estimates of triplet state quantum yields for aromatics. Unfortunately this was not done in the original study on pyridine,²¹ and the low result obtained may in part be due to an insufficient pressure of olefin. The biacetyl sensitization technique also gave no positive results when applied to pyridine, but this may again be in part due to addition of insufficient pressure of the triplet quencher. In the present system we have not attempted the olefin technique because of experimental difficulties in measuring small quantities of the *trans* olefin in the presence of large amounts of the *cis* isomer. The results obtained upon the addition of biacetyl to perfluoropyridine are illustrated in Figure 5. At 2480 Å and 2540 Å no sensitized emission from the biacetyl was visible, but at 2650 Å a very weak phosphorescence was observed which increased linearly with increasing pressure of biacetyl.

Since we have not measured the ratio of fluorescence



5. Sensitized phosphorescence yield Φ_s against biacetyl
e. Pressure of perfluoropyridine =
; λ 2650 Å.

of biacetyl to phosphorescence, it is not valid to assume that the weak emission observed in these experiments is due to triplet-triplet energy transfer between perfluoropyridine and biacetyl. However, if this were the case, the apparent triplet state yield of the pentafluoropyridine under these conditions would be of the order of 0.02.

The results above indicate that the perfluoropyridine may behave in a similar fashion to pyridine itself and to heavily fluorinated benzenes, in that it has a low (in this case zero) fluorescence yield and possibly a very short-lived triplet state whose quantum yield cannot be determined by conventional triplet quenching techniques. The mechanism by which the excited states of perfluoropyridine dissipate their energy cannot be elucidated with the present experimental techniques and must await the completion of more sophisticated kinetic spectroscopy systems at present under development.

Acknowledgments. The authors are grateful to the Royal Society for the award of a grant to cover the purchase of the monochromator and to the Science Research Council for an award to cover purchase of the Farrand Mk 1 Spectrofluorometer. Kh. Al-Ani wishes to thank the British Council for the payment of his fees while studying for the degree of Ph.D and Mr. David Gray for assistance in setting up the experimental system.

(25) J. Lemaire, *J. Phys. Chem.*, **71**, 612 (1967).

Infrared Studies of the Matrix Isolated Photolysis Products of PF₂H and P₂F₄ and the Thermal Decomposition Products of P₂F₄

by Jeremy K. Burdett,¹ Leslie Hodges, Virginia Dunning, and Jerry H. Current*

Department of Chemistry, University of Michigan, Ann Arbor, Michigan 48104 (Received February 13, 1970)

The photolysis of PF₂H in argon matrices at 4°K produced absorptions at 831.4 and 852.1 cm⁻¹ which are assigned to the stretching modes of the PF₂ free radical. An absorption at the lower frequency is also observed when the products of the thermal decomposition of P₂F₄ are isolated in argon matrices. Photolysis of P₂F₄ results in broader absorptions (5–10 cm⁻¹) at 834.0 and 843.5 cm⁻¹ which are ascribed to perturbed PF₂ radicals which are not able to diffuse far from the site of the original P₂F₄ molecule. Seven strong infrared absorptions at 967, 924, 898, 811, 751, 580, 399, and a weaker absorption at 408 cm⁻¹, are assigned to the species PF₃=PF formed by the photolysis of P₂F₄.

Introduction

Unlike its nitrogen analog, P₂F₄ does not exist in equilibrium with its monomer PF₂ in detectable quantities at room temperature. Electron spin resonance experiments² and mass spectrometric data³ show that PF₂ is only formed in detectable quantities when the gas is heated to 200 and 350°, respectively. The eventual products of the gas phase thermal decomposition are PF₃ and PF (polymer).^{4,5}

The radical PF₂ has been observed² by the spin resonance technique both from *in situ* photolysis and gas phase thermal decomposition in a variety of matrices at 20°K. The photolysis and thermal decomposition of PF₂H yield PF₂ radicals² and H atoms in quantities easily detected by spin resonance. No evidence was obtained suggesting the formation of the HPF radical. F atoms in matrices are not observable by esr studies.

Experimental Section

P₂F₄ was prepared by the reaction of PF₂I with mercury as reported by Rudolph, Taylor, and Parry.⁶ PF₂H (PF₂D) was prepared⁷ by the reaction of PF₂I with PH₃ (PD₃) and an excess of mercury.

The apparatus used throughout is a standard double dewar cooled by liquid helium, with CsI inner and outer windows for infrared studies and a quartz window in the rotatable lower section for ultraviolet irradiation purposes. The glass spray-on line was connected by means of a 0.25-in. Swagelok fitting with a Teflon ferrule at the corner of the cell.

A General Electric H4 mercury lamp and a water filter were used to photolyze the samples. Thermal decomposition was initiated on a 3-mm diameter helix of 0.005-in. tungsten wire containing ~20 cm of wire in 11-mm Pyrex tubing extending from 9 to 5 cm from the end of the spray-on line. The calculated total pressure in this section during sample decomposition is 2×10^{-3} cm. Experimentally this arrangement decomposed ~20% of a P₂F₄ sample when the wire was

heated to about 800°. The wire was electrically heated by means of a variable transformer and a 12-V filament transformer. The spray-on rate was regulated with two greaseless Teflon stopcocks and monitored with a mercury manometer. The deposition rate from a 2-l. sample bulb was nominally 1 mmol/hr of total matrix plus reactant.

The temperature of the inner CsI window was monitored by a chromel-constantan thermocouple⁸ potted into the cesium iodide with Woods metal. The temperature of the tungsten helix was estimated *via* its color temperature.

Infrared spectra were taken on a Beckman IR-12 spectrometer and ultraviolet data obtained from a Cary Model 11 ultraviolet-visible spectrometer.

Experiments with PF₂H. PF₂H was not decomposed by radiation of wavelength longer than 250 nm (the CsI cut-off point). However, photolysis through a quartz window ($\lambda > 210$ nm) led to a 75% drop in PF₂H absorption intensity after 7.5 hr. See Figure 1. The electronic transitions of PF₂H are centered at 260 nm and at 218 nm. The argon to PF₂H ratio (*M/R*) was around 900. Three new absorptions appeared at

* To whom correspondence should be addressed at Gulf Research and Development Co., P.O. Drawer 2038, Pittsburgh, Pa. 15230.

(1) Power Foundation Fellow, Magdalene College, Cambridge, England.

(2) M. S. Wei, J. H. Current, and J. Gendell, *J. Chem. Phys.*, **52**, 1592 (1970).

(3) D. Solan and P. L. Timms, *Chem. Commun.*, 1540 (1968).

(4) R. W. Rudolph, Ph.D. Thesis, University of Michigan, Ann Arbor, Mich., 1966.

(5) D. Solan, Ph.D. Thesis, Lawrence Radiation Laboratory, University of California, Berkeley, Calif., 1969.

(6) R. W. Rudolph, R. C. Taylor, and R. W. Parry, *J. Amer. Chem. Soc.*, **88**, 3728 (1966).

(7) R. W. Rudolph and H. W. Schiller, *ibid.*, **90**, 3581 (1968).

(8) L. L. Sparks, R. L. Powell, and W. J. Hall, U. S. Department of Commerce, National Bureau of Standards, Boulder Laboratories, July 1968.

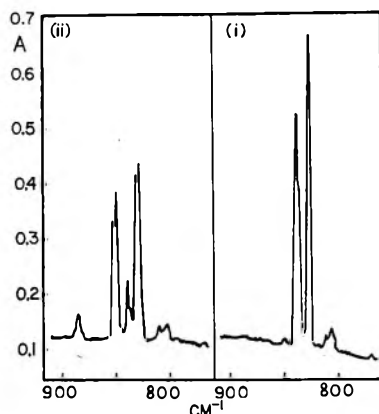


Figure 1. PF_2H behavior on photolysis in an argon matrix ($M/R = 900$) at 4.2°K : (i) before photolysis, (ii) after 7.5 hr irradiation, $\lambda > 210 \text{ nm}$.

795, 831.4, and 852.1 cm^{-1} , as the PF_2H concentration dropped. The first absorption, which is not assigned, was weak and disappeared during the photolysis. The other two, we believe, are the stretching modes of PF_2 . The resulting spectra are shown in Figure 1. The ultraviolet absorption spectrum of PF was identified by comparison with the gas-phase data.⁹ In the matrix a band of 0.02 absorbance unit, of half width 22 nm centered at 330 nm was observed. A separate experiment using PF_2H and PF_2D showed no observable isotope shift on the 853 or 795-cm^{-1} absorptions. This leads to the conclusion that they are not due to a hydrogen containing species. The 832-cm^{-1} region was obscured in the deuterated sample by the overlapping absorptions due to a phosphorus-fluorine stretching mode of PF_2H and PF_2D . The radical PFH therefore seems to be absent from the products. It was not detected in the esr investigation in which PF_2 and H atoms were the only observable products of photolysis.²

A chart showing the intensity behavior of the PF_2H , PF_3 , and PF_2 absorptions with photolysis time is shown in Figure 2. Only 75% of the PF_2H photolyzes, and the concentrations of PF_2H , PF_3 , and the new PF_2 species remain almost constant as the photolysis time increases beyond about 6 hr. This is apparently a dynamic equilibrium controlled by atomic diffusion around each photolysis site.

During this photolysis, the intensities of the PF_3 absorptions at 850.5 and 887 cm^{-1} increase with time indicating migration of fluorine atoms in the matrix. After 7.5 hr of photolysis, the ir absorbances show that for each 100 PF_2H molecules photolyzed, approximately 8 molecules of PF_3 are formed. This ratio is similar to that calculated for the fraction of PF_2H having another PF_2H unit as a nearest or next nearest neighbor.

We believe this defines the average extent of fluorine atom migration in this photolysis experiment since free migration would result in a continuous increase in the

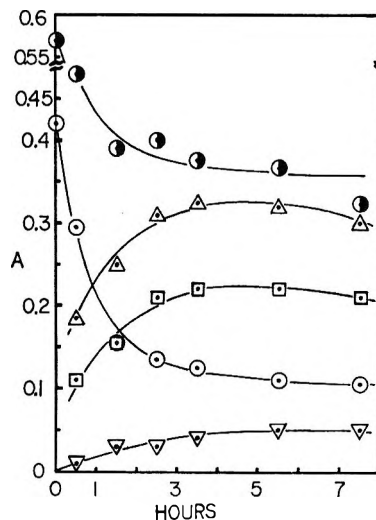


Figure 2. Intensity behavior of infrared absorptions with time, on photolysis of PF_2H ($\lambda > 210 \text{ nm}$): ∇ , PF_3 887 cm^{-1} absorption; \circ , PF_2H 839.6 cm^{-1} absorption; \bullet , PF_2H 828 cm^{-1} absorption; \square , PF_2 831.4 cm^{-1} absorption; \triangle , PF_2 852.1 cm^{-1} absorption).

PF_3 absorption. The photolyses of PF_2 and PF are the probable sources of fluorine atoms.

One hour of irradiation of the partially photolyzed sample with $\lambda > 250 \text{ nm}$ led to a decrease in the intensities of the absorptions at 852.1 and 831.4 cm^{-1} by 23%. The intensities of the PF_3 and the PF_2H bands which are not overlapped by PF_2 absorptions did not change, showing that these concentrations remain constant. This behavior is similar to the results of photolysis of the NF_2 radical.¹⁰ Irradiation ($\lambda > 250 \text{ nm}$) produces a decrease in the intensity of the NF_2 stretching fundamentals, an increase in the NF_3 concentration, and the observation of NF. The parallel behavior on photolysis is further evidence that the two infrared absorptions at 852.1 and 831.4 cm^{-1} are due to the PF_2 radical. Wavelengths greater than 250 nm are effective in photolyzing PF_2 but do not produce PF_2 from PF_2H .

Solan⁵ has reported the rapid photolysis of PF in xenon matrices and apparently a less rapid photolysis in krypton. Thus, ultraviolet evidence for PF from the photolysis of PF_2H in argon is somewhat surprising. The data are consistent if fluorine atom diffusion away from the photolysis site is the limiting step in the destruction of the PF radical; *i.e.*, there is no activation energy for atom combination. The photolysis rates are generally consistent with the expected ease of fluorine atom migration in the various matrices. From the gas-phase result⁹ of Douglas and Frackowiak ($\Delta G^{(1/2)} = 837 \text{ cm}^{-1}$) we might expect the PF vibrational

(9) A. E. Douglas and M. Frackowiak, *Can. J. Phys.*, **40**, 832 (1962).

(10) J. J. Comeford and D. E. Mann, *Spectrochim. Acta*, **21**, 197 (1965).

Table I: Photolysis of PF₂H in an Argon Matrix at 4°K (*M/R* = 900, 2.9 μmol of PF₂H)

After deposition, cm ⁻¹	Absorbance	After 7.5 hr, cm ⁻¹	Absorbance	Assignment
365	0.02	365	0.01	PF ₂ H
384		384		SiF ₄
...	0	795 ^b	0	Transient
803.5		803.5		PF ₂ H aggregate
806.0		806.0		
812		812		
828.0	0.57	828.0	0.32 ^a	
...	0	831.4	0.31 ^a	PF ₂ H
838	0.28	838	0.06	PF ₂
839.6	0.42	839.6	0.105 ^a	PF ₂ H
849.8	0.01	849.8	0.265 ^a	PF ₃
...	0	852.1	0.21 ^a	PF ₂
...	0	887	0.05	PF ₃
1000		1000		Impurity
1014	0.05	1014	0.01	PF ₂ H
1022	0.18	1022	0.13	PF ₂ H, SiF ₄
2270	0.21	2270	0.04	PF ₂ H

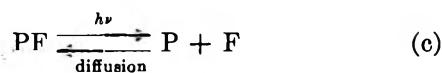
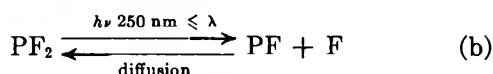
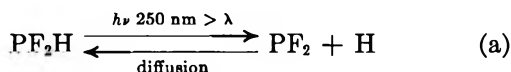
^a Overlapping absorptions. ^b Maximum absorbance of 0.02.

fundamental to lie beneath the lower frequency PF₂H fluorine stretching absorption at 829 cm⁻¹. We have no clear evidence for this but the intensity of this absorption remains rather high throughout the photolysis period.

A summary of the infrared observations is shown in Table I. No new bands which could be attributed to a PF₂ bending mode appeared in the low-frequency spectrum, and no new bands are found in the region associated with ν(P-H). The infrared spectrum of HF was not observed probably because it does not absorb strongly in the infrared.

Matrix Reactions

A simple set of reactions consistent with the observations is



Except for the formation of PF₃, no evidence for atomic diffusion from one photolysis site to another could be observed. HF was not observed and PFH which was expected from reaction "e" is not observed. PFH might be photolizable and thus not attain a significant concentration.



The observed equilibrium indicated by reaction a was unexpected. It shows that H atoms do not diffuse rapidly through an argon matrix to form H₂. This would have resulted in 90% destruction of the PF₂H in 3 hr. Thus, even H-atom diffusion is not free but is either very slow or of a limited range. Indeed, large, stable, hydrogen atom signals were observed in the esr studies of the photolysis of PF₂H in argon at 20°K.²

Studies on PF₂I and PF₃

PF₂I in an argon matrix was found to be stable toward ultraviolet photolysis with λ > 210 nm. The thermal decomposition of PF₂I was shown not to be a useful source of PF₂. The only positively identified product was PF₃. A 16% conversion to PF₃ was obtained using the external heater wire described above. Using a quartz tube (1 cm long by 1.5 mm i.d.) inside the cold cell heated by a coil of platinum wire, the conversion to PF₃ was only 2% at a tube temperature approaching 1300°. Isolation was reasonably good using a dual spray-on arrangement. The observed absorptions of PF₂X species in argon matrices at 4°K are shown in Table II.

Table II: Frequencies (cm⁻¹) of Some PF₂X Species Isolated in Argon Matrices at 4.2°K

PF ₂ H ^a	PF ₂ D	PF ₂ I	Assignment
2270	1656	374	ν(PX)
837.5			
839.7	340	843	ν _{as} (PF)
827.0	329	835	ν _s (PF)
828.0			
b	712 ^b	?	ω _{as} (PX)
1022	764	c	ω _s (PX)
365	361	408	δ _s (FPF)

^a Moderately intense absorptions are observed at 807 and 1014 cm⁻¹ which are apparently due to PF₂H aggregates. ^b Unpublished results of Dunning and Taylor from Raman studies of pure liquid samples indicate ω_{as}(PX) for PF₂H is at 960 cm⁻¹ and for PF₂D is at 706 cm⁻¹. ^c Raman studies on liquid PF₂I indicate that the missing frequency ω_s(PF₂I) is at 202 cm⁻¹. (See ref 4.)

PF₃ similarly was not decomposed by ultraviolet radiation with λ > 210 nm. Attempts to decompose the PF₃ thermally using an external hot wire were unsuccessful.

Experiments with P₂F₄

Photolysis of P₂F₄. Photolysis of a matrix deposited sample of *M/R* = 1600 with a GE H4 mercury lamp with the Pyrex cover retained (thus allowing radiation of λ > 300 nm to pass) produced no observable change in the infrared spectrum after 30 min. Photolysis of the sample through the CsI windows using the same lamp but with the Pyrex cover removed (λ > 250 nm) leads to the drastic changes after 30 min shown in

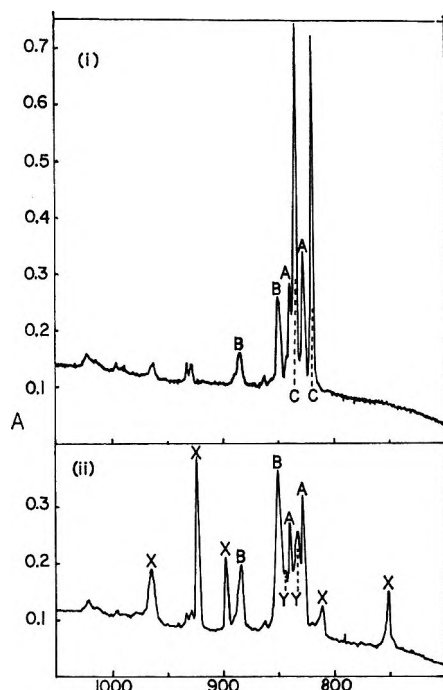


Figure 3. Behavior of P_2F_4 ($M/R = 1600$) on photolysis in an argon matrix at $4.2^\circ K$: high-frequency region (i) before photolysis, (ii) after 30 min irradiation $\lambda > 250$ nm. A = PF_2H , B = PF_3 , C = P_2F_4 , X, Y = new species.

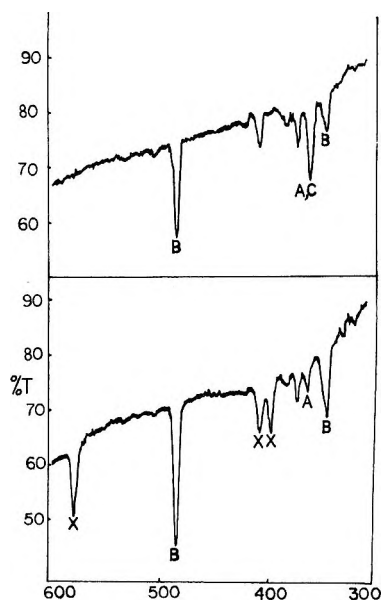


Figure 4. Behavior of P_2F_4 ($M/R = 600$) on photolysis in an argon matrix at $4.2^\circ K$: low-frequency region (i) before photolysis, (ii) after 30 min irradiation $\lambda > 250$ nm. A = PF_2H , B = PF_3 , C = P_2F_4 , X = new species. (This spectrum is of a partially thermally decomposed sample containing 10 times as much PF_3 and twice as much P_2F_4 as that of Figure 3.)

Figures 3 and 4. The bands labeled A are due to PF_2H impurity and do not change in intensity on photolysis in this wavelength region. A summary of the infrared observations is given in Tables III and IV.

Table III: Wave Number and Absorbance Data Associated with Figure 3 on the Photolysis of P_2F_4 ($M/R = 1600$, $5.0 \mu\text{mol}$ of P_2F_4)

Cold deposition		After irradiation		Assignment
cm^{-1}	OD	cm^{-1}	OD	
...		751	0.105	X
...		811.0	0.05	X
819.6	0.638	819.6	0.00	P_2F_4
827.9	0.232	828.0	0.23	PF_2H
...		832.5	0.15	?
...		834.0	0.14	PF_2
834.4	0.65	835.4	(bk) ^a	P_2F_4
839.6	0.18	839.6	0.18	PF_2H
842.4	0.04	842.4	(unobsd) ^b	PF_2I
...		839.3	0.09	PF_2
849.8	0.15	849.8	0.28	PF_3
862.2	0.02	862.2	0.02	PF_2OPF_2
887	0.06	887	0.11	PF_3
...		898	0.13	X
...		924	0.31	X
928	0.03	928	0.03	Impurity
932	0.03	932	0.03	Impurity
963	0.02	963	(unobsd)	PF_2OPF_2
...		967	0.09	X
996	0.015	996	0.015	Impurity
1014	0.01	1014	0.01	PF_2H
1023	0.02	1023	0.02	PF_2H

^a (bk) denotes band unresolvable from noise. ^b (unobsd) denotes band unobservable because of neighboring absorptions.

Table IV: Photolysis of P_2F_4 ($M/R = 600$, Time 30 min, Data Associated with Figure 4)

Cold deposition		After irradiation		Assignment
cm^{-1}	OD	cm^{-1}	OD	
349	0.040	349	0.070	PF_3
364	0.088	364	0.028	PF_2H , P_2F_4
374	0.047	374	0.032	PF_2I
384	0.024	384	0.01	SiF_4
...		399	0.052	X
408	0.034	408	0.050	PF_2I , X
484	0.11	484	0.19	PF_3
505	0.01	505	0.01	PF_2OPF_2
...		580	0.095	X

The P_2F_4 electronic absorptions are observed centered at 299, 260, and ~ 200 nm.

The absorptions due to P_2F_4 at 835 and 820 cm^{-1} have disappeared and the 364-cm^{-1} absorption, which is overlapped by PF_2H , has decreased showing the complete photolysis of P_2F_4 . Eight absorptions labeled X in Figures 3 and 4 have appeared. One of these lines is on top of the 408-cm^{-1} absorption of the PF_2I impurity. During the photolysis period there is an increase in intensity of the PF_3 absorptions in the stretching region, but the ratio of their absorbances remains constant. Thus, no new species absorbing strongly at 887 or 850 cm^{-1} is produced.

When the P_2F_4 had been destroyed by photolysis,

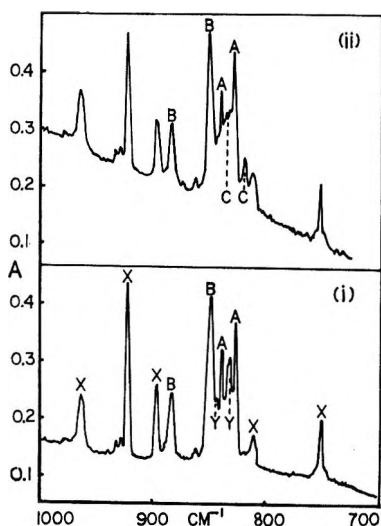


Figure 5. (i) Infrared spectrum of the photolysis products of P₂F₄ ($\lambda > 250$ nm) and (ii) after warming this sample to 20°K and recooling to 4.2°K ($M/R = 1600$). A = PF₂H, B = PF₃, C = P₂F₄, X, Y = new species.

absorptions at 834.0 and 843.5 cm⁻¹ were observed in the spectrum (labeled Y in Figure 3). On warming a sample to 20°K with external infrared lamps, these absorptions disappeared into the background, and P₂F₄ was reformed. See Figure 5. The absorptions, due to the regenerated P₂F₄ could be destroyed by photolysis. In one experiment, the thermal contact deteriorated after an initial photolysis which had produced both X and Y absorptions. Subsequent photolyses resulted in temperature increases (as indicated by the window thermocouple), erratic destruction of Y, with reformation of P₂F₄, and photolysis of P₂F₄ with formation of Y. Some reordering in the matrix and apparent aggregate formation is indicated by the change in slope of the base line in Figure 5 and by shoulders appearing at 833 and 841 cm⁻¹. However, except for 924 cm⁻¹, the X absorptions were not affected by warming to 20°K. The maximum absorbance of the 924-cm⁻¹ absorption was reduced on slight warming of the matrix; however, the line broadened at the same time. The 820-cm⁻¹ absorption is also broader than the original P₂F₄ absorption.

The disappearance of the absorptions at 834.0 and 843.5 cm⁻¹ (the Y bands) on warming the sample to 20°K, and the concurrent appearance of P₂F₄, suggests that these infrared absorptions are due to two PF₂ species trapped in the same matrix cage. The increase in temperature provides the activation energy for recombination. Radicals larger than the fluorine atom are believed to be too large to diffuse through the argon matrices below ~35°K. Photolysis resulting in fission of a P-P bond would leave the phosphorus containing products within a short distance of one another, perhaps only rotated. This is believed to be the reason for the breadth of the Y absorptions and for the

differences between these frequencies and the frequencies observed for the PF₂ radical produced photochemically from PF₂H. In the P₂F₄ experiment the mutual perturbation of the two species within the same matrix cage leads to a different vibrational potential surface than in the isolated case. The effect of such a perturbation should be greater for the antisymmetric stretching mode than for the symmetric counterpart. On this basis, we therefore suggest that for PF₂, $\nu_3 > \nu_1$. This result is analogous to observations¹¹ on SiF₂, where $\nu_3 > \nu_1$. For the first row difluorides, CF₂, NF₂, and OF₂, $\nu_1 > \nu_3$, however.¹² A summary of the vibrational data on PF₂ is shown in Table V.

Table V: PF₂ Frequencies (Argon Matrix)

	Perturbed, cm ⁻¹	Unperturbed, ^a cm ⁻¹
PF ₂ ν_1	834.0	831.4
PF ₂ ν_3	843.5	852.1

^a Using a FPF angle of 99° and assuming a separation of ν_1 and ν_2 (unobserved), force constants for the stretching modes are calculated to be $k_1 = 4.93$ mdyn/Å and $k_{12} = 0.17$ mdyn/Å. Reversing the above assignment leads to $k_1 = 4.94$ mdyn/Å and $k_{12} = 0.42$ mdyn/Å.

An increase in the intensity of both PF₃ absorptions on photolysis stoichiometrically implies formation of the PF radical. Its ultraviolet absorption spectrum was, however, not observed. Only one twentieth of the photolyzed P₂F₄ resulted in PF₃ formation. Again, the PF₃ formation is only a minor side reaction to the primary photolysis process. That the amount produced is approximately equal to the nearest and next nearest neighbor reactant molecules in the matrix is perhaps fortuitous.

The Primary Product of P₂F₄ Photolysis (the X Bands)

The absorptions labeled X in Figures 3 and 4 are apparently associated with one chemical species. They disappear rapidly at the matrix diffusion temperature (~39°K) indicating that X is a reactive species. Warming the sample to 20°K, which causes the reformation of some P₂F₄, did not affect these absorptions.

Their intensities relative to that of the initial P₂F₄ intensity seem to be roughly constant over a dilution range of 1:450 to 1:1600. The relative intensities of the X absorptions were constant for all experiments.

Since diffusion of a phosphorus-containing unit through an argon matrix at 4°K is an unlikely event, the observation of four $\nu(\text{P-F})$ absorptions among the

(11) J. W. Hastie, R. H. Hauge, and J. L. Margrave, *J. Amer. Chem. Soc.*, **90**, 2536 (1969).

(12) D. E. Milligan and M. E. Jacox, *J. Chem. Phys.*, **47**, 703 (1967).

bands labeled X suggests a biphosphorus species and an isomer of P_2F_4 . Their roughly constant intensity relative to P_2F_4 over a large dilution range precludes reaction of two P_2F_4 units.

The vibrational frequencies suggest one fluorine bound to an essentially trivalent phosphorus atom with a low-stretching frequency (811 cm^{-1}) and three nonequivalent fluorine atoms bound to a pentavalent phosphorus atom with high-stretching frequencies ($898, 924, 967\text{ cm}^{-1}$). A species which fits these requirements, and which may be an intermediate in the decomposition of P_2F_4 , is the novel compound $PF_3=PF$. A similar intermediate has been envisaged¹³ for B_2Cl_4 . It is interesting to note that the derivative $(CH_3)_3P=PCF_3$ has been synthesized.¹⁴ A comparison with some other $PF_3=X$ species is shown in Table VI. The ob-

Table VI: Infrared Absorption of Some P^V Species (Frequencies in cm^{-1})

X	PF_3O^a	PF_3S^a	Motion	PF_3^b
967			$\nu(PF_3)$	
898	900	940	$\nu(PF_3)$	1029
924	873	695	$\nu(PF_3)$	948
811			$\nu(PF)$	
751	1415	847	$\nu(PZ)$	
580	485	402	$\delta(PF_3)$	534
408	473	440	$\delta(PF_3)$	575
399	345	276	$\rho(PF_3)$	

^a From K. Nakamoto, "Infrared Spectra of Inorganic and Coordination Compounds," Wiley, New York, N. Y., 1963, p 112. ^b From J. P. Pemsler and W. G. Planet, Jr., *J. Chem. Phys.*, **24**, 920 (1956).

ervation of four $\nu(P-F)$ absorptions implies that non-equivalence of the three fluorine atoms in the PF_3 group and this would be the case if the $P^{III}-F$ bond were not colinear with the $P^{III}-P^V$ bond. The absorption at 751 cm^{-1} may be $\nu(P-P)$. The increased bond order in this species would result in a higher P-P stretching frequency than 541 cm^{-1} , observed⁶ in P_2F_4 . The lack of isotopic data however, prevents a more conclusive vibrational assignment.

It is not probable that any of the 967, 924, and 898 cm^{-1} absorptions are overtones or combination bands. They are the most intense absorptions in the spectrum, which is generally a feature of fundamentals. Further, P_2F_4 and the other molecules studied in this work do not have unusually intense overtones and combinations. The weaker 811 cm^{-1} absorption could be an overtone of the 408 cm^{-1} fundamental but even this seems unlikely for the reasons stated above.

It is also unlikely that all of the infrared allowed stretching modes will be observed for any given molecule. However, this is the case for all of the phosphorus fluorine molecules we have studied and is the most rea-

sonable assumption which can be made to explain the observed spectra.

Solan⁵ has observed similar absorptions in the photolysis of P_2F_4 in krypton and xenon matrices. We believe his absorptions result from the formation of PF_3PF and are not due to P_3F_5 as he suggests. The most conclusive evidence for this is that the new absorptions are independent of the sample dilution and only a small amount of PF_3 is formed in the photolysis.

Thermal Decomposition of P_2F_4

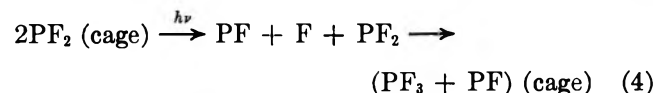
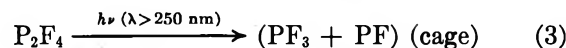
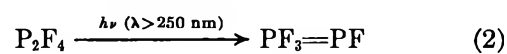
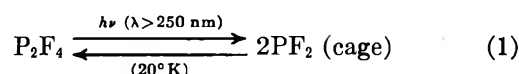
P_2F_4 , diluted with argon, was leaked through the Teflon stopcock, through the heater section, and the products condensed on the inner CsI window at 4.2°K , at a rate of approximately $3000\text{ cm}^3\text{ cm/hr}$. Intensity changes occurred in the $\nu(P-F)$ region of the infrared spectrum when the heater temperature was $\sim 750^\circ$, but resolution of any new bands due to the decomposition products was difficult due to the proximity of the P_2F_4 , PF_3 , PF_2I , and PF_2H absorptions. PF_3 is a decomposition product of P_2F_4 , and PF_2I , and PF_2H are sample impurities. A yellow solid (similar to the decomposition product of many phosphorus-fluorine compounds and referred to as PF polymer) was formed on the glass around the heater. This is presumed to form concurrently with the PF_3 .

At a dilution of $M/R = 600$ there was evidence for a new absorption of around 831.5 cm^{-1} in the thermal decomposition products. This absorption was easily detected after the P_2F_4 was photolyzed to PF_3PF . This is in excellent agreement with the 831.4 cm^{-1} absorption observed on the photolysis of PF_2H and assigned to the unperturbed PF_2 radical. The other stretching mode of PF_2 at 852.1 cm^{-1} is covered by the large excess of PF_3 formed in the thermal decomposition.

Photolysis of these partially decomposed samples gave identical results to those described earlier.

P_2F_4 Reactions

From the above discussion we may summarize the results of the thermal and photolytic decomposition of P_2F_4 as follows



Most of the PF_3 is formed early in the photolysis, thus reaction 3 seems to be more important than reac-

(13) J. Feeney, A. K. Holliday, and F. J. Marsden, *J. Chem. Soc.*, 356 (1961).

(14) A. B. Burg and W. Mahler, *J. Amer. Chem. Soc.*, **83**, 2388 (1961).

tion 4. The fate of the resulting PF has not been determined, since the ultraviolet spectrum of PF is not observed, and the earlier esr studies show no evidence for phosphorus atoms which would be formed by further photolysis. The P and/or PF fragments would remain close to the formed PF₃ molecule, and this perturbation may result in broad, undetectable spectra.



The thermally decomposed samples passed through 5 cm of 7-mm glass tubing before expanding inside the cell. Only a small fraction of the formed radicals ever reached the cold window. The relative importance of (5) and (6) therefore could not be determined. Experi-

ments using heated tubing inside the cell resulted in some aggregation of PF₃ and P₂F₄. These aggregates have broad intense infrared absorptions that effectively block the infrared spectral region of greatest interest and the experiments are of no value. Solan⁵ has used a better furnace design and has evidence for having isolated PF and further evidence for having isolated PF₂ from the thermal decomposition of P₂F₄.

Acknowledgments. We wish to thank Mr. Harvey Schiller for the sample of PF₂I and Dr. Ralph Rudolph for several useful discussions. Dr. David Solan has generously provided us with a copy of his thesis and other information and criticisms which have been most helpful. This work was supported in part by the National Science Foundation.

Effect of Various "Dry Electron" Scavengers on the Radioluminescence of Indole in Polar Solution

by H. B. Steen¹

Norsk Hydro's Institute for Cancer Research, Montebello, Oslo 3, Norway (Received May 19, 1970)

The electron scavengers H₂O₂, ClCH₂COOH, CCl₃COOH, and NaNO₃ have been found to reduce significantly the yield of the X-ray-induced phosphorescence of indole in ethylene glycol-water glass at 77°K when present in concentrations >0.1 M. The reactions involved obey homogeneous competition kinetics. Since the major fraction of this phosphorescence is supposedly due to the geminate recombination between positive indole ions and nonhydrated electrons (e⁻), this effect is attributed to the reaction between the electron scavengers and e⁻. No effect of HCl was found. This is in agreement with the hypothesis of Hamill that H₃O_{aq}⁺ is unreactive toward e⁻. The relative scavenging constants determined by the present experiments agree with those obtained for what is believed to be e⁻ by picosecond pulse radiolysis of aqueous solutions, while they are significantly different from the scavenging constants reported both for "mobile electrons" in strongly acidic glasses as well as for e_{aq}⁻ in water.

Considerable experimental evidence exists that radiation-induced electrons in frozen aqueous media are able to react with molecular entities while they are still in the mobile presolvation state.^{2,3} However, the exact nature of these "mobile electrons" is still obscure.⁴ Recently Hunt, *et al.*,^{5,6} have performed picosecond pulse radiolysis studies of aqueous solutions at room temperature which seem to demonstrate that the precursor of the hydrated electron, *i.e.*, presumably the nonhydrated electron, reacts efficiently with a variety of hydrated electron scavengers except H₃O_{aq}⁺. These phenomena are now attracting renewed interest in consideration of a new model for the radiolysis of water proposed by Hamill.^{7,8} A major assumption of this model is that

electrons may react with molecular entities prior to hydration, that is while they are still moving with thermal energies as quasifree particles. According to this

- (1) Fellow of the Norwegian Cancer Society.
- (2) (a) P. N. Moorthy and J. J. Weiss, *Advan. Chem. Ser.*, **50**, 180 (1965); (b) L. Kevan, "Radiation Chemistry of Aqueous Systems," G. Stein, Ed., Wiley, New York, N. Y., 1968, pp 21-71.
- (3) T. Sawai and W. H. Hamill, *J. Phys. Chem.*, **73**, 2750 (1969).
- (4) P. N. Moorthy, C. Gopinathan, and K. N. Rao, *Radiat. Eff.*, **2**, 175 (1970).
- (5) R. K. Wolff, M. J. Bronskill, and J. W. Hunt, submitted for publication in *J. Phys. Chem.*
- (6) J. W. Hunt, *et al.*, private communication.
- (7) W. H. Hamill, *J. Chem. Phys.*, **49**, 2446 (1968).
- (8) W. H. Hamill, *J. Phys. Chem.*, **73**, 1341 (1969).

hypothesis these "dry electrons" (e^-) should in general react with molecules which are scavengers of hydrated electrons (e_{aq}^-) with the important exception of H_{aq}^+ which should be essentially unreactive toward e^- . The rate constants of such scavengers toward e^- are generally expected to be different from those valid for e_{aq}^- . It is of considerable interest to see if this can be experimentally verified and, if so, to obtain the relevant rate constants.

In the present communication we report experiments which seem to support the above hypothesis. Thus, we have studied the effect of various electron scavengers on the radioluminescence of indole in a polar solution at 77°K. The basis for these experiments is our previous studies of the X-ray-induced luminescence of various aromatic molecules in similar solutions⁹⁻¹¹ from which it was concluded that approximately 90% of the phosphorescence observed during X-irradiation at 77°K results from the recombination between an ionized solute molecule and an electron, the radiative process being the $T_1 \rightarrow S_0$ transition of the neutral solute molecule. This recombination appears to be a geminate process which takes place before solvation occurs. Hence, the effect of various additives on this X-ray-induced phosphorescence should provide a simple test of their efficiencies as scavengers of e^- . It should be emphasized that our previous data seem to exclude that any substantial part of the X-ray-induced phosphorescence observed here results from solvent-solute energy transfer, *e.g.*, from trapping of positive holes by solute molecules followed by neutralization. Thus, a reduction of the X-ray-induced phosphorescence caused by the competition for positive holes between the solute and the scavenger can be disregarded in the present case. Reactions between positive solute ions and scavenger molecules are also ruled out since neither one is able to diffuse in the solvent under the present conditions.

The solvent was a 1:1 mixture of ethylene glycol and water which appears as a rigid and completely transparent glass at 77°K. The concentration of indole was 2×10^{-3} M. The scavengers were H_2O_2 , $ClCH_2COOH$, CCl_3COOH , $NaNO_3$, and HCl which were mixed into the sample solutions within a few minutes before cooling to 77°K. The samples were irradiated in a vacuum with 50-keV X-rays at a dose rate of approximately 50 rads/sec and the emission spectrum was recorded during irradiation. In order to correct for the possible effects of the scavengers on the radiative properties of the solute, we measured also the relative quantum yields of the fluorescence and phosphorescence induced by 270-nm uv light. Thus, it was found that $NaNO_3$, CCl_3COOH , and H_2O_2 markedly reduced these yields. The apparatus and experimental procedure have been described elsewhere.⁹

The yields of fluorescence and phosphorescence were obtained by integration of the respective spectral bands. Taken separately these bands were identical for the two

types of irradiation and, apart from the reduction in intensity, they were not affected by the presence of any of the scavengers except $NaNO_3$. For both types of irradiation $NaNO_3$ produced an additional fluorescence band which presumably reflects the presence of a charge-transfer complex involving the excited solute.

The yield, Y_T , of X-ray-induced excitation of the phosphorescent triplet level is calculated from

$$Y_T = \frac{\phi_F \phi_P^\circ Y_P}{\phi_F^\circ \phi_P Y_P^\circ} Y_T^\circ \quad (1)$$

where Y_P is the yield of X-ray-induced phosphorescence and ϕ_F and ϕ_P are the quantum yields of the uv-induced fluorescence and phosphorescence, respectively. The superscript denotes the yields observed with no scavenger present. Equation 1 is valid only provided the rate of intersystem crossing from the fluorescent singlet level to the phosphorescent triplet level is independent of the scavenger concentration.

It was found that, with one exception, all the scavengers studied significantly reduced Y_T , hence indicating that reactions between scavengers and e^- can compete with recombination. The exception is HCl which, in agreement with Hamill's hypothesis, gives no noticeable reduction of Y_T when present in a concentration of 2 M.

The appropriate Stern-Volmer graphs are presented in Figure 1. It can be seen that the quenching of the X-ray-induced triplet excitation, that is, supposedly the

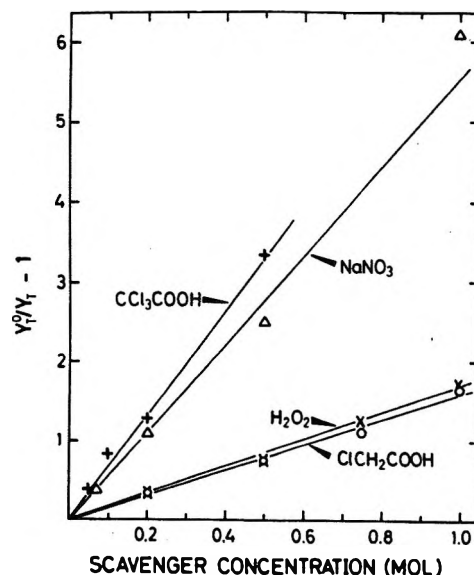


Figure 1. Stern-Volmer graphs of the yield of X-ray-induced excitation of the phosphorescent triplet level of indole in ethylene glycol-water glass containing various electron scavengers at 77°K.

(9) H. B. Steen, *Photochem. Photobiol.*, **6**, 805 (1967).

(10) H. B. Steen, *Radiat. Res.*, **38**, 260 (1969).

(11) H. B. Steen, *ibid.*, **41**, 268 (1970).

Table I^a

Scavenger	C_T, M^{-1}	$C_{37}', \text{rel units}$	k_Q, M^{-1}	$k',^d \text{rel units}$
H ₂ O ₂	1.0 (1.7) ^b	1.0	1.6	1.6
ClCH ₂ COOH	1.1 (1.5) ^c	0.9	1.6	0.85
CCl ₃ COOH	0.26 (0.5) ^c	0.29	6.6	1.1
NaNO ₂	0.31 (0.45) ^b	0.26	5.5	1.4
HCl	>10		<0.2	3.0

^a The scavenger concentration C_{37} needed to reduce the yield of X-ray-induced triplet excitation to 37% and the corresponding quenching constants k_Q . The numbers in parentheses are those obtained by Hunt, *et al.*, and C_{37}' are these values normalized so as to match the present value for H₂O₂. k' are the relative rate constants for e_{aq}^- . ^b See ref 5. ^c See ref 6. ^d See ref 12.

quenching of e^- , obeys homogeneous competition kinetics within the range of concentration studied. The quenching rate constants obtained from the slopes of these curves are given in Table I together with the scavenger concentrations needed to reduce Y_T to $1/e$. The latter values are compared to those found by Hunt, *et al.*, for these scavengers in water at room temperature. It can be seen that the quenching efficiencies are somewhat smaller under the latter conditions. This can be accounted for by the longer lifetime of the nonhydrated ions in the highly viscous solvent used in the present experiments. However, it appears that when compared on a relative scale the quenching efficiencies obtained

here are approximately the same as those found by Hunt, *et al.* This result strongly indicates that the numerical data obtained by these two types of experiments indeed refer to the same reactions, namely the scavenging of e^- .

From Table I it appears that the quenching rate constants obtained here are reciprocally quite different from those known for e_{aq}^- from pulse radiolysis measurements.¹² Kevan² reports that the relative rate constants which he obtained for the scavenging of mobile electrons by various electron scavengers in strongly acidic glasses at low temperatures are fairly similar to those known for e_{aq}^- . Hence, it seems indicated that the nonhydrated electrons observed by Hunt, *et al.*, and in the present work are different both from the mobile electrons discussed by Kevan as well as from the hydrated electrons.

In view of the high "solute" concentrations characterizing living organisms, reactions involving "dry electrons" are likely to have particular importance in radiobiology.

Acknowledgments. The author is deeply indebted to J. W. Hunt for a series of stimulating discussions which initiated the present work. Valuable discussions with M. Kongshaug are also appreciated.

(12) M. Anbar, and P. Neta, *Int. J. Appl. Radiat. Isotop.*, **18**, 493 (1967).

Effect of the Solvent on the Kinetics of Diazotization^{1a}

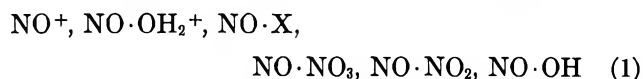
by Z. A. Schelly^{1b}

Department of Chemistry, University of Utah, Salt Lake City, Utah 84112 (Received January 26, 1970)

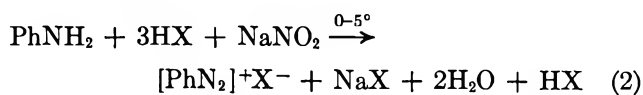
It is shown in methanol-carbon tetrachloride mixtures at 0° that the reaction rate expression developed for diazotization of aniline in pure methanol by Schmid, *et al.*, is further resolvable. Omitting simplifying assumptions concerning the degree of dissociation of the electrolytes present in the reaction mixture, one can detect protonic catalysis which was not found in the earlier work. A rate equation involving H⁺ catalysis is presented. This equation follows automatically from Schmid's reaction mechanism proposed in methanol, that can be confirmed also in methanol-carbon tetrachloride mixtures up to 60% CCl₄ v/v (*D*_{0°} = 15.00). For solvents with lower dielectric constant, the possibility of Ph·NH·NO → Ph·N:N·OH being rate controlling is suggested. Kinetic data have been obtained in pure carbon tetrachloride using an extrapolation method, although the reaction is heterogeneous in this medium. The effect of changing dielectric constant of solvent on the reaction rate is also discussed.

Introduction

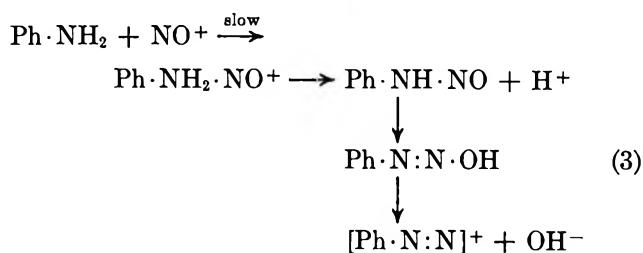
The kinetics and mechanism of diazotization in aqueous solution is well described through the works of Ingold, *et al.*, and Schmid, *et al.*² The latter also investigated this reaction in methanol.³ Summarizing the results obtained in water and in methanol, diazotization is the N-nitrosation of primary aromatic amines resulting in diazonium salts. It is an electrophilic substitution, with nitrosyl ion, NO⁺, as substituent, which can be furnished either as such or in bound form attached to a Brønsted base. The possible or actual carriers of NO⁺ in N-nitrosation are the following



arranged in order of increasing basic strength of the combined base. The nitrosating agents are usually formed from nitrous acid, and the overall reaction of diazotization in an actual experiment can be formulated, for example, as



where X represents a halogen. An excess of acid is necessary to prevent the formation of diazotates from the diazonium ion [PhN₂]⁺. Assuming the nitrosating agent has been supplied, then the first (rate-determining) step of diazotization is the attack of the agent on the lone-pair electrons of the primary amine followed by a sequence of fast steps ending in diazonium ion.



In water as the reaction medium, the first five species of (1) are the actual nitrosating agents. Accordingly, the reaction rate equation contains five terms or less depending on experimental conditions. In methanol, NO·OH₂⁺ is replaced by NO·CH₃OH⁺ (solvated nitrosyl ion or protonated methyl nitrite), and the only actual agent is NO·X. Using aniline and hydrochloric acid as two of the reactants, the reaction rate in methanol can be expressed according to Schmid and Muhr by the simple equation³

$$v = \frac{d(\text{PhN}_2^+)}{dt} = \\ k_0 f_{\text{HCl}}^2 [\text{PhNH}_2^+] [\text{CH}_3\text{ONO}] [\text{Cl}^-] \quad (4)$$

with parentheses symbolizing total and the brackets real concentrations, respectively. *k*₀ is a reaction rate coefficient and *f*_{HCl} is the mean activity coefficient of HCl.

By changing solvent from water to methanol, the reaction mechanism and the rate expression simplify drastically. Although the chemical properties of the two solvents are related to a certain extent, their dielectric constants *D* differ substantially (*D*_{H₂O}^{20°} = 80.36, *D*_{CH₃OH}^{20°} = 33.73). In the present work a systematic study has been performed on the effect of changing dielectric constant on reaction rate and mechanism of diazotization. Also, the effect of extreme changes of reaction medium, *e.g.*, using an aprotic solvent, has been investigated. A series of methanol-carbon tetrachloride mixtures was chosen as solvent

(1) (a) This article is based upon the doctoral dissertation presented to the faculty of Vienna Technical University in 1967. Also presented in part at the 24th Northwest Regional Meeting of the American Chemical Society in Salt Lake City, Utah, June 1969. (b) Correspondence should be addressed to Department of Chemistry, The University of Georgia, Athens, Ga. 30601.

(2) Cf. the review article by H. Schmid, *Chem.-Ztg., Chem. App.*, **86**, 809 (1962), and references cited therein; E. D. Hughes, C. K. Ingold, and J. H. Ridd, *J. Chem. Soc.*, 58 (1958).

(3) H. Schmid and G. Muhr, *Monatsh. Chem.*, **93**, 102 (1962).

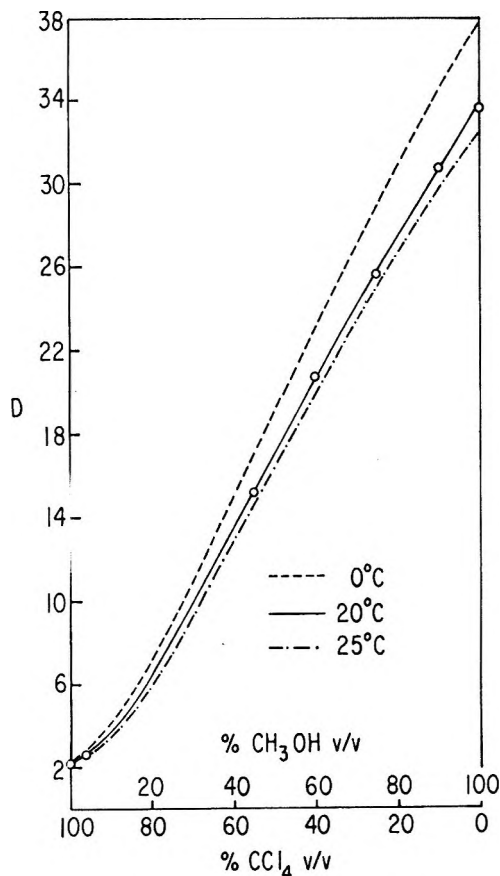


Figure 1. Dielectric constant of the methanol-carbon tetrachloride system at different temperatures.

for this purpose, instead of using several solvents, possibly with quite different chemical properties. The advantages of this system are based on the fact that CH_3OH and CCl_4 are miscible in all proportions. Thus, the dielectric constant of the mixture is variable continuously over a wide range (Figure 1). Consequently, any continuous monotonic function with the general form

$$\Psi = f(D) = F(\text{composition of the mixture}) \quad (5)$$

can be accurately interpolated between a few data points, if Ψ is property of a substance or chemical system dissolved in the mixture. Since CCl_4 can be regarded inert even against NOCl , it acts only as an indifferent diluent, and the chemical properties of the solvent determined by the component methanol are retained for any composition of the mixture (excluding pure CCl_4). In addition, since the composition of the mixtures lies between pure methanol and carbon tetrachloride, one may compare the kinetics in a medium already studied (pure methanol) with those in an aprotic solvent.

Experimental Section

A. Chemicals. All reagents used were analytical grade (purchased from Merck or Riedel de Haën) or

were purified by conventional methods. The concentration of the methanolic NaNO_2 solution was checked according to Fischer.⁴ NOCl was obtained from the Matheson Co., analyzed by the Addison-Thompson method,⁵ and purified from N_2O_4 with potassium chloride.⁶ The concentration of NOCl in pure CCl_4 has been determined by oxidation-reduction titrations. The methanolic HNO_2 was prepared by titration of a methanolic AgNO_3 solution with methanolic HCl with cooling and excluding light. *p*-Hydroxyazobenzene was prepared by Oddo and Puxeddu's method.⁷

B. Apparatus. The dielectric constants were measured at 20° by using Dipolmeter WTW Type DM Ol, and D values for other temperatures were obtained through linear extrapolation by using literature data.⁸ The optical density data were obtained on a Zeiss Spektralphotometer PMQ II. The temperature was controlled to $\pm 0.05^\circ$ with an Ultra Kryostat UK 30.

C. Kinetic Experiments. The reactions were initiated by rapid mixing of two thermostated solutions resulting in a 100-ml reaction mixture. One of the two solutions contained aniline, acid (HCl or NHO_3), and in some cases NaCl and/or NaClO_4 , and the other NaNO_2 or NOCl , respectively. The progress of diazotization has been followed by extracting samples from the reaction mixture and determining the diazonium ion concentration colorimetrically. Reaction in the extracted samples was quenched with the same volume of a strong alkaline methanolic phenol solution with a large excess of phenol. This quenching produces instantaneous formation of *p*-hydroxyazobenzene with theoretical yield with respect to the diazonium ion concentration. The optical density of these solutions was measured at the wavelength of the absorption maximum of the dye (λ_{max} 400 $\text{m}\mu$) and concentrations were obtained from the linear calibration curve. The molar decadic absorptivity of the dye ($\epsilon_{\text{max}}^{20^\circ} = 2.748 \times 10^4 \text{ M}^{-1} \text{ cm}^{-1}$) was determined to be independent of the composition of the reaction mixture after quenching, ranging from pure methanol to 50% CCl_4 v/v.

In long runs, the amount of diazonium ions produced and detected did not reach the theoretical yield (Figure 2), owing to slow decomposition of nitrous acid and diazonium ions and to side reactions of the latter. The two conceivable significant side reactions of diazonium ions are their hydrolysis and their N-coupling with unchanged amines to give diazoamino compounds. To eliminate these possible systematic errors the initial reaction rates v_0 have been determined throughout in

(4) W. M. Fischer, *Z. Anorg. Allg. Chem.*, **78**, 134 (1912).

(5) C. C. Addison and R. O. Thompson, *J. Chem. Soc.*, 218 (1949).

(6) C. W. Wittaker, F. O. Lundstrom, and A. R. Merz, *Ind. Eng. Chem.*, **23**, 1410 (1931).

(7) G. Oddo and E. Puxeddu, *Chem. Ber.*, **38**, 2755 (1905).

(8) "Handbook of Chemistry and Physics," 44th ed, The Chemical Rubber Publishing Co., Cleveland, Ohio, 1963, p 2613; Landolt-Börnstein, "Zahlenwerte und Funktionen," Vol. 2, Part 6, 6th ed, Springer-Verlag, Berlin, 1959, p 632.

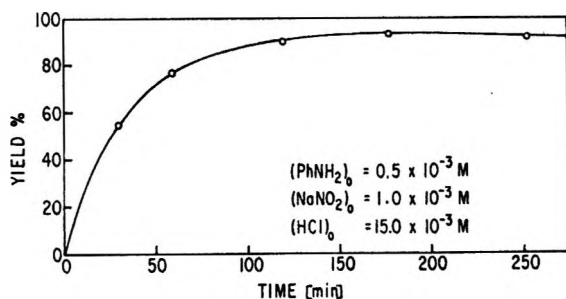


Figure 2. Yield of diazonium ion (as *p*-hydroxyazobenzene) vs. time in a typical long run.

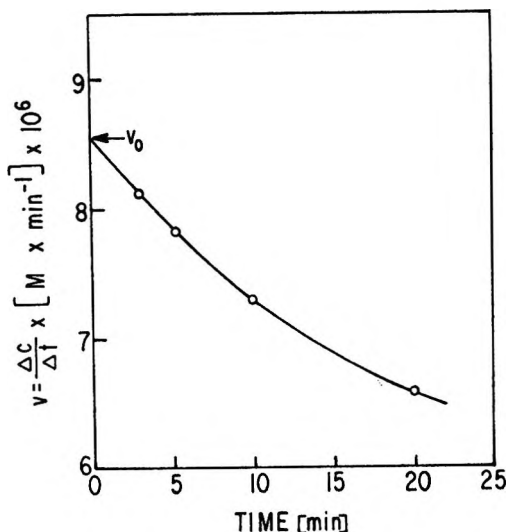


Figure 3. Example for the graphical determination of the initial reaction rate v_0 .

this work by extrapolating the measured average rates to time zero (Figure 3).

Results and Discussion

A. Most of the kinetic experiments have been done in $\text{CH}_3\text{OH}-\text{CCl}_4$ mixtures 1:1 by volume, at 0° . The order of reaction with respect to the different reactants and to the ionic strength $I = \frac{1}{2} \sum z_i^2 c_i$ has been determined by the van't Hoff method. Varying successively the initial concentration c_0 of each component and keeping all other parameters constant at the same time, the slopes of the curves $\log v_0$ vs. $\log c_0$ (Figure 4) give the order with respect to each component. Varying the initial concentration of aniline, sodium nitrite, hydrochloric acid, and the initial ionic strength (Figure 4), one obtains the proportionality

$$v_0 \propto (\text{PhNH}_2)_0 (\text{NaNO}_2)_0 (\text{HCl})_0^x I^y \quad (6)$$

where $0.365 \geq x \geq 0.098$ and $-1.394 \leq y \leq -0.311$, the latter indicating negative salt effects. Varying $(\text{Cl}^-)_0$ and $(\text{H}^+)_0$ (Figure 4) instead of $(\text{HCl})_0$, the proportionality (6) can be replaced by

$$v_0 \propto (\text{PhNH}_2)_0 (\text{NaNO}_2)_0 (\text{Cl}^-)_0 (\text{H}^+)_0^z I^y \quad (7)$$

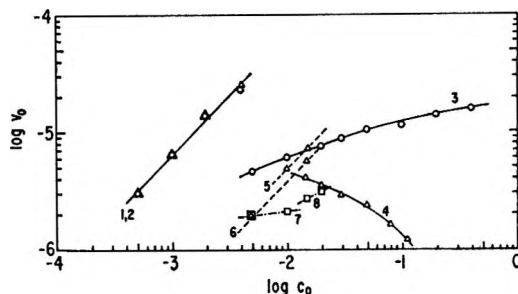


Figure 4. Determination of the order of reaction with respect to the reactants: curve 1, PhNH_2 ; 2, NaNO_2 ; 3, HCl ; 4, I ; 5 and 6, Cl^- ; and 7 and 8, H^+ .

where $0 < z < 1$, indicating protonic catalysis not found in pure methanol.³

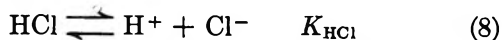
Now let us consider some aspects of the experimental technique used in pure methanol, as well as in the present work. The variation of the initial concentration of a single component, say chloride ion, at a time can be achieved with the usual balancing-of-concentrations method only if values of the degree of dissociation α of electrolytes present in the reaction mixture are known or if all values of α are equal. The knowledge of α is indispensable also for the calculation of ionic concentrations and activity coefficients. A complete dissociation of all electrolytes was assumed in methanol.³ This assumption is, however, unjustified, since for all electrolytes in solvents of lower dielectric constant, dissociation is incomplete at accessible concentrations.⁹ The degrees of dissociation of HCl , NaCl , and NaClO_4 at 0° in pure methanol and in $\text{CH}_3\text{OH}-\text{CCl}_4$ mixture (1:1 by volume) have been estimated based on conductance measurements,¹⁰ where each electrolyte was alone in the solution under its own ionic strength. Values of α have been found to deviate substantially from each other and from unity in methanol. In the $\text{CH}_3\text{OH}-\text{CCl}_4$ mixture ($D_{0^\circ} = 19.1$) dissociation is ever more incomplete; however, the α values for all three electrolytes are equal (the maximum deviation is less than 0.02) and are approximately constant ($\alpha = 0.6 \pm 0.02$) within the range of ionic strength 1.55×10^{-3} to $3.35 \times 10^{-2} M$. Since no information is available about the degree of ionization of $\text{PhNH}_3^+\text{Cl}^-$, it has been assumed to be the same as that of HCl , NaCl , and NaClO_4 . Failure to consider incomplete dissociation in methanol may account for the fact that no H^+ catalysis was detected in this solvent.

B. *Mechanism and Rate Equation.* To be able to postulate a reaction mechanism which is in accord with the empirical rate expression 7, consider all preliminary reactions which have gone to completion or

(9) R. M. Fuoss and C. A. Kraus, *J. Amer. Chem. Soc.*, **55**, 476 (1933).

(10) Z. A. Schelly, Dissertation, Vienna Technical University, 1967.

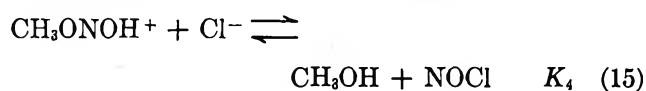
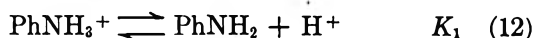
have attained their equilibrium positions, respectively, at zero time. Because of the large excess of methanol,



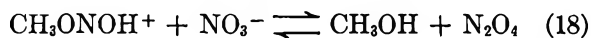
reactions 9 and 10 are very fast and complete, so that

$$(\text{NaNO}_2)_0 \approx [\text{CH}_3\text{ONO}]_0 \quad (11)$$

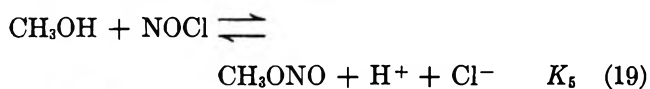
In addition, we have the equilibria



The equilibria 8, 13, and 15 are replaced by



if HNO_3 is used instead of HCl and no Cl^- ions are present in the mixture. However, no diazotization occurs in the absence of halogen ions, indicating that CH_3ONOH^+ and N_2O_4 do not N-nitrosate aniline, unlike their action in water. The equations for equilibria 14 and 15 may be combined so that



where $K_5 = (K_3 \times K_4)^{-1}$.

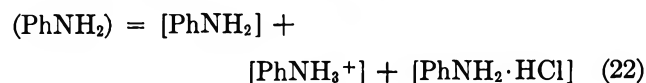
Based on expression 7, the actual diazotizing agent must be a species, for which the real concentration increases with increasing $(\text{NaNO}_2)_0$, $(\text{Cl}^-)_0$, and $(\text{H}^+)_0$. Indeed, in such a case, equilibria 14 and 15 will be shifted in a direction favoring the formation of NOCl . Thus, one can postulate the rate-determining step as being the same as in pure methanol,³ followed by



fast steps given in eq 3. This results in the reaction rate equation

$$v = k[\text{PhNH}_2][\text{NOCl}]f_{\text{PhNH}_2}f_{\text{NOCl}}/f_{\ddagger} \quad (21)$$

where k is a rate constant and f_{\ddagger} is the activity coefficient of the activated complex. Considering that



$[\text{NOCl}]$ can be calculated from equilibrium 19, and the real concentrations in eq 22 from the equilibria 12 and 13, respectively. Substituting the calculated

values into eq 21, and (a) equating the activity coefficients of nonelectrolytes to unity, (b) neglecting the dependence of the activity coefficients of electrolytes on their ionic radii, and (c) symbolizing $f_{\text{H}^+} \times f_{\text{Cl}^-}$ by f_{HCl^2} , one obtains the rate equation

$$v = kK_5^{-1}a_{\text{CH}_3\text{OH}}^{-1} \frac{K_1[\text{H}^+][\text{Cl}^-]}{K_1 + [\text{H}^+] + \frac{1}{K_2}[\text{H}^+][\text{Cl}^-]f_{\text{HCl}^2}} \times (\text{PhNH}_2)[\text{CH}_3\text{ONO}]f_{\text{HCl}^2} \quad (23)$$

where $a_{\text{CH}_3\text{OH}}$ is the activity of methanol. Equation 23 follows automatically from the proposed mechanism. It is compatible with the empirical rate law 7, if one transforms the latter, accounting for the incomplete dissociation of the electrolytes, and utilizing eq 11

$$v \propto [\text{H}^+]^w[\text{Cl}^-]^w(\text{PhNH}_2)_0[\text{CH}_3\text{ONO}]I^{z'} \quad (24)$$

Now $0.8 \leq w \leq 0.9$ and $0.082 \leq z' \leq 0.22$.

Comparing eq 4 and 23, it is obvious that k_0 in (4) is further resolvable, thus

$$k_0[\text{PhNH}_3^+] = kK_5^{-1}a_{\text{CH}_3\text{OH}}^{-1} \times \frac{K_1[\text{H}^+](\text{PhNH}_2)}{K_1 + [\text{H}^+] + \frac{1}{K_2}[\text{H}^+][\text{Cl}^-]f_{\text{HCl}^2}} \quad (25)$$

Since the thermodynamic equilibrium constants K_1 , K_2 , and K_5 at 0° in eq 23 are not known, the rate constant k cannot be calculated. Hence, instead of k the coefficients k' and k'' given by

$$k' = kK_5^{-1} \frac{K_1}{K_1 + [\text{H}^+] + \frac{1}{K_2}[\text{H}^+][\text{Cl}^-]f_{\text{HCl}^2}} \quad (26)$$

$$k'' = k'[\text{H}^+] \quad (27)$$

have been calculated and plotted vs. I (Figure 5). k' is approximately constant at $I > 0.035 M$, in comparison with k'' , which can be considered constant only at very small ionic strength where $I < 0.0125 M$.

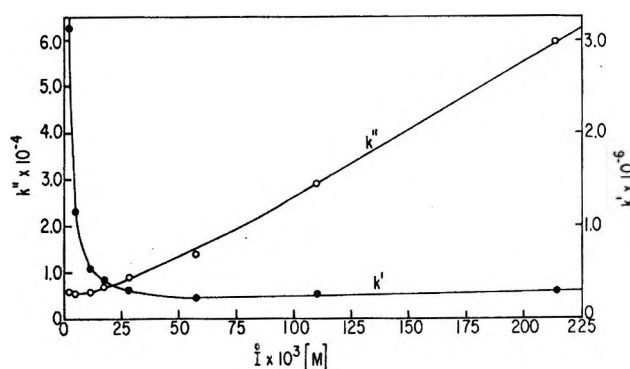


Figure 5. k' and k'' vs. the ionic strength I .

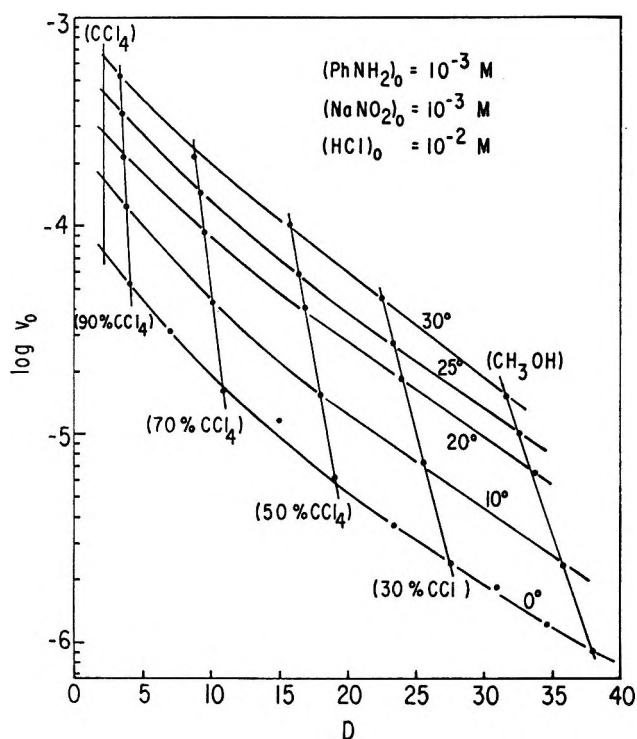


Figure 6. $\log v_0$ vs. D at different temperatures.

C. Variation of the Temperature and the Composition of the Solvent. In these experiments the initial concentrations of all reactants were kept constant, and only the temperature or the dielectric constant of the medium was varied (Figure 6). With decreasing polarity of the solvent the reaction rate shows a steep increase. There are several arguments that would predict the opposite result. (1) The activity coefficients fall with decreasing D of the solvent, which should lead to a smaller rate (cf. eq 21). (2) If the activated complex is more polar than the reactants, the rate constant k should decrease with the D value of the medium.¹¹ The activated complex in the present case is certainly more polar than the reactants since the products are ionic (see eq 20). (3) The activation energy in an ionization reaction does not change rapidly from solvent to solvent; however, the entropy of activation is always negative and becomes more negative as the polarity of the solvent decreases. Thus the rate of reaction should increase with the polarity of the solvent.¹² (4) The preliminary equilibria 8, 12,¹³ and 13 are shifted with decreasing D in favor of association of the species, tending to diminish $[\text{PhNH}_2]$ and $[\text{NOCl}]$, which also should lead to a smaller rate.

However, all these effects (1 through 4) are overwhelmed by the enhancement of the reaction rate caused by the decrease of the activity of methanol, $a_{\text{CH}_3\text{OH}}$ (see eq 23), and by the displacement of equilibrium 19 in favor of higher NOCl concentration, in accord with decreasing dielectric constant of the medium. Also the weaker solvation of the reactants

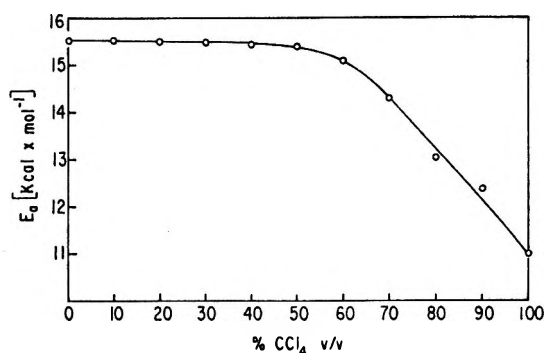


Figure 7. The activation energy E_a vs. composition of the solvent.

amine and NOCl with decreasing polarity of the solvent contributes to the increase of the reaction rate.

D. Activation Energy. The calculated activation energies are plotted vs. composition of the solvent in Figure 7. The insensitivity of the activation energy E_a to the dielectric constant of the medium, in the range between pure methanol and 60% CCl_4 v/v, is a further support for the proposed mechanism, since this property of the activation energy is characteristic for reactions producing ions. If the medium contains more than 60% CCl_4 v/v, E_a decreases significantly because the reactants are less solvated since methanol is not present at sufficient concentration, and/or another step producing no ions becomes rate controlling. If the latter is the case, this step is presumably the rearrangement of the nitrosamine $\text{Ph}\cdot\text{NH}\cdot\text{NO} \rightarrow \text{Ph}\cdot\text{N}\cdot\text{OH}$ (cf. eq 3), probably involving the protonation and subsequent deprotonation of the solvent. With decreasing methanol content of the medium the proton transfer becomes more and more difficult. By choosing the right experimental conditions¹⁴ the tautomerization can be slowed down to such an extent that diazotization practically stops at the nitrosamine stage. Consequently, rate eq 23 is valid with certainty only up to 60% CCl_4 v/v in accord with the mechanism proposed for pure methanol as solvent, and confirmed in $\text{CH}_3\text{OH}-\text{CCl}_4$ mixture, 1:1 by volume.

E. The diazotization of aniline with NOCl in pure carbon tetrachloride¹⁵ results in a heterogeneous mixture, because all polar products such as $[\text{PhN}_2]^+\text{Cl}^-$,

(11) Cf. A. A. Frost and R. F. Pearson, "Kinetics and Mechanism," 2nd ed, Wiley, New York, N. Y., 1965, p 140.

(12) Reference 11, p 137.

(13) K_1 of equilibrium 12 decreases with decreasing polarity of the solvent; e.g., in water at 0° $K_1 = 7.5 \times 10^{-5}$ (K. J. Pedersen, *Kgl. Danske Videnskab. Selskab, Mat.-Fys. Medd.*, 14, 9 (1937); 15, 3 (1937)) in comparison with $K_1 = 3 \times 10^{-7}$ in methanol at 2° (H. Schmid, A. Maschka, and W. Melhardt, *Monatsh. Chem.*, 99, 443 (1968)).

(14) PhNHNO as intermediate in diazotization was proved in ethyl ether at -78° by its uv spectrum by E. Müller and H. Haiss, *Chem. Ber.*, 96, 570 (1963). Under such experimental conditions the nitrosamine can be preserved for days.

(15) On the diazotization of aniline with NOCl in ethyl ether, cf. E. Bamberger, *Chem. Ber.*, 27, 668 (1894).

PhNH₂·HCl, and H₂O precipitate instantaneously, excluding the applicability of homogeneous kinetics. In such a case, one has to account also for transport phenomena and for the development of new phases and interfaces. However, by extrapolating the results obtained in CH₃OH-CCl₄ mixtures, where no precipitation occurs, one can readily obtain rate data (v_0) for 100% CCl₄ as medium (Figure 6). This is possible since all reaction rates determined in the mixtures, as

well as the values obtained for CCl₄ are initial rates, and at time zero diazotization is, even in a medium with $D_{0^{\circ}} = 2.291$, a homogeneous reaction.

Acknowledgements. The author wishes to thank Professor Emeritus H. Schmid for his advice, and Professor E. M. Eyring for helpful discussions and for his interest in this work, that was partially sponsored by AFOSR(SRC)-OAR, USAF, Grant No. 69-1717.

The Reduction of Ruthenium(III) Hexaammine by Hydrogen Atoms and Monovalent Zinc, Cadmium, and Nickel Ions in Aqueous Solutions

by G. Navon¹

Department of Physical Chemistry, The Hebrew University, Jerusalem, and Department of Chemistry, Tel-Aviv University, Tel-Aviv, Israel

and D. Meyerstein

Nuclear Research Center, Negev, Beer-Sheva, Israel (Received April 13, 1970)

The specific rates of reaction of H atoms, Zn⁺, Cd⁺, and Ni⁺ with Ru(NH₃)₆³⁺ were determined. The mechanism of reduction of hexaammine complexes by hydrogen atoms is discussed. It is suggested that hydrogen atoms might penetrate the ligand sphere and form a seven coordinated transition state. The redox potentials of the Zn⁺/Zn²⁺ and Cd⁺/Cd²⁺ couples are estimated as being equal to 2.0 ± 0.4 and 1.8 ± 0.4 V, respectively.

The specific rates of the reactions of hydrogen atoms,²⁻⁴ monovalent zinc, cadmium, and nickel ions,⁵ and hydrated electrons^{5,6} with a series of cobalt(III) complexes have been measured recently. It was found that the reactions of e_{aq}⁻ with all of these complexes are diffusion controlled. However, for the other strong reducing agents, many of the reactions are slower than diffusion controlled and the trend of reactivity toward the different complexes is similar to that found for the much slower reactions by mild reducing agents, *e.g.*, Cr²⁺, Ru(NH₃)₆²⁺, and V²⁺. The results were interpreted as indicating that whereas hydrogen atoms react only *via* the inner-sphere mechanism,²⁻⁴ the monovalent ions have varying mechanisms, being outer sphere for Zn⁺ and mostly inner sphere for Cd⁺ and Ni⁺. Hydrogen atoms are expected to react always *via* the inner-sphere mechanism as a reaction *via* the outer-sphere mechanism would yield either the non-hydrated H⁺ ion and therefore be an endothermic process or require a very high free energy of activation in order to obtain the hydrogen atoms in the configuration of the hydronium ions. However, it was found that H atoms react readily with Co(NH₂)₆³⁺,^{2,3} though it is

generally agreed that the latter complex can be reduced only *via* the outer-sphere mechanism.⁷

With the hope of obtaining more information on the mechanism of reduction of hexaammine complexes by strong reducing agents, the specific rates of reaction of Ru(NH₃)₆³⁺ with H atoms, Zn⁺, Cd⁺, and Ni⁺ have been measured. The choice of this complex ion was made because its reduced form, while having nuclear configuration similar to the analogous cobalt complex, has a completely different structure, having low spin configuration and no electrons in the e_g orbitals. Reduction of this complex by Cr²⁺ and V²⁺ have been recently measured.^{8,9}

(1) To whom correspondence should be addressed.

(2) G. Navon and G. Stein, *J. Phys. Chem.*, **69**, 1390 (1965).

(3) M. Anbar and D. Meyerstein, *Nature*, **206**, 816 (1965).

(4) J. Halpern and T. Rabani, *J. Amer. Chem. Soc.*, **88**, 699 (1966).

(5) D. Meyerstein and W. A. Mulac, *J. Phys. Chem.*, **73**, 1091 (1969).

(6) The specific rates of reaction with e_{aq}⁻ are tabulated in M. Anbar and P. Neta, *Int. J. Appl. Radiat. Isotopes*, **18**, 493 (1967).

(7) H. Taube and E. S. Gould, *Accounts Chem. Res.*, **2**, 321 (1969).

(8) J. E. Endicott and H. Taube, *J. Amer. Chem. Soc.*, **86**, 1686 (1964).

Experimental Section

Reaction with Hydrogen Atoms. Hydrogen atoms were produced in the gas phase and introduced into the aqueous solution using an apparatus which has been described previously.^{10,11} The reduction yields of $\text{Ru}(\text{NH}_3)_6^{3+}$ were determined following Endicott and Taube⁹ by addition of $\text{Co}(\text{NH}_3)_5\text{Br}(\text{ClO}_4)_2$ standard solution and determining its reduction spectrophotometrically at 252 $\text{m}\mu$ taking $\epsilon = 1.64 \times 10^4 \text{ M}^{-1} \text{ cm}^{-1}$ for $\text{Co}(\text{NH}_3)_5\text{Br}^{2+}$ at this wavelength. The calculations of rate constants have been done according to ref 12. The dose rates of introduction of hydrogen atoms into the solution were determined before and after each experiment by following the reduction of 10^{-3} M $\text{K}_3\text{Fe}(\text{CN})_6$ solution.¹²⁻¹⁴ The dose rates were in the range of $1.2\text{--}2.4 \times 10^{-4} \text{ M}^{-1}$ with a reproducibility better than 10%. The concentration of $\text{Ru}(\text{NH}_3)_6\text{Cl}_3$ was 0.01 M in all experiments. This was determined by weighing and spectrophotometrically confirming the value $\epsilon = 530 \text{ M}^{-1} \text{ cm}^{-1}$ at 276 $\text{m}\mu$.¹⁵ No other electrolyte was added to the reaction solution. The reaction time was 15 min for each experiment. The calculated rate constant was independent of dose rate.

Reactions with Monovalent Zinc, Cadmium, and Nickel Ions. The reactions with the monovalent cations were studied by the pulse radiolysis technique. The experiments were carried out by using pulses of 200-mA, 5-MeV electrons with a duration of 0.2–1.2 μsec obtained from the linear accelerator of the Hebrew University of Jerusalem. The experimental setup has been described in detail elsewhere.¹⁶

The monovalent zinc, cadmium, and nickel ions were formed by the reduction of the corresponding bivalent ions by the hydrated electrons. The specific rates of reaction of the monovalent cations with $\text{Ru}(\text{NH}_3)_6^{3+}$ were determined by following the decay of the light absorption due to the monovalent cations in the presence of different concentrations of $\text{Ru}(\text{NH}_3)_6^{3+}$ in the range of 0.05–0.6 mM . Divalent zinc, cadmium, and nickel ions were present as sulfate salts at a concentration of 0.02 M . The experimental procedure has been identical with that described earlier.⁵

Materials. Ruthenium(III) hexaammine chloride from Johnson, Matthey, and Co. was used after two further recrystallizations from dilute hydrochloric acid.^{17,18} All other chemicals were of analytical grade. Water was triply distilled.

Results and Discussion

The results are summarized in Table I. The specific rates of reaction of H atoms, Zn^+ , Cd^+ , and Ni^+ with $\text{Co}(\text{NH}_3)_6^{3+}$ and $\text{Co}(\text{NH}_3)_5\text{H}_2\text{O}^{3+}$ as well as those of $\text{Cr}_{\text{aq}}^{2+}$ and $\text{V}_{\text{aq}}^{2+}$ with the same oxidants are included for comparison. The uncertainty in the absolute values of the specific rates of reaction of hydrogen atoms determined by the present method may amount to a factor of 2.¹² However, their relative values are reliable to a

Table I: Specific Rates of Reduction of $\text{Ru}(\text{NH}_3)_6^{3+}$, $\text{Co}(\text{NH}_3)_6^{3+}$, and $\text{Co}(\text{NH}_3)_5\text{H}_2\text{O}^{3+}$

	E°, V	$\text{Ru}(\text{NH}_3)_6^{3+}$	$\text{Co}(\text{NH}_3)_6^{3+}$	$\text{Co}(\text{NH}_3)_5\text{H}_2\text{O}^{3+}$
Cr^{2+}	0.41 ^b	13 ^d	8.9×10^{-5} ^o	0.5 ^k
V^{2+}	0.25 ^b	42 ^e	3.7×10^{-3} ^o	0.5 ^o
Ni^+		4.0×10^8 ^f	$< 5 \times 10^8$ ^h	$< 5 \cdot 10^8$ ^h
Cd^+	1.8 ± 0.4 ^c	2.2×10^8 ^f	1.72×10^8 ^h	6.2×10^8 ^h
Zn^+	2.0 ± 0.4 ^c	2.2×10^8 ^f	8.4×10^8 ^h	1.56×10^9 ^h
H	2.28 ^c	1.8×10^8 ^f	1.85×10^8 ^{i,j}	4.5×10^8 ^{i,l}

^a Specific rate constants at room temperatures expressed in units of $\text{M}^{-1} \text{ sec}^{-1}$. ^b Reference 4. ^c See text. ^d $\mu = 7.4 \times 10^{-3}$; ref 9. ^e $\mu = 5.3 \times 10^{-3}$; ref 8. ^f Present work, maximal standard deviation $\pm 15\%$. The rates of H atoms at $\mu = 0.06$; of Ni^+ , Cd^+ , and Zn^+ at $\mu = 0.08$. ^o $\mu = 0.4$; ref 25. ^h Reference 5. ⁱ Reference 2. ^j Radiation chemical measurements of this rate constant gave the values of 1.6×10^8 (ref 3) and an upper limit of $1.3 \times 10^6 \text{ M}^{-1} \text{ sec}^{-1}$ (ref 4). ^k $\mu = 1.2$; H. Zwickel and H. Taube, *J. Amer. Chem. Soc.*, **81**, 1288 (1959). ^l Radiation chemical measurement gave an upper limit of $1.0 \times 10^6 \text{ M}^{-1} \text{ sec}^{-1}$ (ref 4).

higher degree. Particularly in the present case, where the three constants for H atoms given in the table have about the same magnitude, the approximations used in the calculation of the rate constants (such as the ignoring of possible scavenger depletion) will affect the results to the same degree. One may conclude that the reported ratio of the rate constants for the reduction of Ru^{III} and Co^{III} hexaammines by atomic hydrogen, which is 1.0, is correct within the experimental error of about $\pm 20\%$.

It is evident from Table I that the specific rate of reaction of all the reducing agents studied, excluding hydrogen atoms with $\text{Ru}(\text{NH}_3)_6^{3+}$, are considerably higher than those with $\text{Co}(\text{NH}_3)_6^{3+}$ and $\text{Co}(\text{NH}_3)_5\text{H}_2\text{O}^{3+}$. This is correct even for the reactions with Zn^+ and Cd^+ which approach the diffusion-controlled limit ($2 \times 10^9 \text{ M}^{-1} \text{ sec}^{-1}$) for these reactions.⁵ The reduction of $\text{Co}(\text{NH}_3)_6^{3+}$ and $\text{Ru}(\text{NH}_3)_6^{3+}$ by other metal ions are commonly believed to proceed *via* the outer-sphere mechanism.⁷ The difference in reactivity between $\text{Co}(\text{NH}_3)_6^{3+}$ and $\text{Ru}(\text{NH}_3)_6^{3+}$ is attributed to the difference in their electronic configuration and not to the small difference in their redox potentials.

(9) J. E. Endicott and H. Taube, *Inorg. Chem.*, **4**, 437 (1965).

(10) G. Czapski and G. Stein, *J. Phys. Chem.*, **63**, 850 (1959).

(11) G. Czapski, J. Jortner, and G. Stein, *ibid.*, **65**, 956 (1961).

(12) G. Navon and G. Stein, *ibid.*, **69**, 1384 (1965).

(13) G. Czapski and G. Stein, *ibid.*, **64**, 219 (1960).

(14) G. Navon and G. Stein, *ibid.*, **70**, 3630 (1966).

(15) H. Hartmann and C. Buschbeck, *Z. Phys. Chem.*, **11**, 120 (1957).

(16) Internal Report of Accelerator Laboratory, Hebrew University, Jerusalem, Israel.

(17) T. J. Meyer and H. Taube, *Inorg. Chem.*, **7**, 2369 (1968).

(18) The same order of magnitude for the ruthenium(II,III) hexaammine exchange rate constant was obtained (G. Navon, unpublished work) by using ¹⁴N nmr line broadening technique.

It has been pointed out by Orgel¹⁹ that electron transfer reactions to Co^{III} complexes are expected to be slow for two reasons. Octahedral Co^{II} complexes have the electronic configuration $t_{2g}^5 e_g^2$ as compared to t_{2g}^6 of Co^{III} complexes. The change of the cobalt spin multiplicity from 1 to 4 during the reduction of Co^{III} is one reason for a slow process. The second reason is that the two electrons in the e_g orbitals, having an antibonding character, should cause an increase in Co^{II}-ligand bond lengths as compared to these in the Co^{III} complexes. Therefore, the reorganization energy during the electron transfer should be appreciable. On the other hand, the ruthenium complex has a low spin configuration in both II and III oxidation states. Furthermore, as only the "nonbonding" t_{2g} orbitals are involved in the electron transfer process, there is reason to believe that the bond lengths in the two oxidation states do not differ appreciably. The difference between the cobalt and ruthenium complexes in relation to electron transfer reactions is also determined by the large difference in the specific rates of self-exchange between the di- and trivalent complexes which are less than $3.3 \times 10^{-12} M^{-1} \text{sec}^{-1}$ in the case of cobalt hexaammines²⁰ and equal to $8.2 \times 10^2 M^{-1} \text{sec}^{-1}$ for the analogous ruthenium complexes.^{17,18}

The equality between the specific rates of Ru^{III} and Co^{III} hexaammines by hydrogen atoms indicates that these reactions are not governed by spin selection rules and also not by reorganization energies as required by application of the Franck-Condon principle to electron transfer reactions.²¹ It has to be concluded therefore that the reductions by hydrogen atoms do not proceed *via* the outer-sphere mechanism. This conclusion seems reasonable if one considers the high amount of reorganization energy which is required for the formation of H_3O^+ from an H atom in a single step. An intermediate complex of H atom with the oxidizing agent, with a subsequent group transfer, or a reaction with the surrounding water molecules is therefore likely to occur. Such a mechanism rather than outer-sphere electron transfer seems to be common to all reduction reactions of atomic hydrogen in aqueous solutions.^{2-4,14} Atomic hydrogen has an exceptionally high redox potential of about $E^\circ = 2.28 \text{ V}$ in aqueous solution.^{22,23} This makes its reactions with $Co(NH_3)_6^{3+}$ and $Ru(NH_3)_6^{3+}$ very exergonic, with free energy changes of about -55 kcal (taking $E^\circ = 0.1 \text{ V}$ for both cobalt²⁴ and ruthenium¹⁷ hexaammines). However, this very large gain in free energy does not seem to account for the similar reactivity of the cobalt and ruthenium complexes toward the hydrogen atoms. For instance, Zn^+ and Cd^+ which also have high redox potentials (see below) react faster with ruthenium hexaamine in comparison with the analog cobalt complex.

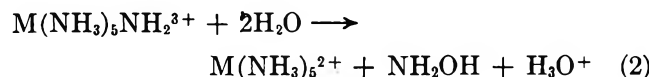
Another exceptional behavior of atomic hydrogen is in the reduction of $Co(NH_3)_5H_2O^{3+}$, which proceeds more slowly than the reduction of $Co(NH_3)_6^{3+}$. (See

Table I.) This is in contrast to all other reducing agents whose reduction rates toward the above complexes have been measured as yet. V^{2+} ,²⁵ $Cr(dipy)_3^{2+}$,²⁶ and $Ru(NH_3)_6^{3+}$,⁸ are known to react with $Co(NH_3)_5H_2O^{3+}$ about 10^2 times faster than with $Co(NH_3)_6^{3+}$. This fact has been taken²⁵ as an evidence that these complexes react by the same mechanism which is by outer-sphere electron transfer. It is interesting to note that a factor of about 10^7 is also predicted from Marcus' theory, taking redox potential values of $E^\circ = -0.33$ ²⁷ and -0.1 V ²¹ for $Co(NH_3)_5H_2O^{3+}$ and $Co(NH_3)_6^{3+}$, respectively, and assuming the same reorganization energy for these two complexes. Cr^{2+} reacts with $Co(NH_3)_5H_2O^{3+}$ faster than with $Co(NH_3)_6^{3+}$ by a factor of about 10^4 . This has been ascribed²⁸ to the availability of the electron pair on the water oxygen for an inner-sphere reaction. The fact that hydrogen atoms react with $Co(NH_3)_5H_2O^{3+}$ at a slower rate than with $Co(NH_3)_6^{3+}$ shows that the available electron pair of the water molecule is not important for the attack by hydrogen atoms and eliminates a bridged mechanism involving the coordinated water molecule.

Two possible alternative mechanisms of reaction can be suggested. (a) A hydrogen abstraction



followed by



Other oxidation products of NH_2 might be obtained. This mechanism seems as unreasonable as the reaction



in which the free energy gain is much larger than in reaction 1, is slow, or does not occur.²⁹ (b) Hydrogen

(19) L. E. Orgel, Report 10th Solvay Conference, Brussels, 289 (1956).

(20) Estimated for room temperature (reference 8) from the results of D. R. Stranks, *Discuss. Faraday Soc.*, 29, 73 (1960).

(21) For a review see: R. A. Marcus, *Annu. Rev. Phys. Chem.*, 15, 155 (1964); N. Sutin, *Annu. Rev. Nucl. Sci.*, 12, 285 (1962).

(22) G. Navon, Ph.D. Thesis, Jerusalem, Israel, 1965. The value usually quoted²³ for this potential, $E^\circ = 2.10 \text{ V}$, is that of the half-reaction $H_{\text{gas}} \rightarrow H_{\text{ac}}^+ + e_{\text{aq}}^-$. The value $E^\circ = 2.28 \text{ V}$ has been estimated for the more relevant half-reaction $H_{\text{aq}} \rightarrow H_{\text{aq}}^+ + e_{\text{aq}}^-$, assuming equal solubility for atomic and molecular hydrogen in water. Note that even a factor of 5 in the assumed solubility of atomic hydrogen amounts only to a change of 0.04 V in the estimated E° .

(23) For example, "Handbook of Chemistry and Physics," 43rd ed, Chemical Rubber Publishing Co., Cleveland, Ohio, 1961; J. H. Baxendale, *Radiat. Res. Suppl.*, 4, 114 (1964).

(24) W. M. Latimer, "Oxidation Potentials," Prentice-Hall, New York, N. Y., 1952.

(25) A. Zwickel and H. Taube, *J. Amer. Chem. Soc.*, 83, 793 (1961).

(26) A. Zwickel and H. Taube, *Discuss. Faraday Soc.*, 29, 73 (1960).

(27) R. G. Yalman, *Inorg. Chem.*, 1, 16 (1962).

(28) H. Taube, *Advan. Inorg. Chem. Radiochem.*, 1, 1 (1959).

(29) D. Katakis and A. O. Allen, *J. Phys. Chem.*, 68, 1359 (1964).

atoms, being very small, might penetrate the coordination sphere of the central cation and become a seventh ligand in the transition state. (That this is possible has been checked on a scale model of the complexes.)

Although the latter mechanism seems to be the most probable for the reaction of hydrogen atoms with hexammine complexes, it should be noted that this mechanism does not fully explain the fact that the specific rates of reaction of H atoms with the $\text{Ru}(\text{NH}_3)_6^{3+}$ and $\text{Co}(\text{NH}_3)_6^{3+}$ are equal.

The redox potentials of the monovalent cations can be roughly estimated from their specific rates of reaction with $\text{Co}(\text{NH}_3)_6^{3+}$ and $\text{Ru}(\text{NH}_3)_6^{3+}$ if one assumes that these reactions are outer-sphere ones and that the Marcus theory can be applied to them. According to Marcus,²² the specific rate of reduction, k_{12} can be calculated using the relations

$$k_{12} = (k_{11}k_{22}K_{12}f)^{1/2};$$

$$\log f = (\log K_{12})^2/4 \log (k_{11}k_{22}/Z^2) \quad (4)$$

where k_{11} and k_{22} are the specific rates of exchange between the oxidized and reduced states of both reactants, K_{12} is the equilibrium constant of the reaction, and $Z = 10^{11} \text{ M}^{-1} \text{ sec}^{-1}$.

For rate constants (k_{obs}) approaching the diffusion-controlled limit (k_{diff}), the following equation must be taken into consideration.³⁰

$$k_{\text{obs}}^{-1} = k_{\text{act}}^{-1} + k_{\text{diff}}^{-1} \quad (5)$$

The activation-controlled constant k_{act} is the one calculated by eq 4. Considering the limiting rate constants obtained for the reactions of monovalent metal ions with cobalt and ruthenium complexes (Table I and ref 5), the rate constants of Zn^+ and Cd^+ with $\text{Ru}(\text{NH}_3)_6^{3+}$ can be taken as the diffusion-controlled rate constant, *i.e.* $k_{\text{diff}} = 2.2 \times 10^9 \text{ M}^{-1} \text{ sec}^{-1}$. Cobalt hexammine(II–III) exchange rate constant is known to be less than $3 \times 10^{-12} \text{ M}^{-1} \text{ sec}^{-1}$.²⁰ Only limits can be given for the monovalent–divalent exchange rate constant k_{22} . As an upper limit, the value $1 \times 10^9 \text{ M}^{-1} \text{ sec}^{-1}$, which approaches the diffusion-controlled limit can be taken and a value of $k_{22} = 1 \text{ M}^{-1} \text{ sec}^{-1}$ seems to be a generous lower limit for such cations having the exchanging electron in an s orbital. Using eq 4 and 5 and the known redox potential of the $\text{Co}(\text{NH}_3)_6^{2+}/\text{Co}(\text{NH}_3)_6^{3+}$ couple the values $E^\circ = 2.0 \pm 0.4 \text{ V}$ and $E^\circ = 1.8 \pm 0.4 \text{ V}$ are calculated for the redox potentials of the $\text{Zn}^+/\text{Zn}^{2+}$ and $\text{Cd}^+/\text{Cd}^{2+}$ couples, respectively. These values are in fair agreement with the values estimated from thermodynamic data;³¹ *i.e.*, 2.5–3.2 V for Zn^+ and 1.9–2.5 V for Cd^+ . The same calculation carried out for the $\text{Ni}^+/\text{Ni}^{2+}$ couple taking

$k_{12} = 4.0 \times 10^8 \text{ M}^{-1} \text{ sec}^{-1}$ for the $\text{Ni}^+ + \text{Ru}(\text{NH}_3)_6^{3+}$ reaction, $k_{11} = 8 \times 10^2 \text{ M}^{-1} \text{ sec}^{-1}$ for the $\text{Ru}(\text{NH}_3)_6^{2+/3+}$ exchange reaction,^{17,18} and assuming $1 < k_{22} < 10^9 \text{ M}^{-1} \text{ sec}^{-1}$ yields $E^\circ = 0.7 \pm 0.4 \text{ V}$. However, in the case of nickel ions it is not clear that the assumption of $k_{22} = 1 \text{ M}^{-1} \text{ sec}^{-1}$ is a lower limit as Ni^+ has a d^9 configuration with a possible Jahn–Teller distortion which does not apply to Ni^{2+} with the d^8 configuration. Therefore, E° for the $\text{Ni}^+/\text{Ni}^{2+}$ couple might approach the upper limit (1.1 V) of the estimated value. The redox potential for the $\text{Ni}^+/\text{Ni}^{2+}$ estimated from thermodynamic data³¹ is much higher (2.7 V) than that obtained in the above calculations.

The redox potentials thus obtained for the $\text{Zn}^+/\text{Zn}^{2+}$ and $\text{Cd}^+/\text{Cd}^{2+}$ can be used to check the Marcus theory for calculating the specific rates of reaction of the hydrated electron³⁰ with the divalent cations. From these specific rates of reaction and Marcus' theory, the redox potentials of the couples $\text{Zn}^+/\text{Zn}^{2+}$ and $\text{Cd}^+/\text{Cd}^{2+}$ were estimated as $E_0 = 1.0 \text{ V}$ and $E^\circ \leq 0.5 \text{ V}$, respectively.³² The discrepancy between the latter values and the values estimated in this study is too large to be adjustable by the assumptions. This together with earlier suggestions based on kinetic data^{32,33} indicates that the Marcus theory is rather limited in explaining the reactions of hydrated electrons.

Finally, from the redox potentials of the couples $\text{Zn}^+/\text{Zn}^{2+}$ and $\text{Cd}^+/\text{Cd}^{2+}$ estimated in the present work and from the known²⁴ redox potentials of 0.76 and 0.40 V for the couples $\text{Zn}^0/\text{Zn}^{2+}$ and $\text{Cd}^0/\text{Cd}^{2+}$, respectively, the redox potentials of the couples Zn^0/Zn^+ and Cd^0/Cd^+ can be estimated as $E^\circ = -0.5 \pm 0.4 \text{ V}$ and $E^\circ = -1.0 \pm 0.4$, respectively. These negative values might explain why there is no evidence for the formation of monovalent zinc or cadmium ions in the dissolution of the metals or the electrolytic reduction of the divalent cations in aqueous solutions in the absence of stabilizing ligands.

Acknowledgments. The authors are indebted to Professor G. Stein for his encouragement and fruitful discussions. This research was supported in part by the U. S. Atomic Energy Commission, Biology Division. We also wish to thank the Linac group at the Hebrew University of Jerusalem for their assistance in carrying out the pulse-radiolytic experiments.

(30) R. A. Marcus, *J. Chem. Phys.*, **43**, 3477 (1965); *Advan. Chem. Series*, **50**, 138 (1965).

(31) J. H. Baxendale and R. S. Dixon, *Z. Phys. Chem. (Frankfurt am Main)*, **43**, 161 (1964).

(32) M. Anbar and D. Meyerstein, *Trans. Faraday Soc.*, **65**, 1812 (1969).

(33) D. Meyerstein and W. A. Mulac, *ibid.*, **65**, 1818 (1969).

The Reactions of Methyl Benzoate and Methyl Formate with Hydrogen Bromide and Hydrogen Iodide^{1a}

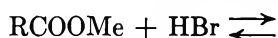
by Richard K. Solly^{1b} and Sidney W. Benson

Department of Thermochemistry and Chemical Kinetics, Stanford Research Institute, Menlo Park, California 94025
(Received January 5, 1970)

The gas phase reactions of methyl benzoate and methyl formate with hydrogen bromide and hydrogen iodide in the temperature range 340–430° are shown to yield the corresponding carboxylic acid and alkyl halide as major products. The methyl ester–hydrogen halide system has been previously reported to yield only acid halide and methanol. The relative amounts of products from the two mechanisms are compared.

Introduction

Stimson and coworkers² have previously postulated that the gas phase reactions of methyl esters with HBr



proceed *via* the acyl bromide and methanol. Appreciable amounts of MeBr were also formed, which was presumed to be formed from the further reaction of MeOH.



During a study of the reactions of iodine atoms with methyl formate³ and methyl benzoate,⁴ we observed that MeI was produced with excess HI. The reaction was followed *in situ* using spectroscopic techniques, but there was no evidence for the formation of benzoyl iodide from methyl benzoate. The reaction of PhCOOMe with HBr was similarly investigated, and only trace amounts of PhCOBr were detected. In this paper, we present our results for PhCOOMe and HCOOMe and propose an alternate mechanism for the formation of MeI or MeBr. With methyl trimethylacetate, this is shown to account for several discrepancies in the kinetics of the reaction with HBr.^{2a}

Experimental Section

Materials. Methyl benzoate and methyl formate from Eastman Kodak and Matheson benzoyl bromide were fractionated on the vacuum line until gas chromatographically pure. Matheson anhydrous HI and HBr were similarly purified by fractional distillation on the vacuum line.

Apparatus. The reaction was investigated in a cylindrical quartz reaction vessel, thermostated with air inside a heated aluminum block. The ultraviolet and visible absorption of the reacting species was monitored with a Cary Model 15 spectrometer, as described previously.⁵ Pressures were measured with a Pace differential transducer using helium as a buffer between the

metal diaphragm and the reaction mixture. For runs below 360°, the reaction vessel was conditioned by the polymerization of 120 Torr of C₂F₄ with di-*tert*-butyl peroxide in the vessel at 200°. Above 360° the Teflon coating was unstable, and a carbon coating was deposited by pyrolyzing pentene for several hours at 440°.

A reaction vessel, packed with pieces of glass tubing so that the surface-to-volume ratio was eight times that of the unpacked vessel, was also used for several runs. The surface of this vessel was treated as for unpacked vessels. Rates measured in the packed vessel, as determined from halogen and noncondensable gas formation, and overall pressure increase were always faster than in the unpacked vessel. Reproducible results could not be obtained, in spite of repeated attempts to condition the vessel. Even at temperatures below 350°, noncondensable gases were formed from PhCOOMe in the presence of HBr and HI.

Procedure. The reaction vessel was evacuated to below 10⁻⁴ Torr prior to a run. The required pressure of degassed PhCOOMe or HCOOMe was admitted to the reaction vessel by heating the storage vessel. After the reagent had been pumped from the heated inlet manifold, HI or HBr was added to the reaction vessel and the total pressure was measured. Owing to the higher vapor pressure of HCOOMe, it was added to the HI or HBr in the majority of runs. Reaction times were determined from the synchronous chart drive and an electric timer. With HI the absorption was followed at 260, 270, and 490 mμ, and at 250 and 260 mμ with HBr. The optical density of PhCOOMe, PhCOOH,

(1) (a) This work was supported in part by Grant AP 00353-04 of the Public Health Service, Division of Air Pollution; (b) Post-doctoral Research Associate; to whom correspondence should be addressed.

(2) (a) J. T. D. Cross and V. R. Stimson, *Aust. J. Chem.*, **21**, 687 (1968); (b) D. A. Kairaitis and V. R. Stimson, *ibid.*, **21**, 1711 (1968).

(3) R. K. Solly and S. W. Benson, *Int. J. Chem. Kin.*, **1**, 427 (1969).

(4) R. K. Solly and S. W. Benson, *ibid.*, submitted.

(5) R. Walsh and S. W. Benson, *J. Amer. Chem. Soc.*, **88**, 4570 (1966).

PhCOBr, MeI, MeBr, HI, and HBr was determined prior to the reaction studies and used to follow the course of the reaction.

The pressure of the reaction mixture was determined by nulling both sides of the differential transducer with He to the estimated reaction pressure. The reaction vessel was momentarily opened to one side of the transducer, and any small difference between the actual and estimated pressure was measured on an oil manometer. By this means, absolute pressures could be measured to 0.1 Torr.

After the He had been pumped from the inlet manifold, the contents of the reaction vessel were condensed in a liquid nitrogen cooled trap. Uncondensed gases were concentrated in a gas buret with a Toepler pump. The liquid nitrogen condensate was fractionally distilled by replacing the liquid nitrogen with an ethanol-liquid nitrogen slush bath (HBr reaction mixture) or an acetone-liquid nitrogen slush bath (HI reaction mixture). The distillate, consisting mostly of HBr or HI, was discarded. The distillate from a salt-ice bath was condensed in a gas pipet with liquid nitrogen prior to gas chromatographic analysis from the vapor phase. Only polymeric residue remained from the HCOOMe reaction mixture, and no attempt was made to analyze this further. The residue from the PhCOOMe reaction mixture was washed from the trap with hexane, and the hexane solution was analyzed by vpc. The residue from some runs was washed from the trap with water. Recrystallization from water gave white crystals having an infrared spectrum (NaCl disk) identical with that of an authentic sample of benzoic acid. A sample of benzoyl bromide was mixed with water and worked up under the same conditions as used for the reaction mixture residue. No evidence for hydrolysis to benzoic acid could be detected.

All vpc analysis was on an F & M Model 810 gas chromatograph equipped with both thermal conductivity and flame ionization detectors. Permanent gases were analyzed on a molecular sieve column, the salt-ice distillate on hallcomid and silicone oil columns, and the hexane solution of the residue on silicone gum rubber.

Results and Discussion

The reaction of PhCOOMe with HBr was followed spectroscopically over the range 245–300 nm. The rate of change of absorbance at 349° was very small. Considering the absorbance changes as being due solely to reaction 2, only 4% of the PhCOOMe had been converted into PhCOBr after 21 hr (run 1, Table I). At



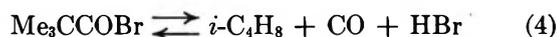
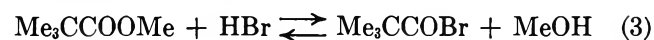
250 nm, $\epsilon(\text{PhCOBr}) \approx 10\epsilon(\text{PhCOOMe}) \gg \epsilon(\text{HBr})$ and $\epsilon(\text{MeBr})$, and the absolute detection limit for PhCOBr is 0.02 Torr. On increasing the reaction temperature to 384°, the maximum conversion of PhCOOMe into PhCOBr was 3% after 100 min (run 4).

The reaction mixture from runs 1 and 4 was condensed in a liquid nitrogen trap and worked up as described in the Experimental Section. At least 16 products were detected by vpc analysis. The major components had peaks with the same retention time as MeBr and PhCOOH, with a peak corresponding to PhCOBr being a minor component. No attempt was made to quantitatively analyze the condensation products, as many are probably formed in the liquid phase. The PhCOOH was further identified by recrystallization from water and comparison of the infrared spectrum with an authentic sample. In a blank run, it was found that at least 5 mg of PhCOOH was required to obtain recrystallization. This is equivalent to a conversion of a minimum of 30% of the PhCOOMe into PhCOOH.

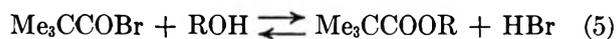
The mechanism proposed by Stimson and coworkers (mechanism 1) offers no route for the formation of PhCOOH. We propose this is formed by a concerted mechanism analogous to reaction 1.



The results reported by Cross and Stimson^{2a} for the reaction of Me₃CCOOMe with HBr are based solely on mechanism 1. They obtained fall-off from pseudo-



first-order behavior in MeC₃COOMe, as would occur if K₃ was a rapid preequilibrium, and k₄ rate determining. However, thermodynamic considerations show that their suggestion (of reaction 4 being reversible) is incorrect. Reaction -4 is negligible compared to reaction 4. Their order dependence on Me₃CCOOMe is first order at low concentrations and zero order at higher concentrations. Small additions of MeOH and H₂O decreased the rate of CO formation, but larger concentrations had no further effect. If we apply the steady-



state approximation to reaction 3, 4, and 5, the rate of formation of *i*-C₄H₈ is given by

$$\frac{d[i\text{-C}_4\text{H}_8]}{dt} = \frac{k_4[\text{HBr}](k_3[\text{Me}_3\text{CCOOMe}] + k_{-5}[\text{Me}_3\text{CCOOR}])}{k_{-3}[\text{MeOH}] + k_4 + k_5[\text{ROH}]} \quad (I)$$

In deriving this expression, reaction -4 is assumed to be negligible. For the case where ROH = MeOH, the rate simplifies to

$$\frac{d[i\text{-C}_4\text{H}_8]}{dt} = \frac{k_4k_3[\text{HBr}][\text{Me}_3\text{CCOOMe}]}{k_{-3}[\text{MeOH}] + k_4} \quad (II)$$

It may be seen that the pseudo-first-order rate in HBr is invariant. Similarly, the inhibiting effect of small

Table I: Reaction of PhCOOMe with HBr

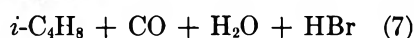
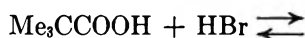
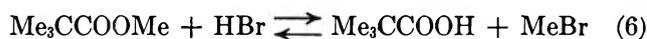
Run	Temp, °C	[PhCOOMe] ₀ , Torr	[HBr] ₀ , Torr	Time, sec	PhCOBr, Torr	Time, sec	ΔP, Torr	Time, sec	[CH ₄] + [CO], Torr
1	349.4	10.3	36.9	76000	0.45	1450	0.0	1650	0.0
2	349.5	14.0	33.0	45600	0.50	1600	0.0	1800	0.1
3	383.9	11.0	31.9	3400	0.32	3200	+0.1	3400	0.4
4	383.8	11.0	44.2	6000	0.35	7000	+0.7	7450	1.1

Table II: Reaction of PhCOOMe with HI

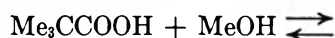
Run	Temp, °C	[PhCOOMe] ₀ , Torr	[HI] ₀ , Torr	Time, sec	ΔP, Torr	Time, sec	[I ₂], Torr	[CH ₄], Torr	[CO], Torr
5	349.5	12.8	39.8	2300	+0.25	2600	6.8	7.5	0.6
6	385.1	10.5	43.6	2300	+2.2	2650	2.9	3.0	2.8

amounts of added MeOH should also be invariant first order.

The observed kinetics for the reaction of Me₃CCOOMe with HBr may be better explained by mecha-



nism 2. Reaction 7 has previously been reported by Cross and Stimson.⁶ The inhibiting effect of MeOH is in esterifying the acid. The esterification of Me₃-



CCOOH with isopropyl alcohol in the presence of HBr has previously been observed.⁷ The formation of isopropyl trimethylacetate on addition of isopropyl alcohol to a reaction mixture of Me₃CCOOMe and HBr has also been reported.⁸

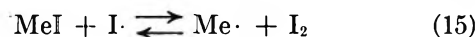
Reactions 6, 7, and 8 do not offer an explanation for the fall-off from first-order behavior with high HBr concentration or the inhibiting effect of H₂O. These effects would suggest that reaction 6 is partly surface catalyzed. Small concentrations of HBr will have first-order absorption characteristics, while larger concentrations will tend toward zero order. The effect of H₂O is to compete with Me₃CCOOH and HBr for reactive surface sites. This is also subject to a surface saturation effect, and the order dependence will tend toward zero at high H₂O concentrations.

At 384° in the reaction of PhCOOMe with HBr (Table I), there is a small pressure increase and the formation of noncondensable gases. This is probably due to radical reactions resulting from the presence of trace amounts of bromine and bromine atoms.



As expected from reactions 9–14, peaks with retention times corresponding to benzaldehyde and benzene were detected in the reaction products.

The reaction of PhCOOMe + HI was also investigated (Table II); but this system is greatly complicated by radical reactions. As with HBr, PhCOOH was a major component of the reaction product. However, even at 350°, appreciable amounts of iodine and methane were formed. In the PhCOOMe-alkyl halide reaction system, whereas bromine atoms will preferentially abstract hydrogen atoms, iodine atoms will preferentially abstract iodine atoms, with a subsequent branching of the iodine atom concentration. Consequently, CH₄ was the major component of the noncondensable gases. Appreciable quantities of CO were also formed,



but this may follow from a radical abstraction reaction analogous to reaction 9, or from the concerted mechanism 1. Any MeOH formed is also subject to radical



decomposition⁸ or esterification with PhCOOH. The



(6) J. T. D. Cross and V. R. Stimson, *J. Chem. Soc. B*, 88 (1967).

(7) J. T. D. Cross and V. R. Stimson, *Aust. J. Chem.*, 21, 701 (1968).

(8) J. T. D. Cross and V. R. Stimson, *ibid.*, 21, 713 (1968).

Table III: Reaction of HCOOMe with HBr

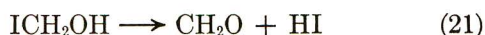
Run	Temp, °C	[HCOOMe] ₀ , Torr	[HBr] ₀ , Torr	Time, sec	ΔP, Torr	Time, sec	[MeBr] ₀ , Torr	[CH ₄] ₀ , Torr	[CO] ₀ , Torr
7	384.4	90.4	42.6	1450	13.4	1650	9.4	3.9	13.4
8	434.7	16.5	41.8	2500	9.2	2700	6.9	10.5	

Table IV: Reaction of HCOOMe with HI

Run	Temp, °C	[HCOOMe] ₀ , Torr	[HI] ₀ , Torr	Time, sec	ΔP, Torr	Time, sec	[I ₂] ₀ , Torr	[CH ₄] ₀ , Torr	[CO] ₀ , Torr
9	339.8	91.0	44.0			950	6.4	6.9	2.0
10	383.5	70.0	58.0	850	9.2	1070	5.1	8.7	10.4
11	383.5	7.0	40.8	1000	0.8	1300	1.1	0.9	1.3

Table V: Reaction of MeOH with HBr

Run	Temp, °C	[MeOH] ₀ , Torr	[HBr] ₀ , Torr	Time, sec	ΔP, Torr	Time, sec	[MeBr] ₀ , Torr	[CO] ₀ , Torr
12	431.9	9.1	51.6	3100	0.0	3500	3.1	0.0



area of the peak with the same retention time as MeOH was less than 0.01% of that due to MeI in reaction 6. The instability of MeOH in the system was shown experimentally by adding 1 Torr to a reaction mixture at 385°. Less than 0.01 Torr was recorded at the flame ionization detector after the normal workup procedure.

Further evidence for mechanism 2 was found in the reaction of HBr and HI with methyl formate. The formation of methyl halide may be measured *in situ*, the absorption no longer being obscured by the aromatic species. As may be seen from Tables III and IV, appreciable quantities of methyl halide were formed with both HBr and HI. There are three possible routes for the formation of MeBr or MeI. It may be formed following radical abstraction from methyl formate.³



Reactions 25 and 26 have been discussed previously,³ and the rate is determined by the concentration of X·. However, competition between reactions 27 and 28 is the critical factor determining the rate of formation of MeX. The ratio of the rate constants k_{27}/k_{28} is approx-

imately 10.⁹ The average concentration ratio, $[\text{X}_2]/[\text{HX}]$, was less than 0.005 for the bromine system and approximately 0.05 for the iodine system, the halogen concentration being measured in the visible region of the spectrum. The low concentration of Br₂ is due to the preferential abstraction of hydrogen atoms by Br·, compared to preferential abstraction of iodine atoms by I·. In the bromine system, for which the ambiguity is less owing to the low Br₂ concentration, any Me· radicals will be trapped as MeH and will not form MeX.

Another route for the formation of MeX is from reaction -28. The H₃C-H bond strength is 104 kcal/mol,^{3,10} compared to 93 for H-COOMe.³ Furthermore, the average concentration of HCOOMe was at least 20 times that of CH₄, so that reaction -30 will not compete with reaction 27.

A third route for the formation of MeX is from reaction 29. This reaction has been previously observed



by Cruickshank and Benson¹¹ and postulated by Cross and Stimson^{2a} to explain the formation of MeBr in their system. However, a blank run in our system (Table V) showed that the rate of reaction 29 was too slow even at 432° to explain the formation of MeBr. The MeBr, and probably part of the MeI, must be formed by the molecular mechanism 2.

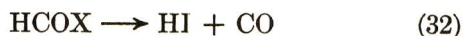


(9) D. M. Golden and S. W. Benson, *Chem. Rev.*, **69**, 125 (1969).

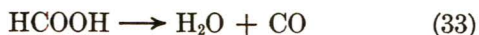
(10) C. A. Goy and H. O. Pritchard, *J. Phys. Chem.*, **69**, 3040 (1965).

(11) F. R. Cruickshank and S. W. Benson, *ibid.*, **73**, 733 (1969).

The formation of CO may be regarded as evidence for a concurrent reaction by mechanism 1. However, CO



may also be formed from the decomposition of formic acid. Arrhenius parameters have been reported for



reaction 33,¹² but they are not consistent with a homogeneous reaction. By analogy with other systems,⁶ reaction 34 is likely to occur in the temperature range 380–430°. Considering run 7, and assuming all the HCOOH decomposes to CO and H₂O, the maximum amount of CO formed *via* reaction 30 is 9.4 Torr. As the measured amount was 13.4 Torr, at least 4 Torr must be formed *via* reaction 31.

Conclusion

The formation of benzoic acid from methyl benzoate is indicative that mechanism 2 is a prominent route in the gas phase decomposition of methyl esters in the presence of HBr or HI. Further evidence for this mechanism is found in the formation of significant quantities of MeBr or MeI from the gas phase reaction of methyl formate with HBr or HI.

By direct measurement of the formation of PhCOBr in the PhCOOMe–HBr system, mechanism 1 was found to be a minor reaction. In the HCOOMe–HBr system, upper and lower limits for the ratio of mechanism 1 to mechanism 2 may be established by assuming no decomposition of HCOOH to CO, and 100% decomposition to CO, respectively. Equating the amount of HCOOH to MeBr, in run 7 the upper and lower limits are 1.4:1 and 0.4:1, respectively.

Our experience with the packed reaction vessel and the inhibition effects reported by Cross and Stimson^{2a} for the Me₃CCOOMe–HBr system would suggest that these reactions are at least partly heterogeneous. Consequently, in this paper the emphasis has been on product identification, rather than kinetic analysis.

The free energy of the reaction forming RCOOH and MeX is also greatly favored over that for formation of RCOX and MeOH. Considering the PhCOOMe–HBr system, and using group values¹³ for the thermodynamic parameters which have not been reported, the free-energy change at 350° for mechanism 1 is 4.8 kcal/mol, compared to –6.2 kcal/mol for mechanism 2.

(12) P. G. Blake and C. Hinshelwood, *Proc. Roy. Soc., Sec. A*, **255**, 444 (1960).

(13) S. W. Benson, F. R. Cruickshank, D. M. Golden, G. R. Haugen, H. E. O'Neal, A. S. Rodgers, R. Shaw, and R. Walsh, *Chem. Rev.*, **69**, 279 (1969).

Kinetics of the Shock-Initiated Decomposition of 1,1-Difluoroethylene

by J. M. Simmie^{1a} and E. Tschuikow-Roux^{1b}

Department of Chemistry, University of Calgary, Calgary, Alberta, Canada (Received May 6, 1970)

The decomposition of 1,1-difluoroethylene has been studied in a single-pulse shock tube over the temperature range of 1290 to 1700°K at total reflected shock pressures of about 3 to 4 kTorr and reaction dwell times of about 10^{–8} sec. At low conversions, below 1480°K, the principal reaction is the unimolecular elimination of HF with the first-order rate constant given by $k = 10^{14.4 \pm 1.1} \exp[-(86,000 \pm 6800)/RT]$ sec^{–1}. At temperatures in excess of 1500°K, corresponding to extents of reaction greater than 5%, the mechanism becomes very complex with over 18 products being observed.

As recently as last year (1969) it was possible to state in a review² of the pyrolysis of alkyl halides in the gas phase that “the direct investigation of the pyrolysis of alkyl fluorides containing a β-carbon–hydrogen bond has not yet been achieved.” However, of late there has been an upsurge of interest in the pyrolytic dehydrofluorination reactions of fluorohydrocarbons. Successful pyrolysis of ethyl fluoride³ and 1-chloro-1-

fluoroethane⁴ has been reported in static systems and of the series CH₃CH_iF_{3–i} (*i* = 0, 1, 2) in a flow system.⁵ In addition, two different kinds of shock tube techniques

(1) (a) Postdoctorate Fellow, 1968–1970; (b) to whom correspondence should be addressed.

(2) A. Maccoll, *Chem. Rev.*, **69**, 33 (1969).

(3) M. Day and A. F. Trotman-Dickenson, *J. Chem. Soc. A*, 233 (1969).

have been used to study dehydrofluorination reactions. In direct studies in this laboratory, we have observed HF elimination from vinyl fluoride⁶ and 1,1-difluoroethane,⁷ while Cadman, *et al.*,⁴ using competitive methods, have reported the Arrhenius parameters for a number of alkyl fluorides. These latter authors have also included more detailed results of previous work,⁸⁻¹⁰ which was based on the application of the Rice-Ramsperger-Kassel-Marcus (RRKM) theory of unimolecular reactions to chemically activated molecule decomposition data.

Chemical activation studies of a number of fluoroalkanes are referenced in a recent paper by Chang and Setser¹¹ on the unimolecular reaction and collisional deactivation of chemically activated 1,2-difluoroethane. Considerably more information on the critical energies for HF elimination, determined by the application of nonequilibrium RRKM theory to chemical activation data, is shortly to be published for the following compounds:¹² $\text{CH}_3\text{CH}_2\text{CHFCH}_3$; $\text{CH}_3\text{CF}_2\text{CH}_3$; $\text{CH}_3\text{CH}_2\text{CH}_i\text{F}_{3-i}$ ($i = 0, 1$), $\text{CH}_i\text{F}_{3-i}\text{CH}_j\text{F}_{3-j}$ ($i = 1, j = 1, 2$ and $i = 2, j = 2$), and $\text{CH}_3\text{CClH}_i\text{F}_{2-i}$ ($i = 0, 1$).

Studies of a more fundamental nature on the product energy states have been performed by Clough, *et al.*¹³ They have examined the vibrational energy distribution of HF, eliminated from nonthermally activated CH_3CF_3 and CH_2CF_2 , in a fast-flow system. They find that the hydrogen fluoride eliminated from Hg-(6^3P_1) photosensitized activation of CH_2CF_2 has considerable excess vibrational and rotational energy. They suggest that the "reverse" activation energy is channeled into the vibrational mode and that the rotational excitation arises from a highly repulsive transition state.

This paper is the second in a series of studies on the kinetics of hydrogen fluoride elimination reactions of alkenyl fluorides.

Experimental Section

Both the modified single-pulse shock tube and the general techniques employed have been fully described in previous communications.^{14,15}

1,1-Difluoroethylene was obtained commercially (Matheson, 99.0% stated minimum purity) and tested for impurities by mass spectrometry and gas chromatography. No significant ($\leq 0.5\%$) impurities were detected; in particular monofluoroacetylene was below the limit of detectability (estimated at ≤ 10 ppm). Reaction mixtures of 1.0 and 2.6% difluoroethylene in argon (Matheson, 99.998% stated purity) were used for kinetic data below 1480°K, and total product analysis above 1500°K, respectively. Samples of the reacted mixture were drawn in the usual manner and analyzed on a gas chromatograph (Varian 1700; 12-ft column of silica gel at 75° with a flow rate of 30 cm^3 He min^{-1}) equipped with flame ionization detectors. For analysis of the products of high-temperature runs, the contents of

part of the low-pressure side of the shock tube (isolated by a ball-valve) were pumped through a copper coil immersed in liquid nitrogen. The trapped compounds were then transferred to Pyrex ampoules which were later sealed off *in vacuo*. These were then run through a coupled mass spectrometer-gas chromatograph (ms-gc).

Results

The decomposition of 1,1-difluoroethylene in shock waves is complex. We have quite arbitrarily divided the pyrolysis results of 1,1- $\text{C}_2\text{H}_2\text{F}_2$ into two ranges: (a) the high-temperature region, above 1500°K, and (b) the low-temperature region $\leq 1480^\circ\text{K}$.

A. *High-Temperature Results.* Shocks into 2.6% 1,1- $\text{C}_2\text{H}_2\text{F}_2$ in argon generating reflected-shock temperatures of more than 1500°K for dwell times of about 1 msec gave over 18 detectable volatile products and, in addition, deposited a carbon film on the walls of the shock tube. The major volatile products are listed in Table I in the order of their elution from a silica gel

Table I: Analysis of Products from High-Temperature Shocks of 1,1- $\text{C}_2\text{H}_2\text{F}_2$

Product identity	Evidence	
	gc	ms
C_2H_6	+	
C_2HF	+	+
C_2F_4	+	+
C_2H_4	+	
$\text{C}_2\text{H}_2\text{F}_2$		Reactant
C_2H_2	+	+
C_2HF_3	+	+
$\text{C}_2\text{H}_3\text{F}$	+	+
$\text{C}_2\text{H}_3\text{F}_3$		+
$\text{C}_4\text{H}_5\text{F}_2$ (?)		+
C_4H_2		+

(4) P. Cadman, M. Day, A. W. Kirk, and A. F. Trotman-Dickenson, *Chem. Commun.*, 203 (1970).

(5) D. Sianesi, G. Nelli, and R. Fontanelli, *Chim. Ind.*, **50**, 619 (1968).

(6) J. M. Simmie, W. J. Quiring, and E. Tschuikow-Roux, *J. Phys. Chem.*, **74**, 992 (1970).

(7) E. Tschuikow-Roux, W. J. Quiring, and J. M. Simmie, *ibid.*, **74**, 2449 (1970).

(8) A. W. Kirk, Ph.D. Thesis, University of Wales, Aberystwyth, 1968.

(9) J. A. Kerr, A. W. Kirk, B. V. O'Grady, D. C. Phillips, and A. F. Trotman-Dickenson, *Discuss. Faraday Soc.*, **44**, 263 (1967).

(10) A. W. Kirk, A. F. Trotman-Dickenson, and B. L. Trus, *J. Chem. Soc. A*, 3058 (1968).

(11) H. W. Chang and D. W. Setser, *J. Amer. Chem. Soc.*, **91**, 7648 (1969).

(12) A. W. Kirk, private communication.

(13) P. N. Clough, J. C. Polanyi, and R. T. Taguchi, *Can. J. Chem.*, in press. We thank Professor Polanyi for a preprint of this paper.

(14) J. M. Simmie, A. J. Quiring, and E. Tschuikow-Roux, *J. Phys. Chem.*, **73**, 3830 (1969).

(15) E. Tschuikow-Roux, J. M. Simmie, and W. J. Quiring, *Astronaut. Acta*, in press.

have been used to study dehydrofluorination reactions. In direct studies in this laboratory, we have observed HF elimination from vinyl fluoride⁶ and 1,1-difluoroethane,⁷ while Cadman, *et al.*,⁴ using competitive methods, have reported the Arrhenius parameters for a number of alkyl fluorides. These latter authors have also included more detailed results of previous work,⁸⁻¹⁰ which was based on the application of the Rice-Ramsperger-Kassel-Marcus (RRKM) theory of unimolecular reactions to chemically activated molecule decomposition data.

Chemical activation studies of a number of fluoroalkanes are referenced in a recent paper by Chang and Setser¹¹ on the unimolecular reaction and collisional deactivation of chemically activated 1,2-difluoroethane. Considerably more information on the critical energies for HF elimination, determined by the application of nonequilibrium RRKM theory to chemical activation data, is shortly to be published for the following compounds:¹² $\text{CH}_3\text{CH}_2\text{CHFCH}_3$; $\text{CH}_3\text{CF}_2\text{CH}_3$; $\text{CH}_3\text{CH}_2\text{CH}_i\text{F}_{3-i}$ ($i = 0, 1$), $\text{CH}_i\text{F}_{3-i}\text{CH}_j\text{F}_{3-j}$ ($i = 1, j = 1, 2$ and $i = 2, j = 2$), and $\text{CH}_3\text{CClH}_i\text{F}_{2-i}$ ($i = 0, 1$).

Studies of a more fundamental nature on the product energy states have been performed by Clough, *et al.*¹³ They have examined the vibrational energy distribution of HF, eliminated from nonthermally activated CH_3CF_3 and CH_2CF_2 , in a fast-flow system. They find that the hydrogen fluoride eliminated from $\text{Hg}(6^3\text{P}_1)$ photosensitized activation of CH_2CF_2 has considerable excess vibrational and rotational energy. They suggest that the "reverse" activation energy is channeled into the vibrational mode and that the rotational excitation arises from a highly repulsive transition state.

This paper is the second in a series of studies on the kinetics of hydrogen fluoride elimination reactions of alkenyl fluorides.

Experimental Section

Both the modified single-pulse shock tube and the general techniques employed have been fully described in previous communications.^{14,15}

1,1-Difluoroethylene was obtained commercially (Matheson, 99.0% stated minimum purity) and tested for impurities by mass spectrometry and gas chromatography. No significant ($\leq 0.5\%$) impurities were detected; in particular monofluoroacetylene was below the limit of detectability (estimated at ≤ 10 ppm). Reaction mixtures of 1.0 and 2.6% difluoroethylene in argon (Matheson, 99.998% stated purity) were used for kinetic data below 1480°K, and total product analysis above 1500°K, respectively. Samples of the reacted mixture were drawn in the usual manner and analyzed on a gas chromatograph (Varian 1700; 12-ft column of silica gel at 75° with a flow rate of 30 cm^3 He min^{-1}) equipped with flame ionization detectors. For analysis of the products of high-temperature runs, the contents of

part of the low-pressure side of the shock tube (isolated by a ball-valve) were pumped through a copper coil immersed in liquid nitrogen. The trapped compounds were then transferred to Pyrex ampoules which were later sealed off *in vacuo*. These were then run through a coupled mass spectrometer-gas chromatograph (ms-gc).

Results

The decomposition of 1,1-difluoroethylene in shock waves is complex. We have quite arbitrarily divided the pyrolysis results of 1,1- $\text{C}_2\text{H}_2\text{F}_2$ into two ranges: (a) the high-temperature region, above 1500°K, and (b) the low-temperature region ≤ 1480 °K.

A. High-Temperature Results. Shocks into 2.6% 1,1- $\text{C}_2\text{H}_2\text{F}_2$ in argon generating reflected-shock temperatures of more than 1500°K for dwell times of about 1 msec gave over 18 detectable volatile products and, in addition, deposited a carbon film on the walls of the shock tube. The major volatile products are listed in Table I in the order of their elution from a silica gel

Table I: Analysis of Products from High-Temperature Shocks of 1,1- $\text{C}_2\text{H}_2\text{F}_2$

Product identity	Evidence	
	gc	ms
C_2H_6	+	
C_2HF	+	+
C_2F_4	+	+
C_2H_4	+	
$\text{C}_2\text{H}_2\text{F}_2$		Reactant
C_2H_2	+	+
C_2HF_2	+	+
$\text{C}_2\text{H}_3\text{F}$	+	+
$\text{C}_2\text{H}_3\text{F}_3$		+
$\text{C}_4\text{H}_5\text{F}_2$ (?)		+
C_4H_2		+

(4) P. Cadman, M. Day, A. W. Kirk, and A. F. Trotman-Dickenson, *Chem. Commun.*, 203 (1970).

(5) D. Sianesi, G. Nelli, and R. Fontanelli, *Chim. Ind.*, **50**, 619 (1968).

(6) J. M. Simmie, W. J. Quiring, and E. Tschuikow-Roux, *J. Phys. Chem.*, **74**, 992 (1970).

(7) E. Tschuikow-Roux, W. J. Quiring, and J. M. Simmie, *ibid.*, **74**, 2449 (1970).

(8) A. W. Kirk, Ph.D. Thesis, University of Wales, Aberystwyth, 1968.

(9) J. A. Kerr, A. W. Kirk, B. V. O'Grady, D. C. Phillips, and A. F. Trotman-Dickenson, *Discuss. Faraday Soc.*, **44**, 263 (1967).

(10) A. W. Kirk, A. F. Trotman-Dickenson, and B. L. Trus, *J. Chem. Soc. A*, 3058 (1968).

(11) H. W. Chang and D. W. Setser, *J. Amer. Chem. Soc.*, **91**, 7648 (1969).

(12) A. W. Kirk, private communication.

(13) P. N. Clough, J. C. Polanyi, and R. T. Taguchi, *Can. J. Chem.*, in press. We thank Professor Polanyi for a preprint of this paper.

(14) J. M. Simmie, A. J. Quiring, and E. Tschuikow-Roux, *J. Phys. Chem.*, **73**, 3830 (1969).

(15) E. Tschuikow-Roux, J. M. Simmie, and W. J. Quiring, *Astronaut. Acta*, in press.

column at 75° together with the nature of the evidence for their presence. In the case of positive gc(+) evidence this means that the retention time of an authentic sample was determined and compared with the unknown compound. For a positive mass spectroscopic identification, agreement with the literature was sought.

B. Low-Temperature Results. The complexity of the reaction at elevated temperatures meant that kinetic data could only be sought at low conversions, in the range of 0.03–5% decomposition. Initial driven gas pressures of 115–150 Torr and driver gas pressures of ca. 4 kTorr gave reflected shock temperatures and pressures of 1290–1480°K and 3.1–3.5 kTorr, respectively. In this range of conditions monofluoroacetylene, CHCF, was the major product of the reaction. Hydrogen fluoride cannot be detected in our apparatus for reasons discussed previously.^{6,7} Small quantities of ethane, ethylene, and acetylene were also formed. We believe that ethane, ethylene, and to some extent acetylene are formed from impurities in the driven gas, argon, since (i) shocking pure argon (*i.e.*, no sample present) also gave these compounds in comparable yields, whereas similar shocks into oxygen or nitrogen gave much reduced yields; (ii) insertion of a molecular sieve-silica gel trap at Dry Ice temperature (–78°) between the argon cylinder and the shock tube again diminished the yields of C₂H₆, C₂H₄, and C₂H₂. In our previous work^{6,7} trace quantities of these compounds had been noted as a puzzling feature. Their occurrence is now satisfactorily explained; in any case, they are unlikely to have significantly perturbed our major findings, particularly since in those sets of runs generally lower temperatures were employed.

To obtain kinetic data it was assumed that the relative gc response for CHCF and 1,1-C₂H₂F₂ mixtures was unity, since an authentic sample of monofluoroacetylene was unavailable to us. This is not an unreasonable approximation because the relative response factor for the mixture C₂H₂ plus C₂H₃F was 1.0 ± 0.1. With this assumption, and the further one that the decomposition was first order in 1,1-C₂H₂F₂, the rate constant *k* was evaluated from the integrated rate law

$$k = (1/t_d) \ln (1 + [C_2HF]/[C_2H_2F_2])$$

The kinetic results are shown in Table II. The Arrhenius equation is shown in Figure 1, in comparison with that found in the dehydrofluorination of vinyl fluoride,⁸ and is given by

$$\log (k, \text{sec}^{-1}) = 14.4 \pm 1.1 - (86,000 \pm 6800)/2.3RT$$

The error limits quoted are standard deviations.^{15a} These data were not corrected for temperature changes caused by the heat of reaction, nor was the cooling correction applied since (a) both these corrections are small in our apparatus¹⁴ and (b) the data are not sufficiently precise to warrant such treatment.

Table II: Results

Mach no.		P _t , kTorr	T _s , °K	t _d , msec	100[C ₂ HF] [1,1-C ₂ H ₂ F ₂]	k [∞] , sec ⁻¹
W ₁₁	W ₂₁					
2.499	1.365	3.27	1482	1.00	4.51	44.1
2.493	1.359	3.24	1476	1.02	3.97	38.2
2.469	1.367	3.09	1463	1.02	3.54	34.1
2.444	1.349	3.21	1428	0.87	1.76	20.1
2.433	1.340	3.13	1414	0.86	1.15	13.3
2.433	1.340	3.16	1411	0.88	1.09	12.3
2.367	1.326	3.53	1341	0.83	0.408	4.91
2.346	1.315	3.20	1318	0.75	0.281	3.74
2.363	1.315	3.31	1333	0.84	0.177	2.11
2.351	1.320	3.23	1321	0.74	0.142	1.92
2.365	1.309	3.13	1329	0.84	0.154	1.83
2.342	1.308	3.40	1311	0.87	0.077	0.89
2.336	1.311	3.30	1317	0.82	0.055	0.67
2.347	1.295	3.27	1311	0.82	0.053	0.65
2.311	1.316	3.32	1287	0.69	0.031	0.45

Thermochemistry

The enthalpy of formation of fluoroacetylene is not at all well established. JANAF tables¹⁶ reports Δ*H*_f[°](CHCF, g) = 30 ± 15 kcal mol⁻¹, whereas two empirical methods of estimation^{17,18} give ≈ 9.5 kcal mol⁻¹. There are strong indications that fluoroalkenes¹⁹ and, *a fortiori*, fluoroalkynes, do not obey a nearest-neighbor interaction only group scheme, so that the estimated values may be widely in error. Nevertheless, since Bryant's method¹⁷ gives reasonable values for Δ*H*_f[°](C₂H₃F) and Δ*H*_f[°](1,1-C₂H₂F₂), we select Δ*H*_f[°](CHCF, g) = 10 kcal mol⁻¹ as a basis for discussion. The heat of formation of 1,1-difluoroethylene has been determined by bomb calorimetry by Neugebauer and Margrave²⁰ and by Kolesov, *et al.*,²¹ as –77.5 and –79.6 cal mol⁻¹, respectively. These values have been recom-

(15a) NOTE ADDED IN PROOF. In a preliminary communication [J. M. Simmie and E. Tschuikow-Roux, *Chem. Commun.*, 773 (1970)] the Arrhenius parameters were reported as: log (*A*, sec⁻¹) = 13.1 and *E* = 335 kJ mol⁻¹ or 80 kcal mol⁻¹. Subsequent work, however, revealed a slight oversight in data reduction. This fact plus additional runs lead to the revised values given in the present paper.

(16) "JANAF Thermochemical Tables," The Dow Chemical Co., Midland, Mich., 1965, and addenda to date.

(17) From W. M. D. Bryant's modification of the method of J. W. Anderson, G. H. Beyer, and K. M. Watson. The values for the various group contributions are taken from G. J. Janz, "Thermodynamic Properties of Organic Compounds," Academic Press, New York, N. Y., 1967.

(18) From J. L. Franklin's method. Group equivalent values taken from J. L. Franklin, J. G. Dillard, H. M. Rosenstock, J. T. Herron, K. Draxl, and F. H. Field, "Ionization Potentials, Appearance Potentials, and Heats of Formation of Gaseous Positive Ions," U. S. Department of Commerce, NSRDS-NBS 26 (1969).

(19) S. W. Benson, F. R. Cruickshank, D. M. Golden, G. R. Haugen, H. E. O'Neal, A. S. Rcdgers, R. Shaw, and R. Walsh, *Chem. Rev.*, **69**, 279 (1969).

(20) C. A. Neugebauer and J. L. Margrave, *J. Phys. Chem.*, **60**, 1318 (1956).

(21) V. P. Kolesov, A. M. Martynov, S. M. Shtekher, and S. M. Skuratov, *Zh. Fiz. Khim.*, **36**, 2078 (1962).

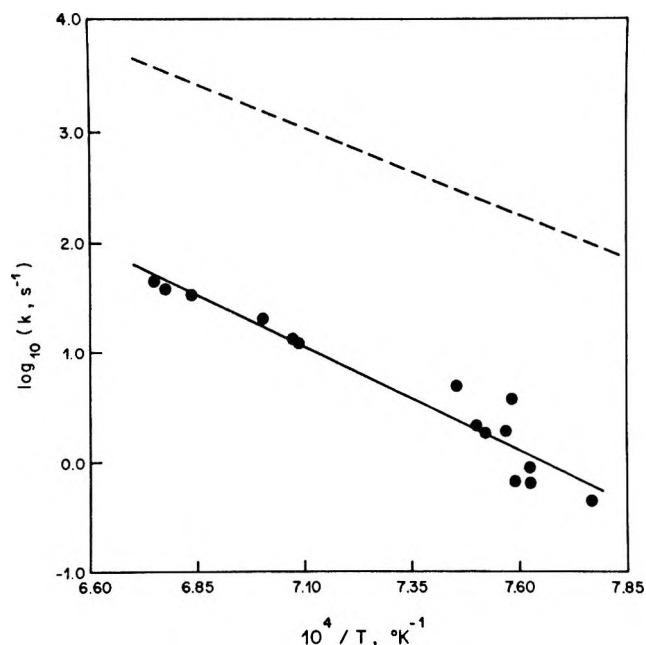


Figure 1. Temperature dependence of rate constants: —, 1,1-difluoroethylene; —, vinyl fluoride.⁹

puted by Lacher and Skinner²² using revised values for $\Delta H_f^\circ(\text{HF}, \text{aq})$ and $\Delta H_f^\circ(\text{CF}_4, \text{g})$, and they recommend $\Delta H_f^\circ(1,1\text{-C}_2\text{H}_2\text{F}_2, \text{g}) = -82.5 \pm 2.4 \text{ kcal mol}^{-1}$. Together with the well known¹⁶ enthalpy of formation of $\text{HF}(\text{g})$, $\Delta H_f^\circ = -64.8 \text{ kcal mol}^{-1}$, the enthalpy change for the reaction is given by

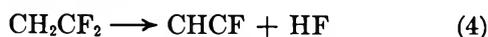


Discussion

Several possible primary processes can be envisioned in the thermal decomposition of 1,1-difluoroethylene. Homolytic bond breaking could include C-H, C-F, and C=C scission



Since the C-H, C-F, and C=C bond dissociation energies are approximately 104,²³ 111,²³ and 125²⁴ kcal mol⁻¹, respectively, homolysis is unlikely to be important unless primary scission is followed by a radical chain process. Molecular elimination of hydrogen fluoride is the only reasonable alternative, and the data observed in the low-temperature region, *i.e.*, at low conversion, support this view



At higher temperatures free-radical reactions increase in importance to such an extent that compounds such as diacetylene C_4H_2 are formed. This latter compound is a typical constituent of the high-temperature pyrolysis of hydrocarbons, particularly in the thermolysis of acetylene.²⁵

It is clear from the results that the decomposition of 1,1-difluoroethylene is complex. In contrast, it was found that molecular elimination of HF is the dominant process in the pyrolysis of vinyl fluoride for up to 30% reaction, proceeding with an activation energy of $\sim 71 \text{ kcal mol}^{-1}$. The present data yield an estimate of about 86 kcal mol^{-1} for the activation energy for 1,1- $\text{C}_2\text{H}_2\text{F}_2$ decomposition. This value can be shown to be of the right magnitude by comparing the rate constants for both systems. At 1323°K , the mean temperature of the two studies, $\log k_{\text{C}_2\text{H}_3\text{F}} \approx 2.30$ and $\log k_{\text{C}_2\text{H}_2\text{F}_2} \approx 0.19$; if the preexponential factors are assumed to be equal then, since $E_{\text{C}_2\text{H}_3\text{F}} = 70.8 \text{ kcal mol}^{-1}$, $E_{\text{C}_2\text{H}_2\text{F}_2} \approx 84 \text{ kcal mol}^{-1}$. This estimate can, of course, only be taken as an approximate guide to the true activation energy, but it does indicate that the activation energy for 1,1-difluoroethylene is significantly greater than that for vinyl fluoride. Jeffers and Shaub²⁶ have used a single-pulse shock tube and Tsang's competitive technique²⁷ to determine the cis-trans isomerization rate constants of 1,2-difluoroethylene. From their data lower limits of 69 and 66 kcal mol⁻¹ for the activation energies of decomposition can be estimated²⁸ for the cis and trans isomers, respectively.

Increasing fluorination at the α -carbon atom for $\text{CH}_2\text{CF}_i\text{H}_{2-i}$ ($i = 1, 2$) thus appears to lead to an increase in the activation energy for HF elimination. The same trend is found in the series of fluoroethanes $\text{CH}_3\text{CF}_i\text{H}_{3-i}$ ($i = 1, 2, 3$) where the substitution of a fluorine atom for hydrogen leads to a simple tenfold decrease in the relative rate constants; *i.e.*, k_{rel} is 1:0.13:0.010⁴ and 1:0.10:0.009⁶ at 1200°K . For the corresponding alkyl chlorides and bromides the rate constants increase with increasing α -halo substitution² (k_{rel} are 1:8.2:32 and 1:9.6:— at 700°K , for chlorides and bromides, respectively). It is now certain that this effect in the alkyl fluorides can be attributed to an increase in the activation energy⁴ rather than to a decrease in the preexponential factor.⁵ Such a statement is supported by calculations^{4,8} on chemical activation data using the nonequilibrium RRKM theory and, from consideration of the

(22) L. R. Lacher and H. A. Skinner, *J. Chem. Soc. A*, 1034 (1968).

(23) $D(\text{CF}_2\text{CH-H}) \approx D(\text{CH}_2\text{CH-H}) = 104 \text{ kcal mol}^{-1}$ from J. A. Kerr, *Chem. Rev.*, **66**, 465 (1966); $D(\text{CH}_2\text{CF-F}) \approx D(\text{CH}_2\text{CH-F}) = 111 \text{ kcal mol}^{-1}$ from ref 6.

(24) J. S. Shapiro and F. P. Lossing, *J. Phys. Chem.*, **72**, 1552 (1968).

(25) E. F. Greene, R. L. Taylor, and W. L. Patterson, Jr., *ibid.*, **62**, 238 (1958).

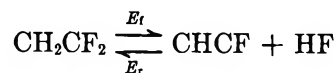
(26) P. M. Jeffers and W. Shaub, *J. Amer. Chem. Soc.*, **91**, 7706 (1969).

(27) W. Tsang, *Int. J. Chem. Kinetics*, **1**, 245 (1969), and references therein.

(28) Jeffers and Shaub²⁶ have shown that side products are negligible for up to 20% isomerization at temperatures of $\sim 1350^\circ\text{K}$. Hence $k_{\text{deo}} \leq k_{\text{isom}}/10$. At 1340°K $k_{\text{cis} \rightarrow \text{trans}} \approx 860 \text{ sec}^{-1}$ and therefore $k_{\text{deo}}^{\text{cis}} \leq 86 \text{ sec}^{-1}$; if the A factors are approximately equal then $E_{\text{deo}}^{\text{cis}} \geq 69 \text{ kcal mol}^{-1}$ since $E_{\text{isom}}^{\text{cis}} = 62.8 \text{ kcal mol}^{-1}$. If $A_{\text{deo}}^{\text{cis}} > A_{\text{isom}}^{\text{cis}} = 10^{12.17} \text{ sec}^{-1}$ and is nearer to the "normal" value of $10^{13.6} \text{ sec}^{-1}$, then $E_{\text{deo}}^{\text{cis}} \geq 71 \text{ kcal mol}^{-1}$. A similar argument can be used to deduce $E_{\text{deo}}^{\text{trans}} \geq 66 \text{ kcal mol}^{-1}$.

effect of replacing H by F on the vibrational frequency pattern and hence on the A factors using the O'Neal and Benson method.²⁹ This is not to say that the experimental values for the HF elimination activation energies determined by Cadman, *et al.*,⁴ are necessarily correct. In particular, their value for 1,1-difluoroethane of 66.6 kcal mol⁻¹ seems rather high since we have found⁷ $E_{\text{HF}} = 61.9 \pm 1.8$ kcal mol⁻¹ for CH₃CHF₂; nevertheless the general trend shown must be correct. Maccoll's ion-pair hypothesis³⁰ and its associated empirical correlations are not all that useful in predicting the correct order of reactivity for polyfluoroalkanes and alkenes. He has shown,³¹ for example, from a consideration of the interplay of electromeric and inductive effects that α -fluoro substitution augments the rate of HF elimination while β -substitution diminishes it. This is contrary to what is observed in α -fluoro-substituted fluoroalkanes as well as fluoroalkenes. We note, however, that an increase in the HF elimination activation energy is paralleled by an increase in the carbon-fluorine heterolytic bond strength for a given series, C₂H₅F: 60, 222 and CH₃CHF₂: 62-67, 262; C₂H₃F: 71, 250 and CH₂CF₂: 86, 259, where the values quoted are the activation energy and the heterolytic bond dissociation energy³² in kilocalories per mole, respectively.

Benson and coworkers³³⁻³⁵ have developed an electrostatic model (point-dipole) for quantitative prediction of the activation energies of four-center addition reactions, $>\text{C}=\text{C}< + \text{HX} \rightarrow >\text{CH}-\text{CX}<$ and $-\text{C}\equiv\text{C}- + \text{HX} \rightarrow -\text{CH}=\text{CX}-$, which, allied with thermochemical data on the enthalpy of reaction, can be used to predict HX elimination activation energies. We⁷ have found evidence, as have others,³⁶ to suggest that the model is not too successful when the alkene or alkyne is highly polar. In this case for 1,1-difluoroethylene



the point-dipole model predicts an activation energy³⁷ of $E_t \simeq E_r + \Delta H_r = 51 + 28 = 79$ kcal mol⁻¹ which is in moderate agreement with the observed value of ~ 36 kcal mol⁻¹. However, the thermochemistry is so uncertain that no definite conclusion can be drawn.

Acknowledgments. This work was supported by the National Research Council of Canada. The assistance of Dr. A. M. Hogg of the University of Alberta in running samples on the combined gc-ms is gratefully acknowledged.

(29) H. E. O'Neal and S. W. Benson, *J. Phys. Chem.*, **71**, 2603 (1967).

(30) (a) A. Maccoll, Special Publication No. 16, The Chemical Society, London, 1962, p 159; (b) A. Maccoll, "Studies of Chemical Structure and Reactivity," J. Ridd, Ed., Methuen, London, 1966.

(31) A. Maccoll, *Discuss. Faraday Soc.*, **44**, 288 (1967).

(32) Activation energies are taken from ref 4 and 6. Heterolytic bond dissociation energies are calculated from electron impact data; ethyl fluoride from ref 3; 1,1-difluoroethane from C. Lifshitz and F. A. Long, *J. Phys. Chem.*, **69**, 3731 (1965); vinyl fluoride and 1,1-difluoroethylene from C. Lifshitz and F. A. Long, *ibid.*, **67**, 2663 (1963).

(33) S. W. Benson and A. N. Bose, *J. Chem. Phys.*, **39**, 3463 (1963).

(34) S. W. Benson and G. R. Haugen, *J. Amer. Chem. Soc.*, **87**, 4036 (1965).

(35) S. W. Benson and G. R. Haugen, *J. Phys. Chem.*, **70**, 3336 (1966).

(36) T. S. Carlton, A. B. Harker, W. K. Natale, R. E. Needham, R. L. Christensen, and J. L. Ellenson, *J. Amer. Chem. Soc.*, **91**, 555 (1969).

(37) E_r is calculated from parameters given in ref 34 and 35 together with an estimated value for the carbon-fluorine longitudinal molar polarizability of $\alpha_L^\circ(\text{C-F}) \approx 1.2 \text{ \AA}^3$ from K. G. Denbigh, *Trans. Faraday Soc.*, **36**, 936 (1940), which is in agreement with a value estimated by R. J. W. LeFèvre, *Adv. Phys. Org. Chem.*, **3**, 1 (1965), and the dipole moment of CHCF from J. K. Tyler and J. Sheridan, *Trans. Faraday Soc.*, **59**, 2661 (1963).

Recoil Tritium Reactions with Methyl Isocyanide and Methyl Cyanide.

Estimates of Energy Deposition for the T-for-H Reaction^{1a}

by C. T. Ting and F. S. Rowland^{1b}

Department of Chemistry, University of California, Irvine, California 92664 (Received April 3, 1970)

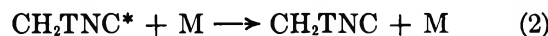
The substitution of energetic T* for H in CH₃NC produces such energetic molecules of CH₂TNC* that none (<1 in 300) are stabilized by gas phase collision prior to isomerization to CH₂TCN or decomposition to CH₂T plus CN. From experiments at 5 atm pressure of argon, it is concluded that less than 1% of the CH₂TNC* molecules have 3.8-eV excitation energy or less. Substitution trajectories corresponding to excitation energies of less than 2–3 eV are apparently forbidden by the detailed dynamics of the substitution process. The substitution of T* for H in CH₃CN forms molecules of CH₂TCN* sufficiently energetic to undergo the thermally unobserved reverse isomerization to CH₂TNC* in small yield. This yield is only observed experimentally under the rapid collisional stabilization conditions of liquid phase densities. Estimates of level densities for CH₂TNC* and CH₂TCN* at energies high enough for rapid isomerization predict a nonzero experimental yield for CH₂TNC in the gas phase, in disagreement with the observations.

Introduction

The replacement of a hydrogen atom in a hydrocarbon by an energetic tritium atom from nuclear recoil is accompanied by the deposition of substantial amounts of internal energy in the resulting tritium-labeled molecule, frequently in amounts sufficient to cause secondary decomposition or isomerization.^{2–4} Detailed study of such T-for-H substitution in cyclobutane, *i.e.*, measurement of the complementary pressure dependence of *c*-C₄H₇T and its decomposition product CH₂=CHT, led to an estimate of 5 eV as the median excitation energy for *c*-C₄H₇T* molecules formed in this system.² At the lowest pressures conveniently usable (about 5 cm) for neutron irradiation of gaseous *c*-C₄H₈,⁵ approximately 54% of the *c*-C₄H₇T molecules had undergone secondary reaction, while the remaining 46% were found as *c*-C₄H₇T. The latter, stabilized molecules could be inferred to possess any amount of energy from zero to the maximum incapable of causing appreciable secondary reaction—for the decomposition of *c*-C₄H₇T* with an activation energy of 62.5 kcal/mol, any excitation energy below about 100 kcal/mol does not lead to appreciable decomposition at 5 cm.⁶

We have sought to extend our information about the lower range of energies of excitation possible from such T-for-H reactions through the use of a different target molecule with a lower energy barrier toward secondary reaction. The availability of detailed pyrolytic studies of isomerization of methyl isocyanide to methyl cyanide—with an activation energy of 38 kcal/mol—made methyl isocyanide an excellent target molecule for such investigations.^{7–9} The sequence of reactions expected for such a recoil tritium system includes the primary substitution reaction (1) and the subsequent competition for CH₂TNC* between collisional deexcitation (2) and isomerization (3). If the excitation

energy were sufficient, one might also anticipate the further decomposition of either CH₂TNC* or CH₂TCN*, as in (4). Among other products routinely anticipated from recoil tritium reaction with CH₃NC are the abstraction product, HT, and the radical substitution reaction forming CH₃T.^{3,4}



We have also briefly investigated the reactions of energetic tritium atoms with methyl cyanide to determine whether the reverse of reaction 3 can be experimentally detected, *i.e.*, the energetically “uphill” and

(1) (a) This research was supported by Atomic Energy Commission Contract No. AT-(11-1)-34, Agreement No. 126, and formed part of the material submitted in the Ph.D. Thesis of C. T. Ting, University of California, Irvine, Calif., 1969. (b) To whom correspondence should be addressed.

(2) E. K. C. Lee and F. S. Rowland, *J. Amer. Chem. Soc.*, **85**, 897 (1963).

(3) F. Schmidt-Bleek and F. S. Rowland, *Angew. Chem., Intern. Ed.*, **3**, 769 (1964).

(4) R. Wolfgang, *Progr. React. Kinet.*, **3**, 97 (1965).

(5) The chief limiting factor is the necessity for stopping an appreciable fraction of the tritium atoms in the gas phase. Tritium atoms recoiling from the reaction ³He(n, p)T have an energy of 192,000 eV and a range of about 1 cm in *c*-C₄H₈ at a pressure of 7 cm. Convenient irradiation of several samples in the same neutron flux (for monitoring of absolute yields) has been confined for us to bulbs of about 2 cm in diameter.

(6) R. W. Carr, Jr., and W. D. Walters, *J. Phys. Chem.*, **67**, 1370 (1963).

(7) F. W. Schneider and B. S. Rabinovitch, *J. Amer. Chem. Soc.*, **84**, 4215 (1962).

(8) F. W. Schneider and B. S. Rabinovitch, *ibid.*, **85**, 2365 (1963).

(9) D. C. Tardy and B. S. Rabinovitch, *J. Chem. Phys.*, **48**, 1282 (1968).

thermally unknown isomerization of CH_2TCN^* to CH_2TNC , following T-for-H substitution in CH_3CN , as in (5) and (6).



Experimental Section

Recoil Tritium Experiments. The preparation, irradiation, and analysis of samples followed regular procedures, utilizing as tritium sources the nuclear reaction $^3\text{He}(n, p)\text{T}$ in gas phase experiments, and $^6\text{Li}(n, \alpha)\text{T}$ in the liquid phase.^{3,4} The upper limit on pressure in gas phase samples was set by the characteristics of the standard vacuum line used in these experiments.

Radiogas Chromatography. The standard analytical techniques of radiogas chromatography were applied,^{10,11} using a 3-ft column of 4% tetraglyme coated on Fluoropak 80. This column gave a good separation of the labeled polar products, with only moderate "tailing" problems as illustrated in Figures 1 and 2. Molecular HT and the light hydrocarbons were separated with a propylene carbonate-on-alumina (PCA) column. The illustrated separations utilized a column-switching technique¹¹ in which HT and CH_3T passed through both the Fluoropak column (twice) and the PCA column, while all others passed only through the Fluoropak column.

Preparation of Methyl Isocyanide.¹² Methyl isocyanide was formed by dropwise addition of *N*-methylformamide (Matheson Coleman and Bell, chromatography quality) into a solution of toluene-*p*-sulfonyl chloride (Eastman Organic Chemicals) and quinoline (Matheson Coleman and Bell, synthetic grade) at 75° and 60 mm pressure, and purified first by distillation and then by preparative gas chromatography. It was stored in the dark to avoid photoinduced polymerization reactions.

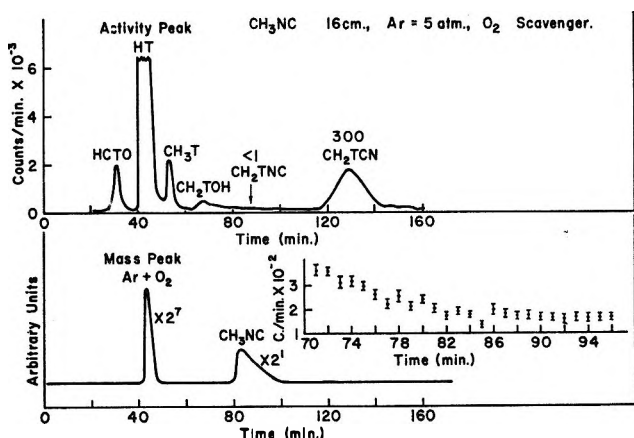


Figure 1. Radiogas chromatogram of radioactive products from recoil tritium reaction with CH_3NC in the gas phase: CH_3NC , 16 cm; argon, 5 atm; O_2 , 3 cm. Upper line: radioactivity; lower line: thermal conductivity; inset: expansion of radioactivity graph in the region of CH_3NC peak.

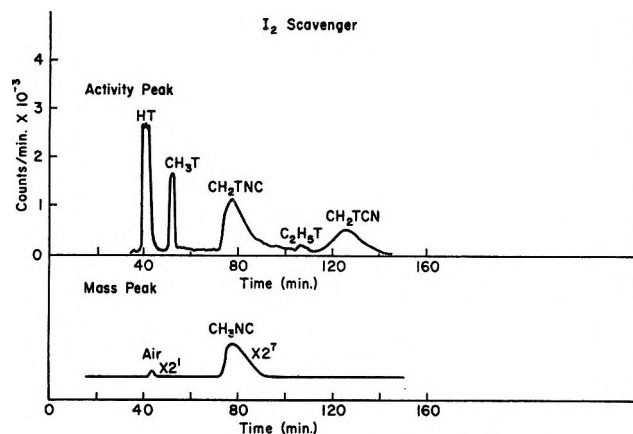


Figure 2. Radiogas chromatogram of radioactive products from recoil tritium reaction with CH_3NC in the liquid phase, I_2 -scavenged. Upper line: radioactivity; lower line: thermal conductivity.

Methyl cyanide (spectroscopic grade) was supplied by Eastman Organic Chemicals and was used without further purification.

Results and Discussion

Gas Phase Yield of CH_2TNC . The yield of CH_2TNC is negligibly low in all gas phase experiments, as shown in Table I. Upper limits on the CH_2TNC yield have been estimated from the fluctuations in measured radioactivity in the CH_3NC region on the tail of the CH_2TOH peak, as illustrated in Figure 1. In these O_2 -scavenged experiments, CH_2TOH is undoubtedly evidence for an abundant yield of CH_2T from the decomposition of CH_2TNC^* and/or CH_2TCN^* , the two sources being indistinguishable insofar as CH_2T formation is concerned.

In contrast, both CH_2TCN and CH_2TNC are found in all liquid phase experiments, as shown in Table I. (We draw no conclusions without extensive further experimentation from the apparent difference in ($\text{CH}_2\text{TNC}/\text{CH}_2\text{TNC}$) ratio for I_2 - and DPPH-scavenged samples.)

We assume, from the observation of CH_2TNC in the liquid phase and by analogy to a wide variety of other recoil tritium systems (hydrocarbons, alkyl halides, alcohols, etc.),^{3,4} that reaction 1 actually occurs as a primary step in the gas phase and that the CH_2TNC^* molecules so formed have a brief existence following this substitution event. The absence of CH_2TNC among the detectable labeled products in the gas phase then leads to a simple qualitative conclusion about the energetics of this reaction. Essentially all CH_2TNC^* molecules formed by the substitution of T-for-H in CH_3NC are left with so much excitation energy that they isom-

(10) J. K. Lee, E. K. C. Lee, B. Musgrave, Y.-N. Tang, J. W. Root, and F. S. Rowland, *Anal. Chem.*, **34**, 741 (1962).

(11) J. W. Root, E. K. C. Lee, and F. S. Rowland, *Science*, **143**, 676 (1964).

(12) J. Casanova, Jr., R. E. Schuster, and N. D. Werner, *J. Chem. Soc.*, 4280 (1963).

Table I: Relative Yields of Labeled Products from the Reactions of Recoil Tritium Atoms with Methyl Isocyanide

Irradiation conditions	Products (HT = 100)				
	CH ₃ TNC	CH ₂ TCN	CH ₃ T	C ₂ H ₅ T	CH ₂ TOH
Gases (cm) ^a					
CH ₃ NC (16)	<0.05	7.6	3.7	3.7	<0.01
CH ₃ NC (16), O ₂ (3)	<0.05	8.4	3.6	<0.06	1.3
CH ₃ NC (16), O ₂ (3), Ar (380)	<0.05	15.9	4.3	<0.03	1.8
Liquids					
CH ₃ NC	19.8	14.3	7.2	<0.1	<0.05
CH ₃ NC + I ₂	30.4	11.6	9.6	<0.3	<0.03

^a Each gas sample also contained 1-2 cm of ³He.

erize (and/or decompose) prior to a stabilizing collision with another gaseous molecule. Since such collisions occur in about 10⁻⁹ to 10⁻¹⁰ sec, the molecular lifetimes for CH₂TNC* formed in this system fall overwhelmingly into the time scale of ≤ 10⁻¹⁰ sec.

The conversion of molecular lifetimes into molecular excitation energies can be accomplished by assuming that the excited molecules decompose through equilibrium unimolecular decay, as treated theoretically by Rice, Ramsperger, Kassel, and Marcus.^{13,14} This assumption of the applicability of RRKM theory is on shakier grounds than in the earlier cyclobutane system, for we do not have any evidence here for excited molecules with lifetimes of ≥ 10⁻⁹ sec. However, estimates of *minimum* excitation energies corresponding to maximum lifetimes in the 10⁻¹⁰ sec region are probably of satisfactory validity. If an excited molecule were to survive for 10⁻¹⁰ sec, we believe that the RRKM calculation is a plausible method for evaluation of the corresponding excitation energy. If an excited molecule were to survive for only 10⁻¹¹ or 10⁻¹² sec, we assume only that such molecules have *more* excitation energy on the average than those which can exist without stabilizing collisions for 10 or 100 times longer. Whether a reaction occurring in 10⁻¹² sec represents random unimolecular decay corresponding to the RRKM assumptions is a moot point and is not involved in our estimates of *minimum* excitation energies.

Excitation Energies. The RRKM rate constant for isomerization of CH₃NC* to CH₃CN has been given as a function of excitation energy by Tardy and Rabinovitch⁹ and extended to higher excitation energies by the same methods.¹⁵ In this calculation, the excitation energies corresponding to various rate constants are (sec⁻¹, kcal/mol): 10⁸, 43; 10⁹, 55; 10¹⁰, 78; 2 × 10¹¹, 120. (For our semiquantitative purposes, we ignore the small isotopic difference in the rate constant for isomerization between CH₃NC* and CH₂TNC* at equivalent excitation energies. Detailed calculations are also available for CD₃NC*.⁸)

The observed gas phase yields of excited RT* molecules from the reaction of T* with RH can be expressed as the integral of

$$\int_{E_{\min}}^{E_{\max}} \frac{n(E)\omega dE}{(\omega + k_E)}$$

in which $n(E)$ is the distribution of excitation energies for RT* following the substitution reaction, k_E is the rate constant for removal of RT* by secondary reaction, and ω is the rate of collisional deexcitation in reciprocal seconds. In the case of CH₂TNC* from CH₃NC, the value of this integral is zero within the limits of error, and the only quantitative evaluation that can be made is a lower limit on the energy of excitation for these molecules. We assume that the processes of energy loss in collisional deexcitation of these molecules are the same as for the thermally excited molecules on which the RRKM calculations are based. The calculation also assumes that RT* cannot be reformed by reversal of the initial secondary reaction; this question of reversibility is discussed in detail below.

By assuming a monoenergetic "spike" of excitation energies, an upper limit can be placed on the fraction of CH₂TNC* molecules in this spike by calculating its fractional stabilization together with the requirement that the overall fraction of stabilized molecules must *not* be detectable in radio gas chromatographic analyses such as Figure 1. Since CH₂TNC* molecules with 2 eV excitation energy or less are essentially completely stabilized at 16 cm pressure, the detection limit that CH₂TNC/CH₂TCN < 1:150 furnishes directly the conclusion that less than 1 molecule in 150 of CH₂TNC* has 2 eV or less excitation energy. For higher excitation energies, the fractional limits are less restrictive since complete stabilization would not be anticipated at 16 cm pressure. Nevertheless, the limits are quite informative: not more than 1 in 50 has less than 2.8 eV energy; not more than 1 in 10 has less than 4 eV excitation. Clearly, the overwhelming percentage of T-for-H substitution reactions with CH₃NC create very highly excited molecules of CH₂TNC*.

(13) D. L. Bunker, "Theory of Elementary Gas Reaction Rates," Pergamon Press, Elmsford, N. Y., and Oxford, 1966.

(14) B. S. Rabinovitch and D. W. Setser, *Advan. Photochem.*, **3**, 53 (1964).

(15) C. T. Ting, Ph.D. Thesis, University of California, Irvine, Calif., 1969.

Assuming that the measured collisional stabilization efficiencies are the same at higher energies as those found in thermal experiments (Ar is 0.17 as efficient as CH_3NC),⁹ the experiments with 5 atm of argon are the equivalent of about 81 cm of CH_3NC , and the average collisional frequency is almost 10^{10} sec^{-1} . The corresponding estimates for excitation energy limits are then: less than 1 molecule in 300 of CH_2TNC^* has less than 2.4 eV while not more than 1 in 100 has less than 3.8-eV excitation energy after primary substitution of T-for-H in argon-moderated CH_3NC . It is perhaps worth emphasizing that no evidence has been obtained for the stabilization of *any* molecules of CH_2TNC in any gas phase experiments. Thus, the statement that <1% of CH_2TNC^* molecules have 3.8-eV excitation energy is only an upper limit upon the fractional yield, and no evidence exists that *any* molecules have as little as 3.8-eV excitation energy.

The most important conclusion arising from these experiments is the simple, qualitative statement that the mechanism of replacement of H by energetic T is essentially limited to trajectories in which energy deposition of several electron volts *must* occur for the resulting molecule. Of course, this statement is strictly applicable only to the particular case of CH_3NC , but the ubiquity of substantial excitation energies for a large fraction of many other T-for-H molecules leads us to believe that the statement is of general application: trajectories involving substitution of T-for-H with product excitations less than 2–3 eV are essentially forbidden by the detailed dynamics of the substitution process.

Compatibility of Various Excitation Energy Distributions Following T-for-H Substitution. The conclusion that <1% of CH_2TNC^* molecules have 4 eV or less of excitation energy is not completely incompatible with the published data on the decomposition of excited $c\text{-C}_4\text{H}_7\text{T}^*$, but it does impose severe constraints on a distribution of excitation energies designed for simultaneous satisfaction of both sets of data. The fractional survival of $c\text{-C}_4\text{H}_7\text{T}$ at 0.1 atm implies that about half of such molecules have less than 5 eV excitation energy, and our present scant knowledge of such processes cannot automatically eliminate a distribution of excited molecules heavily weighted between 4 and 5 eV. However, the $c\text{-C}_4\text{H}_7\text{T}^*$ and CH_3T^* distributions, the latter obtained from $\text{T}^* + \text{CH}_4$,^{16,17} are not mutually compatible, nor have we any present theories for such T-for-H reactions which would imply that the same distribution of excitation energies should result from T-for-H substitution in all molecules.

We believe that these apparent differences in excitation energy distributions can be explained either by (a) genuine differences in energy deposition, varying with the structure of the molecule involved; or (b) by errors introduced through extrapolation of RRKM rate constants far beyond the energies for which they have been shown to fit experimental data. (Basically, most of

these constants are fitted to thermal data and correspond to excitation energies not too far above the respective activation energies.) These suggestions are not mutually exclusive, and we, in fact, believe that both are quite likely to be partially correct hypotheses. However, the possible error in long extrapolations from 2 to 4–5 eV or higher prevents any firm conclusion that the excitation energy distributions must be different for the excited T-for-H products in CH_4 , $c\text{-C}_4\text{H}_8$, and/or CH_3NC .

The Reactions of Energetic Tritium Atoms with Methyl Cyanide. Radiogas chromatographic analysis of the labeled products from recoil tritium reactions with $\text{CH}_3\text{-CN}$ shows the formation of both CH_2TCN and CH_2TNC in I_2 -scavenged liquid phase samples, with a $\text{CH}_2\text{TNC}/\text{CH}_2\text{TCN}$ ratio of about 0.04. Gas phase experiments again fail to show any stabilized CH_2TNC . Following the direct T-for-H substitution reaction (5) with CH_3CN , an excitation energy of 80–100 kcal/mol should be sufficient to cause isomerization of CH_2TCN^* to CH_2TNC^* —activation energy = $38 + 17 = 55 \text{ kcal/mol}$ —and insufficient for decomposition to $\text{CH}_2\text{T} + \text{CN}$.¹⁸ However, the excited molecules of CH_2TNC^* just formed obviously possess sufficient energy to re-isomerize back to the original CH_2TCN and will do so unless stabilized by collision. The 17 kcal/mol difference in activation energies is sufficiently large that the re-isomerization should be very much faster than the original isomerization itself.

Reversible Isomerizations: The Nonequilibrium Paradox. Most other measurements of secondary reactions following recoil tritium substitution have involved decomposition into two fragments,^{2–4} and entropy considerations ensure that reversal of this process has a negligible probability for occurrence. However, the newly isomerized molecules in this study still contain all of the original atoms *and* all of the excitation energy and are potentially capable of re-isomerization back to the original structural arrangement. For example, when a molecule of CH_2TNC^* with 100-kcal/mol excitation energy isomerizes to CH_2TCN^* with a rate constant of approximately $5 \times 10^{10} \text{ sec}^{-1}$, the newly formed molecule of CH_2TCN^* now possesses 117 kcal/mol excitation energy above the ground state of CH_2TCN and is easily capable of re-isomerization to CH_2TNC . Presumably, these isomerizations should proceed back and forth establishing an equilibrium to be disturbed only by removal of some of the excitation energy by collision with another molecule. If this deexciting collision were to remove *all* of the excitation energy, or at least sufficient

(16) D. Seewald and R. Wolfgang, *J. Chem. Phys.*, **47**, 143 (1967).

(17) Y.-N. Tang and F. S. Rowland, *J. Phys. Chem.*, **72**, 707 (1968).

(18) The heats of formation of CH_3NC and CH_3CN are given as 35.9 and 19.1 kcal/mol, respectively, for a difference of 16.8 kcal/mol. Using $\Delta H_f = 111 \text{ kcal/mol}$ for CN, the decomposition to $\text{CH}_3 + \text{CN}$ is endothermic by 109 and 126 kcal/mol for CH_3NC and CH_3CN , respectively; see S. W. Benson, "Thermochemical Kinetics," Wiley, New York, N. Y., 1968.

energy to prevent further isomerization, then the deexciting collisions might be expected to leave stabilized CH_2TCN and CH_2TNC with the proportions present in the isomerization equilibrium.

The two molecules, CH_2NC and CH_3CN , have very similar vibrational frequencies,¹⁹ as befits two such similar molecules, and hence have quite similar patterns of level densities when compared to the respective ground states. Crudely, one can estimate that the rates of isomerization from CH_2TNC to CH_2TCN and reverse will have the same A factors and will differ only in the activation energies of the reactions. If, for example, the isomerization from CH_2TNC is given by

$$k_1 = A \left(1 - \frac{E^*}{E^* + \Delta} \right)^{s-1}$$

for an excitation energy Δ kcal/mol greater than the potential barrier, then the reverse isomerization from CH_2TCN should be given by

$$k_2 = A' \left(1 - \frac{E^* + 17}{E^* + 17 + \Delta} \right)^{s-1}$$

The $(3N - 6)$ degrees of freedom ensure that s has the same value of 12 for both molecules, while the similarities in vibrational frequencies require that $A \cong A'$. Consequently, this calculation indicates an equilibrium ratio of states for $\text{CH}_2\text{TNC}/\text{CH}_2\text{TCN}$ of $[(E^* + \Delta)/(E^* + 17 + \Delta)]^{11}$, or approximately 1:9 for $\Delta = 40$ kcal/mol—corresponding to a rate constant of about 10^{10} sec^{-1} for isomerization of CH_2TNC^* and about 10^9 sec^{-1} for the return. Lesser values of Δ provide somewhat higher ratios but no longer correspond to rate constants sufficiently fast to guarantee even one initial isomerization prior to the first gas phase collision. Even for $\Delta = 5$ kcal/mol, the level density ratio is only 1:40, while the corresponding isomerization rate constant of 10^8 sec^{-1} would clearly result in the stabilization in the gas phase as CH_2TNC of >90% of such initially excited molecules. A serious paradox arises from the

<1:300 ratio of surviving CH_2TNC and CH_2TCN molecules—a level density of <1:300 does not occur for simple calculations at any energy corresponding to favorable competition for isomerization *vis-a-vis* immediate collisional stabilization of the newly formed excited molecule.

The partial isomerization of CH_2TNC^* to CH_2TCN in the liquid phase is reasonable since many initially formed CH_2TNC^* molecules will be collisionally stabilized before isomerization can occur. The small yield of CH_2TNC from CH_2TCN^* is also consistent with this picture, for simple calculations such as given above indicate that excitation energies of 100–110 kcal/mol for CH_2TCN^* ($\Delta = 45$ –55 kcal/mol) correspond to equilibrium ratios of $\text{CH}_2\text{TNC}/\text{CH}_2\text{TCN}$ of less than 1:10, and stabilization by collision of a fraction of such molecules is sufficient to account for the observed liquid phase yields of CH_2TNC .

An explanation for the failure to find some CH_2TNC in the gas phase (e.g., 1:9 to 1:40 relative to CH_2TCN), as indicated by these simple equilibrium calculations, is not given here. The question of the energy loss per collision of the excited molecule does not enter into this qualitative problem: while an excited molecule of CH_2TCN^* or CH_2TNC^* may very well not lose more than 10–15 kcal/mol in its initial collision, there is no excitation energy for which isomerization can occur that satisfies the <1:300 ratio in observed yields. Accurate level density calculations do not change the quantitative discrepancies between equilibrium predictions and observed yields either, and we conclude only that the complete absence of CH_2TNC in the gas phase seems paradoxical and without adequate explanation at the present time.

(19) M. G. K. Pillai and F. F. Cleveland, *J. Mol. Spectrosc.*, **5**, 212 (1960). The doubly degenerate $\nu_8(\text{e})$ is 361 cm^{-1} for CH_3CN vs. 270 cm^{-1} for CH_2NC , while the nondegenerate $\nu_2(\text{a}_1)$ and $\nu_4(\text{a}_1)$ are 2287 vs. 2166 and 920 vs. 945 cm^{-1} for the same comparison. The remaining five frequencies (three doubly degenerate) vary by less than 1% each between these two molecules. Data for tritiated species are not available.

Energy Transfer in Alkali Halide Matrices^{1a}

by Mohan Khare and Everett R. Johnson^{1b}

Department of Chemical Engineering, University of Maryland, College Park, Maryland (Received January 22, 1970)

The radiation-induced decomposition of KNO_3 dispersed in a KBr matrix has been studied to determine the mechanism of energy transfer in these systems. It is observed that $-G(\text{NO}_3^-)$ is as much as 100 times that for the pure salt depending on the concentration of KNO_3 in the system. The enhanced decomposition of the KNO_3 in these systems is due to the transfer of energy but the matrix material with an energy gap less than 4.0 eV is ineffective in causing enhanced decomposition, indicating the importance of the role of excitons in the energy transport process. Further support for exciton mechanism is found in temperature dependence studies and preirradiation of the matrix material.

Jones² has shown that when KNO_3 embedded in a KBr matrix (similar to KBr pellet technique for ir studies) is irradiated, the decomposition of KNO_3 is far in excess of that which occurs in the pure salt when the energy absorbed by the KNO_3 is calculated on the basis of its electron fraction in the total system. The cause of the increased decomposition of KNO_3 in this system is presumably due to some of the energy absorbed by the KBr being transferred to the KNO_3 . Energy transfer by "inert" systems is well known. For example when organic compounds (azoethane, hexane, isopropyhexane, to name a few) adsorbed on silica are irradiated, it is observed that the decomposition of the adsorbate is very large compared to the decomposition of the pure material³ (again the energy absorbed by the adsorbate is calculated on the basis of its electron fraction in the total system). Although the evidence for energy transfer in these systems is substantial, there appear to be some conflicting data concerning the mechanisms. Sagert and Robinson⁴ and Wong and Willard⁵ have interpreted their results in terms of electron migration, whereas Rabe, Rabe, and Allen³ infer that their results can best be interpreted on the basis of exciton transfer.

We have investigated energy transfer in systems composed of nitrates embedded in various inorganic matrices both as a function of temperature and composition in an attempt to resolve the mechanism of energy transfer in these systems.

Experimental Section

Reagent grade chemicals were used as purchased except for KBr. The KBr was recrystallized several times in triply distilled water and dried in a vacuum oven at 100°. Pellets were prepared by grinding together a known amount of the salts and forming in a Beckman Die at 25,000 psi (we will refer to this method of making pellets as the "grinding" technique). Pellets were also formed using the technique of Jones⁶ by adding a small amount of a solution of the additive (KNO_3 , for example) to a slurry of the matrix material and drying, with stirring, using an infrared lamp as the

heat source. For example, about 1 cc of a dilute KNO_3 solution would be added to a slurry of KBr, the slurry stirred until dry. The resulting powder was heated in a vacuum oven at 100° for 24 hr and then pelleted in the usual manner of making a KBr pellet (this technique will be referred to as the Jones method). Jones determined by this method that up to about 0.2 mol % nitrate ion could be introduced into the KBr lattice. The grinding technique also resulted in NO_3^- being introduced into the KBr lattice; however, the amount was usually small, the majority of the nitrate being dispersed as small crystals in the KBr matrix.

Nitrite was determined by the method of Shinn. In this method sulfanilamide is diazotized and coupled with *N*-(1-naphthyl)ethylenediamine hydrochloride to form a colored azo compound. The molar extinction coefficient at 536 m μ was 52,000. Ferric ion was determined by direct absorption at 305 m μ using a molar extinction coefficient of 2201.

Dosimetry was determined by ferrous sulfate oxidation using a *G* value (molecules of product formed per 100 eV absorbed) of 15.45 molecules of ferrous ion oxidized per 100 eV absorbed. The radiation source was a cylinder of cobalt-60. Most irradiations were performed using a rotating sample holder placed inside the center of the source which ensured uniform irradiation.

The dose absorbed by the KNO_3 in the various systems was calculated on the basis of its electron fraction in the total system; *i.e.*, absorbed dose \times mole fraction of $\text{KNO}_3 \times$ electrons per mole of KNO_3 /electrons per mole of matrix material. No correction was made for

(1) (a) Research conducted under the auspices of the U. S. Atomic Energy Commission Contract No. AT(40-1)-3660; (b) to whom correspondence should be addressed.

(2) A. R. Jones, *J. Chem. Phys.*, **35**, 751 (1961).

(3) For general reference see J. G. Rabe, B. Rabe, and A. O. Allen, *J. Phys. Chem.*, **70**, 1098 (1966), and E. A. Roja and R. R. Hentz, *ibid.*, **70**, 2919 (1966).

(4) N. H. Sagert and R. W. Robinson, *Can. J. Chem.*, **46**, 2075 (1968).

(5) P. K. Wong and J. E. Willard, *J. Phys. Chem.*, **72**, 2623 (1968).

(6) A. R. Jones and R. L. Durfee, *Radiat. Res.*, **15**, 546 (1961).

the differences in the mass absorption coefficients of the dosimeter solution and the various samples (matrix material plus nitrate).

Results

Pellets made from different sources of KBr gave different quantitative results, but qualitatively the results were the same. By this is meant simply that the effect of temperature, preirradiation of the KBr, doping, etc., qualitatively gave the same results with the different sources of KBr; however, absolute G values were different. For example, a sample of KBr used as purchased gave a G value of 26 for a 0.05 wt % KNO_3 pellet irradiated to an absorbed dose of 0.172×10^{21} eV/g. Pellets made from recrystallized KBr and irradiated similarly gave a G value of 68; pellets prepared using the method of Jones with recrystallized KBr containing the same wt % KNO_3 gave a G value of about 100 for an absorbed dose of 0.172×10^{21} eV/g. The bulk of our experiments was done with KBr recrystallized three times from triply distilled water using the grinding technique; however, we also include experiments done with other sources of KBr which will be identified in the appropriate discussion.

$G(\text{NO}_2^-)$ as a function of absorbed dose at varying percentages of KNO_3 in the KBr matrix is shown in Figure 1. The highest G value observed was 169.5 at an absorbed dose of 0.172×10^{21} eV/g for a pellet formed by grinding together KNO_3 and KBr to give a final concentration of 0.005 wt % KNO_3 . As can be seen, $G(\text{NO}_2^-)$ is very sensitive to absorbed dose; $G(\text{NO}_2^-)$ being virtually constant beyond an absorbed dose of about 1×10^{21} eV/g of KNO_3 . The results shown in Figure 1 are mean values of two or more pellets formed from the same mixture irradiated simultaneously; *i.e.*, a known amount of KNO_3 is added to a known amount of KBr and the mixture is ground to a fine powder, the resulting mixture providing sufficient material to form seven to ten pellets. The results from pellets formed from a particular mixture irradiated to the same dose seldom differed by more than 10%, the usual reproducibility being better than 5%.

Energy transfer to other nitrates was also determined to be certain that this effect was not unique to KNO_3 . The decomposition of other nitrates in KBr and RbBr matrices is summarized in Table I. Some of the results obtained with KNO_3 in the same systems are included for comparison. The results given in Table I are for an absorbed dose of 0.172×10^{21} eV/g.

The decomposition of KNO_3 dispersed in a variety of matrices was done to determine the relationship of ease of energy transfer in these systems and the energy gap of the matrix material. All pellets contained the same wt % KNO_3 (0.05%), and all were irradiated to the same absorbed dose (0.172×10^{21} eV/g). These results are summarized in Table II. In the NiO and ZnO systems there was small amount of decomposition of

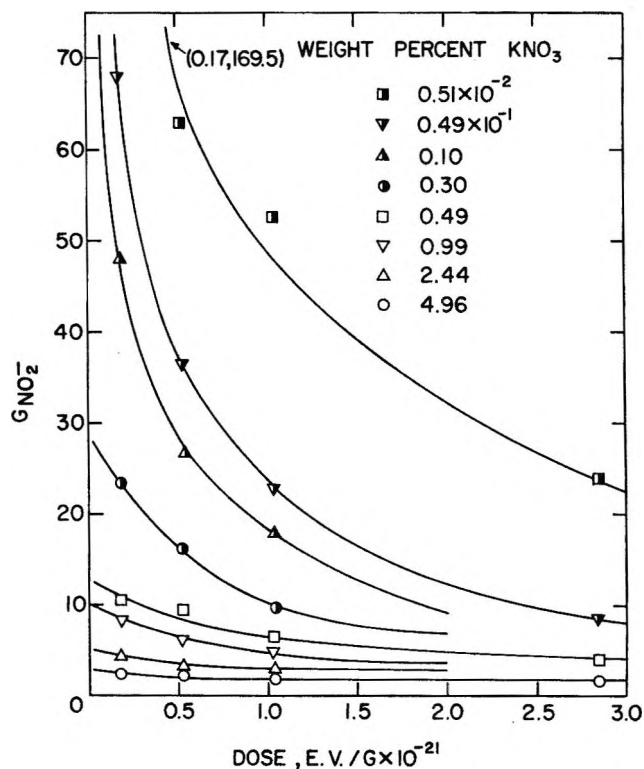


Figure 1. $G(\text{NO}_2^-)$ as a function of absorbed dose for pellets of varying wt % KNO_3 .

Table I

System	Mole fraction of nitrate	Dose, eV/g	$G(\text{NO}_2^-)$
NaNO_3 (pure)		0.172×10^{21}	0.24
NaNO_3 -KBr	0.692×10^{-3}	0.172×10^{21}	87.6
NaNO_3 -RbBr	0.92×10^{-3}	0.172×10^{21}	266.2
$\text{Ba}(\text{NO}_3)_2$ (pure)		0.172×10^{21}	1.89
$\text{Ba}(\text{NO}_3)_2$ -KBr	0.227×10^{-3}	0.172×10^{21}	52.5
$\text{Ba}(\text{NO}_3)_2$ -RbBr	0.315×10^{-3}	0.172×10^{21}	230.0
KNO_3 (pure)		0.172×10^{21}	1.47
KNO_3 -KBr	0.582×10^{-3}	0.172×10^{21}	68.0
KNO_3 -RbBr	0.529×10^{-3}	0.172×10^{21}	274.0
AgNO_3 (pure)		0.172×10^{21}	$\sim 0.15^a$
AgNO_3 -KBr	0.05×10^{-3}	0.172×10^{21}	65.3

^a Data from T. H. Chen and E. R. Johnson, *J. Phys. Chem.*, **66**, 2249 (1962).

KNO_3 ; however, both of these oxides when irradiated interfered with the determination of nitrite ion by the Shinn method. It is apparent, however, that matrix material with an energy gap less than 4.0 eV was not effective in causing decomposition of KNO_3 .

The effect of temperature on the decomposition of KBr pellets containing 0.05 wt % KNO_3 was also determined. These results are summarized in Table III and Figure 2.

An Arrhenius plot of the data (Figure 2) gave an activation energy of 6.63 kcal/mol. A plot of the data using a different source of KBr (KBr as purchased)

Table II

System	$G(\text{NO}_2^-)$	First exciton absorption peak (eV) for the matrix material	Energy gap of matrix material, eV
LiBr-KNO ₃	50.4	7.0	8.5
NaBr-KNO ₃	13.3	6.5	7.7
KBr-KNO ₃	68.0	6.6	7.8
RbBr-KNO ₃	274.8	6.47	7.7
CsBr-KNO ₃	263.4	6.63	7.8
KF-KNO ₃	71.3	9.8	10.9
KCl-KNO ₃	25.5	7.7	8.5
MgO-KNO ₃	68.2	7.3	7.3
NiO-KNO ₃	Some	3.7	3.7-3.9
ZnO-KNO ₃	Some	3.44	~3.9
TiO ₂ -KNO ₃	Less than 2.0	3.25	3.2

Table III: Effect of Temperature on the Decomposition of KBr-KNO₃ Pellets Containing 0.05 Wt % KNO₃

Temp, °C	Absorbed dose, eV/g	Mean $G(\text{NO}_2^-)$
25	0.172×10^{21}	68.0 (68.0) ^a
100	0.181×10^{21}	207.0 (66.8)
150	0.195×10^{21}	340.3 (64.5)

^a Since the absorbed dose varied in these experiments, the figures given in parentheses are for the room temperature decomposition of pellets containing 0.05 wt % KNO₃ irradiated to the absorbed doses shown.

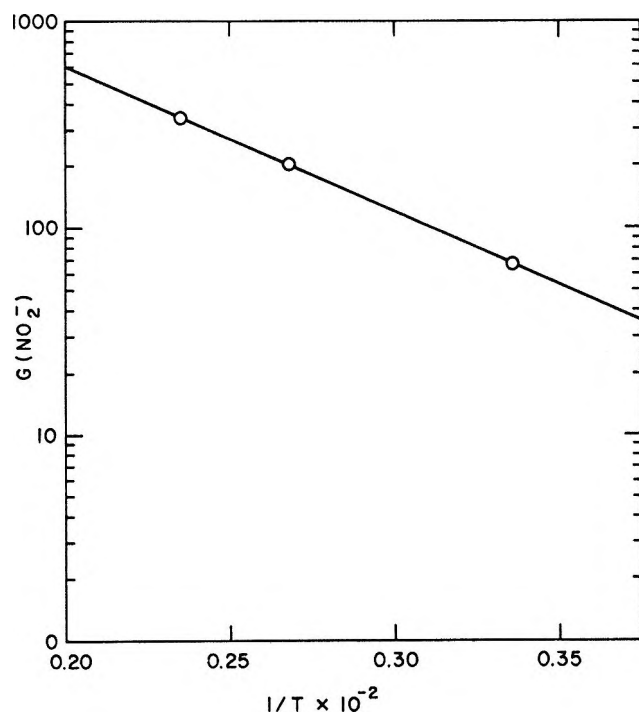


Figure 2. $G(\text{NO}_2^-)$ as a function of temperature. Results are for pellets containing 0.05 wt % KNO₃.

gave a curve, which although it had different G values, at the different temperatures, had the same slope. This value is far in excess of the activation energy observed for the radiation-induced decomposition of pure KNO₃ or other nitrates. The values found by Cunningham for pure KNO₃ was 1.63 kcal/mol. $G(\text{NO}_2^-)$ at an absorbed dose of 0.172×10^{21} eV/g for pellets containing 0.05 wt % KNO₃ irradiated at -192 and 0° were approximately the same as $G(\text{NO}_2^-)$ for samples irradiated similarly at 25° . Dosimetry at the low temperatures was not as accurate as at the higher temperature; however, it was unlikely that the error exceeded $\pm 15\%$. These results would indicate that there are two processes which occur, one of which requires no thermal activation or at most a few hundred calories per mole.

The role of surface in the energy transfer process was studied by varying the surface-to-volume ratio of the pellets and by irradiating pellets in different atmospheres. Changing the surface-to-volume ratio was accomplished by simply changing the pellet thickness. A fivefold decrease in the surface-to-volume ratio produced about a 20% increase in $G(\text{NO}_2^-)$; however, a small error in dosimetry was present which could well account for most of this increase. The effect of ambient atmosphere was studied by irradiating pellets containing 0.05 wt % KNO₃ in air, vacuum, helium, N₂O, and H₂O. Pellets were placed in ampoules, sealed to a vacuum line, and evacuated under gentle heating to remove adsorbed gases. The pellets were maintained under vacuum for about 5 hr prior to adding the respective gases. Irradiating the pellets under vacuum, in air, or in helium produced no significant change in $G(\text{NO}_2^-)$. A small decrease (less than 8%) in $G(\text{NO}_2^-)$ was observed for samples irradiated in an atmosphere of N₂O (about 2 atm pressure) or H₂O (about 25 mm pressure).

Cunningham⁷ had observed a decrease in $G(\text{NO}_2^-)$ in KNO₃ doped with varying amounts of Ag⁺. He attributed the decrease in $G(\text{NO}_2^-)$ to the scavenging of low-energy electrons by the Ag⁺, thus preventing dissociative electron capture by nitrate ions. The effect of doping with Ag⁺ was studied in the KBr-KNO₃ systems using a 0.2 wt % solution of AgBr in KBr made by adding a weighed amount of AgBr to molten KBr. The melt was cooled and ground to a fine powder. Pellets containing 0.05 wt % KNO₃ (based on the weight of the AgBr-KBr) were then made and irradiated to varying doses. The results are summarized in Table IV.

Table IV: Effect of Doping on $G(\text{NO}_2^-)$ in KBr-KNO₃ Pellets

Absorbed dose, eV/g	$G(\text{NO}_2^-)$	
	Ag ⁺ -doped pellets	Undoped
0.172×10^{21}	138	68
1.032×10^{21}	43.6	17.0

(7) J. Cunningham, *J. Amer. Chem. Soc.*, **85**, 2716 (1963).

The effect of annealing and preirradiation on the matrix material indicated that the ability of the KBr to transfer energy could not be completely destroyed by preirradiation. Pellets containing 0.05 wt % KNO_3 were prepared by mixing the KNO_3 with KBr that had been previously irradiated to a total adsorbed dose of 1.032×10^{21} eV/g. The pellets so made were then irradiated to an absorbed dose of 0.172×10^{21} eV/g. $G(\text{NO}_2^-)$ decreased to 60% of the value of that for pellets made with the normal KBr and irradiated to the same absorbed dose. If the irradiated KBr was annealed at 170° for 48 hr prior to forming a pellet, $G(\text{NO}_2^-)$ was raised to its usual value. This effect was confirmed in a number of experiments. The decrease in $G(\text{NO}_2^-)$ as a result of preparing pellets with irradiated KBr could be magnified by using KBr that had been irradiated to larger absorbed doses than that referred to above; however, in no case could $G(\text{NO}_2^-)$ be reduced to less than 30. This may be due to the fact that the heat generated in the pelleting process is sufficient to cause some annealing of the irradiated KBr.

Discussion

The data reported here we believe support an energy transfer mechanism involving exciton transfer rather than one involving dissociative capture of low energy electrons. Nitrate ions show two absorption bands in the uv. There is an intense band at 2630 \AA and another less intense band at 3000 \AA . Absorption of energy in these regions induces dissociation of the nitrate ion to give nitrite plus oxygen atoms.^{8,9} It would appear



therefore that a minimum of about 4 eV is required to cause dissociation of nitrate ions. The position of the first exciton absorption peak in the various matrix materials is shown in Table II. Although there does not appear to be a direct correspondence between the energy of the absorption peak and efficiency of energy transfer, there is no doubt that a certain minimum energy is required to effect energy transfer. NiO, ZnO, and TiO_2 with absorption peaks at 3.7, 3.44, and 3.05 eV, respectively, have essentially zero efficiency in this regard. We do not know why the CsBr and RbBr lattices should exhibit such substantially greater efficiency than the other bromate lattices. Possibly this may be due to the purity. It is not due to the ease of exchange of NO_3^- ion with bromide (as occurs in the grinding process) since pellets made using Jones' technique give essentially the same results.

The data shown in Table I indicate that it is the matrix lattice that affects the extent of nitrate ion decomposition; i.e., $G(\text{NO}_2^-)$ has a mean value of about 70 for nitrates in the KBr lattice and about 250 in RbBr lattice. It appears therefore that the cation associated with the different nitrates does not play any significant role in these systems.

The loss of ability of KBr and other matrix materials³ to transfer energy as a result of irradiation appears to occur at an absorbed dose of about $0.5\text{--}1 \times 10^{21}$ eV/g. We attributed this, for several reasons, to the buildup of exciton-trapping sites which prevents further transfer of energy as the primary cause rather than the occurrence of a back-reaction of nitrite with the oxygen simultaneously formed.

Pellets made with preirradiated KBr show a decrease in $G(\text{NO}_2^-)$ of about 60% compared to pellets made with ordinary (or irradiated and subsequently annealed) KBr. This indicates to us that something has occurred to the KBr when irradiated which decreases its ability to transfer energy. The number of low-energy electrons produced per unit of energy absorbed should be the same regardless of whether the KBr has been preirradiated or not. Hence, unless there is some species produced in KBr during irradiation which can scavenge these low-energy electrons, we are inclined to believe that holes, electron excess centers, and other trapping sites that are known to be produced in the alkali halides act as exciton-scattering centers and so prevent the energy transfer process.

Rabe, Rabe, and Allen,³ in their studies on the radiation-induced decomposition of azoethane adsorbed on silica gel, determined a direct relation between the buildup of F center concentration (as determined by chemical analysis) in NaCl and the decrease in azoethane decomposition (azoethane adsorbed on silica gel) as a function of adsorbed dose (see Figure 3). The concentration of F centers appears to saturate in NaCl and other halides at an absorbed dose of about $0.5\text{--}1.0 \times 10^{21}$ eV/g and at saturation the concentration is about $0.5 \times 10^{18} \text{ cm}^{-3}$.^{3,10,11} Electron excess (color centers) and defect centers (holes) were also observed in the KBr- KNO_3 system using the method of Burns and

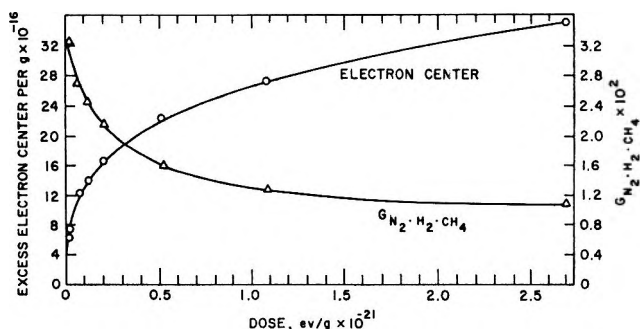


Figure 3. The decomposition of azoethane adsorbed on silica gel and electron excess center formation as a function of absorbed dose; from J. G. Rabe, B. Rabe, and A. O. Allen, *J. Phys. Chem.*, **70**, 1098 (1966).

- (8) L. K. Narayanswamy, *Trans. Faraday Soc.*, **31**, 1411 (1935).
 (9) P. Doigan and T. W. Davis, *J. Phys. Chem.*, **56**, 764 (1952).
 (10) M. Hasekaylo and D. Otterson, *J. Chem. Phys.*, **21**, 552, 1434 (1953).
 (11) W. G. Burns and T. F. Williams, *Nature*, **175**, 1043 (1955).

Williams.¹¹ Pellets containing 0.05 wt % KNO_3 were irradiated to varying doses and added to KI solutions, and the concentration of I_3^- was determined colorimetrically. Nitrite ion reacts in these systems in a complex manner, and though we were unable to obtain good quantitative data, the results certainly indicated that these centers are formed in the KBr-KNO_3 system during irradiation and that the initial concentrations of these centers are proportional to absorbed dose. Ladov and Johnson¹² in their studies on the oxygen isotope effect in the radiolysis of KNO_3 invoke an energy transfer mechanism to explain the abnormally high isotope effect observed in the initial stages of the decomposition. They too observed that the energy transfer process falls off with increasing absorbed dose and appears to become insignificant at an absorbed dose of about 0.5×10^{21} eV/g. They attributed this decrease to a buildup of trapping sites in the KNO_3 lattice which prevents further energy transfer. From their data they estimate that the number of these trapping sites is about 0.5×10^{18} cm^{-3} . Recently Yamada, Hasegawa, and Miura¹³ reported on the formation of anion radicals on γ -irradiated silica gel. O_2 , SO_2 , CO_2 , and tetracyanoethylene (TCNE) were added to silica gel which had been previously irradiated, and the signals for O_2^- , CO_2^- , SO_2^- , and $(\text{TCNE})^-$ were detected. These authors observed a substantial increase in signal strength for the radical anions when the silica gel with the adsorbate was postirradiated with uv light in the 2000–4000-Å range. This was interpreted as being due to the electrons trapped in the silica gel being released and migrating to the surface forming anion radicals. These results would appear to indicate that silica gel readily traps electrons into relatively deep lying traps (3–4 eV) since light above 4000 Å was relatively ineffective in releasing these trapped electrons. The evidence therefore appears to indicate that electron excess centers and or electron defect centers are involved in the process which inhibits energy transfer in these systems.

As to the possibility that back-reaction ($\text{NO}_2^- + \frac{1}{2}\text{O}_2 \rightleftharpoons \text{NO}_3^-$) is responsible for the decrease in $G(\text{NO}_2^-)$ with absorbed dose, it is observed that for an absorbed dose of 0.172×10^{21} eV/g the pellets containing 0.005 wt % KNO_3 have undergone 4.3% decomposition, whereas those containing 0.05 and 0.3 wt % KNO_3 have undergone 1.03 and 0.6% decomposition, respectively. The per cent decomposition (based on nitrite found) as a function of absorbed dose is shown in Figure 4. It is apparent that the onset of a large decrease in $G(\text{NO}_2^-)$ occurs at approximately the same dose and is independent of the concentration of NO_2^- . Unless some unusual mechanism is invoked for the radiation-induced back-reaction it would be impossible to account for such a large variation in per cent decomposition with concentration. In pure KNO_3 , $G(\text{NO}_2^-)$ decreases with absorbed dose as a result of the back-reaction; however,

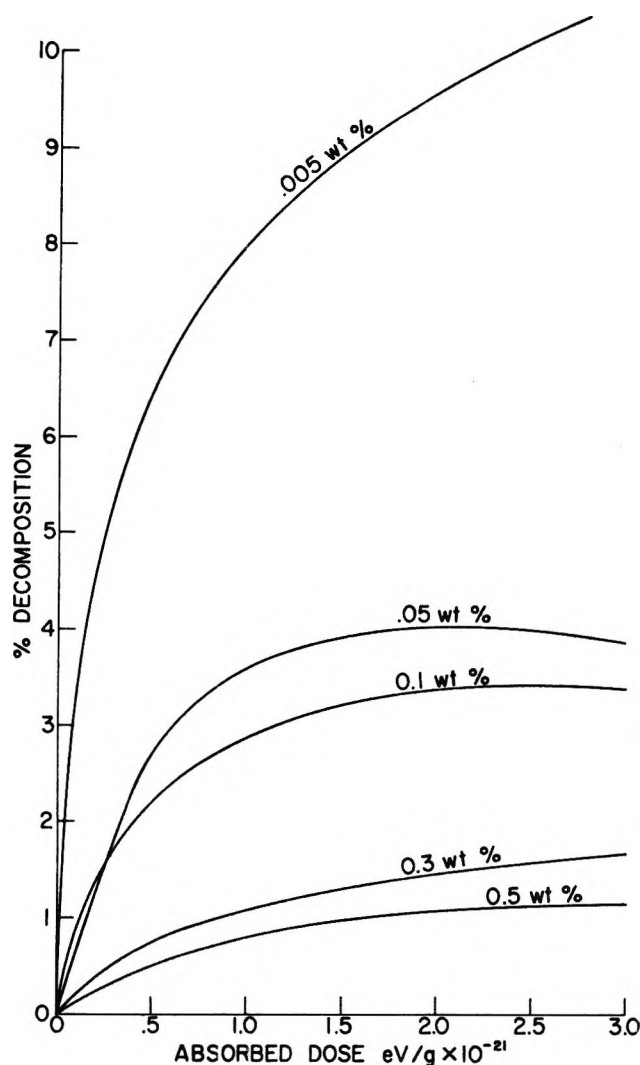


Figure 4. Per cent decomposition as a function of absorbed dose in pellets containing various concentrations of KNO_3 .

in the dose range of 0.172 – 2.8×10^{21} eV/g, $G(\text{NO}_2^-)$ shows only an 8% decrease.

As indicated previously a plot of $G(\text{NO}_2^-)$ vs. temperature appears to give two curves which intersect at about 25° . At the low-temperature side the curve has essentially zero slope or at most a slope which would give an activation of about 200 or so cal/mol. The photochemical and radiation-induced decompositions of the azides also exhibit this phenomenon.^{14,15} The temperature coefficient observed in these studies for the decomposition above 0° is far in excess of that observed for the radiation-induced decomposition of pure KNO_3^- ; hence, the observed activation energy must be related

(12) E. N. Ladov and E. R. Johnson, *J. Amer. Chem. Soc.*, **91**, 7601 (1969).

(13) Y. Yamada, A. Hasegawa, and M. Miura, *Bull. Chem. Soc. Jap.*, **42**, 1836 (1969).

(14) J. M. Grocock and F. C. Tompkins, *Proc. Roy. Soc., Ser. A*, **223**, 267 (1954).

(15) H. G. Heal, *Trans. Faraday Soc.*, **53**, 210 (1957).

to some other process. The effect of temperature on the decomposition of KNO_3 in the KBr-KNO_3 system cannot be explained on the basis of F center destruction since the activation energy for removal of an electron from an F center to the conduction band requires about 1.5–2.0 eV, which is far in excess of the 0.13 eV found in these studies. This amount of energy, however, is more in line with the energy required to remove an electron from an excited F center (or other electron traps). It is also in line with the activation energies observed in photoconductivity studies. The effect of temperature could possibly be interpreted in terms of enhanced diffusion (or exchange of nitrate ion into the KBr lattice); however, some annealing experiments appear to indicate that this cannot be the reason for the enhanced decomposition at the higher temperature. Another possibility is the effect of temperature on the absorption peaks. It is generally observed in the alkali halides that exciton absorption peak energies shift toward lower energies as the temperature is raised. We do not appear to find 1:1 correspondence with efficiency of energy transfer and the energy of the exciton absorption peak in the different bromides; however, we do not know how the presence of lower energy bands in a particular lattice will affect its ability to transfer energy. We are inclined to associate the observed activation energy with removal of electrons from excited trapping sites (corresponding to a loss of electron excess and defect centers) since this amount of energy is more in line with this type of process. These sites then no longer act as exciton trapping sites and, hence, the increased decomposition.

The increase in $G(\text{NO}_2^-)$ when the KBr matrix material is doped with Ag^+ ion is difficult to assess. The absorption spectra of Ag^+ -doped KBr show three new bands, 5.12, 5.35, and 5.8 eV.¹⁶ These levels are all significantly lower than those in pure KBr or KBr at higher temperatures (by about 20–25%). Even though there appears to be no correlation between ease of energy transfer and exciton absorption peak energies, our studies are not sufficiently extensive to preclude the possibility that this substantially lower energy (5.12 eV) or the introduction of impurity levels may be sufficient to cause enhanced energy transfer in the KBr matrix material.

The decrease in $G(\text{NO}_2^-)$ with increasing KNO_3 (Figure 5) concentration appears best explained on basis of an increase in scattering centers (defects) introduced into the KBr . Gibbon and Kuczynski¹⁷ have shown that the pelleting process in pure KCl and KI produces grain boundaries which may act as defect sinks; *i.e.*, F center concentration is greatly enhanced when newly pressed pellets are irradiated; however, annealing can decrease this. In the pelleting process there is a distortion of the KBr lattice at the KNO_3 - KBr interface causing defects which can act as exciton-scattering sites. Increasing the amount of KNO_3 increases the

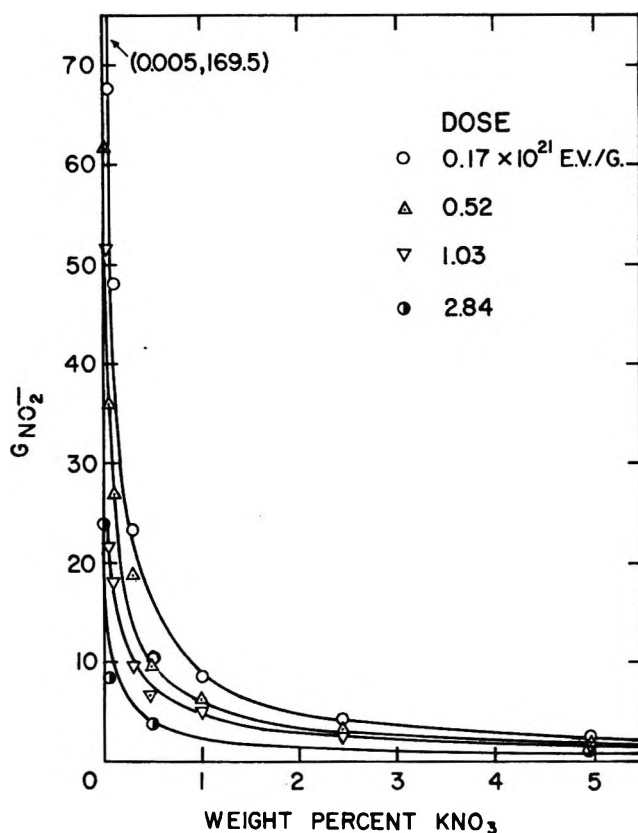


Figure 5. $G(\text{NO}_2^-)$ as a function of wt % KNO_3 for different absorbed doses.

number of these defect sites since the pellets are made by thoroughly mixing microcrystals of KNO_3 and KBr and pressing these into pellets.

The evidence for energy transfer *via* excitons we believe is substantial. The results of Sagert and Robinson⁴ and Wong and Willard⁵ may, at least to some extent, be also explained by low-energy electrons being trapped on the surface. These electrons are released during the irradiation process on the surface or in certain defect sites close to the surface. Lunsford and Jayne^{18,19} were able to detect trapped electrons and radical ions such as CO_2^- and O_2^- on MgO which had been irradiated with 2537-Å light. This energy (4.9 eV) is far below the first exciton absorption peak in MgO , and hence, these electrons arose from impurity states in the MgO . Electrons so trapped in surface states may react with adsorbed molecules, providing the electron affinities of the molecules are sufficiently high to cause capture as in the case of O_2 to form O_2^- or dissociative capture as in the case of N_2O . Our ex-

(16) J. H. Schulman and W. D. Compton, "Color Centers in Solids," Macmillan, New York, N. Y., 1962, pp 175–178.

(17) C. F. Gibbon and G. C. Kuczynski, *J. Chem. Phys.*, **46**, 814 (1967).

(18) J. H. Lunsford and J. P. Jayne, *J. Phys. Chem.*, **69**, 2182 (1965).

(19) J. H. Lunsford and J. P. Jayne, *J. Chem. Phys.*, **44**, 1487 (1966).

periments with N_2O and H_2O , though negative, do not exclude the possibility of the role of surface electrons in our studies since our degassing procedure may not have been adequate. They do, however, indicate that scavangeable electrons play a minor role in the decomposition in the $KBr-KNO_3$ system. Scavangeable electrons

are present on the surface of irradiated alkali halides since it is known that when ethylene is distilled onto irradiated $NaCl$ which has been degassed by simple evacuation, the irradiated salt will induce polymerization in the ethylene,¹¹ indicating the presence of electron excess and defect centers on the $NaCl$ surface.

Thermal Decomposition of the Perchlorate Ion in a Potassium Chloride Matrix¹

by I. C. Hisatsune* and D. G. Linnehan

Department of Chemistry, Whitmore Laboratory, The Pennsylvania State University, University Park, Pennsylvania 16802 (Received June 15, 1970)

The thermal decomposition of ClO_4^- isolated in a pressed KCl disk has been studied by infrared spectroscopy. Although all previous investigators have reported only first-order decomposition kinetics, we found the decay to be a second-order reaction, $2ClO_4^- \rightarrow 2ClO_3^- + O_2$, with Arrhenius parameters of $\log A$ ($M^{-1} \text{sec}^{-1}$) = 12.90 ± 0.13 and $E = 44.31 \pm 0.43$ kcal/mol for the temperature range 450–550°. In this temperature range, ClO_3^- also decomposed by a second-order process with a reaction activation energy of about 30 kcal/mol. The only observable product in the infrared spectrum of the latter reaction system was a small amount of ClO_4^- . When ClO_4^- and ClO_3^- were present together in appreciable concentrations, the decay of both ions was no longer a second-order reaction but followed a reaction order closer to one. However, the first-order rate constants varied from run to run by about one order of magnitude depending on the relative concentrations of both ions. No BrO_3^- was detected during the decomposition of ClO_4^- in a KBr matrix, and the rates were comparable to those from the KCl matrix. The decomposition in a KI matrix produced ClO_3^- and IO_3^- , and the rates were faster by about two orders of magnitude.

Introduction

The existence of numerous publications describing the decomposition of solid potassium perchlorate, including the most recent one by Cordes and Smith,² suggests that the kinetics of this well studied reaction is not yet understood. Indeed, the activation energies reported for this reaction extend from a low value of 37 kcal/mol to about 70 kcal/mol,^{3,4} and, although there seems to be a universal agreement that the decomposition is a first-order reaction, the Arrhenius frequency factors vary by about ten orders of magnitude.^{3,5} Since it appeared to us that more experimental data from the measurement of sample weight changes or of the evolved gases during the reaction are not likely to clarify the decomposition mechanism, we have restudied this reaction by the more direct method of infrared spectroscopy which enables us to measure simultaneously the changes in concentrations of the reactant ClO_4^- and the intermediate ClO_3^- .² To facilitate the infrared measurement and to reduce the difficulties arising from multiple phases⁶ usually present in the decomposition of pure

$KClO_4$, we have employed the alkali halide pressed disks as the reaction media.⁷ We present here the results from a kinetic study of the perchlorate ion isolated in the KCl matrix

Experimental Section

The potassium halides used as matrices were Harshaw infrared optical grade salts. Fisher reagent grade

* To whom all correspondence should be addressed.

(1) This work was supported by PHS Grant EC-97 from the Environmental Control Administration and by Grant AFOSR-907-67 from the AFOSR(SRC)-OAR, USAF.

(2) H. F. Cordes and S. R. Smith, *J. Phys. Chem.*, **72**, 2189 (1968).

(3) A. E. Simchen and A. Glasner, *Bull. Soc. Chim. Fr.*, **20**, 127 (1953).

(4) A. E. Harvey, C. J. Wassink, T. A. Rodgers, and K. H. Stern, *Ann. N. Y. Acad. Sci.*, **79**, 971 (1960).

(5) A. Glasner and A. E. Simchen, *Bull. Soc. Chim. Fr.*, **18**, 233 (1951).

(6) M. M. Markowitz and D. A. Boryta, *J. Phys. Chem.*, **69**, 1114 (1965).

(7) I. C. Hisatsune, *Nippon Kagaku Zasshi*, **89**, 1143 (1968).

KClO₃ was used directly, but KClO₄ came from three different sources. Sample I was a portion of the material used earlier by Seward and Otto⁸ in their study of the perchlorate decomposition in fused sodium hydroxide. This sample had been prepared by two recrystallizations of the Fisher reagent grade salt and subsequent drying of the crystals at 180–190° in a vacuum for seven days. The dried crystals had been pulverized and then stored in a desiccator. The source of sample II was Matheson Coleman and Bell (MCB) reagent grade compound, and it was recrystallized once from an ion-exchanged distilled water. Four recrystallizations of MCB reagent gave sample III.

The experimental procedures for the fabrication of the pressed KCl disks containing ClO₄⁻ in high dilution and for the use of these disks in the decomposition study are described in detail elsewhere.⁹ Most of the original experimental data are summarized in the same reference. We have also reported earlier the matrix isolation of ClO₄⁻ ion in a KCl lattice.⁷

Results

Matrix Isolation of ClO₄⁻. Whether KClO₄ was dispersed in the KCl disk by the freeze-dry method or by the grinding technique,⁷ the initial ir spectrum of the disk showed only a broad band in the Cl–O stretch region near 1120 cm⁻¹. However, as the disk was heated to decompose the solute, this broad band was replaced by a pair of sharp bands at 1133 and 1119 cm⁻¹. In KBr and KI matrices freeze-drying alone was sufficient to produce similar sharp pairs of bands at 1123–1109 cm⁻¹ and 1112–1099 cm⁻¹, respectively. Previously, Krynauw and Schutte¹⁰ had observed and assigned the band pairs in KBr and KI, and we make a similar assignment of the KCl matrix band pair to the degenerate stretch fundamentals of the matrix isolated ³⁶ClO₄⁻ and ³⁷ClO₄⁻ ions.

Since the matrix isolation of the perchlorate ion in KCl and the concomitant growth of the 1133–1119 cm⁻¹ band pair could not be produced without considerable decomposition of the solute, there was no correlation between the observed peak optical density of the band pair and the initial solute concentration in the unheated disk. Thus, the concentration calibration curve necessary for the kinetic study was constructed by taking the integrated intensity of the band pair in KCl to be the same as that in the KBr matrix where the solute can be isolated without decomposition. This assumption of similar integrated intensities in these two matrices appears reasonable in view of the intensity values found for the matrix-isolated cyanate ion.¹¹ Also, the ³⁶ClO₄⁻ ir band in KCl (1133 cm⁻¹) had a band width of 3.8 cm⁻¹ compared to a width of 4.2 cm⁻¹ in a KBr matrix (1123 cm⁻¹) while the band width in KI (1112 cm⁻¹) was 5.2 cm⁻¹. For the integrated intensity of the degenerate stretch band of ClO₄⁻ in KBr, we took the experimental value reported by Krynauw and Schutte.¹⁰

Table I: Peak Molar Extinction Coefficients of ClO₄⁻ Infrared Bands in Potassium Halide Matrices^a

	Extinction coefficient, $M^{-1} \text{ cm}^{-1}$		
	KCl	KBr	KI
$\nu_2(^{36}\text{Cl})$	9550 ± 260 ^b (1133)	9550 ± 260 (1123)	5890 ± 50 (1112)
$\nu_3(^{37}\text{Cl})$	3320 ± 100 ^b (1119)	3320 ± 100 (1109)	2030 ± 20 (1099)
$\nu_4(^{36}\text{Cl}, ^{37}\text{Cl})$	900 ± 100 ^b (640)		500 ± 150 (628)

^a Values in parentheses are peak frequencies in cm⁻¹. ^b See text for origin of these values.

These authors also measured the integrated intensity in KI, which we confirmed experimentally.

The peak molar extinction coefficients, $(1/CL) \log I_0/I$ where C is the molar concentration and L is the path length in centimeters, of the ir bands of ClO₄⁻ ion in the potassium halide matrices are summarized in Table I. The peak optical density calibration points for KBr fell on the same Beer's law line as did those for the KCl matrix, so the same extinction coefficient is listed for both matrices. The degenerate bend fundamental, which showed no isotopic components, was not measured for the KBr matrix but its intensity appeared to be similar to that for the KCl matrix.

Peak molar extinction coefficients for the ClO₃⁻ ion, a reaction intermediate, were determined also by assuming equal integrated intensities in both KCl and KBr matrices. From the integrated intensities reported by Krynauw and Schutte¹⁰ for this ion in KBr, we obtained peak extinction coefficients in KCl of 3240 ± 40, 1280 ± 10, and 250 ± 100 M⁻¹ cm⁻¹ for $\nu_3(^{36}\text{Cl}, 1015 \text{ cm}^{-1})$, $\nu_3(^{37}\text{Cl}, 1005 \text{ cm}^{-1})$, and $\nu_1(^{36}\text{Cl}, ^{37}\text{Cl}, 956 \text{ cm}^{-1})$, respectively.

Decomposition of ClO₄⁻ in KCl Matrix. In the early phase of this investigation, matrix isolation of the ClO₄⁻ ion was effected simply by heating a newly pressed KCl disk at about 370° for several days until the solute exhibited only the sharp band pair at 1133 and 1119 cm⁻¹. This process caused much decomposition of the solute and the formation of the ClO₃⁻ ion before the kinetics could be studied quantitatively. Also, the low initial optical density of the 1133-cm⁻¹ band permitted the decay kinetics to be followed only for a short reaction period, and the presence of the ClO₃⁻ ion introduced additional complications since this intermediate itself was found to decompose into the ClO₄⁻ ion. The optical density changes appeared to follow first-order

(8) R. P. Seward and H. W. Otto, *J. Phys. Chem.*, **65**, 2078 (1961).

(9) D. G. Linnehan, "The Thermal Decomposition of the Perchlorate Ion in a Potassium Chloride Matrix," M.S. Thesis, Pattee Library, The Pennsylvania State University, Dec 1969.

(10) G. N. Krynauw and C. T. H. Schutte, *Z. Phys. Chem. (Frankfurt am Main)*, **55**, 121 (1967).

(11) V. Schettino and I. C. Hisatsune, *J. Chem. Phys.*, **52**, 9 (1970).

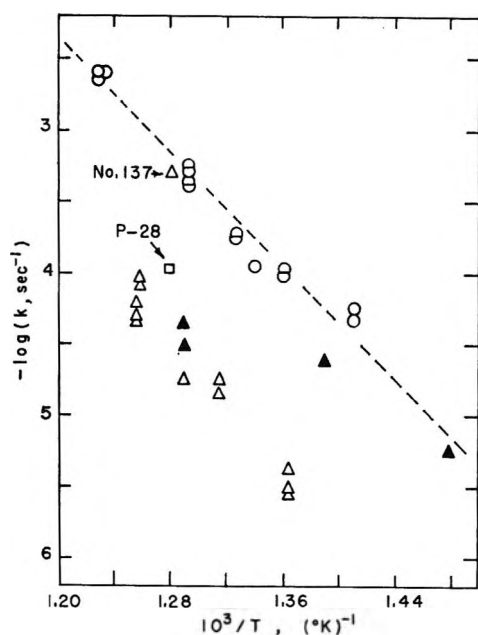


Figure 1. First-order decay rate constants for ClO_4^- in KCl matrix: Δ , sample I; \circ , sample II; \square , run P-28 (Figure 4) of sample III; \blacktriangle , from KClO_3 -KCl disks.

kinetics, and both 1133 and 1119- cm^{-1} bands gave similar rate constants. However, the experimental points showed considerable scatter and often a noticeable decrease in the decay rate toward the end of the reaction. Furthermore, ClO_4^- samples I and II gave rate constants differing by about one order of magnitude as shown in Figure 1. Sample I disks which gave the lower rate constants were characterized by a relatively high concentration of the ClO_3^- intermediate (0.1 to 0.3 optical density unit for the 1015- cm^{-1} band) while the maximum ClO_3^- optical densities observed during the reaction in sample II disks were all less than 0.1. One unusual sample I disk (run no. 137) gave a first-order rate constant at 507° which fell among the sample II values (see Figure 1), but the maximum optical density of the ClO_3^- ion during this run was only 0.071, well below those found in other sample I disks.

To increase the initial concentration of the matrix isolated ClO_4^- and at the same time to minimize the formation of the ClO_3^- intermediate, the experimental procedure of disk fabrication was modified. We found that these requirements were essentially met by disks prepared from powder mixtures that had been heated at about 400° for several hours prior to pressing. Additional sample II disks and some sample III disks were prepared by this new procedure, and most of these disks now showed a second-order decay of the 1133 and 1119- cm^{-1} bands. An example of this second-order ClO_4^- decomposition is illustrated in Figure 2 for a reaction carried out at 522°. The intermediate ClO_3^- ion was still formed during this decomposition, and its 1015- cm^{-1} band optical density is plotted against that of the reactant 1133- cm^{-1} band in Figure 3. The cor-

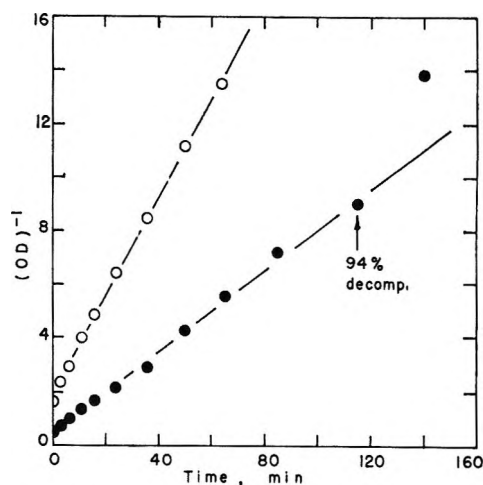


Figure 2. Second-order decay of ClO_4^- (sample II) in KCl matrix at 522°: \bullet , $^{35}\text{ClO}_4^-$ ($k = 4.5 M^{-1} \text{sec}^{-1}$); \circ , $^{37}\text{ClO}_4^-$ ($k = 3.9 M^{-1} \text{sec}^{-1}$). Data from 1.00-g disk of 13 mm diameter.

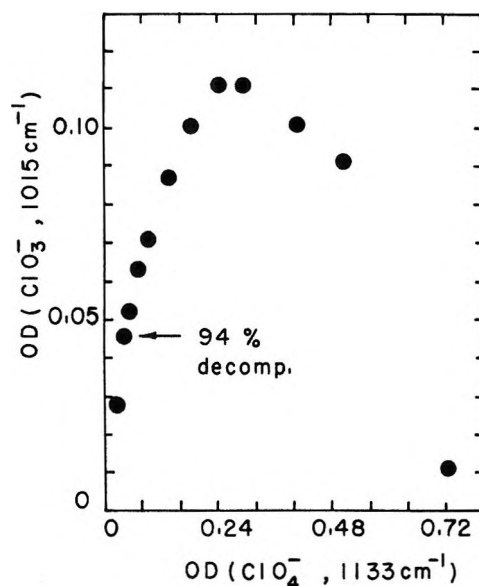


Figure 3. Changes in optical densities of ClO_3^- and ClO_4^- ions at 522°. Data from kinetic run of Figure 2 but the mass of the KCl disk is 0.400 g.

rected optical densities⁷ in this figure correspond to those from a KCl disk weighing exactly 0.4 g while the standard disk weight was taken as 1 g for the data in Figure 2.

The maximum observed in the chlorate concentration for reactions at temperature above about 500° was often greater than that shown in Figure 3, and experimental points from such a run gave a poor fit to the second-order kinetic equation. In fact, its reaction order analysis indicated that the decomposition of the ClO_4^- ion was approximately second order during the growth stage of the ClO_3^- ion but it changed to an order closer to 1 during the decay stage of ClO_3^- . In runs where the ClO_3^- maximum was high and near the beginning

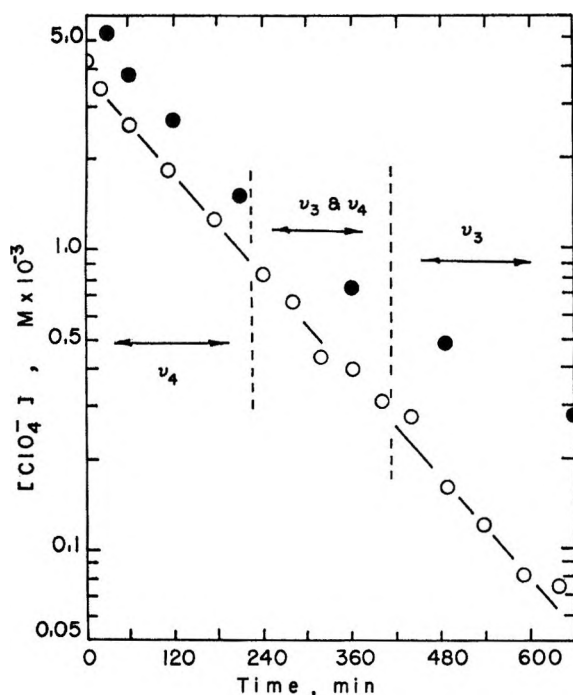


Figure 4. First-order decay of 1.58 mg/g of KClO_4 in KCl at 510° : \circ , run P-28; \bullet , run P-32. See text.

of the reaction, the overall reaction order for ClO_4^- decay was often neither first nor second but had an intermediate value. Run P-32 of Figure 4 is an example of a decomposition in which the reaction order was about 1.5. In this run, as well as in run P-28 shown in the same figure, the weak degenerate bending mode fundamental at 640 cm^{-1} had to be used to follow the initial part of the reaction. Both runs were made with disks containing identical initial concentration of the solute, but P-32 disk was made from a preheated powder, whereas P-28 disk was not preheated. The infrared spectrum of the latter disk resembled the spectrum of crystalline KClO_4 throughout most of the decomposition. The first-order rate constant from run P-28 is included in Figure 1. Much ClO_3^- was present in both disks during the reaction.

The second-order rate constants from sample II and III disks showing relatively low yields of ClO_3^- intermediate are summarized in Figure 5. We have also calculated and displayed in this figure (opened circles and triangle) second-order rate constants from the initial rates of reactions which showed a first-order ClO_4^- decay and gave low ClO_3^- concentration during the reaction (Figure 1). The Arrhenius parameters from the least-squares fit of these data were $\log A$ ($\text{M}^{-1}\text{sec}^{-1}$) = 12.90 ± 0.13 and $E = 44.31 \pm 0.43$ kcal/mol. The solid line drawn through the points in Figure 5 corresponds to these Arrhenius parameters, and a line with the same activation energy has been inserted in Figure 1 for the sample II data points. The first-order frequency factor for the latter data is about $\log A$ (sec^{-1}) = 9.2.

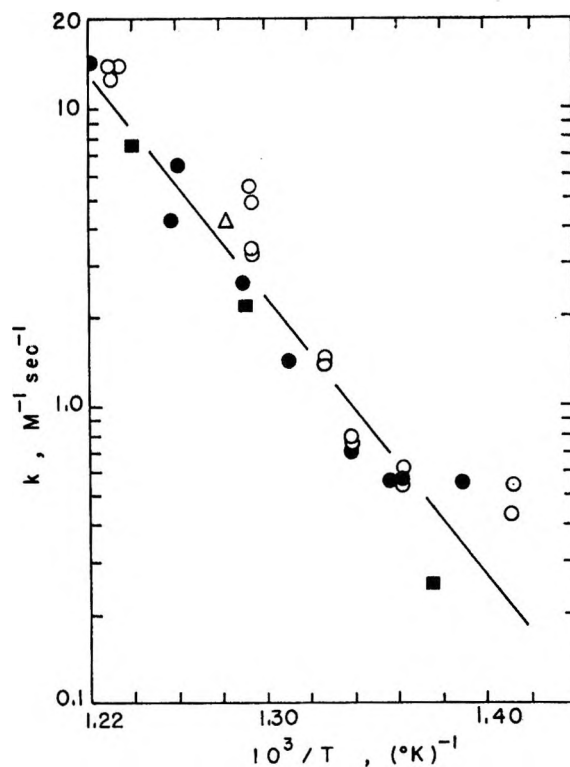


Figure 5. Second-order decay rate constants for ClO_4^- in KCl matrix: \bullet , sample II; \blacksquare , sample III; \circ , from sample II first-order data (Figure 1); Δ , from run 137 data (Figure 1).

The stoichiometric relationship between ClO_4^- and ClO_3^- was determined from optical density correlation plots like that shown in Figure 3. From seven disks which gave second-order decay kinetics, the $d[\text{ClO}_3^-]/d[\text{ClO}_4^-]$ ratios from the growth and decay stages of the ClO_3^- ion were -0.92 ± 0.13 and $+1.9 \pm 0.2$, respectively.

Decomposition of ClO_4^- in KBr and KI Matrices. The decomposition of ClO_4^- in KBr and KI matrices was examined qualitatively. No BrO_3^- was detected during the reaction in KBr, but much ClO_3^- was produced. As in the KCl case, disks with low ClO_3^- concentrations gave second-order decay kinetics while those with high concentrations of this intermediate followed a reaction order closer to one. The decomposition rates and rate constants for the KBr matrix, however, were comparable to those obtained from the KCl disks.

First-order kinetics was observed for the decay of ClO_4^- in a KI matrix. The rates were about two orders of magnitude greater than the rates in the KCl matrix. Consequently there was very little decay of the intermediate ClO_3^- , and 1.06 ± 0.12 mol of this ion was produced from each mole of ClO_4^- . One mole of iodate ion was also produced in this reaction from 2.8 ± 0.6 mol of ClO_4^- .

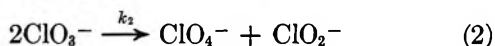
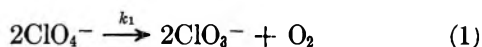
Decomposition of ClO_3^- in KCl Matrix. Qualitative study of the decomposition of ClO_3^- isolated in a KCl matrix was also carried out. This reaction was found

to be second order in ClO_3^- with a rate constant of $10^{8.3} \exp(-30 \text{ kcal}/RT) M^{-1} \text{ sec}^{-1}$ for the temperature range $450\text{--}550^\circ$. The ClO_4^- ion was observed as a minor product ($\sim 10\%$ yield), but in four disks its concentration was sufficient to follow the decomposition. The ClO_4^- decay was first order, and the rate constants which fell into two sets according to the concentration of ClO_3^- present during the reaction are included in Figure 1.

The rates of second-order decay of ClO_3^- in KBr and KI matrices were comparable to the rates in the KCl matrix. However, when a high concentration of ClO_4^- was present with the ClO_3^- as in the case shown in Figure 3, the decay of the latter ion in both KCl and KBr matrices was not a second-order but approximately a first-order reaction.

Discussion

A decomposition mechanism for the ClO_4^- ion, which is consistent with our experimental results, must include the following bimolecular reactions.



Reaction 1 is suggested by the observed second-order decay of ClO_4^- in kinetic runs where $[\text{ClO}_3^-]$ was low during the reaction and by $d[\text{ClO}_3^-]/d[\text{ClO}_4^-] = -0.92 \pm 0.13$ for the growth stage of ClO_3^- intermediate (see Figure 3). The detection of ClO_4^- during the decomposition of ClO_3^- isolated in a KCl matrix and the second-order kinetics of this decomposition when the concentration of ClO_4^- intermediate was low suggest reaction 2. The second product of this reaction is presumably unstable and cannot be trapped in the matrix at our decomposition temperatures of $450\text{--}550^\circ$. Our experimental data also indicate that reactions 1 and 2 may be the principal steps in the formation and decay of the intermediate ClO_3^- during the decomposition of ClO_4^- . Since the rates of formation and decay of the intermediate ClO_3^- are the same at the observed maximum in $[\text{ClO}_3^-]$, we have $k_1[\text{ClO}_4^-]_{\text{max}}^2 = k_2[\text{ClO}_3^-]_{\text{max}}^2$. Our experimental values⁹ of k_1 , $[\text{ClO}_3^-]_{\text{max}}$, and $[\text{ClO}_4^-]_{\text{max}}$ give $k_2 = 10^{9.4} \exp[-32 \text{ kcal}/RT] M^{-1} \text{ sec}^{-1}$ which is in reasonable agreement with the second-order decomposition rate constant obtained from KCl disks with ClO_3^- .

When the concentrations of ClO_4^- and ClO_3^- were comparable, the decomposition of ClO_4^- was no longer a second-order reaction (Figures 1 and 4). Reactions 1 and 2 show that such deviations are expected, but they do not provide an interpretation of the approximate first-order decay of ClO_4^- observed under these experimental conditions. Neither are these equations

adequate to explain the first-order decay of ClO_3^- when $[\text{ClO}_4^-]$ was relatively high. More extensive kinetic studies of the decompositions of ClO_3^- , ClO_2^- , and perhaps ClO^- are necessary to determine what additional reactions to include with reactions 1 and 2 to provide a satisfactory interpretation of our kinetic data on ClO_4^- .

The decomposition rates of ClO_4^- in the KBr matrix were not markedly different from those in KCl. Thus, reactions 1 and 2 appear to be the principal steps in the KBr matrix also, and the effect, if any, of the chloride ion in the decomposition of ClO_4^- is comparable to that of the bromide ion. However, our experimental results from the KI matrix indicate that the iodide ion accelerates the decomposition of ClO_4^- more so than it does the decay of ClO_3^- . In this matrix the experimental reaction stoichiometry was



and the decay of ClO_4^- was a first-order reaction.

Apparently, there has been no report in the literature of a second-order decomposition kinetics of the perchlorate ion. However, Cordes and Smith² have recently interpreted their first-order kinetic results in terms of reaction 1 as being a homogeneous bimolecular solid state reaction. They proposed for this reaction a transition state with a reasonable structure $(\text{O}_3\text{ClOOCIO}_3)^{2-}$. Their first-order rate constants varied by about one order of magnitude depending on the sample as did ours, and they consistently observed CO_2 as a minor product. This gas was also observed in some of our disks which exhibited a gray color. It appears that carbon-containing impurities in reagent grade salts, in the laboratory atmosphere, and in distilled water may be the sources of the CO_2 gas.^{7,12} The success we had in reducing the initial $[\text{ClO}_3^-]$ by preheating in air the $\text{KClO}_4\text{--KCl}$ powder mixture before pressing may be due in part to the elimination of some carbon impurities by oxidation. Although impurities are known to affect strongly the decomposition of the perchlorate ion, the kinetics observed by previous investigators may be influenced by the presence of the chlorate ion in their reaction systems.

Acknowledgments. We are pleased to acknowledge the support given us by the Bureau of Radiological Health of the PHS Environmental Control Administration and by the Directorate of Chemical Sciences of the U. S. Air Force Office of Scientific Research. We wish to thank James J. Stacy for carrying out some preliminary studies as a B.S. degree thesis research and for assisting us in some of our experimental work.

(12) D. L. Bernitt, K. O. Hartman, and I. C. Hisatsune, *J. Chem. Phys.*, **42**, 3553 (1965).

Ultrasonic Absorption in Aqueous Solutions of Polyethylene Glycol^{1a}

by L. W. Kessler,^{1b} W. D. O'Brien, Jr., and F. Dunn

Bioacoustics Research Laboratory, University of Illinois, Urbana, Illinois 61801 (Received February 16, 1970)

Ultrasonic absorption spectra have been determined for aqueous solutions of polyethylene glycol, a linear molecule which assumes a random coil configuration, as a function of molecular weight (62–20,000) and frequency (1.5–163 MHz). The broad frequency range employed in this investigation revealed the presence of multiple relaxation processes. Similarities between the absorption dependence upon frequency and molecular weight of polyethylene glycol and dextran, another macromolecule which assumes a similar spatial configuration in solution, are pointed out. It is concluded that the observed ultrasonic absorption cannot be fully accounted for by shear viscoelasticity and that the presence of a bulk viscosity must be taken into account.

Introduction

The ultrasonic velocity of propagation and absorption coefficient characteristic of aqueous solutions of macromolecules are of interest in the fields of physical chemistry and biophysics to the extent that these properties are useful in studying the kinetic behavior of chemical and structural equilibria having reaction rate constants between 10^{-9} and 10^{-4} sec.^{2a} These equilibria may be perturbed by changes in temperature, pressure, or density produced by the sound wave. The molecular process whose characteristic time determines the rate at which equilibrium is restored, after the perturbation, is referred to as a relaxation process.^{2b} It has been observed that perturbations of configurational equilibria may result in significant acoustic absorption³ and definite changes in absorption and velocity that correlate with structural alterations have also been reported.^{4,5} This study was undertaken to continue the investigation of the ultrasonic absorption spectra of aqueous solutions of macromolecules which assume similar configurations but which differ chemically. Polyethylene glycol (PEG), a synthesized long-chain flexible macromolecule, was chosen for this purpose since it assumes a random coil configuration in aqueous solution as does another macromolecule, dextran, which has already been studied.^{6,7} In addition, since PEG is readily obtainable in several narrow molecular weight fractions, the effect of polymerization on the acoustic properties of the solution could be studied.

Theory

The adiabatic propagation of a longitudinal acoustic wave through a fluid medium results in time-varying localized perturbations in thermodynamic equilibria at rates which depend on the sound frequency, f , and maximum interaction for any particular equilibrium occurs when $f = f_0 = (2\pi\tau)^{-1}$, where τ is the characteristic relaxation time of the reaction being perturbed. This leads to a time lag between an applied pressure and the resulting change in density. Consequently, molecular energy level populations are perturbed at the expense of

acoustic wave energy, and the process results in absorption. The absorption that is experimentally observed may result from multiple independent or coupled relaxation processes which can yield a spectrum of relaxation times.

Shear viscosity was one of the first properties to be recognized as responsible for the absorption of sound in fluids.⁸ Although it was realized at the time that a liquid may possess bulk viscosity as well, this was not considered, as no direct method was available for its measurement. The well-known equation describing the absorption of sound by a viscous liquid is

$$\alpha = \frac{2\pi^2 f^2}{\rho V^3} (\eta_v + \frac{4}{3}\eta_s) \quad (1)$$

where ρ and V are the undisturbed density and the low-frequency speed of sound, and η_v and η_s are the bulk and shear viscosities, respectively. Variation in the viscosity with frequency is due to relaxation; however, for water the viscous relaxation times are thought to be of the order 10^{-12} sec,^{9,10} which is almost two orders of magnitude beyond the currently attainable range of acoustic measurements.

(1) (a) Portions of this work were extracted from the thesis submitted by L. W. K. in partial fulfillment of the requirements for the Ph.D. degree in Electrical Engineering, University of Illinois, 1968. (b) To whom correspondence should be addressed at Research Department, Zenith Radio Corp., 6001 W. Dickens Avenue, Chicago, Ill. 60639.

(2) (a) F. Dunn, P. D. Edmonds, and W. J. Fry, "Absorption and Dispersion of Ultrasound in Biological Media" in "Biological Engineering," H. P. Schwan, Ed., McGraw-Hill Book Co., New York, N. Y., 1969; (b) M. Eigen and L. deMayer, "Relaxation Methods" in "Technique of Organic Chemistry," Vol. 8, part 2, S. L. Friess, et al., Ed., Interscience, New York, N. Y., 1963.

(3) G. Schwarz, *J. Mol. Biol.*, **11**, 64 (1965).

(4) L. W. Kessler and F. Dunn, *J. Phys. Chem.*, **23**, 4526 (1969).

(5) R. Zana, R. Cerf, and S. Candau, *J. Chim. Phys.*, **60**, 869 (1963).

(6) S. A. Hawley and F. Dunn, *J. Chem. Phys.*, **50**, 3523 (1969).

(7) S. A. Hawley, L. W. Kessler, and F. Dunn, *J. Acoust. Soc. Amer.*, **38**, 521 (1965).

(8) G. G. Stokes, *Trans. Cambr. Phil. Soc.*, **8**, 287 (1845).

(9) L. Hall, *Phys. Rev.*, **73**, 775 (1948).

(10) H. S. Frank and W. Y. Wen, *Discuss. Faraday Soc.*, **24**, 133 (1957).

The shear viscosity exhibited by a dilute solution of long-chain flexible polymers results from the frictional resistance opposing the flow of solvent molecules past polymer segments and the resistance to perturbation of the configurational equilibrium of the polymer. Further, the bulk viscosity is due to resistance of the polymer molecules against changing the volume they occupy in the solvent in response to a pressure change, and it is dependent on solvent-polymer interactions which may not affect the shear viscosity. Adequate physical models which would predict the observed frequency dependence of bulk viscosity have not yet been developed for aqueous systems because of the inadequate knowledge of the specific solvent-polymer interactions. The polymer model used to calculate the dynamic shear viscosity consists of a linear arrangement of $N + 1$ identical beads each having mass m connected alternately by N massless link segments.¹¹ If complete flexibility is allowed at each bead, the mean-squared distance between the ends of the chain, \bar{L}^2 , is given by the statistical random walk result for large N ¹¹

$$\bar{L}^2 = \bar{b}_0^2 N \quad (2)$$

where \bar{b}_0^2 is the mean-squared segment length. Since complete flexibility cannot be allowed, \bar{b}_0^2 is replaced by \bar{b}_{eff}^2 .

The dynamic shear viscosity of an infinitely dilute solution of Gaussian coiled polymers is given by^{12,13}

$$\eta^* = \eta_0 + \frac{CN_A}{M_w} KT \sum_{k=1}^N \frac{\tau_k}{1 + i\omega\tau_k} \quad (3a)$$

$$\eta^* = \eta' + i\eta'' \quad (3b)$$

where η_0 is the shear viscosity of the solvent, C is the concentration of polymer molecules, M_w is the weight-average molecular weight of the polymer, N_A is Avogadro's number, T is the absolute temperature, K is Boltzmann's constant, and the summation is carried out over all N segments of the polymer. In eq 3b, η'' can be considered as elasticity. The relaxation time, τ_k , depends on hydrodynamic interactions¹²⁻¹⁵ which may be taken into account by the expansion parameter¹² ϵ by

$$\frac{\bar{b}_{\text{eff}}^2}{\bar{b}_0^2} = N^\epsilon \quad (4)$$

The relaxation times are given by

$$\tau_k = \frac{M_w \eta_0 [\eta]_0}{\left(\sum_{k=1}^N \lambda^{-1} \right) N_A K T \lambda_k} \quad (5)$$

where $[\eta]_0$ is the intrinsic viscosity of the solution at $\omega = 0$, given by¹²

$$[\eta]_0 = (2.84 \times 10^{23}) \frac{\bar{L}^3}{M_w} \quad (6)$$

and the λ_k 's are tabulated as a function of ϵ in ref 14.

Ultrasonic Technique

The amplitude of a plane, progressive sinusoidal wave decays exponentially as it propagates through a lossy, homogeneous, infinitely extended medium according to

$$P(x,t) = P_0 \exp(-\alpha x) \exp[i(\omega t - kx)] \quad (7)$$

where P is the instantaneous value of the acoustic pressure amplitude as a function of distance x and time t , and k is the wave number. The pulse technique employed in this study to measure the absorption coefficient in liquids simulates the free field condition expressed by eq 7 for finite sample sizes, provided that the pulse length in the medium is short compared with the acoustic path length. In addition, the error in the absorption coefficient due to the spectrum of frequencies associated with a pulse train is negligible if the pulse is at least $30\pi/\omega$ sec in length.¹⁶

Two techniques were employed in the present study to measure the absorption coefficient over the frequency range from 1.5 to 163 MHz. The first technique,^{17,18} an automated version of that originally described by Pellam and Galt,¹⁶ can be employed into the low megahertz frequency range depending on the magnitude of the absorption relative to the attenuation due to diffraction. For example, for a 1-in. diameter transducer the above considerations limited operation to 9 MHz. Over the frequency range from 9 to 69 MHz two matched 3-MHz fundamental frequency X-cut quartz transducers are set parallel and coaxial to each other in the liquid to be studied. Each transducer is edge-mounted with its front face in direct contact with the liquid and its back face exposed to an air-filled cavity. One transducer emits pulses of ultrasonic energy, while the other transducer is employed as a detector. The acoustic path length is varied by displacing one transducer relative to the other at constant velocity. The amplitude of the received acoustic pulse varies according to eq 7, and the amplitude of the electrical signal from the receiving transducer is recorded on a logarithmic recorder whose chart displacement is synchronized to the moving transducer. Over the frequency range from 75 to 165 MHz, a pair of 15-MHz fundamental, X-cut quartz transducers bonded to fused quartz delay rods are substituted for the 3-MHz transducers.

In this variable path length technique, the absorption could be determined to within $\pm 3\%$ in water over the approximate frequency range from 15 to 100 MHz.

(11) C. Tanford, "Physical Chemistry of Macromolecules," Wiley, New York, N. Y., 1961.

(12) B. H. Zimm, *J. Chem. Phys.*, **24**, 269 (1956).

(13) P. E. Rouse, *ibid.*, **21**, 1272 (1953).

(14) V. Bloomfield and B. H. Zimm, *ibid.*, **44**, 315 (1966).

(15) A. Peterlin, *J. Polym. Sci., Part A2*, **5**, 179 (1967).

(16) J. R. Pellam and J. K. Galt, *J. Chem. Phys.*, **14**, 608 (1946).

(17) S. A. Hawley, Ph.D. Thesis, University of Illinois, Urbana, Ill., 1966.

(18) L. W. Kessler, S. A. Hawley, and F. Dunn, *J. Acoust. Soc. Amer.*, **41**, 1591 (1967).

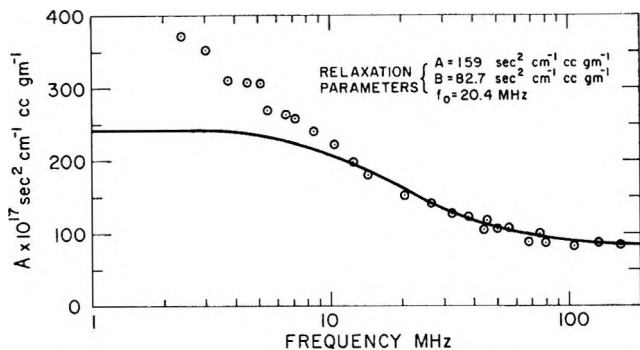


Figure 5. Best-fit single relaxation curve for M_w 20,000 and M_w 4500, above 10 MHz.

To elucidate the mechanism(s) responsible for the ultrasonic absorption, the contribution of dynamic shear viscosity must be considered. Heretofore it was thought that such a process was unimportant for this material for two reasons.²⁵ First, on the basis of their data (which were all above 10 MHz), the mechanism was concluded to be a single relaxation process, and second, the relaxation times predicted theoretically were more than an order of magnitude larger than those observed. Contributing to this last factor is an error in their calculation of τ_k wherein the static viscosity of the solution η is used in place of that of the solvent, η_0 .²⁶

The dynamic shear viscosity contribution to the absorption coefficient is discussed below on the basis of the Bloomfield-Zimm theory.¹⁴ Subsequent comparison with the contribution predicted by the Rouse theory¹³ and the Zimm theory¹² resulted in only slight differences in the overall absorption. PEG molecules are assumed to be extended, nonfree-draining, flexible polymers and each structural unit is assumed to be the monomer unit, although larger segments could also have been used.¹¹ The effective segment length, b_{eff} , is calculated from the ratio of the intrinsic viscosity, predicted on the basis of b_0 for nonfree-draining coils, to that observed, and from eq 6 and 2 the following relationship is obtained

$$\frac{[\eta]_0^{theor}}{[\eta]_0^{obs}} = \left[\frac{b_0}{b_{eff}} \right]^3 \quad (11)$$

The intrinsic viscosity was reported in aqueous solutions of PEG at 20.0°²⁸ and found to be related to molecular weight by the following relationship

$$[\eta]_{obs} = 2.0 + 0.033(M_w)^{0.72} \quad (12)$$

Table I lists the properties of PEG polymer chains used to compute the relaxation times, and Table II lists the relaxation times for the first four modes of viscoelastic relaxation. The viscoelastic absorption is evaluated from the following equation where $\Delta\alpha_s$ is the difference

$$A_s = \frac{\Delta\alpha_s}{Cf^2} = \frac{15.65 \times 10^{-5}}{M_w} \sum_{k=1}^N \frac{\tau_k}{1 + \omega^2\tau_k^2} \quad (13)$$

Table I: Properties of PEG Polymer Chains

M_w	N	$[\eta]^a$ cc/g	$[\eta]^b$ cc/g	b_{eff} , Å	ϵ
20,000	455	43.2	11.7	6.78	0.14
4,500	102	16.1	5.48	6.30	0.15
1,450	33	8.23	3.16	6.07	0.184
400	9	4.47	1.63	6.16	0.306

^a Intrinsic viscosity calculated from eq 12. ^b Intrinsic viscosity calculated from eq 6.

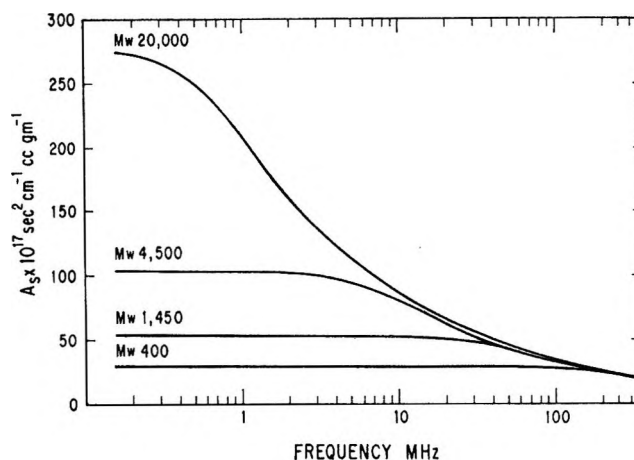


Figure 6. Computed absorption due to shear viscosity relaxation.

in the shear absorption coefficients between the solution and the solvent, and this result is plotted in Figure 6 for the three highest molecular weight fractions.

Comparison of Figure 6 with the experimentally observed results (Figure 1) suggests that the dynamic shear viscosity alone does not describe completely the observed ultrasonic absorption since the theoretical prediction accounts for only a fraction of that actually observed. For this comparison, the ordinates of Figures 1 and 6 are related by the equation $A = A_s - 84 \times 10^{-17} \text{ sec}^2 \text{ cm}^{-1} \text{ cc g}^{-1}$ for a solution of concentration 0.2 g/cc. Since the frequency dependence of the absorption due to shear viscoelasticity may not be an unreasonable description of that observed, considering the high concentrations of the solutions employed, it appears possible, as suggested by Hawley and Dunn,⁶ that the normal modes of the molecule determine the mode of coupling to other relaxation processes. The absorption, not accounted for by shear viscoelastic relaxation, can be accounted for by volume viscosity due to thermal or structural relaxation processes.²⁹ Thermal relaxation occurs if the temperature fluctuations which follow the sound wave perturb a molecular

(28) C. Sadron and P. Rempp, *J. Polym. Sci.*, **XXIX**, 127 (1958).

(29) J. Lamb in "Physical Acoustics," Vol. II, Part A, W. P. Mason, Ed., Academic Press, New York, N. Y., 1965, Chapter 4.

Table II: Predicted Relaxation Times for Shear Viscoelastic Relaxation

M_w	τ_1 , sec	τ_2 , sec	τ_3 , sec	τ_4 , sec
20,000	16×10^{-8}	4.9×10^{-8}	2.5×10^{-8}	1.6×10^{-8}
4,500	12×10^{-9}	3.7×10^{-9}	1.9×10^{-9}	1.2×10^{-9}
1,450	23×10^{-10}	7.0×10^{-10}	3.6×10^{-10}	2.2×10^{-10}
400	42×10^{-11}	12×10^{-11}	6.3×10^{-11}	3.8×10^{-11}

equilibrium. Typical examples of such a process are chemical relaxation and rotational isomerism. Thus far, however, each thermal relaxation process observed has been best described by a single relaxation time. Structural relaxation occurs when the hydrostatic pressure or density fluctuations disturb a molecular level configurational equilibrium which results in a volume change, *i.e.*, a pressure-dependent arrangement of atoms in the solution. Structural relaxation is usually characterized by a broad spectrum of relaxation times²⁹ and is probably responsible for the excess absorption in aqueous solutions of PEG. At high frequencies, however, the nonzero limiting value of A_s of $171 \times 10^{-17} \text{ cm}^{-1} \text{ sec}^2 \text{ cc g}^{-1}$ could also be due to an internal viscosity of the polymer chain,¹⁶ but the data available do not permit the magnitude of this contribution to be calculated.

Two possible mechanisms of structural relaxation in aqueous PEG solutions are considered. First, η_v can be due to perturbation of the polymer-solvent complex by the sound wave. More specifically, either the structure of the hydration layer surrounding the polymer chain or the amount of hydration is pressure dependent. This mechanism has already been attributed to the excess absorption in aqueous solutions of dextran⁶ and has also been proposed for PEG.²⁶ Second, η_v can be caused by a perturbation of the short-range structural configuration of the polymer chain which would result in a change in the radius of gyration of the flexible polymer. Two structural configurations exist for PEG, the zig-zag and the meandering forms,³⁰ for the low and the high molecular weight fractions, respectively. On the basis of entropy considerations the meandering form resides in a higher energy level, and it is possible that when the higher molecular weight fractions are subjected to ultrasonic stress, the structural equilibrium is shifted toward the zig-zag configuration. Suppose that each segment of the polymer chain that occupies the meandering form can be considered as a unit which is capable of structural relaxation in the ultrasonic range. Then, if interactions between units can be neglected, the ultrasonic absorption would be linearly dependent on the number of units present. Since the structure of all the high molecular weight PEG chains is predominantly the meandering configuration,³⁰ the number of relaxing units relative to the molecular weight of the polymer is constant. Therefore, on the assumption that the absorption is determined by the

presence of relaxing units, the absorption in aqueous solutions of high molecular weight fractions of PEG would depend on the mass concentration of the solution and not upon the molecular weight. This type of behavior is supported experimentally by Figure 7 which shows that above M_w 4500, A is independent of molecular weight. Since the lower molecular weight fractions are composed of smaller percentages of meandering structures, the absorption per concentration decreases. This molecular weight dependence is similar to that observed for dextran⁶ except that in that case the absorption approaches that of the monomer at higher frequencies,

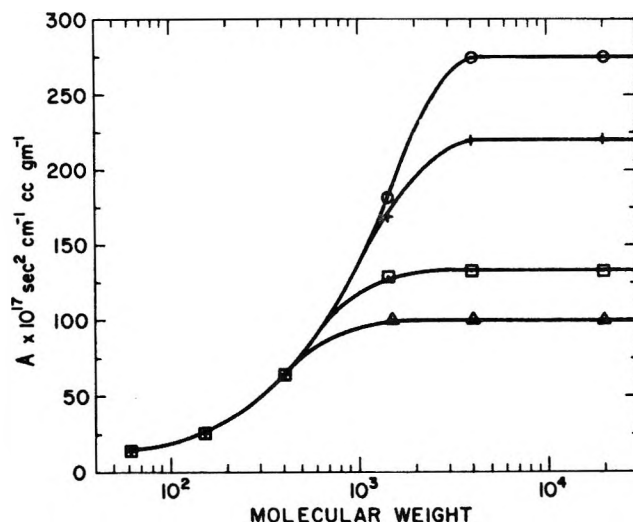


Figure 7. Dependence of absorption on molecular weight: ⊞, all frequencies; ○, 6 MHz; +, 10 MHz; □, 30 MHz; Δ, 60 MHz.

whereas in PEG it does not. This could be due to additional relaxation processes that occur in a higher frequency range or due to an internal viscosity of the polymer. Also, with regard to the presence of relaxing units it is noteworthy that the absorption spectrum for M_w 1450 approaches that for M_w 4500 and M_w 20,000 at about 35 MHz in both Figures 1 and 6. In contrast, viscoelastic theory predicts that the absorption spectra for M_w 4500 and M_w 20,000 should begin to diverge substantially in the neighborhood of 10 MHz, but this

(30) G. O. Curme, "Glycols," Reinhold, New York, N. Y., 1952, pp 180, 181.

is not observed experimentally. This implies the possibility of distinct relaxation processes occurring over the frequency range investigated.

Acknowledgement. The authors acknowledge grate-

fully the support of this research in part by a grant from the Institute of General Medical Sciences, National Institutes of Health, and in part by the Office of Naval Research, Acoustics Program.

Electron Spin Resonance Spectra and Catalytic Activity of Molybdenum Oxide on Various Supports

by K. S. Seshadri and L. Petrakis

Gulf Research & Development Company, Pittsburgh, Pennsylvania 15230 (Received April 9, 1970)

Hexavalent molybdenum in the oxide form incorporated either by impregnation or coprecipitation into magnesium oxide, alumina, or magnesium aluminate, and subsequently reduced at elevated temperatures was investigated by electron spin resonance spectroscopy (esr), and its catalytic activity was tested by the vapor phase aldol condensation of *n*-butyraldehyde. The yield of certain products was found to correlate with the esr signal intensity, both showing the same functional dependence on molybdenum content that reached a maximum at 9 wt % in MoO₃. The esr spectra showed considerable variation with preparation procedure, nature of support, pretreatment, and reduction temperatures. The species responsible for the esr signal were identified as Mo⁵⁺, and spectral parameters were extracted. No hyperfine structure components due to the odd isotopes of molybdenum were observed in the solid samples. However, such a hyperfine structure is observed in the isotropic spectra resulting from the acid solutions of the catalysts. When frozen, these acid solutions yield highly anisotropic spectra which are described by an axially symmetric spin Hamiltonian.

Introduction

Catalytically active species are often paramagnetic and, therefore, can be studied by esr spectroscopy. Possible information that can be obtained about the active species includes qualitative identification of the valency and the nature of the site occupied, quantitative determination of the active species, and elucidation of the role of such variables as nature of support, calcination temperature, preparative procedure, reduction conditions, etc., on the appearance of the spectra. The availability of such information, of course, would be very significant in that it could provide some insight into fundamental aspects of heterogeneous catalysis. However, the extraction of the pertinent spectroscopic parameters from polycrystalline samples (catalysts) is seldom an easy task. For, unlike well-defined single crystals, powder spectra can have all the complications of the solid state (*e.g.*, anisotropy of *g* and hfs) for which there is little hope of separating these various complicating effects. When esr spectroscopy is used to study catalysts, a number of questions arise. Might not the spectroscopic parameters be expected to change radically with the nature of the support? How severe are changes that are introduced by variations in calcination temperatures, reduction temperatures, or in preparation

procedures such as coprecipitation and impregnation? Can the valence and nature of the active site be identified unambiguously? Can the various spectroscopic parameters be correlated with criteria of catalytic efficiency and selectivity of the systems for various reactions? We have studied the spectra of molybdenum oxide in a number of hosts in an attempt to answer some of these questions.

Molybdenum(V) in suitable media has been found to catalyze the polymerization of ethylene and has been studied by esr spectroscopy. A correlation between the esr spectra and the catalytic activity has been established.¹ Spin resonance of Mo(V) has also been reported in the host lattice of TiO₂² and in aqueous acid solutions.³ The catalytic activity of molybdenum oxide, particularly of Mo₂O₃, has not been extensively explored. MoO₃, Bi₂O₃-MoO₃, and some nonstoichiometric Mo oxides have been used in the catalytic oxidation of 1-butene to butadiene.⁴ The oxidation of

(1) V. A. Dzs'ko, E. M. Emel'yanova, Yu. I. Pecherskaya, and V. B. Kazanski, *Dokl. Akad. Nauk SSR*, **150**, 829 (1963).

(2) (a) R.-T. Kyi, *Phys. Rev.*, **128**, 151 (1962); (b) T.-T. Chang, *ibid.*, **136**, A1413 (1964).

(3) M. M. Abraham, J. P. Abriata, M. E. Foglio, and E. Pasquini, *J. Chem. Phys.*, **45**, 2069 (1966).

other olefins has been studied by Adams,⁵ and Sachtler and de Boer⁶ have studied the conversion of propylene into acrolein on bismuth molybdate. During these reactions, the reduction of hexavalent molybdenum and later oxidation is postulated, and the formation of pentavalent molybdenum is not excluded.⁴ The case for the catalytic importance of molybdenum and the pertinence of esr spectroscopy as a tool in such studies have been well established. Our main concern in this study has been to define and to understand the spectral changes that occur and to evaluate the extent to which such information may be of help in catalytic problems.

Experimental Section

Sample Preparation. The molybdenum oxide-MgO samples used in the present work were prepared by first precipitating $\text{Mg}(\text{OH})_2$ upon mixing a hot solution of $\text{Mg}(\text{NO}_3)_2$ with NaOH solution. The precipitate was dried at 100° for several hours and then wetted with a solution of ammonium molybdate and dried again at 100°. The dried sample was heated in air at 500° until it was completely dehydrated. Then it was reduced in a current of hydrogen at the required temperature for 2 hr. Reduction has been carried out at 200, 400, 490, and 600°. Al_2O_3 -molybdenum oxide and MgAl_2O_4 -molybdenum oxide samples were prepared by a procedure similar to the above using Bayerite and magnesium aluminate as the starting materials.

Molybdenum oxide-MgO samples were also made by coprecipitation. A mixture of magnesium nitrate and ammonium molybdate solutions was treated with NaOH solution till the pH reached 11. Presumably, the molybdate gets precipitated as magnesium molybdate along with $\text{Mg}(\text{OH})_2$. The liquid phase was removed by filtration, and the subsequent treatment of the precipitate was similar to the procedure described above.

To prepare the acid solution of the samples, the reduced product was dissolved in concentrated HCl and warmed. Any undissolved portion was removed by filtration, and the filtrate was diluted to appropriate volume such that the resulting solution was 10 M in acid.

Esr Measurements. The esr measurements were performed on a Varian V4500 spectrometer operating at 9.5 kHz. The magnetic field was modulated at 100 kHz, and the first derivative of the spectra was recorded. Peak-to-peak modulation amplitudes from 2 to 5 G were used in recording the spectra. The sample tubes were of Pyrex glass of 4 mm o.d. and 2 mm i.d., and they were filled with the powder in air to a height greater than the depth of the resonant cavity, evacuated under moderate vacuum, and sealed. The magnetic field was measured with a proton gauss meter. In addition, a spectrum in the K-band region has also been obtained. A sample of pitch in KCl (1%) was used as a calibration standard.

The integrated intensities were obtained by double

integration of the first derivative spectra using a computer program. The relative values of intensities in arbitrary units are reported. In several samples we have measured the number of spins per gram using the dual sample cavity and a mechanical mixture of MoCl_5 - Al_2O_3 as intensity standard. We have obtained the X-band spectrum of one of the samples at 77°K using the Varian liquid nitrogen Dewar (V-4546) and at variable temperatures from room to -160° at intervals of 20°. We have also studied the same sample at room temperature at different microwave power levels.

The solution spectra were obtained by using either the Varian flat quartz electrolytic cell or by placing the solution in a Pyrex glass capillary which in turn is placed in a quartz esr tube. The latter arrangement was used to get the spectrum of frozen solutions. Refrigeration was achieved by using the Varian liquid nitrogen, low-temperature accessories.

Catalytic Activity. The catalytic activity of the samples was tested using the vapor phase aldol condensation of *n*-butyraldehyde. A 15-cc sample was packed into a reactor and treated with hydrogen at 375° for 5 hr. Then the temperature was reduced to 250°, *n*-butyraldehyde was introduced with hydrogen as the carrier gas, and the reaction was carried out for 2 hr. The liquid products were collected and analyzed on a gas chromatograph. The catalytic activity was expressed in terms of milligrams of product formed per gram of catalyst in the course of 2 hr. The BET surface area was measured with nitrogen at liquid nitrogen temperature and compared with catalytic activity.

Results and Discussion

The first derivative of the esr absorption was recorded for molybdenum supported on MgO, alumina, and MgAl_2O_4 . The samples were prepared either by coprecipitation or impregnation and were subjected to various pretreatments in addition to reductions being effected at various temperatures. Considerable spectral changes take place, and these will be discussed below in detail.

In our experiments with sample preparation, it was found that the unreduced sample had the color of the carrier material, and the reduced samples were darker in color, the degree of coloration depending on the concentration and the carrier material. In the case of magnesium oxide as the calcination temperature was increased, the color deepened and became bluish at 1000°. The spectra of Al_2O_3 -molybdenum oxide and MgO-MoO₃ containing 8% MoO₃ are shown in Figure 1. The width between points of maximum slope is 79 G with Al_2O_3 as the carrier material, 76 G in MgAl_2O_4 , and

(4) (a) Ph. A. Batist, C. J. Kapteijns, B. C. Lippens, and G. C. A. Schuit, *J. Catal.*, **7**, 33 (1967); (b) Ph. A. Batist, B. C. Lippens, and G. C. A. Schuit, *ibid.*, **5**, 55 (1966).

(5) C. R. Adams, *Proc. Int. Congr. Catal.*, **3rd**, Amsterdam, 1964, **1**, 240 (1965).

(6) W. H. M. Sachtler and N. H. de Boer, *ibid.*, **1**, 252 (1965).

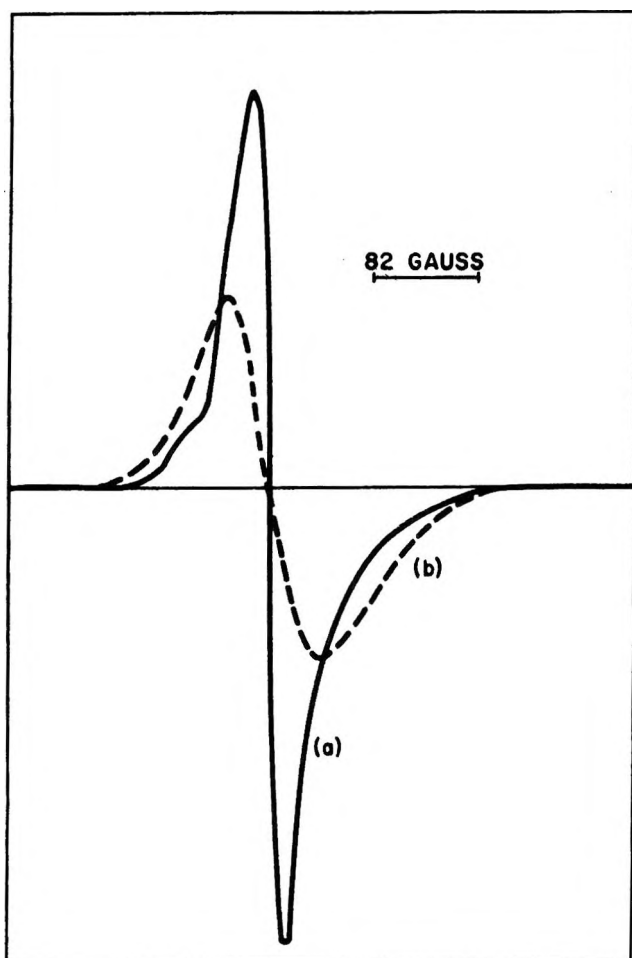


Figure 1. ESR spectra of 8% MoO₃ in (a) MgO and (b) Al₂O₃.

34 G in MgO. (The concentration of MoO₃ in MgAl₂O₄ is 1%.) The lines are definitely asymmetric, and the g value with MgO as the carrier material is 1.928, 1.929 on Al₂O₃, and 1.927 on MgAl₂O₄. There is no significant variation in the g value with the carrier material. Measurements carried out at 23 kHz also gave an asymmetric line (Figure 2) with a width between points of

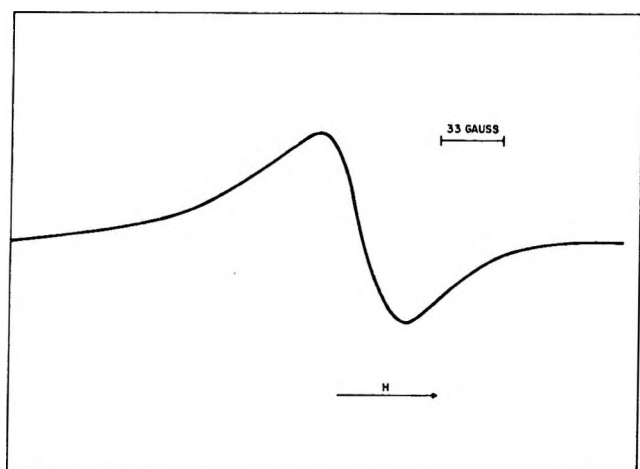


Figure 2. ESR spectra of 8% MoO₃ in MgO in K-band region.

maximum slope of 50 G. The g value is equal to 1.923. The equality of g at two frequencies is an indication that we are dealing with true asymmetry and not a broadening due to the superposition of different esr signals with slightly different g values.

There is no definitive evidence as to the environment of Mo⁵⁺, but molybdenum is probably on the surface coordinated to the carrier material, and the larger magnetic moment of ²⁷Al may be responsible for the larger width in the case of Al₂O₃ and magnesium aluminate.

Molybdenum can exist in any of four valences 6+, 5+, 4+, and 3+ corresponding to d⁰, d¹, d², and d³ configurations. Hexavalent molybdenum is diamagnetic and, therefore, gives no esr signal. Tetravalent molybdenum, even if it were paramagnetic, would not be expected to be observed except at very low temperatures. Also, it would be expected that any observed resonance due to d² would have a large zero-field splitting and, therefore, a very broad signal.⁷ Indeed, to the best of our knowledge, the spectrum of Mo(IV) has not been observed. Therefore, the observed signals must be due to Mo(V) and/or Mo(III).

Several studies of esr spectra of Mo(III) have been reported. Griffiths, Owen, and Ward⁸ have studied hydrated and unhydrated chloro and fluoro complexes of Mo(III) and report isotropic g values around 1.96. Landry⁹ has studied Mo(III) in aluminum-zinc phosphate glass and reports a very broad spectrum with a strong peak at g_{eff} of 5.19. Ramaseshan and Suryan¹⁰ have studied an unhydrated chloro complex of Mo(III) and have observed resonance at $g_{\text{eff}} = 1.76$. The two extreme values differing largely from $g \cong 2$ are effective or experimental values, and they reflect large zero-field splittings and crystal field effects. The true g value of Mo(III) is around 1.96. Thus, Mo³⁺ in less than cubic symmetry can be readily eliminated as a contributor to the resonances reported here. However, the possibility, in principle at least, remains that Mo³⁺ has diffused in the cubic MgO lattice and is contributing to resonances observed here. It is our contention that these resonances are predominantly, if not exclusively, due to Mo(V). This is considered at some length below.

Hexavalent oxide of Mo has been reduced by H₂ at 500° for long periods¹¹ and has been examined by X-ray. No phase corresponding to the oxide MoO_{1.5} has been observed, from which it is reasonable to conclude that it is improbable that hexavalent molybdenum oxide can be reduced to trivalent oxide by hydrogen around 500°. We have studied the samples at low temperatures and

(7) (a) K. D. Bowers and J. Owen, *Rept. Progr. Phys.*, **18**, 304 (1955); (b) R. J. Kokes, "Experimental Methods in Catalytic Research," R. B. Anderson, Ed., Academic Press, New York, N. Y., 1968, pp 436-475.

(8) J. H. E. Griffiths, J. Owen, and I. M. Ward, *Proc. Roy. Soc., Ser. A*, **219**, 526 (1953).

(9) R. J. Landry, *J. Chem. Phys.*, **48**, 1422 (1968).

(10) S. Ramaseshan and G. Suryan, *Phys. Rev.*, **84**, 593 (1951).

(11) L. Kihlberg, *Acta Chem. Scand.*, **13**, 954 (1959).

at different microwave power levels. As the temperature is lowered, there is only enhancement of signal intensity, without any appearance of additional lines. Although we were unable to saturate the signal, a linear increase in the signal amplitude with microwave power is observed. These results suggest that the samples studied contain predominantly, if not exclusively, one paramagnetic species capable of resonance absorption at room temperature. As already mentioned, we have used three different supports and have studied several samples which are precalcined to different temperatures prior to reduction. Despite these variations, the resonance absorption is always observed around $g = 1.928$. If Mo(III) were present to any significant extent, one would expect the spectra to show some changes as a function of calcination temperature and nature of support. Intuitively at least, one expects that at the higher precalcination temperatures the Mo(III) spin diffusing into the cubic MgO lattice is more numerous than at the lower temperature and, therefore, some more pronounced absorption around $g = 1.96$. Similar arguments can be made for the various supports and the amounts of total Mo incorporated into the lattice. But no such variations in the g_{eff} are observed at all. The constancy of the g value can thus be taken as an indication that a single species is predominantly responsible for the observed resonance. Results of independent weight loss measurements in our laboratory by microbalance techniques¹² indicate that supported MoO₃ on reduction gives mainly tetra- and pentavalent oxides. All these arguments may not prove the exclusive presence of Mo(V), but they strongly indicate that if Mo(III) is indeed present, it must be present in very small amounts compared to Mo(V). The solution spectra of these materials provide additional corroborative evidence to support this contention. This evidence will be presented below.

The appearance of the signal itself as well as the integrated total intensity depends very significantly on the amount of molybdenum, on reduction temperature, and on precalcination temperature. The integrated intensities of the esr signal as a function of MoO₃ concentration are shown in Figure 3 for the samples prepared by impregnation. Figure 4 shows the same variation for the samples prepared by coprecipitation and calcined prior to reduction, under the same reduction condition specified above. From these results, it may be observed that for a given reduction temperature or calcination temperature, the integrated intensity reaches a maximum at about 9% of MoO₃, and for a given concentration, more spins are produced when reduced at 600° than at 490°. The effect of calcination temperature on the signal intensity is marked at 900 and 1000° while at other temperatures there is no appreciable change. The decrease in intensity at 900 and 1000° is definitely due to the evaporation of MoO₃, and samples containing MoO₃ could be heated to as high as

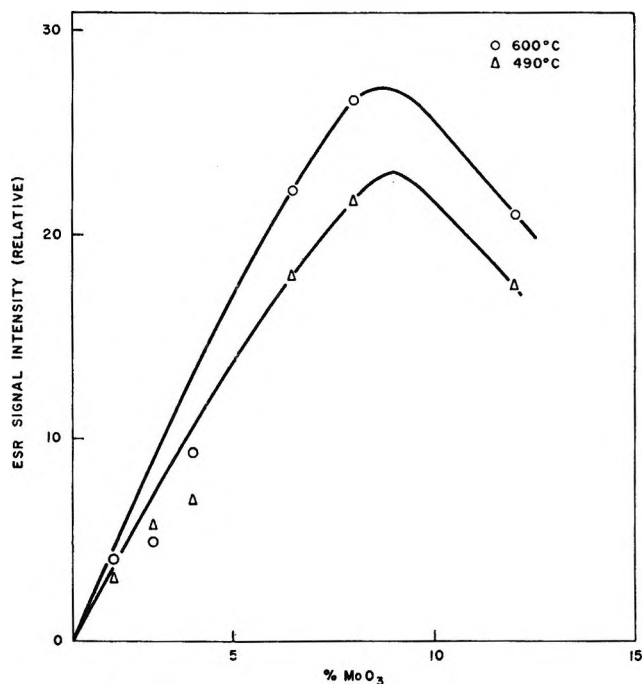


Figure 3. Dependence of integrated esr signal intensity on total molybdenum content at reduction temperatures: (a) 490° and (b) 600°.

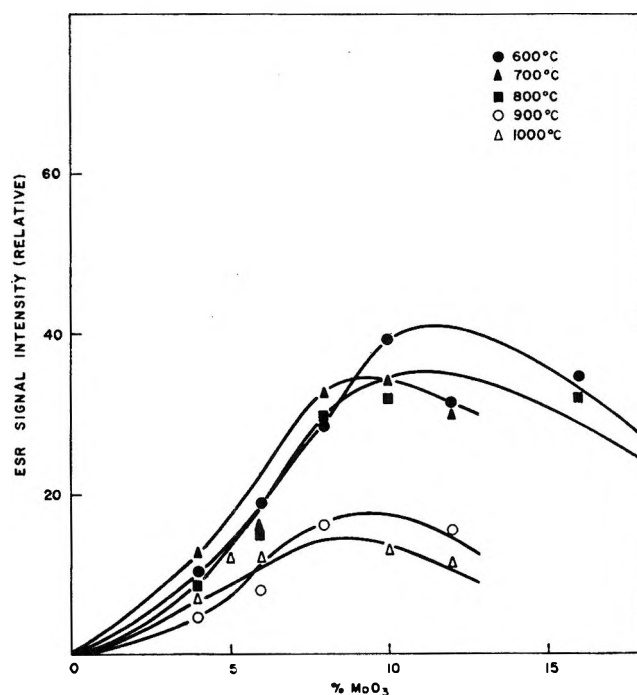


Figure 4. Dependence of integrated esr signal intensity on total molybdenum content at different calcination temperatures.

800° without any significant loss of the oxide. Since it was observed that the reduction proceeds to a greater extent at 600° than at 490°, a 9% sample in MgO, prepared by impregnation, was reduced at 200, 400, and

(12) K. S. Seshadri, F. E. Massoth, and L. Petrakis, *J. Catal.*, in press.

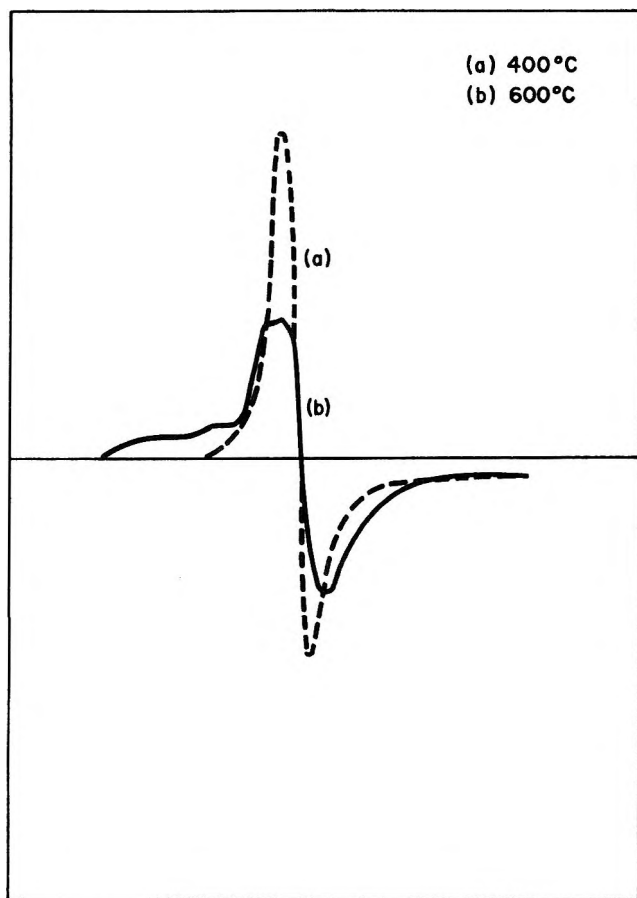


Figure 5. ESR spectra of 9% MoO₃ in MgO reduced at two different temperatures: (a) 400° and (b) 600°.

600°. The esr spectra of the latter two samples are shown in Figure 5. There is practically no reduction at 200°. The signal arising from the sample reduced at 400° is less intense, narrower, and more symmetrical than the signal from the sample reduced at 600°. As the reduction temperature is increased, more spins are produced, increasing interaction among themselves and the host material and thus broadening the signal. In Figure 5b shoulders are observed on the low-field side of signal.

Distinct spectral changes are also observed with increasing calcination temperatures. The spectra of a reduced sample in MgO at two calcination temperatures are shown in Figure 6. There is no significant change in the width between points of maximum slope and in g value. But at calcination temperatures of 700° (Figure 6a, $g = 1.926$) or lower, the spectra are very much similar to the one shown in Figure 5b. The shoulders disappear as the calcination temperature is increased to 800° (Figure 6b, $g = 1.928$), and they are not observed in the sample reduced at 400° (Figure 5a). They are also not observed in the case of Al₂O₃ and MgAl₂O₄. Similar spectral features have been observed by Poole, *et al.*,¹³ and they have attributed such shoulders to different phases. The X-ray spectra of our samples show

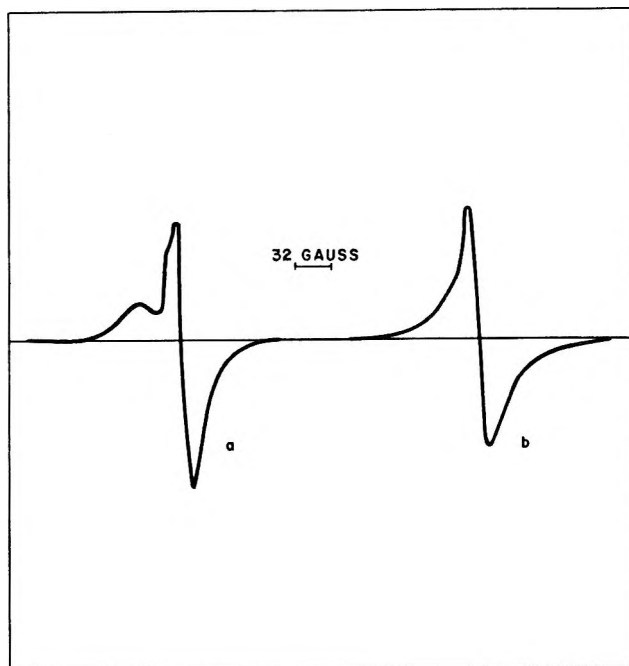


Figure 6. ESR spectra of MgO-MoO₃ at two different precalcination temperatures: (a) 700° and (b) 800°.

only the pattern due to MgO, and so we cannot with certainty attribute the shoulders to different phases. These shoulders are probably due to clusters. When reduced at 400°, the Mo(V) ions are at low concentration, and so they are isolated. As the reduction temperature is increased, more spins are produced, favoring the formation of clusters. At a still higher precalcination temperature, molybdenum oxide is probably redistributed on the surface; when the spins are produced, they are isolated, precluding the formation of clusters. On the surface of Al₂O₃, the spins are isolated perhaps by other species like OH groups adsorbed on the surface. It is known¹⁴ that on prolonged evacuation at 800°, all the OH groups are removed from the surface of MgO while only about 80% of them are removed from that of Al₂O₃.¹⁵ Based on this observation, it is reasonable to assume that the Al₂O₃ surface is covered to a greater extent with OH groups and possibly water molecules at a given temperature than MgO surface. In any case, since this spectral feature is dependent on temperature and surface characteristics, it cannot be due to different orientations of crystal or molecular axis with respect to the external magnetic field.

Further corroborative evidence that the observed spectra on the various surfaces are due to molybdenum(V) is provided by the results obtained from studying the HCl acid solution spectra of these samples

(13) C. P. Poole, W. L. Kehl, and D. S. MacIver, *J. Catal.*, **1**, 407 (1962).

(14) P. J. Anderson and P. L. Morgan, *Trans. Faraday Soc.*, **60**, 930 (1964).

(15) J. B. Peri, *Actes Congr. Int. Catalyze*, **2°**, Paris, 1960, 1333 (1961).

both at room and lower temperatures. The characteristics of the spectra definitely indicate the presence of Mo(V). The room temperature spectrum shows a sharp line due to the even isotope on which is superimposed an isotropic fine structure of six lines due to the odd isotopes. By inspecting the spectra, values for g and A are obtained directly, and they are 1.948 ± 0.004 and 53.6 ± 1.0 G, respectively. The complex spectrum at a lower temperature can be described by the spin

$$H = g_{\parallel}\beta H_z S_z + g_{\perp}\beta(H_x S_x + H_y S_y) + A I_z S_z + B(I_x S_x + I_y S_y)$$

Hamiltonian where $S = 1/2$ and $I = 0$ for even isotopes and $I = 5/2$ for odd isotopes. By examining the spectrum we have obtained $g_{\parallel} = 1.960$, $g_{\perp} = 1.937 \pm 0.004$, $A = 83.0 \pm 1.0$, and $B = 44.8 \pm 3.0$ G. Our values are in good agreement with $g_{\parallel} = 1.96$, $g_{\perp} = 1.938 \pm 0.005$, $A = 80$, and $B = 49$ G reported by Garif'yanov and Fedotov,¹⁶ who have studied aqueous solutions of $(\text{NH}_4)_2(\text{MoCl}_5)$ and $g_{\parallel} = 1.972 \pm 0.004$, $g_{\perp} = 1.942 \pm 0.005$, $A = 81 \pm 1$, and $B = 34 \pm 4$ G reported by Abraham, *et al.*,³ who have investigated reduced HCl solutions of MoO_3 . The values from our low-temperature spectra yield $g = 1/3(2|g_{\perp}| + |g_{\parallel}|) = 1.945$ and $1/3(|A| + |2B|) = 57.5$ and agree within experimental error with the experimental values of g and A measured at room temperature. We have also recorded the spin resonance spectra of molybdenum pentachloride in hydrochloric acid solution. The values of g and A are 1.945 ± 0.001 and 50.4 ± 1.0 G, respectively, which again are in good agreement with g and A values of $\text{MoO}^{3+}\text{-MgO}$ acid solutions at room temperature.

The acid solution of the reduced samples in all probability contains the complex $[\text{MoOCl}_5]^{2-}$. We have observed the formation of green and brown solutions when the solid samples are dissolved in HCl. Though both the green and the brown solutions contain Mo(V), the brown solution invariably gives a weaker esr signal than the green solution. There is enhancement of signal intensity when the brown solutions are diluted with acid. Hare, *et al.*,¹⁷ have studied the esr spectra of $(\text{NH}_4)_2(\text{MoOCl}_5)$ in HCl solutions ranging from 12 to 2 M in acid and have compared their results with the magnetic susceptibility measurements by Sacconi and Cini¹⁸ and electronic spectral results by Haight.¹⁹ They have concluded that the acid solution contains several species, all containing pentavalent molybdenum, out of which only the monomer of MoO^{3+} gives an esr spectrum. Its concentration is 100% in 12 M acid solution, decreases with decrease in acid concentration, and reaches zero in 2 M acid solution. This scheme would be in agreement with our observations. Also, we have observed a 1:1 correspondence in the variation of signal intensity in the solid and in solution with per cent MoO_3 when 4, 9, and 14% $\text{MoO}_3\text{-Al}_2\text{O}_3$ samples were dissolved in HCl and diluted to the same concentration in acid. This would seem to rule out the possibility of any equi-

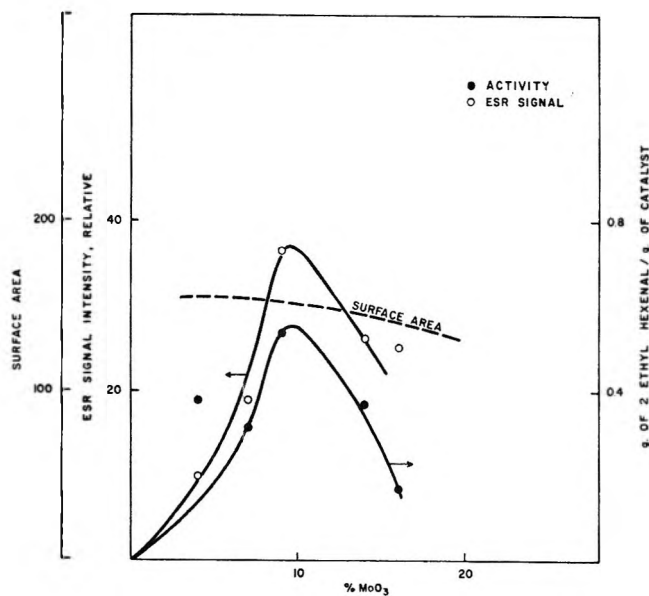


Figure 7. Correlation of the activity of $\text{MoO}^{3+}\text{-MgO}$ with signal intensity.

libria among different valence forms of Mo in solid samples.

The catalytic activity of the samples prepared has been tested using the vapor phase aldol condensation of *n*-butyraldehyde. In Figure 7 the activity of the $\text{MoO}^{3+}\text{-MgO}$, the integrated intensities of the sample, and BET surface area are plotted against the molybdenum oxide content in the sample. Several products are formed during the reaction, but the yield of 2-ethylhexenal, since it is the major product, has been used to express the catalytic activity. Within the accuracy of measurement, surface area practically remains constant with concentration. In another set of experiments, the catalytic activity of $\text{MoO}^{3+}\text{-Al}_2\text{O}_3$ was tested, and the results are given in Figure 8. With Al_2O_3 as the carrier material, two new products in significant amount were formed, and the yield of one of them, identified as a cyclic ketone with a molecular formula $\text{C}_{12}\text{H}_{20}\text{O}$, is used to express the activity. In both situations, the catalytic activity as measured in each case by the amount of the main product has the same functional dependence on MoO_3 content as the intensity of the esr signal. The existence of such a correlation, of course, cannot automatically be construed as having established a direct relationship between the Mo^{5+} and this particular reaction. For example, the different distribution of products for the two different supports studied is evidence that other factors probably enter the picture. It is interesting, nevertheless, that

(16) N. S. Garif'yanov and V. N. Fedotov, *Zh. Strukt. Khim.*, **3**, 711 (1962).

(17) C. R. Hare, I. Bernal, and H. B. Gray, *Inorg. Chem.*, **1**, 831 (1962).

(18) L. Sacconi and R. Cini, *J. Amer. Chem. Soc.*, **76**, 4239 (1954).

(19) G. P. Haight, Jr., *J. Inorg. Nucl. Chem.*, **24**, 663 (1963).

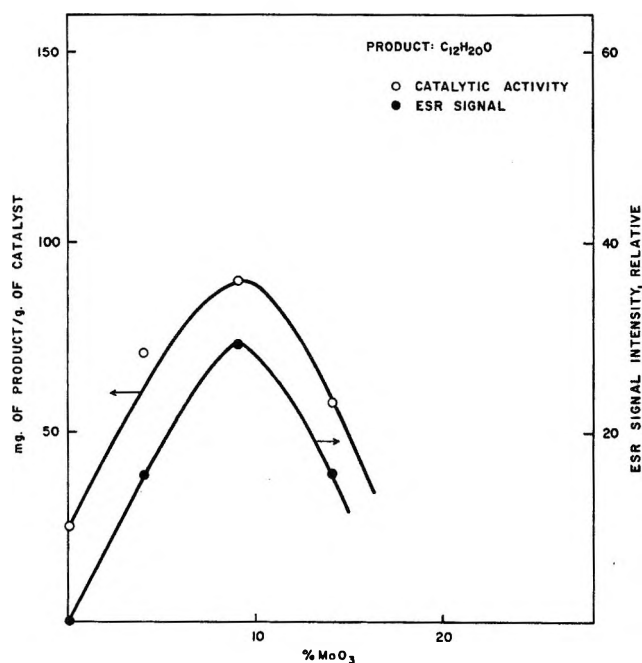


Figure 8. Correlation of the activity of $\text{MoO}_3^{3+}-\eta\text{-Al}_2\text{O}_3$ with signal intensity.

in both of these situations a maximum in esr signal intensity and degree of conversion appears at the same point, *i.e.*, about 9% MoO_3 in the support. This is indicative, of course, that at least common factors affect both the Mo^{5+} production and the degree of conversion. It is interesting to speculate as to why the intensity itself should reach a maximum at all. This is not unique and has been observed both with free-radical ions and transition metal ions. A likely possibility is that dimerization may be taking place or perhaps complexation, *e.g.*, with surface impurities, and thereby quenching the paramagnetism of the samples. Dimerization also changes the configuration of Mo(V) from d^1 to d^2 , and for reasons mentioned above the resonance signal due to the latter is hard to observe at room temperature leading to decrease in paramagnetic signal intensity. Alternatively, it might be argued that for the relatively lower Mo(V) content in the higher Mo -containing samples, there might be present some bulk MoO_3 which on reduction would not form Mo(V) but rather MoO_2 .²⁰ Magnetic susceptibility measurements of solid samples should be able to resolve some of these problems.

The number of spins per gram in some representative samples ($1.1\text{--}4.9 \times 10^{19}$ spins) is similar in magnitude to what has been reported by Dzs'ko, *et al.*,¹ in their molybdenum work and is comparable to what has been reported by Kazanski and Turkevich²¹ in their work on chromium(V).

The spent samples, after their catalytic efficiency had been tested, were examined by esr spectroscopy and there was an enhancement in signal intensity and a de-

crease in half-width. In addition, in the case of Al_2O_3 , the esr spectrum contained a free-radical signal indicating coking on Al_2O_3 . The enhancement of the signal may be partly due to further reduction by hydrogen. X-Ray spectra of fresh and spent samples show only lines due to MgO , but the lines in the spectrum of spent samples are more intense. Diffusion of surface species into the lattice is likely to enhance the intensity of X-ray lines. Such changes will isolate the paramagnetic species, thus decreasing the half-width of the esr signal.

Molybdenum has several isotopes (92, 94, 96, 98, and 100) with $I = 0$ and isotopes (95 and 97) with $I = 5/2$. The latter constitute $\sim 25\%$ of the total naturally abundant molybdenum. One would then expect to see hyperfine structure in the spectra in which case one could have an additional handle in the attempt not only to conclusively identify the species giving rise to the resonance but also, and more importantly, provide some quantitative indication of the sites occupied. At no time—including our own measurements—has the hfs due to the $I = 5/2$ isotopes of molybdenum been observed except in single crystals at liquid N_2 temperature. It is known that the energy levels of Mo^{6+} are similar to those of V^{4+} and Ti^{3+} . The five degenerate orbitals are split into an upper doublet and a lower triplet by cubic field. Fields of lower symmetry further split the triplet into a lower singlet and an upper doublet. In solution, this splitting is facilitated by an axially symmetric field, and since resonance is observed at room temperature, this splitting must be sufficiently large ensuring a long relaxation time. But at room temperature, an isotropic spectrum is observed with a sharp central line which strongly suggests that the cubic field is stronger than the axial component. If a similar situation existed in solids also, we should have observed resonance with hyperfine structure. Our attempts to bring out the hyperfine structure by varying the preparative procedure and going to very low concentrations have not been successful. Mo^{6+} has been studied in rutile² where the local symmetry of each Ti ion is orthorhombic, and it has been concluded that Mo ions go into host lattice substitutionally. For Mo(V) in rutile, absorption has been observed only at 77° and 4.2°K . Our samples are by no means solid solutions, and we have observed resonance at room temperature. Griffiths, *et al.*,⁸ have studied the esr spectrum of $\text{K}_3[\text{Mo}(\text{CN})_8]$ powder and have observed a line at $g = 2.005 \pm 0.005$. The eight cyanide molecules lie on the corners of a dodecahedron, and on a crystal field model the five d orbitals are split into a lower singlet and an upper quartet at much higher energy. The separation is so large it corresponds to a long relaxation time permitting resonance absorption even at 290°K . The

(20) J. Masson and J. Nechtschein, *Bull. Soc. Chim. Fr.*, 3933 (1968).

(21) V. B. Kazanski and J. Turkevich, *J. Catal.*, **8**, 231 (1967).

conditions in our samples probably are quite similar. Mo(V) is in an electric field of very low symmetry facilitating spin resonance absorption at room temperature. This introduces anisotropic conditions. This and dipole-dipole interactions probably combine to suppress the hyperfine structure.

In one of our experiments, the sample was heated to 400° *in vacuo* and at this temperature was exposed to air, resulting in decrease in esr signal intensity. This suggests that MoO^{3+} is on the surface. We suspect that this decrease is due to partial oxidation of MoO^{3+} . The line width remains unchanged, which is reasonable. Any substantial change in the line width is unlikely following only a slight oxidation of pentavalent molybdenum. MoO^{3+} is supposed to be unstable, and as it is formed, it gets coordinated with the surface atoms and is stabilized. By extracting the magnetic parameters from the observed signal, it is possible to understand the local electric field in which Mo(V) is situated. The analysis of the line can be done by fitting the experimental spectrum to a theoretical function by a computer program. We have observed that a better fit is obtained when all the three components of the g tensor are different. This suggests that the field is of very low symmetry or the paramagnetic species are in environments of different symmetry.

We have calculated a spectrum using the computer program described by Johnston and Hecht²² with "experimental" $g_{||} = 1.891$ and $g_{\perp} = 1.940$ to fit an observed spectrum of $\text{MoO}^{3+}\text{-MgO}$, and the best fit was obtained with complete anisotropy of g tensor, $g_x = 1.945$, $g_y = 1.939$, and $g_z = 1.877$. It is likely that the initial choice of g_{\perp} and $g_{||}$ will influence the final fit. So we varied g_{\perp} and $g_{||}$ within reasonable limits and always ended up with completely anisotropic tensor.

Summary and Conclusions

The main thrust of this work has been to provide a detailed look into the nature of paramagnetic species of bulk catalysts. There is no doubt that esr spectroscopy can be a powerful tool in the study of systems of catalytic interest. Important changes appear in the spectral features due to the nature of the support, the method of preparation, pretreatment, and reduction conditions. Spectroscopic parameters such as g and hfs can identify the species responsible for esr signals and indicate the symmetry of the site occupied. More detailed calculations with spectra, hopefully richer in detail than those reported here (*e.g.*, working with nuclear species, such as niobium with higher abundances of nuclei with non-vanishing nuclear spins so the hfs might be observed), and *in situ* experiments to observe spectral changes upon treatment should provide definite, quantitative delineation of the correlations between the paramagnetism of the species and catalytic conversions reported here. Finally, the definite changes in the spectral features observed here, besides the promise they hold, also warn that considerable care must be exercised in making comparisons and drawing conclusions about the precise role of particular paramagnetic species in catalytic reactions.

Acknowledgment. Grateful acknowledgment is made of helpful discussions with Mr. William L. Kehl, Dr. Harold E. Swift, and Mr. John E. Bozik, who also made available the apparatus for testing the catalytic activity of the samples. We wish to thank Mr. Arthur V. Fareri and Mr. William E. Magison for their assistance with the experimental work.

(22) T. S. Johnston and H. G. Hecht, *J. Mol. Spectrosc.*, **17**, 98 (1965).

Molecular Structure of Dilute Vitreous Selenium-Sulfur and Selenium-Tellurium Alloys

by A. T. Ward

Xerox Corporation, Research Laboratories, Rochester, New York 14603 (Received April 17, 1970)

The dependence of the molecular constitution of dilute vitreous Se-S and Se-Te alloys upon alloy concentration has been elucidated¹ by applying to these alloys the concept of equilibrium copolymerization developed by Tobolsky and Owen,² and modified by Myers.³ Raman spectroscopic evidence justifying this approach is reviewed. Sample calculations of the relative abundances of selenium monomer (Se_8), comonomer (mixed $\text{Se}_\gamma\text{S}_{8-\gamma}$ or $\text{Se}_z\text{Te}_{8-z}$ octaatomic rings), and copolymer (mixed Se-S or Se-Te chains) are shown and the results compared with those obtained by Raman spectroscopy. Sample calculations of copolymer chain length are also included and the interpretation of glass transition temperatures in terms of these new results is discussed.

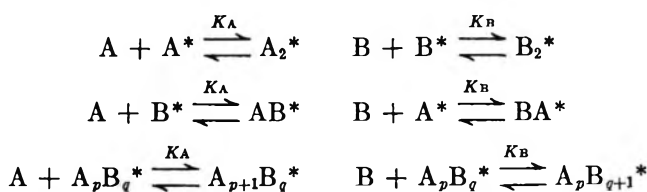
A recent paper by Schottmiller, *et al.*,¹ on the effects of valency on electrical transport in vitreous binary alloys of selenium has identified the importance of thermodynamic and spectroscopic measurements in the elucidation of transport mechanisms in amorphous materials. The results of such experiments have achieved special significance in the case of dilute selenium alloys containing the isoelectronic additives S and Te. For these systems it was found possible to correlate the electron transport properties directly with the composition-dependent variation of the Se_8 monomer concentration estimated from thermodynamic arguments. These thermodynamic estimates were based on the theory of equilibrium copolymerization developed by Tobolsky and Owen² and modified by Myers.³ The same calculations permitted generation of the relative abundances and degree of polymerization of all the molecular species present in the alloy. Strong support for the validity of the results has been derived from laser Raman spectroscopy and from calorimetric determinations of the glass transition temperature. The purpose of this paper is to explain the significance of the Myers modification of the Tobolsky-Owen theory and to demonstrate, through sample calculations, the application of the modified theory to the Se-S and Se-Te alloys. The importance of laser Raman spectroscopy, both for identifying the molecular species present and for assessing their relative abundances, is reiterated and the interpretation of glass-transition temperatures in terms of the new results is discussed.

Equilibrium Copolymerization Theory. The copolymerization of sulfur with selenium and of tellurium with selenium may be assumed to follow case II of the general theory described by Tobolsky and Owen; *i.e.*, in the liquid phase monomer A copolymerizes with monomer B through the following reactions to form an activated polymeric species as the final product.

(initiation)



(propagation)



According to Tobolsky and Owen, K_A' , K_B' and K_A , K_B may be taken as the equilibrium constants for the initiation and propagation reactions, respectively, of the corresponding homopolymerization equilibria. In the case of the sulfur-selenium copolymerization these workers assumed the initial monomer species to be the octaatomic ring molecules S_8 and Se_8 identified in the homopolymerizations. Myers³ has shown that this assumption leads to poor agreement between observed and calculated values of the polymerization transition threshold temperature in sulfur-rich sulfur-selenium alloys. Better agreement is obtained when the exact nature of the copolymerizing species is taken into account, *i.e.*, when the copolymerization is assumed to involve S_8 and Se_2S_6 (the latter being the most abundant selenium-containing ring observed spectroscopically in sulfur-rich alloys).⁴ In the Myers calculation this required that the propagation equilibrium constant for homopolymerization of Se_8 be replaced by the corresponding equilibrium constant for Se_2S_6 . The latter

(1) J. Schottmiller, M. Tabak, G. Lucovsky, and A. Ward, *J. Non-Cryst. Solids*, **4**, 161 (1970).

(2) A. V. Tobolsky and G. D. T. Owen, *J. Polym. Sci.*, **59**, 329 (1962).

(3) A. T. Ward and M. B. Myers, *J. Phys. Chem.*, **73**, 1374 (1969).

(4) A. T. Ward, *ibid.*, **72**, 4133 (1968).

was estimated by assigning to the Se_2S_6 equilibria the entropy of propagation of S_8 and the enthalpy of propagation of Se_8 ; *i.e.* the configurational change occurring during the propagation reaction was assumed to be insensitive to the presence of two "foreign" atoms in the 8-membered ring while the enthalpy change was assumed to be determined by the strength of the weakest bond.

Raman Spectroscopy. In order to extend these ideas to the alloys of present interest it was first necessary to identify the probable participants in the copolymerization. This was achieved by Raman spectroscopic characterization of the appropriate melt-quenched glasses. Details of the experimental method may be found in the paper by Schottmiller, *et al.*¹

The results of the Raman investigation are shown in Figure 1 where portions of traces of the anti-Stokes region Raman spectra are shown for various alloy compositions in the Se-S and Se-Te systems. Each trace has been normalized to the same maximum peak intensity because experimental variables, particularly optical geometry, effectively prohibit comparisons of absolute scattering intensity. The relative intensities of Raman peaks in the same trace do, however, provide a unique indication of the composition dependence of the molecular structure.

The characteristic spectrum of either melt-quenched or evaporated amorphous selenium in the 150–400- cm^{-1} region consists of a single, well defined peak at 250

cm^{-1} , attributed to the high-frequency symmetric vibration of Se_8 monomer rings⁵ with a shoulder at 235 cm^{-1} attributed to Se_n polymeric chains. Inspection of Figure 1 reveals that addition of S to Se introduces a new spectral feature at 355 cm^{-1} which contributes 2–3% of the total scattering from $\text{Se}_{0.95}\text{S}_{0.05}$ and 9% of the total scattering from $\text{Se}_{0.80}\text{S}_{0.20}$. Similarly, in the case of Se-Te alloys, addition of Te introduces only one new feature, a well defined peak at 216 cm^{-1} which contributes 20% of the total scattering from $\text{Se}_{0.95}\text{Te}_{0.05}$ and 40% of the total scattering from $\text{Se}_{0.90}\text{Te}_{0.10}$.

The line width of the new feature for both types of alloy is slit-width limited and compares closely with that of the peak at 250 cm^{-1} due to Se_8 . Raman spectral features in this region associated with fundamental vibrations of polymeric entities are generally much broader than this,^{1,4} and are not slit-width limited. Consequently, in both cases, the new feature may be assumed to be due to a monomeric rather than to a polymeric species. This, together with the identification of $\text{Se}_Y\text{S}_{8-Y}$ monomers in sulfur-rich S-Se alloys,⁴ is considered good evidence for the existence of similar mixed octaatomic rings in the alloys under consideration; *i.e.*, the Raman line at 355 cm^{-1} in Se-S alloys is assumed to be associated with the high-frequency symmetric A_1 mode of the ring $\text{Se}_Y\text{S}_{8-Y}$ and the line at 216 cm^{-1} in Se-Te alloys is assumed to be associated with the corresponding mode of the ring $\text{Se}_Z\text{Te}_{8-Z}$. The values of Y and Z have been determined by a frequency interpolation method discussed in a previous paper.⁴ According to this method the normal vibration frequencies of mixed rings vary as the reciprocal square root of the molecular weight modified by a factor which takes into account the composition dependence of the force constants. For example, in the case of $\text{Se}_Z\text{Te}_{8-Z}$.

$$\frac{\nu_{\text{Se}_Z\text{Te}_{8-Z}}}{\nu_{\text{Se}_8}} = \left[1 - \frac{A(8-Z)}{8} \right] \left[\frac{M_{\text{Se}_8}}{M_{\text{Se}_Z\text{Te}_{8-Z}}} \right]^{1/2} \quad (1)$$

where ν indicates vibrational frequency and M indicates molecular weight. A is a constant determined by substituting $Z = 0$. This substitution requires a knowledge of the vibration frequencies of the hypothetical molecule Te_8 which, unlike its sulfur and selenium analogs appears to be incapable of stable existence at room temperature. Accordingly, the $\text{Te}_8(A_1)$ frequency has been estimated by assuming that, for the A_1 modes: $\nu_{\text{Te}_8}/\nu_{\text{Se}_8} = \nu_{\text{Se}_8}/\nu_{\text{S}_8} = 0.53$. The validity of this assumption is supported by the observation that a similar relationship holds for the A_1 modes of the extended trigonal chain molecules S_n , Se_n , and Te_n : *viz.*

$$\nu_{\text{Te}_n}/\nu_{\text{Se}_n} = \nu_{\text{Se}_n}/\nu_{\text{S}_n} = 0.51$$

Making the appropriate substitutions in eq 1 leads to the value $A = 0.32$. Figure 2 shows $\nu_{\text{Se}_Z\text{Te}_{8-Z}} (A_1)$

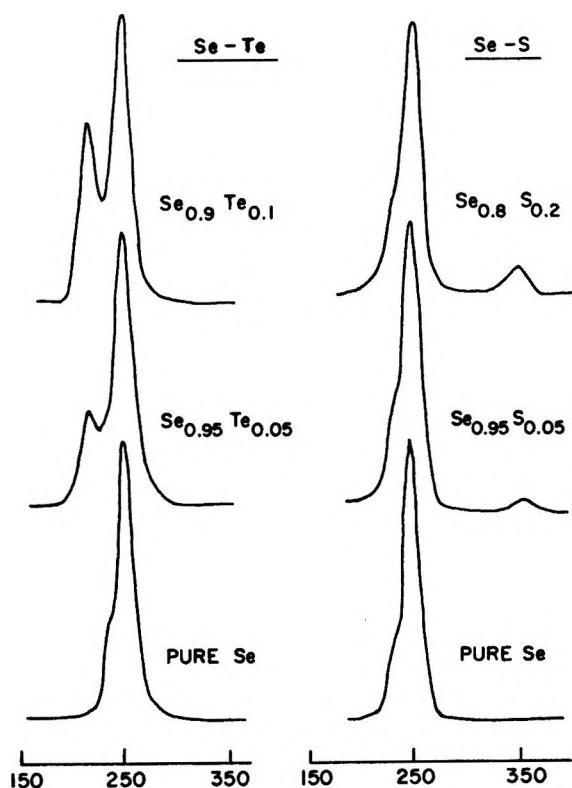


Figure 1. Normalized anti-Stokes Raman spectra of vitreous Se-Te and Se-S alloys.

(5) G. Lucovsky, A. Mooradian, W. Taylor, G. B. Wright, and R. C. Keezer, *Solid State Commun.*, 5, 113 (1967).

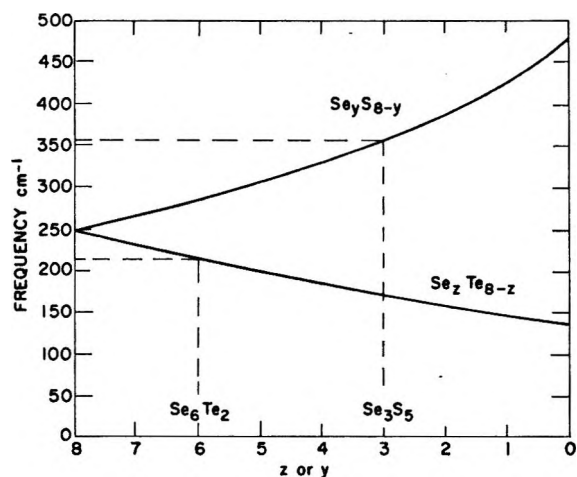


Figure 2. Variation of the octaatomic Se ring vibration frequency with degree of substitution of S or Te for Se.

calculated as a function of Z using this value of A . The corresponding data for $\nu_{\text{Se}_y\text{S}_{8-y}}$ (A_1) taken from ref 4 are plotted on the same scale. Comparison of the frequency values of 216 and 355 cm^{-1} observed for the Se-Te and Se-S alloys, respectively, with the curves plotted in Figure 2 leads to the conclusion $Z = 6$ and $Y = 3$, i.e., the relevant mixed ring species are assumed to be Se_6Te_2 and Se_3S_5 . Actually, as will be shown later, the end result does not depend critically on Z or Y .

Sample Calculations of Molecular Abundance. The relative abundances of selenium rings, mixed rings, and copolymer chains as a function of alloy composition may now be calculated by making the appropriate substitutions in the following equations.

$$K_A A + K_B B = 1 \quad (2)$$

$$\left[\frac{A_0 - A}{B_0 - B} \right] = \frac{K_A A}{K_B B} \quad (3)$$

Here A_0 , B_0 are the concentrations, in mol kg^{-1} , of the alloy components prior to copolymerization and A , B are the corresponding concentrations in the alloy at the temperature of interest. A complete derivation of eq 2 and 3 may be found in the paper by Tobolsky and Owen.² K_A and K_B , the equilibrium constants for the propagation reactions described previously, are calculated from the relationship

$$\log K = \frac{\Delta S^\circ}{R} - \frac{\Delta H^\circ}{RT} \quad (4)$$

For Se-S alloys the propagation reactions involve Se_8 and Se_3S_5 . The corresponding parameters are

$$\Delta S_p^\circ = 5.47 \text{ cal deg mol}^{-1}$$

$$\Delta H_p^\circ = 2.27 \text{ kcal mol}^{-1}$$

Table I: Equilibrium Constants for Copolymerization Initiation and Propagation Evaluated at the Melting Point for Se-S and Se-S Alloys

Atomic % S	T_{mp} , °K	K_A	K_B	K_A'	K_B'
0	490	1.52		8.3×10^{-7}	
5	483	1.47	0.97	5.7×10^{-7}	5.7×10^{-7}
10	473	1.39	0.92	3.3×10^{-7}	3.3×10^{-7}
15	468	1.36	0.90	2.6×10^{-7}	2.6×10^{-7}
20	458	1.29	0.83	1.5×10^{-7}	1.5×10^{-7}
Atomic % Te					
0.2	490			8.3×10^{-7}	2.4×10^{-4}
1	490			8.3×10^{-7}	2.4×10^{-4}
2	490	1.52	2.19	8.3×10^{-7}	2.4×10^{-4}
5	490	1.52	2.19	8.3×10^{-7}	2.4×10^{-4}
8	500	1.59	2.28	1.4×10^{-6}	5.4×10^{-4}
10	500	1.59	2.28	1.4×10^{-6}	5.4×10^{-4}



$$\Delta S_p^\circ = 4.63 \text{ cal deg mol}^{-1}$$

$$\Delta H_p^\circ = 2.27 \text{ cal deg mol}^{-1}$$

where subscript p indicates propagation. These values are also taken from the Tobolsky-Owen paper. Note that Se_3S_5 is assigned the propagation enthalpy of Se_3 and the propagation entropy of S_3 .

Recall that the temperature of interest is taken to be the melting point temperature because it is the molecular configuration in equilibrium at this point which is assumed to be frozen on cooling to the solid state. Values for the melting points of Se-S alloys have been taken from the work of Ringer.⁶ These, together with the corresponding values of K_A and K_B , are shown in Table I as a function of nominal alloy composition.

Consider now 100 atoms of the alloy $\text{Se}_{0.96}\text{S}_{0.05}$ existing as Se_3S_5 and Se_8 prior to copolymerization. The atomic distribution is as follows.

S(as Se_3S_5)	Se(as Se_3S_5)	Se(as Se_8)
5	3	92

This corresponds to a weight per cent of $\text{Se}_3\text{S}_5 = 0.0516$ and a weight per cent of $\text{Se}_8 = 0.948$. Using the molecular weights $\text{Se}_3\text{S}_5 = 397$ and $\text{Se}_8 = 632$ these weight percentages convert to the initial concentrations $A_0(\text{Se}_8) = 1.503 \text{ mol kg}^{-1}$ and $B_0(\text{Se}_3\text{S}_5) = 0.13 \text{ mol kg}^{-1}$. Equations 2 and 3 may now be solved simultaneously giving $A(\text{Se}_8) = 0.634 \text{ mol kg}^{-1}$, $B(\text{Se}_3\text{S}_5) = 0.0685 \text{ mol kg}^{-1}$.

Consider now the initial and final atomic distributions per kilogram of alloy.

	Se_3S_5	Se_8	Se_pS_q
Initial	20.8 g (S); 30.8 g (Se)	948.4 g	0.0 g
Final	10.9 g (S); 16.2 g (Se)	400 g	573 g

(6) W. E. Ringer, *Z. Anorg. Chem.*, **32**, 183 (1902).

The initial and final contributions of Se_3S_5 and Se_8 are known and therefore the amount of copolymer produced may be calculated because the total mass remains constant. Furthermore, the amounts of S and Se in the copolymer must correspond to the respective mass decreases in the monomers. That is, the copolymer contains $(20.8 - 10.9 \text{ g}) = 9.9 \text{ g}$ (S), equivalent to 0.039 mol of sulfur monomer, and 563 g (Se), equivalent to 0.891 mol of selenium monomer. This completes the information needed to compute the mole fractions of all the molecular constituents of the alloy. The identical procedure has been used to calculate these mole fractions for alloys containing 0–20 atomic % of sulfur at intervals of 5 atomic %. The results are shown graphically in Figure 3.

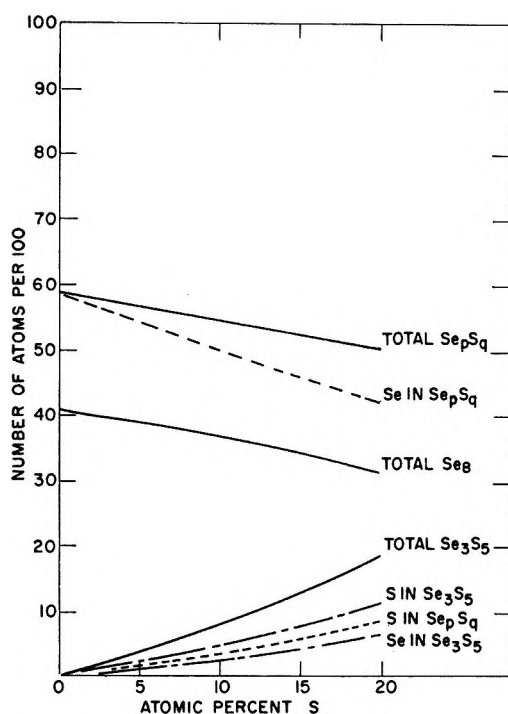


Figure 3. Atomic and molecular distribution in vitreous Se-S alloys.

Application of the method to Se-Te alloys requires additional assumptions concerning the enthalpy of propagation for Se_6Te_2 . This species, for the same reasons as discussed previously in the case of Se_3S_5 , is assigned the enthalpy of propagation of the hypothetical molecule Te_3 (for which no thermodynamic data are available). The necessary assumptions are: (1) that the enthalpy of propagation for Te_3 is approximately 10% of the enthalpy of initiation as in the case of Se_8 and S_8 ; (2) the enthalpy of initiation for Te_3 is proportional to the Te-Te single bond energy as in the case of Se_8 and S_8 ; and (3) the Te-Te single bond energy can be estimated by bond length-bond energy correlations. With these assumptions $E_{\text{Te-Te}}$ can be estimated as $32 \pm 0.5 \text{ kcal mol}^{-1}$ giving $\Delta H_{\text{initiation}} = 19.4 \pm 0.3 \text{ kcal}$

mol^{-1} and $\Delta H_{\text{propagation}} = 1.9 \text{ kcal mol}^{-1}$. The latter is almost certainly an upper limit and, as will be shown later, a downward revision of this figure can only lead to an enhancement of the trends which evolve from the equilibrium copolymerization calculation.

The appropriate parameters involved in Se-Te alloy copolymerizations of Se_8 and Se_6Te_2 are therefore

$$\begin{aligned} & \text{Se}_8 \\ \Delta S_p^\circ &= 5.47 \text{ cal deg mol}^{-1} \\ \Delta H_p^\circ &= 2.27 \text{ kcal mol}^{-1} \\ & \text{Se}_6\text{Te}_2 \\ \Delta S_p^\circ &= 5.47 \text{ cal deg mol}^{-1} \\ \Delta H_p^\circ &= 1.9 \text{ kcal mol}^{-1} \end{aligned}$$

Values for the melting points of Se-Te alloys⁷ and the corresponding values of K_A and K_B calculated according to eq 4 are shown as a function of nominal alloy composition in Table I. The procedure for calculating the relative abundances of the various molecular and polymeric constituents of Se-Te alloys now follows exactly the procedure outlined earlier for the Se-S system.

Consider the case of $\text{Se}_{0.9}\text{Te}_{0.1}$. The atomic distribution of 100 atoms of this alloy prior to copolymerization is as follows.

Te(as Se_6Te_2)	Se(as Se_6Te_2)	Se(as Se_8)
10	30	60

This corresponds to a weight per cent of $\text{Se}_6\text{Te}_2 = 0.435$ and a weight per cent of $\text{Se}_8 = 0.565$. Using the molecular weights $\text{Se}_6\text{Te}_2 = 729$ and $\text{Se}_8 = 632$ these weight percentages convert to the initial concentrations $A_0(\text{Se}_8) = 0.895 \text{ mol kg}^{-1}$ and $B_0(\text{Se}_6\text{Te}_2) = 0.596 \text{ mol kg}^{-1}$. Simultaneous solution of eq 2 and 3 gives $A(\text{Se}_8) = 0.357 \text{ mol kg}^{-1}$ and $B(\text{Se}_6\text{Te}_2) = 0.190 \text{ mol kg}^{-1}$. The initial and final atomic distributions per kilogram of alloy are therefore

	Se_6Te_2	Se_8	Se_pTe_q
Initial	152 g (Te); 283 g (Se)	565 g	0.0 g
Final	48.5 g (Te); 90 g (Se)	226 g	635.5 g

Furthermore, the copolymer must contain $(152 - 48.5 \text{ g}) = 103.5 \text{ g}$ (Te), equivalent to 0.101 mol of tellurium monomer, and 532 g (Se), equivalent to 0.841 mol of selenium monomer. The mole fractions of all the alloy constituents may hence be calculated. Mole fractions for 2, 5, 8, and 10 atomic % Te alloys have been calculated in this way and the results are shown graphically in Figure 4.

(7) M. Hansen, "Constitution of Binary Alloys," McGraw-Hill, New York, N. Y., 1968.

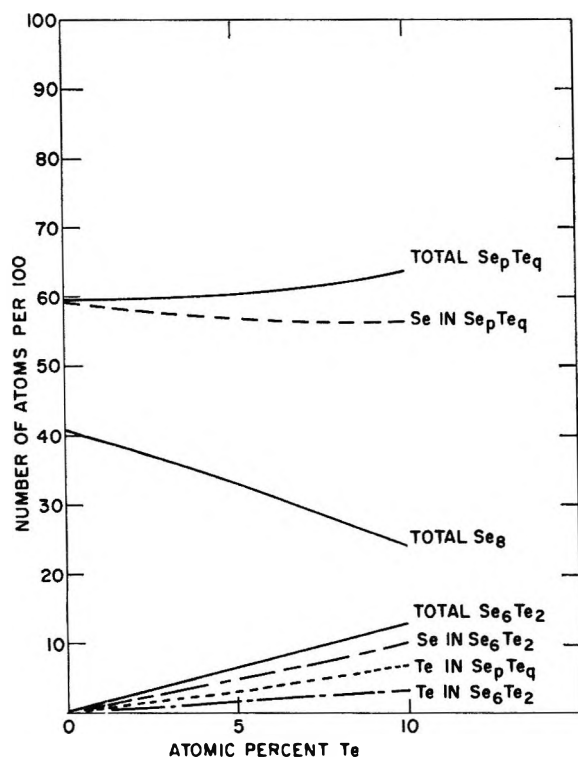


Figure 4. Atomic and molecular distribution in vitreous Se-Te alloys.

Sample Calculations of Chain Length

According to case II of the Tobolsky-Owen equilibrium copolymerization theory, the copolymer number-average chain length P in units of eight atoms is given by

$$P = \left[\frac{(A_0 - A) + (B_0 - B)}{K_A A + K_B B} \right]^{1/2} \quad (5)$$

In the case of Se-S copolymers $K_A' = K_B' = K'(Se_8)$ since the initial ring-opening reaction for both Se_8 and Se_3S_5 is assumed to involve fission of a Se-Se bond. K_A' and K_B' are therefore determined by the thermodynamic parameters appropriate to selenium, *viz.*

$$\log K_A = \log K_B = \frac{\Delta S_I^\circ}{R} - \frac{\Delta H_I^\circ}{RT} \quad (6)$$

$\Delta H_I^\circ = 24.9 \text{ kcal mol}^{-1}$, $\Delta S_I^\circ = 23.0 \text{ cal deg}^{-1} \text{ mol}^{-1}$, and subscript I indicates initiation. For Se-Te copolymers $K_A' = K'(Se_8)$ but $K_B' = K'(Se_6Te_2) = K'(Te_8)$ because, again, fission of the weakest bond is assumed responsible for ring-opening. The entropy of the initiation reaction is assumed to be the same for all eight-membered chalcogenide rings, *i.e.*, $\Delta S_I^\circ = 23.0 \text{ cal deg}^{-1} \text{ mol}^{-1}$, because the configurational change occurring during ring-opening is essentially independent of the nature of the ring atoms.⁸ The value of the enthalpy of initiation for Te_8 (and Se_6Te_2), estimated previously from the energy of the Te-Te single bond, is taken as $19.4 \text{ kcal mol}^{-1}$. Thus, for Se-Te alloys K_A' and K_B' are again given by eq 6 except in the latter case ΔH_I°

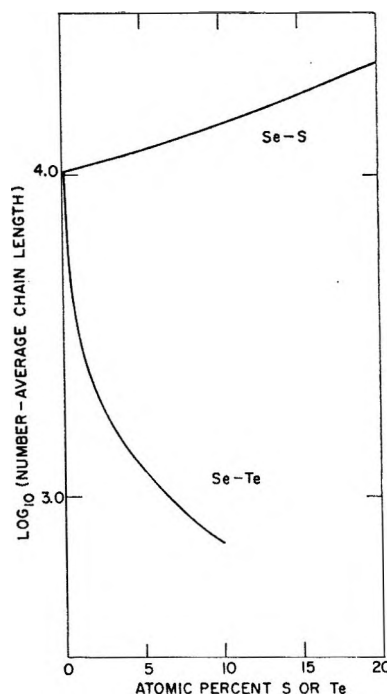


Figure 5. Variation of number-average chain length with composition in vitreous Se-S and Se-Te alloys.

$= 19.4 \text{ kcal mol}^{-1}$ and $\Delta S_I^\circ = 23.0 \text{ cal mol}^{-1} \text{ deg}^{-1}$. Values of melting point initiation reaction equilibrium constants so calculated are included in Table I. The number-average chain lengths calculated according to eq 5 are shown in Figure 5 for both types of alloy. The logarithm of the absolute number-average chain length (rather than the number-average chain length in eight atom units) is plotted against nominal alloy composition in the dilute range.

Discussion

Inspection of the molecular abundances shown by solid lines in Figures 3 and 4 reveals that the effect on amorphous selenium of introducing the isoelectronic additives S and Te is basically similar. The dominant effect is a buildup of a single mixed ring species either Se_3S_5 or Se_6Te_2 , accompanied by a corresponding decrease in the Se_8 ring population. However, Te is clearly much more effective than S in reducing the Se_8 ring population; in Se-Te alloys the proportion of atoms present as Se_8 rings is reduced to half its value in amorphous selenium at the point corresponding to $\sim 12\%$ Te, whereas in Se-S this reduction would not occur until the S concentration reached $\sim 40\%$, assuming a linear extrapolation. Note that, at any given concentration of the isoelectronic additive, the proportion of atoms present as mixed rings is higher in the Se-Te than in the Se-S case, in qualitative accord with the Raman scattering results. A more quantitative correlation cannot be made at this time because of the difference in

(8) A. Eisenberg and A. V. Tobolsky, *J. Polym. Sci.*, **46**, 19 (1960).

scattering efficiency of Te-Te and S-Se bonds. As mentioned previously, the significance of these results becomes apparent in correlations between molecular structure and electrical transport properties suggested by Schottmiller, *et al.*¹ According to this work, the composition dependence of the electron mobility, as determined by time-resolved transient photoconductivity measurements on these and other vitreous binary alloys of selenium, appears to correlate quantitatively with the composition dependence of the Se_8 ring concentration. Additional calculations based on the assumption of the existence of Se_4S_4 or Se_2S_6 instead of Se_3S_5 , and of Se_5Te_3 instead of Se_6Te_2 , do not significantly alter these conclusions. Indeed, a variation of ± 1 in Y or of -1 in Z causes a deviation of less than $\pm 5\%$ in the curves shown in Figure 3. Apparently the form of these curves depends only on the presence of at least one S-S or Te-Te bond in the comonomer. A variation of $+1$ in Z would, however, give rise to a somewhat different situation because of the lack of a Te-Te bond in the Se_7Te species.

In addition to these changes in monomer concentration there is a significant change in the fraction of atoms present in polymeric form. The polymer fraction decreases in the case of Se-S and increases in the case of Se-Te as the concentration of alloying additive is increased. As pointed out by Myers and Felty,⁹ this variation should be reflected in the composition dependence of the glass transition temperature. That this is indeed the case is supported by the correlation in Figure 6 which shows a plot of glass transition temperature, T_g , against polymer fraction. The T_g data were obtained by Myers and Felty⁹ and by Myers¹⁰ using differential scanning calorimetry. While the plot is not linear, the continuous increase in T_g with polymer fraction in a composition range where the number-average chain length may be varying dramatically (see Figure 5) strongly suggests that T_g is not sensitive to chain length when the chains are sufficiently long, *e.g.*, greater than 10^3 atoms. However, it would seem reasonable to suppose that, for a system such as Se-Te in which the polymer fraction is increasing linearly while the chain length is decreasing logarithmically, eventually a composition will be reached where the influence of chain length will dominate the behavior of T_g . At this point T_g should decrease rather rapidly so that stable glass formation at room temperature in the Se-Te system should become increasingly difficult as the Te concentration is increased. Conversely, it should be easier to grow Te-rich than Se-rich Se-Te single crystals as has indeed been found by Keezer, Griffiths, and Vernon.¹¹

Inspection of the atomic distributions shown by

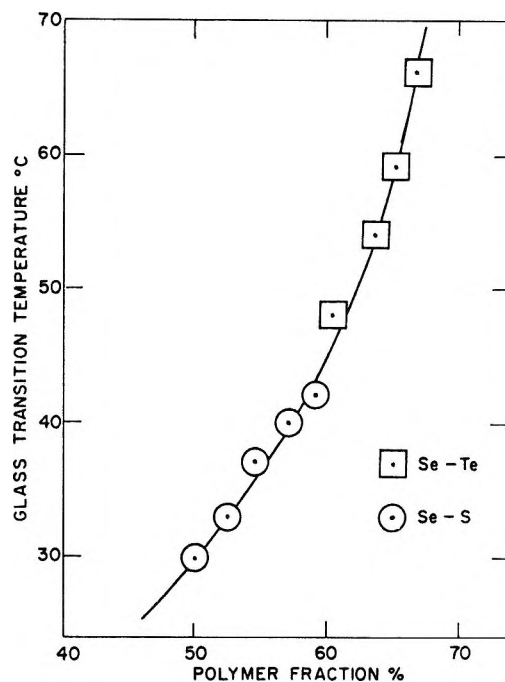


Figure 6. Variation of the glass transition temperature with polymer fraction in Se-S and Se-Te alloys.

dashed, broken, and dotted lines in Figures 3 and 4 reveals that for any nominal alloy concentration S enters eight-membered rings preferentially while Te enters copolymer chains preferentially. This trend is consistent with the known preference of elemental sulfur for the eight-membered ring state at all temperatures below 160° and the known preference of elemental tellurium for the extended chain state in the solid and liquid phase. As mentioned previously the effect, if any, of a downward revision of the initiation and propagation enthalpy values for Se_6Te_2 can only be in a direction favoring the tendencies indicated above. Actually, the effect of changing H_p° is almost insignificant: a 0.1 kcal decrease producing a net change in the atomic distribution of less than one atom per hundred for each specie. However, decreasing H_1° by the same proportion, *i.e.*, by 1 kcal, produces a decrease in the number-average chain length of about 25%.

Acknowledgement. The author wishes to thank M. B. Myers for making available the alloy samples used in the experimental phases of this work and for contributing unpublished data on the glass transition temperatures of Se-Te alloys.

(9) M. B. Myers and E. J. Felty, *Mater. Res. Bull.*, **2**, 535 (1967).

(10) M. B. Myers, private communication.

(11) R. C. Keezer, C. H. Griffiths, and J. P. Vernon, *J. Cryst. Growth*, **3**, 4, 755 (1968).

Solute and Solvent Structure Effects in Volumes and Compressibilities of Organic Ions in Solution

by L. H. Laliberté and B. E. Conway^{1a,b}

Chemistry Department, University of Ottawa, Ottawa, Canada (Received May 4, 1970)

Previous studies on the apparent molal volumes ϕ_v and adiabatic compressibilities $\phi_{K(S)}$ of organic N-containing ions have been extended to aliphatic dialkylamines, the related (cyclic) piperidines, and pyridines. In the case of tetraalkylammonium salts, new data obtained down to low concentrations by means of a dilatometer are reported, and at the lowest concentration ϕ_v begins to vary with concentration according to the Debye-Hückel limiting law. With hydrophilic alkylammonium ions, the concentration dependence of ϕ_v is more like that of simple inorganic salts. The $\phi_{K(S)}$ behavior of di-*n*-alkylamine salts shows alternations of the value of $\phi_{K(S)}$ with increasing number of CH₂ groups, but pyridine and piperidine and their homologs give linear relations. The relative electrostrictions at the N⁺ centers are also evaluated for various organic N⁺ cations. On the basis of $\phi_{K(S)}$ measurements on tetraalkylammonium and pyridine salts an extrapolation method is proposed that enables estimation of the individual ionic contributions in the observed $\phi_{K(S)}$ values for the salts.

Introduction

In previous papers^{2,3} we have shown how the complementary use of partial molal volume \bar{V} and apparent molar adiabatic compressibility $\phi_{K(S)}$ studies on aqueous solutions of organic ions can give interesting information on specificities in ion-solvent interaction connected with the structure of the organic solute and on the reciprocal effects which arise in the solvent due to the reaction of the solute ions on the processes determining the lattice structure equilibrium in the solvent (solvent structure promotion and structure breaking⁴ and the associated changes in spin-lattice relaxation times⁵). Previous work has been concerned with simple inorganic ions,⁶ tetraalkylammonium (TAA),^{2,7-11} and alkylammonium salts² as well as salts derived from pyridine and its homologs.^{3,12,13}

In the present paper we report extensions of the previous investigations^{2,3} with regard to determinations of the apparent molar functions ϕ_v and $\phi_{K(S)}$ for piperidine salts and the neutral bases and for a series of other selected salts chosen with regard to specificities in their interaction with the solvent, *e.g.*, the series of dialkylammonium hydrohalides and triethyl- and triethanolammonium bromide. Additivity relations in the pyridine and TAA series have also been investigated particularly in the case of $\phi_{K(S)}$ measurements. Here, a system for examining the results is required which will enable, by means of a suitable extrapolation procedure, individual ionic contributions in $\phi_{K(S)}$ or $\phi_{K(S)}^\circ$ to be derived in an analogous way to that developed for the individual ionic partial volumes.¹¹

Experimental Section

1. *Preparation and Purification of Compounds for Study.* TAA and pyridine salts were purified and re-

crystallized as described previously.^{3,11,12} Reagent grade piperidine and 1-methylpiperidine were distilled under a nitrogen atmosphere at reduced pressure prior to use. Piperidinium and 1-methylpiperidinium chlorides were prepared by bubbling dried HCl gas into a cold (0°) solution of the respective bases in ethanol under a nitrogen atmosphere. The products were recrystallized from ethanol, and their compositions were checked by means of a Cl⁻ analysis. 1,1-Dimethylpiperidinium iodide was prepared by slowly adding methyl iodide to a solution of 1-methylpiperidine in ethanol. The product was recrystallized from ethanol and the purity was checked by I⁻ analysis. Piperi-

(1) (a) Commonwealth Visiting Professor (1969-1970) at the Universities of Southampton and Newcastle-upon-Tyne, England; (b) to whom correspondence should be addressed at Ottawa.

(2) B. E. Conway and R. E. Verrall, *J. Phys. Chem.*, **70**, 3952 (1966); see also R. E. Verrall and B. E. Conway, *ibid.*, **70**, 3961 (1966).

(3) B. E. Conway and L. H. Laliberté, "Hydrogen Bonded Solvent Systems," A. K. Covington and P. Jones, Ed., Taylor and Francis Ltd., London, 1968, p 139.

(4) G. Némethy and H. A. Scheraga, *J. Chem. Phys.*, **36**, 3401 (1962).

(5) G. Engel and H. G. Hertz, *Ber. Bunsenges. Phys. Chem.*, **72**, 808 (1968).

(6) J. Padova, *J. Chem. Phys.*, **40**, 691 (1964); see also F. Vaslow, *J. Phys. Chem.*, **70**, 2286 (1966); **71**, 4585 (1967).

(7) L. A. Dunn, *Trans. Faraday Soc.*, **64**, 2951 (1968).

(8) F. Franks and H. T. Smith, *ibid.*, **64**, 2962 (1968); **63**, 2586 (1967).

(9) W. Y. Wen and S. Saito, *J. Phys. Chem.*, **68**, 2639 (1964).

(10) L. G. Hepler, J. M. Stokes, and R. H. Stokes, *Trans. Faraday Soc.*, **61**, 20 (1965).

(11) B. E. Conway, J. E. Desnoyers, and R. E. Verrall, *ibid.*, **62**, 2738 (1966).

(12) B. E. Conway and R. G. Barradas, *Electrochim. Acta*, **5**, 319, 349 (1961).

(13) B. E. Conway and L. G. M. Gordon, *J. Phys. Chem.*, **73**, 3609 (1969).

dinium iodide was prepared in solution by titrating piperidine with aqueous HI. The HI had been purified by distillation from red phosphorus. The I^- content of the HI solution was established by a volumetric analysis.

Diethyl-, di-*n*-propyl-, and di-*n*-butylammonium chlorides were prepared by bubbling dry HCl gas into an ethanolic solution of the amine. Reagent grade diethylamine, dipropylamine, and dibutylamine were each distilled under a nitrogen atmosphere, the dibutylamine at reduced pressure. The hydrochlorides were recrystallized from an ethanol (10%)–diethyl ether mixture, and the purity was checked by Cl^- analysis.

Triethylammonium and triethanolammonium bromides were prepared by bubbling HBr gas into a cold solution of the amine in ethanol. The first salt was recrystallized from ethanol and the second from 3:1 ethanol–water mixture. The melting points agreed with literature values. Tetramethylammonium tetrafluoroborate obtained from Aldrich Chemicals was recrystallized from hot water. The tetra-*n*-alkylammonium bromide series from CH_3 to *n*- C_4H_9 , were Eastman reagent grade materials which were recrystallized as described previously.¹¹

2. ϕ_v and $\phi_{K(S)}$ Measurements. The previously described² techniques were employed; a differential ultrasonic velocity apparatus described earlier² was used to evaluate the difference of speed of ultrasound in the solvent and solution at a given temperature, from which the $\phi_{K(S)}$ was determined at various concentrations. Special attention was given to improving the uniformity of temperature of the long bath² by provision of multiple stirrers in the outer and inner solution baths and a special extended heater system (Figure 1). All measurements were conducted at $25 \pm 0.01^\circ$.

The solutions to be studied were made up directly in the test vessel by adding weighed amounts of solute to a known weight of solvent. The concentrations (molalities) were converted into molarities by means of density data which had been obtained previously in ϕ_v mea-

surements. Loss of solvent by evaporation was minimized by keeping most of the long opening along the top of the test vessel covered with a Plexiglas lid.

The velocity differences ΔU were obtained with an absolute accuracy of $\pm 0.02 \text{ m sec}^{-1}$. Test runs were performed on KCl solutions and a value of $-45.5 \times 10^{-4} \text{ ml (g-mol bar)}^{-1}$ was obtained for the partial molar adiabatic compressibility. This compared favorably with the results of Owen and Kronick, $-44 \pm 1 \times 10^{-4} \text{ ml (g-mol bar)}^{-1}$ ¹⁴ and those of Gucker, *et al.*,¹⁵ $-45.6 \times 10^{-4} \text{ ml (g-mol bar)}^{-1}$.

The ϕ_v measurements were made by means of the differential buoyancy balance employed previously² using the techniques referred to in an earlier paper² for attainment of maximum accuracy. Determinations of ϕ_v down to concentrations below 0.02 *M* were necessitated in the case of TAA salts for attainment of the Debye–Hückel limiting law region so that reliable extrapolations to infinite dilution could be made. For this purpose, measurements were made between 0.05 and 0.002 *M* by means of a special magnetically operated dilatometer described elsewhere.¹⁶ The dilatometer was maintained in a water thermostat at 25° controlled to $\pm 0.001^\circ$ in a large cupboard thermostated to $\pm 0.5^\circ$. Corrections for the compression caused by the hydrostatic head of liquid in the capillary of the dilatometer were negligible for most measurements.

3. Hydrolysis Corrections. Since the piperidines are strong bases, their salts did not hydrolyze (K_a ca. 7×10^{-12}), and no corrections to the volumes and compressibilities were required, as was the case with the pyridinium salts.³ The neutral bases, on the other hand, react with water significantly to form the protonated species ($K_B = 1.32 \times 10^{-1}$ for piperidine). If the measurements are made in alkaline solution, it can be shown that the degree of hydrolysis α is K_B/C_{OH^-} , where C_{OH^-} is the concentration of KOH in the solvent. For piperidine in 0.1 *N* KOH, $\alpha = 0.0132$ and since no K_B value was available for 1-methylpiperidine the same α value was assumed to hold. The above considerations led to corrections of 0.1 and 0.15 ml in the apparent molar volumes of piperidine and 1-methylpiperidine, respectively.

Results

1. Extrapolation Procedures. a. Partial Molar Volumes. Extrapolations of the ϕ_v data were carried out by means of the following equation^{2,11}

$$\phi_v - 1.868c^{1/2} = \bar{V}_2^\circ + jc \quad (1)$$

using the limiting slope given by Redlich and Meyer.¹⁷

(14) B. B. Owen and P. L. Kronick, *J. Phys. Chem.*, **65**, 84 (1961).

(15) F. T. Gucker, C. L. Chernick, and P. Roy-Chowdhury, *Proc. Nat. Acad. Sci. U. S.*, **55**, 12 (1966).

(16) B. E. Conway and L. H. Laliberté, *Trans. Faraday Soc.*, in press.

(17) O. Redlich and D. M. Meyer, *Chem. Rev.*, **64**, 221 (1964).

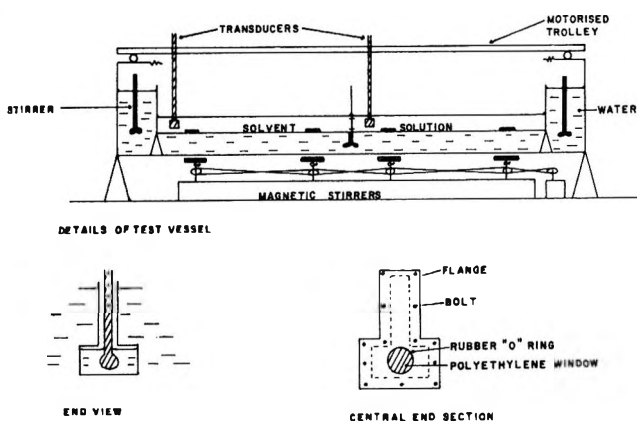


Figure 1. Schematic representation of mechanical assembly used in differential velocity measurements, and details on the test vessel used.

Extrapolations of ϕ_v as a function of $c^{1/2}$ were also carried out.

b. *Partial Molar Adiabatic Compressibilities.* An equation for apparent molar adiabatic compressibility can be obtained by differentiating eq 1 with respect to pressure and neglecting the jc term, *i.e.*

$$-\phi_{K(S)} = \frac{\partial \phi_v}{\partial P} = \frac{\partial \phi_v^\circ}{\partial P} + \left[\frac{\partial S_v}{\partial P} + \frac{\beta_s S_v}{2} \right] c^{1/2} \quad (2)$$

or

$$\phi_{K(S)} = \phi_{K(S)}^\circ + S_{K(S)} c^{1/2} \quad (3)$$

where

$$S_{K(S)} = - \left(\frac{\partial S_v}{\partial P} + \frac{\beta_s S_v}{2} \right)$$

[If the term jc is included and differentiated, an equation similar to eq 2 results but with the additional term $[(\partial j/\partial P) + j\beta]c$. In the case of neutral solutes both the ϕ_v and $\phi_{K(S)}$ data were plotted empirically as a function of c for lack of any theoretically justified extrapolation equation.]

Since β_s is a function of concentration, the slope $S_{K(S)}$ should not be constant; however, this variation is less than the uncertainty in the slope for the concentration range used in this work, so that eq 3 can be regarded as linear in $c^{1/2}$.

2. *Partial Molar Volumes.* a. *Protonated N+ Centers.* The ϕ_v data for the piperidinium salts were plotted according to eq 1 and \bar{V}_2° values were obtained. These data are given in Table I. The slope of the plots

Table I: Values of \bar{V}_2° and j in Eq 1

Salt	$\bar{V}_2^\circ \pm 0.05$, ml (g-mol) ⁻¹	$j \pm 0.02$ ml l. g-mol ⁻¹
1,1-Dimethylpiperidinium iodide	158.68	0.0 up to $c = 0.40$
1-Methylpiperidinium chloride	125.51	0.0 up to $c = 0.55$
Piperidinium chloride	106.67	0.0 up to $c = 0.75$
Compound	\bar{V}_2° , ml g-mol ⁻¹	$(d\phi_v/dc)_{c \rightarrow 0}$, ml l. g-mol ⁻¹
Piperidine in 0.1 N KOH	91.10	0.0
1-Methylpiperidine in 0.1 N KOH	109.91	0.0

of the apparent molar volume *vs.* $c^{1/2}$ for all three salts approaches the limiting law value in the concentration range studied as shown in Figure 2. Also given in Table I are the \bar{V}_2° values for the two corresponding neutral bases obtained from the plot shown in Figure 3.

The partial molar volumes of selected *n*-alkylammonium halide salts were examined to study further the specific structural effects associated with coordination of N^+ centers by alkyl groups and H atoms and thus to

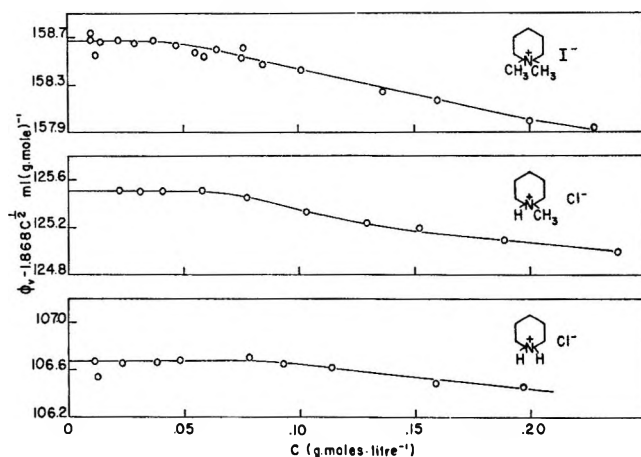


Figure 2. Plot of $\phi_v - 1.868c^{1/2}$ as a function of concentration for 1,1-dimethylpiperidinium iodide, 1-methylpiperidinium chloride, and piperidinium chloride at 25°.

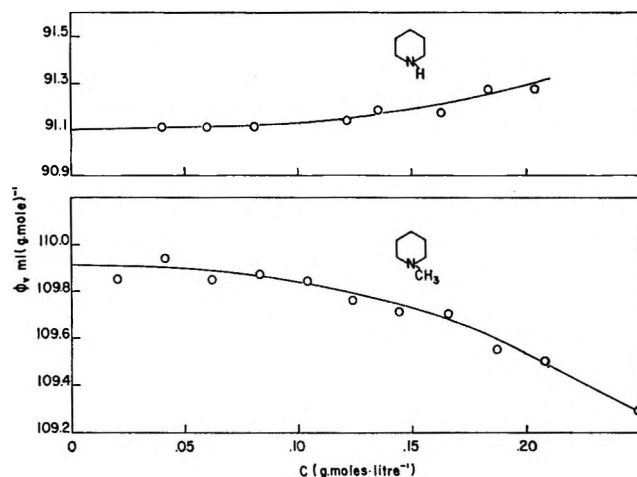


Figure 3. Plot of apparent molar volume ϕ_v as a function of concentration for piperidine and 1-methylpiperidine in 0.1 N KOH at 25°.

complement the volume data already gathered in this laboratory^{2,3,11} and by others^{7-10,18} for related compounds. The apparent molar volumes of the salts in the series R_2NH_2Cl , where $R = C_2H_5^-$, $n-C_3H_7^-$, and $n-C_4H_9^-$, were determined and are shown in Figure 4. As may be seen from Figure 4, the deviations from the limiting law slope of $1.868 \text{ ml l.}^{1/2} (\text{g-mol})^{-1/2}$ increase with increasing size of the R group. In Figure 5 the plot of ϕ_v against $c^{1/2}$ for $(\text{HO}C_2H_4)_3NH^+Br^-$ shows that the introduction of a polar-OH group into the alkyl residues of the molecule causes it to behave like a "normal" 1:1 electrolyte as opposed to the behavior of $(C_2H_5)_3NHBr$ (Figure 5) which exhibits a large negative deviation from the Debye-Hückel limiting law for ϕ_v . The \bar{V}_2° data for the compounds shown in Figures 4 and 5 are listed in Table II. The \bar{V}_2° datum for Me_4NBF_4 is also included in Table II.

(18) J. E. Desnoyers and M. Arel, *Can. J. Chem.*, **45**, 359 (1967).

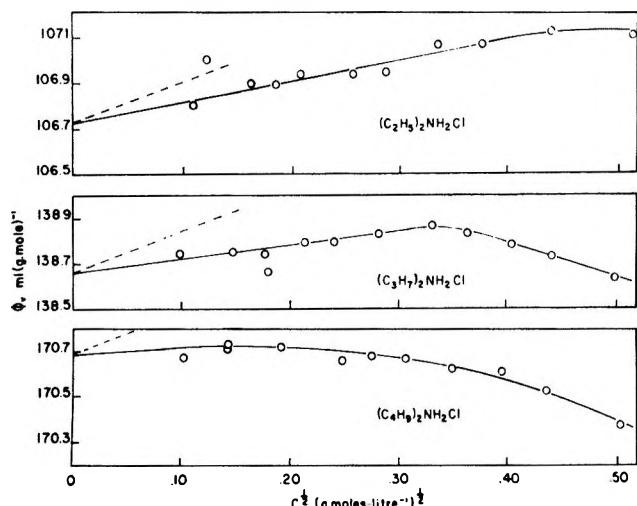


Figure 4. Plot of apparent molar volume ϕ_v against $c^{1/2}$ for $(C_2H_5)_2NH_2Cl$, $(C_3H_7)_2NH_2Cl$, and $(C_4H_9)_2NH_2Cl$ at 25° .

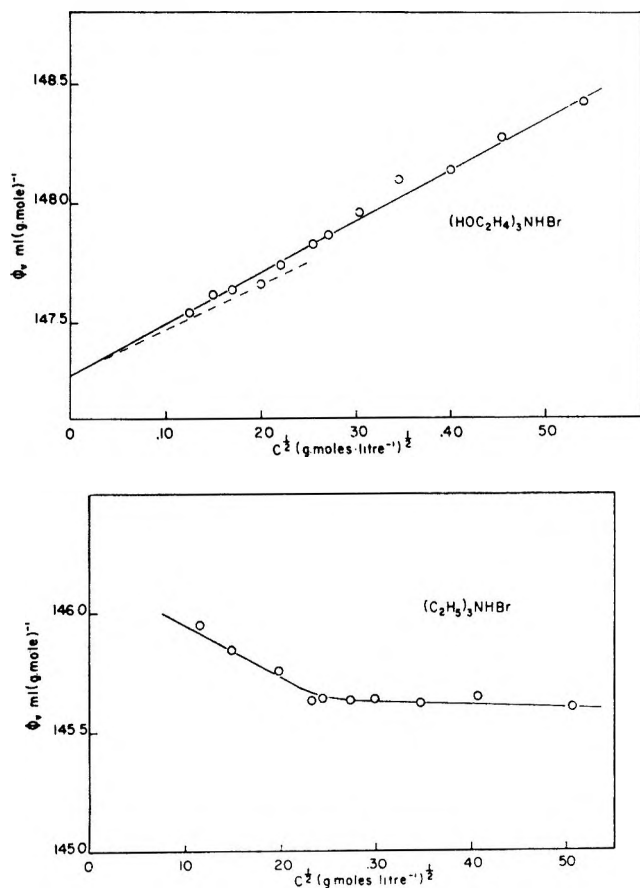


Figure 5. Plot of apparent molar volume ϕ_v against $c^{1/2}$ for triethanolammonium and a plot of apparent molar volume ϕ_v against $c^{1/2}$ for triethylammonium bromide at 25° .

b. Quaternized N^+ Centers. The partial molar volumes of tetraalkylammonium (TAA) salts have been studied extensively, both in this laboratory^{2,11} and elsewhere.^{7-10,19} The present measurements were primarily confined to the high dilution region, *i.e.*, $0.002 < c < 0.01 M$; however, because of the type of dilatometer used,¹⁶ it was also necessary to have accu-

Table II: Values of \bar{V}_2° for a Series of Alkylammonium Salts

Salt	$\bar{V}_2^\circ = 0.05 \text{ ml (g-mol)}^{-1}$
NH_4Cl	36.27
$(C_2H_5)_2NH_2Cl$	106.73
$(n-C_3H_7)_2NH_2Cl$	138.66
$(n-C_4H_9)_2NH_2Br$	170.68
$(C_2H_5)_3NHB r$	146.17
$(HOC_2H_4)_3NHB r$	147.28
$(n-C_3H_7)_3NHB r^a$	193.65
$(CH_3)_4NBF_4$	132.60

^a Derived from the data of Conway and Verrall² for the Cl^- and I^- salts.

rate ϕ_v data in the region $0.10 < c < 0.5 M$. Therefore the existing data in this high concentration region were extended and augmented where needed.

The first member in the series, $(CH_3)_4NBr$, exhibits a positive slope ($d\phi_v/dc^{1/2}$) at quite high ($\leq 0.1 M$) concentrations and has been shown to follow the Debye-Hückel limiting law¹⁰ quite well. Dilatometric measurements were carried out on $(C_2H_5)_4NBr$, $(n-C_3H_7)_4NBr$, and $(n-C_4H_9)_4NBr$ in H_2O and in one case in D_2O at 25° . The results for $(C_2H_5)_4NBr$ in D_2O have also been reported elsewhere.¹⁶ Figure 6 shows the behavior of ϕ_v plotted against $c^{1/2}$ for $(C_2H_5)_4NBr$ in H_2O and D_2O . The relation is linear up to $c = 0.04 M$ and has a slope of $1.65 \pm 0.2 \text{ ml l.}^{1/2} (\text{g-mol})^{-1/2}$, the ϕ_v plots for D_2O being parallel to those of H_2O in this concentration range. The present results for $(n-C_3H_7)_4NBr$

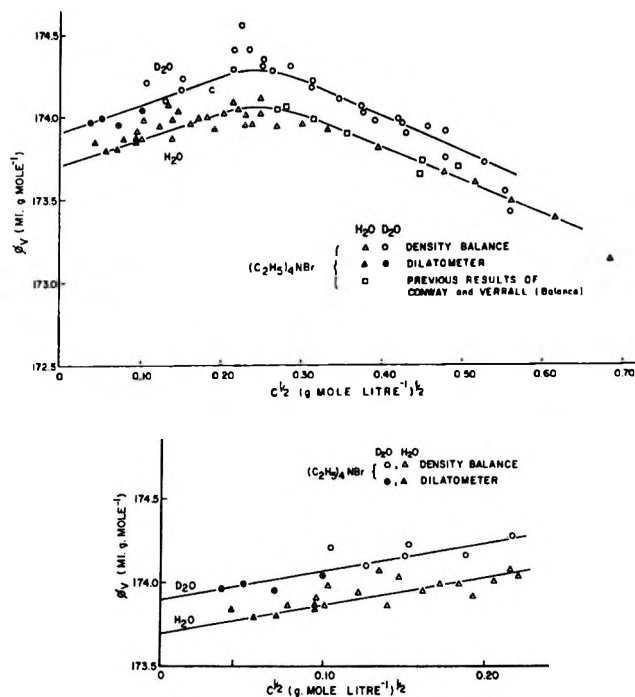


Figure 6. A plot of apparent molar volume ϕ_v against $c^{1/2}$ for tetraethylammonium bromide in H_2O and D_2O at 25° .

(19) H. E. Wirth, *J. Phys. Chem.*, **71**, 2922 (1967).

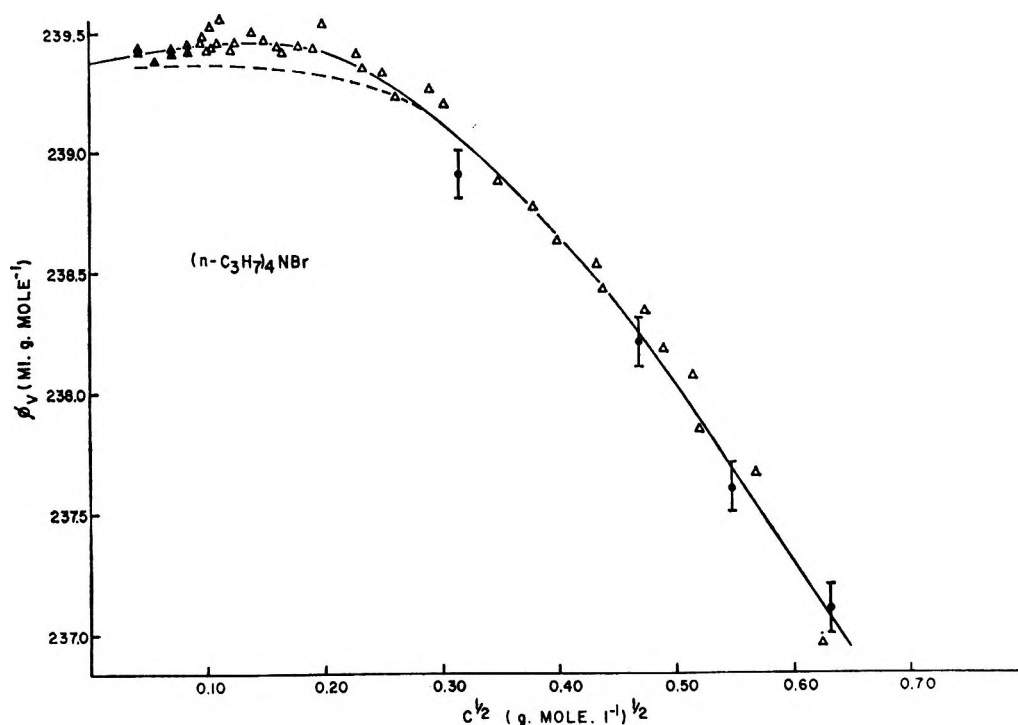


Figure 7. Plot of apparent molar volume ϕ_v against $c^{1/2}$ for tetra-*n*-propylammonium bromide in H_2O . Present results: dilatometer, \blacktriangle ; buoyancy balance, \triangle ; Wen and Saito \times ,⁹ Franks and Smith,⁸ ---.

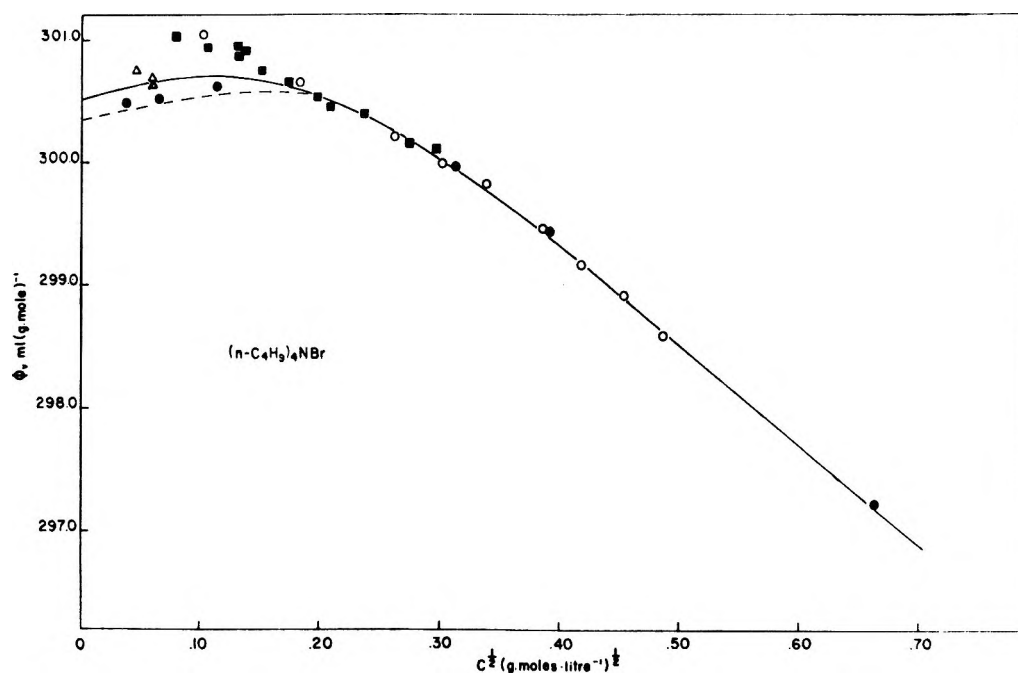


Figure 8. Plot of apparent molar volume ϕ_v against $c^{1/2}$ for tetra-*n*-butylammonium bromide in H_2O at 25° . Present results: dilatometer, \triangle ; buoyancy balance, O ; Conway and Verrall,¹¹ \blacksquare ; Dunn,⁷ \bullet ; Franks and Smith,⁸ ---.

have been plotted in Figure 7 together with those of Wen and Saito⁹ and Franks and Smith.⁸ The plot of ϕ_v against $c^{1/2}$ goes through a maximum with $(\partial\phi_v/\partial c^{1/2})$ being positive below *ca.* 0.015 *M*. The limiting law slope is not reached even at the high dilutions used, the highest positive slope being *ca.* $+0.7 \pm 0.2$ ml $l^{1/2}$ $(g\text{-mol})^{-1/2}$. The concentration range over which a straight line of positive slope can be drawn is so small

that a scatter of ± 0.02 ml $(g\text{-mol})^{-1}$ in ϕ_v introduces an appreciable uncertainty in the value of the slope. Dilatometric measurements on $(n\text{-}C_4H_9)_4NBr$ have recently been reported²⁰ and are in agreement with the results of the present determinations on this compound (Figure 8).

(20) L. A. Dunn, *Trans. Faraday Soc.*, **64**, 1898 (1968).

Table III: Values of \bar{V}_2° for the Tetra-*n*-alkylammonium Bromides in H₂O at 25°

Salt	$\bar{V}_2^\circ, \text{ml (g-mol)}^{-1}$		
	a	b	c
(CH ₃) ₄ NBr	114.26 ^d	114.40	114.25
(C ₂ H ₅) ₄ NBr	173.70 ± 0.05	173.65	173.6 ± 0.10
(<i>n</i> -C ₃ H ₇) ₄ NBr	239.38 ± 0.05	239.15	
(<i>n</i> -C ₄ H ₉) ₄ NBr	300.41 ± 0.10	300.35	300.40

^a Present work; ϕ_v data obtained dilatometrically down to $c = 0.002 M$. ^b Franks and Smith;⁸ ϕ_v data obtained on magnetically operated densitometer down to $c = 0.002 M$. Hepler, Stokes, and Stokes;¹⁰ ϕ_v data obtained dilatometrically down to $c = 0.01 M$. Dunn;⁷ ϕ_v data obtained dilatometrically down to $c = 0.0015 M$. ^c Wirth;¹⁹ ϕ_v data obtained dilatometrically down to $c = 0.002 M$. ^d Conway, Verrall, and Desnoyers;¹¹ ϕ_v data obtained on a differential buoyancy balance down to $c = 0.01 M$.

The results for \bar{V}_2° obtained in this study on the TAA bromides have been listed in Table III together with the data of other workers, where extrapolations were made from sufficiently high dilutions. As may be seen from Figures 6 and 7 and also from Table III, there is good agreement between the present results and those of other workers. For results obtained at high dilutions, measurements obtained dilatometrically are the most precise; for example, good agreement in the ϕ_v data was found for *n*-Bu₄NBr and Et₄NBr where two dilatometric determinations could be compared (Table III).

c. Apparent Molar Adiabatic Compressibilities. The $\phi_{K(S)}$ data for the piperidinium salts were plotted according to eq 3 (Figure 9a) and the $\phi^\circ_{K(S)}$ and $S_{K(S)}$ values obtained are shown in Table IV. The plot is linear for piperidinium chloride but for 1-methylpiperidinium chloride the linear section extends only to $c = 0.10 M$. The $\phi_{K(S)}$ data for the two neutral piperidines in 0.1 *N* KOH were plotted as a function of concentration (Figure 9b) and the $\phi^\circ_{K(S)}$, together with the limiting slopes $(d\phi_{K(S)}/dc)$, are shown in Table IV.

The $\phi_{K(S)}$ data for the alkylammonium salts were plotted according to eq 3, and the $\phi_{K(S)}^\circ$ values, together with the slopes $S_{K(S)}$, were obtained. These data are shown in Table IV and are plotted in Figures 9c and 9d. Also included in Table IV are $\phi^\circ_{K(S)}$ data for the salt Me₄NBF₄ which was investigated on account of the similar ionic radii of its cation and anion.

Discussion

1. Limiting Law Behavior and the Dependence of ϕ_v on Concentration. To examine structural effects in the partial molar volume of organic salts at infinite dilution, it is necessary to make extrapolations to unusually low concentrations on account of the anomalous concentration dependence¹¹ of ϕ_v (negative slope) exhibited, *e.g.*, by TAA salts above 0.04–0.05 *M*. The anomalous slopes S_v arise on account of the long-range hydrophobic

Table IV: Values of $10^4\phi_{K(S)}$ and $S_{K(S)}^\circ$ in Eq 3 (25°)

Salt	$10^4\phi_{K(S)} \pm 0.25, \text{ml (g-mol bar)}^{-1}$	$S_{K(S)}^\circ, \text{ml l.}^{1/2} (\text{g-mol})^{3/2} \text{bar}^{-1}$
Piperidinium chloride ^a	-22.0	+8.6
1-Methylpiperidinium chloride	-20.9	+15.0
(C ₂ H ₅) ₂ NH ₂ Cl	-25.1	+4.0
(<i>n</i> -C ₃ H ₇) ₂ NH ₂ Cl	-17.9	+3.8
(<i>n</i> -C ₄ H ₉) ₂ NH ₂ Cl	-25.0	+11.0
NH ₄ Cl	-25.6	+18.0
(C ₂ H ₅) ₃ NHBr	-5.6	+7.4
(HOC ₂ H ₄) ₃ NHBr	-8.6	+9.0
(CH ₃) ₄ NBF ₄	+18.0	+7.0
(CH ₃) ₄ NI ^a	+3.3	+17.2

Values of $10^4\phi_{K(S)}$ and $(d\phi_{K(S)}/dc)_{c \rightarrow 0}$ (25°) for Neutral Piperidines

Compound	$10^4\phi_{K(S)} \pm 0.25, \text{ml (g-mol bar)}^{-1}$	$(d\phi_{K(S)}/dc)_{c \rightarrow 0}, \text{ml l. (g-mol)}^{-2} \text{bar}^{-1}$
Piperidine in 0.1 <i>N</i> KOH	-0.40	0.0
1-Methylpiperidine in 0.1 <i>N</i> KOH	+0.30	+0.7

^a From the data of Verrall and Conway.²

interactions which the cations of these salts exhibit in water. Figures 6, 7, and 8 show the situation with regard to ϕ_v from previous work in this and other laboratories in relation to the new dilatometric data obtained at very low concentrations. Evidently the ϕ_v data approach ϕ_v° with the correct slope providing that data are obtained at sufficiently high dilutions. Figure 8 shows the situation more clearly in the limiting law region for H₂O and D₂O (*cf.* ref 16) with the plots based on many points. With the more hydrophilic secondary and tertiary *n*-alkylammonium, pyridinium, and piperidinium salts, the limiting law slope was already approached at concentrations >0.01 *M* and in some cases $d\phi_v/dc^{1/2}$ retains the normal positive sign up to moderate concentrations. Various interpretations of the anomalous slopes have been given.^{11,19,21}

2. Additivity in the Volumes. Comparison of \bar{V}_2° values in a series of related compounds studied in a given solvent provides a good basis for examination of the additivity (or deviations therefrom indicating specificities and solute-solvent interactions) of the volume function since the solute molecules are always present in corresponding states (*e.g.*, comparison of volumes of substances in the pure compounds at a given temperature is not so satisfactory since the compounds under these conditions are not in corresponding states nor are the intermolecular interactions usually comparable; in excess of solvent, these interactions are more nearly constant). In previous work^{2,11} we have

(21) R. N. Diamond, *J. Phys. Chem.*, **67**, 2513 (1963).

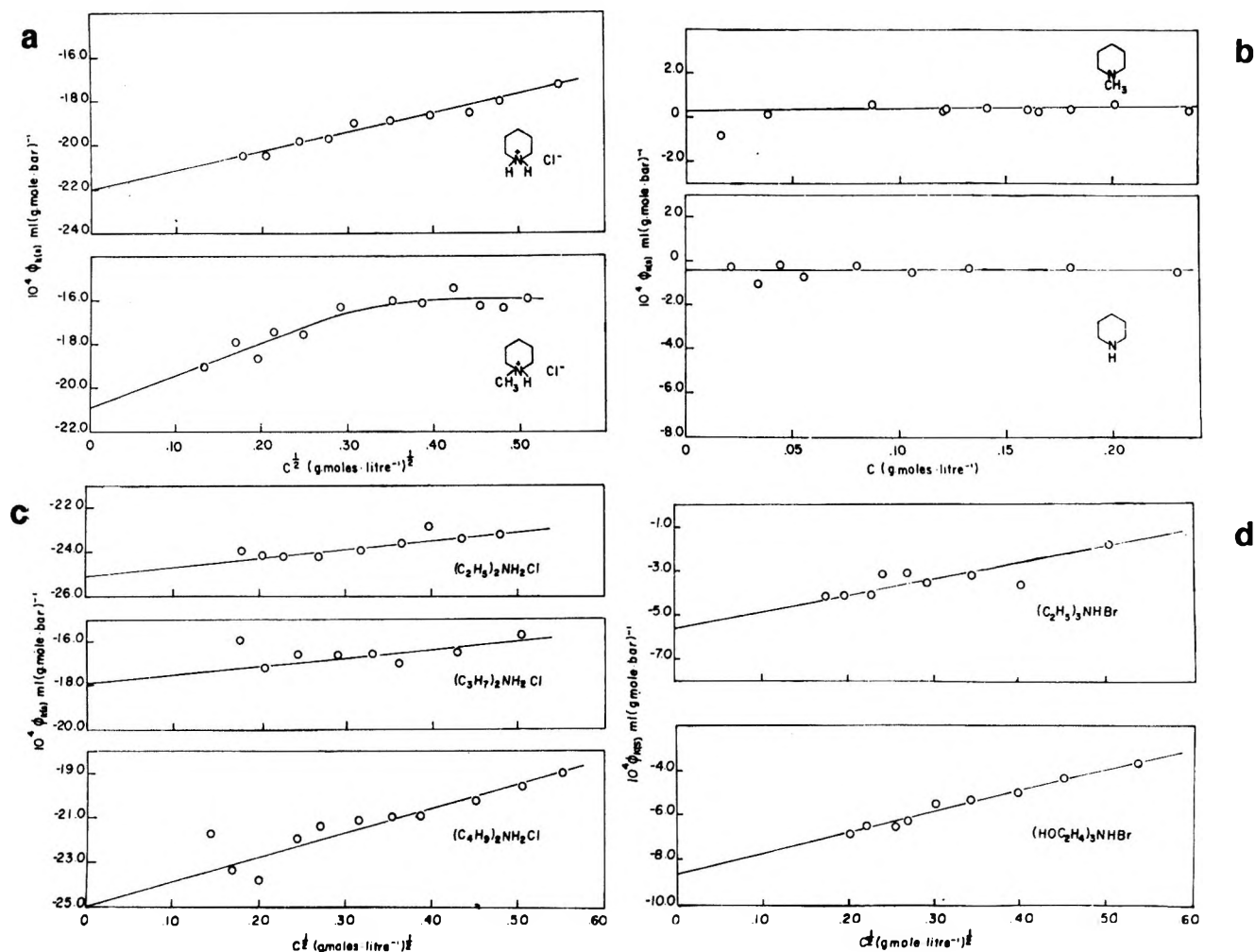


Figure 9. (a) Plot of apparent molar adiabatic compressibility $\phi_{K(S)}$ as a function of concentration for piperidinium chloride and 1-methylpiperidinium chloride at 25°. (b) Plot of apparent molar adiabatic compressibility $\phi_{K(S)}$ as a function of concentration for piperidine and 1-methylpiperidine in 0.1 N KOH at 25°. (c) Plot of apparent molar adiabatic compressibility $\phi_{K(S)}$ against $C^{1/2}$ for $(\text{C}_2\text{H}_5)_2\text{NH}_2\text{Cl}$, $(n\text{-C}_3\text{H}_7)_2\text{NH}_2\text{Cl}$, and $(n\text{-C}_4\text{H}_9)_2\text{NH}_2\text{Cl}$ at 25°. (d) Plot of apparent molar adiabatic compressibility $\phi_{K(S)}$ against $C^{1/2}$ for $(\text{C}_2\text{H}_5)_3\text{NHBr}$ and $(\text{HOOC}_2\text{H}_5)_3\text{NHBr}$ at 25°.

examined the additivity of \bar{V}_2° for TAA cations, for pyridine and its homologs, and for the derived salts.³ The additivity can be characterized by a b coefficient^{2,11} which measures the specific volume increment per gram of CH_2 groups in successive additions of CH_2 in various homologous series of ions or corresponding neutral molecules.

The data for the R_2NH_2^+ series, where R is varied from methyl to n -butyl, together with that for the RNH_3^+ series studied by Desnoyers and Arel¹⁸ (where R varies from methyl to n -octyl) lead in both cases to b values which are considerably lower than those for the methyl-substituted ammonium ion series $[\text{Me}_{4-x}\text{NH}_2^+]$.² This reflects the greater shielding effect (with respect to hydration) of the higher alkyl substituents in these two series.

The RNH_3X and $\text{R}_2\text{NH}_2\text{X}$ series of salts differ from the TAA halides in that there must be a significant electrostriction term in their volumes due to the direct

accessibility of the N^+ center. Assuming that the TAA salts do not themselves cause any electrostriction,² it is possible to determine the (relative) electrostriction caused by the partially alkyl-substituted salts mentioned above. This was done by measuring the deviation at a given value of the molecular weight of the cation W^+ (*i.e.*, for isomeric ions) of the volume of the salt concerned from the line characterizing the linear additivity relation¹¹ for the TAA salts. The results of these calculations are shown graphically in Figure 10, where the relative electrostriction $V_{e(+)}$ caused by the cation is plotted against its molecular weight. In the series of RNH_3X salts,¹⁸ the electrostriction reaches a constant value of $-3.5 \text{ ml}(\text{g-mol})^{-1}$ after R becomes larger than an n -propyl group. If the substituent is smaller than a propyl group, the influence of the field at the charge center can evidently still be manifested in the average properties of a water molecule at that coordination position. From the results obtained on

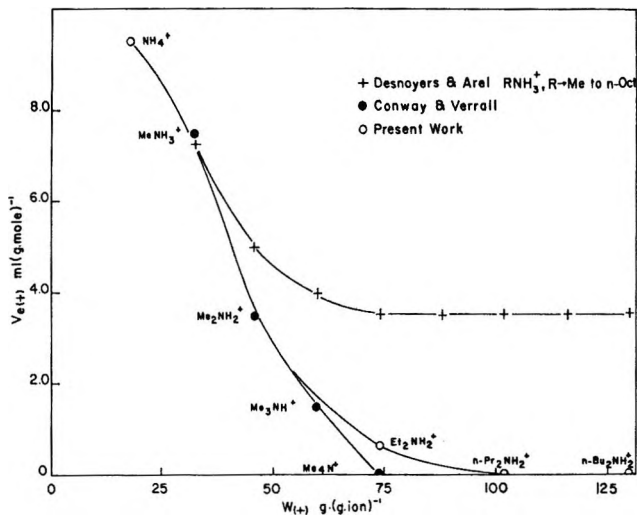


Figure 10. Plot of relative electrostriction $V_{e(+)}$ caused by n -alkylammonium cations against molecular weight W_+ of the cation. (Zero line for the ordinate axis, $V_{e(+)} = 0$, corresponds to a reference line for the TAA salt series.) Data for the $\text{Me}_{4-n}\text{NH}_2^+$ series are from previous work of Conway and Verrall.²

the $\text{R}_2\text{NH}_2\text{Cl}$ salt series studied in the present work, it is apparent that when the two R groups are larger than C_2H_5 the electrostriction is virtually eliminated. This must be attributed to the ability of the two alkyl groups to shield the positive charge on the nitrogen center. However, it is of interest to note that when only one alkyl group is present,¹⁸ even when it is a long chain, appreciably more electrostriction remains (Figure 10). Behavior similar to that observed with the dialkylammonium salts was found with the trialkylammonium ions Et_3NH^+ and $(n\text{-Pr})_3\text{NH}^+$. The series of methyl-substituted ammonium ions studied by Conway and Verrall² show, however, the effect of progressive blocking of the charged center.

The difference in b values in going from the methylammonium series to the TAA series suggests that each CH_2 group eliminates a degree of electrostriction of solvent equivalent to $14 \times (1.115 - 1.284)$, i.e., $-2.37 \text{ ml mol}^{-1}$. This is equivalent (cf. the previous calculations²²) to the effect of a local field of $ca. 2.7 \times 10^5 \text{ esu}$ which is reasonable for an exposed NH^+ center (radius $ca. 1.05 \text{ \AA}$), since 90% of the electrostriction arising at charged centers of small radius can be shown to occur within one H_2O diameter from the center.²² A similar calculation for the pyridine-HCl salts showed³ that substitution of methyl groups on the pyridine ring adjacent to the charged nitrogen eliminated an electrostriction of solvent equivalent to -1.6 ml mol^{-1} . This lower value of the decrease in the electrostriction reflects the indirect nature of the blocking effect at the charged center which arises in the case of the ring-substituted pyridinium ions. With the N -methylpyridinium salts, effective primary hydration of the charged nitrogen is prevented; for this case, ring substitution eliminates only $-0.42 \text{ ml mol}^{-1}$ of electrostriction.

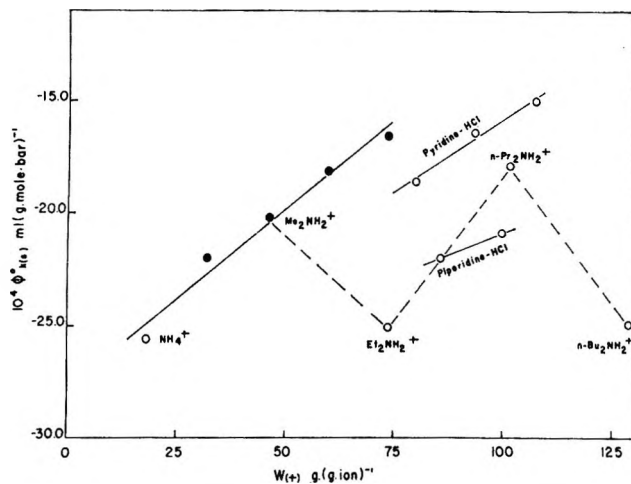


Figure 11. Plot of $\phi_{K(S)}^0$ against the molecular weights of cations in the series of hydrochlorides studied.

Similarly, in the R_2NH_2^+ and RNH_3^+ series, the addition of CH_2 groups is being made at some distance from the charged center, so that only $ca. -0.50 \text{ ml mol}^{-1}$ of net electrostriction is eliminated per CH_2 group added.

3. *Partial Molar Adiabatic Compressibilities. a. Additivity and Structural Effects.* In discussing the trends in the compressibility results, the model proposed previously² and applied to hydration of various ions^{2,3} has been employed, where electrostricted water around small ions and the supposed "icelike" water surrounding hydrophobic solutes was regarded as essentially incompressible, while "structure-broken" water was assumed to be relatively more compressible. A more dynamical picture of the ion-water interactions is afforded by the nmr spin-lattice relaxation behavior⁶ which provides a complementary characterization of these thermodynamic effects in terms of individual molecular properties, e.g., ions which increase structure or so-called "icelike"-ness in water, increase the relaxation times.

The values of the apparent molar adiabatic compressibilities $\phi_{K(S)}$ at infinite dilution for the series of hydrochloride salts of various bases studied were plotted against the molecular weights of the cations and are shown in Figure 11. Also included in this figure are data for the methyl-substituted ammonium ion series from CH_3NH_3^+ to $(\text{CH}_3)_4\text{N}^+$, determined by Conway and Verrall.² In the ring-substituted pyridine-HCl series,³ $\phi_{K(S)}$ also increases in a linear manner with the molecular weight of the cation, W_+ , and the same trend is observed with the two piperidine-HCl salts. In the series Me_2NH_2^+ to $n\text{-Bu}_2\text{NH}_2^+$, the behavior is more complex and illustrates the rather structure-specific effects which determine $\phi_{K(S)}$.

While the methylammonium ion series (NH_4^+ to Me_4N^+) shows² a uniform trend of $\phi_{K(S)}$ with increasing

(22) J. E. Desnoyers, R. E. Verrall, and B. E. Conway, *J. Chem. Phys.*, **43**, 243 (1965); *Z. Phys. Chem. (Leipzig)*, **230**, 157 (1965).

coordination of the N^+ center by CH_3 groups, the behavior of the secondary aminium ions $R_2NH_2^+$ from $R = Me$ to $R = n-Bu$ shows an alternating change of $\phi_{K(S)}^\circ$ (well outside experimental error) between successive members of the series. In particular, the change from hydrophilic to more hydrophobic hydration as the alkyl chains are lengthened occurs in a nonlinear manner because of the asymmetrical structure of the salts and leads to the observed alternating $\phi_{K(S)}^\circ$ values. The hydration behavior of the N^+ center is evidently very susceptible to its local environment, and it is apparent that the compressibility variations from one type of ion to another are much more sensitive than are the volume variations (Figure 10) to specificities of structure of the molecular ions and to the solvent structure⁴ and related changes⁵ which such ions produce in water.

b. Extrapolation Procedure for Individual Ionic Compressibilities. In the present work, we have been concerned with developing a method for obtaining absolute individual ionic partial molar adiabatic compressibilities. An extrapolation procedure was developed by Conway, Verrall, and Desnoyers¹¹ for determination of individual partial gram ionic volumes. The values so obtained are in quite close agreement with the results of recent ultrasonic potential measurements of Zana and Yeager.²³ A related method was developed for individual $\phi_{K(S)}^\circ$ values and is presented below.

The total partial molar volume of a salt at infinite dilution can be written

$$\bar{V}_2^\circ = \bar{V}_+^\circ + \bar{V}_-^\circ \quad (4)$$

where \bar{V}_+° and \bar{V}_-° are the individual partial molar volumes at infinite dilution of the cation and anion, respectively. The volume of the cation can further be broken down into various contributions

$$\bar{V}_+^\circ = V_{in(+)} + V_{e(+)} + V_{s(+)} \quad (5)$$

where $V_{in(+)}$ is the intrinsic volume of the ion; $V_{e(+)}$ is the electrostriction of the solvent caused by the field of the ion and will be negligible for the series of TAA ions, while $V_{s(+)}$ is the structural contribution to the volume due to the inclusion of the ion in a cavity in the solvent (negative effect) and to any increase in "icelikeness" of the solvent (positive effect). There is evidence that the term $V_{s(+)}$ only becomes important for $n-Bu_4NBr$, in which case it is negative.^{24,25}

The partial molar adiabatic compressibility is the pressure derivative of the partial molar volume at constant entropy

$$-\phi_{K(S)}^\circ = \left(\frac{\partial \bar{V}_2^\circ}{\partial P} \right)_s = \left(\frac{\partial \bar{V}_+^\circ}{\partial P} \right)_s + \left(\frac{\partial \bar{V}_-^\circ}{\partial P} \right)_s \quad (6)$$

which can be written as

$$\phi_{K(S)}^\circ = \bar{V}_+^\circ \left[\frac{1}{\bar{V}_+^\circ} \left(\frac{\partial \bar{V}_+^\circ}{\partial P} \right)_s \right] + \phi_{K(S)(-)}^\circ \quad (7)$$

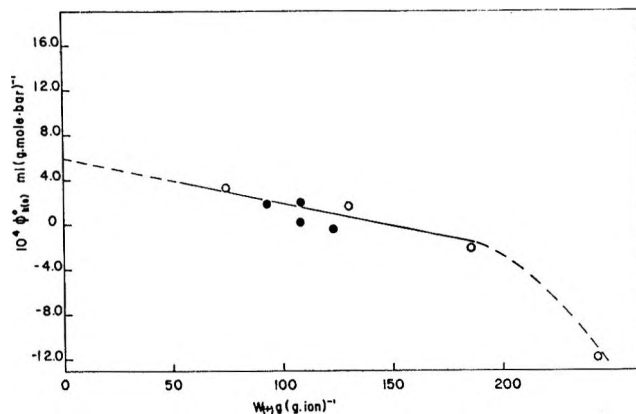


Figure 12. Plot of $\phi_{K(S)}^\circ$ at infinite dilution against the molecular weight of the cations for a series of tetra-*n*-alkylammonium iodides (based on data of ref 2) (O) and pyridinium iodides (●).

where the term $-(1/\bar{V}_+^\circ) (\partial \bar{V}_+^\circ / \partial P)_s$ is a specific compressibility and will be written as $\bar{\beta}_+^\circ$. For the series of salts, Me_4NI to Pr_4NI ,² and for four *N*-alkyl-substituted pyridinium iodides,³ $\bar{\beta}_+^\circ$ is essentially a constant equal to the total partial molar compressibility divided by the total partial molar volume. The observation that $\bar{\beta}_+^\circ$ is approximately constant implies that the nature but not necessarily the extent of hydration remains constant in the series. In fact $10^6 \bar{\beta}_+^\circ = -0.7 \pm 1.0$ bar⁻¹ for the series of iodide salts referred to above.

Equation 7 can therefore be written as

$$\phi_{K(S)}^\circ = V_{in(+)} \cdot \bar{\beta}_+^\circ + \phi_{K(S)(-)}^\circ \quad (8)$$

where $V_{e(+)}$ and $V_{s(+)}$ have been assumed to be negligible for the reasons discussed above. Finally, eq 8 can be written with $V_{in(+)}$ in terms of W_+ if we assume that $V_{in(+)} = W_+/d_+$, where d_+ is a proportionality constant having the dimensions of density and implying that the ions in the series have the same mean density.

$$\phi_{K(S)}^\circ = W_+ \left(\frac{\bar{\beta}_+^\circ}{d_+} \right) + \phi_{K(S)(-)}^\circ \quad (9)$$

The data were plotted according to eq 9 (Figure 12) and a fairly straight line was obtained up to the W_+ value corresponding to $(n-Pr)_4NBr$. From the intercept, a value of $+6.0 \pm 1.0 \times 10^{-4}$ ml (g-mol bar)⁻¹ was obtained for $\phi_{K(S),I^-}^\circ$. A similar plot using the previously published data² for the TAA bromides yielded a value of -3.8 ± 1.0 for $10^4 \phi_{K(S),Br^-}^\circ$. These two results agree with the thermodynamically determinable difference in $10^4 \phi_{K(S)}^\circ$ between an iodide and a bromide salt with a common cation, as listed in Table V. In the above plot, the datum for $(n-Bu)_4NBr$ does not fall on the line and, in fact, exhibits a more negative com-

(23) R. Zana and E. Yeager, *J. Phys. Chem.*, **70**, 954 (1966); **71**, 521 (1967).

(24) F. J. Millero and W. Drost-Hansen, *ibid.*, **72**, 1758 (1968).

(25) M. E. Friedman and H. A. Scheraga, *ibid.*, **69**, 3795 (1965).

Table V: Values of Individual Partial Gram Ionic Volumes, Compressibilities, and Expansibilities

Ion	\bar{V}°_{ion} $\pm 0.2, \text{ ml}$ $(\text{g-mol})^{-1} \text{ }^a$	$10^2 \times$	$10^4 \times$
		$\left(\frac{\partial \bar{V}^{\circ}_{ion}}{\partial T}\right)_P,$ ml (g-mol) $\text{deg}^{-1} \text{ }^b$	$\left(\frac{\partial \bar{V}^{\circ}_{ion}}{\partial P}\right)_T,$ $\pm 1.0,$ ml (g-mol) $\text{bar}^{-1} \text{ }^c$
H ⁺	-5.7	-1.2	-3.9
NH ₄ ⁺	12.8 ^c	-3.0	+13.4 ^c
CH ₃ NH ₃ ⁺	30.2	...	+10.0
(CH ₃) ₂ NH ₂ ⁺	48.9	...	+7.6
(CH ₃) ₃ NH ⁺	67.0	...	+5.9
(CH ₃) ₄ N ⁺	83.4 ^c	+3.1	+3.8
(C ₂ H ₅) ₄ N ⁺	142.8 ^c	+5.2	+4.4
(C ₃ H ₇) ₄ N ⁺	208.5 ^c	+9.3	+8.3
(C ₄ H ₉) ₄ N ⁺	270.1 ^c	+17.5	+17.9
(C ₂ H ₅) ₂ NH ₂ ⁺	83.1 ^c	...	+13.0 ^c
(C ₃ H ₇) ₂ NH ₂ ⁺	115.1 ^c	...	+5.7 ^c
(C ₄ H ₉) ₂ NH ₂ ⁺	147.1 ^c	...	+12.8 ^c
BF ₄ ⁻	49.0 ^c	...	-21.8 ^c
Cl ⁻	23.6	+4.8	+12.2 ^c
Br ⁻	30.9	+3.5	+3.8
I ⁻	42.2	...	-6.0 ^c
K ⁺	3.2 ^c	+3.5	+33.3 ^c
Pyridinium	67.4 ^c	...	+6.4 ^c
1-Me-pyridinium	84.6 ^c	...	+7.5 ^c
1,2-Di-Me-pyridinium	100.4 ^c	...	+6.1 ^c
1,2,6-Tri-Me-pyridinium	116.0 ^c	...	+5.6 ^c
1-Et-pyridinium	101.8 ^c	...	+8.0 ^c
Piperidinium	83.1 ^c	...	+9.8 ^c
1-Me-piperidinium	101.9 ^c	...	+8.7 ^c
1,1-Dimethylpiperidinium	116.5

^a Conway and Verrall.² ^b Millero and Drost-Hansen.²⁴
^c Present results.

compressibility² (*cf.* ref 24 for the expansibility which deviates similarly for this ion).

It has been mentioned above that the $\phi^{\circ}_{K(S)}$ reflects more sensitively than do the volumes any specificities in ion-solvent interactions. Hence, it must be recognized that the procedure for evaluation of individual ionic contributions in $\phi^{\circ}_{K(S)}$ may not be so unambiguous as in the case of the analogous extrapolation of \bar{V}_2° data. For example, a progressive structural contribution

$V_{s(+)}$ in $\phi^{\circ}_{K(S)}$, varying with molecular weight of the cation, might still be present in the data of Figure 12. However, since the data for the pyridinium series as well as for the TAA series, which have rather different molecular structures, seem to fall with reasonable consistency on the same line, the procedure seems justified. Within the above limitations, we estimate that the uncertainty in the $\phi^{\circ}_{K(S)}$ value for the iodide ion in water at 25° is $\pm 1.0 \times 10^{-4}$ ml (g-mol bar)⁻¹ as indicated in Table V.

Using the values of $\phi^{\circ}_{K(S)}$ ion determined above, a scale of values for other ions may be derived. These data, together with the individual partial gram ionic volumes \bar{V}°_{ion} and expansibilities^{6,24} E°_{ion} , are summarized in Table V.

The quantity $-(\partial \bar{V}^{\circ}_{ion}/\partial P)$ is made up of three terms which involve the pressure derivatives of V_{in} , V_e , and V_s . $(\partial V_{in}/\partial P)$ will be negative or close to zero since it involves the compressibility of the ion itself and the dead space between the ion and the solvent molecules. For the larger TAA ions, $V_{e(+)}$ will be negligible; therefore, we are left with a relatively large positive value for $(\partial V_{s(+)} / \partial P)$. This is in accord with current thoughts about the hydration of hydrophobic groups, since the structural volume term, V_s , is thought to be made up of a positive contribution due to the local enhancement of structure in the solvent and a negative contribution due to the inclusion of the ion in cavities formed in the solvent. If, as has been proposed, V_s is negative,^{24,25} positive values of $(\partial V_{s(+)} / \partial P)$ and $(\partial V_{s(+)} / \partial T)$ ²⁴ would indicate that the enhancement of solvent structure ceases to be significant with increasing temperature and pressure from which it is to be concluded that the ions are less able to influence the formation of solvent cages.

Acknowledgments. Grateful acknowledgment is made to the National Research Council of Canada for support of the early part of this work and to the Department of Energy, Mines and Resources for its support in 1969-1970. L. H. L. acknowledges the award of a National Research Council Scholarship (1966-1969).

Diffusion of Several Transition Metal Ions in the Adsorbed Layer of Sodium Polyacrylate As Studied by Polarography

by Hiroyuki Kojima and Shizuo Fujiwara*

Department of Chemistry, Faculty of Science, The University of Tokyo, Hongo, Tokyo 113, Japan
(Received April 28, 1970)

The limiting currents for Mn(II), Co(II), Ni(II), Cu(II), and Zn(II) ions were measured, using sodium polyacrylate as a supporting electrolyte. These data are used to obtain diffusion coefficients for the metal ions. It is to be noted that the diffusion coefficients are quite small in comparison to those for metal ions with simple inorganic salts as supporting electrolytes. It is shown that sodium polyacrylate is adsorbed on the surface of the dropping mercury electrode. In view of these results, a simple model is proposed for the diffusion. A metal ion is coordinated with carboxylic groups on the sodium polyacrylate molecule and repeats jumping from one to another site, thus being transferred to the electrode. On the basis of the above model, the free energies of activation for the diffusion were estimated, using Eyring's theory. The values of the free energy are strongly dependent on the species of the metal ions. It should be noted that the free energy of complexation for these ions varies in a quite similar way. The effects on the free energy of activation for the diffusion of the addition of sodium perchlorate and of the change in the degree of neutralization of polyacrylic acid are consistent with the results obtained from the potentiometric titration. These results show that the model proposed above is reasonable for the system under investigation.

Introduction

The polarographic method is useful in elucidating transport processes for metal ions in solution. Miller and his coworkers¹⁻⁴ have recently investigated the effects of polyelectrolytes adsorbed on the surface of the mercury dropping electrode on the polarographic currents of inorganic depolarizers, using polyvinylpyridine, bovine serum albumin, or DNA. Lapanje and Oman⁵⁻⁸ have investigated the binding of cadmium or thallos ion with polystyrenesulfonic acid, polyacrylic acid, or pepsin.

In the present study, the limiting currents for Mn(II), Co(II), Ni(II), Cu(II), and Zn(II) ions are measured, using sodium polyacrylate (Na-PA) as a supporting electrolyte. From these data the diffusion coefficients for the metal ions are obtained, using Ilkovič's equation. A simple model is proposed for the diffusion, and the free energy of activation for the diffusion has been estimated for the metal ions on the basis of the above model. The present results will be useful in discussing transport processes in biological systems.

Experimental Section

Samples. Sodium polyacrylate (Na-PA) is purified by the following processes. Na-PA is precipitated with methanol from the aqueous solution and redissolved in 1 *N* sodium hydroxide. After repeating this procedure five times, the product is dried *in vacuo*. The sample thus obtained is dissolved in distilled water and passed through a column of the acid-type cation-exchange resin. Finally, the eluate is neutralized using a standard NaOH solution. The carboxylic content of Na-PA is determined by this titration. The degree of

polymerization of the sample which is used in the present experiment is about 2700-7500.

Apparatus and Procedure. The d.c. polarograms are obtained using a Yanagimoto polarograph Model P8-A, the scan rate being 5 min/V. Current-time curves during the single drop life at a fixed potential are obtained using an apparatus which has been constructed in this laboratory⁹ and spectrum computer Model JRA-5 of the Japan Electron Optics Co. The flow rates of mercury are 1.62 and 1.72 mg at mercury column heights of 60 and 70 cm, respectively. Dissolved oxygen is removed as usual by bubbling nitrogen gas through the solution. Sample solutions for the measurement of polarographic current are prepared by mixing the standard solution of Na-PA with that of metal ions. The concentration of metal ions was determined by titration with EDTA. Sample solutions contain 3.6×10^{-2} *N* Na-PA and about 1 mM of metal chlorides. Solutions of polyacrylic acid at various degrees of neutralization are prepared by adding sodium

* To whom correspondence should be addressed.

- (1) I. R. Miller, *J. Phys. Chem.*, **69**, 2740 (1965).
- (2) Y. F. Frei and I. R. Miller, *ibid.*, **69**, 3018 (1965).
- (3) M. A. Frommer and I. R. Miller, *ibid.*, **72**, 2862 (1968).
- (4) I. R. Miller and D. Bach, *Biopolymers*, **4**, 705 (1966).
- (5) S. Lapanje and S. Oman, *Makromol. Chem.*, **53**, 46 (1962).
- (6) S. Lapanje, S. Oman, and C. Miklavc, "Physicalische Chemie Biogener Makromoleküle," Vol. II, Akademie-Verlag, Berlin, 1964, p 55-60.
- (7) S. Lapanje, *Biopolymers*, **2**, 585 (1964).
- (8) S. Lapanje, *ibid.*, **4**, 85 (1966).
- (9) S. Fujiwara, Y. Umezawa, and T. Kugo, *Bull. Chem. Soc. Jap.*, **41**, 2223 (1968).

hydroxide to solutions of polyacrylic acid. All polarographic measurements are made at $22.5 \pm 0.5^\circ$.

Results and Discussion

Formation of the Adsorbed Layer. The limiting currents of metal ions are strongly reduced when Na-PA is used as a supporting electrolyte. As a typical example, the polarogram of the CoCl_2 -Na-PA system is shown in Figure 1, where the reduction wave for the Co(II) ion is obtained at about -1.6 V. It should be noted that the current intensity for this system is very much smaller than that for usual systems where supporting electrolytes are simple inorganic ions. In Table I, the current intensities for the systems which

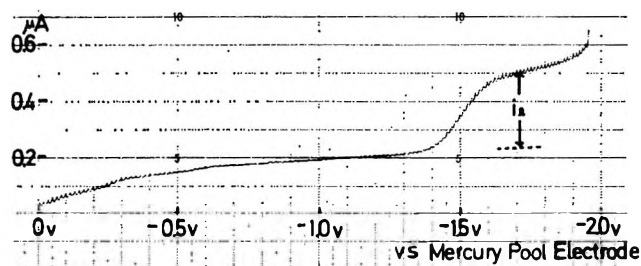


Figure 1. Polarogram of Co(II) ion with Na-PA as a supporting electrolyte. i_L denotes the intensity of limiting current: 1 mM CoCl_2 and 0.036 N Na-PA.

Table I: The Intensities of the Limiting Current for Several Systems with Supporting Electrolytes of 0.5 N NaClO_4 and 0.036 N Na-PA

	Intensity, μA , of NaClO_4 , 0.5 N (A)	Intensity, μA , of Na-PA, 0.036 N (B)	Ratio B/A
MnCl_2 , 1 mM	6.1	0.23	3.8×10^{-2}
CoCl_2 , 1 mM	5.4	0.25	4.6×10^{-2}
NiCl_2 , 1 mM	6.2	0.20	3.2×10^{-2}
CuCl_2 , 1 mM	5.1	0.02	0.4×10^{-2}
ZnCl_2 , 1 mM	5.7	0.15	2.6×10^{-2}

contain $3.6 \times 10^{-2} \text{ N}$ Na-PA are compared to those for the systems which contain 0.5 N NaClO_4 . As seen in Table I, the intensities observed in the former systems are one-tenth to one-hundredth of those for the latter systems.

These results suggest that Na-PA is adsorbed on the surface of the mercury electrode, inhibiting depolarizers to reach the electrode surface. In fact, each drop of the dropping mercury electrode keeps its spherical form on the mercury pool of the counter electrode without merging in it. Measurements of the current-time curve have been shown to be useful in investigating adsorption phenomena on the surface of the dropping mercury electrode. According to Kuta and Smoller,¹⁰ the current-time curve has a sharp peak at the initial

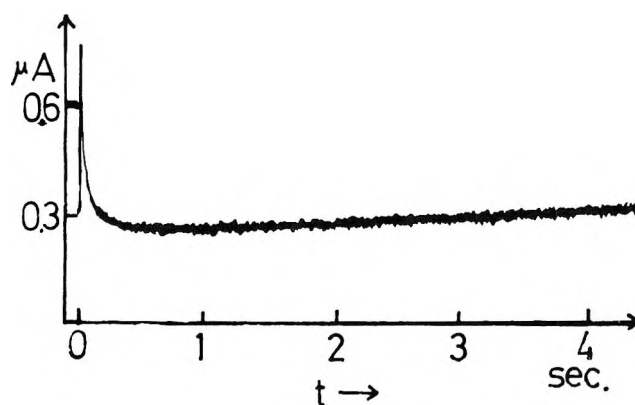


Figure 2. Current-time curve at -1.5 V in the system of ZnCl_2 -Na-PA: 1 mM ZnCl_2 and 0.036 N Na-PA.

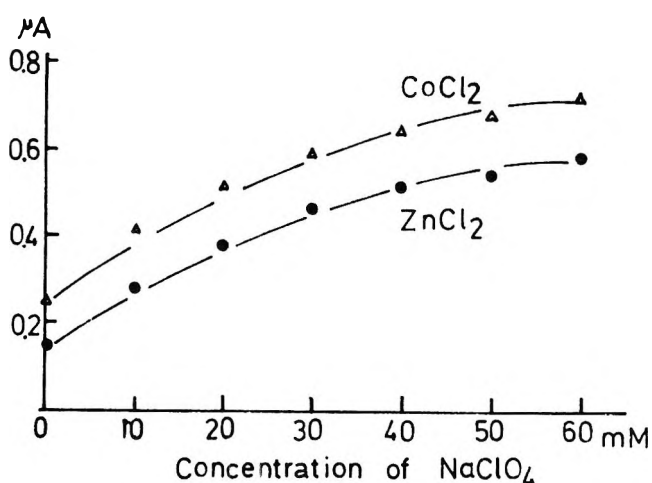


Figure 3. Effect of neutral salts on the limiting current for Zn(II) or Co(II) ion: 1 mM ZnCl_2 or CoCl_2 , 0.036 N Na-PA, and 10 – 60 mM NaClO_4 .

period when the surface coverage is incomplete. The current-time curve for the ZnCl_2 -Na-PA system is given in Figure 2, where a very short but relatively high impulse can clearly be seen at the initial period. The intensity of this impulse increases almost proportionally to the square root of the mercury column height. Hence, it can be concluded that the surface of the dropping mercury electrode is covered with the adsorbed layer of Na-PA after the impulse is depressed.

Characterization of the Limiting Current. Although the systems under investigation show a high resistance of about $70 \text{ k}\Omega$, a contribution from the migration current could not be detected. As shown in Figure 3, the limiting currents for the Zn(II) and Co(II) ions are increased by the addition of sodium perchlorate. This result eliminates the possibility of a contribution from the migration current; if the limiting current involves this contribution, the current intensity must decrease by the addition of the neutral salt. It is well established that the migration current increases with an in-

(10) J. Kuta and I. Smoller, *Progr. Polarography*, **1**, 41 (1962).

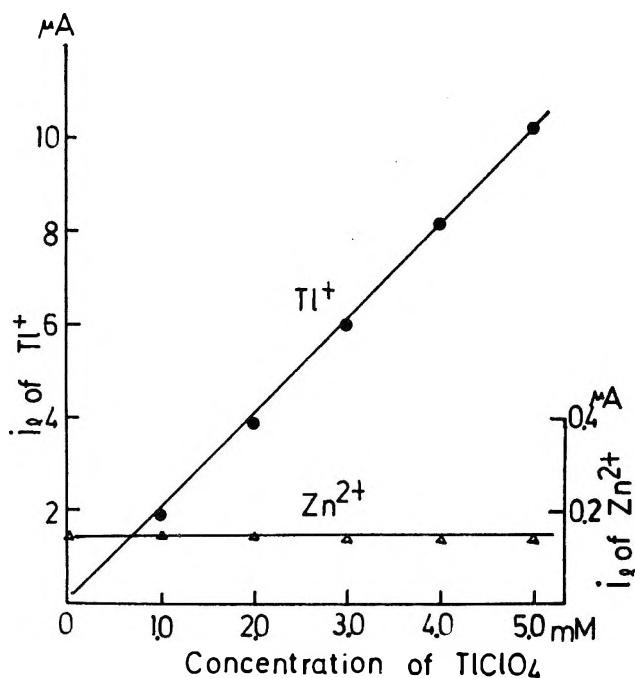


Figure 4. Effect of the iR drop of the solution on the limiting current for Zn(II) ion: 1 mM ZnCl₂, 0.036 N Na-PA, and 0–5 mM TiClO₄.

crease in the iR drop of solutions (exaltation effect).¹¹ As shown in Figure 4, the limiting current for the Zn(II) ion does not change on addition of the Tl(I) ion to the solution. These results confirm that the migration current does not make an important contribution to the limiting current.

The intensity of the diffusion current may be given by Ilkovič's equation

$$I_d = 4 \sqrt{\frac{7\pi}{3}} \left(\frac{3}{4\pi d} \right)^{2/3} nFD^{1/2} C m^{2/3} t^{1/6} \quad (1)$$

where d is the density of mercury, m the rate of the mercury flow, D the diffusion coefficient, and t the drop time. If eq 1 holds for the systems under investigation, the current intensity should be proportional to the square root of the mercury column height, h . Figure 5 shows the dependence of the current intensity on the mercury column height. This result is consistent with eq 1.

The $\log i$ vs. $\log t$ plot of the current–time curve for the ZnCl₂–Na-PA system is given in Figure 6. This plot satisfies Ilkovič's relation; *i.e.*, $\log i$ is proportional to $\log t$ with a slope of $1/6$. If the kinetic current contributes to the limiting current under investigation, the slope of this plot should deviate from $1/6$ and approach to $2/3$.¹⁰ The slopes observed for the other ions are also found to be $1/6$. The above results clearly indicate that the limiting current for the Na-PA system is diffusion controlled, obeying eq 1.

Diffusion Coefficients. Using eq 1, the diffusion coefficients of metal ions in the solutions of Na-PA were

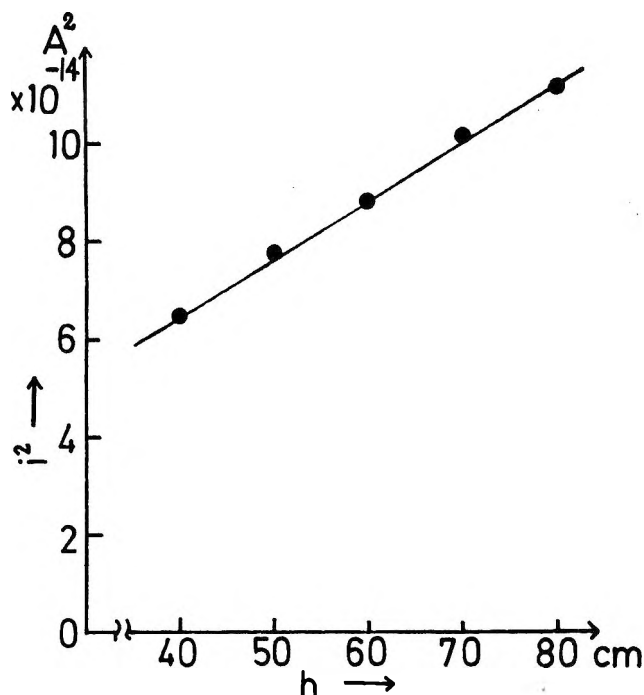


Figure 5. Dependence of the intensity of the limiting current on the mercury column height: 1 mM CoCl₂ and 0.036 N Na-PA. Mercury column height, h , 40–80 cm.

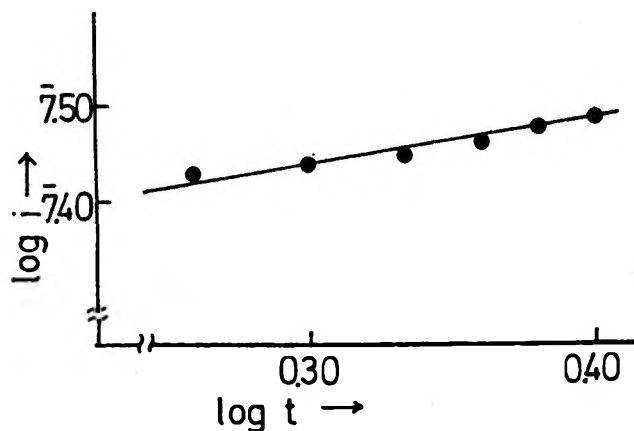


Figure 6. $\log i$ vs. $\log t$ plot for the ZnCl₂–Na-PA system at -1.5 V: 1 mM ZnCl₂ and 0.036 N Na-PA.

obtained. Table II summarizes the values of D , the diffusion coefficient, for Mn(II), Co(II), Ni(II), Cu(II), and Zn(II) ions in the Na-PA systems. All these systems contain 3.6×10^{-2} N Na-PA and about 1 mM metal chlorides. The values of D at mercury column heights of 60 and 70 cm agree with each other within experimental error. Since the limiting current is small in the case of Cu(II) ion, the error of the D value is larger than those in the other systems. In Table I, it is to be noted that the values of D are strongly dependent on the species of ions. Small D values are obtained

(11) See, for example, J. Heyrovsky, "Principle of Polarography," Academic Press, New York, N.Y., 1960.

Table II: Diffusion Coefficients for the Systems with Na-PA As a Supporting Electrolyte

Ion species	h , cm	t , sec	$-E$, V ^a	I_d , A	C , mol/cc	D , cm ² /sec
MnCl ₂	60	3.6	1.8	0.235×10^{-6}	1.00×10^{-6}	$(9.5 \pm 0.3) \times 10^{-9}$
	70	3.1	1.8	0.240×10^{-6}	1.00×10^{-6}	$(9.5 \pm 0.3) \times 10^{-9}$
CoCl ₂	60	3.9	1.7	0.250×10^{-6}	1.01×10^{-6}	$(1.0 \pm 0.2) \times 10^{-8}$
	70	3.4	1.7	0.270×10^{-6}	1.01×10^{-6}	$(1.1 \pm 0.2) \times 10^{-8}$
NiCl ₂	60	4.2	1.5	0.195×10^{-6}	1.09×10^{-6}	$(5.2 \pm 0.2) \times 10^{-9}$
	70	3.6	1.5	0.200×10^{-6}	1.09×10^{-6}	$(5.3 \pm 0.3) \times 10^{-9}$
CuCl ₂	60	5.2	0.5	0.020×10^{-6}	1.00×10^{-6}	$(6 \pm 3) \times 10^{-11}$
	70	4.4	0.5	0.020×10^{-6}	1.00×10^{-6}	$(6 \pm 3) \times 10^{-11}$
ZnCl ₂	60	4.4	1.5	0.155×10^{-6}	0.956×10^{-6}	$(2.4 \pm 0.3) \times 10^{-9}$
	70	3.9	1.5	0.160×10^{-6}	0.956×10^{-6}	$(2.4 \pm 0.3) \times 10^{-9}$

^a E is a potential at which the drop time and current intensity are measured.

for Cu(II) and Zn(II) ions which have been shown to form strong coordination bonds with carboxylic groups.¹² This point will be discussed in more detail later.

Mechanism of the Diffusion of Metal Ions. The results of Table II are specific for the systems with the supporting electrolyte of Na-PA. It has been shown that these metal ions form complexes with Na-PA.¹³⁻¹⁶ If the metal ion-Na-PA complexes are transported as a whole, diffusion coefficients should be almost independent of the ion species. In contrast to this, free ions would contribute only to a small extent to the limiting current, because the complexation constants are quite large in these systems.¹⁷

In view of the above results, a following model is proposed for the transport process of ions. Metal ions form complexes with carboxylic groups in Na-PA which is adsorbed on the surface of the dropping mercury electrode, and the metal ions jump from one site to another. Then, the diffusion coefficients may be related to the rate of crossing the potential barrier intervening the two sites. According to Eyring's theory,¹⁸ the diffusion coefficient may be given as

$$D = \lambda^2 \frac{kT}{h} \exp\left(-\frac{\Delta G^\ddagger}{RT}\right) \quad (2)$$

where h , k , T , and R mean the Planck constant, the Boltzmann constant, the absolute temperature, and the gas constant, respectively. ΔG^\ddagger is the free energy of activation for diffusion, and λ is the distance between the successive equilibrium positions.

When the value of λ is taken to be 3 Å, which is the distance between the neighboring carboxylic groups in Na-PA, ΔG^\ddagger can be calculated from the observed D values. In Figure 7, ΔG^\ddagger thus obtained is compared with the free energies of complexation of the metal ions with malonic acid and succinic acid.^{12,19} These dibasic acids were chosen as model chelating reagents for Na-PA. As Figure 7 shows, the dependence on ionic species of ΔG^\ddagger is quite similar to that of the free energy of complexation, $-\Delta G_f$. It should be noted that ΔG^\ddagger is the difference in free energy between the complex-

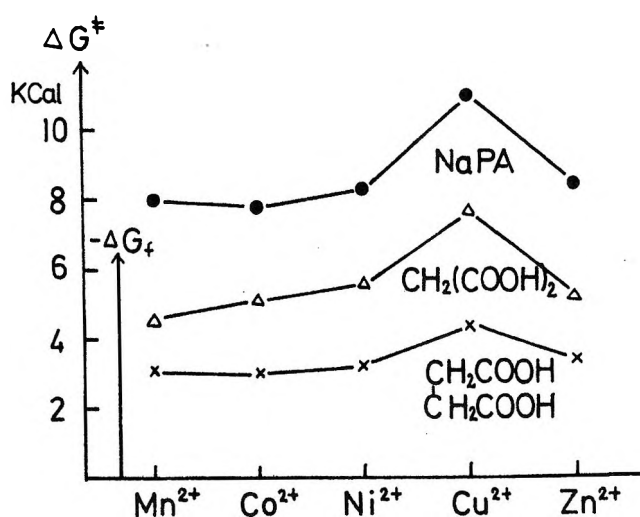


Figure 7. Free energies of activation for diffusion compared to the free energies of complexation: ΔG^\ddagger , free energy of activation for diffusion in the system with the supporting electrolyte of 0.036 *N* Na-PA; $-\Delta G_f$, free energy of complexation with succinic acid or malonic acid.

forming state and the transition state. These results are consistent with the mechanism proposed above. A schematic representation of the above model is drawn in Figure 8.

(12) G. H. Nancollas, "Interactions in Electrolyte Solutions," Elsevier, Amsterdam, 1966, p 185.

(13) F. T. Wall and S. J. Gill, *J. Phys. Chem.*, **58**, 1128 (1954).

(14) H. P. Gregor, L. B. Luttinger, and E. M. Loebel, *ibid.*, **59**, 34 (1955).

(15) A. M. Kotliar and H. Morawetz, *J. Amer. Chem. Soc.*, **77**, 3692 (1955).

(16) J. V. McLaren, J. D. Watts, and A. Gilbert, *J. Polym. Sci., Part C*, **16**, 1903 (1967).

(17) This has been shown to be due to a large contribution from electrostatic free energy. According to Gregor and his coworkers,¹⁴ the complexation constant is in the range 10^9 - 10^{11} for a polyacrylic acid-copper complex, the complexation constant being defined as $K = [\text{Cu}(\text{COO})_2]/[\text{Cu}^{2+}][-\text{COO}^-]^2$.

(18) S. Glasstone, K. J. Laidler, and H. Eyring, "The Theory of Rate Processes," McGraw-Hill, New York, N. Y., 1941.

(19) V. S. K. Nair and G. H. Nancollas, *J. Chem. Soc.*, 4367 (1961); A. McAuley and G. H. Nancollas, *ibid.*, 989 (1963); A. McAuley and G. H. Nancollas, *ibid.*, 4458 (1961).

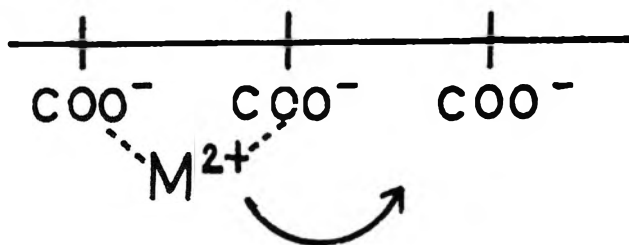


Figure 8. Schematic representation for the diffusion of divalent ions in the adsorbed layer of Na-PA.

Dependence of ΔG^\ddagger on the Concentration of an Added Salt and the Degree of Neutralization of Polyacrylic Acid. The values of ΔG^\ddagger are much larger than the free energy of complexation of malonic acid or succinic acid. It has been shown in divalent metal ion-polyacrylic acid systems, that *electrostatic free energy* greatly enhances the free energy of complexation.^{14,20} This suggests that ΔG^\ddagger for the diffusion discussed in the previous section contains a contribution from the electrostatic free energy. As Figure 3 shows, a large increase is observed in the limiting currents for the metal ions when NaClO_4 is added. This result suggests that the barrier for diffusion of the metal ions is lowered by the addition of the neutral salt, which partially shields the electrostatic field produced by the carboxylic groups in the polyions.

Furthermore, when the degree of neutralization of polyacrylic acid is decreased, the intensity of the limiting current for the ions is increased. This is because ΔG^\ddagger is reduced with a decrease in the number of ionized groups in the polymer molecule.

The influences of ionic strength and of the degree of neutralization on the electrostatic free energy have been studied by many workers by means of potentiometric titration.²¹ In general, the pH of a polyacid solution is expressed in terms of a change in electrostatic free energy corresponding to the ionization process as

$$\text{pH} = \text{p}K_0 - \log \left[\frac{1 - \alpha}{\alpha} \right] + 0.434 \Delta G_{e1} / RT \quad (3)$$

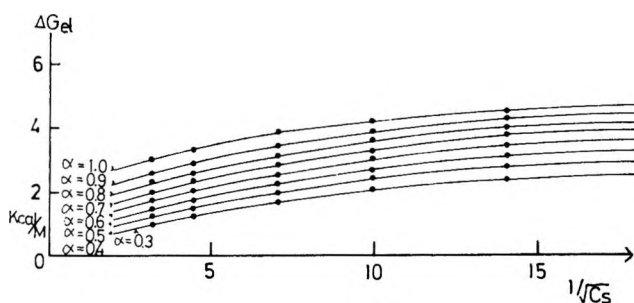


Figure 9. Relationship between ΔG_{e1} and the ionic strength of the solvent at various degrees of neutralization of polyacrylic acid. Each value of ΔG_{e1} is obtained from data of Nagasawa and his coworkers²² using eq 3, where the value of $\text{p}K_0$ is assumed to be 4.32. The values of ΔG_{e1} are those extrapolated to infinite dilution of the polymer. C_s denotes the concentration of sodium chloride.

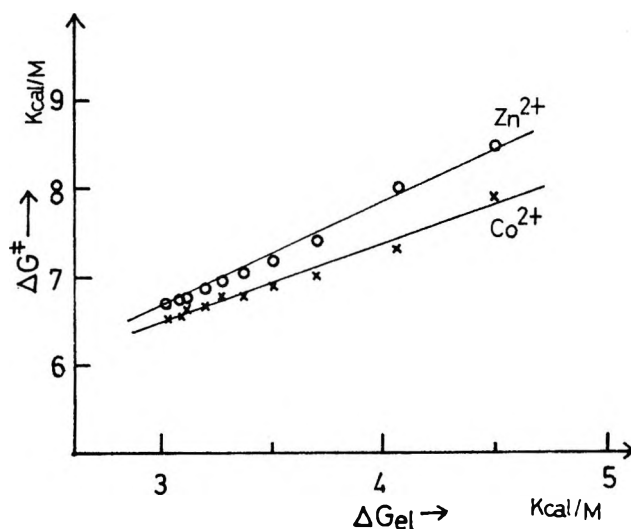


Figure 10. Relationship between ΔG^\ddagger for Zn(II) and Co(II) ions and ΔG_{e1} at various concentrations of neutral salt. Sodium perchlorate (10–90 mM) is added as a neutral salt to the system where 1 mM ZnCl_2 or CoCl_2 is used as the depolarizer and 0.036 N Na-PA is used as the supporting electrolyte.

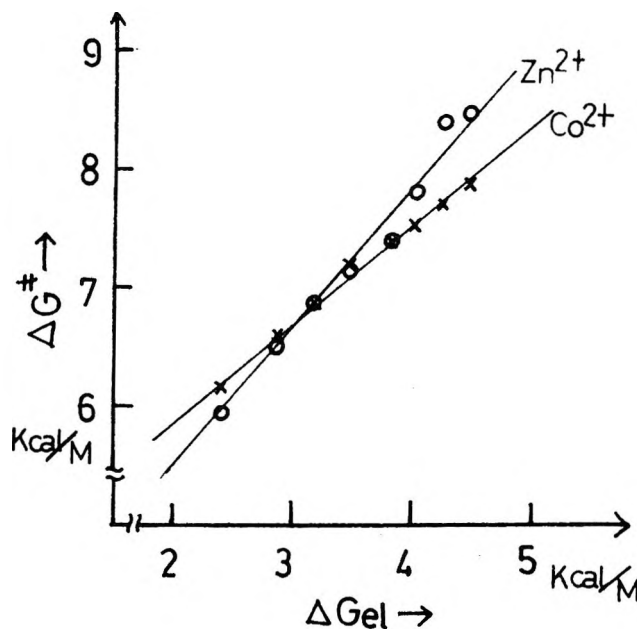


Figure 11. Relationship between ΔG^\ddagger for Zn(II) and Co(II) ions and ΔG_{e1} at various degrees of neutralization ($\alpha = 0.4\text{--}0.9$); 1 mM of ZnCl_2 or CoCl_2 is used as the depolarizer.

where $\text{p}K_0$ is the negative logarithm of the intrinsic dissociation constant, α is the degree of neutralization, and ΔG_{e1} is the change in electrostatic free energy of the system. If the value of $\text{p}K_0$ is estimated by extrapolating α to zero, ΔG_{e1} can be evaluated from the potenti-

(20) H. Morawetz, "High Polymers," Vol. XXI, Wiley, New York, N. Y., 1965.

(21) See, for example, S. A. Rice and M. Nagasawa, "Polyelectrolyte Solutions," Academic Press, New York, N. Y., 1961.

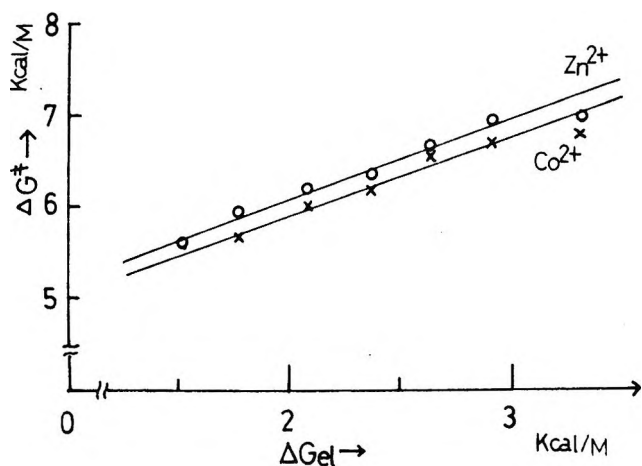


Figure 12. Relationship between ΔG^\ddagger for Zn(II) and Co(II) ions and ΔG_{e1} at various degrees of neutralization ($\alpha = 0.4-0.9$). Sodium perchlorate (40 mM) is added to the systems at various degrees of neutralization.

ometric titration. Nagasawa and his coworkers²² reported the titration curves for polyacrylic acid at various ionic strengths. From these data, the relationship between ΔG_{e1} and the ionic strength of the solvent at

various degrees of neutralization of polyacrylic acid can be obtained as shown in Figure 9. Using the results of Figure 9, the values of ΔG_{e1} corresponding to the present experiment are obtained. Figure 10 shows a ΔG^\ddagger vs. ΔG_{e1} plot, where ΔG^\ddagger is obtained for Zn(II) and Co(II) ions, using the Na-PA systems containing 10–90 M NaClO₄. Figure 11 shows a ΔG^\ddagger vs. ΔG_{e1} plot when the degree of neutralization of polyacrylic acid is varied ($\alpha = 0.9-0.4$). In Figure 12, the result is shown when 40 mM of sodium perchlorate is added to the systems at various degree of neutralization. In Figures 10–12, it is clearly exhibited that ΔG^\ddagger is proportional to ΔG_{e1} with a slope of about unity. These results indicate that a decrease in ΔG^\ddagger comes from that in ΔG_{e1} . In other words, the present results are consistent with the results obtained from the potentiometric titration.

In conclusion, it appears that the present model for the diffusion is reasonable for the system under investigation.

Acknowledgments. We are greatly indebted to Dr. Y. Arata for valuable discussions.

(22) M. Nagasawa, T. Murase, and K. Kondo, *J. Phys. Chem.*, **69**, 4003 (1965).

Electronic Spectra of the Oxyanions of Selenium in Solution

by A. Treinin and J. Wilf

Department of Physical Chemistry, The Hebrew University, Jerusalem, Israel (Received May 19, 1970)

The electronic spectra of SeO_3^{2-} , HSeO_3^- , SeO_4^{2-} , and HSeO_4^- were analyzed by studying their response to environmental effects. The first absorption band in each spectrum is assigned to an allowed sub-Rydberg transition involving the nonbonding electrons on the oxygen atoms. In the spectra of SeO_3^{2-} , HSeO_3^- , and SeO_4^{2-} this band is followed by a charge-transfer-to-solvent (ctts) band. The ctts bands of the dinegative ions appear to be twice as sensitive as that of HSeO_3^- towards solvent effects, whereas their temperature sensitivities are nearly the same. pH and temperature effects yield some thermodynamic data on the equilibria $\text{HSeO}_n^- \rightleftharpoons \text{H}^+ + \text{SeO}_n^{2-}$. The vertical ionization potential and the effective crystallographic radius of HSeO_3^- are derived from the analysis of solvent effects on its ctts band. Under the conditions employed the uv spectra do not reveal the formation of new species, such as dimers or esters.

The aim of this research is to examine the effect of electrical charge on electronic spectra of closely related anions. Solutions of mono- and dinegative oxyanions of selenium, readily converted into each other by pH adjustment, display considerable absorptions in readily accessible spectral regions. The solutions are rather stable and pure tetraalkylammonium salts can be prepared that dissolve in alcohols and acetonitrile. Thus environmental effects on the spectra could be studied in detail. Some studies of this type were

already conducted with oxyanions of phosphorus,¹ but their scope was somewhat limited owing to relatively low absorptions and insolubility of the salts employed in pure organic solvents.

Previous information on the spectra of oxyselenides² is meagre and in some discord with our results. Here

(1) M. Halmann and I. Platzner, *J. Chem. Soc.*, 1440 (1965); H. Benderly and M. Halmann, *J. Phys. Chem.*, **71**, 1053 (1967).

(2) H. Ley and E. K6rig, *Z. Phys. Chem. Abt. B*, **41**, 365 (1938).

we present an analysis of electronic transitions in SeO_3^{2-} , HSeO_3^- , SeO_4^{2-} , and HSeO_4^- . The first three display charge transfer-to-solvent (ctts) transitions; this gives us an opportunity to examine environmental effects on ctts bands of polyvalent anions and compare them with theory.³ Some thermodynamic data are derived from spectroscopic results.

Experimental Section

Materials. The Na_2SeO_3 (B.D.H.) was recrystallized from concentrated aqueous solution by adding acetonitrile. A second recrystallization proved to have no effect on the spectrum. NaHSeO_3 (B.D.H.) was recrystallized from CH_3CN ; both materials exhibited the same spectrum at the same pH.

$\text{N}(\text{C}_2\text{H}_5)_4\text{HSeO}_3$ and $(\text{N}(\text{C}_2\text{H}_5)_4)_2\text{SeO}_3$ were prepared by neutralization of H_2SeO_3 (Riedel-De Haen) with a solution of $\text{N}(\text{C}_2\text{H}_5)_4\text{OH}$ (Fluka, Purum; some yellow impurities were removed from this solution by several extractions with CH_3CN); pH 6 and 10.5 were chosen as end points for their preparation, respectively. Water was expelled under reduced pressure and the dry materials recrystallized from CH_3CN . The biselenite was then dried under vacuum at 40° . The selenite was redissolved in a solution of $\text{N}(\text{C}_2\text{H}_5)_4\text{OH}$, water evaporated, and the material was thoroughly dried. In this way an excess of $\text{N}(\text{C}_2\text{H}_5)_4\text{OH}$ was added to the selenite; the pH of $10^{-3} M$ in water was 10.5. This was done so as to avoid conversion of SeO_3^{2-} to HSeO_3^- in the organic solvents employed.

Na_2SeO_4 (Analar) was used without further purification. $(\text{N}(\text{C}_2\text{H}_5)_4)_2\text{SeO}_4$ was prepared by neutralization of H_2SeO_4 (Riedel De Haen) with $\text{N}(\text{C}_2\text{H}_5)_4\text{OH}$ (pH 6 as end point), the material crystallized from concentrated solution by adding CH_3CN , rinsed with CH_3CN , and dried under vacuum at 40° .

The purity of tetraethylammonium salts was checked by measuring their spectra in aqueous solutions; the spectra were identical with that of the sodium salts (see, e.g., Figure 5, which also indicates that $\text{N}(\text{C}_2\text{H}_5)_4\text{OH}$ present in excess did not contribute to the absorption). The tetraethylammonium salts were used to introduce the oxyselenide ions into organic solvents. The following experiment was performed to check the identity of ionic species in CH_3CN : further addition of $\text{N}(\text{C}_2\text{H}_5)_4\text{OH}$ to selenite had no effect on its spectrum while a little concentrated HClO_4 changed the spectrum to that of biselenite in the same solvent. Concentrated HClO_4 was also used to convert SeO_4^{2-} to HSeO_4^- while adding only little H_2O to the organic solvent. (The pH of acidic solutions was below 1, as measured with indicator paper.)

The organic solvents were of spectroscopic grade. Special care was taken to dry CH_3CN because traces of water exerted a considerable effect on the spectra of SeO_3^{2-} and SeO_4^{2-} . For this purpose CH_3CN (Matheson Coleman and Bell) was shaken with anhydrous

CaSO_4 for 70 hr. (Similar results were obtained with CuSO_4 .) Water was triply distilled, D_2O (99.7%, Fluka, Puriss) was used without further purification, and all other materials were of Analar grade.

Measurements. Spectra were measured with a 450 Perkin-Elmer spectrophotometer equipped with a thermostated cell compartment to keep temperature constant within $\pm 0.1^\circ$. Absorption cells with 10 mm, 1 mm, and variable path length (down to 0.1 mm) were employed. Absorbance up to 1.8 could be read without distinct deviations from Lambert's law. The instrument was flushed with N_2 for measurements below 190 nm.

pH was measured with a Metrohm pH meter ($\Delta\text{pH} \pm 0.01$). Perchloric acid, phosphate, and borate buffers were employed to vary the pH in the range 0–11.5.

Results

All the oxyselenide ions were found to obey Beer's law over all the wavelength region studied. Range of concentrations studied was 10^{-2} – $10^{-4} M$ in water and in organic solvents. With HSeO_3^- in water the law was checked from $10^{-5} M$ to $1 M$ and no deviation was detected; this is in contrast to the behavior of HSO_3^- , which dimerizes to $\text{S}_2\text{O}_5^{2-}$ under such conditions.⁴ Another difference lies in the stability of HSeO_3^- towards oxidation by O_2 : no change in spectra was displayed by air containing solutions after 48 hr, while HSO_3^- was considerably oxidized under the same treatment.

From the pH effect on the spectra of aqueous systems the thermodynamics of



could be studied.

A sharp isosbestic point is exhibited by the selenite system (Figure 1). The selenate system appears to

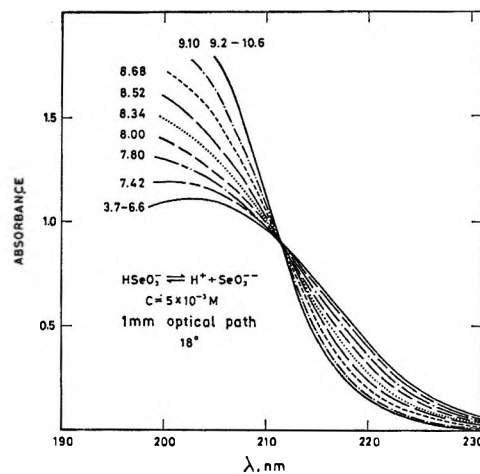


Figure 1. Isosbestic point displayed by the HSeO_3^- – SeO_3^{2-} system.

(3) A. Treinin, *J. Phys. Chem.*, **68**, 898 (1964).

(4) R. M. Golding, *J. Chem. Soc.*, 3711 (1960).

Table I: Thermodynamic Data for the Equilibrium $\text{HSeO}_n^- \rightleftharpoons \text{H}^+ + \text{SeO}_n^{2-}$

	T, °C	$\text{HSeO}_3^- \rightleftharpoons \text{H}^+ + \text{SeO}_3^{2-}$		$\text{HSeO}_4^- \rightleftharpoons \text{H}^+ + \text{SeO}_4^{2-}$	
		Present work	Previous data	Present work	Previous data
pK	10	8.50 ± 0.02		1.80 ± 0.02	1.82 ^b
	20	8.43 ± 0.02	8.0 ^b	1.84 ± 0.04	1.86 ^b
	25	8.39 ± 0.03 ^a	8.32 ^b 6.60 ^c		1.88 ^b
	30	8.37 ± 0.03			1.70 ± 0.01 ^d
	50	8.23 ± 0.03			
ΔG° (kcal/mol)	25	11.4 ± 0.4		2.5	
ΔH° (kcal/mol)	25	2.8 ± 0.2	1.1 ^c		-2.2 ^c
ΔS° (eu)	25	-29 ± 2	-26.5 ^c		-16.3 ^c

^a From the plot of pK against 1/T. ^b "Stability Constants," Special Publication No. 17, The Chemical Society, London; see this reference for more data. ^c W. M. Latimer, "Oxidation Potentials," 2nd ed, Prentice-Hall, Englewood Cliffs, N. J., 1952, p 83. ^d A. K. Covington and J. V. Dobson, *J. Inorg. Nucl. Chem.*, **27**, 1435 (1965).

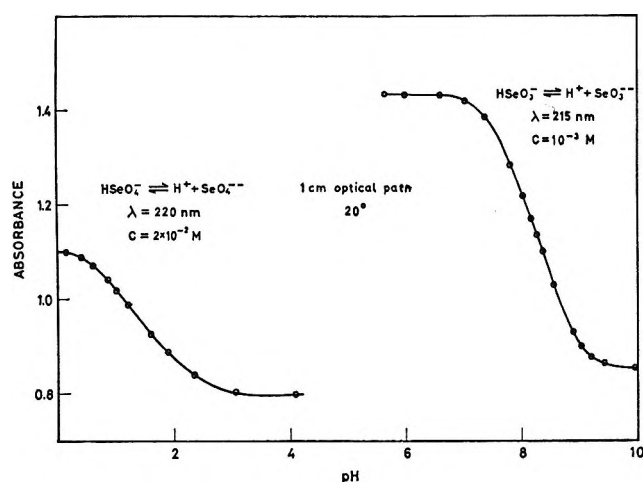


Figure 2. Typical "titration curves" displayed by the HSeO_3^- - SeO_3^{2-} and HSeO_4^- - SeO_4^{2-} systems.

reach such a point below 185 nm (see Figure 3). Figure 2 shows a typical "titration curve" for each system. The pK of equilibrium 1 was determined by means of the approximation

$$\text{p}K_1 = \text{pH} - \log \frac{D_{\text{HSeO}_n^-} - D}{D - D_{\text{SeO}_n^{2-}}} + \frac{3A\sqrt{I}}{1 + \sqrt{I}} \quad (2)$$

where $D_{\text{HSeO}_n^-}$, $D_{\text{SeO}_n^{2-}}$ and D are the absorbance values of the system when present in its acidic form, alkaline form, and at the given pH, respectively; the last term is the simplified correction for $\log \gamma_{\text{HSeO}_n^-} / \gamma_{\text{SeO}_n^{2-}}$ (γ = activity coefficient). The ionic strength I was calculated by successive approximations from the amounts of electrolytes introduced and equilibrium constants. The second term on the right (eq 2) was determined from plots of $D_{\text{HSeO}_n^-} - D$ against $D - D_{\text{SeO}_n^{2-}}$ at the same pH and different wavelengths.⁵ Calculations were carried out for three pH values within $\text{p}K \pm 1.0$. From the dependence of pK on temperature ΔH_1° and ΔS_1° were determined for HSeO_3^- (Table I). The values of A at various temperatures were taken

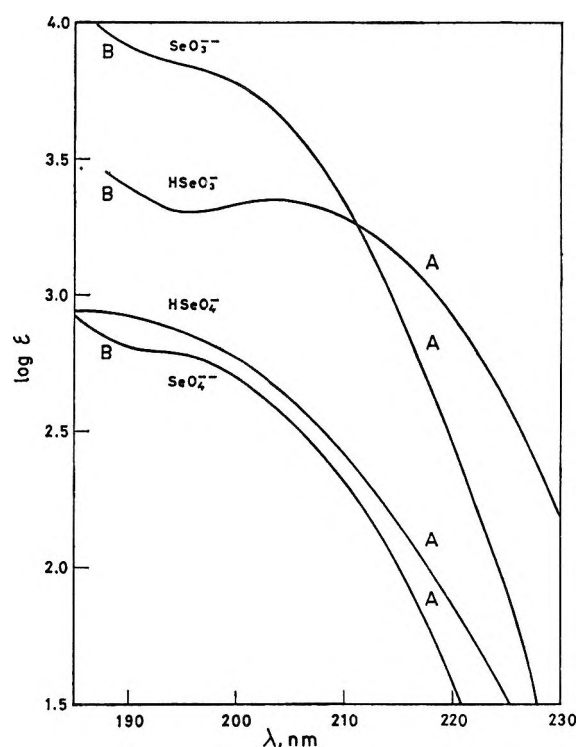


Figure 3. Absorption spectra of the oxyselenide ions at 20°C.

from ref 6. The results with HSeO_4^- were less reliable (low pH and high ionic strengths, up to 0.3 M); pK appeared to increase with temperature but ΔH and ΔS could not be determined. The results are summarized in Table I; agreement with previous data is satisfactory.

Environmental Effects. Figure 3 records the spectra of oxyselenides in water. HSeO_3^- , SeO_3^{2-} , and SeO_4^{2-} each displays two overlapping quite intense bands (designated A and B), which are best resolved in the spectrum of HSeO_3^- . The two bands respond differently to

(5) See e.g., J. Jortner and G. Stein, *Bull. Res. Council. Isr., Sect. A*, **6**, 239 (1957).

(6) R. A. Robinson and R. H. Stokes, "Electrolyte Solutions," 2nd ed, Butterworths, London, 1959, p 468.

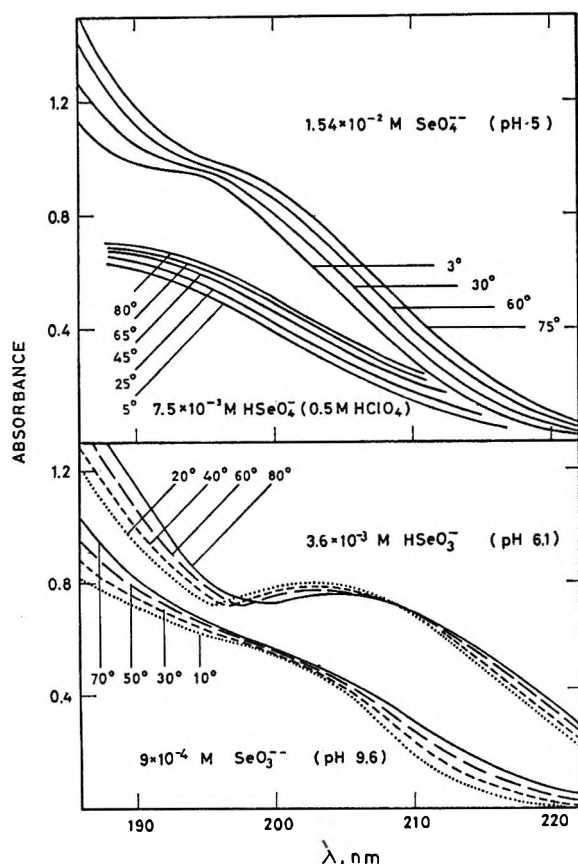


Figure 4. Temperature effects on spectra of the oxyseleide ions.

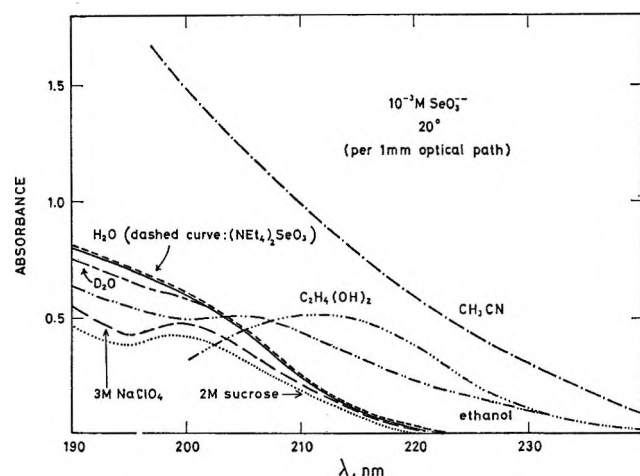


Figure 5. Solvent effects on the spectrum of SeO_3^{2-} .

changes in environment, the single band of HSeO_4^- exhibiting the band-A-type of behavior.

Figure 4 shows effects of temperature on the spectra and Table II records $-d(h\nu)/dT$ at various absorptivities. Band B is somewhat more sensitive with $-d(h\nu)/dT \sim 20 \text{ cm}^{-1} \text{ deg}^{-1}$ regardless of ionic charge. The difference in $d(h\nu)/dT$ brings about a shift in the isosbestic point for SeO_3^{2-} - HSeO_3^- to longer wavelengths with rise in temperature.

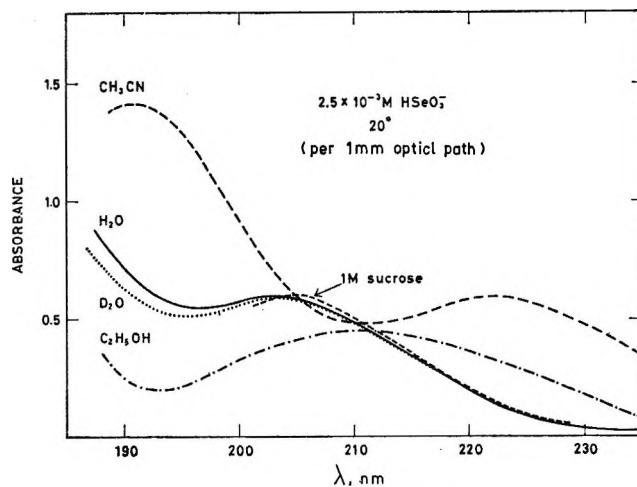


Figure 6. Solvent effects on the spectrum of HSeO_3^- .

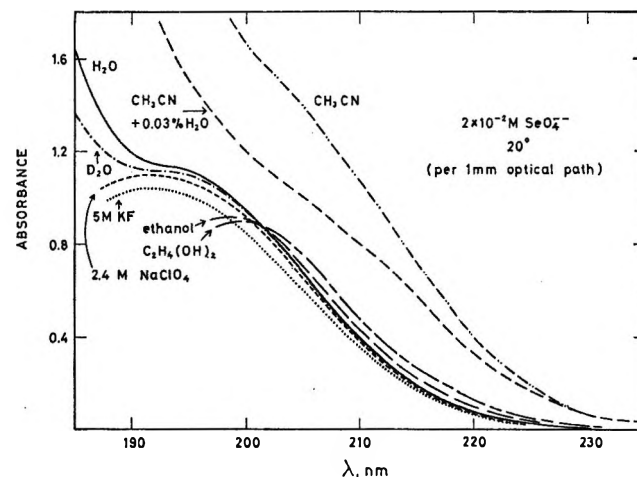


Figure 7. Solvent effects on the spectrum of SeO_4^{2-} .

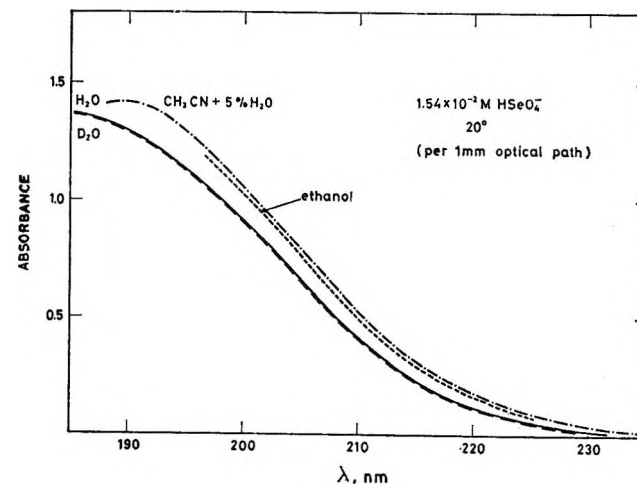


Figure 8. Solvent effects on the spectrum of HSeO_4^- .

A more pronounced distinction between A and B is shown by solvent effects (Figures 5-8). Band A undergoes the regular "blue shift" with $h\nu$ increasing in the order $\text{CH}_3\text{CN} < \text{glycol} < \text{ethanol} < \text{H}_2\text{O} \sim \text{D}_2\text{O}$. On the other hand, the order for B is: $\text{CH}_3\text{CN} < \text{H}_2\text{O} <$

Table II: Spectral Data and Environmental Effects^a

Ion	ϵ , $M^{-1} \text{ cm}^{-1}$	$-d(h\nu)/dT$, $\text{cm}^{-1} \text{ deg}^{-1}$	β	λ_{max} , ϵ_{max} , and oscillator strength f^c
SeO_3^{2-}	3000 (A)	11		A in ethanol: 206 nm, 5100 $M^{-1} \text{ cm}^{-1}$, $f = 0.12$
	5000 (A)	6		
	6000 (B)		1.5	
	6500 (B)		1.5 ^b	
	8000 (B)		2.0 ^b	
HSeO_3^-	9000 (B)	19	1.9 ^b	A in ethanol: 211 nm, 1800 $M^{-1} \text{ cm}^{-1}$, $f = 5.5 \times 10^{-2}$ B in CH_3CN : 191 nm, 5600 $M^{-1} \text{ cm}^{-1}$, $f = 0.17$
	1000 (A)	8		
	2800 (B)		1.0	
	3300 (B)	19		
	4000 (B)		1.2 ^b	
SeO_4^{2-}	6000 (B)		0.9 ^b	A in ethanol: 199 nm, 450 $M^{-1} \text{ cm}^{-1}$, $f = 9.8 \times 10^{-3}$
	100 (A)	13		
	300 (A)	11		
	650 (B)		1.45, 2.0 ^b	
HSeO_4^-	700 (B)	20	2.0 ^b	
	300 (A)	15		
	500 (A)	17		

^a A and B signify the first and second absorption bands, respectively. ^b The ratio of solvent shifts $\Delta\nu_x/\Delta\nu_I^-$ for the oxyseleide ion X and I^- , on replacing H_2O by D_2O . ^c See reference 8.

$\text{D}_2\text{O} < \text{ethanol} < \text{glycol}$, *i.e.*, the characteristic sequence for cttts transitions.⁷ The opposing effects of alcohols on A and B bring about the separation of A as a distinct band and so some of its properties could be determined (Table II).⁸ In CH_3CN both bands are considerably red shifted and in the case of HSeO_3^- band B also emerges well defined with $\lambda_{\text{max}} = 191 \text{ nm}$ and $\epsilon_{\text{max}} 5600 M^{-1} \text{ cm}^{-1}$ (Figure 6). On gradually adding water to CH_3CN or alcohol the whole spectrum is shifted (Figure 9) in a way which indicates that the effect is essentially physical. Thus under the conditions employed no new species are formed which absorb in this region, like dimers or esters.⁹

The cttts nature of B is clearly demonstrated in Figure

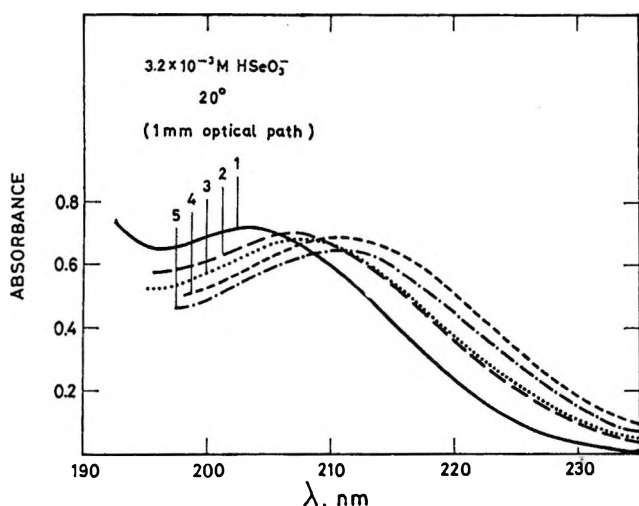


Figure 9. Band A of HSeO_3^- in mixed solvents: water (1), water + 50% ethanol (2), water + 50% methanol (3), water + 95% ethanol (4), water + 95% methanol (5).

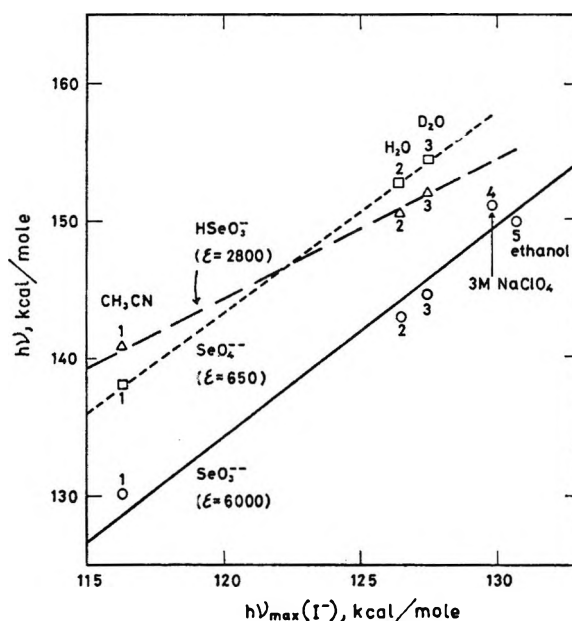


Figure 10. $h\nu$ of the oxyseleide ions at the specified absorptivities against $h\nu_{\text{max}}(\text{I}^-)$ in the same solvents (20°).

10 which records transition energy at a specified absorptivity against $h\nu_{\text{max}}$ of I^- in the same solvent *i.e.*, against the cttts value of the solvent.¹⁰ Mixed solvents were not included in this correlation because in the same

- (7) M. J. Blandamer and M. F. Fox, *Chem. Rev.*, **70**, 59 (1970).
 (8) f was calculated using the approximation $f = 4.32 \times 10^{-9} \times 1.06 \epsilon_{\text{max}} \Delta\nu^{1/2}$ (C. Sandorfy, "Electronic Spectra and Quantum Chemistry," Prentice-Hall, Englewood Cliffs, N. J., 1964).
 (9) A. Simon and R. Paetzold, *Z. Anorg. Allgem. Chem.*, **303**, 46 (1960); R. Paetzold and E. Ronsch, *ibid.*, **315**, 64 (1962); R. Paetzold, *ibid.*, **325**, 47 (1963).
 (10) I. Burak and A. Treinin, *Trans. Faraday Soc.*, **59**, 1490 (1963).

mixture the solvation layers of I^- and SeO_n^{2-} should have different compositions, that of SeO_n^{2-} being much richer in water. Indeed, a little water added to solution of SeO_3^{2-} and SeO_4^{2-} in CH_3CN had a striking effect on their spectra, bringing them close to that in water (Figure 7), whereas the effect on I^- in CH_3CN was relatively small. However, added solutes do fit into the lines (Figure 10), showing that at the concentrations employed the light absorbing ions are essentially surrounded by water molecules. The relatively large effect of sucrose and ClO_4^- is also typical for cttts transitions.¹¹

The slopes of the lines in Figure 10 (designated β) are also recorded in Table II. They measure the sensitivity of band B to solvent effects at the specified absorptivity.¹⁰ With the pair H_2O - D_2O β could be determined farther from the overlap zones of B with A (Table II).

Discussion

The high energy bands of SeO_3^{2-} , $HSeO_3^-$, and SeO_4^{2-} (bands B) display the characteristic properties of cttts bands. However, detailed information concerning these bands is rather limited because only the ascending branches were observed, and they are overlapped by other bands. The solvent sensitivity β and $-d(h\nu)/dt$ are known to depend on absorptivity ϵ (or more correctly on ϵ/ϵ_{max}); the former increases¹⁰ and the latter decreases¹² with ϵ . Thus strict comparison with theory is impossible if ϵ_{max} is unknown. The overlap problem is more serious than that of resolving the spectrum into its components. The proximity of a cttts state to another excited state is likely to result in their "mixing," *i.e.*, in their losing some of their "pure" character. Still some support to the theory can be inferred from our results.

A. For anions with radii $R_x \sim R_{I^-}$ and charges -1 and -2 , β_{max} should be close to 1 and 2, respectively.³ This is in agreement with our results for the ratio of solvent shifts $\Delta\nu_x/\Delta\nu_{I^-}$, on replacing H_2O by D_2O (Table II). For dinegative ions the values of β derived from Figure 10 are appreciably lower (Table II). This is probably due to (i) overlap effects (with SeO_3^{2-} at $\epsilon \sim 6000$ the pair H_2O - D_2O also yields $\beta = 1.5$); (ii) traces of water still present in the organic solvents.

B. The little dependence of $d(h\nu)/dt$ on charge (Table II) is also in accord with theory.³

Knowing $h\nu_{max}$ of $HSeO_3^-$ in CH_3CN (150 kcal/mol) we could estimate its vertical ionization potential E and its effective crystallographic radius R (thermochemical radius¹³). When CH_3CN is replaced by H_2O , $h\nu$ of $HSeO_3^-$ (at $\epsilon = 2800 M^{-1} cm^{-1}$) is shifted by 10 kcal/mol. Assuming that this also applies to the peak (a shift of 10.4 kcal is displayed by $h\nu_{max}$ of I^- ¹⁰) we obtain $h\nu_{max}(HSeO_3^-) = 160$ kcal/mol. From the parameters of the lines in Figure 10, E can be evaluated. The theoretical expression for the intercept is¹⁵

$$\text{intercept} = E - \beta E_{I^-} + 34(\beta - 1) \text{ (kcal)} \quad (3)$$

The intercept of the line for $HSeO_3^-$ is 24 kcal/mol; putting $\beta = 1$ and $E_{I^-} = 71$ kcal¹⁴ we obtain $E = 4.15$ eV. (The electron affinity pertaining to equilibrium configuration should be somewhat lower.) The theoretical expression for $h\nu_{max}$ of a cttts band in aqueous solution is¹⁵

$$h\nu_{max} = E - L + 0.77e^2/r_0 - 1.58 \text{ (eV)} \quad (4)$$

where L is the solvation energy of the radical and $r_0 = 1.25R$. Inserting $h\nu_{max} = 6.95$ eV, $E = 4.15$ eV, $L = 0.3$ eV (as that of several polyatomic radicals¹⁵), we derive $R_{HSeO_3^-} = 1.9 \text{ \AA}$. The same value can be estimated from other crystallographic data:¹⁶ $R_{SO_3^{2-}} = 2.0 \text{ \AA}$; adding to it the difference $R_{SeO_3^{2-}} - R_{SO_3^{2-}} = 0.13 \text{ \AA}$, we estimate $R_{SeO_3^{2-}} = 2.15 \text{ \AA}$. On protonation the radii of CO_3^{2-} and SO_4^{2-} are reduced by 0.22 and 0.24 \AA , respectively; assuming the same effect for SeO_3^{2-} , we obtain $R_{HSeO_3^-} \sim 1.9 \text{ \AA}$.

The low-energy bands of the four oxyselenide ions appear to be allowed sub-Rydberg transitions involving excitation of the nonbonding electrons on the oxygen atoms to antibonding orbitals mainly centered on the selenium atom. Such transitions should display the regular "blue shift" type of solvent effects and can be rather sensitive to temperature. This agrees with our results, but the effect of protonation is rather perplexing. The transition energy of band A follows the order $HSeO_n^- < SeO_n^{2-}$. The opposite order is expected since protonation involves complete binding of a pair of nonbonding electrons. Indeed the opposite order is displayed by the systems⁷ SO_4^{2-} - HSO_4^- ; SO_3^{2-} - HSO_3^- ; CO_3^{2-} - HCO_3^- ; HPO_4^{2-} - $H_2PO_4^-$. Moreover, the cttts bands of the oxyselenides behave regularly⁷ with $h\nu$ increasing in the order: $SeO_4^{2-} < HSeO_4^-$, $SeO_3^{2-} < HSeO_3^-$ and $SeO_2^{2-} < SeO_4^{2-}$. Following is a possible explanation of this anomaly.

SeO_4^{2-} and SeO_3^{2-} possess the same valence shell configurations as SO_4^{2-} and SO_3^{2-} , respectively. Their lowest energy transitions involve degenerate orbitals¹⁷ which should split when the symmetry is lowered. Such splitting was actually observed in the spectra of several tetrahedral anions, *e.g.*, CrO_4^{2-} when protonated,¹⁸ the low-energy component of $HCrO_4^-$ having lower transition energy than the correlated band of CrO_4^{2-} . This may also be the case with the oxyselenide

(11) G. Stein and A. Treinin, *Trans. Faraday Soc.*, **56**, 1393 (1960).

(12) G. Stein and A. Treinin, *ibid.*, **55**, 1091 (1959).

(13) A. F. Kapustinskii, *Quart. Rev. (London)*, **10**, 283 (1956).

(14) R. S. Berry, C. W. Riemann, and G. N. Spokes, *J. Chem. Phys.*, **37**, 2278 (1962).

(15) G. Stein and A. Treinin, *Trans. Faraday Soc.*, **55**, 1086 (1959).

(16) G. A. Krestov, *J. Struct. Chem.*, **3**, 391 (1962).

(17) R. Manne, *J. Chem. Phys.*, **46**, 4645 (1967).

(18) A. Carrington and M. C. R. Symons, *Chem. Rev.*, **63**, 443 (1963).

ions, where mixing of this component with the cttts state can contribute to its relatively high intensity and shift it further to the red. A similar analysis was given to the spectrum of $S_2O_3^{2-}$,¹⁹ but the spectra of SO_4^{2-} and HSO_4^- were interpreted only in terms of cttts transitions.⁷ The nature of electronic transitions in SO_3^- and HSO_3^- is still unknown; formation of solvated

electrons on excitation cannot be taken as a criterion for cttts transitions.²⁰ A detailed examination of environmental effects on the spectra of oxysulfide and oxytelluride ions is now being conducted in our laboratory.

(19) R. Sperling and A. Treinin, *J. Phys. Chem.*, **68**, 897 (1964).

(20) L. Dogliotti and E. Hayon, *ibid.*, **72**, 1800 (1968).

Formation of Ions and Excited States in the Laser Photolysis of Solutions of Pyrene¹

by J. T. Richards, G. West, and J. K. Thomas*

Chemistry Division, Argonne National Laboratory, Argonne, Illinois 60439 (Received June 16, 1970)

The formation of ions and excited states of pyrene has been investigated using 347.1-nm light from a Q-switched Korad KIPQ ruby laser. In hydrocarbon solutions transient absorbing species were observed which by lifetime and spin-orbit coupling studies were assigned to singlet-singlet and triplet-triplet transitions. Three singlet maxima were observed at 470 nm, 365 nm, and 254 nm; the latter corresponds to a bound state above the gas-phase ionization potential of pyrene. Oxygen was found to react with both the singlet and triplet states with the following rate constants: $k_{(O_2+P^S)} = 1.9 \times 10^{10} M^{-1} sec^{-1}$, $k_{(O_2+P^T)} = 2.4 \times 10^9 M^{-1} sec^{-1}$. It was also found that oxygen efficiently enhances the intersystem crossing. In methanol and ethanol solutions of pyrene in addition to singlet and triplet states of pyrene, solvated electrons and positive ions of pyrene were observed. The ionization of the pyrene was found to occur by a biphotonic process; possible mechanisms for this process have been considered.

Introduction

The photolysis of solutions of pyrene has been of interest to the photochemist for many years, mainly because of the long lifetime of the singlet excited state and because of the relative ease with which this excited singlet state forms excimers. The absorption spectrum of the triplet state has been characterized by flash photolysis² and steady-state methods,³ while recently the spectrum of the excited singlet state and excimer have been observed by laser photolysis⁴⁻⁶ and flash photolysis.⁷ A recent study⁸ has also indicated that ionization of pyrene is possible by multiphotonic processes at high light intensities. The object of the present study is to investigate the role of solvent and light intensity in the formation of excited states and ions in the photolysis of solutions of pyrene.

Experimental Section

Cyclohexane and 3-methylpentane 3MH (Phillips Petroleum Co.) were dried prior to use by passage through a 3-ft column of activated alumina. Ethanol (I.S.U.) and methanol (Mallinckrodt) were analytical grade and were used as received. Distillation of the

alcohols from solutions containing the sulfate salt of 2,4-dinitrophenylhydrazine, to remove aldehydes, gave identical results to the untreated material. Pyrene (Eastman Organic Chemical Co.) was purified by two recrystallizations from ethanol and was resublimed under vacuum prior to use. Xenon, helium, oxygen, carbon dioxide, nitrous oxide, and sulfur hexafluoride were obtained from Matheson Scientific Co. The py-

* To whom correspondence should be addressed at Chemistry Department and Radiation Laboratory, University of Notre Dame, Notre Dame, Ind. 46556.

(1) Work performed under the auspices of the U. S. Atomic Energy Commission.

(2) G. Porter and M. W. Windsor, *Proc. Roy. Soc. Ser. A*, **245**, 238 (1958).

(3) W. Heinzelmann and H. Labhart, *Chem. Phys. Lett.*, **3**, 20 (1969).

(4) J. R. Novak and M. W. Windsor, *Proc. Roy. Soc. Ser. A*, **308**, 95 (1968).

(5) G. Porter and M. Topp, *ibid.*, **315**, 163 (1970).

(6) C. R. Goldschmidt and M. Ottolenghi, *J. Phys. Chem.*, **74**, 2041 (1970).

(7) Y. Nakato, N. Yamamoto, and H. Tsubomura, *Chem. Phys. Lett.*, **2**, 57 (1968).

(8) S. B. Babenko, V. A. Benderskii, and V. I. Goldanskii, *JETP Letters*, **10**, 129 (1969).

rene solutions were prepared by the syringe technique which has already been described in detail.⁹

The laser photolysis apparatus and analytical techniques have already been described for the 265-nm output of a quadrupled neodymium laser.¹⁰ In this work a ruby rod was used in the same Korad KIPQ laser system. The total output of the frequency-doubled light at 347.1 nm was measured as 80 mJ using a T.R.G. bolometer. In order to obtain high photon densities the 347.1-nm beam was focused onto the irradiation cell by means of a suitable focal length quartz lens. The energy input to the photolysis cell was measured by using solutions of anthracene in cyclohexane of identical optical density at 347.1 nm to the solutions under investigation. The yield of the triplet of anthracene was measured spectrally, using $\epsilon_{\max}^{425 \text{ nm}} = 65,000 \text{ L M}^{-1} \text{ cm}^{-1}$,¹¹ corresponding to a $\phi_{(\text{triplet})} = 0.7$. This provides a measure of the energy input to the system under the prevailing experimental conditions.

Pyrene in Cyclohexane. Two typical oscilloscope pictures of the transitory species observed in the laser photolysis of deaerated pyrene in cyclohexane are shown as A and B in Figure 1. A is taken at 360 nm and shows a species which is produced with the 15-nsec laser pulse, subsequently decaying exponentially. B, taken at 415 nm, shows a species which grows in intensity following the laser pulse and also the fluorescence observed in the absence of the analyzing light beam. If the OD at the end of the laser pulse and OD at several microseconds are plotted vs. wavelength the spectra shown in Figure 1 are obtained. The spectrum at the end of the pulse shows three distinct maxima at 254 nm, 365 nm, and 470 nm. (In order to obtain the spectra at $\lambda < 300 \text{ nm}$, it was necessary to use very low concentrations of pyrene ($\sim 10^{-6} \text{ M}$) since at higher pyrene concentrations the

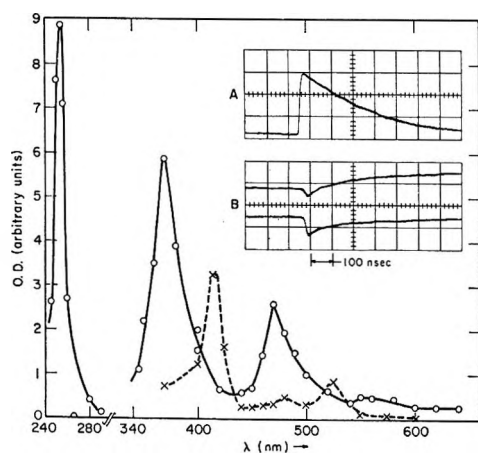


Figure 1. Transient absorption spectra obtained by 347.1-nm laser photolysis of $1.4 \times 10^{-4} \text{ M}$ pyrene in cyclohexane: \circ , spectrum at end of laser pulse, band pass 1.2 nm; \otimes , spectrum after $1 \mu \text{ sec}$ ($\times 5$), band pass 1.2 nm. NB [pyrene] = 10^{-6} M for $\lambda < 300 \text{ nm}$. A, oscilloscope trace taken at 360 nm; B, oscilloscope traces taken at 415 nm upper trace with light on, lower trace with light off.

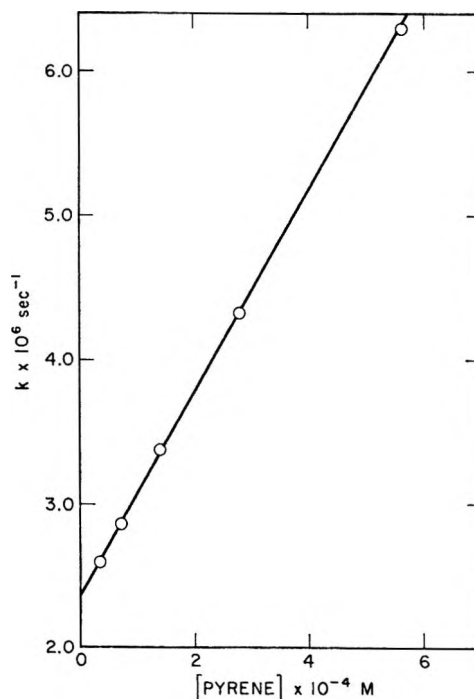
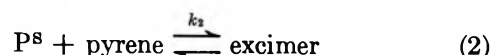
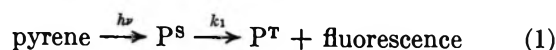


Figure 2. The effect of pyrene concentration on the first-order decay rate of the pyrene singlet absorption monitored in cyclohexane solutions at 470 nm.

ground-state absorption precludes observation of transient species.) The spectrum at several microseconds after the pulse shows maxima at 415 nm, 480 nm, and 525 nm and is in agreement with that attributed to the triplet state of pyrene.² The intensities of both spectra increase linearly with the laser intensity over a fivefold range.

The general shapes of the spectra in Figure 1 are not changed by pyrene concentration; however, the rate of decay of the end of pulse spectrum increases with pyrene concentration above 10^{-4} M . The decay of the short-lived absorption monitored at either 257 nm, 365 nm, or 470 nm is always identical with that of the fluorescence monitored at 400 nm. A plot of the rate of decay of the spectrum vs. pyrene concentration is shown in Figure 2. The data suggest that the spectrum at the end of the pulse is that of the excited singlet state of pyrene, and that the fluorescence at 400 nm is monomer fluorescence. The effect of pyrene on the lifetime is then due to excimer formation



The rate of decay of the excited singlet is given by $k = k_1 + k_2 [\text{pyrene}]$ which gives $k_1 = 2.36 \times 10^6 \text{ sec}^{-1}$ and

(9) J. K. Thomas, S. Gordon, and E. J. Hart, *J. Phys. Chem.*, **68**, 1524 (1964).

(10) R. McNeil, J. T. Richards, and J. K. Thomas, *ibid.*, **74**, 2290 (1970).

(11) E. J. Land, private communication.

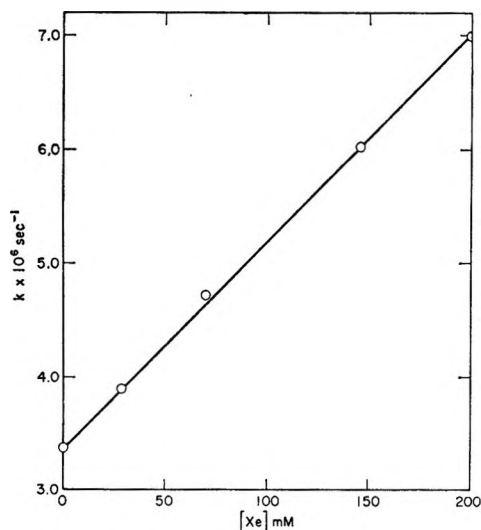


Figure 3. The effect of xenon concentration on the first-order decay rate of the pyrene singlet absorption monitored at 470 nm in $1.4 \times 10^{-4} M$ pyrene in cyclohexane solutions.

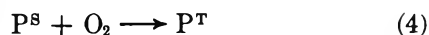
$k_2 = 7.1 \times 10^9 M^{-1} \text{sec}^{-1}$. These values are in good agreement with those obtained by Birks, *et al.*,¹² from fluorescence measurements.

Effect of Xenon on Singlet Decay. The rate of decay of the excited singlet spectrum is also increased by the presence of xenon gas in solution with a concomitant increase in the rate of growth and yield of the triplet state. The variation of the first-order rate constant with xenon concentration for a solution of $1.4 \times 10^{-4} M$ pyrene is shown in Figure 3. The reactions contributing to this decay are (1) and (3).



The data in Figure 3 give k_3 as $1.84 \times 10^7 M^{-1} \text{sec}^{-1}$, which compares favorably with the value of $2.2 \times 10^7 M^{-1} \text{sec}^{-1}$ obtained by fluorescence measurements in ethanol.¹³

Effect of Oxygen in Singlet and Triplet Decay. Oxygen also increases the rate of decay of the singlet excited states, the relevant data being shown in Figure 4. If the reaction rate of the singlet with O_2 is k_4 , then $k_4 = 1.9 \times 10^{10} M^{-1} \text{sec}^{-1}$ from Figure 4.



Oxygen also reacts with the triplet state, the relevant data being shown in Figure 5. If this rate constant is k_5 , then $k_5 = 2.4 \times 10^9 M^{-1} \text{sec}^{-1}$ from Figure 5.



A point of special interest here is the fact that as the rate of reaction with O_2 of the singlet is much faster than the triplet with O_2 , it is possible to monitor the triplet yield immediately following the laser pulse under conditions where the singlet reaction with oxygen is complete. Figure 6 shows the end of a pulse spectrum obtained with $10^{-4} M$ pyrene in cyclohexane and $10^{-2} M$

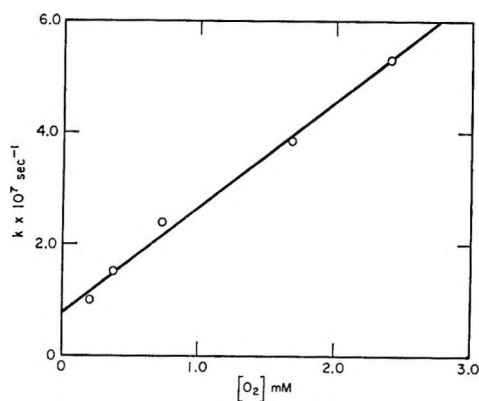


Figure 4. The effect of oxygen concentrations on the first-order decay rate of the pyrene singlet fluorescence monitored at 400 nm in $1.4 \times 10^{-4} M$ pyrene in cyclohexane solutions.

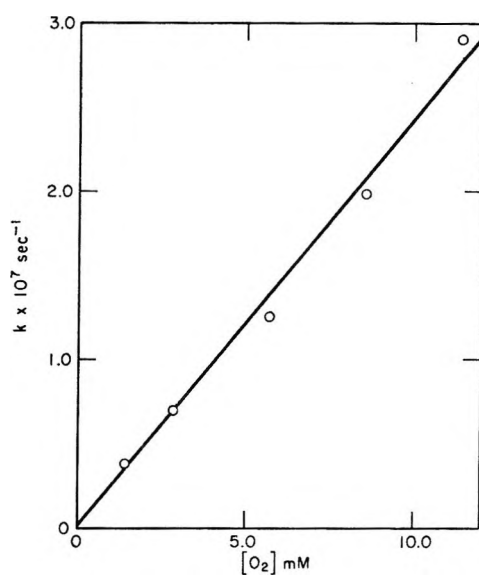


Figure 5. The effect of oxygen concentration on first-order rate of decay of the pyrene triplet absorption monitored at 415 nm in $1.6 \times 10^{-4} M$ pyrene in cyclohexane solutions.

oxygen; this is identical with that obtained at long times in the absence of O_2 . Note however that in the absence of O_2 (oscilloscope trace taken at 415 nm for $1.0 \times 10^{-4} M$ pyrene in argon-saturated cyclohexane) following an initial downward deflection of the trace caused by fluorescence the triplet absorption signal grows steadily over a period of about 600 nsec. In the presence of O_2 (oscilloscope trace taken at 415 nm for $1.0 \times 10^{-4} M$ pyrene in oxygen-saturated cyclohexane) the triplet signal rises to its maximum value (about twice the value of that in the absence of O_2) almost instantaneously (~ 20 nsec) owing to an enhanced rate of intersystem crossing and then rapidly falls again because of oxygen quenching of the triplet state. *Clearly oxygen strongly enhances the*

(12) J. B. Birks and H. Munro, *Progr. React. Kinet.*, **4**, 239 (1967).

(13) A. R. Horrocks, A. Kearvell, K. Tickle, and F. Wilkinson, *Trans. Faraday Soc.*, **62**, 3393 (1966).

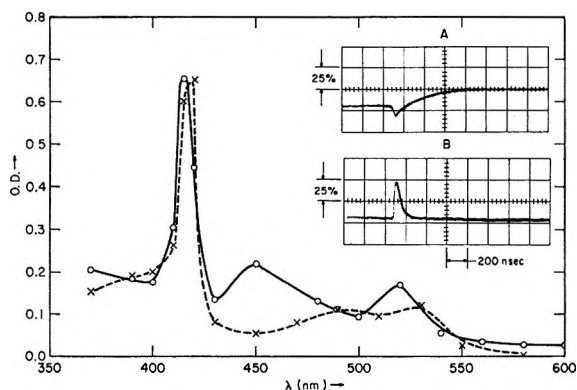


Figure 6. End of pulse transient absorption spectra obtained by 347.1-nm laser photolysis of oxygen-saturated pyrene solutions: \times , $1.0 \times 10^{-6} M$ pyrene in cyclohexane, band pass 1.2 nm; \circ , $1.0 \times 10^{-6} M$ pyrene in methanol, band pass 1.2 nm. A, an oscilloscope trace taken at 415 nm for $1.0 \times 10^{-4} M$ pyrene in argon-saturated cyclohexane; B, oscilloscope trace taken at 415 nm for $1.0 \times 10^{-4} M$ pyrene in oxygen-saturated cyclohexane.

rate of intersystem crossing from singlet to triplet in pyrene.

In view of the slow rate of fluorescence emission and of intersystem crossing in the absence of O_2 , it is fair to conclude that, in the presence of O_2 essentially all the singlet states are converted to the triplet state in a period of 20 nsec or less. Thus, in the presence of O_2 , the triplet yield is unity. The observed twofold enhancement by oxygen then implies a quantum yield for triplet of about 0.5 in the absence of oxygen. This is consistent with a value of 0.56 reported for $10^{-4} M$ pyrene solutions by other workers.³ Essentially similar data were also obtained using 3MH as a solvent.

Pyrene in Ethanol and Methanol. The transitory spectra obtained in the laser photolysis of pyrene in methanol are shown in Figure 7. Analogous data are obtained in ethanol solution. A comparison of these

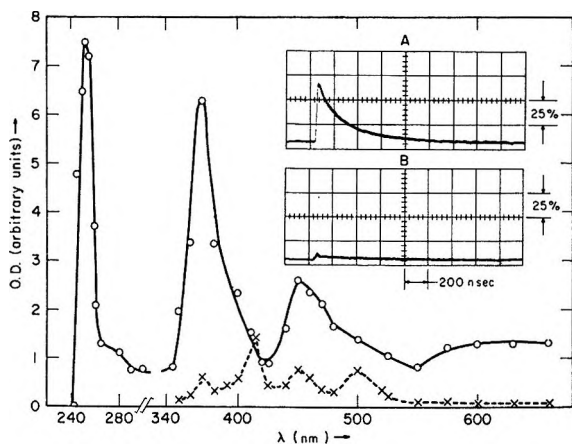


Figure 7. Transient absorption spectra obtained by 347.1-nm laser photolysis of $1.0 \times 10^{-4} M$ pyrene in methanol: \circ , spectrum at end of laser pulse, band pass 1.2 nm; \otimes , spectrum after $1 \mu\text{sec}$, band pass 1.2 nm. A, oscilloscope trace taken at 630 nm; B, oscilloscope trace taken at 630 nm with $10^{-2} M$ acid added.

data with those in cyclohexane, Figure 1, shows the two excited singlet peaks at 252 nm and 360 nm, while the peak at 470 is now shifted to 450 nm. Another broad absorption is obtained in the red part of the spectrum. The triplet spectrum also shows the 450-nm band. A and B in Figure 7 show the decay of the red band monitored at 630 nm in methanol solution (A) and in methanol solution containing $10^{-2} M$ perchloric acid (B). This band is destroyed by acid while the singlet and triplet spectra and the 450-nm band are unaffected. Typical scavengers of solvated electrons, *e.g.*, nitrous oxide, carbon dioxide, and SF_6 , also remove the red absorption band; hence it is suggested that this is the absorption of the solvated electron in methanol. Pulse radiolysis studies¹⁴ show that the absorption of the solvated electron is indeed similar to that obtained from 550 to 650 nm in the present work with a peak at 650 nm. The 450-nm band may be identified as the cation of pyrene, which has a peak in this region also.¹⁵ In agreement with this assignment, the 450-nm peak decays more rapidly in solutions saturated with ammonia and at high concentrations of alkali. The yield of solvated electrons depends on the square of the light intensity over a threefold range. The yield of excited singlet state and solvated electrons *vs.* pyrene concentration is shown in Figure 8. At low concentrations up to

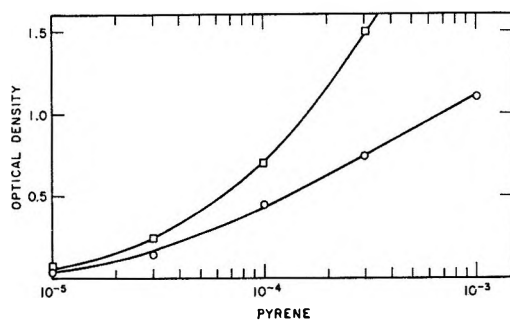


Figure 8. Yield of pyrene singlet monitored at 360 nm and yield of solvated electrons monitored at 630 nm in methanol as a function of pyrene concentration: \circ , electron yield; \square , pyrene singlet yield.

$10^{-4} M$ both singlet and electron yield increase in an identical manner with increasing pyrene concentration. At higher pyrene concentrations the electron yield increases less rapidly than the singlet yield. This may be explained as being due to the higher optical densities at concentrations above $10^{-4} M$, leading to lower effective light intensities, which affect the electron yield to a greater extent than the singlet yield due to the dependence of the former yield on (intensity).² It may be concluded that the electron yield and excited singlet yield show similar dependence on pyrene concentration.

(14) J. K. Thomas, *Radiat. Res. Rev.*, **1**, 183 (1968).

(15) W. Ij. Aalbersberg, G. J. Hoijink, E. L. Mackor, and W. P. Weijland, *J. Chem. Soc.*, 3052 (1959).

Essentially similar data were obtained using ethanol as a solvent.

Xenon gas does not affect the yield of positive ion or the electron yield, while oxygen or 0.1 *N* CH₃I does not affect the positive ion yield. Both these solutes lead to enhanced triplet yields and a greatly reduced singlet lifetime.

It may be added that solvated electrons are produced in the laser photolysis of 10⁻⁴ *M* 1,2-benzanthracene, anthracene, and TMPD in methanol. With anthracene and TMPD the singlet lifetime is considerably shorter than the pulse duration.

Discussion

The laser photolysis of pyrene in cyclohexane and in ethanol leads to transitory spectra which may be ascribed to singlet-singlet and triplet-triplet transitions of pyrene. The spectrum of the triplet is identical with that obtained by conventional photolysis techniques while a part of the excited singlet spectrum agrees with previous laser work⁵ (470 nm peak) and flash photolysis⁶ (365 and 470 nm peak). An additional peak is observed at 254 nm which lies at an energy 8.6 eV above the ground state. This is ~1.0 eV above the gas-phase ionization potential of 7.5 eV. No significant absorption is seen at a point in the spectrum corresponding to the gas-phase ionization potential, *i.e.*, $\lambda \sim 300$ nm. The sharp symmetrical peak of the 254-nm band indicates a transition to a bound state of pyrene which is well above the gas-phase ionization potential. The accelerated decay of the excited singlet state by xenon and pyrene is in quantitative agreement with similar measurements using the fluorescence of the excited singlet state. The accelerated decays of the excited singlet and triplet state by oxygen are reminiscent of similar oxygen effects with other molecules. The present data clearly show that the reaction of oxygen with the excited singlet state of pyrene efficiently produces the triplet state, rather than an intermediate complex or direct quenching.

In alcohol solutions the solvated electrons and cations of pyrene are produced along with excited states. The dependence of the ionic yield on the square of the light intensity shows that a biphotonic process is operating here. Three biphotonic mechanisms may be considered: (a) the absorption of a second 347.1-nm photon by the excited singlet state, (b) the absorption of a second 347.1-nm photon by the triplet, and (c) a direct two-

photon absorption by the ground state to give a high energy state which ionizes.

The first process (a) may be ruled out as CH₃I and O₂, which make the lifetime of the excited singlet short compared to the pulse, have no effect on the positive ion yield. It may be argued that the ionization in the case of anthracene is similar to that in pyrene because anthracene shows similar behavior even in the absence of excited singlet quenchers owing to its inherently short singlet lifetime which is much shorter than the pulse length. Mechanism (b) involving the triplet state is also unlikely as the production of triplet states in pyrene by intersystem crossing is 100 times slower than the pulse duration. Consequently, there is little triplet present during the laser pulse. The presence of O₂ increases the triplet yield by twofold and produces it in a short time compared to the pulse. However, O₂ has no effect on the pyrene cation yield. From these experiments it must be concluded that mechanism (c) is responsible for the production of ions. The customary calculations¹⁶ of biphotonic processes in organic molecules show that the yield of ionization in the present experiments should be 10⁴ smaller than that found experimentally, since the absorption cross section for two photon absorption *via* a virtual intermediate state is exceedingly low. However, these calculations are applicable to a system which is transparent to the laser photons, whereas pyrene does actually absorb light at the 347.1-nm laser wavelength. The energy of a state corresponding to the absorption of two 347.1-nm laser photons is 7.25 eV, *i.e.*, ~0.3 eV below the gas-phase ionization potential of pyrene. It may be concluded that the 0.3 eV of energy necessary to ionize the 7.25-eV state is provided by the solvation energy of the electron which amounts to about 1.7 eV in alcohols. An alternative way of expressing this is to say that in alcohol solutions the effective ionization potential of pyrene might be appreciably less than the gas-phase value, perhaps by as much as 1.7 eV, the solvation energy of the electron. Then in this case the direct absorption of two 347.1-nm photons will produce direct ionization of the pyrene. However, the electron is not solvated in hydrocarbons at room temperature, which explains the lack of photoionization in cyclohexane solutions.

Acknowledgments. G. West wishes to thank Argonne National Laboratory for a scholarship.

(16) D. Kleinman, *Phys. Rev.*, **125**, 87 (1962).

Reduction of Cobalt(III) in Cobaltamines Induced by the Decomposition of Persulfate Ion

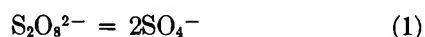
by James Dee White and H. Taube*

Department of Chemistry, Stanford University, Stanford, California 94305 (Received May 25, 1970)

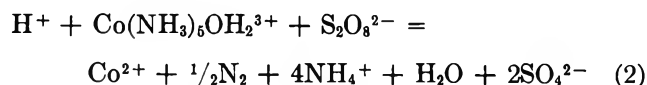
The stoichiometric relations proposed by Thusius and Taube¹ for the production of N₂ from cobaltamines induced by the decomposition of S₂O₈²⁻: H⁺ + Co(NH₃)₅OH₂³⁺ + S₂O₈²⁻ = Co²⁺ + 1/2N₂ + 4NH₄⁺ + H₂O + 2SO₄²⁻ has been confirmed under conditions such that the production of CO₂ is virtually eliminated. The stoichiometric relation Co^{III}:S₂O₈²⁻:N₂ = 2:2:1 has been extended to Co(NH₂)₄(OH₂)₂³⁺ as substrate. Production of N₂O is also observed, amounting to 5% of the gas in the case of the pentaammine and 15% when the tetraammine is the substrate. When Co(NH₂)₂(OH₂)₄³⁺ is substrate, aside from adventitious CO₂, O₂ is the only gaseous product. The stoichiometric relation Co^{III}:S₂O₈²⁻:O₂ was observed to be 2:2:3, but it is not certain whether this is invariant with concentration conditions. In the reaction producing N₂ only that amount of S₂O₈²⁻ which would have decomposed in the absence of Co^{III} is implicated. For each of the amines, it is assumed that SO₄⁻ produced in the decomposition of S₂O₈²⁻ produces Co^{IV}. Nitrogen tracer experiments show that the formation of the N-N bonds in N₂ is an intermolecular process, and it is suggested that N₂ arises from the production of NH in the coordination sphere of Co^{IV}. Nitrogen and oxygen tracer experiments show that the formation of the N-O bond in N₂O is intramolecular. The reaction Co^{IV} → Co²⁺ + NH₂OH is suggested as the primary step leading to N₂O production. Co^{IV} is implicated as the agent which takes NH to N₂, and as producing isomerization in *trans*-nitrogen labeled Co(NH₃)₅OH₂³⁺.

Introduction

Earlier studies¹ have shown that the decomposition of S₂O₈²⁻ in the presence of Co(NH₃)₆³⁺ or Co(NH₃)₅OH₂³⁺ induces the reduction of the cobaltamine to Co²⁺, with NH₄⁺ and N₂ appearing as the major nitrogen-containing products. At low Co^{III} concentration, the rate of production of Co²⁺ increases with [Co^{III}], but when this is in the millimolar range, the rate reaches a saturation value determined only by the rate of the reaction^{2,3}



The main net change in the rate saturation region for the pentaammine as substrate is



It should be noted that only that amount of S₂O₈²⁻ is brought into reaction which in the absence of the cobaltamine would have decomposed to SO₄²⁻ and O₂.

The experiments by Thusius and Taube¹ indicated that N₂O in minor amounts was also formed, but conclusions on the contribution by this reaction and on some other significant aspects of the chemistry of the system were obscured by the fact that CO₂, arising from the oxidation of adventitious organic matter, was present in substantial amounts among the gaseous products. We have returned to the study of these systems and have succeeded in reducing the amount of CO₂ so that it is only a minor component of the product gases, making it possible to get quantitative data on

the reaction producing N₂O. The work has been extended to encompass the tetraammine and diammine complexes of Co^{III}, and it includes nitrogen and oxygen tracer studies which help to clarify the mechanism of production of N₂ and N₂O.

Experimental Section

Preparation of the Complexes. [Co(NH₃)₅OH₂](ClO₄)₃. Carbonatopentaamminecobalt(III) nitrate⁴ was treated with cold 2 M perchloric acid, and the solid which formed was recrystallized three times from 0.1 M perchloric acid. *Anal.* Calcd for [Co(NH₃)₅OH₂](ClO₄)₃: H, 3.7; N, 15.4; ClO₄, 64.8. Found: H, 3.7; N, 15.3; ClO₄, 64.7.

trans-[Co(NH₃)₄(¹⁵NH₃)OH₂](ClO₄)₃. The compound [Co(NH₃)₆SO₃]₂SO₃ was prepared according to the synthesis of Werner and Gruger.⁵ A modification of Sargeson's procedure^{6,7} was used for the synthesis of the ¹⁵N-labeled complex.

[Co(NH₃)₅SO₃]₂SO₃ was dissolved in concentrated hydrochloric acid and immediately precipitated with

* To whom correspondence should be addressed.

(1) D. D. Thusius and H. Taube, *J. Phys. Chem.*, **71**, 3845 (1967).

(2) I. M. Kolthoff and J. K. Miller, *J. Amer. Chem. Soc.*, **73**, 3055 (1951).

(3) W. K. Wilmarth and A. Haim in "Peroxide Reaction Mechanisms," J. O. Edwards, Ed., Wiley-Interscience, New York, N. Y., 1962.

(4) A. Lamb and K. Mysels, *J. Amer. Chem. Soc.*, **67**, 468 (1945).

(5) A. Werner and H. Gruger, *Z. Anorg. Chem.*, **16**, 406 (1898).

(6) D. A. Buckingham, I. I. Olsen, and A. M. Sargeson, *J. Amer. Chem. Soc.*, **89**, 5129 (1967).

(7) A. M. Sargeson, private communication.

ethanol. The precipitate was recrystallized from a solution of concentrated hydrochloric acid and lithium chloride, then from an ammoniacal solution with ethanol, washed with ether, and treated with 3% aqueous LiOH for 5 min. *trans*-[Co(NH₃)₄(OH)SO₃] crystallized upon the addition of ethanol.

Freshly prepared [Co(NH₃)₄(OH)SO₃] (0.63 g) was added to a solution containing 0.5 g ¹⁵NH₄Cl (99.5% ¹⁵N) and 0.26 g of LiOH in 50 ml of H₂O. *trans*-[Co(NH₃)₄(¹⁵NH₃)SO₃]Cl was crystallized from solution. After 10 min ethanol was added to complete the crystallization. After drying, the *trans*-[Co(NH₃)₄(¹⁵NH₃)SO₃]Cl was dissolved in a solution of LiCl in concentrated HCl. The solution was heated on a water bath for approximately 10 min. After cooling in an ice bath, ethanol was added to precipitate *trans*-[Co(NH₃)₄(¹⁵NH₃)Cl]Cl₂. This material was dissolved in 0.1 M HClO₄ and treated with a solution of mercuric perchlorate. The resulting solution was ion-exchanged and *trans*-[Co(NH₃)₄(¹⁵NH₃)OH₂](ClO₄)₃ was precipitated with 72% HClO₄.

The ¹⁵N-labeled complex was recrystallized twice and stored under vacuum in a desiccator at ca. 0°. The precaution of keeping the temperature low was taken in order to minimize isomerization of the complex.⁷

Proton nmr was used to determine the purity of the complex using Sargeson's peak assignments.⁶ No *cis*-¹⁵NH₃ protons were observed. In addition, the extinction coefficients at 490 and 345 mμ were determined.⁸ The value of ε found at λ 490 and 345 nm were 47.4 and 44.8, to be compared to the literature values of 47.5 and 44.8.

[Co(NH₃)₄(OH₂)₂](ClO₄)₃. This salt was prepared by Schlessinger's procedure.⁹ Carbonatotetraammine (30 g) was dissolved in 600 ml of cold deionized water and 40 ml of 72% HClO₄ was then added slowly. Precipitation of the salt was induced by the addition of ethanol; the solid was collected and was further purified by recrystallizing from dilute perchloric acid solution. *Anal.* Calcd: H, 3.47; N, 12.14; ClO₄, 64.7. Found: H, 3.51; N, 12.15; ClO₄, 64.7.

Equilibration^{10a} between *cis* and *trans* forms of the tetraammine has been reported to be quite rapid. Experiments done since this work was completed and other auspices^{10b} suggest that the tetraammine exists in the *cis* form. Attempts to prepare the *trans* form have proved to be unsuccessful.

[Co(NH₃)₂(OH₂)₄](ClO₄)₃. The blue variety of K[Co(NH₃)₂(CO₃)₂] was prepared according to Mori's procedure.¹¹ K[Co(NH₃)₂(CO₃)₂] (10 g) was dissolved in 100 ml of cold 1 M HClO₄. The resulting solution was filtered and charged onto a thermostated column of Dowex 50X2 100–200 mesh cation exchange resin. Cold 1 M HClO₄ was used to elute Co^{II}. A violet species was eluted with 2 M HClO₄. On the basis of its spectrum and ion-exchange behavior we believe this

material to be a dihydroxy bridged dimer of the diammine; it will be reported on in greater detail in a separate publication.

To obtain monomeric diammine, a solution of the dimer was condensed using a rotary evaporator with no external heating of the solution. After reducing the solution to a small volume, it was further concentrated on a vacuum line until solid material formed. The solid is very hygroscopic and difficult to weigh; it was immediately put into solution for later use.

Because of the difficulty in manipulating the solid, analyses were performed on solutions. The ratios of Co_T:Co^{III}:NH₃ in two separate preparations proved to be: 1.00:0.99:1.98, 1.00:1.02:1.98. Co_T represents total cobalt and Co^{III} represents that present in the 3+ oxidation state. The methods of determining these quantities will be dealt with presently.

Stock Reagents. Water. Deionized water was distilled three times in consecutive glass stills, the first distillation being from alkaline permanganate. The water was further treated by adding K₂S₂O₈, 3 g/l. of water, refluxing for 8 hr, and then distilling the water. The liquid so obtained was used for the persulfate reactions and for recrystallizing the complex compounds used in this research.

Cerium(IV). Primary standard grade ammonium hexanitrate cerate, obtained from the G. Frederick Smith Chemical Co., in H₂SO₄ served as the source of Ce^{IV}.

Iron(II). Mallinckrodt analytical grade Fe(NH₄)₂(SO₄)₂·6H₂O dissolved in 2 N H₂SO₄ was used as a reducing agent.

Dichromate. Primary Standard potassium dichromate (Mallinckrodt) was used in Co^{III} determinations.

Buffer System. In most of the experiments, a phosphate buffer was used, made up using AR sodium monobasic phosphate and sodium dibasic phosphate. The total level of phosphate was 0.054 M.

Potassium Hydrogen Phthalate. Matheson Coleman and Bell's alkimetric standard K.H.P. was used to standardize NaOH solutions.

All other chemicals were readily available ACS reagent grade and were used without further purification.

Analyses

Cobalt(II). Cobalt(II) was determined spectrophotometrically as the thiocyanate complex in acetone according to Kitson's method.¹²

Cobalt(III). Excess Fe(NH₄)₂(SO₄)₂ in 2 N H₂SO₄

(8) A. M. Zwickel, Ph.D. Dissertation, University of Chicago, 1954.

(9) G. Schlessinger, *Inorg. Syn.*, **6**, 173 (1960).

(10) (a) R. G. Yalman and T. Kuwana, *J. Phys. Chem.*, **59**, 298 (1955); (b) J. D. White and T. W. Newton, to be published.

(11) M. Mori, M. Shibato, E. Kyono, and T. Adachi, *Bull. Chem. Soc. Jap.*, **29**, 883 (1956).

(12) R. E. Kitson, *Ancl. Chem.*, **22**, 664 (1950).

was added to the Co^{III} solution and back-titrated with $\text{Cr}_2\text{O}_7^{2-}$ using sodium diphenylamine sulfonate as the indicator.¹³

Total Cobalt (Co_T). This was determined by the Kitson¹² method.

Persulfate. Excess $\text{Fe}(\text{NH}_4)_2(\text{SO}_4)_2$ in 2 N H_2SO_4 was added to the persulfate solution and back-titrated potentiometrically with Ce^{IV} .

Cerium(IV). The Ce^{IV} concentration was determined spectrophotometrically using extinction coefficients measured by Robson¹⁴ and Medalia and Byrne.¹⁵

Dichromate. A solution of potassium dichromate was made alkaline with NaOH to convert the dichromate to chromate and the concentration was spectrophotometrically determined at 373 $\text{m}\mu$.¹⁶

Iron(II). Ferrous ion was determined potentiometrically with either Ce^{IV} or $\text{Cr}_2\text{O}_7^{2-}$ using diphenylamine sulfonate as an indicator.

Ammonia. A known volume of aquoamminecobalt(III) solution was reduced with FeSO_4 . Sodium hydroxide pellets were added and the liberated ammonia was distilled into a standardized perchloric solution. The acid was then titrated with a sodium hydroxide solution with methyl red serving as the indicator.

Chloride. Chloride was determined gravimetrically as silver chloride.¹⁷

H_2^{18}O . The Co_2 equilibration method described by Hunt¹⁸ was used to determine the ^{18}O content of enriched water.

Methods

Reactions with Persulfate. Water distilled from persulfate was stored in a glass-stoppered bottle with a cover over the stopper to prevent dust from contaminating the neck of the bottle. Glassware which was used for handling reagents was cleaned with a warm solution of $\text{Na}_2\text{Cr}_2\text{O}_7$ in concentrated H_2SO_4 , rinsed profusely with water distilled from persulfate, and dried in an oven at ca. 100°.

Cobalt complexes were recrystallized from perchloric acid solutions, which were made from water distilled from persulfate. A trace of sodium persulfate was added to the cobalt solutions before heating to oxidize organic impurities. Care was taken at all stages to minimize contamination by particulate matter.

Kinetics of Reactions with Persulfate. For the reactions with persulfate, the desired amounts of sodium persulfate, disodium phosphate, and monosodium phosphate were added to redistilled (from persulfate) water and the mixture was heated in a constant temperature bath at 50° for 4 to 6 hr to oxidize organic impurities. It should be noted that only 2% or so of the $\text{S}_2\text{O}_8^{2-}$ decomposes in this interval of time. After cooling the solution to room temperature, the pH was adjusted to 3.5 by dropwise additions of perchloric acid and sodium hydroxide. The solution was heated for 1 hr at 50°.

The cobalt complex was weighed from a weighing bottle and added to a known aliquot of the persulfate solution, which had been allowed to reach ambient temperature.

Upon dissolution of the complex, the solution was placed in a constant temperature bath at 50° to initiate the reaction. The initial rate of Co^{II} production was followed by taking aliquots from the solution, chilling, and determining the amount of Co^{II} using the Kitson method.¹² Optical densities were determined with a Cary 14 recording spectrophotometer. In all runs, the sample optical density was corrected by using a Co^{III} ammine blank of appropriate concentration.

The initial rate of the reaction producing reduced cobalt was determined from the slope of the plot Co^{II} vs. time. Rate constants for the process are defined as

$$k = \frac{d[\text{Co}^{\text{II}}]}{dt[\text{S}_2\text{O}_8^{2-}]}$$

Analysis of the Gaseous Products of the Reactions with Persulfate. The reaction vessel consisted of a round-bottomed flask with a constricted neck ending in a standard top joint, and a side arm topped with break-seal. The reaction vessel was cleaned with a warm solution of $\text{Na}_2\text{Cr}_2\text{O}_7$ in concentrated H_2SO_4 and rinsed profusely with quadruply distilled water. The vessel was then filled with a persulfate solution and heated for 6 hr at 50°. The vessel was emptied, a known amount of cobalt complex was added directly from a weighing bottle, and then the persulfate solution of known concentration. The solution was degassed by vacuum techniques, whereupon the vessel was sealed off at the constriction with a torch.

The reaction was initiated by placing the vessel in a bath at 50° and was allowed to proceed for a time varying from 15 to 60 min. The reaction was quenched by freezing the solution in a Dry Ice-acetone bath. The vessel was attached to a vacuum line, the break-seal was opened, and the gas was transferred by means of a Toepler pump through a trap cooled in liquid nitrogen to a gas buret where the amount of gas was measured. The noncondensable gases were transferred to a Urey tube. To collect the condensable gases, Dry Ice-acetone was substituted for liquid nitrogen in the trap.

The gases were analyzed either by means of a mass spectrometer or a gas chromatograph.

Results

$\text{Co}(\text{NH}_3)_5\text{OH}_2^{3+}$. Some experiments were performed to check on the rate law

(13) D. A. Skoog and D. M. West, "Fundamentals of Analytical Chemistry," Holt, Rinehart and Winston, New York, N. Y., 1963, p 457.

(14) R. Robson and H. Taube, *J. Amer. Chem. Soc.*, **89**, 6487 (1967).

(15) A. I. Medalia and B. Byrne, *Anal. Chem.*, **23**, 453 (1951).

(16) E. A. Deutsch, Ph.D. Dissertation, Stanford University, 1967.

(17) See ref 13, p 202.

(18) H. R. Hunt, Ph.D. Dissertation, University of Chicago, 1957.

Table I: Analytical Results on the Products of the Reaction of $\text{Co}(\text{NH}_3)_5\text{OH}_2^{3+}$ with $\text{S}_2\text{O}_8^{2-}$

Expt ^a	$[\text{S}_2\text{O}_8^{2-}]$, <i>M</i>	$[\text{Co}^{\text{III}}]$, 10^3 <i>M</i>	Time, min	μmol of Co^{2+}	μmol of N_2	μmol of N_2O	μmol of CO_2
1	0.15	4.61	60.0	5.40	2.59	0.14	0.02
2	0.30	25.4	60.0	10.90	5.27	0.24	0.04
3	0.73	5.76	16.0	7.21	3.25	0.14	0.05
4	0.73	4.97	15.5	6.75	3.17	0.14	0.02
5	1.03	6.00	15.0	9.18	4.07	0.26	0.26
6	1.03	4.87	15.0	9.24	3.98	0.26	0.26

^a $T = 5^\circ$; pH 3.5; the reaction volume was 10 ml in all cases.

$$\frac{d[\text{Co}^{2+}]}{dt} = k[\text{S}_2\text{O}_8^{2-}]$$

at concentrations of $[\text{S}_2\text{O}_8^{2-}]$ higher than those used by Thusius and Taube.¹ In a series at 50° and pH 3.5 with $[\text{Co}^{\text{III}}] = 4 \times 10^{-3}$ *M* (note that the rate is within 5% of saturation¹ at 1×10^{-3} *M* Co^{III}) and with $[\text{S}_2\text{O}_8^{2-}] = 0.15, 0.15, 0.53,$ and 1.03 *M*, k ($\text{sec}^{-1} \times 10^6$) was found to be 0.99, 1.00, 1.01, and 1.03, respectively. As concluded in the earlier work, any contribution to the reaction in the "saturation" region by a second-order process is small indeed.

An experiment was performed to determine whether significant complexation of Co^{III} by $\text{S}_2\text{O}_8^{2-}$ takes place. A solution containing $\text{Co}(\text{NH}_3)_5\text{OH}_2^{3+}$ (5×10^{-3} *M*) and $\text{K}_2\text{S}_2\text{O}_8$ (0.1 *M*) was heated at 50° for 2 hr and scans of the absorption were made approximately every 15 min. The spectrum did not alter significantly with time, except for the 10–15% decrease resulting from the reduction of Co^{III} . This is not a very sensitive test of complex formation, but the experiment does indicate at least that there is no major complexation of Co^{III} with $\text{S}_2\text{O}_8^{2-}$.

The results of determinations of stoichiometry are shown in Table I, and an analysis of the stoichiometric data appears in Table II.

Table II: Stoichiometric Relations for $\text{Co}(\text{NH}_3)_5\text{OH}_2^{3+} + \text{S}_2\text{O}_8^{2-}$

Expt	$\frac{(\text{N}_2\text{O})}{(\text{N}_2\text{O} + \text{N}_2)}$	$\frac{\text{Co}^{2+\text{obsd}}}{\text{Co}^{2+\text{calcd}}}$	Equip oxid ^a agents consumed, $\times 10^6$	Equip ($\text{N}_2 + \text{N}_2\text{O}$) formed ^b $\times 10^6$
1	0.051	0.94	16.2	16.7
2	0.044	0.94	32.5	33.5
3	0.041	1.02	21.2	20.6
4	0.042	0.98	20.8	20.1
5	0.061	1.00	27.7	26.7
6	0.061	1.04	27.6	26.0

^a $[\text{Co}^{2+}] + 2[\text{S}_2\text{O}_8^{2-}]$ decomposed = equiv $[\text{Co}^{\text{III}}]$ and $[\text{S}_2\text{O}_8^{2-}]$ used. $[\text{S}_2\text{O}_8^{2-}]$ decomposed was calculated using the expression $d[\text{S}_2\text{O}_8^{2-}]/dt = k[\text{S}_2\text{O}_8^{2-}]$ where $k = 1.0 \times 10^{-6}$ sec^{-1} , the value measured in the absence of Co^{III} . ^b $[\mu\text{mol}$ of $\text{N}_2 \times 6 + \mu\text{mol}$ of $\text{N}_2\text{O} \times 8]$ = equiv of $(\text{N}_2\text{O} + \text{N}_2)$ formed.

The second column of Table II shows that the N_2O content is rather invariant to concentration conditions. In the third column are shown values of the ratio $\text{Co}^{2+\text{obsd}}/\text{Co}^{2+\text{calcd}}$ where $\text{Co}^{2+\text{calcd}}$ is obtained on the basis of assuming that 2 mol of Co^{2+} is produced for each mole of N_2 (*cf.* eq 2) and 4 mol for each mol of N_2O (the results are not sensitive to the stoichiometry assumed for this reaction). The entries in column 4 are obtained by calculating the number of equivalents of $\text{S}_2\text{O}_8^{2-}$ which would have decomposed in the absence of Co^{III} and adding to them the number of equivalents of Co^{III} consumed, these together making up the number of equivalents of oxidizing agent consumed. The last column shows the number of equivalents needed to produce the N_2 and N_2O which formed, 6 equiv being required for each mole of the former and 8 each for each mole of the latter.

An experiment was done by letting $[\text{Co}(\text{NH}_3)_5\text{OH}_2]^{3+}$ (10^{-2} *M*) react with $\text{S}_2\text{O}_8^{2-}$ (1 *M*) in H_2^{18}O (1.52 atom% enriched) for 15 min at 53° and pH 3.5. The cobalt complex, persulfate ion, and phosphate were all used at normal levels of enrichment. If there were no induced exchange, the residual aquo complex would have proceeded 18% of the way to isotopic equilibrium with the solvent. The N_2O was found by mass spectrometric measurements to contain 0.72 atom% ^{18}O . Making allowance¹⁹ for the incorporation of ^{18}O into the complex by spontaneous exchange, the result shows that N_2O derived no more than 17% of its oxygen from the solvent. Though there is a possibility that oxygen from $\text{S}_2\text{O}_8^{2-}$ or phosphate appears in the N_2O , it seems a remote one and it will be assumed that the N_2O derives its complement of oxygen of normal isotopic composition from the coordination sphere of the complex.

Two experiments were performed by heating *trans*- $\text{Co}(\text{NH}_3)_5(\text{NH}_3)_4\text{OH}_2^{3+}$ (5×10^{-3} *M*) in $\text{S}_2\text{O}_8^{2-}$ (0.2 *M*) at 50° and 53° for 60 and 100 min, respectively (pH 3.5). In the first experiment the ratios $^{14}\text{N}_2$, $^{14}\text{N}^{15}\text{N}$, $^{15}\text{N}_2$ were determined and were found to be 16:8:1, precisely the value expected for random formation of nitrogen from one part of ^{15}N and four parts of

(19) H. R. Hunt and H. Taube, *J. Amer. Chem. Soc.*, **80**, 2642 (1958).

^{14}N . The CO_2 content of the gas was too high to lead to good values of the isotopic ratios in N_2O . Accordingly, the gas obtained in the second experiment was distilled onto solid NaOH to absorb CO_2 . The ratio $^{14}\text{N}^{14}\text{NO}$, $^{14}\text{N}^{15}\text{NO}$ and $^{15}\text{N}^{14}\text{NO}$, $^{15}\text{N}^{15}\text{NO}$ was found to be 40:11:1. The ^{15}N content is much below that expected for random distribution of the isotopes.

The unreacted complex from the second experiment was precipitated, dissolved in DMSO, and the proton nmr spectrum was taken.⁶ This showed that the $^{15}\text{NH}_3$ was randomly distributed in the complex. A blank experiment was done in which *trans*- $\text{Co}(\text{NH}_3)_4(\text{OH}_2)_2^{3+}$ was heated for 110 min at 53° in a solution at pH 3.5 in the absence of $\text{S}_2\text{O}_8^{2-}$. The proton nmr of the cobalt salt showed that the $^{15}\text{NH}_3$ label was not scrambled in the experiment, and we thus conclude that scrambling is induced by the decomposition of $\text{S}_2\text{O}_8^{2-}$. The blank, incidentally, confirms for rather extreme conditions the conclusion reached by Buckingham, *et al.*,⁶ to wit, that substitution in the pentaammine complex in acidic solution takes place without isomerization.

$\text{Co}(\text{NH}_3)_4(\text{OH}_2)_2^{3+}$. The rate of production of Co^{2+} in the reaction of $\text{Co}(\text{NH}_3)_4(\text{OH}_2)_2^{3+}$ with $\text{S}_2\text{O}_8^{2-}$ follows the pattern found with $\text{Co}(\text{NH}_3)_5\text{OH}_2^{3+}$. At low concentrations of Co^{III} , the rate is sensitive to this variable, but becomes independent of it when $[\text{Co}^{\text{III}}]$ exceeds approximately $4 \times 10^{-3} \text{ M}$. (*cf.* Table III.)

Table III: Rate of Co^{2+} Production for $\text{Co}(\text{NH}_3)_4(\text{OH}_2)_2^{3+} + \text{S}_2\text{O}_8^{2-}$ ^a

$[\text{S}_2\text{O}_8^{2-}]$, <i>M</i>	$[\text{Co}(\text{NH}_3)_4(\text{OH}_2)_2^{3+}]$, $\times 10^4 \text{ M}$	$k^a \times 10^4$, sec^{-1}
0.15	1.0	0.35
0.15	2.0	0.43
0.15	4.0	0.62
0.15	20.0	0.78
0.15	20.0	0.76
0.15	30.0	0.87
0.15	40.0	1.01
0.15	50.0	0.99
0.15	100.0	1.00
0.24	304.0	1.01
0.60	351.8	0.98
1.05	215.0	0.98
1.03	500.0	1.00

^a $T = 50.0^\circ$; pH 3.5; $k = (d[\text{Co}^{2+}]/dt)/[\text{S}_2\text{O}_8^{2-}]$.

The rate of reaction is strictly first order in $[\text{S}_2\text{O}_8^{2-}]$ over the whole range studied.

In Table IV the results of experiments devoted to determining the products of the reaction are summarized.

The stoichiometry was analyzed just as it was for the reaction of $\text{Co}(\text{NH}_3)_5\text{OH}_2^{3+}$ with $\text{S}_2\text{O}_8^{2-}$ and the results

Table IV: Analytical Results on the Products of the Reaction of $[\text{Co}(\text{NH}_3)_4(\text{OH}_2)_2]^{3+}$ with $\text{S}_2\text{O}_8^{2-}$

Expt ^a	$[\text{Co}(\text{NH}_3)_4(\text{OH}_2)_2]^{3+}$, $\times 10^2$, <i>M</i>		μmol Co^{2+}	μmol^b N_2	μmol^b N_2O	μmol^b CO_2
	$[\text{S}_2\text{O}_8^{2-}]$, <i>M</i>	<i>M</i>				
1	0.15	0.45	5.44	2.20	0.57	0.02
2	0.24	5.07	8.60	2.88	0.85	0.03
3	0.24	11.9	8.62	2.63	0.80	0.02
4	0.24	2.45	8.68	2.70	0.90	0.04
5	1.03	2.4	36.5	12.63	2.27	0.10
6	1.03	4.96	24.0	8.28	1.53	0.90

^a $T = 50^\circ$, pH 3.5. ^b In all cases the volume is 10 ml and the time is 60 min, except in number 6 where the time is 40 min.

Table V: Stoichiometric Relations for the Reaction of $\text{Co}(\text{NH}_3)_4(\text{OH}_2)_2^{3+}$ with $\text{S}_2\text{O}_8^{2-}$

Expt	$\frac{\text{N}_2\text{O}}{\text{N}_2\text{O} + \text{N}_2}$	$\frac{\text{Co}^{2+}_{\text{obsd}}}{\text{Co}^{2+}_{\text{calcd}}}$	Equiv oxid agent consumed $\times 10^6$	Equiv ($\text{N}_2 + \text{N}_2\text{O}$) formed $\times 10^6$
2	0.23	0.94	25.9	24.1
3	0.23	0.96	25.9	22.2
4	0.25	0.97	25.9	24.9
5	0.15	1.06	110.5	93.9
6	0.16	1.05	73.4	61.9

are shown in Table V. The columns mean the same as those in Table II.

The ratios in the third column of Table V are calculated on the basis that 2 mol of Co^{2+} are produced for each mole of N_2 and 4 mol for each mole of N_2O . Except for experiment 1, which deviates from the others, the values of $\text{Co}^{2+}_{\text{obsd}}/\text{Co}^{2+}_{\text{calcd}}$ are 1.0 within experimental error. However, the contribution of the reaction producing N_2O is small enough so that when allowance is made for experimental error, the ratio of 4:1 for Co^{2+} to N_2O cannot be taken as proven.

In column 4, the oxidizing agent consumed, as before, is calculated as equal to the number of equivalents of $\text{S}_2\text{O}_8^{2-}$ having decomposed to SO_4^- in the time interval of the experiment, together with the Co^{III} reduced. The entries in column 4 match those in 5 reasonably well. The deviations in experiments 5 and 6 are partly accounted for by the production of CO_2 . That in experiment 1 is again unexplained. The agreement, such as it is, in major part is accounted for by the stoichiometry of the reaction producing N_2 and again, the results are not a sensitive test of the stoichiometry proposed for the production of N_2O .

$\text{Co}(\text{NH}_3)_2(\text{OH}_2)_4^{3+}$. Two experiments were done with $\text{Co}(\text{NH}_3)_2(\text{OH}_2)_4$ and $\text{S}_2\text{O}_8^{2-}$. The results of Table VI show a striking change in stoichiometry compared to the higher amines. Oxygen now accounts

Table VI: Product Analyses for $[\text{Co}(\text{NH}_3)_2(\text{OH}_2)_4]^{3+} + \text{S}_2\text{O}_8^{2-}$ ^a

$\mu\text{mol of Co}^{2+}$	$\mu\text{mol of O}_2$	$\mu\text{mol of CO}_2$	$\text{S}_2\text{O}_8^{2-}$ ^b con- sumed	Equip of (Co^{III} + $\text{S}_2\text{O}_8^{2-}$) reduced $\times 10^6$	Equip of O_2 formed $\times 10^6$
5.92	4.12	0.09	5.4	16.7	16.5
5.60	4.12	0.09	5.4	16.5	16.5

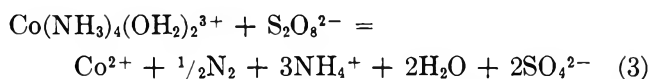
^a $T = 50^\circ$, pH 3.5, $[\text{S}_2\text{O}_8^{2-}] = 0.15 M$, $[\text{Co}^{\text{III}}] = 4.26 \times 10^{-2} M$, time = 60 min, vol = 10 ml. ^b Calcd from rate of spontaneous decomposition.

for 97% of the gaseous products, and N_2 and N_2O are each less than 1% of the gas.

Oxidation-reduction balance is quite satisfactory, again on the basis that reaction 1 governs the extent of reaction. Approximately 1 mol of Co^{2+} is formed for each mole of $\text{S}_2\text{O}_8^{2-}$ which disappears.

Discussion

The results we have obtained confirm¹ the stoichiometry as expressed by eq 2 for the production of N_2 from $\text{Co}(\text{NH}_3)_5\text{OH}_2^{3+}$. Because the production of N_2 is the major net reaction at rate "saturation" also for the tetraammine, we can conclude that in this case as well the ratio of Co^{III} consumed to $\text{S}_2\text{O}_8^{2-}$ consumed to N_2 produced is 2:2:1, the equation for the net change then being



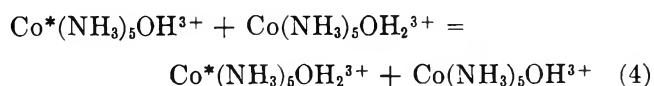
The point needs perhaps to be emphasized again¹ that the rate of production of Co^{2+} at saturation is precisely $\frac{1}{2}$ the rate of SO_4^- production as measured by the rate of decomposition of $\text{S}_2\text{O}_8^{2-}$ in the absence of Co^{III} . Thus, the total oxidizing capacity is accounted for by the total rate of SO_4^- production, measured as above, together with the Co^{III} consumed. It follows, then, that unless some oxidation products are left unaccounted for, only the $\text{S}_2\text{O}_8^{2-}$ which decomposes to SO_4^- is implicated in the net change. This, in turn, means that no reactant (say Co^{III}), no product (say Co^{2+}), and no intermediate attacks $\text{S}_2\text{O}_8^{2-}$ to bring more into reaction than corresponds to the rate of spontaneous decomposition.

Turning now to a consideration of the mechanism of the reactions, we leave aside for the time being the question of the identity of the radical, be it HO or SO_4^- , which attacks Co^{III} . For the immediate discussion we need only assume that a powerful $1e^-$ oxidant is present, capable of oxidizing Co^{III} to Co^{IV} . The earlier work¹ indicates that the attack by the intermediate on Co^{III} involves, in effect, the removal of a hydrogen atom from a water molecule in the coordination sphere of the complex and from coordinated ammonia when no water molecules are present. Unless the immediate cobalt-

containing product is decomposed instantly, and evidence to be presented suggests that it does not do so, the process is equivalent to generating Co^{IV} in the complex ion. The chemistry of the various reactions which have been encountered will be considered in terms of reactions of Co^{IV} .

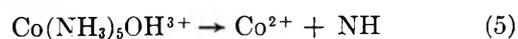
To explain the $6e^-$ oxidation of NH_3 to N_2 , a consideration of the constraints which govern the reactions of these intermediates with other substances present in the system is in order. The point has already been made that the intermediates do not attack $\text{S}_2\text{O}_8^{2-}$; if they did, more $\text{S}_2\text{O}_8^{2-}$ would be brought into reaction than corresponds to process 1. Owing to the high reactivity of SO_4^- or HO , these species at saturation are kept at very low concentration, and their reactions with nitrogen or oxygen-containing intermediates are extremely improbable. The two oxidants which it will be necessary to consider as candidates for the oxidation of N or O intermediates are Co^{III} and Co^{IV} , the former favored because of its higher concentration and the latter because of its very much higher reactivity. As will be shown, the stoichiometry in each case demands that Co^{IV} rather than Co^{III} be the intermediate active in oxidizing the nitrogen and oxygen-containing intermediates to stable products.

To understand the stoichiometry, it will be necessary to assume that Co^{IV} is present at significant concentrations, (high enough, that is, to oxidize intermediate nitrogen radicals) and thus that it has a moderately long lifetime. Other evidence for the conclusion is provided by the experiments on the redistribution of $^{15}\text{NH}_3$ between cis and trans positions in $\text{Co}(\text{NH}_3)_5\text{OH}_2^{3+}$. The decomposition of $\text{S}_2\text{O}_8^{2-}$ has been shown to accelerate the reaction enormously. This effect can be understood if it be supposed that the isomerization takes place readily in the Co^{IV} complex, and if, moreover, electron transfer between Co^{III} and Co^{IV} takes place.



If reaction 4 occurs, each Co^{IV} during its lifetime can bring about isomerization within a large number of molecules of the Co^{III} complex.

The significance of the experiment using *trans*- $[\text{Co}(^{15}\text{NH}_3)(\text{NH}_3)_4\text{OH}_2]^{3+}$ in diagnosing the mechanism of N_2 formation is to some extent vitiated by the induced isomerization within the molecule. But one important conclusion can still be drawn. Since each molecule of the complex contains only one $^{15}\text{NH}_3$, the fact that $^{15}\text{N}^{15}\text{N}$ is formed in statistical proportions shows that N-N bond formation is an inter-, rather than an intramolecular process. We concur with Thusius, *et al.*,¹ in assuming that NH is produced by decomposition of the Co^{IV} complex



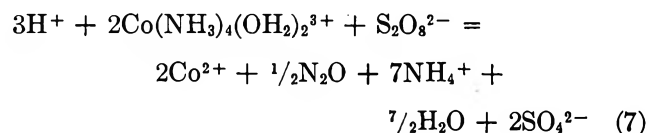
(Only the products of changes in oxidation state are shown.) In view of the fact that the isotopic composition of the N_2O shows that isomerization of the complex is not instantaneous, we must assume that there is virtually no discrimination between *cis* and *trans* positions in oxidizing coordinated NH_3 to NH , or that there is randomization in solution by a process such as $*NH + NH_4^+ = NH + *NH_4^+$. The stoichiometry is accounted for if Co^{IV} oxidizes NH to N_2 , it being thereby reduced to $Co(NH_3)_5OH_2^{3+}$



but is violated if NH reduces Co^{III} , or if Co^{IV} is reduced to Co^{II} . Reaction 6 as written has only stoichiometric, not mechanistic, significance (it is possible, for example, that NH produces N_2H_2 before it is oxidized).

The experimental basis for imposing the constraint that the nitrogen intermediates do not attack $S_2O_8^{2-}$ has already been emphasized, but having suggested NH as an intermediate, we are obliged to ask whether it is reasonable that this species seek out Co^{IV} in preference to $S_2O_8^{2-}$, though the latter is present at much higher concentrations. Not enough is known about the chemistry of NH to support a critical evaluation of the ad hoc assumption pertaining to the reactivity of the species toward Co^{IV} and $S_2O_8^{2-}$. It is perhaps worth pointing out, however, that if NH is taken to be in a triplet rather than singlet state, the assumption that it is relatively unreactive to $S_2O_8^{2-}$ does not appear to be as alarming as would otherwise be the case.

The stoichiometric results obtained on the production of N_2O are not nearly as clear cut as those for the production of N_2 . For the pentaammine, the extent of the reaction producing N_2O is so small that the data provide no test of stoichiometry. Even for the tetraammine, there are, as we shall see, difficulties in deciding upon the stoichiometry. The experimental results were examined on the assumption that four Co^{2+} are produced for each N_2O . The product ratio 4:1 under the proviso that $S_2O_8^{2-}$ is the only oxidant in addition to Co^{III} and that the only redox products are Co^{2+} , SO_4^{2-} , and N_2O would require the stoichiometry expressed by eq 7 for the reaction with $Co(NH_3)_4(OH_2)_2^{3+}$



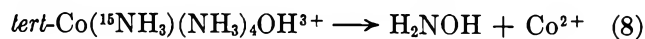
The stoichiometry expressed by equation 7, however, is not compatible with the rate data shown in Table III. Even were $S_2O_8^{2-}$ consumed in the reaction only at the rate corresponding to the spontaneous decomposition, since two Co^{III} are reduced for each $S_2O_8^{2-}$ which reacts, the specific rate of Co^{2+} production at saturation should be *ca.* $1.2 \times 10^{-6} \text{ sec}^{-1}$, whereas only $1.0 \times 10^{-6} \text{ sec}^{-1}$ is recorded.

Of the two kinds of data, stoichiometric and kinetic,

the former seem the less dependable. This appraisal is strengthened by the fact that experiment 1 of Table V, which as has already been noted, deviates from the others, is nicely compatible with a ratio of $2Co^{2+}/N_2O$, and thus with the rate data. It seems likely that the products of reaction are not fully accounted for and, moreover, that the additional reaction paths are not reproducible from experiment to experiment. Further experiments are called for searching for NO_2^- and NO_3^- among the reaction products.

Even with the important matter of stoichiometry left in an unsatisfactory state, some rather definite conclusions about mechanism can be reached. The isotopic experiments show that the bulk of the oxygen in N_2O is derived from the coordination sphere of the complex, and that there is a preference for nitrogen in NH_3 *cis* to H_2O in the complex to be converted to N_2O . The calculation for the oxygen tracer experiment was made on the assumption that water exchange between the complex and solvent is not accelerated when $S_2O_8^{2-}$ is present, but in view of the induced redistribution of NH_3 in the coordination sphere, it is likely that oxygen is also induced. Any such additional exchange would mean that the actual extent of complex-oxygen incorporation exceeds that calculated. Since isomerization is known to take place, the actual preference for *cis*- NH_3 in forming N_2O also exceeds that calculated. The fact that there is any preference shows that the redistribution of NH_3 was not complete by the time a substantial amount of N_2O was formed.

Since the nitrogen isotopic distribution in N_2O is different from that in N_2 , we conclude that NH is not an intermediate in forming N_2O . (NH might be assumed, for example, to attack water in the coordination sphere of the complex). A reaction which is consistent with all the evidence is the following



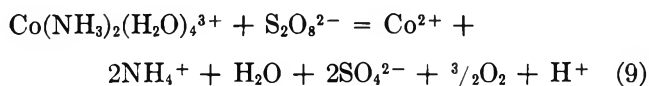
where eq 8 expresses the observed preference for *cis*- NH_3 on N_2O and, as before, it is assumed that Co^{IV} is formed by the attack of SO_4^- on Co^{III} . However, if the stoichiometry embodied in reaction 7 is not insisted upon, the stringent requirement that only Co^{IV} oxidize the intermediates is relaxed. If, in fact, two rather than four Co^{2+} are produced for each N_2O , NH_2OH can be taken as being oxidized to NH_2OH by $S_2O_8^{2-}$, and the rate data are now compatible with the stoichiometric data.

Reaction 8 assumes intramolecular bond formation between N and O, and as the reverse of oxidative addition can be called reductive elimination.²⁰ What the spin state of the cobalt is just prior to the bond rearrangement is a matter of some interest. It cannot be taken for granted that Co^{IV} remains in a low-spin con-

(20) It is likely that bond formation between O and N is preceded by dissociation of a proton from NH_3 . This process is probably facile in the Co^{IV} complex by virtue of the high charge on the metal ion.

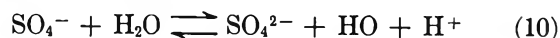
figuration. The induced isomerization in $\text{Co}(\text{NH}_3)_6\text{OH}_2^{3+}$ indicates an unusual lability for the species and therefore that a high spin state is close in energy to the presumed low spin ground state.

When $\text{Co}(\text{NH}_3)_2(\text{OH}_2)_4^{3+}$ is acted upon by the radical products of the decomposition of $\text{S}_2\text{O}_8^{2-}$, there is again good balance between the number of oxidizing equivalents ($\text{Co}^{\text{III}} + \text{SO}_4^-$ produced by spontaneous decomposition of $\text{S}_2\text{O}_8^{2-}$) and the equivalents of oxidized product formed by O_2 . The induction factor given by the ratio $\text{Co}^{2+}/\text{S}_2\text{O}_8^{2-}$ is found to be 1.1 in one of the experiments and 1.0 in the other. If we take the factor to be 1.0, the equation expressing the net change takes the form



It is tempting to ascribe the abrupt change in stoichiometry which occurs in changing from the tetraammine to the diammine as substrate to NH_3 being lost from Co^{IV} diammine species before NH_3 can be produced or an N-O bond can be formed. Ammonia as the stronger field ligand is expected to stabilize a low-spin state more than does water, and it would not be surprising to find the high-spin state to be the ground state of Co^{IV} when only two ammonia molecules are left in the coordination sphere. Though these ideas seem reasonable, we have difficulty incorporating them into a mechanism which reproduces the stoichiometry of reaction 7. Each SO_4^- produced from $\text{S}_2\text{O}_8^{2-}$ at saturation will produce one Co^{IV} . If each Co^{IV} immediately loses NH_3 , it is at once fated to become Co^{2+} (Co^{3+} aqueous, it should be noted, is unstable under the experimental conditions), and thus the induction factor would be 2.0. We have not found it possible to devise a simple, reasonable mechanism consistent with the induction factor of 1.0. An induction factor of 1.0 requires precisely $\frac{1}{2}$ of the Co^{IV} to be reduced to Co^{2+} and the other $\frac{1}{2}$ to reappear as a Co^{III} ammine com-

plex. More work will need to be done varying the conditions to see if the induction factor is invariant, and moreover, to check into the possibility that triamminecobalt(III) or tetraamminecobalt(III) complexes form. There having been at the time no dependable estimate of the rate at which equilibrium represented by eq 10 is established



Thusius, *et al.*,¹ arbitrarily assumed that equilibrium was maintained, and since $[\text{H}^+]$ and $[\text{SO}_4^{2-}]$ were both low in their experiments, took HO to be the species which attacks the Co^{III} complex. The specific rate of reaction 10 in the forward direction has been estimated by Pennington and Haim²¹ as about 10^3 to 10^4 sec^{-1} . Since the specific rate for the reaction of SO_4^- with the cobaltammines is not known, even with a value for the rate of reaction 10 on hand, it is impossible to decide whether HO or SO_4^- attacks the complex. At sufficiently high Co^{III} , SO_4^- will certainly be scavenged before it can react with water. If we assume that already at the outset of the saturation region SO_4^- reacts with Co^{III} before producing HO, the data call for a specific rate of the order 10^6 to $10^7 \text{ M}^{-1} \text{ sec}^{-1}$ for the reaction of SO_4^- with a cobaltamine.

As mentioned before, if the intermediate is completely scavenged by Co^{III} , it is irrelevant, for the purposes of stoichiometry, whether the intermediate is HO or SO_4^- , but the point is itself of some interest and will be worth investigating. Careful studies of the stoichiometry and kinetics in the concentration region short of saturation can help to settle the manner and can serve as a check on some of the proposals of mechanism made here.

Acknowledgment. Financial support for this research by the Atomic Energy Commission, Grant AT 04 3 325, PA 6, is gratefully acknowledged.

(21) D. E. Pennington and A. Haim, *J. Amer. Chem. Soc.*, **90**, 3700 (1968).

Chemisorption of Hydrogen and Ethylene and Hydrogenation of Ethylene on Zinc Oxide

by D. Narayana, Jagdish Lal, and V. Kesavulu*

Regional Research Laboratory, Hyderabad-9, India (Received September 4, 1968)

The catalytic activity of zinc oxide for hydrogenation of ethylene can be enhanced by treatment with hydrogen above 300°. The activity of the oxide for hydrogenation is closely related to its activity for type A chemisorption of hydrogen. This form of hydrogen chemisorption causes a slight decrease in the conductivity of the oxide and appears to be covalently bound to the surface sites. The ionic form of hydrogen chemisorption which accompanies the type A chemisorption at 60° does not take part in the hydrogenation reaction. Below about 100°, ethylene adsorption leads to a slight decrease in the conductivity of the oxide, while at higher temperatures the conductivity increases. At 60°, three forms of ethylene adsorption on zinc oxide can be distinguished. The first type which leads to a decrease in the conductivity of the oxide appears to be the active form taking part in the hydrogenation reaction. The second type which increases conductivity is slow and irreversible and is not participating in the reaction at 60°. The third form which has no effect on the conductivity of the oxide appears to be physically adsorbed. The surface defects in the form of excess zinc atoms produced by activation are considered to be the sites at which the type A chemisorption of hydrogen, the associative chemisorption of ethylene, and the hydrogenation of ethylene take place.

Introduction

It has been shown¹⁻³ that hydrogen chemisorption on zinc oxide is a complex process leading to simultaneous formation of more than one chemisorbed species on the surface. Ethylene chemisorption on metals⁴ and on alumina⁵ occurs both in "associative" and in "dissociative" forms. It is likely that ethylene on zinc oxide also gives rise to these two forms of chemisorption. In the present study an attempt is made to distinguish the different forms of hydrogen and ethylene chemisorptions and to determine the active forms responsible for hydrogenation of ethylene on zinc oxide. Chemisorption and hydrogenation studies are combined with the measurement of conductivity changes in the solid.

It has been suggested¹ that the sites active in the type A chemisorption of hydrogen on zinc oxide are also responsible for the catalytic activity of the oxide for hydrogenation reactions. That the catalytic activity of zinc oxide for the H₂-D₂ exchange reaction is closely related to its activity for the type A chemisorption of hydrogen has been shown. Whether a similar connection exists between this form of hydrogen chemisorption and other hydrogenation reactions on the oxide is not known. This point needs to be examined. In this connection, it may be noted that, though both hydrogen chemisorption and the H₂-D₂ exchange reaction on zinc oxide are affected by doping the oxide with mono- and trivalent metals,^{6,7} a similar doping has no effect on the rate of the C₂H₄ + H₂ = C₂H₆ reaction catalyzed by zinc oxide at 150°.⁸

Experimental Section

Chemisorption and conductivity changes were measured on a sample of zinc oxide powder (5.773 g) pre-

pared by heating zinc oxalate in a current of dry oxygen at 420°. The experimental setup and the cell used for simultaneous measurement of chemisorption and conductivity have been described elsewhere.³ The pressure changes during chemisorption were followed with a dibutyl phthalate manometer. Conductivity was measured using an a.c. bridge with a precision of 1% in the range 1 ohm to 1 megohm at 10 kHz. A Pt-13% Rh-Pt thermocouple was used to measure temperature.

Kinetic studies of the hydrogenation reaction were carried out in a separate apparatus which included arrangements for preheating and circulating the reaction mixture. A 1.54-g sample of the catalyst was used. The rate of the reaction was followed by measuring pressure changes on a mercury manometer, and the products were analyzed with a gas chromatograph.

Ethylene, prepared by dehydrating alcohol over alumina, was purified by distillation at -130° and by repeated freezing and evacuation. Hydrogen and helium were purified as indicated earlier.³

* To whom correspondence should be addressed.

- (1) V. Kesavulu and H. A. Taylor, *J. Phys. Chem.*, **64**, 1124 (1960).
- (2) R. P. Eischens, W. A. Pliskin, and M. J. D. Low, *J. Catal.*, **1**, 180 (1962).
- (3) D. Narayana, V. S. Subrahmanyam, J. Lal, M. Mahmood Ali, and V. Kesavulu, *J. Phys. Chem.*, **74**, 779 (1970).
- (4) R. P. Eischens and W. A. Pliskin, *Advan. Catal.*, **10**, 1 (1958).
- (5) J. L. Carter, P. J. Lucchesi, J. H. Sinfelt, and D. J. C. Yates, *Proc. Third Intern. Congr. Catalysis, Amsterdam*, **1**, 644 (1964).
- (6) A. Cimino, E. Cipollini, and E. Molinari, *Naturwissenschaften*, **43**, 58 (1956).
- (7) E. Molinari and G. Parravano, *J. Amer. Chem. Soc.*, **75**, 5233 (1953).
- (8) J. Aigueperse and S. J. Teichner, *J. Catal.*, **2**, 359 (1963).

Results

Preliminary Experiments. Adsorption isobars for hydrogen on zinc oxide have two well-defined maxima, one at 50° (type A) and another at 230° (type B). If type A chemisorption of hydrogen is responsible for hydrogenation on zinc oxide as suggested earlier,¹ then ethylene-hydrogen reaction should take place at temperatures at which type A chemisorption occurs rapidly. A few test runs made to check this revealed that zinc oxide can catalyze the reaction even at room temperature. Gas chromatographic analysis showed ethane to be the only product, and the amounts of ethane formed corresponded to those deduced from the pressure changes. Since type A chemisorption of hydrogen occurs rapidly and reversibly above 50°, most of the kinetic runs of the hydrogenation reaction were carried out above this temperature. Runs made at 60° showed that the reaction follows first-order kinetics both with respect to hydrogen and with respect to ethylene.

Since the capacity of zinc oxide for type A chemisorption can be enhanced¹ by heating the oxide in hydrogen and evacuating above 300°, a few runs were made with a fresh sample (1.54 g) to see how the variation in type A activity of zinc oxide affects the hydrogenation reaction. Figure 1 gives pressure as a function of time for three kinetic runs at 60° with stoichiometric mixtures of ethylene and hydrogen (32.2 mm each). These runs were preceded by hydrogen treatment and evacuation at 340° and followed by chemisorption measurements at 50° (type A) and at 230° (type B). The chemisorption measurements were made by first measuring the amount of hydrogen adsorbed in 1 hr at 50° and then raising the temperature to 230° and noting the amount adsorbed at this temperature after 1 hr. The initial pressure in all the

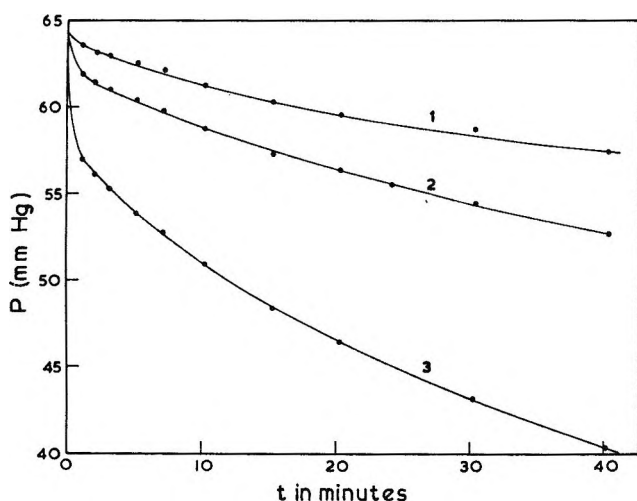


Figure 1. Kinetics of the ethylene-hydrogen reaction on zinc oxide at 60° at three different type A activities.

tion of time for three kinetic runs at 60° with stoichiometric mixtures of ethylene and hydrogen (32.2 mm each). These runs were preceded by hydrogen treatment and evacuation at 340° and followed by chemisorption measurements at 50° (type A) and at 230° (type B). The chemisorption measurements were made by first measuring the amount of hydrogen adsorbed in 1 hr at 50° and then raising the temperature to 230° and noting the amount adsorbed at this temperature after 1 hr. The initial pressure in all the

Table I

	—Hydrogen chemisorption—		Ethylene-hydrogen reaction Initial rate, mm/min
	Type A, ml (STP)	Type B, ml (STP)	
1.	0.02	0.12	0.34
2.	0.05	...	0.43
3.	0.17	0.10	0.90

chemisorption experiments was 20.12 mm. The volumes of hydrogen adsorbed along with the initial rates of the ethylene-hydrogen reaction are given in Table I. In the second chemisorption experiment, while heating, the temperature of the catalyst went above 230°, and so the quantity adsorbed as type B was not measured.

These results confirm that the hydrogenation activity of zinc oxide is closely related to its activity for type A chemisorption of hydrogen. There is hardly any change in the type B chemisorption as has been noted earlier.¹

Hydrogen Chemisorption. The chemisorption experiments were carried out after activating the oxide (5.773 g) by repeated treatment with hydrogen and evacuation at 340°. Between experiments the oxide was evacuated for 4 hr at 340°. Figure 2 shows the pressure dependence of conductivity and chemisorption of hydrogen at 60°. The results are similar to those found at 50°³ except that the irreversible part of the chemisorption is slightly more than that at 50°. Chemisorption of hydrogen is accompanied by a slow increase in conductivity. This conductivity change is irreversible. It is not affected by desorption of hydrogen. Even evacuation for 0.5 hr at 60° does not diminish the conductivity. The irreversible part of the chemisorption responsible for the conductivity change is the ionic form which appears to be the same as the

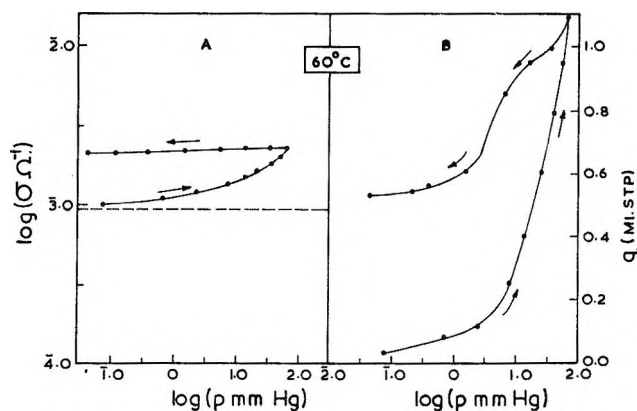


Figure 2. Pressure dependence of conductivity (A) and hydrogen chemisorption (B) on zinc oxide at 60°. The broken line in A represents the conductivity of the oxide before chemisorption.

ir-inactive slow chemisorption⁹ observed by Eischens and coworkers at room temperature. In the present study it has been noted that the ionic form of hydrogen chemisorption occurs to a considerable extent at room temperature and that its amount increases slowly with time.

The reversible part of the chemisorption at 60° corresponding to type A appears to be covalently bound to the surface sites. Since this chemisorption is accompanied by the ionic form which causes an increase in conductivity, it would be difficult to detect any conductivity change caused by type A alone. The previous results¹ on chemisorption kinetics showed that type A chemisorption occurs even at -78°. Since the ionic form of hydrogen chemisorption decreases with decreasing temperature, chemisorption and conductivity measurements at -78° may show the effect due to type A. Figure 3 shows the pressure dependence of conductivity at -78°. Hydrogen chemisorption causes a decrease in the conductivity of the oxide. The points for decreasing pressures do not represent equilibrium values. Only 10 min was allowed for each point. On evacuating for 15 min, the conductivity returns to the base value, showing that the chemisorption is reversible.

Ethylene Chemisorption. In the experiments on ethylene chemisorption and hydrogenation of ethylene, the oxide was subjected to a standard pretreatment of heating in hydrogen (100 mm) for 0.5 hr and evacuating for 4 hr at 340°. This treatment was found to be sufficient to restore the activity of the oxide fully.

Large amounts of ethylene are adsorbed rapidly at room temperature, and this decreases with increasing temperature. Below about 100° ethylene chemisorption leads to a slight decrease in the conductivity of the oxide, while at higher temperatures the conductiv-

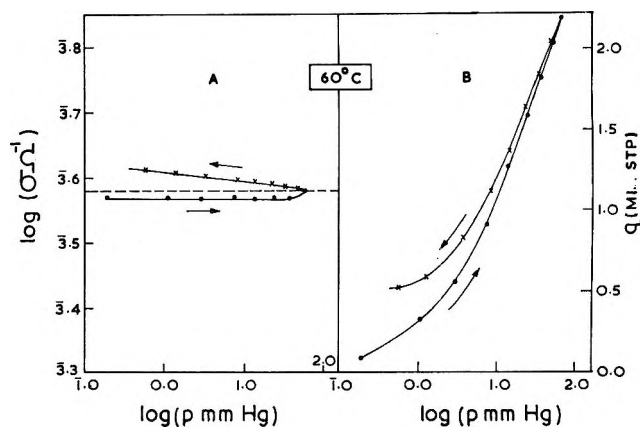


Figure 4. Pressure dependence of conductivity (A) and ethylene chemisorption (B) on zinc oxide at 60°. The broken line in A represents the conductivity of the oxide before chemisorption.

ity increases. The kinetics of ethylene adsorption is characterized by rapid initial adsorption followed by a slow adsorption. At lower temperatures the slow process is negligible, while at higher temperatures it becomes appreciable. Thus at 30°, 99% of the adsorption is over within the first minute, while at 200° only 30% of the total quantity is adsorbed in the first minute.

Figure 4 shows the pressure dependence of conductivity and chemisorption of ethylene at 60°. The broken line in Figure 4A represents initial conductivity of the oxide before chemisorption. Most of the conductivity drop has taken place with the very first addition ($q_{\text{ads}} = 0.10 \text{ ml}$). Further adsorption produces no change in conductivity. Toward the end of adsorption and during desorption conductivity change occurs in the opposite direction. On evacuating, conductivity does not return to its base value. This shows that the adsorption responsible for the conductivity increase is irreversible. If now fresh ethylene is introduced into the cell, the conductivity drops again, and the magnitude of the drop from the new base conductivity is exactly equal to the original drop. On evacuating immediately, the conductivity returns to the new base value. These facts show that there are at least three types of ethylene adsorption at 60°. The first leading to a decrease in conductivity is fast and reversible, the second causing conductivity increase is slow and irreversible, and the third which forms the bulk of the adsorption is fast and reversible and has no effect on the conductivity.

Ethylene-Hydrogen Interaction. If zinc oxide is allowed to chemisorb hydrogen at 230° and then cooled

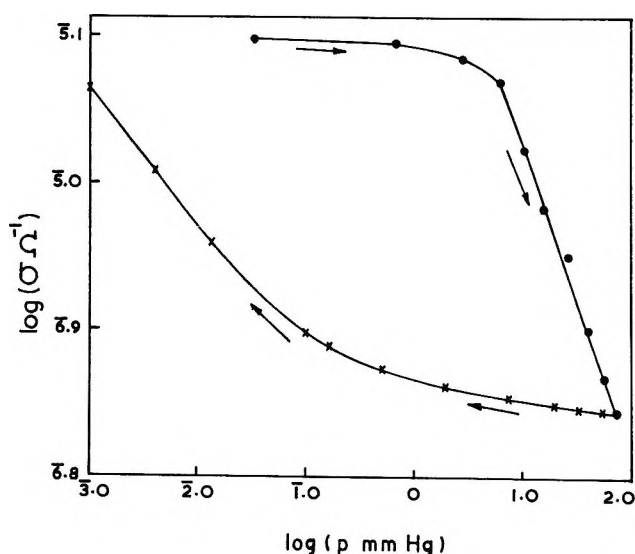


Figure 3. Pressure dependence of conductivity for hydrogen chemisorption at -78°.

(9) Eischens, *et al.*,² attributed the ir-inactive slow chemisorption to the formation of H^+ ions on the surface. A similar conclusion has been reached by us also.³ However, since they assumed that there is no increase in the conductivity of the oxide, Eischens and coworkers had to postulate a trapping mechanism for the conduction electrons. The results presented here and in ref 3 show that there is no need for assuming such a mechanism.

to 60° without evacuating the gas, the enhanced conductivity produced by the ionic form remains. On evacuating the gas at 60°, the amount chemisorbed as type A is removed while practically all of the ionic form of hydrogen remains on the surface along with the enhanced conductivity. If ethylene is now introduced, a slight decrease in conductivity occurs as would happen on a bare surface. This shows that the part of ethylene chemisorption responsible for the decrease in conductivity is not affected by the presence of ionic hydrogen on the surface. On evacuation, the conductivity increases again and reaches a value close to that prevailing before the introduction of ethylene. This indicates that there is little interaction between ionic hydrogen and ethylene. This may be contrasted with the behavior of oxygen toward the ionic form of hydrogen. If oxygen is introduced instead of ethylene, the conductivity due to ionic hydrogen is destroyed immediately and cannot be recovered by evacuation.

In Figure 5 are summarized the results of three experiments on the interaction of adsorbed ethylene and hydrogen at 60°. First hydrogen ($P_0 = 22.60$ mm) was introduced into the cell, and the chemisorption and conductivity changes were followed for 100 min. Then ethylene ($P_0 = 19.20$ mm) was introduced on the top of hydrogen, and the measurement of pressure and conductivity changes was continued. In the second experiment, the order of introducing the gases was reversed keeping the initial partial pressures the same as in the first. Since the adsorption equilibrium for ethylene is reached rapidly, hydrogen was introduced after 20 min instead of after 100 min. In the third experiment, a mixture of the two gases (in the same volume ratio) was introduced. The results show that, irrespective of whether the surface is bare or is covered with adsorbed ethylene or hydrogen, the same kinetics is observed for the ethylene-hydrogen reaction. Preadsorbed ethylene

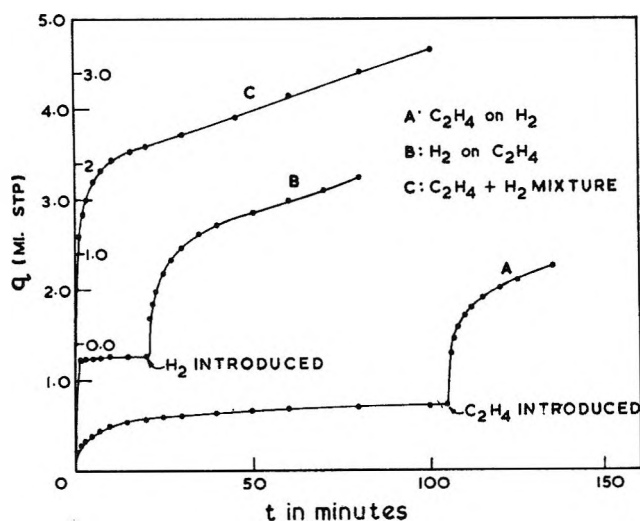


Figure 5. Interaction between ethylene and hydrogen at the zinc oxide surface at 60°. The zero of curve C is shifted up, and the scale is shown inside the figure.

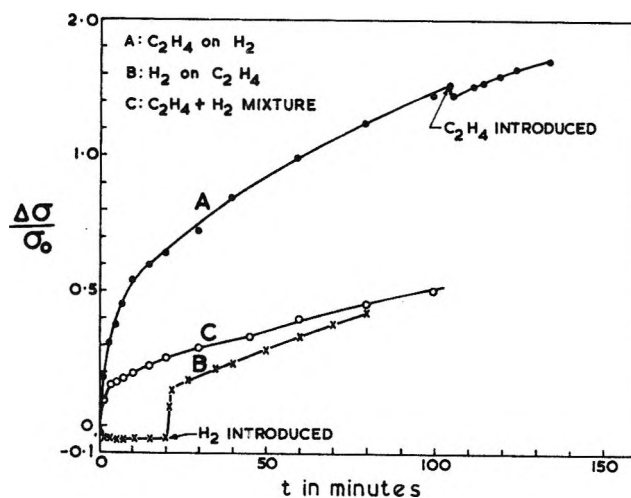


Figure 6. Conductivity changes in zinc oxide produced by ethylene and hydrogen and their interaction at 60°. These measurements were carried out during the experiments reported in Figure 5.

does not act as a poison. It may be noted that, under the conditions employed here, the "dissociative" form of ethylene chemisorption would be negligible. Preadsorbed hydrogen also does not enhance the rate of the reaction. This is in agreement with the results of the kinetic studies carried out before and after covering the surface with ionic hydrogen; the rate of the reaction is unaltered. Initial rates obtained from the curves in Figure 5 give the same value for all the three cases, which is close to 6.0×10^{18} molecules/min. The initial rates were obtained by extrapolating to zero time the rates obtained after the first minute.

Figure 6 shows the conductivity changes observed in the above three experiments. It is seen that the presence of the ionic form of hydrogen does not affect the associative chemisorption of ethylene which leads to a slight decrease in conductivity (curve A), whereas the ionic form of hydrogen chemisorption is hindered by the presence of adsorbed ethylene (curves B and C).

Discussion

The Nature of the Active Sites. It has been shown that zinc oxide has to be activated by treatment with hydrogen at elevated temperatures for developing the activity for type A chemisorption of hydrogen,¹ for H_2 - D_2 exchange reaction,⁷ and for hydrogenation of ethylene (Figure 1). It is obvious that the active sites responsible for these catalytic processes are not present initially, but are generated during activation. That hydrogen causes a chemical reduction of the surface layers of the oxide under the conditions of activation has been noted.^{1,10} Removal of oxygen atoms from the basal planes of the oxide crystallites would leave zinc atoms in their lattice positions on the surface. It has been

(10) D. G. Thomas and J. J. Lander, *J. Phys. Chem. Solids*, 2, 318 (1957).

shown that these excess zinc atoms act as surface donors causing enhanced conductivity³ as do adsorbed zinc atoms on zinc oxide.¹⁰ The following equilibrium may, therefore, be expected at the surface of an activated oxide



It is likely that the surface defects in the form of excess Zn or Zn⁺ are responsible for the catalytic property of the oxide. That the free electrons do not play any significant role in the catalytic activity of the oxide is indicated by the fact that altering the conductivity of the oxide by doping with mono- and trivalent metals⁸ and by hydrogen chemisorption (ionic form) is without effect on the catalytic activity of the oxide. Surface Zn²⁺ and O²⁻ ions of the lattice have been proposed¹¹ as possible sites for hydrogen chemisorption. This is unlikely since the unactivated surface (presumably stoichiometric) is inactive. Further, because of its d¹⁰ configuration, Zn²⁺ is not likely to be catalytically active. Kemball¹² has shown that zinc films have no catalytic activity toward the NH₃-D₂ exchange reaction.

Hydrogen Chemisorption. The catalytically active type A chemisorption of hydrogen occurs rapidly and reversibly in the low-temperature region, and above 50° its amount decreases. At -78°, it appears to form a stable covalent complex with the surface sites. The slight negative conductivity effect produced by hydrogen chemisorption at -78° suggests that the active sites are probably Zn atoms. In such a case, the equilibrium 1 would be shifted to the left causing a decrease in the free electron density. At higher temperatures, the Zn(H₂) complex would become unstable and lead to the rupture of the Zn-H bonds facilitating the migration of the H atoms to other sites to give rise to ionic chemisorption or desorption.

In the infrared spectrum of hydrogen chemisorbed on zinc oxide at 30°, Eischens, *et al.*,² have observed two bands at 2.86 and 5.85 μ which they have attributed to O-H and Zn-H vibrations, respectively. It has been seen that both type A and ionic forms of hydrogen chemisorption occur at this temperature. It is likely that type A passes through other intermediate stages before giving rise to the ionic form. It would be, therefore, interesting to study the ir spectrum at -78° at which temperature a stable Zn(H₂) complex appears to be formed. A knowledge of the spectrum at -78° and its variation with temperature should be helpful in determining the structure of the complex and the changes which make it unstable and reactive.

Ethylene Chemisorption. There are at least three types of ethylene adsorption at 60°. The first which occurs rapidly and reversibly and produces a decrease in the conductivity of the oxide probably occurs as "associative" chemisorption on the same Zn sites and pro-

vides the surface species responsible for the hydrogenation reaction. The second which occurs slowly and irreversibly and produces a positive effect on conductivity appears to be "dissociative" chemisorption and does not contribute to the reaction as happens on alumina.⁵ The third which forms the bulk of the adsorption at 60° is fast, reversible, and has no effect on conductivity. This appears to be physical adsorption. It may be assumed that the associatively chemisorbed ethylene is in rapid equilibrium with the physically adsorbed form.

Ethylene-Hydrogen Reaction. The fact that the same rate for the reaction is observed whether the surface is bare or is covered with chemisorbed ethylene or hydrogen shows that the slow chemisorptions of ethylene and hydrogen are not involved in the reaction. Since the associative chemisorption of ethylene is not affected by the presence of ionic hydrogen (Figure 6), it may be inferred that the sites on which this type of ethylene chemisorption takes place are different from those involved in the ionic form of hydrogen. The slight negative effect on conductivity produced by ethylene suggests that the sites are probably Zn atoms. It may also be noted that the presence of chemisorbed ethylene interferes with the ionic form of hydrogen chemisorption. This is understandable since, for the ionic chemisorption, H atoms from Zn sites are required¹³ and these sites are engaged in ethylene and hydrogen chemisorptions (associative and type A), and the hydrogen from the sites is used up in the hydrogenation reaction. The assumption of competitive adsorption of ethylene and hydrogen on the same kind of sites is also in accordance with the observed kinetics of the reaction.

Acknowledgment. D. N. and J. L. are thankful to the Council of Scientific and Industrial Research, New Delhi, for awarding junior and senior research fellowships.

Addendum: Comments on the Papers of Dent and Kokes

Recently A. L. Dent and R. J. Kokes have presented their results on the chemisorption of hydrogen and ethylene and hydrogenation of ethylene on zinc oxide at room temperature [*J. Phys. Chem.*, **73**, 3772 and 3781 (1969)]. They have used infrared studies to supplement the chemisorption and kinetic measurements. The two sets of results, theirs and ours, complement each other. Some of the findings and conclusions are similar and others different.

Hydrogen Chemisorption. Dent and Kokes also find that hydrogen chemisorption on zinc oxide occurs in two forms. Type I which corresponds to type A of

(11) E. Wicke, *Z. Elektrochem.*, **53**, 279 (1949).

(12) C. Kemball, *Proc. Roy. Soc., Ser. A*, **214**, 413 (1952).

(13) V. Kesavulu and H. A. Taylor, *J. Phys. Chem.*, **66**, 54 (1962).

this paper is fast and reversible and is the active form taking part in the hydrogenation reaction. Type II which is slow and irreversible corresponds to the ionic form. This does not participate in the hydrogenation reaction. However, they find that the type II has a slight promotional activity on the reaction. On the other hand, we find that the surface saturated with the ionic form does not affect the rate of the reaction. Resolution of this difference requires further study. It may be that evacuation at 60° removes some of the active form of type II chemisorption responsible for the promotional activity.

Dent and Kokes do not agree with the conclusion of Eischens, *et al.*,² that the slow, irreversible chemisorption (type II) is "protonic." However, the conductivity measurements³ show that this chemisorption is protonic, supporting the conclusion of Eischens and coworkers. The fact that this chemisorption does not produce any appreciable change in the background transmission probably indicates that the ir technique is not as sensitive as the conductivity measurements in detecting small changes in the carrier concentration.

Ethylene Chemisorption. Dent and Kokes have noted: "adsorption of ethylene gave rise to no ir bands that were not masked by or ascribable to bands of the unsaturated hydrocarbon." They therefore concluded that only one type of ethylene chemisorption

occurs on zinc oxide at room temperature. On the other hand, conductivity measurements show the occurrence of three types of ethylene adsorption at 60°. These forms also occur at room temperature, but, at this temperature, the slow and irreversible form which causes conductivity increase occurs much more slowly than at 60°.

Active Sites. Dent and Kokes have presented an interesting model of the active sites on zinc oxide. The active sites, isolated Zn-O pairs, are thought to be formed when Zn²⁺ ions get embedded in the close-packed O²⁻ layer on 000 $\bar{1}$ face of zinc oxide. There is no clearcut evidence in favor of their assumption that no nonstoichiometry is involved in the formation of the active sites. The possibility of removal of oxygen from the surface layers under the conditions of activation and evacuation employed by them cannot be ruled out. Our model consists of isolated Zn atoms on the surface produced by removal of oxygen during activation and evacuation. The fact that hydrogen retains its molecular identity in adsorption-desorption and in hydrogenation is not consistent with the ir spectrum obtained during hydrogenation. To get more meaningful information from the ir data, it may be necessary to study the spectrum at low temperatures where the mobility of the chemisorbed species is restricted.

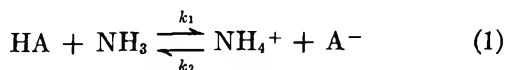
NOTES

A Kinetic Study of the Reactions of Water with Sodium and Cesium in Methylamine

by R. R. Dewald* and O. H. Bezirjian

Department of Chemistry, Tufts University,
Medford, Massachusetts 02155 (Received June 10, 1970)

Kinetic measurements for the reactions of sodium with water,^{1,2} alcohols,²⁻⁴ and other weak acids^{5,6} in liquid ammonia led to the conclusion that these reactions occur in the two stages represented by eq 1 and 2



where HA represents water, ethyl, and *tert*-butyl

alcohol, urea, and hydrazine. For a steady-state concentration of ammonium ions, the rate law

$$\frac{-d(\text{M})}{dt} = \frac{k_1 k_3 (\text{M})(\text{HA})}{k_2 (\text{A}^-) + k_3 (\text{M})} \quad (3)$$

is derived where (e_{am}^-) = (M), the metal concentration. On the other hand, kinetic data for the reaction of cesium with water in ethylenediamine have been analyzed on the assumption that two parallel second-order reactions are operative.^{7,8} Moreover, preliminary re-

* To whom correspondence should be addressed.

- (1) R. R. Dewald and R. V. Tsina, *Chem. Commun.*, 647 (1967).
- (2) R. R. Dewald and R. V. Tsina, *J. Phys. Chem.*, **72**, 4520 (1968).
- (3) W. L. Jolly, *Advances in Chemistry Series*, No. 50, American Chemical Society, Washington, D. C., 1965, p 27.
- (4) R. R. Dewald, *Proceedings of Colloque Weyl II*, Ithaca, N. Y., Butterworths, Washington, D. C., 1970, in press.
- (5) W. L. Jolly and L. Prizant, *Chem. Commun.*, 1345 (1968).
- (6) J. Belloni, *Int. J. Radiat. Phys. Chem.*, **1**, 411 (1969).

sults for the reaction of sodium with water in ethylenediamine indicate that the reaction is first order with respect to sodium while apparently greater than first order in water.^{7,8}

Studies of the optical,⁹⁻¹⁴ electrochemical,¹⁵⁻¹⁸ and magnetic^{13,19,20} properties of the alkali metals in primary amines indicate that the nature of these systems differs markedly from the metal-ammonia system. The observed properties of metal-amine solutions are also very metal dependent in contrast to metal-ammonia solutions. The nature of the metal-amine solution has been a matter of considerable controversy of which there is yet no general agreement.

Experimental Section

Methylamine (Matheson 99.8%) was purified by a procedure described elsewhere.¹⁸ Water samples, starting with doubly distilled conductance water, were prepared by a method already described.²

The progress of the reactions was followed conductometrically. Bright platinum electrodes were found to be suitable for making the measurements. The cell constants were determined by established procedures.¹⁶ The procedures used in preparing the metal-amine solutions and taking the resistance measurements were similar to that described elsewhere.¹⁸ Temperatures, -70° , were maintained by a Harris Manufacturing Co. Model 1Le BC2-075 convection fluid test chamber using Dow Corning No. 200 silicone fluid.

The initial concentrations of the sodium- and cesium-methylamine solutions were determined from reported conductance data.¹⁸ Next, a fragile glass ampoule containing the weighed water sample was broken, the solution mixed, and the resistance of the mixture measured as a function of time. The resistance-time data were evaluated following methods outlined elsewhere.²¹

The stability of the metal-amine solutions in the absence of added water in this study can be considered to be comparable to stability reported elsewhere.¹⁸ In one experiment with excess cesium ($[Cs] \approx 1.4 \times 10^{-3} M$ and $[H_2O] \approx 8.0 \times 10^{-4} M$) the resistance of the solution increased rapidly for about the first hour after addition of the water and then resistance of the blue solution was found to increase only by about 2% in 3 days after the initial reaction period. Hence the results reported herein should reflect the reaction of water with the metal solutions and not the decay rates of the solutions without water.

Results and Discussion

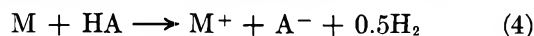
The reaction of cesium with water in methylamine was found too rapid for study by our conventional method at -50° using reactant concentrations similar to those given in Table I. However, the rate was slow enough to permit study at -70° . The kinetic data obtained for the cesium-water reaction could best be ex-

Table I: Kinetic Data for the Reaction of Cesium with Water in Methylamine

Run no.	$10^4[Cd], M$	$10^4[H_2O], M$	$10^4k_1, M^{-1} \text{ sec}^{-1}$	k_2/k_3
66	1.56	4.85	4.0	3.6
82	2.11	2.31	3.8	4.0
88	2.43	8.06	4.2	5.5
90	2.49	5.93	4.7	1.9
	4.2 ± 0.3^a	3.8 ± 0.5^a

^a Average error.

plained in terms of reactions 1 and 2, where NH_3 is replaced by CH_3NH_2 , and eq 3. Figure 1 shows a semilog plot of $[Cs]$ vs. time for a typical experiment. The solid line is the theoretical curve based on the calculated values of k_1 and k_2/k_3 and eq 3, assuming (M) is the total cesium concentration. The notation (M) used in this report refers to the total metal concentration and not any particular species that might be present in the metal solution. The concentrations of A^- used in eq 3 were estimated from the stoichiometry of the equation



where M is either Cs or Na, and HA is water. Also, more than one species⁹⁻¹⁴ is probably present in the cesium solution and thus only part of the metal might be functioning as the reducing agent. This may account for the differences between the theoretical curve and the experimental plot shown in Figure 1. Table I gives a summary of the kinetic data for the reaction of cesium with water in methylamine at -70° .

The reaction of sodium with water in methylamine was found to be much slower than that for cesium. This is evident from Figure 1. All experiments using sodium metal were carried out using a large excess of

(7) L. H. Feldman, R. R. Dewald, and J. L. Dye, *Advances in Chemistry Series*, No. 50, American Chemical Society, Washington, D. C., 1965, p 163.

(8) J. L. Dye, *Accounts Chem. Res.*, **1**, 306 (1968).

(9) M. Gold and W. L. Jolly, *Inorg. Chem.*, **1**, 818 (1962).

(10) R. R. Dewald and J. L. Dye, *J. Phys. Chem.*, **68**, 121 (1964).

(11) S. Matalon, S. Golden, and M. Ottolenghi, *ibid.*, **73**, 3098 (1969).

(12) M. Ottolenghi, K. Bar-Eli, and H. Linschitz, *J. Chem. Phys.*, **43**, 206 (1965).

(13) L. R. Dalton, J. D. Rynbrandt, E. M. Hansen, and J. L. Dye, *ibid.*, **44**, 3969 (1966).

(14) I. Hurley, T. R. Tuttle, Jr., and S. Golden, *ibid.*, **48**, 2818 (1968).

(15) R. R. Dewald and J. L. Dye, *J. Phys. Chem.*, **68**, 128 (1964).

(16) R. R. Dewald and J. H. Roberts, *ibid.*, **72**, 4224 (1968).

(17) R. R. Dewald, *ibid.*, **73**, 2615 (1969).

(18) R. R. Dewald and K. W. Browall, *ibid.*, **74**, 129 (1970).

(19) C. A. Hutchinson, Jr., and R. C. Pastor, *J. Chem. Phys.*, **21**, 7659 (1953).

(20) K. Bar-Eli and T. R. Tuttle, Jr., *ibid.*, **40**, 2508 (1964).

(21) A. A. Frost and R. G. Pearson, "Kinetics and Mechanism," 2nd ed, Wiley, New York, N. Y., 1961, p 29.

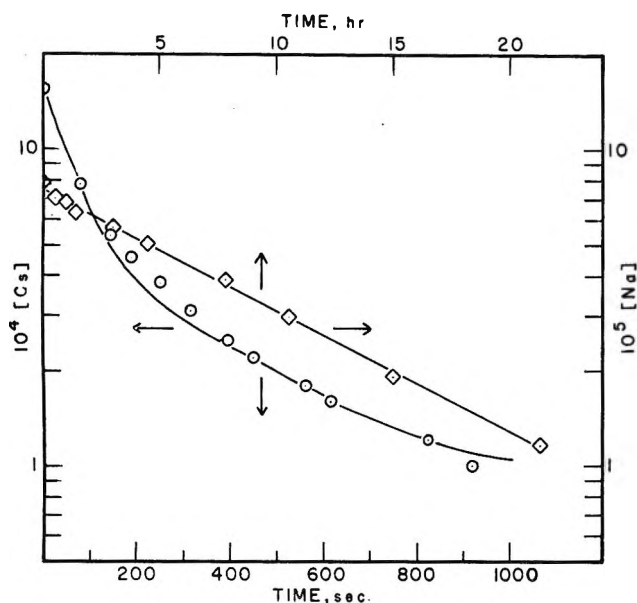


Figure 1. Semilogarithmic plots of metal concentration vs. time for the reaction of cesium and sodium with water at -70° in methylamine: \circ , run no. 66, cesium; \square , run no. 65, sodium.

water such that its concentration could be considered constant, and in all experiments the reaction was pseudo-first order in the sodium concentration as shown in Figure 1. A plot of the log of the pseudo-first-order rate constant vs. $\log (\text{H}_2\text{O})$ gives a straight line with slope of unity. The rate constant is found to be $1.0 \pm 0.1 \times 10^{-3} \text{ M}^{-1} \text{ sec}^{-1}$ at -70° . Table II gives a sum-

Table II: Kinetic Data for the Reaction of Sodium with Water in Methylamine at -70°

Run no.	$10^4 [\text{Na}]$, <i>M</i>	$10^3 [\text{H}_2\text{O}]$, <i>M</i>	$10^3 k$, $\text{M}^{-1} \text{ sec}^{-1}$
65	8.65	24.0	1.0
84	24.0	14.8	1.0
86	35.5	7.56	1.1
100	34.5	82.8	1.0

mary of the kinetic data for the reaction of sodium with water in methylamine.

One possible explanation for the marked difference in the observed kinetic behavior of sodium and cesium with water in methylamine could be the difference in the rates at which the reducing species formed by dissolution of the metals react with methylammonium ion. If the rate for the reaction of Na species with the methylammonium ion is slow, then the rate expression becomes

$$-\frac{d(\text{Na})}{dt} = k_1 \frac{(\text{H}_2\text{O})(\text{Na})}{k_2 (\text{OH}^-)} \quad (5)$$

Moreover, sodium hydroxide is probably only slightly soluble in methylamine as in liquid ammonia,²² and the

(OH^-) term can be considered constant. This will then lead to the observed pseudo-first-order kinetics when $[\text{H}_2\text{O}] \gg [\text{Na}]$.

Solutions of sodium in amines exhibit predominantly an absorption band at 660 nm¹⁰⁻¹⁴ with perhaps a very small infrared absorption while solutions of cesium show an infrared band ($\lambda_{\text{max}} \approx 13,000 \text{ \AA}$) and another band at about 975 nm.^{18,23} General agreement appears to exist in attributing the infrared band to a solvated electron.^{11,24} Recently, it has been suggested that the bands at 660 and 975 nm should be attributed to Na^- and Cs^- metal ions,¹¹ respectively. These assignments are also consistent with reported conductance data.^{15,18} Therefore, we conclude that the difference in rates of reaction 2 suggested in this work for sodium and cesium solutions reflect the nature of the reactivities of the dissolved species.

Acknowledgment. This research was supported by the National Science Foundation under Grant No. GP 8322. O. H. B. is also grateful to the National Science Foundation for support through its Summer Research Participation for College Teachers Program.

(22) M. Skossarewsky and N. Tchitchinadze, *J. Chim. Phys.*, **14**, 11 (1916).

(23) R. C. Douthit, Ph.D. Thesis, Michigan State University, 1959.

(24) J. L. Dye and R. R. Dewald, *J. Phys. Chem.*, **68**, 135 (1964).

Vapor Phase Association of Methanol. Vapor Density Evidence for Trimer Formation

by Venghuot Cheam, Sutton B. Farnham, and Sherril D. Christian*

Department of Chemistry, The University of Oklahoma, Norman, Oklahoma (Received March 25, 1970)

Recent reports from this laboratory have described a method for treating several types of data on the association of alcohols by assuming the presence of only two associated species—the linear trimer and the cyclic octamer—as the predominant polymeric forms.^{1,2} Vapor pressure, infrared, and proton magnetic resonance data for several alcohol-organic solvent systems and *PVT* data for methanol vapor have been nicely correlated by using this association model. Nonetheless, there is by no means general agreement regarding the size or geometry of alcohol aggregates in either vapor or condensed phases;³ therefore, we decided to

* To whom correspondence should be addressed.

(1) E. E. Tucker, S. B. Farnham, and S. D. Christian, *J. Phys. Chem.*, **73**, 3820 (1969).

(2) E. E. Tucker, Ph.D. Dissertation, The University of Oklahoma, Norman, Okla., 1969.

investigate the self-association of methanol using an accurate vapor density technique developed in this laboratory. One important advantage of the vapor density method—as opposed to spectral, heat capacity, or PVT measurements, for example—is that values of the average molecular weight of associating vapors can be inferred directly from experimental data, independent of any association model or functional form selected for fitting data. This communication describes results obtained for methanol vapor at 25°, at pressures ranging from a few Torr nearly to saturation.

Experimental Section

The use and theory of silica microbalances have been treated by numerous previous investigators. For example, Johnson and Nash⁴ used a magnetically operated balance to study the vapor-phase association of acetic and trimethylacetic acids. Bradley⁵ and Carmichael⁶ have described in detail the operation, performance, and theory of various fused-silica balances. Our balance frame and beam are similar to those described by Bradley, except that at each end of the balance, Pyrex bulbs are attached to the silica beam by means of graded silica-to-Pyrex seals. At one end of the beam there is a closed bulb and at the other an open bulb having nearly the same total surface area.⁴ The balance fits into a grease-free chamber, to which methanol samples can be added through a mercury-covered, sintered-glass disk;⁷ pressures are measured either with a mercury manometer or a Texas Instruments Inc. precision pressure gauge.¹ The entire apparatus is immersed in a water bath controlled to $\pm 0.01^\circ$. The change in gas density in the chamber is detected by observing the change in height of a blackened pointer (attached to the closed bulb) with a cathetometer (to ± 0.01 mm).

The balance was calibrated by using pure nitrogen as a standard; within the limits of accuracy attainable, it was adequate to treat N_2 as an ideal gas. The gas was bubbled through the glass disk until a density in the desired range was obtained. After a few minutes, both the pressure and the density reached constant values and the pointer height, R , and the corresponding pressure, p_{N_2} , were recorded. Series of pairs of values of R , p_{N_2} were obtained by adding or pumping out small quantities of nitrogen. These data were fit by least-squares analysis in the form

$$R = a + bP_{N_2} + cP_{N_2}^2 + dP_{N_2}^3 \quad (1)$$

to determine the empirical constants a , b , c , and d . Following the initial calibration run, methanol vapor was added to the system and sets of values of R and the pressure of methanol, p , were recorded. Corresponding to each measured value of R , it was possible to calculate p_{N_2}' (the pressure of nitrogen required to give the same density as that of the alcohol sample) by solving eq 1 numerically. This value of p_{N_2}' (which was termed the equivalent nitrogen pressure) could then be used to

compute the vapor density or substituted into the expressions $\langle M \rangle = p_{N_2}'M_{N_2}/p$ and $\pi = p_{N_2}'M_{N_2}/32.04$ to obtain the average molecular weight ($\langle M \rangle$) and the formal pressure (π).⁸ After each series of measurements on methanol, the system was recalibrated with nitrogen in order to check the reproducibility of the results. Values of p_{N_2}' consistent to within 0.04 Torr were obtained in this way.

Results and Discussion

Figure 1 is a plot of the average molecular weight of methanol as a function of total pressure at 25.00°. A striking feature of the curve is that the limiting slope, extrapolated to zero pressure, is quite small. It is difficult to see how any reasonable fit of the data could yield a value of the dimer formation constant, K_2 , greater than about 5×10^{-5} Torr⁻¹ or 1.0 l. mol⁻¹.⁹

In analytically fitting data, we first considered only the region from 0 to 90 Torr (in which it has been dem-

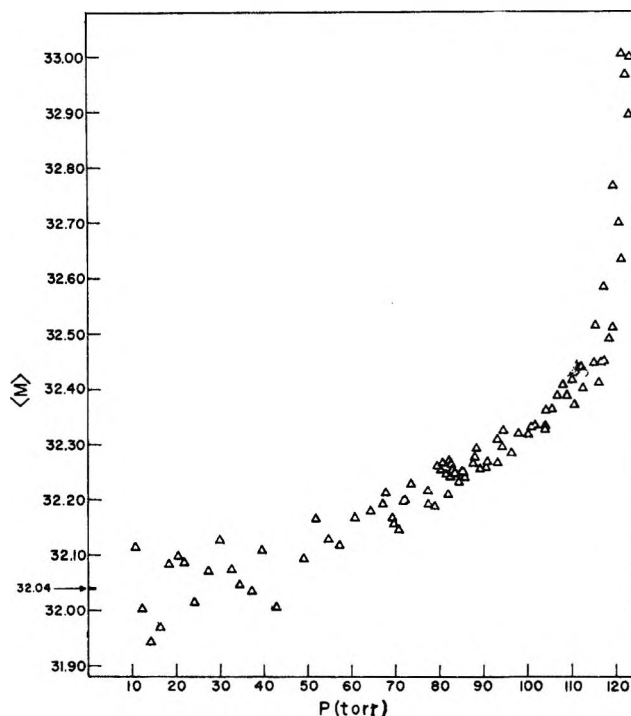


Figure 1. Molecular weight of methanol vapor as a function of pressure at 25°.

(3) References to several vapor phase studies of methanol association are given by N. S. Berman, *A.I.Ch.E. J.*, **14**, 497 (1968); condensed phase studies are cited by A. N. Fletcher and C. A. Heller, *J. Phys. Chem.*, **71**, 3742 (1967), and in ref 1.

(4) E. W. Johnson and L. K. Nash, *J. Amer. Chem. Soc.*, **74**, 547 (1950).

(5) R. S. Bradley, *J. Sci. Instrum.*, **30**, 84 (1953).

(6) H. Carmichael, *Can. J. Phys.*, **30**, 524 (1952).

(7) A. A. Taha, R. D. Grigsby, J. R. Johnson, S. D. Christian, and H. E. Affsprung, *J. Chem. Educ.*, **43**, 432 (1966).

(8) Formal pressure is defined as the total, or formal, concentration of methanol multiplied by RT .

(9) The dimer formation constant, K_2 , can be shown to be equal to the limiting slope of a plot of $\langle M \rangle$ against p , divided by the molecular weight of monomeric methanol (32.04).

onstrated by a gravimetric adsorption experiment that the adsorption of methanol vapors on Pyrex buoyancy bulbs is not sufficient to interfere in vapor density experiments).¹⁰ If we assume that all the deviation from ideal behavior is attributable to the formation of associated species, it is possible to relate both the formal pressure and the total pressure to the partial pressure of the methanol monomer, p_M , by the equations

$$\pi = p_M + 2K_2 p_M^2 + 3K_3 p_M^3 + \dots \quad (2)$$

and

$$p = p_M + K_2 p_M^2 + K_3 p_M^3 + \dots \quad (3)$$

in which the individual terms on the right-hand side represent formal and partial pressures of the various methanol species which are present. For any given choice of assumed species, it is possible to choose an initial set of values of the association constants and solve eq 3 point by point to obtain trial values of p_M . Using these p_M values and the assumed values of the formation constants, one may calculate the expected value of formal pressure, π_i^{calcd} , for each point and compute the root mean square deviation in formal pressure

$$\text{RMSD} = \sqrt{\frac{\sum_{i=1}^n (\pi_i - \pi_i^{\text{calcd}})^2}{n - \text{par.}}}$$

where par. is the number of parameters, for the entire collection of n pairs of measurements.¹¹ By means of a numerical optimization procedure, it is possible to vary the values of the association constants in such a way as to determine the absolute minimum in RMSD, corresponding to the best values of the association constants for the given choice of assumed species.¹

Table I shows results obtained with several plausible selections of combinations of species up to 90 Torr of methanol. Of the three single aggregate sets, the 1-3 model is the best choice. In the case of the 1-2-3 model, K_2 is a small negative number having a standard error several times the value of the constant itself and K_3

nearly equals the value obtained using the 1-3 model. The 1-2-3-4 model leads to negative values of K_2 and K_4 (-3×10^{-5} Torr⁻¹ and -2.1×10^{-9} Torr⁻³, respectively) and an unexpectedly large positive value of K_3 (about double that obtained with the 1-3 or 1-2-3 models). Models involving species larger than the tetramer (such as 1-3-6 and 1-3-8) did not lead to an improvement in the statistical fit of data, and the formation constants for the higher polymers are slightly negative. In fact, no three or four species model provides a better fit of data than the monomer-trimer model. Our data, therefore, support the conclusion that the predominant associated species, up to pressures of 90 Torr, is the methanol trimer. The value of K_3 reported here is approximately 10% smaller than that reported previously, based on *PVT* data.

Data at higher pressures were also correlated with various association models. Adsorption errors may be expected to become significant above 110 Torr, although the microbalance was designed to compensate for adsorption insofar as possible by using a counterbalancing open bulb having nearly the same total surface area as the closed buoyancy bulb. We estimate that uncompensated adsorption effects, at pressures up to 116 Torr, do not lead to errors in the reported $\langle M \rangle$ values of more than 0.05. Using all data points for pressures less than 116 Torr, the following RMSD values were obtained for various models which include the trimer: 1-3, RMSD = 0.0537 Torr; 1-3-2, RMSD = 0.0535 Torr; 1-3-6, RMSD = 0.0532 Torr; 1-3-8, RMSD = 0.0530 Torr; 1-3-9, RMSD = 0.0528 Torr. In all of these correlations the computed value of K_3 agrees with the value reported in Table I for the 1-3 model to within 10%; and for all of the 1-3- n models, the relative concentration of the n -mer (compared to trimer) is less than 10% at the highest pressures.

We believe that the vapor density results reported here provide significant new information about the extent and nature of the association of methanol.¹² The important advantage of the buoyancy method is that in fitting data with any given association model, the only unknowns are the equilibrium constants for formation of the various polymeric species. There are no additional unknown parameters, such as apparatus constants or absorptivities and other constants specific for individual aggregates, which tend to blur differences in the models which are being compared for fitting data.

Acknowledgment. This work was supported by National Science Foundation Grant No. GP-8029.

Table I: RMSD and Equilibrium Constant Values for Various Sets of Assumed Methanol Species at 25°

Species	Equilibrium constants ^{a, b}	RMSD, Torr
1-2	$K_2 = (7.46 \pm 0.17) \times 10^{-5}$ Torr ⁻¹	0.0621
1-3	$K_3 = (4.61 \pm 0.08) \times 10^{-7}$ Torr ⁻²	0.0470
1-4	$K_4 = (3.69 \pm 0.08) \times 10^{-9}$ Torr ⁻³	0.0592
1-2-3	K_2 (negative value)	
	$K_3 = (4.38 \pm 0.71) \times 10^{-7}$ Torr ⁻²	0.0474
1-2-3-4	K_2 (negative value)	0.0477
	$K_3 = (9.0 \pm 1.4) \times 10^{-7}$ Torr ⁻²	
	K_4 (negative value)	

^a Uncertainties in equilibrium constant values are standard errors. ^b K_i refers to the equilibrium constant for the reaction $i\text{-MeOH} = (\text{MeOH})_i$.

(10) V. Cheam, Ph.D. Dissertation, The University of Oklahoma, Norman, Okla., in preparation.

(11) Values of π_i were assigned equal weight throughout the entire pressure range, consistent with the experimental uncertainties in measurement of the equivalent nitrogen pressure.

(12) Tabular data corresponding to the results shown in Figure 1 are available from ADI Auxiliary Publications Project, Photoduplication Service, Library of Congress, Washington, D. C. 20540.

A Proton Nuclear Magnetic Resonance Technique for Determining the Surface Hydroxyl Content of Hydrated Silica Gel

by Victor M. Bermudez

U. S. Naval Research Laboratory, Washington, D. C. 20390
(Received May 13, 1970)

The surface hydroxyl content of silica gel and other silica-based adsorbents is of great theoretical and practical interest in studies of gas and liquid adsorption and of catalysis. Several chemical and physical techniques for measuring this quantity have evolved, but each involves certain difficulties which make the accuracy of the result open to question. Application of BET theory to N_2 and H_2O adsorption isotherms¹ suffers from uncertainty about the effective area of an adsorbed molecule and the uniformity of the surface coverage. Quantitative reactions with the silanol group, using D_2O ,² $SOCl_2$, BCl_3 , $AlCl_3$,³ CH_3Li ,⁴ B_2H_6 ,⁵ Ca^{2+} , and $LiAlH_4$,⁶ are all subject to steric effects and questions concerning the stability of the reaction products. Furthermore, all these techniques are affected by the pore size of the solid adsorbent. In this note, we propose a simple nmr method which avoids all these complications; we discuss its range of validity and apply it successfully to data obtained by Kamiyoshi,⁷ which are particularly well suited to this approach.

The hydrated silica gel surface is covered with randomly⁸ placed silanol groups (chemisorbed water) to which molecular water is attached *via* hydrogen bonds (physically adsorbed water). From the observation that the transverse relaxation time of the silanol protons is constant over a wide range of temperature and content of physically adsorbed water,⁸⁻¹⁰ it is known that silanol groups are immobile and that silanol protons do not exchange among themselves. This is especially true when physically adsorbed water prevents the formation of silanol-silanol hydrogen bonds.¹¹ Woessner and Zimmerman,¹² quoting dielectric and nmr relaxation results, show that physically adsorbed water undergoes rapid reorientation with a time constant similar to that of the liquid. It is also known^{9,12,13} that, at room temperature and at coverages between about 0.5 and 3 statistical monolayers of physically adsorbed water, the longitudinal relaxation times of the protons in the system,¹⁴ the transverse relaxation time of protons in the adsorbed layers, and the proton lifetime at either site are all much greater than the transverse relaxation time (T_{2s}) of a silanol proton, 2×10^{-4} sec.^{8,9} Under these conditions, it is also true that the difference in line widths is very much greater than the difference in chemical shifts of the protons in the two phases.

Under these circumstances, the observed line width ($1/T_2'$) is given by

$$\frac{1}{T_2'} = \frac{P_s}{T_{2s}} \quad (1)$$

where P_s is the probability that a proton will be found in a surface silanol group and T_{2s} is the transverse relaxation time of the silanol proton. Writing P_s in terms of $[OH]$ and $[H_2O]$, the concentration of surface hydroxyl groups and of physically adsorbed water, in units of g/100 g of gel, we obtain

$$T_2' = \frac{[OH] + 2[H_2O]}{[OH]} T_{2s} = T_{2s} + \frac{2T_{2s}}{[OH]} [H_2O] \quad (2)$$

At this point it is necessary to comment on the range of validity of the foregoing treatment. Equation 1 is correct only in the limit of rapid exchange, when $2\pi(\Delta\nu) \ll 1/\tau$, where $\Delta\nu$ is the difference in chemical shifts of protons at the two sites and $1/\tau$ is the proton exchange frequency. Woessner and Zimmerman¹² estimate $1/\tau$ to be about 10^3 sec⁻¹ and δ (measured using a 26.5 MHz spectrometer) to be somewhere between 0 and 4 ppm. The quantity $(2\pi\tau)^{-1}$ is equivalent to a chemical shift of about 6.0 ppm. Although more than one resonance can be distinguished below 0°, due to reduction of $1/\tau$, only a single signal is seen at room temperature.¹⁵⁻¹⁷ Hence, the assumption of rapid exchange appears to be correct, at least at room temperature and above, although more precise knowledge of δ would be useful. Equation 1 is not applicable at high surface coverages, those at which the protons in the adsorbed water greatly outnumber the silanol protons and relaxation times other than T_{2s} must be considered, or at low coverages, less than about 0.3 monolayer, below which two

- (1) S. Brunauer, D. L. Kantro, and C. M. Weise, *Can. J. Chem.*, **34**, 1483 (1956).
- (2) V. Ya. Davydov, A. V. Kiselev, and L. T. Zhuravlev, *Trans. Faraday Soc.*, **60**, 2254 (1960).
- (3) H. P. Boehm, M. Schneider, and F. Arendt, *Z. Anorg. Allgem. Chem.*, **320**, 43 (1963).
- (4) J. J. Fripiat and J. Uytterhoeven, *J. Phys. Chem.*, **66**, 800 (1962).
- (5) C. Naccache and B. Imelik, *Bull. Soc. Chim. Fr.*, 553 (1961).
- (6) V. M. Chertov, *et al.*, *Russ. J. Phys. Chem.*, **40**, 283 (1966).
- (7) K. Kamiyoshi, *J. Phys. Radium*, **20**, 60 (1959).
- (8) D. E. O'Reilly, H. P. Leftin, and W. K. Hall, *J. Chem. Phys.*, **29**, 970 (1958).
- (9) J. R. Zimmerman and J. A. Lasater, *J. Phys. Chem.*, **62**, 1157 (1958).
- (10) V. I. Kvlivdize, *et al.*, *Kinet. Katal. USSR*, **3**, 73 (1962).
- (11) F. H. Hambleton, J. A. Hockey, and J. A. G. Taylor, *Trans. Faraday Soc.*, **62**, 795 (1966).
- (12) D. E. Woessner and J. R. Zimmerman, *J. Phys. Chem.*, **67**, 1590 (1963).
- (13) J. R. Zimmerman, B. G. Holmes, and J. A. Lasater, *ibid.*, **60**, 1157 (1956).
- (14) For an explanation of the assignment of observed lifetimes to specific proton sites, see H. Resing, *Advan. Mol. Relaxation Processes*, **1**, 109 (1968).
- (15) V. I. Kvlivdize, *Dokl. Phys. Chem.*, **157**, 673 (1964).
- (16) V. I. Kvlivdize and V. F. Kiselev, *J. Struct. Chem. (USSR)*, **8**, 191 (1967).
- (17) V. V. Strelko, B. M. Mitsyuk, and Z. Z. Vysotskii, *Theor. Exp. Chem. (USSR)*, **3**, 148 (1967).

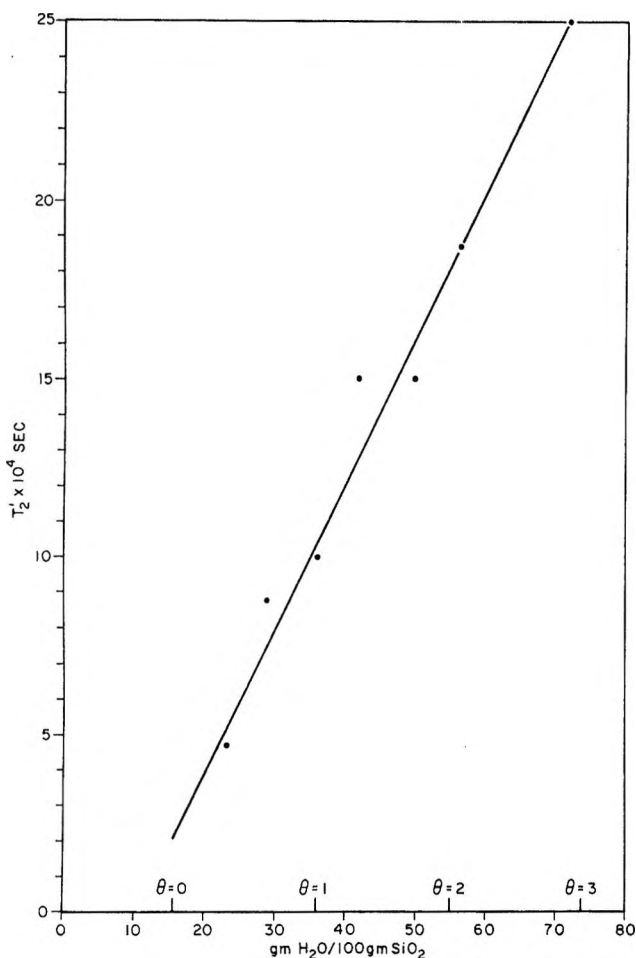


Figure 1. Observed line width parameter vs. physically adsorbed water content, obtained from ref 7. Values of θ indicate fraction of a statistical monolayer (see text).

coexisting environmental states cannot be defined.¹² However, at room temperature and between about 0.5 and 2 or 3 monolayers of physically adsorbed water, the dominant contribution to line width comes from T_{2s} and eq 2 should fit the observed line width. Note that when most of the silanol protons are replaced by Ca^{2+} , the resonance is much sharper at low adsorbed water content and much less dependent on the extent of coverage.¹⁷

Kamiyoshi⁷ has provided the necessary data for a type of gel having a surface area of about $800 \text{ m}^2/\text{g}$.¹⁸ Figure 1 represents a plot of these data, which are qualitatively similar to those of other authors for gels of unknown surface area.^{17,19} The observed line widths have been converted from field to frequency units ($\Delta\omega(\text{sec}^{-1}) = 2\pi\Delta\nu = 26.75 \times \Delta H$ (in mG)). The negative intercept can be traced to the method of determining water content, drying 6 hr at 110° , which removes all physically adsorbed water but also dehydrates some silanol groups and eliminates some internal water. Hence, each point in Figure 1 is displaced too far to the right on the concentration axis by about 15 g of $\text{H}_2\text{O}/100 \text{ g}$ of SiO_2 based on the anticipated value of the intercept.

Table I: A Comparison of the Results of Different Methods for Determining the Surface Hydroxyl Content of Silica Gel

Method	Surface area (m^2/g)	10^{-6} mol OH/ m^2	Ref
H_2O adsorption/BET	658	6.1	1
D_2O exchange/mass spectrum	750	8.2	2
Reaction with B_2H_6	820	9.5	5
Reaction with LiAlH_4	634	10.1	6
Nmr	800	7.0	This work

This does not affect the slope, which is the parameter of interest, and has taken into account in determining the values of fractional surface coverage (θ). A better way to measure the adsorbed water content would be prolonged evacuation at room temperature, which removes only the truly physically adsorbed water.²⁰

From the surface area of the gel, the known value of T_{2s} (2×10^{-4} sec), and the slope, paying attention to concentration units, we obtain a value of surface hydroxyl content of 7.0×10^{-6} mol of OH/ m^2 . In Table I, this result is compared with those obtained with gels of similar surface area by other methods.

The data in Table I were obtained with different gels; hence, the variation in the values of hydroxyl content reflects differences in the gels as well as in the methods of measurement. Nevertheless, it is clear that the nmr method gives a reasonable result and that it is much less ambiguous than the other techniques, since it involves measurements performed on the undisturbed silica surface. It would be very useful to compare the results of these different methods on the same type of gel.

Acknowledgment. The author wishes to thank Dr. M. N. Kabler and Dr. H. Resing for much helpful discussion.

- (18) M. H. Waldman, *J. Phys. Radium*, **17**, 426 (1956).
- (19) D. Geschke, *Z. Naturforsch.*, **23A**, 689 (1968).
- (20) G. J. Young, *J. Colloid Sci.*, **13**, 67 (1958).

A Formulation of the Reaction Coordinate

by Kenichi Fukui¹

Department of Chemistry, Illinois Institute of Technology, Chicago, Illinois 60616 (Received June 17, 1970)

Since the discovery of orbital symmetry control^{2,3} in determining the favorable path of chemical reactions, the concept of the reaction coordinate has been used in the molecular orbital theory of chemical reactivity more frequently than before. The symmetry arguments of

(1) To whom correspondence should be addressed at Department of Hydrocarbon Chemistry, Kyoto University, Japan.

molecular orbitals (MO), in particular of the HO (highest occupied) MO and the LU (lowest unoccupied) MO, have been made in relation to the favorable path of chemical reactions,⁴⁻⁸ and the nature of HOMO-LUMO interaction has been understood in connection with the change of molecular geometry along the reaction coordinate.^{9,10} The conservation of orbital symmetry along the reaction coordinate has been discussed in connection with the stereoselection rule.^{3,11}

In this connection, it is desirable to formulate the "reaction coordinate." Although in actual sense this can obviously never be a simple concept, a conventional definition would be helpful. We tentatively define the reaction coordinate as a curve passing through the initial and the transition points and orthogonal to energy equipotential contour surface. A reaction coordinate, defined as such, may be called "intrinsic reaction coordinate."

Let the number of nuclei of the reacting system be N . There are $3N - 6$ independent internuclear distances which are enough to determine the potential energy W . These variables are denoted by $x_1 x_2 \dots x_m$ ($n = 3N - 6$). An equipotential surface can be given by a hypersurface in the n -dimensional $x_1 x_2 \dots x_n$ space as $c = W(x_1 x_2 \dots x_n)$ with respect to a given electronic state in which c is a constant value of potential energy. The points corresponding to the initial, final, transition, and intermediate states must satisfy the condition

$$\frac{\partial W}{\partial x_1} = \frac{\partial W}{\partial x_2} = \dots = \frac{\partial W}{\partial x_n} = 0 \quad (1)$$

These points together are referred to as "equilibrium points." The sets x_i ($i = 1, 2, \dots, n$) representing these points are, respectively, denoted by $\xi_i^{(\text{init})}$, $\xi_i^{(\text{fin})}$, $\xi_i^{(\text{trans})}$, and $\xi_i^{(\text{interm})}$.¹² The reaction coordinate as defined above is given by a solution of the following simultaneous differential equations which passes through the points $\xi_i^{(\text{init})}$, $\xi_i^{(\text{trans})}$, and $\xi_i^{(\text{fin})}$.

$$dx_1 / \frac{\partial W}{\partial x_1} = dx_2 / \frac{\partial W}{\partial x_2} = \dots = dx_n / \frac{\partial W}{\partial x_n} \quad (2)$$

The derivation of eq 2 is obvious. The tangential plane of the surface $c = W(x_1 x_2 \dots x_n)$ at a point x_i is given by $\sum_i (\partial W / \partial x_i)(X_i - x_i) = 0$ where X_i are the current coordinates. If we represent a reaction coordinate as $x_1 = T_1(t)$, $x_2 = T_2(t)$, \dots , $x_n = T_n(t)$ using a parameter t , the tangent of this curve at the point x_i will be $(X_1 - x_1)/(dT_1/dt) = (X_2 - x_2)/(dT_2/dt) = \dots = (X_n - x_n)/(dT_n/dt)$, and the condition that this line should be perpendicular to the above-mentioned tangential plane is nothing but eq 2.

Since the reaction coordinate is orthogonal to the tangential plane of the equipotential surface, the potential energy value on this tangential plane has always an extremum¹³ at the point crossing the reaction coordinate.

Equation 2 is worthwhile since this will connect the chemical concept of reaction path to numerical computation in combination with the recent growth of possibility of obtaining the values of W for a reacting system with a tolerable reliability. But this equation is also useful in getting some qualitative information about the nature of reaction coordinate.

Equation 2 represents an extremely simple fact that the direction of displacement conforms to the direction of "force," namely the vector $(-\partial W / \partial x_1, -\partial W / \partial x_2, \dots, -\partial W / \partial x_n)$. In this manner, at a nonequilibrium point, the driving force for a configuration change acts in the direction of extremum potential energy change. The coordinate, ρ , in the direction of configuration change at any point is thus simply given by

$$\frac{\partial W}{\partial \rho} = \text{extremum} \quad (3)$$

If we designate the direction cosines of a coordinate as $l_1 l_2 \dots l_n$ and regard the potential energy gradient in this direction as a function of l_j , eq 3 leads to the relation

$$\frac{1}{l_1} \frac{\partial W}{\partial x_1} = \frac{1}{l_2} \frac{\partial W}{\partial x_2} = \dots = \frac{1}{l_n} \frac{\partial W}{\partial x_n} \quad (3')$$

determining the l_j 's for the reaction coordinate ρ at any point.

Any nonequilibrium point on a reaction coordinate has *one* direction satisfying eq 3. Along the reaction coordinates the curvature of potential energy increase has to be *maximum* with respect to the variation of direction; this is a requisite for the occurrence of a chemical reaction with an energy barrier to be overcome.

A particular situation may arise at an equilibrium point ξ_i at which all $\partial W / \partial x_i$ vanish. At a point close to ξ_i , say $\xi_i + \Delta x_i$, however, we have

(2) K. Fukui, "Molecular Orbitals in Chemistry, Physics, and Biology," P.-O. Löwdin and B. Pullman, Ed., Academic Press, New York, N. Y., 1964, p 513.

(3) R. B. Woodward and R. Hoffmann, *J. Amer. Chem. Soc.*, **87**, 395 (1965), and their papers cited in *Angew. Chem. Int. Ed. Engl.*, **8**, 781 (1969).

(4) K. Fukui, *Bull. Chem. Soc. Jap.*, **39**, 498 (1966).

(5) K. Fukui and H. Fujimoto, *ibid.*, **39**, 2116 (1966).

(6) K. Fukui and H. Fujimoto, "Mechanisms of Molecular Migrations," Vol. 2, B. S. Thyagarajan, Ed., Interscience, New York, N. Y., 1969, p 117.

(7) L. Salem, *Chem. Brit.*, 449 (1969); *Chem. Phys. Lett.*, **3**, 99 (1969).

(8) L. Salem and J. S. Wright, *J. Amer. Chem. Soc.*, **91**, 5947 (1969).

(9) K. Fukui and H. Fujimoto, *Bull. Chem. Soc. Jap.*, **41**, 1989 (1968).

(10) K. Fukui and H. Fukimoto, *ibid.*, **42**, 3399 (1969).

(11) R. G. Pearson, *Theor. Chim. Acta*, **16**, 107 (1970).

(12) Here a stable initial state refers to the ground-state reaction. In an excited state, the possibility of involvement of a chemical relaxation which may start from a nonequilibrium point cannot entirely be rejected.

(13) For this path to have a definite physical meaning of reaction coordinate, this extremum should be an absolute minimum.

$$W/\partial x_i \sim \sum_j (\partial^2 W / \partial x_i \partial x_j)_{x_k = \xi_k} \Delta x_j$$

In order for this point to lie on one reaction coordinate, it follows from eq 2 that

$$\frac{\Delta x_1}{\sum_j \left(\frac{\partial^2 W}{\partial x_1 \partial x_j} \right)_{x_k = \xi_k} \Delta x_j} = \frac{\Delta x_2}{\sum_j \left(\frac{\partial^2 W}{\partial x_2 \partial x_j} \right)_{x_k = \xi_k} \Delta x_j} = \dots = \frac{\Delta x_n}{\sum_j \left(\frac{\partial^2 W}{\partial x_n \partial x_j} \right)_{x_k = \xi_k} \Delta x_j} = \text{const.} = \frac{1}{\kappa}$$

which immediately leads to the secular equation

$$\begin{vmatrix} b_{11} - \kappa & b_{12} & \dots & b_{1n} \\ b_{21} & b_{22} - \kappa & \dots & b_{2n} \\ \dots & \dots & \dots & \dots \\ b_{n1} & b_{n2} & \dots & b_{nn} - \kappa \end{vmatrix} = 0$$

$$\left(b_{ij} = b_{ji} = \left(\frac{\partial^2 W}{\partial x_i \partial x_j} \right)_{x_k = \xi_k} \right)$$

giving Δx_i by which we can determine the direction of displacement. Accordingly, in this case we have instead of eq 3

$$\frac{\partial^2 W}{\partial \rho^2} = \text{extremum} \quad (4)$$

as the condition to be satisfied by a reaction coordinate ρ .¹⁴ This means, similar to eq 3', that the direction cosines l_j of the reaction coordinate ρ are specified as satisfying the relation

$$\frac{1}{l_1} \frac{\partial}{\partial x_1} \sum_j l_j \frac{\partial W}{\partial x_j} = \frac{1}{l_2} \frac{\partial}{\partial x_2} \sum_j l_j \frac{\partial W}{\partial x_j} = \dots = \frac{1}{l_n} \frac{\partial}{\partial x_n} \sum_j l_j \frac{\partial W}{\partial x_j} \quad (4')$$

Once the system starts to displace along one of these reaction coordinates, the route is controlled by eq 2 up to a transition-state or another equilibrium point.

At an equilibrium point, we have in general n directions which satisfy eq 4. At a stable equilibrium point (e.g., corresponding to $\xi_i^{(inv)}$, $\xi_i^{(in)}$, or $\xi_i^{(interm)}$, $\partial^2 W / \partial \rho^2$ is positive in the direction of all of n such directions. At a transition-state point $\partial^2 W / \partial \rho^2$ is negative in direction of the reaction coordinate and positive in the others.

Lastly, it is interesting to consider the symmetry of the reaction coordinate^{3,11} by the use of eq 2. Equation 2 prescribes completely the locus of the motion of nuclei along the intrinsic reaction coordinate. Equation 2 shows that the direction of displacement of nuclear positions is in conformity with the direction of gradient of the potential energy of the entire reacting system. In other words, the reaction coordinate always belongs to the totally symmetric representation of the

point group to which the symmetry of the nuclear arrangement belongs. Therefore, it is self-evident that the symmetry, if any exists in the system, is conserved in the deformation along the reaction coordinate. In this way, it results that each reaction coordinate has a definite symmetry of its own.

The relation between the symmetry possessed by a system and the symmetry of the MO's associated with that system is a matter of common knowledge. According to the group-theoretical requirement, the molecular orbital symmetry is necessarily conserved along one reaction coordinate throughout, provided the symmetry of the reaction coordinate is conserved throughout. In this way, the principle of conservation of orbital symmetry is derived from eq 2. This in fact made possible the dexterous use of the correlation diagrams by Woodward and Hoffmann.³

But it should be noted that the orbital symmetry is conserved in relation to every possible reaction coordinate which obeys the control of eq 2, no matter whether it is of high energy or low energy. Therefore, the principle of conservation of orbital symmetry itself cannot tell us the reason why a particular reaction path proves to be favorable and another unfavorable on the correlation diagram. In order to explore this reason, we have to look into the nature of the change in potential energy of the system along the reaction coordinate.

Bader^{15,16} and Pearson¹⁷ showed in regard to many examples that at an equilibrium point the value of $\partial^2 W / \partial \rho^2$ is seriously reduced if the reaction coordinate ρ belongs to the same irreducible representation as the direct product of the representations of HOMO and LUMO of the entire reacting system. The mechanism of self-accelerating reduction of the interaction energy according to the proceeding of reaction along the reaction coordinate has been clarified^{2,4-10} in relation to the HOMO-LUMO interaction between the reactants. In the case of two-molecule reactions, the interrelation between these two approaches is self-evident. In intramolecular reactions, too, the correspondence is a matter of approximation if we use the partition technique⁶ in the reacting molecule. The localized nature¹⁰ of usual chemical reactions almost permits us in many cases to consider an intramolecular reaction as a reaction between two parts of one molecule.

Acknowledgment. This work was carried out during the author's stay at Illinois Institute of Technology as a National Science Foundation Senior Foreign Scientist Fellow. The author thanks Dr. S. I. Miller of IIT and Dr. H. Fujimoto of Kyoto University for helpful comments.

(14) In some cases, the secular equation factors, and Δx_i 's separate into several noncombining groups.

(15) R. F. W. Bader, *Mol. Phys.*, **3**, 137 (1960).

(16) R. F. W. Bader, *Can. J. Chem.*, **40**, 1164 (1962).

(17) R. G. Pearson, *J. Amer. Chem. Soc.*, **91**, 1252, 4947 (1969).

Intramolecular Hydrogen Bond Formation in *o*-Trifluoromethylphenol

by Frank C. Marler, III, and Harry P. Hopkins, Jr.*

Department of Chemistry, Georgia State University,
Atlanta, Georgia 30303 (Received June 24, 1970)

The formation of an intramolecular hydrogen bond between a hydroxyl proton and a fluorine atom on a neighboring group has received considerable attention in recent years.¹⁻⁷

Infrared studies on this type of system have been hampered by the small shift in the OH stretching frequency which is normally observed^{8,9} when a hydrogen bond is formed between a covalently bound fluorine and a hydroxyl hydrogen. All previous studies, to our knowledge, have been performed on molecular systems in which a five-membered ring results from the hydrogen bond formation. The geometry of the five-membered ring and the size of the fluorine atom¹⁰ present an unfavorable situation for the formation of a hydrogen bond, if formed at all,^{1-3,10} in these systems. In an effort to determine if intramolecular hydrogen bond formation between a covalently bound fluorine and hydroxyl hydrogen is influenced by ring size, high resolution infrared studies were performed on *o*-trifluoromethylphenol, a system in which a six-membered ring will be formed if intramolecular hydrogen bonding occurs.

Experimental Section

The spectra were recorded with a Beckman IR-12 spectrometer and a VLT-2 variable temperature unit. The trifluoromethylphenols studied were obtained from the Peninsular ChemResearch, Inc., and purified by vacuum distillation or sublimation. Samples of the *o*-trifluoromethylphenol were triply vacuum sublimed and sealed in glass ampoules under nitrogen until the solutions were prepared. The final purity of the *o*-trifluoromethylphenol was determined by a pH titration in aqueous solution to be 99% or better. In order to prepare solutions containing a minimum quantity of water, spectroscopic grade isooctane which had been dried over molecular sieve was mixed in a dry bag under nitrogen with the samples sealed in the glass ampoules. The resulting solutions were then transferred to the infrared cells in the dry bag under nitrogen. Compensation for the solvent bands in the 3600-cm⁻¹ region was accomplished with a variable path length cell in the reference beam of the spectrometer.

Results

The infrared spectra of phenol and the three isomers of trifluoromethylphenol were recorded in the 3600-cm⁻¹ region in isooctane solutions dilute enough so that no intermolecular association could be detected. For phe-

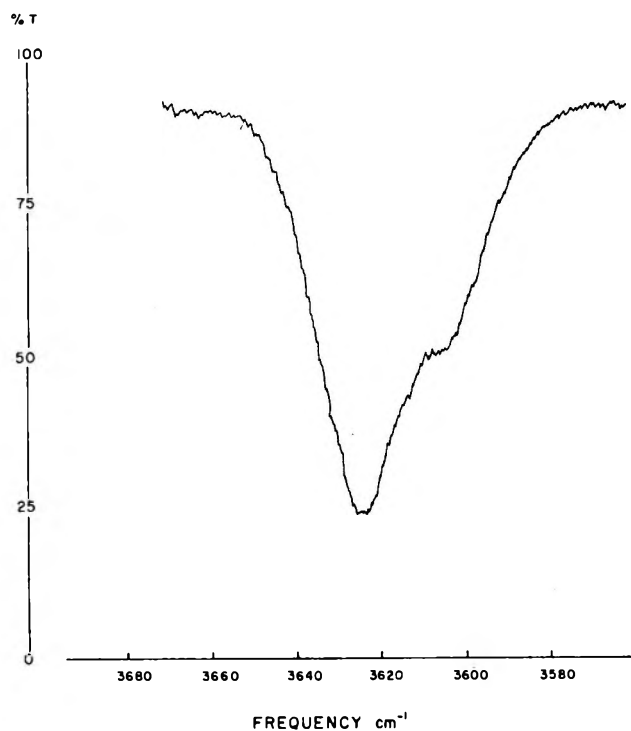


Figure 1. Infrared spectrum of *o*-trifluoromethylphenol in isooctane in the 3600-cm⁻¹ region.

mol and the *m*- and *p*-trifluoromethylphenols symmetrical bands with approximately Lorentzian shapes were observed with maxima at 3619.5, 3617.5, and 3622.0, respectively. The band corresponding to the OH stretching mode for *o*-trifluoromethylphenol was asymmetric and is shown in Figure 1. The observed spectra could be reproduced by two overlapping Lorentzian bands with maxima at 3606 and 3624 cm⁻¹. A series of spectra were determined for an identical solution at several different temperatures. Using an iterative procedure, the relative areas of the bands were determined and the ratio of the band centered at 3624 to that at 3606 was evaluated for each temperature studied. The temperatures and the corresponding ratios are given in Table I.

The shoulder which appears on the band assigned to

* To whom correspondence should be addressed.

- (1) H. Bourana-Bataille, P. Sauvageau, and C. Sandorfy, *Can. J. Chem.*, **41**, 2240 (1963).
- (2) A. W. Baker and W. W. Kaeding, *J. Amer. Chem. Soc.*, **81**, 5904 (1959).
- (3) E. A. Allan and L. W. Reeves, *J. Phys. Chem.*, **66**, 613 (1962).
- (4) J. H. Richards and S. Walker, *Trans. Faraday Soc.*, **55**, 220 (1959).
- (5) P. J. Krueger and H. D. Mettee, *Can. J. Chem.*, **42**, 326 (1964).
- (6) P. J. Krueger and H. D. Mettee, *ibid.*, **42**, 340 (1964).
- (7) D. A. K. Jones and J. G. Watkinson, *Proc. Chem. Soc. London*, 2371 (1964).
- (8) D. A. K. Jones and J. G. Watkinson, *J. Chem. Soc. London*, 2366 (1964).
- (9) P. J. Krueger and H. D. Mettee, *Can. J. Chem.*, **42**, 288 (1964).
- (10) L. J. Bellamy and R. J. Pace, *Spectrochim. Acta, Part A*, **25**, 319 (1969).

Table I: Ratios of the Integrated Intensity of the trans to the cis Bands

Temp. °C	Ratio
25	2.1333
10	1.8975
-15	1.4959
-25	1.3368
-30	1.2565

the OH stretching mode of *o*-trifluoromethylphenol is assigned to the cis isomer where intramolecular hydrogen bonding could stabilize this conformation. If the ratio of the extinction coefficients of the cis (3606 cm⁻¹) and trans (3624 cm⁻¹) bands is approximately constant over the temperature range studied, the ratios given in Table I are related to the equilibrium constants for interconversion merely by a constant. A plot of the log of the ratios given in Table I vs. the reciprocal of the absolute temperature is shown in Figure 2. From the slope of the straight line obtained, the enthalpy difference between the cis and trans conformation was determined by standard thermodynamic relationship to be 1.4 kcal/mol.

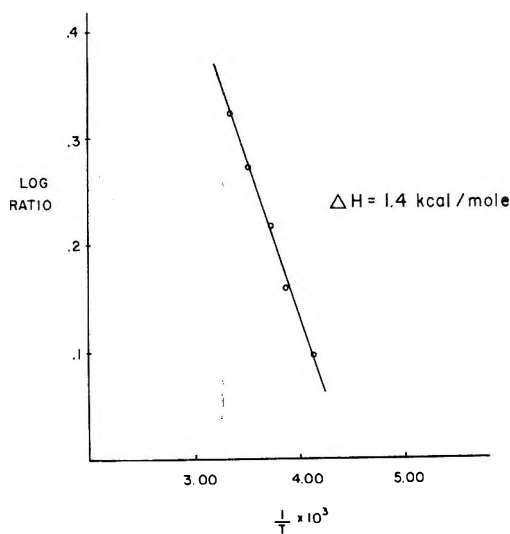


Figure 2. A plot of the log of the ratios tabulated in Table I vs. $1/T^{\circ}\text{K}$.

A separation of 18 cm⁻¹ between the cis and trans conformation is considerably less than that found for intermolecular association of phenol with a covalently bound fluorine⁹ (39.7 cm⁻¹). However, the frequency change is almost identical with that reported for the intramolecular association postulated for monofluoroethanol⁵ (15.5 cm⁻¹) and trifluoroethanol⁶ (19.0 cm⁻¹). The enthalpy difference derived from these data is significantly smaller than found in the above examples (2.13, 2.07, and 3.32 kcal/mol, respectively). From these

comparisons it appears that an increase in ring size from five to six members does not influence appreciably the magnitude of the hydrogen bond interaction.

These results cannot be adequately compared with the *o*-fluorophenol system since the OH stretching mode in this system appears to have no detectable asymmetry. They do suggest, however, that the interactions in the cis isomer of *o*-fluorophenol are too weak to result in an observable frequency shift.

Diaphragm Cell Diffusion Studies with Short Prediffusion Times

by Michael J. Pika

Chemistry Department, University of Tennessee, Knoxville, Tennessee 37916 (Received May 27, 1970)

The diaphragm cell has proven to be a very useful tool in the study of liquid diffusion.¹⁻⁵ The basic feature of a diaphragm cell is the porous membrane, which is usually a glass frit separating an upper and a lower compartment containing liquids of different composition. If the concentration of diffusing species is initially zero in the upper compartment, the classical analysis⁶ shows that from the duration of the diffusion experiment, t , and the concentration of the diffusing species in the upper and lower compartments at the end of the run, denoted by W and V , respectively, the diffusion coefficients may be calculated from the equation

$$D = (1/\beta t) \ln \left(\frac{1 + fW/V}{1 - W/V} \right) \quad (1)$$

Here, β is a cell constant determined by calibration, and f is defined by

$$f = \frac{V^u + V_D/2}{V^L + V_D/2} \quad (2)$$

where V^u and V^L are the volumes of the upper and lower compartments, respectively, and V_D is the volume of the frit. The derivation of eq 1 assumes the concentration distribution in the frit is linear throughout the experiment, although it has been shown⁷ that as long as the

(1) J. N. Northrop and M. L. Anson, *J. Gen. Physiol.*, **12**, 543 (1928).

(2) A. R. Gordon, *Ann. N. Y. Acad. Sci.*, **46**, 285 (1945).

(3) R. H. Stokes, *J. Amer. Chem. Soc.*, **72**, 763 (1950).

(4) J. G. Albright and R. Mills, *J. Phys. Chem.*, **69**, 3120 (1965).

(5) R. Mills and L. A. Woolf, "The Diaphragm Cell," Australian National University Press, Canberra, Australia, 1968.

(6) See R. A. Robinson and R. H. Stokes, "Electrolyte Solutions," Academic Press, New York, N. Y., 1959, Chapter 10.

(7) C. Barnes, *Physics*, **5**, 4 (1934).

initial concentration distribution is linear, eq 1 is still valid in all practical cases.

For the purpose of developing an initial linear concentration distribution, a prediffusion step is introduced into the experimental procedure. In a tracer experiment (*i.e.*, where the diffusing species is present in small concentration and moves in an essentially homogenous environment), the upper compartment and the diaphragm are initially filled with solution devoid of tracer species. Solution containing the tracer (labeled solution) is placed in the lower compartment, and diffusion is allowed to proceed for prediffusion time, τ . Next, the solution in the upper compartment is removed, and the compartment is rinsed with unlabeled solution. Fresh unlabeled solution is then placed in the upper compartment, and the actual diffusion run is started. The assumption is that after a sufficiently long prediffusion time, the concentration distribution in the frit is linear and eq 1 is valid.

The question is, of course, how long must the prediffusion time be to preclude serious error due to the failure of eq 1. The usual procedure^{2,5,8} is to determine a "rough but safe" lower limit for τ from the Gordon inequality, $D\tau/l^2 > 1.2$, where D is the diffusion coefficient in cm^2/sec and l is the "apparent thickness" of the frit ($l \approx 1.6 \times \text{actual thickness}$). For the usual type of frit, $l \approx 0.4 \text{ cm}$, and if $D = 2 \times 10^{-5} \text{ cm}^2/\text{sec}$, τ is of the order of 3 hr. However, if $D = 2 \times 10^{-6} \text{ cm}^2/\text{sec}$, the estimated preliminary diffusion time is 30 hr. Thus, the diaphragm cell technique does not appear to be practical when the diffusion coefficients are small, particularly if short-lived isotopes are to be studied or the solution undergoes slow chemical decomposition. However, there is evidence which suggests that the Gordon inequality overestimates the time required to establish a linear concentration distribution.⁹

The purpose of this note is to present the results of a combined theoretical and experimental investigation of the effect of variation in prediffusion time on the "apparent" diffusion coefficient calculated from eq 1. A theoretical "correction" to be applied to eq 1 for short prediffusion times will be derived. Experimental data will be presented which indicate the theoretical correction is accurate within $\pm 30\%$ or better. The practical result of this study is that a prediffusion time smaller by a factor of five than those given by the Gordon inequality may be used without introducing serious error.

Theory

The following discussion refers to a tracer diffusion experiment where the tracer is originally in the lower compartment and is allowed to diffuse into the upper compartment. The diaphragm is devoid of tracer at the start of prediffusion. Both compartments are taken to have the same volume. The theory developed here is basically an extension of the earlier work of

Barnes.⁷ The general procedure is to first evaluate the concentration distribution in the frit at the start of the diffusion run. The distribution function derived contains a nonlinear term depending on τ . Next, this distribution function is used to relate the concentrations of diffusing species in the upper and lower compartments to the product Dt . Algebraic manipulation of the resulting equation then yields the diffusion coefficient as a sum of two terms. The first term is the right-hand side of eq 1, while the second term is the theoretical "correction" for a short prediffusion time. The symbols used are defined as follows.

$$\lambda \equiv V_D/V^u = V_D/V^L$$

V_0 = concentration of tracer in the lower compartment at the start of the diffusion run (*i.e.*, at $t = 0$); V_0' = concentration of tracer in the lower compartment at the start of prediffusion; W_τ = concentration of tracer in the upper compartment at the conclusion of prediffusion; $W_0 = 0$ = concentration of tracer in the upper compartment at the start of the diffusion run; a = effective volume of a frit of unit area; $U_0(x)$ = concentration of a tracer in the frit at position x ($0 \leq x \leq a$) at the conclusion of prediffusion (and at the start of the diffusion run).

Barnes⁷ has given several solutions of the problem of diffusion through a membrane based upon a solution of Fick's second law subject to the appropriate boundary conditions. In the case where the concentration distribution in the frit is initially linear (gradient filled case), Barnes' equations reduce to eq 1 for all practical purposes, with the cell constant being given by $\beta = 2\lambda(1 - \lambda/6 + \lambda^2/45)/a^2$. Another situation considered by Barnes was the case in which the frit is initially free of tracer, and no prediffusion period is used. In this case (solvent-filled case), omitting the small quadratic terms in λ and the vanishingly small series term, Barnes' results may be written in the form

$$D = D^1 + (1/\beta\tau) \ln [(1 - \lambda/6)/(1 - \lambda/2)] \quad (3)$$

where D^1 represents the value of the diffusion coefficient calculated from eq 1.

We now consider the solution of the diffusion problem in the more general case where the initial concentration distribution in the frit is determined by the prediffusion conditions. Our solution will correspond to the systematic retention of all significant terms linear in λ ; the quadratic terms in λ will be omitted. From the equations given by Barnes, we find that the concentration distribution in the frit at the start of the diffusion run is given by

(8) A. L. Geddes and R. B. Pontius in "Physical Methods of Organic Chemistry," Part 2, A. Weissberger, Ed., Interscience Publishers, Inc., New York, N. Y., 1960, p 895.

(9) R. Mills, L. A. Woolf, and R. O. Waats, *A.I.Ch.E. J.*, **14**, 671 (1968).

$$U_0(x) = V_0(1 - x/a) + W_\tau x/a - (2V_0'/\pi) \sum_{n=1}^{\infty} \frac{e^{-\xi_n \tau}}{n} \sin(n\pi x/a) \quad (4)$$

where

$$\xi_n = Dn^2\pi^2/a^2 \quad (n = 1, 2, \dots) \quad (5)$$

and

$$W_\tau = (V_0'/2)(1 - e^{-\beta D \tau}) \quad (6)$$

Following the procedure outlined by Barnes with $U_0(x)$ given by eq 4, and using the approximation $V_0' = V_0$ in eq 4, we find

$$V = (V_0/2)[1 - 4\lambda S_1/\pi^2 + W_\tau \lambda/2V_0 + (1 - 4\lambda S_2/\pi^2 - W_\tau \lambda/6V_0)e^{-D\beta t}] \quad (7)$$

$$W = (V_0/2)[1 - 4\lambda S_1/\pi^2 + W_\tau \lambda/2V_0 - (1 - 4\lambda S_2/\pi^2 - W_\tau \lambda/6V_0)e^{-D\beta t}] \quad (8)$$

with

$$S_1 \equiv \sum_{\substack{n \\ \text{odd}}} \frac{e^{-\xi_n \tau}}{n^2} \quad (9)$$

$$S_2 \equiv \sum_{\substack{n \\ \text{even}}} \frac{e^{-\xi_n \tau}}{n^2} \quad (10)$$

Rearrangement of eq 7 and 8 to eliminate V_0 and using the good approximation, $W_\tau \approx V_0\beta D\tau/2$, yields the desired result

$$D = D^1 + (1/\beta t) \ln [(1 - \alpha_2)/(1 - \alpha_1)] \quad (11)$$

where D^1 is, again, the value of D calculated from eq 1. The symbols α_1 and α_2 represent the functions

$$\alpha_1 \equiv (4S_1/\pi^2 - \beta D\tau/4)\lambda \quad (12)$$

$$\alpha_2 \equiv (4S_2/\pi^2 + \beta D\tau/12)\lambda \quad (13)$$

When α_1 and α_2 are small compared to unity, the function $D - D^1$ may be simplified to

$$D - D^1 = \frac{\lambda}{\beta t} \left[\frac{4}{\pi^2} (S_1 - S_2) - \beta D\tau/3 \right] \quad (14)$$

The presence of S_1 and S_2 reflect the lack of "filling" the frit to a linear concentration profile, while the presence of $\beta D\tau$ reflects the partial "emptying" of the frit at the start of diffusion when the upper solution containing tracer is replaced with fresh unlabeled solution. The terms involving S_1 and S_2 may be significant if the prediffusion time is very short, while the term in $\beta D\tau$ is significant only when the prediffusion time is of the same order of magnitude as the length of the diffusion run.

It should be noted that the calculation of $D - D^1$ by eq 11 requires a preliminary estimate of D to evaluate α_1 and α_2 . As a first approximation, $D \cong D^1$ may be used to evaluate α_1 and α_2 . Also, the parameter a is

needed to evaluate S_1 and S_2 . The approximation, $\beta \cong 2\lambda/a^2$, may be used for this purpose.

It is a simple matter to verify that our solution reduces to the solvent filled case as $\tau \rightarrow 0$, as it should. When $\tau = 0$, $S_1 = \sum_{\substack{n \\ \text{odd}}} 1/n^2 = \pi^2/8$, and $S_2 = \sum_{\substack{n \\ \text{even}}} 1/n^2 = \pi^2/24$. Therefore, as $\tau \rightarrow 0$, $\alpha_1 \rightarrow \lambda/2$, $\alpha_2 \rightarrow \lambda/6$, and eq 11 reduces to the solvent-filled case.

Experimental Section

To demonstrate the essential validity of eq 11, one tracer diffusion run was made with each of two diaphragm cells. In each cell, a small volume of solution containing trace amounts of $^{24}\text{Na}^+$, $^{45}\text{Ca}^{2+}$, and $^{88}\text{Y}^{3+}$ was added to the solution in the lower compartment. For each cell, the concentration ratios W/V were determined for the three isotopes by taking advantage of the short half-life of $^{24}\text{Na}^+$ and the counting characteristics of the isotopes. Diffusion coefficients were then calculated using eq 11. The diffusion conditions were chosen so that the function $D - D^1$, for each isotope, was significant for cell 1 but insignificant for cell 2'.

Magnetically stirred diaphragm cells of the Stokes design,³ with Teflon bottom plugs,⁴ were used in the experiments. The stirring rate was 60 rpm. The calibration constants, β , were evaluated in the usual way by allowing 0.5 *N* potassium chloride to diffuse into pure water.

The potassium chloride and sodium chloride were reagent grade chemicals. The potassium chloride was recrystallized once from water. All solutions were filtered through a fine glass frit before use and were then degassed. Triple-distilled water was used in this research. The 1.00 *m* sodium chloride solution was prepared from weighed quantities of the dried salt and distilled water. The radioactive isotopes, yttrium-88 and calcium-45, were obtained from the Isotopes Division of Oak Ridge National Laboratory, Oak Ridge, Tenn. The sodium-24 used in this research was prepared by irradiation of reagent grade sodium carbonate using the Oak Ridge research reactor at Oak Ridge National Laboratory. The radioactive purities of the yttrium-88 and of the sodium-24 samples were verified by checking their respective γ -ray spectra.

The following procedure was employed. Trace amounts of the radioactive species, $^{24}\text{Na}^+$, $^{88}\text{Y}^{3+}$, and $^{45}\text{Ca}^{2+}$ were added to 1.00 *m* sodium chloride in the lower compartment. Diffusion was allowed to proceed for a prediffusion time, τ . The upper compartments were then emptied and rinsed four times with 20-ml portions of 1.00 *m* sodium chloride. The diffusion run was begun when the final filling of the upper compartment was started. Within a few hours after the conclusion of the diffusion run, "initial" counting rates of weighed samples of the upper and lower compartments were determined on a well type sodium iodide scintillation counter. After sufficient time had elapsed

for the sodium-24 to decay away, the same samples were again counted on the sodium iodide counter to give final counting rates. To detect a possible change of counting efficiency between the initial counting period and the final counting period, a standard solution of yttrium-88 was counted each time. The initial and final counting rate data, plus the experimental observation that the β decay of calcium-45 did not register on the sodium iodide counter, allowed calculation of X_{Na^+} and $X_{\text{Y}^{3+}}$, where X denotes the ratio W/V . Appropriate decay corrections were made for decay of sodium-24 during the initial counting period and for the decay of yttrium-88 between the time of the initial counting period and the time of the final counting period. To evaluate $X_{\text{Ca}^{2+}}$, samples from the upper and lower compartments were counted on a Model 314 EX Packard Tri-Carb liquid scintillation counter using the scintillation cocktail described by Bray.¹⁰ The experimentally determined counting efficiency of yttrium-88 on the Tri-Carb (measured relative to the efficiency on the sodium iodide counter) allowed the contribution of the yttrium-88 to the observed counting rates to be eliminated, since the yttrium-88 counting rate on the sodium iodide counter was known. Corrections for background were, of course, applied in all of the counting experiments. The counting rates were low enough so that coincidence corrections were not needed. The experimental values of X are given in Table I along with other relevant ex-

Table I: Experimental Parameters

Parameter	Cell 1	Cell 2'
β	0.13985	0.12000
λ	0.0148	0.013
f	1.0124	0.9117
τ , sec	2.28×10^3	3.765×10^4
t , sec	3.750×10^4	4.956×10^4
$10^2 \times X(\text{Na}^+)$	3.172 ± 0.014	3.878 ± 0.027
$10^2 \times X(\text{Ca}^{2+})$	1.887 ± 0.012	2.420 ± 0.019
$10^2 \times X(\text{Y}^{3+})$	1.454 ± 0.008	1.975 ± 0.005

perimental data. The error limits on the X values correspond to a 90% confidence limit, *considering counting errors only*. To provide a test of the theory under conditions where $D - D^1$ is large, both the prediffusion time and the diffusion time for cell 1 were kept very short, while the prediffusion time for cell 2' was long enough for a linear concentration profile to be established. Unfortunately, this procedure also has the effect of making the results very sensitive to any small disturbance of the frit during handling. However, past experience in this laboratory indicates that the "error" in the D^1 values reported here introduced by "frit disturbance" should be less than the corresponding "error" introduced by the uncertainty in the counting data.

Results and Discussion

From the data in Table I, a value of D^1 was calculated using eq 1, and the "correction term", $D - D^1$, was calculated using eq 11. To evaluate α_1 and α_2 , the value of D^1 from cell 2' was used as an approximation for D . The approximation, $a^2 = 2\lambda/\beta$ was used to evaluate a^2 . The results of these calculations were then combined to give a value of the diffusion coefficient, D . Since, for cell 1, the "correction term" is significantly larger than the experimental uncertainty in the value of D , a test of the theory may be made by comparing a diffusion coefficient obtained from cell 1 with the corresponding quantity obtained from cell 2'. The results of this comparison are given in Table II,

Table II: Comparison of Theory with Experiment: Tracer Diffusion Coefficients in 1.00 *N* Aqueous NaCl at 25°

Ion	$-10^5(D - D^1)$ theory		$10^5 D$	
	Cell 1	Cell 2'	Cell 1	Cell 2'
$^{24}\text{Na}^+$	0.030	-0.004	1.247 ^a	1.244 ^a
$^{45}\text{Ca}^{2+}$	0.049	-0.002	0.773	0.777
$^{88}\text{Y}^{3+}$	0.056	-0.002	0.614	0.633

^a For sodium-22, $10^5 D_{\text{Na}^+} = 1.236$ [R. Mills, *Rev. Pure Appl. Chem.*, **11**, 78 (1961)].

where theoretical values of $D - D^1$ and the corresponding diffusion coefficients are listed. Each entry represents the result of a single experiment. We note that good agreement between the cell 1 and cell 2' diffusion coefficients is found for both $^{24}\text{Na}^+$ and $^{45}\text{Ca}^{2+}$. For $^{88}\text{Y}^{3+}$, however, the cell 1 value is about 3.1% lower than the cell 2' value. This difference may be due to experimental error. However, the possibility of a small defect in the theory cannot be ignored. More extensive experimentation would be needed to settle this point. Since we expect no significant isotope effect between $^{24}\text{Na}^+$ diffusion and $^{22}\text{Na}^+$ diffusion,¹¹ it is significant to note that the diffusion coefficient for $^{24}\text{Na}^+$ determined in this research is in good agreement with the literature value for $^{22}\text{Na}^+$. With due consideration of the experimental uncertainties, we conclude, from the data, that the theoretical expression for $D - D^1$ is in error by no more than ~30% for the range of $D\tau$ values spanned by the data. Thus, the data, although sparse, do demonstrate that the theoretical expression for $D - D^1$ is, at worst, semiquantitative. Indeed, the expression for $D - D^1$ may be quantitative. However, in the absence of additional data, it would seem advisable to restrict the use of eq 11 to systems

(10) G. A. Bray, *Anal. Biochem.*, **1**, 279 (1960).

(11) Preliminary measurements in this laboratory have indicated that there is no significant isotope effect (*i.e.*, above ~0.5%) between $^{24}\text{Na}^+$ and $^{22}\text{Na}^+$ diffusion in 4.0 *M* NaCl. Therefore, we also expect the absence of an isotope effect in 1.00 *M* NaCl.

where an error of $\sim 30\%$ in $D - D^1$ has a negligible effect on D . In practice, this is not a serious restriction. To carry out more stringent tests of the $D - D^1$ correction, one should use diaphragm cells having values of λ considerably larger than the cells used here.

The results of this research demonstrate that one may use prediffusion times significantly less than those calculated from the Gordon inequality. For example, in the case of Na^+ diffusion in 1.00 M NaCl, the Gordon prediffusion time is about 4 hr. Yet, as the data in Table II indicate, accurate diffusion data may be obtained when the prediffusion time is only about 0.5 hr, provided the correction term, $D - D^1$, is used. The practical significance of this research is more obvious when diffusion coefficients are very small. For exam-

ple, if $D = 2 \times 10^{-6}$ cm²/sec, the Gordon prediffusion time is about 30 hr for our diaphragm cells, which are typical of those in common use. However, by using the correction term, $D - D^1$ (assumed to be accurate within 30%) diffusion data accurate to within 1% may be obtained even when the prediffusion time is only 5 hr and the diffusion time is 24 hr.

Acknowledgments. Acknowledgment is made to the donors of the Petroleum Research Fund, administered by the American Chemical Society, and to the University of Tennessee Faculty Research Fellowship Fund for partial support of this research. The author wishes to thank Dr. G. E. Boyd and Oak Ridge National Laboratory for the use of laboratory facilities.

COMMUNICATIONS TO THE EDITOR

Photodissociation of an e_{aq}^- Complex in Hydrogen-Saturated Alkaline Solutions

Sir: We have discovered an unstable transient species in continuously photolyzed H_2 -saturated NaOH solutions at pH 11. This species may be ionized by light of wavelengths as long as 340 nm and produces e_{aq}^- , the hydrated electron. Since the concentration of e_{aq}^- produced on photoionization increases with added Na^+ concentration, we tentatively attribute this species to a dissociable complex involving Na^+ and e_{aq}^- . Assuming its structure to be $(\text{Na}^+ \cdot e^-)_{\text{aq}}$ we write



However, at this stage, an impurity- e_{aq}^- complex, H^- , or excited water cannot be excluded.

The apparatus used for creating and detecting this species is diagrammed in Figure 1. It consists of a sensitive e_{aq}^- detector, an Hg vapor lamp for generating a steady-state concentration of e_{aq}^- , and an analyzing xenon flash lamp. The tungsten lamp (a), Suprasil irradiation cell (b), 700-nm filter (c), photomultiplier (d), 400-channel analyzer (e), and XY recorder (f) constitute the e_{aq}^- detecting system. With it we may study transient e_{aq}^- signals with a sensitivity of 0.1 nM. Hydrated electrons are continuously generated in the irradiation cell (b) at a rate of about 10 nM/sec by a low-pressure Hg vapor lamp (g). A xenon lamp (h) provides a 50-joule light flash of 30- μ sec half-width and generates about 50 nM e_{aq}^- when placed at a distance of 20 cm from cell b. Lamps g and h produce and transmit light down to <200 nm.

We interpose Corning filters 0-52 and 0-53 in holder i in order to absorb the shorter wavelengths. See the inset of Figure 2 for the optical transmission properties of these filters. In juxtaposition with (i) about 300 nM e_{aq}^- is produced by the xenon flash without the cutoff filters. The reliability of this unit is greatly improved over the earlier model¹ by accumulating the signals from several carefully controlled flashes for each experiment. The e_{aq}^- signals are stored in the 400-channel analyzer and read out on an XY recorder.

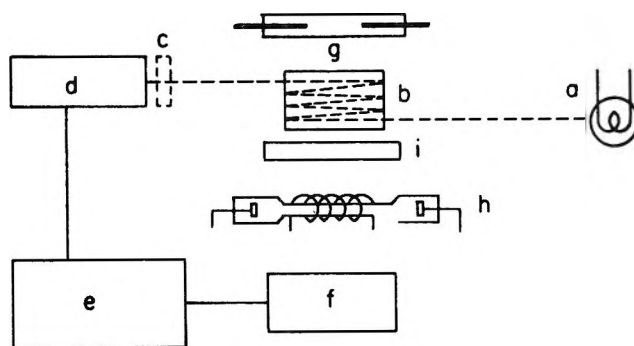


Figure 1. Schematic drawing of e_{aq}^- photogeneration apparatus: (a) tungsten lamp, (b) a 5-cm Suprasil "irradiation cell" with an associated optical system providing seven light passes (35-cm path length), (c) a filter combination transmitting 700-nm light, (d) photomultiplier, (e) 400-channel analyzer, (f) XY recorder, (g) low-pressure Hg vapor lamp with uv transmitting jacket, (h) xenon flash lamp, and (i) light filter holder.

(1) K. Schmidt and E. J. Hart, *Advan. Chem. Ser.*, **81**, 267 (1968).

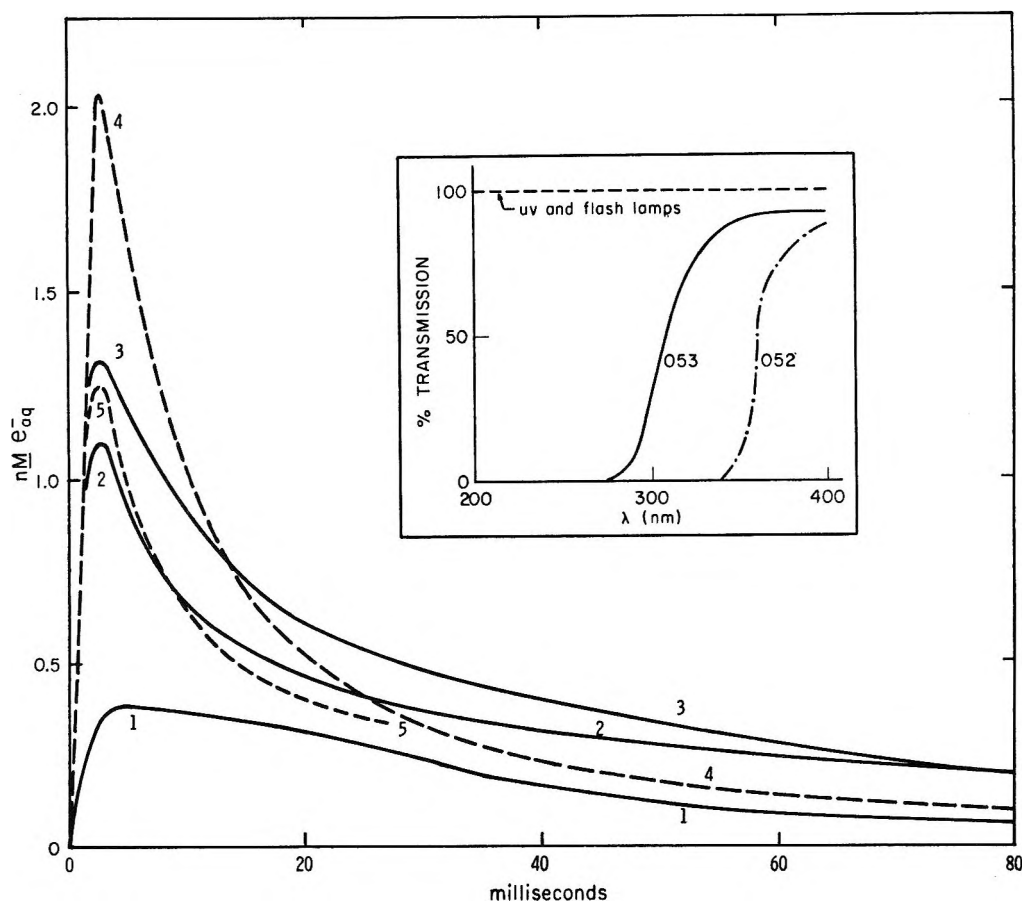


Figure 2. Photodissociation of e_{aq}^- complex in photolyzed H_2 -saturated solution of pH 11: curve 1, black filter (noise and pickup), or 0-53, Hg lamp off, or 0-52, Hg lamp on, 1 A; curve 2, 0-53, Hg lamp on, 1 A; curve 3, 0-53, Hg lamp on, 2 A; curve 4, 0-53, Hg lamp on, 2 A, $10^{-2} M NaClO_4$ added; curve 5, 0-52, Hg lamp on, 1 A, $10^{-2} M NaClO_4$ added. Inset: transmission of Hg vapor lamp, xenon flash lamp, and Corning filters 0-52 and 0-53

Curves 1-5 of Figure 2 reveal our results. They are traces of e_{aq}^- formation and decay curves averaged from five xenon lamp flashes by the method described above. They were taken with the Hg lamp operating at a "normal" 1 A, at 2 A, or with a closed shutter so that no light from the steady mercury lamp reached the cell. Under this latter condition e_{aq}^- is not produced by the xenon flash with filter 0-53, having a cut-off at 280 nm, since the signal produced is identical with that obtained with an opaque "black" filter. We attribute the signal of curve 1 to noise and to electrical and magnetic pickup by the photomultiplier when the xenon lamp is discharged.

The e_{aq}^- signal from a species in the photolyzed solution is evident by comparing trace 2 with 1. This comparison demonstrates that e_{aq}^- is generated by a xenon flash at $\lambda > 280$ nm, but only when the solution is being irradiated by the mercury lamp. The strength of the signal also increases with current supplied to the mercury lamp. (Compare traces 2 and 3.)

That Na^+ enhances the signal is shown by comparing trace 4 with 3 and trace 5 with 1. Traces 4 and 5 were obtained from the H_2 -saturated pH 11 solution to which $0.01 M NaClO_4$ was added. The comparison of

trace 3 with 4 shows that the e_{aq}^- signal is nearly doubled by light of $\lambda > 280$ nm in the presence of $0.01 M NaClO_4$. Even at 340 nm e_{aq}^- is generated in these $NaClO_4$ solutions when the mercury lamp is on. (Compare trace 5 with 1.)

We interpret our results as the photodissociation of an unstable $(Na^+ \cdot e^-)_{aq}$ complex and represent the process by reaction 1. This "neutral" species has its counterpart in the "monomer" units postulated in metal-ammonia solutions.² Our assignment is chiefly based on the enhancement by added $NaClO_4$. There could also be a contribution from the ClO_4^- although traces 2 and 3 show that ClO_4^- is unnecessary to produce the e_{aq}^- signal.

The dielectron, $(e_2^{2-})_{aq}$, has been postulated as a species dissociable into e_{aq}^- by light of $\lambda > 800$ nm.³ We may unequivocally exclude $(e_2^{2-})_{aq}$ as the species responsible for our result. Because our flash lamp has a high intensity of light of $\lambda > 800$ nm where $(e_2^{2-})_{aq}$ is believed to absorb, we would have obtained a signal

(2) W. L. Jolly, *Advan. Chem. Ser.*, **50**, 27 (1965).

(3) N. Basco, G. A. Kenney, and D. C. Walker, *Chem. Commun.*, 917 (1969).

with a xenon flash transmitting light of $\lambda > 340$ nm as long as the Hg lamp was on. The absence of a signal using the 0-52 filter with the lamp on is the basis for this conclusion. (See curve 1 of Figure 2.)

Other conceivable species could be impurities, H^- , and excited water. Impurities are difficult to exclude since their concentration is increased with the addition of $NaClO_4$. At this stage H^- is also a candidate, but this ion may be easily tested by increasing the pH to a point where the steady-state concentration of H atoms is vanishingly small. Since our optical system transmits light well into the first fundamental band of water it is conceivable that a small concentration of a dissociable "excited" water may contribute to this effect. However, the large enhancement by Na^+ indicates that this source of e_{aq}^- is unlikely.

At the present time we know only that this species absorbs around 300 nm. It is tempting to associate it with the absorbing "monovalent" species produced by e_{aq}^- reaction with bivalent ions such as Zn^{2+} , Cd^{2+} , Mn^{2+} , and Pb^{2+} .⁴ Each of these "monovalent" ions has an intense absorption band centered at 310 nm. We plan to investigate the photodissociation of these ions by our apparatus.

If e_{aq}^- forms a complex with Na^+ a new area of photochemical research opens up encompassing the alkali and alkaline earth ions as well as other unstable reduced complexes.

(4) G. E. Adams, J. H. Baxendale, and J. W. Boag, *Proc. Chem. Soc.*, 241 (1963).

BHABHA ATOMIC RESEARCH CENTRE
TROMBAY, BOMBAY, INDIA

C. GOPINATHAN

ARGONNE NATIONAL LABORATORY
ARGONNE, ILLINOIS

E. J. HART
K. H. SCHMIDT

RECEIVED July 20, 1970

Isentropic Compressibility of Ideal Solutions

Sir: In a recent publication,¹ Blandamer and Waddington defined the excess isentropic compressibility $[(K_s')^E]$ of a liquid mixture as the difference between the observed isentropic compressibility $[K_s']$ and that of an ideal solution $[(K_s')_{id}]$ as in eq 1. The isentropic compressibility of an ideal solution was represented as the mole fraction (x_i) average of the isentropic compressibilities of the pure liquids $[(K_s')_i^\circ]$.

$$(K_s')^E = K_s' - (K_s')_{id} \quad (1)$$

$$(K_s')_{id} = \sum x_i (K_s')_i^\circ \quad (2)$$

$$K_s' = -(\partial \ln V / \partial P)_s \quad (3)$$

$$K_t = -(\partial \ln V / \partial P)_t \quad (4)$$

Jacobson² used an expression similar to eq 2, but with volume fractions instead of mole fractions. Neither of these expressions is correct.

The isentropic compressibility of any solution is related to the isothermal compressibility $[K_t]$ by the ratio of the heat capacities at constant volume and constant pressure, as in eq 5. The isothermal compressibility of an ideal solution can easily be shown to equal the volume-fraction (v_i) average of the isothermal compressibilities of the pure liquids, and the heat capacity to equal the mole-fraction average of the heat capacities of the pure liquids. For an ideal binary solution, the isentropic compressibility is correctly represented by eq 6. Values of C_v° for the pure liquids can be calculated from C_p° , K_t° , the molar volume, and the coefficient of thermal expansion $[\alpha = (\partial \ln V / \partial T)_p]$, using eq 7, as suggested by Lewis and Randall.³ Since accurate values of K_t° are not available for all liquids, and since there is likely to be some discrepancy between values of K_s' calculated from sound velocity experiments and those calculated from eq 5 and 7, we suggest that the value of K_t° to be used for calculations of the excess isentropic compressibilities based on sound velocity measurements might best be calculated from K_s' for the pure liquid.

$$K_s' = K_t(C_v/C_p) \quad (5)$$

$$(K_s')_{id} = (v_1 K_{t1}^\circ + v_2 K_{t2}^\circ)(x_1 C_{v1}^\circ + x_2 C_{v2}^\circ) / (x_1 C_{p1}^\circ + x_2 C_{p2}^\circ) \quad (6)$$

$$C_p - C_v = \alpha^2 V T / K_t \quad (7)$$

In Figure 1, we show the excess isentropic compressibilities calculated from eq 1 and 6 for the systems methanol-water, ethanol-water, *n*-propanol-water, *tert*-butanol-water, and acetone-water. On each of these plots we indicate the composition at which the ultrasonic absorption is a maximum (PSAC).⁴ Blandamer and Waddington attempted to show a correlation between the PSAC and the position of zero excess isentropic compressibility in terms of the real and imaginary components of the total isentropic compressibility. A much more substantial correlation between the PSAC and the position of the minimum excess isentropic compressibility can be seen in our plots using the correct expression for the ideal solution term. A striking failure of this correlation is the absence of a PSAC for the system methanol-water.

(1) M. J. Blandamer and D. Waddington, *J. Phys. Chem.*, **74**, 2569 (1970).

(2) B. Jacobson, *Ark. Kemi*, **2**, 177 (1950).

(3) G. N. Lewis and M. Randall (revised by K. S. Pitzer and L. Brewer), "Thermodynamics," 2nd ed, McGraw-Hill, New York, N. Y., 1961, p 107.

(4) C. J. Burton, *J. Acoust. Soc. Amer.*, **20**, 186 (1948).

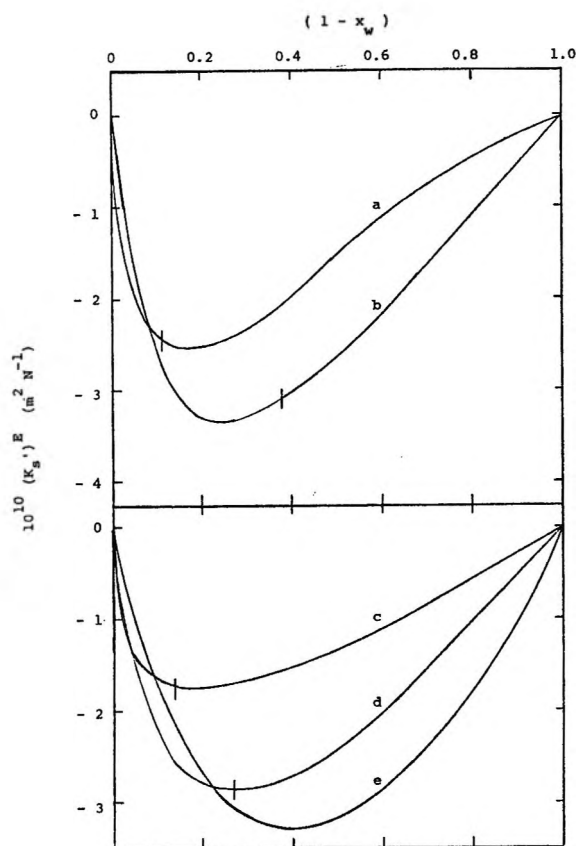


Figure 1. Excess isentropic compressibilities for the systems: (a) *tert*-butyl alcohol–water at 27°. Data are scaled from graph in ref 4. Density data are extrapolated from the data of A. Doroshevski, *J. Russ. Phys. Chem. Soc.*, **43**, 66 (1911); listed in J. Timmermans, "Physico-chemical Constants of Binary Systems in Concentrated Solutions," Vol. 4, Interscience, New York, N. Y. 1960; (b) acetone–water at 20° (ref 2); (c) *n*-propyl alcohol–water at 20° (ref 2); (d) ethanol–water at 20° (ref 2); (e) methanol–water at 20° (ref 2). The vertical hash marks on the curves indicate the composition at which the maximum ultrasonic absorption occurs (PSAC, ref 4).

(Dr. Blandamer has indicated to the editors that he concurs with the authors' comments on ref 1 of this communication.)

* To whom correspondence should be addressed.

DEPARTMENT OF CHEMISTRY
UNIVERSITY OF MISSOURI, ROLLA,
ROLLA, MISSOURI 65401

GARY L. BERTRAND*
LARRY E. SMITH

RECEIVED JUNE 29, 1970

Electronic Excitation Energy Transfer in Dye–Polyanion Complexes

Sir: The shift in the absorption spectra of cationic dyes upon interaction with polyanions (metachromasia) is the basis of a wide range of cytological and histochemical methods for identifying these materials in cells and

tissues.¹ Dye aggregation, rather than interaction between the ionic site and the dye, has been shown to be the major driving force in such interactions.² Changes in the fluorescence properties of the dye have also been noted, but this aspect has received little detailed study. A limitation of the dye-binding technique in quantitative study is the tendency of the emission to fade rapidly.³ In emission studies attention has been mainly devoted to DNA–acridine orange complexes, in an attempt to understand the powerful mutagenic activity of acridine dyes.⁴ Little is known about the mechanism of fluorescence quenching of cationic dyes by polyanions, and this is the objective of our investigation.

When acridine orange is added to dilute aqueous solutions of dextran sulfate or heparin the absorption and emission spectra depend on the ratio P/D where P is the number of available anionic sites and D is the number of dye molecules in solution. When $P/D \sim 1$ the dye has an absorption spectrum very similar to the aggregated dye in polymer free solution. When $P/D \gg 1$ the absorption spectrum is similar to that of the free monomeric dye. Unlike the spectral shift to the blue observed in absorption, increase of acridine orange concentration results in the buildup of a new emission band at longer wavelengths arising from excited dimer molecules. There is no detectable emission from excited states of larger aggregates.

The main features of both the emission and absorption spectra can be explained by the theory of exciton splitting.^{5,6} An upper singlet state of a monomer splits on N -fold aggregation into an N -fold band of levels with a band width depending on the intensity of monomer absorption as well as the relative orientations and separation of the dye molecules. The behavior of acridine orange molecules on interaction with the polyanions mentioned above is consistent with this theory and with the dye molecules forming laminar or card-pack aggregates. Apart from the strong exciton coupling which results in the blue shift in absorption, weak coupling is to be expected and should lead to rapid excitation energy transfer effects.

Experiments have been carried out on the quenching of fluorescence from acridine orange bound to polyanions by very low concentrations (10^{-8} to $10^{-7}M$) of methylene blue or thionine. In Figure 1 the Stern–Volmer plots for the quenching of acridine orange on dextran sulfate fluorescence are shown. F is the

(1) For an evaluation see J. W. Kelly, *Acta Histochem., Suppl.*, **1S**, 56 (1958).

(2) J. S. Moore, G. O. Phillips, D. M. Power, and J. V. Davies, *J. Chem. Soc. A*, 1155 (1970).

(3) P. J. Stoward, "Luminescence in Chemistry," E. J. Bowen, Ed, Van Nostrand, London, 1968, pp 222.

(4) I. Isenberg, R. B. Leslie, S. L. Baird, R. Rosenbluth, and R. Bersohn, *Proc. Nat. Acad. Sci. U. S.*, **52**, 374 (1964).

(5) A. S. Davydov, "Theory of Molecular Excitons (trans. by M. Kasha and M. Oppenheimer)," McGraw-Hill, New York, N. Y., 1962.

(6) M. Kasha, *Radiat. Res.*, **20**, 55, (1963).

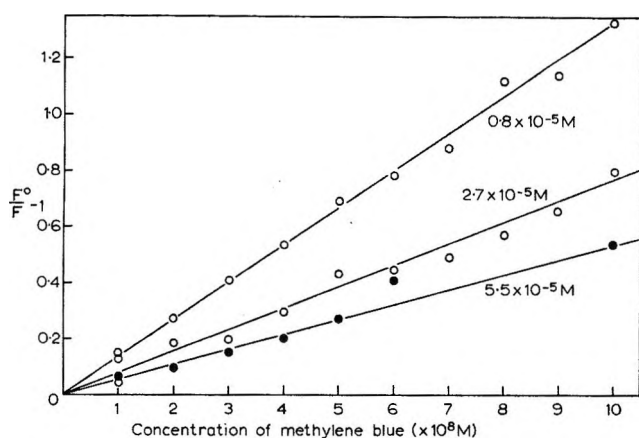


Figure 1. Stern-Volmer relationships for the quenching of the fluorescence of dextran sulfate-acridine orange complexes by methylene blue at various acridine orange concentrations. Dextran sulfate concentration 2×10^{-4} equivalent anionic sites per liter.

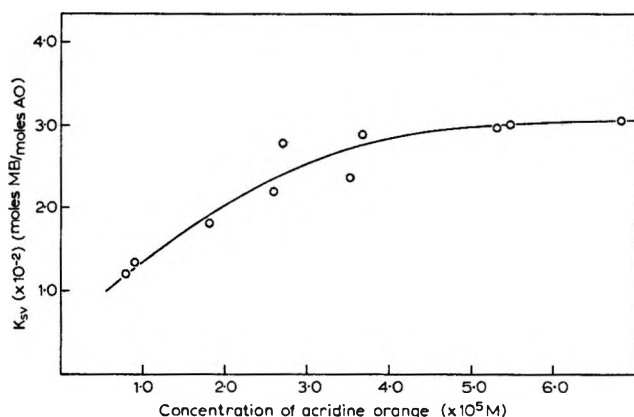


Figure 2. Variation of the Stern-Volmer constants, K_{sv} , with concentration of acridine orange for dextran sulfate-acridine orange complexes.

fluorescence intensity in the presence of quencher and F° the value in the absence of quencher. The values of K_{sv} (mole ratio units) which are given by the slopes of the plots multiplied by the acridine orange concentration do not depend significantly on the P/D ratio in the range 4–20, but increase with acridine orange concentration in the range $0.8\text{--}7 \times 10^{-5} M$ (Figure 2). Table I summarizes K_{sv} values obtained with both methylene blue and thionine on two polyanions. The exciting wavelength was chosen so that predominantly acridine orange dye aggregates were excited and the aggregation was unchanged by the small amounts of methylene blue or thionine present. In addition no evidence for the formation of mixed aggregates between acridine orange and quenching dye could be found.

K_{sv} measures the effectiveness of the methylene blue and thionine in the deactivation of excited states which give rise to dimer emission relative to the specific rate of decay in the absence of quenching dye. The values of K_{sv} are high and approach the maximum value of

Table I

Polyanion	Acridine orange concentration $\times 10^5 M$	P/D	Acceptor	K_{sv} (mole ratio units) $\times 10^{-2}$
Dextran sulfate ^a	5.3	10	Methylene Blue ^b	2.97
Dextran sulfate	5.5	4	Methylene Blue	3.03
Dextran sulfate	2.4	10	Thionine	2.24
Dextran sulfate	2.3	5	Thionine	2.59
Heparin	3.9	10	Methylene Blue	2.77
Heparin	3.6	5	Methylene Blue	2.84

^a Temperatures: 24° (dextran sulfate); 20° (heparin).

^b Acceptor concentrations varied between 10^{-8} and $10^{-7} M$.

about 4×10^4 found for quenching of anthracene fluorescence by naphthacene in anthracene crystals.^{7,8} "Energy hopping" between dye aggregates, similar to that postulated for organic crystals, must occur until, among other possibilities, trapping occurs at a dimer aggregate and fluorescence from the lower level of the first excited singlet state occurs.

Analysis of the results of the quenching experiments with heparin shows that energy migration from one polyanion-dye complex to another occurs. A typical heparin molecule used in these experiments had a molecular weight of about 10^4 and about 70 anion sites per molecule. From results given in Table I an acridine orange concentration of $3.9 \times 10^{-5} M$ and a mole ratio of 1.9×10^{-3} for methylene blue to acridine orange gives a 30% quenching. At $P/D = 10$ there is one methylene blue molecule for each 5200 sites and therefore at least 22 heparin molecules must, on average, be involved in each quenching act. If methylene blue molecules were only able to quench excited states of acridine orange on the same molecule as it was located there would only be 1.5% quenching. It can be shown by calculation that both diffusive and long-range Forster type energy transfer are not sufficiently effective to explain the observations under the experimental conditions. There must be a weak or intermediate exciton coupling between dye molecules on different polyanions in clusters formed under the conditions of solution. This interpretation is consistent with the lack of significant change in the effectiveness of energy transfer between aggregates when the P/D ratio is changed. The effect of increasing acridine orange concentration on the value of K_{sv} is probably due to quenching of the fluorescent dimer state by transfer to lower excited levels of higher aggregate.

The demonstration of rapid electronic energy transfer, apart from improving understanding of the behavior of

(7) J. B. Birks, "The Theory and Practice of Scintillation Counting," Pergamon, Oxford, 1964, p 259.

(8) D. C. Northrop and O. Simpson, *Proc. Roy. Soc. Ser. A.*, **234**, 136, (1956).

dyes used in fluorescence microscopy and histochemistry, provides a valid model for energy transfer under biological conditions. The extremely facile intermolecular energy transfer between aggregates, in particular, raises interesting possibilities about such processes being operative in the connective tissue matrix, where the polyanions are in similar association with a range of polycations.

It has also been found possible to render dye-polyanion systems resistant to fading under conditions of illumination. The small amounts of methylene blue or thionine added do not affect the absorption spectra, but seem to decrease the photodecomposition or photooxidation reactions of acridine orange in the presence of air. The decrease in fading brought about by methylene blue is much more marked than the quenching of dimer fluorescence. This useful finding is consistent with very rapid energy transfer involving a number of excited states. The high efficiency of transfer makes it possible for energy transfer from higher excited states to occur.

Acknowledgment. This work was supported in part by a grant from the Medical Research Council and the United States Department of Agriculture PL 480 Grant FG-UK-147.

* To whom correspondence should be addressed.

DEPARTMENT OF CHEMISTRY
THE UNIVERSITY, NOTTINGHAM, ENGLAND

R. B. CUNDALL
C. LEWIS

DEPARTMENT OF CHEMISTRY AND
APPLIED CHEMISTRY
THE UNIVERSITY SALFORD, M5 4WT, ENGLAND

P. J. LLEWELLYN
G. O. PHILLIPS*

RECEIVED JULY 25, 1970

Chemical Equilibrium and the Anti-Helmholtz Function. A Statistical Interpretation

Sir: Recently Duffin and Zener have discussed the problem of chemical equilibrium as formulated in the language of geometric programming.¹ They establish that the usual method of minimizing the Helmholtz free energy with respect to concentration of products and reactants is equivalent to maximizing an "anti-Helmholtz" function with respect to the activities of the atomic species present in the system. They also give a statistical mechanical interpretation of this approach in terms of the method of Darwin and Fowler. The well known relation between the "selector variables" of the Darwin-Fowler method and chemical activities suggests an alternate statistical interpretation of their results which clearly reveals the relationship between the atomic activities and the anti-Helmholtz function.

Let e_i ($i = 1$ to m) be the number of atoms of the i th atomic component in the system and $Z(\{e\})$ be the

canonical partition function for the set of atomic components $\{e\}$. The atomic composition of the system is, of course, unchanged by chemical reaction. The grand partition function $\Xi(\{\nu\})$ is then given by

$$\Xi(\{\nu\}) = \sum_{\{e\}} Z(\{e\}) \pi_i e^{\beta \nu_i e_i} \quad (1)$$

where ν_i is the chemical potential of the i th atomic species and β is the statistical temperature. The function $\Xi(\{\nu\})$ is essentially the Laplace transform of $Z(\{e\})$. Inverting the transform, we have

$$Z(\{e\}) = \left(\frac{1}{2\pi i}\right)^m \pi_j \left\{ \int_{\nu'_j - i\infty}^{\nu'_j + i\infty} d\nu_j \right\} \Xi(\{\nu\}) \pi_i e^{-\beta \nu_i e_i} \quad (2)$$

where ν'_j can be conveniently chosen (within the convergence limit) on the real axis of ν_j .

We can evaluate Ξ by making use of the fact that the only important contributions to Ξ come from energy levels which result from the atoms being associated in stable species. Let n_i ($i = 1$ to n) be the number of molecules of the i th stable compound and write the stoichiometric relations for the decomposition of molecules to atoms in the form

$$\sum_{i=1}^n n_i a_{ij} = e_j \quad (j = 1 \text{ to } m)$$

where a_{ij} are stoichiometric coefficients. Then

$$\Xi(\nu) = \sum_{\{e\}} Z(\{e\}) \pi_i e^{\beta \nu_i e_i} = \sum_{\{n\}} Z(\{n\}) \pi_i \lambda_i^{n_i} \quad (3)$$

where $\lambda_i = \pi_j e^{\beta \nu_j a_{ij}}$ is the activity of the i th molecular species. In the last equality we have made use of the fact that only atomic configurations corresponding to stable compounds give an important contribution to the sum. If we substitute eq 3 into eq 2 and evaluate the resulting integrals by the method of steepest descents, we obtain an expression for Z in terms of the minimum of the function $Z^*(\{\nu\}) = \Xi/\pi_i e^{\beta \nu_i e_i}$ with respect to the atomic chemical potentials $\{\nu\}$. This is equivalent to the maximization of the anti-Helmholtz function $F^* = -1/\beta \ln Z^* = \sum_i \nu_i e_i - PV$ where PV is the pressure-volume product.

As an example, in the case considered by Duffin and Zener, when all the species are ideal gases, then

$$\Xi = \sum_{\{n\}} \pi_i (z_i \lambda_i)^{n_i} / n_i! = \exp(\sum_i z_i \pi_j e^{\beta \nu_j a_{ij}})$$

where z_i is the molecular partition function of the i th stable species. From eq 3 we have

$$Z = \left(\frac{1}{2\pi i}\right)^m \pi_j \left\{ \int_{\nu'_j - i\infty}^{\nu'_j + i\infty} d\nu_j \right\} \exp(\sum_i z_i \pi_j e^{\beta \nu_j a_{ij}}) e^{-\beta \nu_i e_i}$$

which when computed by the method of steepest descents yields the result of Duffin and Zener

$$Z = \min \left\{ \frac{\exp(\sum_i z_i \pi_j e^{\beta \nu_j a_{ij}})}{\pi_i e^{\beta \nu_i e_i}} \right\}$$

(1) R. J. Duffin and C. Zener, *J. Phys. Chem.*, **74**, 2419 (1970).

This is the statistical analog of the maximization of the anti-Helmholtz function for the equilibrium between reacting ideal gases.

INSTITUTE FOR ATOMIC RESEARCH
AND DEPARTMENT OF CHEMISTRY
IOWA STATE UNIVERSITY
AMES, IOWA 50010

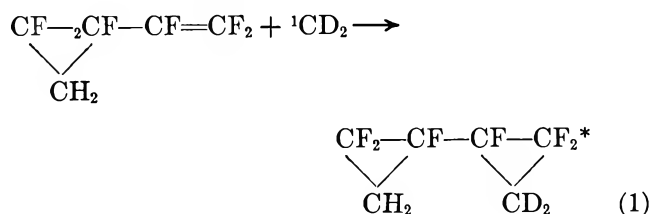
D. K. HOFFMAN

RECEIVED AUGUST 24, 1970

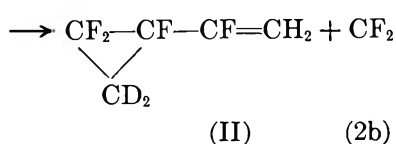
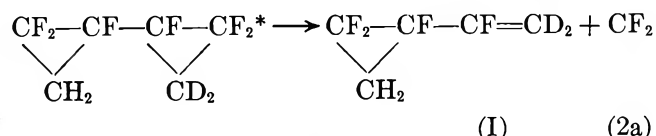
Intramolecular Energy Relaxation. A Novel and Direct Test of the RRK-RRKM Postulate^{1a}

Sir: Working theories of unimolecular decomposition² assume that internal energy relaxation occurs on a time scale that is short relative to decomposition; effective randomness of the internal energy distribution in excited molecules leads to the prediction of random incidence of decomposition events. Considerable evidence of various kinds and of varying degrees of cogency has now been accumulated that supports the general validity of this postulate,³ although there can be no doubt that failure must occur for sufficiently short-lived species.

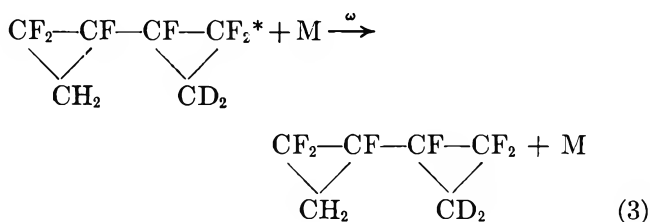
We have for some time been attempting to make an even more direct and quantitative experimental test of intramolecular energy relaxation than has hitherto existed. To this end we have applied the technique of chemical activation in order simultaneously to symmetrize and activate a substrate molecule of interest. The substrate finally chosen for study was hexafluorovinylcyclopropane (HVC). Addition of CD₂ to HVC produces symmetrical, vibrationally excited hexafluorobicyclopopyl (HBC)



where the asterisk signifies vibrational excitation. Deuterium atoms were used as a tracer to distinguish the original and product rings and otherwise differ unimportantly from H atoms. The excited HBC may decompose by disruption of the product ring (eq 2a) which was the



original site of activation or by rupture of the original ring (eq 2b).⁴ Equal amounts of decomposition of the two rings is direct evidence for internal energy randomization prior to decomposition. Variation of pressure of the system and the rate of collisional stabilization ω of the hot HBC molecule (eq 3)



provides a time scale against which the rate of internal relaxation can be measured. Obviously one wishes to shorten this time scale by pushing the system to higher and higher pressures; this kind of experiment has the advantage over others that have been made recently at high pressure^{5,6} in that three-body effects which can vitiate the latter⁶ as valid tests of the energy-randomization postulate will be self-canceling by the present test.

In these experiments, HVC was prepared by the photolysis at 2800 Å of a ketene-perfluorobutadiene mixture. This fluorocarbon system is preferable to its hydrocarbon analog, which we first investigated, since the reactions of methylene are cleaner with the fluorocarbon; also, decomposition of the hot product proceeds uniquely by split-off of a CF₂ moiety,⁴ rather than by a variety of ring isomerization reactions that ensue for the hydrocarbon analog. The HVC was purified and photolyzed again with ketene-*d*₂ in the presence of excess CO bath gas which contained 0.5% O₂. These diatomics inhibited complicating reaction of any ³CH₂ formed.^{7,8} After careful and complete gas chromatographic separation of the tetrafluorovinylcyclopropane products from all other components of the reaction mixture, analysis was made with a MS9 mass spectrometer. Rupture of products I and II by electron impact produces cyclopropyl and vinyl ions and results

(1) (a) Work supported by the National Science Foundation; (b) Standard Oil predoctoral fellow.

(2) (a) L. Kassel, "Kinetics of Homogeneous Gas Reactions," Reinhold, New York, N. Y. 1952; (b) R. A. Marcus and O. K. Rice, *J. Phys. Colloid Chem.*, **55**, 894 (1951).

(3) The first striking evidence was given by J. N. Butler and G. B. Kistiakowsky, *J. Amer. Chem. Soc.*, **82**, 759 (1959); for a review see L. D. Spicer and B. S. Rabinovitch, *Ann. Rev. Phys. Chem.*, **21**, 349 (1970).

(4) N. C. Craig, T. Hu, and P. H. Martyn, *J. Phys. Chem.*, **72**, 2234 (1968).

(5) D. W. Placzek, B. S. Rabinovitch, and F. H. Dorer, *J. Chem. Phys.*, **44**, 279 (1966).

(6) J. Aspden, N. A. Kawaja, J. Reardon, and D. J. Wilson, *J. Amer. Chem. Soc.*, **91**, 7580 (1969).

(7) B. A. DeGraff and G. B. Kistiakowsky, *ibid.*, **71**, 1553 (1967); **71**, 3984 (1967).

(8) J. W. Simons and B. S. Rabinovitch, *J. Phys. Chem.*, **68**, 1322 (1964).

in ion peaks at $m/e = 47$ and 95 from I and $m/e = 45$ and 97 from II; unfortunately, the masses corresponding to the vinyl group do not have a unique origin and the intensities of these peaks are confirmatory rather than diagnostic.

The energy of the excited bicyclopropyl parent is not known exactly but may be estimated to average 95–100

kcal mol⁻¹; the tail of the energy distribution carries energies to above 100 kcal mol⁻¹. The critical threshold for reaction is known⁹ to be less than 50 kcal mol⁻¹, so that the excess energy above threshold is a like amount in this case. Table I shows the product ratios over a 100-fold range of pressures. Their constancy with pressure variation is evident. A minor mass-spectral H–D isotope effect may be expected to be present but has no influence on the interpretation. The highest pressure corresponds to a relaxation time for collisional stabilization of $\sim 10^{-10}$ sec. The validity of the theoretical postulate regarding internal energy randomization is borne out to the extent tested.

The work will be extended to higher pressures and to reverse isotopic substitution.

Table I: Product Ratios on Decomposition of HBC

Pressure, mm	47/45 ^a	95/97 ^b
0.80	1.07 ± 0.08 ^c	1.21 ± 0.06 ^c
1.0	1.07 ± 0.06	1.21 ± 0.05
4.0	1.06 ± 0.10	1.24 ± 0.08
9.2	1.12 ± 0.03	1.23 ± 0.04
20	1.18 ± 0.03	1.22 ± 0.02
60	1.18 ± 0.01	1.26 ± 0.02
310	1.10 ± 0.11	

^a Uncorrected mass spectral ratios. ^b 13% of a 97 → 95 overlay correction, only, applied; a more complete correction does not change the ratio significantly. ^c Standard deviation of individual analyses.

(9) F. P. Herbert, J. A. Kerr, and A. F. Trotman-Dickenson, *J. Chem. Soc.*, 5710 (1965).

DEPARTMENT OF CHEMISTRY
UNIVERSITY OF WASHINGTON
SEATTLE, WASHINGTON 98105

J. D. RYNBRANDT^{1b}
B. S. RABINOVITCH

RECEIVED AUGUST 26, 1970

Journal of Chemical and Engineering Data

October 1970, Vol. 15, No. 4

TABLE OF CONTENTS

- 465** Editorial
- 466** Thermodynamic and Physical Properties of Monomethylamine-Lithium Thiocyanate System
Robert A. Macriss, Dharamvir Punwani, William F. Rush, and Wendell J. Biermann
- 471** Isobaric Vapor-Liquid Equilibria for the Systems Glycerol-Water and Glycerol-Water Saturated with Sodium Chloride
David H. T. Chen and A. Ralph Thompson
- 474** Enthalpies of Tetralin and Mixtures of Tetralin and n-Pentane
J. M. Lenoir, K. E. Hayworth and H. G. Hipkin
- 480** Vapor-Liquid Equilibria. Systems p-Xylene-Furfural and Ethylbenzene-Furfural
Pushpinder Singh Puri and K. S. N. Raju
- 483** Volumetric Behavior, Vapor Pressures, and Critical Properties of Cyclopropane
David C.-K. Lin, I. Harold Silberberg, and John J. McKetta
- 492** Liquid-Vapor Equilibria in the Sodium-Lead System
Albert K. Fischer and Stanley A. Johnson
- 495** Melting Point Intervals of Sulfur Allotropes
Malcolm Thackray
- 497** Phosphorus-31 NMR Data for Some Miscellaneous Compounds
Samuel O. Grim, Anthony W. Yankowsky, Salvatore A. Bruno, William J. Bailey, Edward F. Davidoff, and Tobin J. Marks
- 499** Partial Molal Volumes of p-Toluenesulfonic Acid, Sodium p-Toluenesulfonate, Iodic Acid, and Sodium Iodate in Aqueous Solutions at 25° C.
Oscar D. Bonner and Ralph W. Gable
- 501** Apparatus for Measurement of Isobaric Dew and Bubble Points and Vapor-Liquid Equilibria. Methanol-Water and Water-Dioxane Systems
Masahiro Kato, Hitoshi Konishi, and Mitsuho Hirata
- 505** Enthalpy of Alkali Metal Fluoroborates from 298-1000° K. Enthalpies and Entropies of Fusion and Transition
Arthur S. Dworkin and Max A. Bredig
- 508** Saturation Pressures of Cesium to Temperatures and Pressures Approaching Critical State
C. T. Ewing, J. R. Spann, J. P. Stone, E. W. Steinkuller, and R. R. Miller
- 510** Vapor Pressure of D₂O from 106 to 300° C.
Chia-Tsun Liu and William T. Lindsay, Jr.
- 514** Equation of State for Saturated Liquids
Harold G. Rackett
- 518** Specific Heat of Aluminum from Zero to Its Melting Temperature and Beyond. Equation for Representation of the Specific Heat of Solids
Edgar H. Buyco and Fred E. Davis
- 523** Estimates of Thermodynamic Properties of H₂O in Equilibrium with H, H₂, O, O₂, and OH. Temperature 1000° to 6000° C and Pressure 10 to 250,000 Bars
Clair E. Chapin
- 527** Solubility of F₂, NF₃, and O₂ in Anhydrous Liquid HF
R. T. Rewick, W. E. Tolberg, and M. E. Hill
- 531** Isobaric Binary Vapor-Liquid Equilibria. Systems Acetic Acid-Ethylbenzene and Acetic Acid-p-Xylene
O. P. Bagga and K. S. N. Raju
- 534** Thermodynamic Properties of Acetone, Dimethyl Sulfoxide, and Their Solutions by Rayleigh Light Scattering
Linda L. Haynes, Raymond L. Schmidt, and H. Lawrence Clever
- 536** Some Properties of the Systems 1-Chlorobutane-1-Chlorooctadecane and 1-Chlorobutane-1-Chlorohexane at 25° C
E. L. Heric and B. M. Coursey
- 539** Abrupt Changes in Cadmium Activity with Composition for Dilute Copper and Gold Alloys
Donald R. Conant and Harold S. Swofford, Jr.
- 542** Binary Freezing Point Diagrams for Some Methyl Ketones and Their Complete Solubilities in Acetone, Methanol, Benzene, and Carbon Tetrachloride
August V. Bailey, Donald Mitcham, and Ewald L. Skau
- 546** Temperature Dependence of Diffusion and Viscosity in Aqueous Urea Solutions
John C. MacDonald and James J. Guerrero

- 548** Thermodynamics of Hydrochloric Acid in 8.03, 20.76, 44.04, 70.28, and 87.71 Weight % 2-Propanol-Water Mixtures from E.M.F. Measurements at 0°, 15°, 25°, and 35° C
Rabindra N. Roy and Alfred Bothwell
- 553** Enthalpy of Formation of Bromotrinitromethane
George A. Carpenter, Martin F. Zimmer, Edward E. Baroody, and Robert A. Robb
- 556** Natural Convection Heat Transfer from a Horizontal Cylinder to a Reacting Gas. $\text{N}_2\text{O}_4 \rightleftharpoons 2\text{NO}_2$ System
Frank T. Brown, Boo-Goh Ong, and David M. Mason
- 560** Enthalpy of Formation of Ammonium Hydrogen Monoamidophosphate, $\text{NH}_4\text{HPO}_3\text{NH}_2$
Zachary T. Wakefield, Basil B. Luff, and Robert B. Reed
- 562** Apparent Molal Volumes of Aqueous Sodium Tetraphenylboron Solutions from 0° to 60° C
Frank J. Millero
- ORGANIC SECTION
- 567** Effect of Molecular Structure on Infrared Spectra of Six Isomers of Bipyridine
Carol K. Pearce, Dietmar W. Grosse, and William Hessel
- 570** Methyl Esters of Comphoric and Isocomphoric Acids
David J. Stanonis and Walter D. King
- 573** Isolation of an Intermediate during Formation of 4,4',4''-Trinitrohydrobenzamide in the Reaction of 4-Nitrobenzaldehyde with Ammonia
Anne-Marie Weidler-Kubanek
- 574** NMR Structure Determination of Some New 4-Hydroxyxanthone Derivatives
Piero Valenti, Giulio Ceccarelli, and Paolo Da Re
- 578** 2-Alkyl-3-Phenylcinchoninic Acids and Related Products
Eldon H. Sund and Henry R. Henze
- 579** Synthesis and NMR Data for Dialkyl and Diaryl Trichloromethylphosphonates
K. Darrel Berlin and N. K. Roy
- 581** New Method for Preparing Alkyl (Amino-s-triazinyl)phosphonates
Jerry P. Moreau and Leon H. Chance
- 583** Solubilities of Some Normal Saturated and Unsaturated Long-Chain Fatty Acid Methyl Esters in Acetone, n-Hexane, Toluene, and 1,2-Dichloroethane
August V. Bailey, James A. Harris, and Evald L. Skau
- 586** Sodium Alkylbenzenesulfonates from Phenols
James E. Cooper and James M. Paul
- 589** A New Synthesis for a Highly Halogenated Styrene
Leonard O. Moore
- 590** Some 2,5- and 5,6-Dihalonicotinic Acids and Their Precursors
Frank L. Setliff
- 592** Nitration of 1-Benzylpyrrole.
Shyam Sunder and C. DeWitt Blanton, Jr.
- 593** Synthesis and Characterization of 2-Ureylene-4,6-diamino-s-triazines
John E. Herweh and William Y. Whitmore
- 595** Salting Out of Aqueous Procaine Hydrochloride by Sodium Chloride at 25° C
Robert F. Platford
- 598** Errata
- 599** New Data Compilations
- 600** Author Index
- 604** Subject Index